Geology, Geochronology, and Tectonic Significance of the Blair River inlier, Northern Cape Breton Island, Nova Scotia

by

Brent V. Miller

Submitted in partial fulfillment of the requirements
for the degree of Doctor in Philosophy

at

Dalhousie University
Halifax, Nova Scotia
May, 1997

© Copyright 1997 by Brent V. Miller

National Library of Canada
Bibliothèque nationale du Canada

Acquisitions and Bibliographic Services
Acquisitions et services bibliographiques

395 Wellington Street
Ottawa ON K1A 0N4
Canada
395, rue Wellington
Ottawa ON K1A 0N4
Canada

Your file Votre référence

Our file Notre référence

The author has granted a non-exclusive licence allowing the National Library of Canada to reproduce, loan, distribute or sell copies of this thesis in microform, paper or electronic formats.

L'auteur a accordé une licence non exclusive permettant à la Bibliothèque nationale du Canada de reproduire, prêter, distribuer ou vendre des copies de cette thèse sous la forme de microfiche/film, de reproduction sur papier ou sur format électronique.

The author retains ownership of the copyright in this thesis. Neither the thesis nor substantial extracts from it may be printed or otherwise reproduced without the author's permission.

L'auteur conserve la propriété du droit d'auteur qui protège cette thèse. Ni la thèse ni des extraits substantiels de celle-ci ne doivent être imprimés ou autrement reproduits sans son autorisation.

0-612-24755-4

Canada

TABLE OF CONTENTS

LIST OF FIGURES

LIST OF TABLES

ABSTRACT

The Blair River inlier of northern Cape Breton Island, Nova Scotia includes four major Proterozoic units. The protolith of the tonalitic to dioritic Sailor Brook orthogneiss is no younger than 1217 Ma and metamorphic zircon associated with granulite-facies metamorphism of this unit crystallised at 1035 +12/-10 Ma. Igneous zircon in the Lowland Brook Syenite crystallised at 1080 +5/-3 Ma, but this unit was not significantly affected by Proterozoic metamorphism and deformation. The Red River Anorthosite Suite is a Proterozoic massif-type anorthosite that contains a central core of massive anorthosite and grades outward, through leucogabbro and layered mafic rocks, to rare pyroxenite. High-temperature, relatively low-pressure metamorphism of the suite occurred at 996 +6/-5 Ma, but its effects are rarely distinguishable due to a strong amphibolite-facies overprint and intense alteration. Charnockitic rocks are lithologically and chemically gradational with the layered unit, possibly due to contact metamorphism and metasomatism of the anorthosite suite during intrusion of the charnockite. The biotite-rich, garnet-bearing, granitoid Otter Brook gneiss yielded an igneous age of 978 +6/-5 Ma.

Silurian thermal activity in the Blair River inlier is recorded by magmatism associated with the undeformed Sammys Barren granite at 435 +7/-3 Ma and by metamorphic mineral ages. U-Pb analysis of metamorphic titanite from amphibolite-facies overprint assemblages in the Sailor Brook gneiss, Lowland Brook Syenite, Red River Anorthosite Suite, a gneissic anorthosite, and the Otter Brook gneiss, along with igneous titanite from the Red River syenite and Fox Back Ridge diorite/granodiorite, all yield cooling ages of ca. 425 Ma. Lower-temperature cooling ages are provided by hornblende from the Fox Back Ridge unit (417 ± 6 Ma), rutile from the Red River Anorthosite Suite (410 ± 2 Ma), muscovite from the Meat Cove marble (428 ± 7 Ma), and phlogopite from a calc-silicate lens in the Otter Brook gneiss (410 ± 6 Ma).

The Blair River inlier is interpreted to be a fragment of Grenvillian basement derived from a promontory on the proto-Atlantic continental margin of North America. Its tectonostratigraphic position at the western margin of a condensed section of the Appalachian orogen in Cape Breton Island is confirmed by a host of geophysical data. Similarities in rock types, ages, and isotopic characteristics with the Grenville Province support a cratonic Laurentian origin for the Blair River inlier and these features contrast sharply with accreted terranes of the Appalachian orogen. The Blair River inlier preserves no indication of Taconian (Ordovician) events, and Acadian (Devonian) or Alleghanian (Carboniferous) events appear to be limited to high-level faulting associated with the amalgamation of the neighbouring Aspy terrane. Widespread Silurian metamorphism and localised magmatism of this inlier identical in age to similar events recognised elsewhere in the northern Appalachian orogen, and indicates involvement of the Blair River inlier in the Silurian culmination of Appalachian orogenesis.

ACKNOWLEDGEMENTS

I thank my supervisory committee, Dr. Rebecca Jamieson, Dr. Sandra Barr, and Dr. Robert Raeside for their insightful supervision of this project and their many helpful comments on the text of the dissertation. My field assistants, Tasos Gramatikopolis, Robert Bekkers, and Gary MacDougall were an invaluable help. Thanks also to laboratory technicians, Don Osborn, Bob Mackay, Keith Taylor, Sherry Dunsworth, who helped to make data acquisition easier and more accurate. I am grateful to the many students, faculty and staff at Acadia and Dalhousie Universities who have provided intelligent discussion and incisive suggestions. I would like to acknowledge specifically Adoon Wunapeera and Robert Bekkers, who completed related studies in northern Cape Breton Island and Chris White for his generosity and constant willingness to share his extensive knowledge of northern Appalachian geology, and home-brew. Completion of this project would not have been possible without the unwavering support and encouragement of my entire family, notably my parents, Sandra and James Miller and my grandparents, Ruth and Don Cole and Martha Miller.

CHAPTER 1 - Introduction

1.1 Introduction

From the Middle Proterozoic to the mid-Paleozoic, the eastern margin of ancient North America (Laurentia) was subjected to extremes of tectonic processes; two major orogenic episodes, both culminating in continent-continent collision, were separated in time by the development of a passive continental margin. The most extensive record of this period of geological activity is preserved in a band of basement inliers and their sedimentary cover sequences that extend discontinuously from Alabama to Newfoundland (Figure 1.1) along the western flank of the Appalachian orogen. The inliers expose Middle to Late Proterozoic rocks derived from the cratonic basement of easternmost Laurentia (Hatcher, 1984; Bartholomew and Lewis, 1992; Rodgers, 1995), which is otherwise buried beneath Paleozoic sedimentary rocks of the Appalachian foreland basin. East of the band of inliers are outboard terranes accreted to Laurentia during Paleozoic orogenies.

Laurentian basement inliers in the Appalachian orogen contain distinctive lithologies including granulite-facies gneiss, anorthosite, charnockite, and mangerite (Bartholomew, 1984 and papers therein; Owen and Erdmer, 1990). These rock types are common in the Grenville Province, but are largely absent from the Appalachian outboard terranes. Their ages, where known or inferred, are comparable to the characteristic ages of plutonism and metamorphism in the Grenvillian orogen (ca. 1200-960 Ma; e.g., Owen and Erdmer, 1989; 1990; Karabinos and Aleinikoff, 1990; Currie et al., 1991, Rankin et al., 1989).

The Blair River inlier (formerly Blair River Complex of Barr and Raeside, 1989) of northwestern Cape Breton Island (Figure 1.1) lies within the Appalachian geological province but

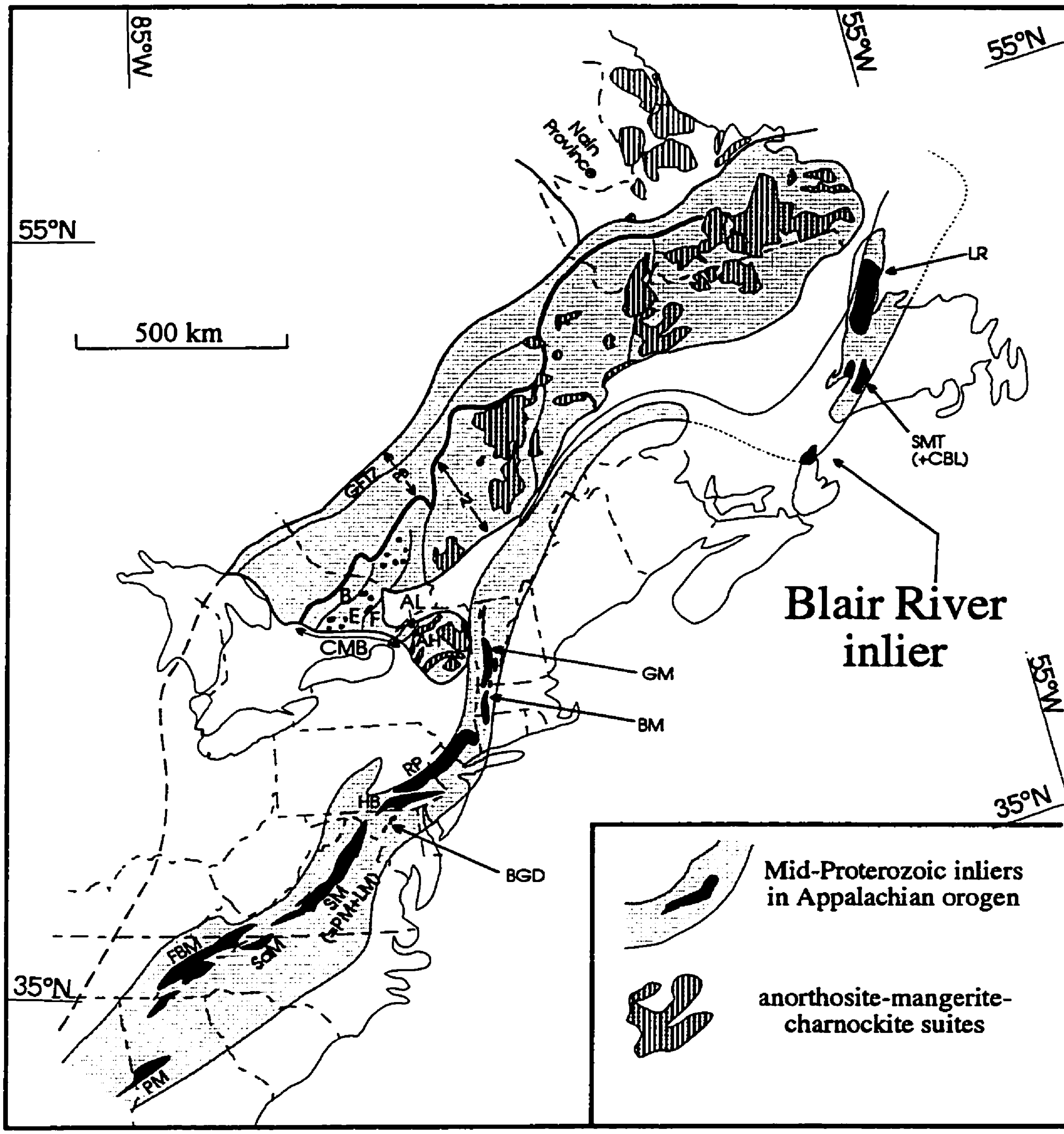

Figure 1.1 - Distribution of Middle Proterozoic rocks in the Appalachian orogen. Modified after Rankin (1976) and Bartholomew and Lewis (1992). SLP = St. Lawrence promontory, QR = Quebec re-entrant. The inferred eastern limit of Laurentia is the positive gravity anomaly (after Rodgers, 1995; Rankin et al., 1989)

includes granulite-facies gneiss, an anorthosite suite, charnockite, and pyroxene-bearing syenite. These rocks are distinct from the Appalachian outboard terranes in Cape Breton Island (Barr and Raeside, 1986; 1989), but similar to rock types in the Grenville Province and in Grenvillian basement inliers in the Humber Zone of western Newfoundland (e.g., Owen and Erdmer, 1990). The Blair River inlier has the characteristics of Grenvillian basement to the Appalachian orogen, and has the potential of preserving a long record of the geological history of eastern Laurentia.

1.2 Tectonic zones in the Appalachian orogen

On a broad scale, the northern and Newfoundland Appalachian orogen comprises three principal components: 1) remnants of the Laurentian continental margin, including Grenvillian basement rocks overlain by rift-drift-passive margin sedimentary sequences, 2) the Central Mobile Belt, a variety of oceanic remnants including terranes associated with the Iapetus Ocean, oceanic arc complexes, and possible microcontinents, and 3) remnants of Gondwana and peri-Gondwanan arcs. The latter two major components are the generalised "Appalachian outboard terranes" with origins outside of, though not necessarily distant from, Laurentia. These crustal fragments form a variety of lithotectonically discrete terranes and zones (Williams, 1979; Williams and Hatcher, 1982; Horton et al., 1989; Williams et al., 1988; Barr and Raeside, 1989; van Staal and Fyffe, 1991; Colman-Sadd et al., 1992; Keppie, 1993). The deformed Laurentian margin is termed the Humber Zone in the northern (Canadian) Appalachian orogen, makes up part of the "Taconian" zone in the central Appalachian orogen (Maine to New Jersey), and in the southern Appalachians (Pennsylvania to Alabama) its remnants occupy the Blue Ridge Province in the Cumberland zone of Hibbard and Samson (1995), and Humber Zone equivalents in the subsurface beneath the Inner Piedmont.

The Appalachian orogen is classically divided in time and, less discretely, in space (generally younging outward from the craton) into large-scale orogenic bands designated the Taconian (Middle and Late Ordovician), Acadian (Late Silurian-Middle Devonian), and Alleghanian (Carboniferous-Early Permian) orogenies (Rodgers, 1970; Williams and Hatcher, 1982; Bradley, 1983). Detailed studies that integrate precise geochronology with structural and petrologic data, demonstrate that this paradigm is overly simplistic. Current evidence suggests considerable diachroneity in the timing, style, and intensity of the once-presumed laterally equivalent tectonic episodes in different parts of the Appalachian orogen, (e.g., Rodgers, 1970; Dunning et al., 1990a; Keppie, 1993; Sevigny and Hanson, 1993; Wintsch et al., 1993). Furthermore, considerable debate exists as to the tectonic significance of the orogenic events.

1.3 Historical perspectives of the relationship between northern Appalachian tectonic zones and the Blair River inlier

Early workers proposed a lithologic correlation between gneissic and meta-igneous rocks in northern Cape Breton Island (now separated as the Blair River inlier) and basement rocks of western Newfoundland (now the Humber Zone; e.g., Neale 1963; 1964; Neale and Kennedy 1965; Cameron, 1966; Jenness 1966; Brown 1973; Currie 1975; Macdonald and Smith 1979; Smith and Macdonald, 1983; Dupuy et al., 1986). However, the tectonic significance of the correlation was poorly understood at the time.

Despite the lithologic correlation with Laurentian rocks in western Newfoundland, early tectonic zone models considered all of Cape Breton Island to be part of the Gondwanan-affinity Avalon terrane. These models necessitated a deflection in the strike of terrane boundaries from Newfoundland through the Cabot Strait and north of Cape Breton Island (Figure 1.2a; Williams, 1978; Williams and Hatcher, 1982; 1983; Nance, 1986; Keppie and Dallmeyer, 1989). The position of the other terrane boundaries in the Cabot Strait and Gulf of St. Lawrence was a topic that received little discussion. This interpretation

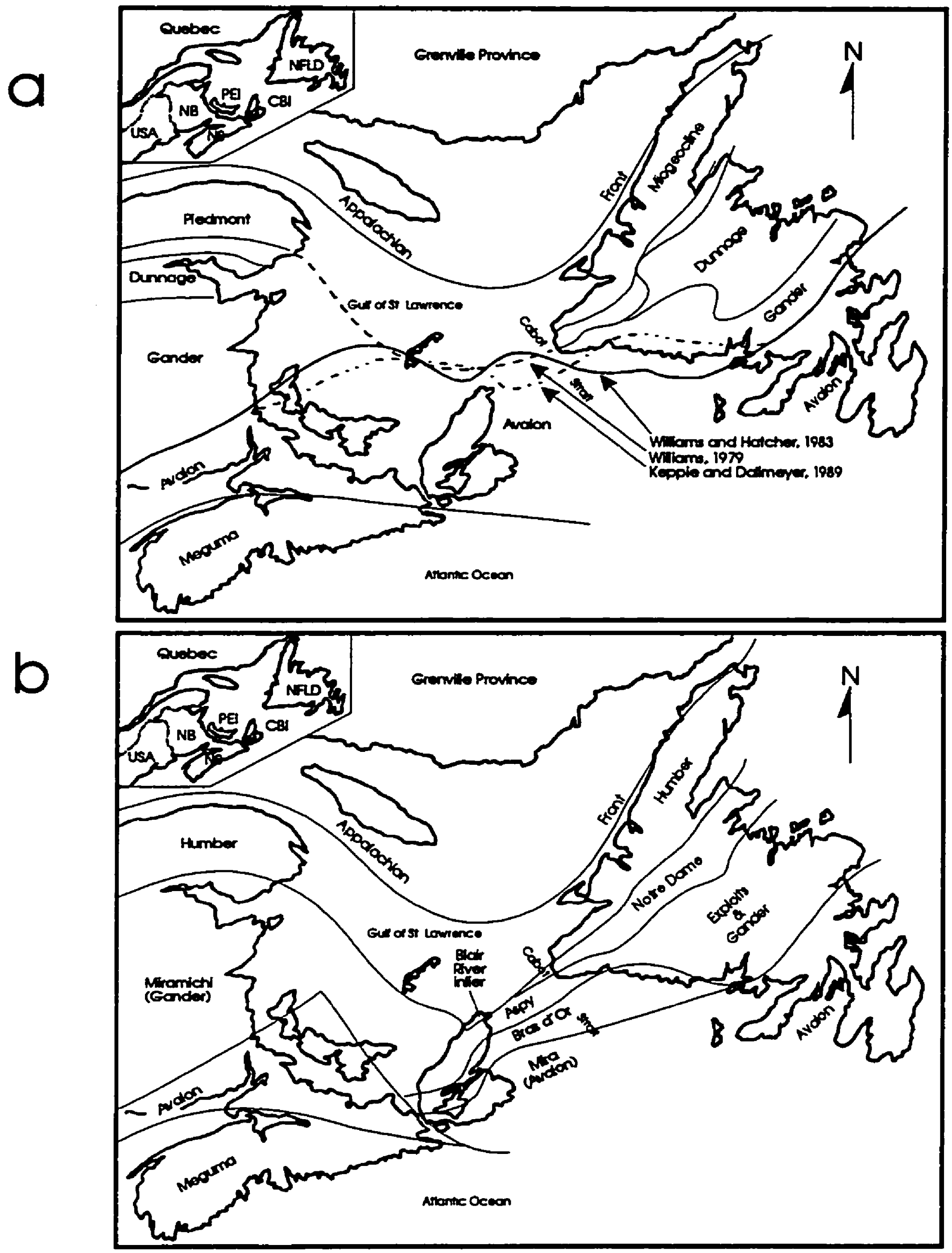

Figure 1.2 - Examples of historical differences in northern Appalachian tectonic zones. (a) Early interpretations of the tectonic zones in the northern Appalachian orogen that considered Cape Breton Island part of the Avalon terrane. Zones are after Williams and Hatcher (1983) and Avalon-Gander terrane boundaries are after authors noted on the figure. (b) Later tectonic zones (from Barr and Raeside, 1986; 1989) that were corroborated, in part, by geophysical data published in the late 1980's.

of tectonic zones made it easier to discount the significance of Grenvillian-type rocks in northern Cape Breton Island because, unlike the other basement inliers that were thought to be underlain by autochthonous Laurentian craton (e.g., Hatcher and Zeitz, 1980), the locations of terrane boundaries in the Gulf of St. Lawrence (cf., Figure 1.2a) implied that Grenvillian basement did not extend far enough into the orogen to provide an underlying source region for the Blair River inlier.

A variety of geophysical data became available in the late 1980's that helped to support a correlation between the Blair River inlier and the Humber Zone in western Newfoundland. Deep seismic profiles from Lithoprobe East transects combined with industrial shallow seismic data (Loncarevic et al., 1989; Marillier et al., 1989; Durling and Marillier, 1990; Stockmal et al., 1990; Langdon and Hall, 1994) showed that autochthonous Laurentian lower crust extends, at depth, much farther into the Gulf of St Lawrence than was previously thought, to at least as far south and east as northernmost Cape Breton Island (Figure 1.3). Furthermore, linear gravity and magnetic anomalies, which reflect major lower and upper crustal structures such as terrane boundaries and tectonic zones (e.g., Loncarevic et al., 1989; Marillier et al., 1989; Marillier and Verhoef, 1989; Miller, 1990), clearly strike from southern Newfoundland through the Cabot Strait and into, rather than around, Cape Breton Island (Figure 1.4).

Based primarily on geological considerations, Barr and Raeside (1986; 1989) and Barr et al. (1987a; 1987b) revived the correlation of the Blair River inlier with the Humber Zone as part of their redefinition of tectonic zones in the northern Appalachian orogen and defined more clearly the tectonic significance of the correlation. Their interpretation has since been used in tectonic models (Stockmal et al., 1987; 1990, Lin et al., 1994). The repositioned tectonic zones (Figure 1.2b), as constrained partly by the geophysical data, require that Cape Breton Island contain a condensed section of the Appalachian orogen (e.g., Barr and Raeside, 1986; 1989) between the Laurentian Blair River inlier and the Avalonian Mira terrane, as opposed to the Appalachian zones meandering awkwardly and arbitrarily north of the

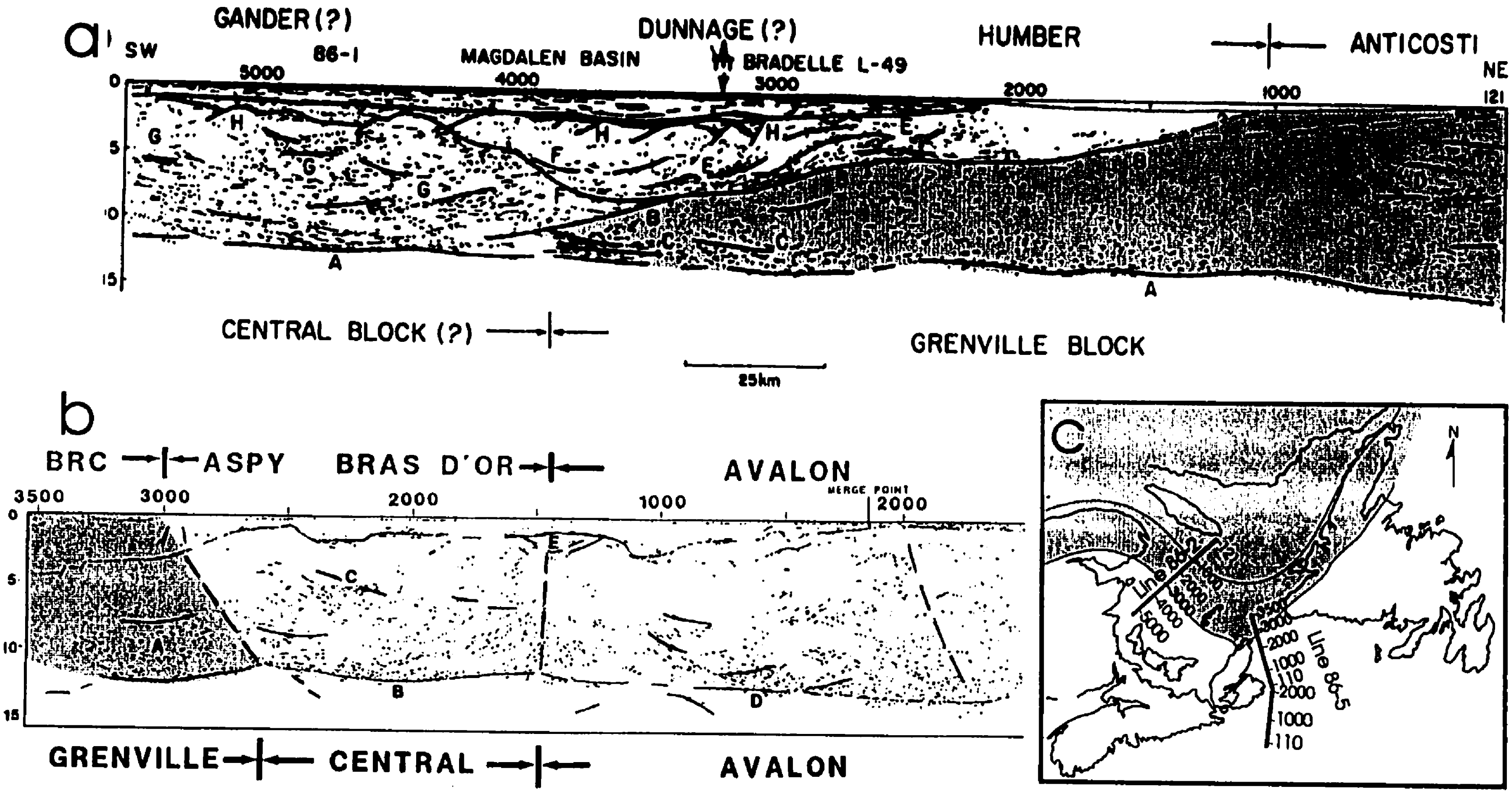

Figure 1.3 - Interpreted Lithoprobe East deep seismic lines that suggest Grenvillian basement extends farther into the Appalachian orogen than previously believed. (a) Lithoprobe East line 2, as interpreted by Marillier et al. (1989). (b) Lithoprobe East line 5, as interpreted by Loncarevic et al (1989). (c) Terrane map of Barr and Raeside (1989) showing locations of seismic lines. Numbered tick marks correspond to shot points shown on the lines.

a

b

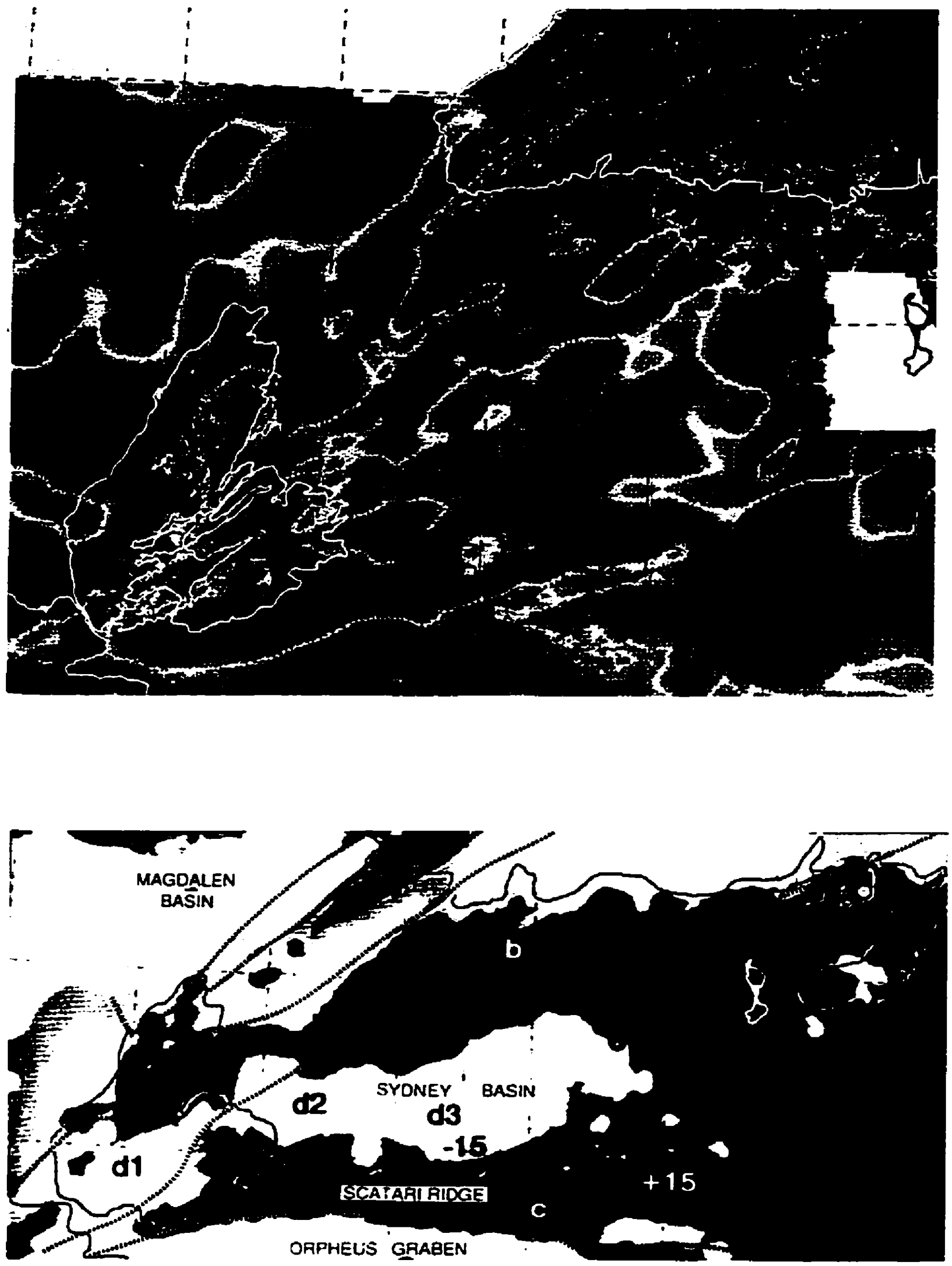

Figure 1.4 - Geophysical data that suggest structural continuity between Cape Breton Island and southern Newfoundland. (a) Total-field magnetic anomaly map from Loncarevic et al. (1989). (b) Bouguer anomaly map from Loncarevic et al. (1989).

island. However, some authors have not accepted the Grenvillian affinity and/or the Laurentian parentage of the Blair River inlier, based partly on the implications for the relations of the other Appalachian terranes in Cape Breton Island (e.g., Murphy et al., 1989; Keppie et al., 1992; Keppie, 1993; Lin, 1993; Chen et al., 1995; Lynch, 1996). Some of these workers continue to include the Blair River inlier in the Avalon terrane or in a composite thrust terrane in the Central Mobile Belt of the Appalachian orogen, whereas others debate the tectonostratigraphic relationships between the Aspy, Bras d' Or, and Mira terranes in Cape Breton Island (Figure 1.2).

1.4 Grenvillian basement exposures in the Appalachian orogen

Middle Proterozoic basement rocks and late Proterozoic to mid-Paleozoic volcanic and sedimentary cover rocks in the Appalachian orogen preserve an extensive record of geological activity along the eastern margin of ancient North America. These rocks record the effects of Grenvillian orogenesis on the North American craton, break-up of a Proterozoic supercontinent (Hoffman, 1991), development of a passive margin, and Appalachian orogenesis on the eastern margin of Laurentia.

Exposures of Grenvillian basement rocks in the Appalachian orogen form a discontinuous band of fault- or unconformity-bounded inliers between Alabama and Newfoundland (Figure 1.1). The band of inliers in the northern and central Appalachian orogen coincides closely with a prominent regional positive gravity gradient (Figure 1.1; Hatcher and Zeitz, 1980; Cook and Oliver, 1981; Haworth et al., 1981; Rodgers, 1995) located near the core of the Appalachian orogen. The Blue Ridge anticlinorium is displaced to the north and west of the gravity gradient but the, probably more closely autochthonous, Pine Mountain block is adjacent to the gradient. Only the, controversially Laurentian, Goochland terrane (Farrar, 1984; Rankin et al., 1993; Hibbard and Samson, 1995) is exposed east of the gravity gradient.

The gravity gradient is thought to mark the eastern extent of the Laurentian craton beneath the Appalachian orogen (Hatcher and Zietz, 1980) and its sinuous trend reflects the shape of late Proterozoic to early Paleozoic continental break-up, perhaps along zones of extension linking hot-spot generated triple junctions (Burke and Dewey, 1973; Rankin, 1976). The trend of the gravity gradient outlines a series of promontories and re-entrants in the buried edge of Laurentia (Thomas, 1977; Rankin, 1976). The northern, central, and southern segments of the Appalachian orogen each contain a major promontory/re-entrant pair. The northern Appalachian orogen contains the largest pair, the St. Lawrence promontory and the Quebec re-entrant (Figure 1.1). The Blair River inlier is exposed at the apex of the promontory.

Oroclinal bends in the trend of the band of Grenvillian basement inliers broadly coincide with the promontories and re-entrants, although the curvature is somewhat muted compared to that of the gravity gradient (Figure 1.1). These observations are widely interpreted to indicate that the shape of the inherited Laurentian continental margin had a strong influence on the geometry and development of Paleozoic orogenic events, including emplacement of basement inliers (Hibbard, 1982; Hatcher, 1984; Bartholomew and Lewis, 1988; Rodgers, 1995). But only the southern Blue Ridge Province was thrust a large distance (>100; Hatcher, 1978; Bartholomew, 1983) over the cratonic edge during the Paleozoic.

The Blair River inlier has all the necessary characteristics to be included in the band of inliers. The inlier contains Grenvillian rock types, it lies near the western flank of the Appalachian orogen adjacent to the positive gravity gradient that marks the eastern extent of Laurentia, and to the south and east are accreted Appalachian outboard terranes. The Blair River inlier is unique, however, in that it directly overlies the apex of the largest and sharpest promontory of the buried Laurentian cratonic edge.

1.5 Research justification and purpose of study

The Grenville orogen in eastern North America is nearly twice as long and half-again as wide as its exposure in the Grenville Province; most of the orogen is buried beneath Paleozoic sedimentary rocks or the Appalachian orogen (Figure 1.1). The basement inliers in the Appalachian orogen, therefore, provide important constraints on the pre-Paleozoic shape of, and a broader understanding of the ages and compositions of the rocks that comprised, a large area eastern Laurentia. For example, the primarily orthogneissic inliers in the Blue Ridge Province are probably not an extension of the Central Granulite Belt of the Grenville Province, but may comprise a previously unrecognised Grenvillian subdivision (Rankin et al., 1993). The basement inliers in New England may be a continuation of the Adirondack Mountains (part of the Central Granulite Belt) but lack distinctive igneous rocks like anorthosite and charnockite. The lithologies, ages, and metamorphic conditions in the Long Range Inlier correspond closely to the Grenvillian rocks in eastern Labrador and northern Quebec (Owen and Erdmer, 1989; 1990; Owen, 1991). Moore (1986) suggested that the recognition of oceanic rocks and suture zones between the allochthonous terranes and parts of the opposing continent could resolve the debate (at that time) over the continent-continent collision versus intracratonic nature of the Grenvillian orogeny. He further speculated that the suture zone might be located in (or under) the Appalachian orogen and that the Central Metasedimentary Belt may be a klippe rooted southeast of the Grenville Province. If so, the basement inliers may preserve a clearer record of Grenvillian continent-continent collision and may contain the only remnants of the opposing continent. The Blair River inlier, being located at, and most likely derived from, the apex of the largest protrusion from cratonic North America is an important sample of Grenvillian rocks with which to test the hypotheses of Moore (1986). The Blair River inlier can also provide important constraints for extending the understanding of lithological variations and the timing of Proterozoic thermal events in parts of the Grenville orogen that are exposed only in the Appalachian inliers.

Despite the potential of basement inliers to preserve an extensive record of the history of tectonic processes along the eastern margin of Laurentia, "...a number of them have yet to receive anything but cursory work as geologists have pursued what seemed like more timely and momentous geological problems in the Appalachians" (Bartholomew, 1984; pg. v). In the twelve years since the comprehensive compilation of Bartholomew (1984), most workers in the western flank of the Appalachian orogen have focused on the Paleozoic sedimentary sequences, and the basement rocks have received relatively little study. As Rankin et al. (1993; pg. 397) noted,

> "Our understanding of Grenvillian history of the Laurentian Appalachians is very limited. Recognition of many of the rocks as pre-Appalachian basement alone is a major accomplishment in many areas where Paleozoic redeformation has been intense. Where sufficiently well-studied and uncomplicated by later events, the Laurentian basement records a very complex sequence of events in the 1.35-Ga to 900-Ma time period."

Although a Paleozoic thermal overprint is evident from petrographic studies, the age of Appalachian metamorphism is poorly constrained in most of the inliers, allowing for ambiguities and apparent contradictions in the timing of orogenesis along the strike of the orogen. Furthermore, some inliers (or units within an inlier) are defined as "Grenvillian" on the basis of rock type alone (e.g., Drake, 1984; Piasecki, 1991; Valières et al., 1978), inferred geologic correlations and imprecise or questionable radiometric ages (e.g., Rb-Sr whole-rock; Davis et al., 1962; Fullagar and Odom, 1973; Helenek and Mose, 1984).

Despite lingering contradictory tectonic models, the Blair River inlier, as one of the Grenvillian basement blocks in the Appalachian orogen, can provide important constraints on the geometry and timing of northern Appalachian tectonic events, and thereby constrain tectonic models. However, the Blair River inlier had not been mapped systematically as a discrete lithotectonic unit, bounding and internal structures were not well documented, both Grenvillian and Appalachian metamorphic conditions were poorly constrained, and the ages of units could only be inferred from geological correlations and one imprecise radiometric age. Therefore, the specific objectives of this thesis dissertation are to:

1) present the results of 1:10,000 scale mapping in the Blair River inlier, subdividing and redefining previously described units where necessary (presented at 1:50,000 scale, Map A in back pocket)

2) document rock types, field relations, compositional variations, chemistry, and structure of the units that comprise the Blair River inlier and its bounding fault zones (Chapter 2)

3) describe the geochemical characteristics of gneissic and plutonic rocks (Chapter 3)

4) determine the ages of major units in order to test the Grenvillian affinity of the Blair River inlier, and to evaluate the timing and degree of involvement in Appalachian orogenesis (Chapter 4)

5) provide constraints on metamorphic conditions of major units (Chapter 5)

6) compile new and existing data on the Blair River inlier to provide a synthesised interpretation of its relationship to the Grenvillian orogeny and its role in northern Appalachian orogenesis (Chapter 6).

CHAPTER 2 - Lithologic Units, Field Relations, Petrography, and Structure

2.1 Introduction and previous work

The Blair River inlier consists of the pre-Middle Devonian rocks in the crystalline core of the northwestern Cape Breton Highlands. The inlier is flanked to the north and west by Carboniferous sedimentary units of the Horton and Windsor groups and by rhyolite, basalt, and sedimentary rocks of the Devonian to Early Carboniferous (Barr et al., 1995; Smith and Macdonald, 1981) Fisset Brook Formation (Figure 2.1). The contact between the Blair River inlier and the cover rocks is locally interpreted as a nonconformity (Bradley and Bradley, 1984), but is faulted in most locations. The Blair River inlier is separated from the Aspy terrane to the southwest by the Red River fault zone and to the southeast by the Wilkie Brook fault zone (Figure 2.1).

The most detailed published map of the Blair River inlier prior to this study was that of Raeside and Barr (1992). Their map formed the basis for the present project and their unit names are followed here as closely as possible. The present study, however, recognises lithologic subdivisions within previously undivided units, repositions the boundaries of some units, and suggests new or more appropriate unit names in order to describe more precisely the association between, and lithologic variation within, the inlier. The Blair River inlier is so named in order to retain, as a single lithotectonic entity, the pre-Devonian units north of the Red River fault zone and west of the Wilkie Brook fault zone.

As mapped here, the Blair River inlier consists of eight major lithologic units that comprise about 85% of the map area. The major units in the complex are the Sailor Brook gneiss, Otter Brook gneiss, Polletts Cove River gneiss, Lowland Brook Syenite, Red River Anorthosite Suite and an associated charnockite unit, and the Fox Back Ridge diorite/granodiorite. Smaller units include

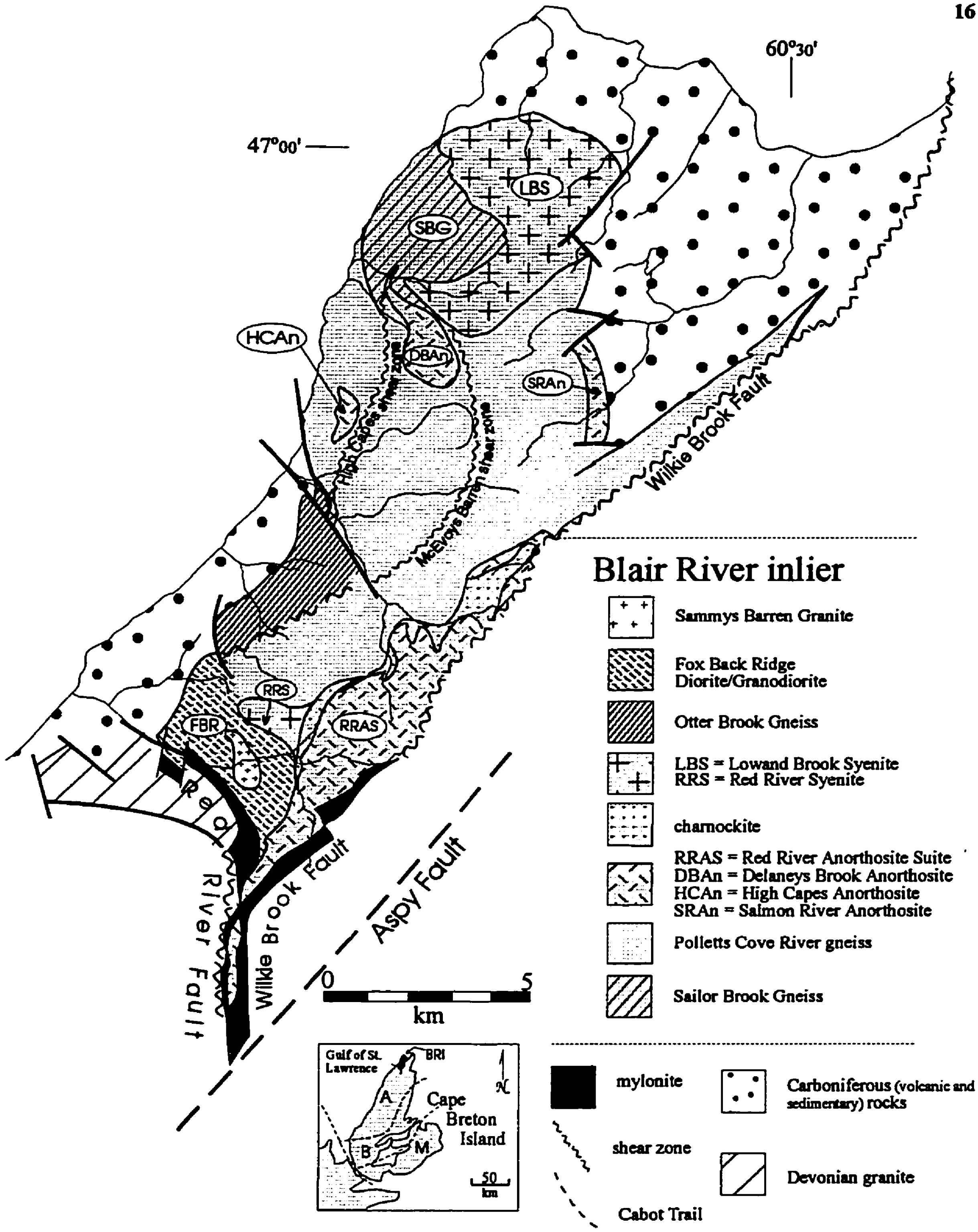

Figure 2.1 - Generalised geologic map of the Blair River inlier. Inset: BRI = Blair River inlier, A = Aspy terrane, B = Bras d Or terrane, M = Mira terrane.

the Delaneys Brook, High Capes, and Salmon River anorthosite bodies, Sammys Barren granite, Red Ravine syenite, small bodies and dikes of coarse grained metagabbro, marble and calc-silicate rocks, relatively undeformed and unmetamorphosed fine-grained mafic and felsic dikes, and various fault zone rocks (Figure 2.1).

A significant change from the map of Raeside and Barr (1992) is the identification of the Sailor Brook gneiss and Otter Brook gneiss as distinct map units and the separation of these units from the Polletts Cove River Group. The remainder of the Polletts Cove River Group is here renamed the Polletts Cove River gneiss. This unit is heterogeneous, consisting of variably deformed igneous rocks and gneisses of many different compositions and states of deformation with inferred igneous protoliths that are not further divisible at the present map scale and are not recognisably stratified.

In the southeastern part of the map area, Smith and Macdonald (1983) included anorthosite and gabbroic rocks in the Red River Anorthosite Complex. However, the term "suite" is more appropriate than "complex" because this large-scale map unit comprises lithologically distinctive and separable igneous subunits that are interpreted to be genetically related (Macdonald and Smith, 1979; Dupuy et al., 1986; Bekkers, 1993). Therefore, this unit is here termed the Red River Anorthosite Suite. The suite as now mapped includes some of the rocks mapped as diorite by Neale (1964), thought to be metasedimentary or metavolcanic rocks by Jenness (1966), considered country rock by Mitchell (1979), and mapped as gabbro, gneiss, and granulite by Smith and Macdonald (1983).

Raeside and Barr (1992), following the work of Smith and Macdonald (1983), combined monzodiorite, diorite, and dioritic gabbro in the southern part of the map area into a unit they termed the Red River monzodiorite. The present study recognises that their map unit includes amphibolite, massive and layered gabbro, and metagabbro, all of which are here interpreted to be part of the Red River Anorthosite Suite. The recognition of preserved or relict orthopyroxene-bearing "monzodiorite and related rocks" associated with, but not part of, the anorthosite suite are here defined as charnockite. The diorite and remaining monzodiorite and granodiorite are here considered a separate unit termed the Fox Back Ridge diorite/granodiorite. Undeformed granite and syenogranite layers, dikes, veins, and small pods in the Fox Back Ridge diorite/granodiorite were mapped by Smith and Macdonald (1983) and are probably related to a small body of granite that is here termed the Sammys Barren granite.

The Aspy Fault escarpment is the most prominent topographic feature in northern Cape Breton Island (Figure 2.2a), and some early workers considered it to be a major geologic boundary (Neale, 1963; Cameron, 1966; Wiebe, 1972). Neale and Kennedy (1975), however, recognised the similarity of basement and cover rocks across this fault and suggested that the major lithologic boundary exists elsewhere, possibly unexposed. Macdonald and Smith (1979) and Smith and Macdonald (1983) mapped fault and mylonite zones sub-parallel to, but west of, the Aspy Fault. Raeside et al. (1986) interpreted these structures as a major fault system, the Wilkie Brook fault zone, separating the then unnamed Blair River inlier from the Aspy terrane. They also defined the Red River fault zone as the southern boundary of the Blair River inlier.

Field mapping in northern Cape Breton Island was conducted by the author at a scale of 1:10,000 in the summers of 1990 and 1991. During the two field seasons, 519 samples were collected from throughout the Blair River inlier wich were added to the 739 samples collected by

Figure 2.2 - Photographs illustrating the physiography of northwestern Cape Breton Island.

(a) Aspy Fault escarpment which was, at one time, considered a major geological boundary but is now known to be a Carboniferous or younger normal fault that does not greatly offset the geology of the Aspy terrane.

(b) aerial photograph of McEvoys Barren. Similar barrens in the central portion of the Blair River inlier make further subdivision of the Polletts Cove River gneiss difficult due to lack of outcrop.

(c) deeply incised tributaries of Blair River.

(d) examples of the types of outcrops in many of the smaller brooks and tributaries.

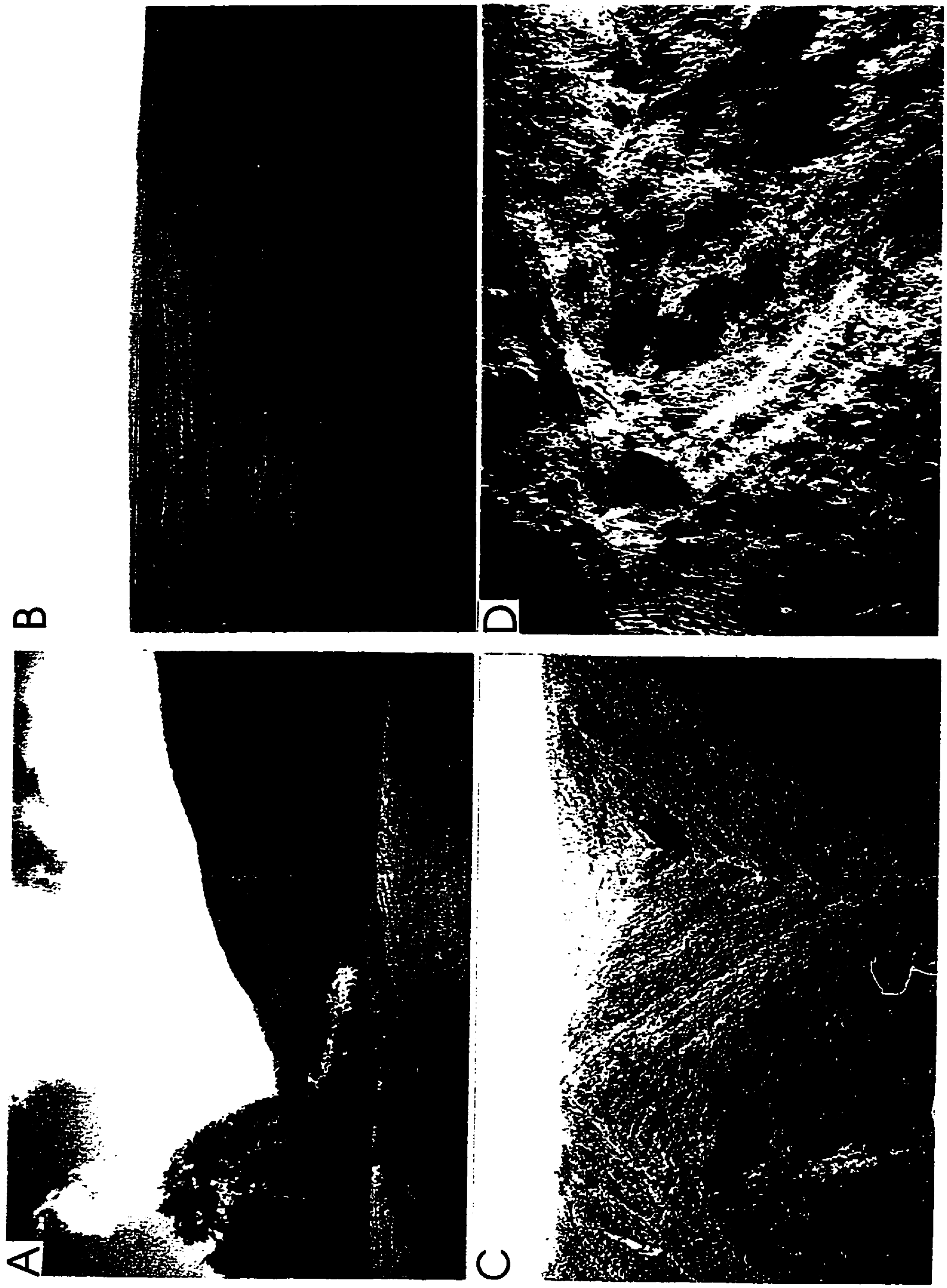

Figure 2.2

R. Raeside, S. Barr, C. White, and F. Dennis between 1985 and 1989. Thin sections were made from 375 of these samples, selected to represent the lithological diversity of the complex.

The central strip of the Blair River inlier, the Polletts Cove River gneiss, could not be further divided due to sparse outcrop and difficult access. Bogs and spruce forests cover much of the highlands plateau (Figure 2.2b) and outcrops are restricted largely to deeply incised gorges (Figure 2.2c). Few field photographs are included here because many exposures are along gorge walls, are small moss- or lichen-covered outcrops, or are submerged in poorly illuminated brooks (e.g., Figure 2.2d).

The units in the Blair River inlier are described below, in order of their known or inferred ages.

2.2 Rock types, petrography, and contact relations

Sailor Brook gneiss

The Sailor Brook gneiss (Figure 2.1) is a heterogeneous unit distinguished as a granular, granulite-facies gneiss that is hard, massive, and locally migmatitic. Some of the characteristic rock types are shown in Figure 2.3a,b and include fine- to medium-grained granular gneiss with compositions of tonalite, quartz diorite, and granodiorite (~60%). Minor rock types include granular or foliated amphibolite (~20%), granoblastic one- and two-pyroxene banded gneiss (~8%), granular and foliated granitic gneiss (~5%), chlorite-epidote-muscovite schist (~5%), and subophitic metagabbro (~1%). These lithologies are intimately mixed and it is not possible to subdivide them at the 1:10,000 scale of field mapping of the present study. Granular gneiss contains weak metamorphic banding defined by the concentration of equant mafic minerals, but in many samples granular mineral relicts are discernible in lensoid patches in the dominant gneissic

Figure 2.3 - Representative samples from the Sailor Brook gneiss.

(a) examples of Sailor Brook gneiss coarse-granular granodioritic gniess (top-left, BVM91-526), weakly banded diorite gneiss with granitic leucosomes (top-right, BVM91-773), coarse granular diorite (bottom-left, RR85-2047a), and weakly foliated granodiorite gneiss (bottom-right, BVM91-527).

(b) boulder of migmatitic gneiss.

(c) intrusion breccia in Sailor Brook gneiss near the (now faulted) contact with the Lowland Brook Syenite. This photograph is of a boulder, but the same relationship is seen in several, less photogenic, nearby outcrops.

(d) examples of mafic xenoliths in the Lowland Brook Syenite (BVM91-753, CW85-103, SB85-1048).

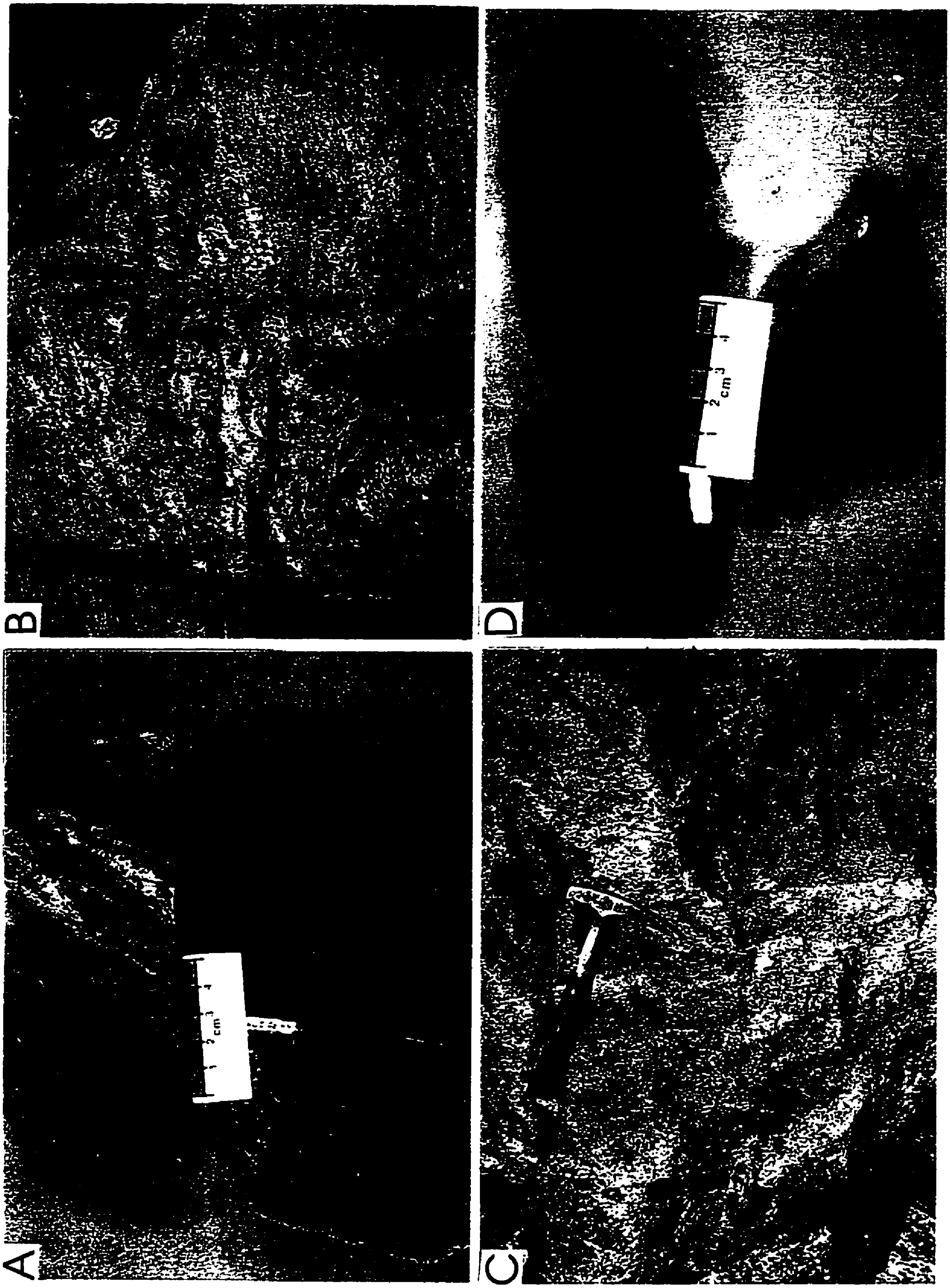

Figure 2.3

foliation. Granular gneiss is most common in the centre of the unit on the southern branch of Sailor Brook and near the contact with, or as xenoliths in, the Lowland Brook Syenite (Map A). The Sailor Brook gneiss is a mappable unit only in the northwestern portion of the Blair River inlier, but similar intermediate to mafic granulite gneiss is present in the Polletts Cove River gneiss.

Samples of mafic and intermediate granular gneiss are medium-grained and unfoliated but weakly compositionally banded, with granoblastic plagioclase, quartz, hornblende, clinopyroxene, and orthopyroxene. Several mafic samples preserve two-pyroxene metamorphic mineral assemblages. Two-pyroxene granulites contain pale-green augite (15-20%), hypersthene (8-15%), plagioclase[1] ($An_{\sim33\text{-}42}$, 30-40%), K-feldspar (~15%), quartz (8%), radiating acicular rims of orange-brown biotite (~2%) around Fe-Ti oxide minerals, and large blocky grains of olive-green to brown hastingsitic hornblende (~5%). A secondary fibrous pale-green hornblende (magnesio-hornblende or actinolite) is commonly an epitaxial overgrowth on pyroxenes. Zircon and apatite are rare accessory minerals. Augite grains are roughly equant, range from 0.25 to 0.75 mm in diameter, and are the best preserved of the two pyroxenes, although they are commonly partly altered to fine-grained amphibole (uralitized) with or without exsolved rutile concentrated in discrete lamellae. Rutile and/or ilmenite are exsolved evenly throughout 0.25-0.75 mm equant orthopyroxene (schillerization), giving it the lustre typical of bronzite (Figure 2.4a). Both alteration textures are distinguishable even in highly altered and moderately deformed rocks,

[1] Plagioclase compositions were determined on grains from a wide variety of samples by electron microprobe analysis, others were determined by standard optical techniques. Applied to the same grain both methods agree within <10% An.

Figure 2.4 - Examples of mineral textures in the Sailor Brook gneiss (PP = plane polarized light, XP = crossed polars)

(a) two-pyroxene granulite containing orthopyroxene (with schiller texture), clinopyroxene (with coarser rutile exsolution), and Fe-Ti oxide minerals with radial acicular biotite (BVM91-527; PP, Scale bar = 1 mm).

(b) granoblastic hypersthene-granulite with banding defined by pyroxene-rich layer (SB85-1048; PP, Scale bar = 1 mm).

(c) macroscopically well foliated, but microscopically granoblastic, amphibolite. (SB85-1109; PP, Scale bar = 1 mm).

(d) granular amphibolite with Hbl+Qtz mosaics (left half, BVM91-535; PP, Scale bar = 1 mm) and foliated amphibolite with flattened mosaics and recrystallised massive amphibole grains (right half, CW85-107; PP, Scale bar = 1 mm). Titanite, instead of orange brown-biotite, rims Fe-Ti oxide minerals in these amphibolite samples.

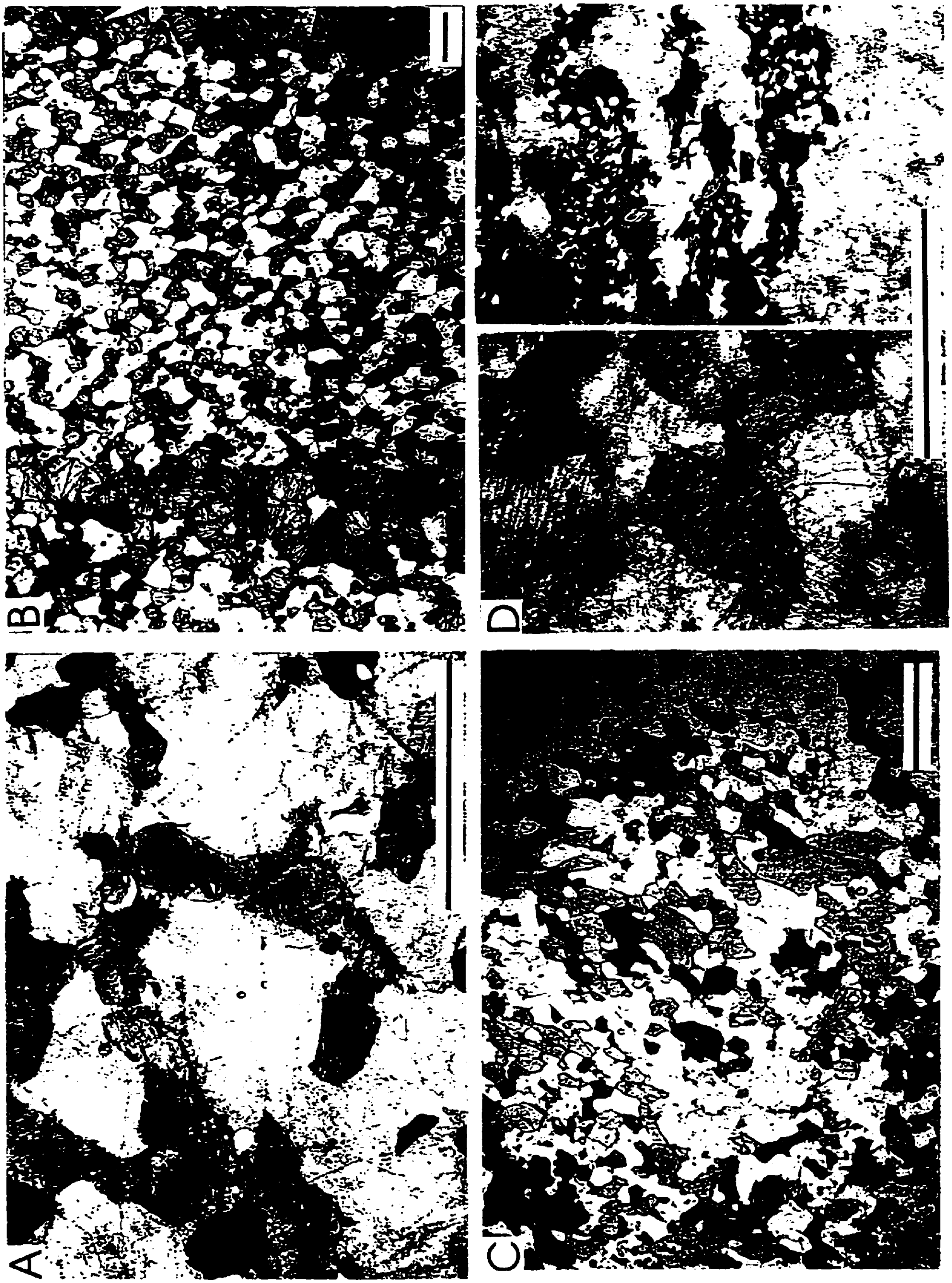

Figure 2.4

allowing for the identification of pre-existing mineral assemblages in many of the samples from this unit. Olive-green to brown hornblende grains appear to be derived from altered pyroxene because they are similar in shape and size to the pyroxenes, have poorly developed amphibole cleavage, and contain many small opaque inclusions that mimic Ti-oxide exsolution textures in the pyroxenes.

Migmatitic leucosome contains large (up to ~2.5 mm; ~20%) anhedral quartz grains, smaller (~0.2-0.5 mm) subhedral plagioclase ($An_{\sim 25}$, ~40%) and K-feldspar (~30%) with a granitic texture. Both types of feldspar are highly altered. Mafic minerals are few (<1% total), but include hornblende xenocrysts from the melanosome, biotite, epidote and chlorite. The leucosomes have diffuse edges but are parallel to the granular layering (Figure 2.3b).

Granulite xenoliths in the Lowland Brook Syenite preserve fresh, to slightly altered, hypersthene (En_{55}), augite ($Di_{\sim 75}$), plagioclase (An_{67}), Fe-Ti oxide minerals and quartz, all comprising a granoblastic texture with a weak layering defined by the concentration of pyroxenes (Figure 2.4b). They occur near or within undeformed nebular melt pods, and appear to be the melanosome residuum of extreme migmatization. These samples contain up to 50% coarse-grained orange-brown biotite, granoblastic polygonal microperthitic feldspars (25%), equant clinopyroxene (10%), and a coarse, dark-yellow epidote-group mineral (5%).

Granitic lithologies in the Sailor Brook gneiss are rare, but where present have a granular foliation with a slight foliation defined by clusters of Fe-Ti oxide minerals, zones of recrystallized feldspar, and recovered quartz ribbons. These felsic gneisses contain large (0.75-1.25 mm), equant perthitic and antiperthitic feldspar (~50%), smaller (~0.25 mm) separate microcline (~7%) and plagioclase (~7%) forming a recrystallized matrix, xenoblastic, lensoid, or ribbon quartz (25%), Fe-Ti oxide minerals (~3%), and large (0.25-0.8 mm) apatite grains (~2%).

Most samples from the Sailor Brook gneiss contain amphibolite-facies assemblages, and many preserve textures, relict mineral proportions, and pseudomorphic grain sizes and shapes comparable to those of the high-grade rocks. Several amphibolite samples are macroscopically foliated with anastomosing lensoid mafic clots or polycrystalline augen, but in thin section contains very fresh-looking green-brown hornblende and a granoblastic texture (Figure 2.4c). More commonly, amphibole-rich samples are altered pyroxene granulites. Mosaics of amphibole, quartz, and in some cases plagioclase are pseudomorphous after clinopyroxene (Figure 2.4d), which is preserved rarely as fragments or cores in the mosaics. Massive amphibole grains retain vestiges of pyroxene cleavage, or contain Fe-Ti oxide inclusions that mimic pyroxene cleavage. Amphibole in these samples makes up ~30-50% of the rock and is complexly zoned in irregular patches. Separate grains within the same mosaic, or differently pleochroic parts of massive grains, range in composition from tschermakite to actinolite. Feldspars are highly altered but retain a granular texture. Brown to tan biotite is rare in the overprinted granulites, occurring mainly as a tertiary alteration mineral along late fractures, and is commonly partly altered to chlorite. Titanite commonly rims Fe-Ti oxides and, in some samples, appears to be pseudomorphous after the rims of orange-brown biotite in the high-grade rocks (Figure 2.4). Felsic bands (relict leucosomes?) consist of recrystallized and xenoblastic, highly to moderately sericitized, plagioclase (An_{22-34}), minor non-perthitic K-feldspar, and quartz.

Highly foliated mafic rocks are located near or in shear zones and contain a strong schistose foliation defined by chlorite and biotite altering to chlorite. Low-strain zones in some samples preserve hornblende partly altered to chlorite and relict mosaic textures. Feldspars are highly sericitized and saussuritized but retain equant grain shapes from their presumed high-grade precursors. Quartz grains are deformed into polycrystalline ribbons or oblate lenses and subgrains have sutured subgrain boundaries.

Where exposed, the contact between the Sailor Brook gneiss and the Lowland Brook Syenite is a series of brittle faults. However, on Sailor Brook there are several outcrops of intrusion breccia consisting of mafic granular gneiss intruded by syenite (Figure 2.3c) near the faulted contacts. Mafic granoblastic xenoliths (Figure 2.3d) of texturally and mineralogically similar gneiss are present in the syenite as far as 1.5 km from the contact with the Sailor Brook gneiss. Several outcrops in the syenite contain lineated, but not highly foliated, micaceous mafic enclaves (biotite-epidote-plagioclase) in massive, undeformed syenite. The intrusion breccia suggests an originally intrusive contact between the Lowland Brook Syenite and the Sailor Brook gneiss and the xenoliths in the syenite are here correlated with the Sailor Brook gneiss based on lithological similarities.

Zones of highly sheared chlorite-epidote-albite schist and localised mafic mylonite (sheared Sailor Brook gneiss?) separate the Sailor Brook gneiss from the Polletts Cove River gneiss. On Sailor Brook, a well exposed 50 m wide zone of straight gneiss (blastomylonite) is located within the Sailor Brook gneiss, but is extrapolated to separate the Delaneys Brook anorthosite and the Lowland Brook Syenite and to link with the McEvoys Barren shear zone (Map A).

Polletts Cove River gneiss

An area of undivided gneissic and plutonic rocks forms the core of the Blair River inlier (Polletts Cove River gneiss, Figure 2.1) and is exposed along Polletts Cove River, Blair River, their tributaries, and along sea cliffs in the High Capes area. There is no exposure over large areas of the highlands plateau (e.g., Polletts Cove River gneiss east of the Otter Brook gneiss and McEvoys Barren shear zone; see Figure 2.2b), making detailed mapping difficult and correlations between exposures in widely separated brooks difficult. The unit is heterogeneous and includes rocks with a wide range of compositions, metamorphic grades, and states of deformation that are intimately mixed and that could not be included in the major gneissic or plutonic units or further subdivided at the present scale of mapping. Some of the rocks may have a semipelitic sedimentary protolith as inferred by Raeside and Barr (1992). The Polletts Cove River gneiss includes rare calc-silicate lenses associated with shear zones and one sample that contains Ath+Phl+Pl.

The characteristic lithologies on Polletts Cove River are quartzofeldspathic and both massive and foliated amphibolite gneisses intruded by granitic dikes and network veins (Figure 2.5a,b) as well as variably deformed and altered rocks presumed to be the equivalents of the amphibolites. On Blair River, the Polletts Cove River gneiss is generally characterised by monotonous green-grey mafic gneiss and chloritic schist with deformed granitic pegmatites, locally as sheared asymmetric boudins (Figure 2.5c,d). In detail, however, the rock types are more variable; some examples of the gneissic rocks from the Polletts Cove River gneiss are shown in Figure 2.6a,b. The gneissic rocks on both Polletts Cove River and Blair River lack any recognisable stratigraphy or identifiable metasedimentary layering.

Several generations of small gabbro bodies and diabase dikes intruded the Polletts Cove River gneiss. The latest generation is an undeformed fine-grained diabase that cuts gneissic and schistose fabrics and is probably related to the Fisset Brook Formation. Rarer metagabbroic rocks are coarse grained and preserve relict subophitic textures (Figure 2.6c). Outcrops and samples that

Figure 2.5 - Outcrops of gneissic rocks in the Polletts Cove River gneiss.

(a) massive amphibolite cut by thin granitic veins

(b) banded amphibolite gneiss; both (a) and (b) are typical of the Polletts Cove River gneiss on Polletts Cove River

(c) green-grey gneiss with asymmetric pegmatite boudin

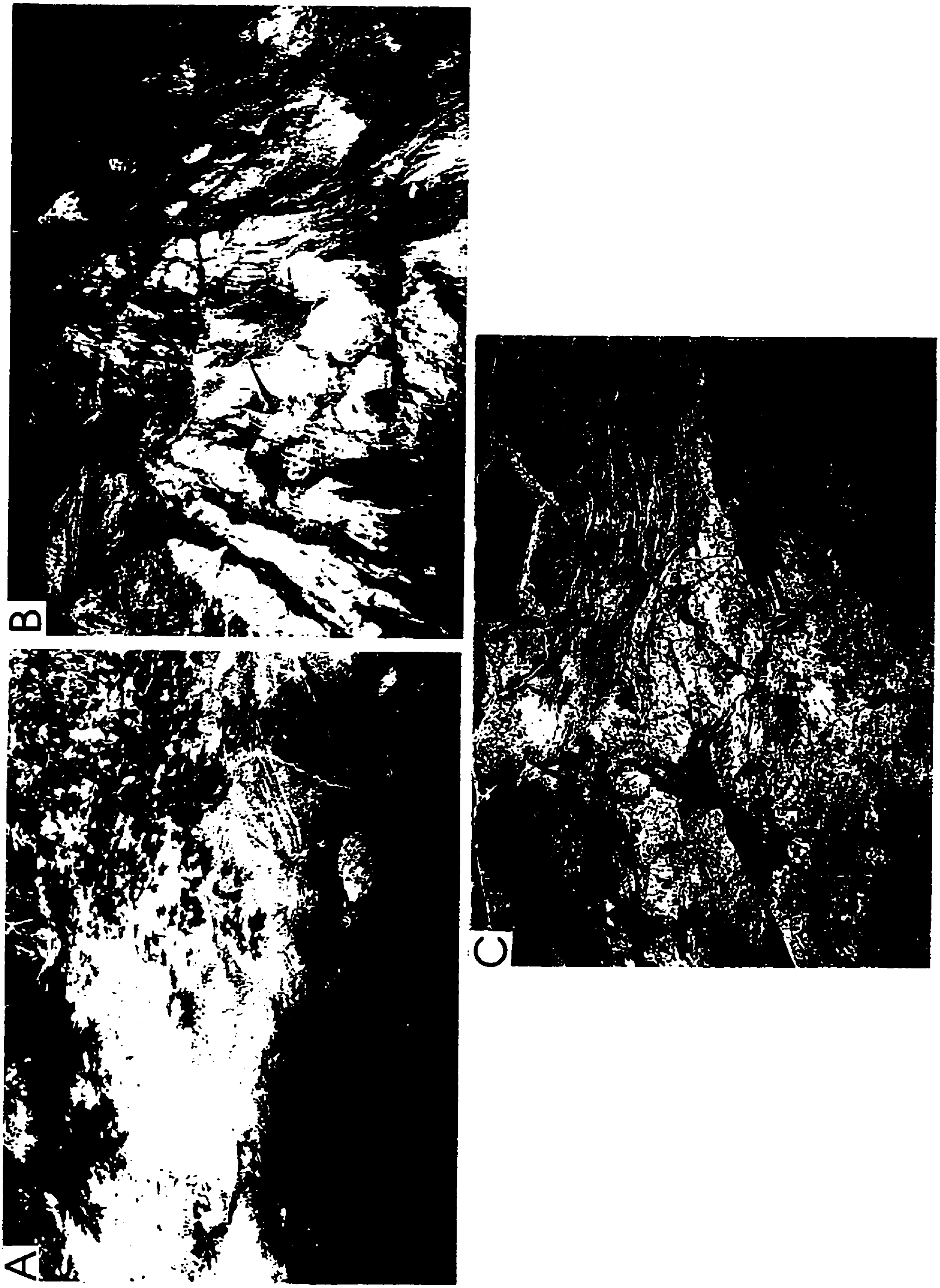

Figure 2.5

Figure 2.6 - Hand samples illustrating the lithological variation in the Polletts Cove River gneiss.

(a) amphibolite gneiss (RR85-2049, CW85-118a, CW85-119, BVM91-637, CW85-148, BVM90-141)

(b) examples of the lithologic variation of gneissic rocks (BVM90-092, BVM91-701, BVM91-691, BVM90-093, BVM91-704, SB85-1099)

(c) metagabbro (RR85-2105, BVM91-545)

(d) boulders of sheared anorthosite and leucogabbro

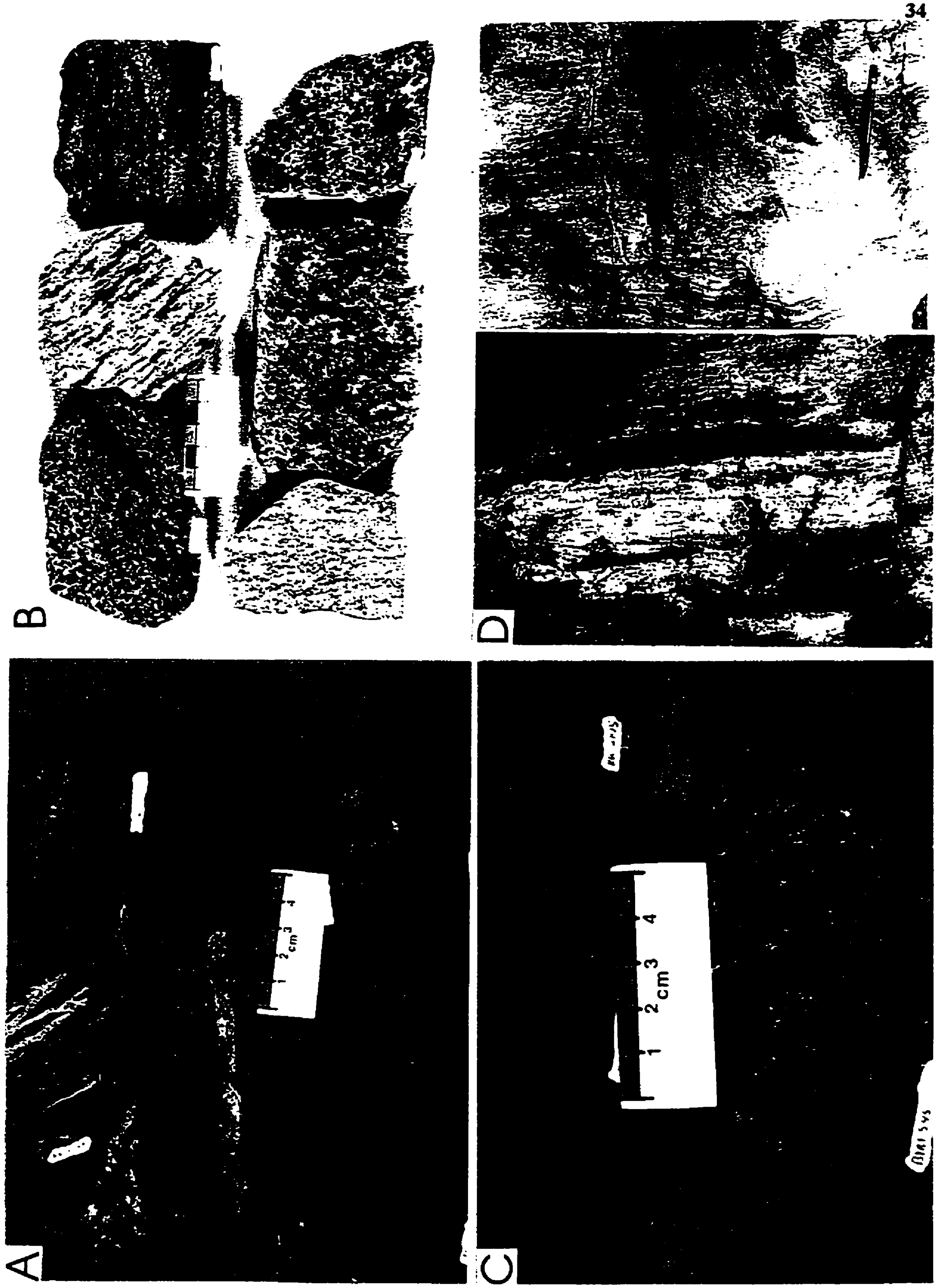

Figure 2.6

appear to be similar to the Sailor Brook gneiss and Otter Brook gneiss are either too small or too isolated to be shown separately at the present map scale. Small highly sheared outcrops of anorthosite and leucogabbro (Figure 2.6d) are present throughout the Polletts Cove River gneiss and some coarse-grained feldspathic gneisses are similar to altered samples from the Lowland Brook Syenite.

Contacts between the Polletts Cove River gneiss and other units are either faulted or not exposed. The contact with the Fox Back Ridge diorite/granodiorite is constrained only by widely separated outcrops of each unit. The contact with the Red River Anorthosite Suite is a zone of breccia and chlorite-epidote schist that is 20-50 m wide and dips gently southeast. Although other workers (Mitchell, 1979; Dupuy et al., 1986) considered this to be a sheared intrusive contact, no xenoliths, intrusion breccia, or anorthosite apophyses in the "country rock" were observed. The contact is here interpreted as a fault, with no implications as to original relationships.

Many small shear zones are present in the Polletts Cove River gneiss, but only a few are extensive enough to map over large distances. Lineaments on contoured orthophoto maps help to constrain the trace of some shear zones, but only those lineaments that are also reasonably constrained by field observations are mapped as faults (Figure 2.1 and Map A). Known and inferred shear zones trend approximately N to NNE and include the boundary shear zone with the Otter Brook gneiss, the McEvoys Barren shear zone, the High Capes shear zones, and a small band of chloritic schist and phyllonite on Blair River. The McEvoys Barren shear zone is here interpreted to link with the zone of mylonite or blastomylonite (described above) between the Lowland Brook Syenite and the Delaneys Brook anorthosite, but this extrapolation requires projection across a large area devoid of outcrop and is, therefore, speculative. The High Capes shear zone separates a western coastal block that includes a small anorthosite body, coarsely perthitic felsic gneisses, and subophitic metagabbro from the remainder of the Polletts Cove River gneiss.

Amphibolites in the Polletts Cove River gneiss are medium- to fine-grained and contain variable amounts of hornblende, quartz, and feldspar. Most commonly, they contain large (~0.75 mm) olive-green magnesio-hornblende (~50-75%), some of which are poikiloblastic with equigranular inclusions of quartz and plagioclase, in a matrix of xenoblastic plagioclase (15%, An_{25-35}) and quartz (10%), multigranular clusters of titanite (<5%), and accessory minerals including Fe-Ti oxide with titanite rims and apatite. Alteration to chlorite, epidote, and sericite is common along fractures. Highly foliated amphibolites contain the same mineral assemblage, but with up to 20% green-brown, preferentially aligned biotite replacing hornblende. The granitic network veins in the amphibolite contain large (2.5 mm) grains of coarse-patch antiperthite (15%) in a finer grained (0.25-0.75 mm) recrystallized matrix of microcline (30%) and subequigranular plagioclase (20% An~22) with elongate xenoblastic quartz (35%).

Metagabbroic rocks in the Polletts Cove River gneiss occur as dikes and small bodies. They have an altered subophitic texture in which randomly oriented plagioclase (An_{40}) laths are inclusions in or intergrown with multigranular aggregates of hornblende pseudomorphous after clinopyroxene. Aggregates are separated by coarse plagioclase laths giving a spotted appearance in outcrops and hand samples. Skeletal clinopyroxene grains are rarely preserved in the centres of the aggregates.

Granular intermediate gneisses contain slightly to highly sericitized equigranular plagioclase (30-55%) and quartz (10-25%), and either blocky olive-green hornblende, Hbl-Qtz mosaics after pyroxene, or Act+Chl+Qtz mosaics pseudomorphous after Hbl-Qtz mosaics. The textures and grain sizes are similar to those of the Sailor Brook gneiss, and these rocks appear to have been similar high-grade gneisses overprinted by amphibolite-facies metamorphic mineral assemblages.

Anorthosite in the Polletts Cove River gneiss is ubiquitously altered. Large (1-2.5 mm) plagioclase porphyroclasts are surrounded by fine-grained saussurite and sericite that has preferentially replaced recrystallized matrix plagioclase. Fe-Ti oxide minerals in the altered matrix have titanite rims, but lack rims where they are inclusions in plagioclase porphyroclasts. Other anorthosite samples are altered throughout to sericite and saussurite. One sample preserves, between highly altered patches, medium-grained (0.3 mm) equigranular plagioclase with straight 120° grain boundaries that are similar to the cumulate textures described below. Wispy, pale-green mafic layers contain aligned fibrous chlorite and epidote.

Other leucocratic rocks of uncertain origin contain significant quartz (40-60%), two feldspars (albite and orthoclase), little or no mafic minerals (chlorite and one sample with garnet) and are commonly highly sheared and altered. One sample is a coarse graphic granite and another is a microcline syenogranite with euhedral titanite. A sample from Lockhart Brook contains xenoblastic oligoclase (80%), coarse prismatic anthophyllite (10%), phlogopite (5%), and an opaque oxide mineral (5%).

Most of the leucocratic or granitic rocks occur in Greys Hollow Brook or Wilkie Brook (in or near the Wilkie Brook fault zone) where they may be related to granites in the Aspy terrane. The least altered foliated biotite-hornblende amphibolites are also from near or in the Wilkie Brook fault zone and may also be derived from the Aspy terrane where these rock types are common in the Cape North Group (Wunapeera, 1992). Foliated amphibolites from well within the Blair River inlier are typically highly to partly altered with sericitized plagioclase and ragged amphibole partly replaced by (rather than coexisting stably with) biotite and partly altered to chlorite and epidote along late fractures.

Red River Anorthosite Suite

The Red River Anorthosite Suite (Figure 2.1) is the largest of several anorthosite bodies and tectonite slivers in the Blair River inlier. Ashwal (1993) classified the Red River Anorthosite Suite as a Proterozoic massif-type anorthosite based on reports from earlier workers (Jenness, 1966; Dupuy et al., 1986). The suite contains a central core of massive meta-anorthosite that grades into more mafic meta-leuconorite, anorthositic diorite, or leucogabbro and is bordered to the west by interlayered meta-anorthosite, metatonalite, meta-leucogabbro, amphibolite, pyroxenite, and rocks of charnockitic affinity. To the east, the suite is truncated by the Wilkie Brook fault zone. All units in, or associated with, the suite are metamorphosed and altered, and rarely preserve primary igneous textures, but many samples preserve relict igneous mineralogies from which an estimate of the protolith composition may be inferred[2].

Notably absent from the Red River Anorthosite Suite are olivine, massive oxides or sulphides, chromite, and significant apatite. Thus, the suite lacks troctolitic lithologies commonly associated with some, particularly labradorite-type, massif anorthosite suites (e.g., Anderson and Morin, 1968; Emslie, 1985). The mafic rocks in the suite, notably the layered unit, do not appear to have the economic metals potential of some layered gabbro bodies (e.g., Gross, 1968; Anderson,

[2] Following convention, the metamorphosed igneous rocks of the Red River Anorthosite Suite are hereafter referred to by their inferred igneous protolith name for simplicity and clarity.

1968) or phosphorous ore as in some intermediate rocks associated with anorthosite bodies (e.g., Kolker, 1982).

Bekkers (1993) distinguished five lithologic subdivisions in the Red River Anorthosite Suite; anorthosite, anorthositic gabbro and gabbro, layered unit, Greys Hollow charnockite, and Wilkie Brook charnockite. However, most workers separate charnockite from spatially associated anorthosite and gabbro units in order not to imply a comagmatic relationship, and this convention is followed here; the charnockites are described in a subsequent section. The Red River Anorthosite Suite here includes rocks ranging from anorthosite to leucogabbro to pyroxenite and their inferred metamorphosed equivalents. These lithologies are separated into map units of massive anorthosite, leucogabbro, layered rocks, and pyroxenite (Map A).

A steep escarpment marks the northwestern edge of the anorthosite suite, producing a distinct (on contoured orthophoto maps) topographic expression that is outlined by the two large eastern branches of Polletts Cove River. Both branches contain large (up to 3 m^3) boulders of anorthosite that were derived from steep cliffs above the river, but sheared and catacastic mafic rocks of the Polletts Cove River gneiss crop out in the river bed. Small brooks to the south and east of Polletts Cove River and its southern tributary flow across the escarpment and the contact between the Red River Anorthosite Suite and the Polletts Cove River gneiss is exposed or can be constrained closely in these brooks. In these tributaries, the contact veers upstream from the trend of the escarpment, producing a lobate map pattern as the result of deeply incised stream valleys intersecting a gently dipping contact with the Polletts Cove River gneiss. The small brooks to the north and west of Polletts Cove River and its southern tributary expose the undivided gneissic unit.

Where the contact with the Polletts Cove River gneiss is exposed, it is a 20-50 m wide, gently southeast-dipping zone of breccia and chlorite-epidote schist. Some workers interpreted this to be a sheared intrusive contact (Mitchell, 1979; Smith and Macdonald, 1983; Dupuy et al., 1986), but neither xenoliths in the anorthosite, nor intrusion breccia, nor anorthosite apophyses in the "country rock" were recognised. Therefore, the contact is here interpreted to be a low-angle fault with no implications as to prior relationships. None of the contacts with the Fox Back Ridge diorite/granodiorite are exposed. In the southernmost tip of the Blair River inlier several units, including the Red River Anorthosite Suite, are complexly interleaved by shearing associated with convergence of the Wilkie Brook and Red River fault zones.

Plagioclase compositions in the Red River Anorthosite Suite appear to be controlled partly by lithology, and to a greater extent by the degree of alteration and metamorphism. Anorthosite and leucogabbro contain calcic andesine or labradorite ($An_{\sim 40-50}$) and in the layered unit and pyroxenites, plagioclase is more sodic ($An_{\sim 30-45}$). In general, labradorite and bytownite compositions are preserved in the least altered anorthosite near the centre of the body and the lowest An-content plagioclase is concentrated nearer the edges where rocks are more commonly sheared and highly altered.

Anorthosite

Massive anorthosite crops out in the central portions of the Red River Anorthosite Suite and is most commonly buff-white or pale-pink. Anorthosite is commonly so thoroughly altered that individual grains cannot be identified at the hand-sample scale (Figure 2.7a). Bands of alteration and cataclasis, characterised by thin (0.5 to 2 cm) zones of intense sericitization along fractures and by cracks filled with either epidote-group minerals or coarse tremolite and phlogopite, trend

Figure 2.7 - Anorthosite samples and mineral textures in the Red River Anorthosite Suite.

(a) altered pale pink or buff white massive anorthosite (RB91-025, RB91-063, RB91-060, RR85-2047, RB91-080).

(b) least altered massive anorthosite with pink or blue spots of iridescent labradorite and streaky or lensoid mafic mineral clusters (RB91-052, BVM91-584, RB91-076).

(c) massive anorthosite with flattened mafic mineral clusters (probably recrystallized orthopyroxene megacrysts)

(d) plagioclase textures in Type 1 anorthosite (RB91-063)

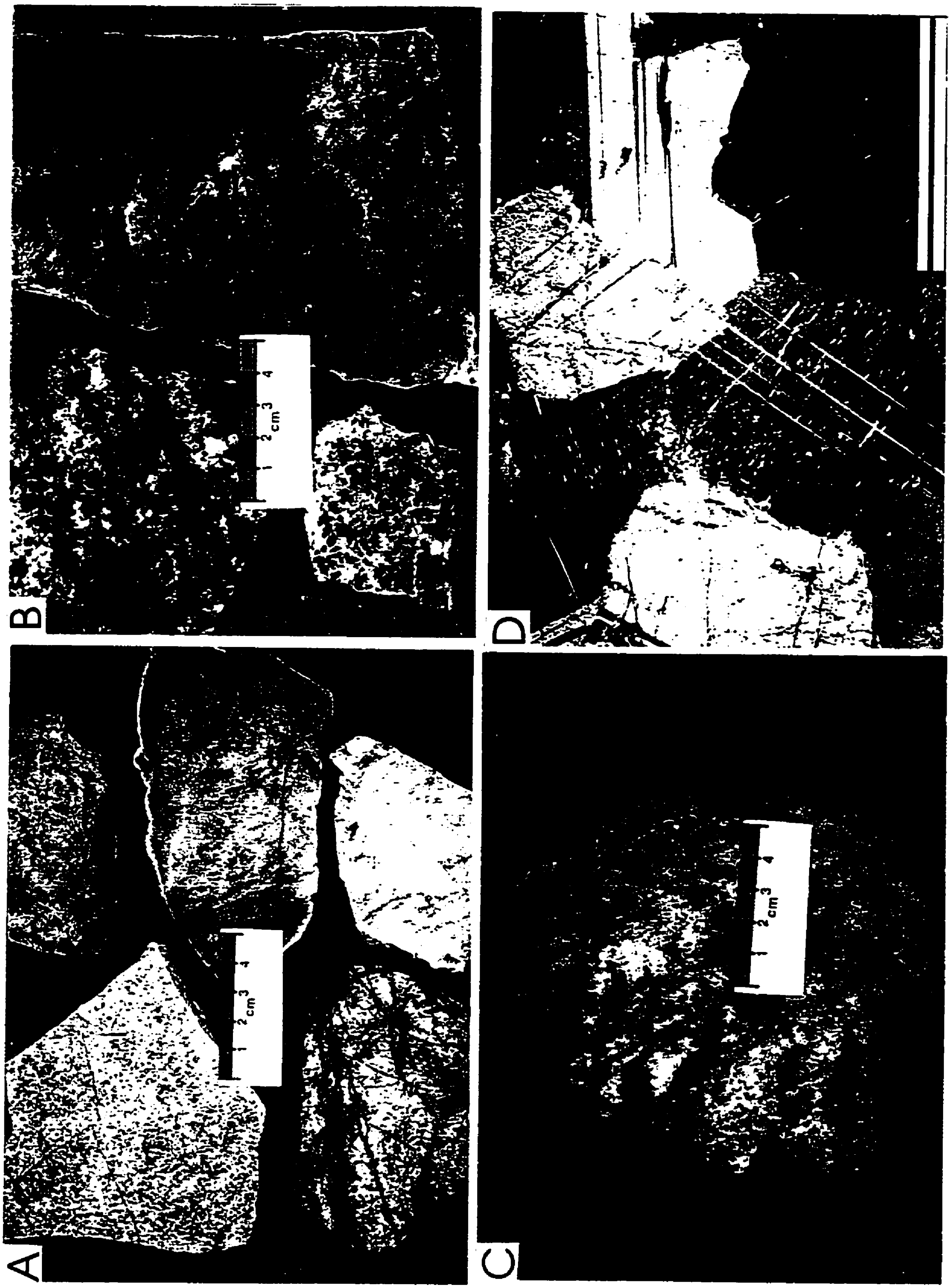

Figure 2.7

Figure 2.7 (continued)

(e) plagioclase textures in Type 2 anorthosite (RB91-076; XP, scale bar = 1mm)

(f) photomicrograph of textures in Type 3 anorthosite (SB86-3139a; XP, scale bar = 1mm)

(g) photomicrograph of textures in Type 4 anorthosite (SB86-3139a; PP, scale bar = 1mm)

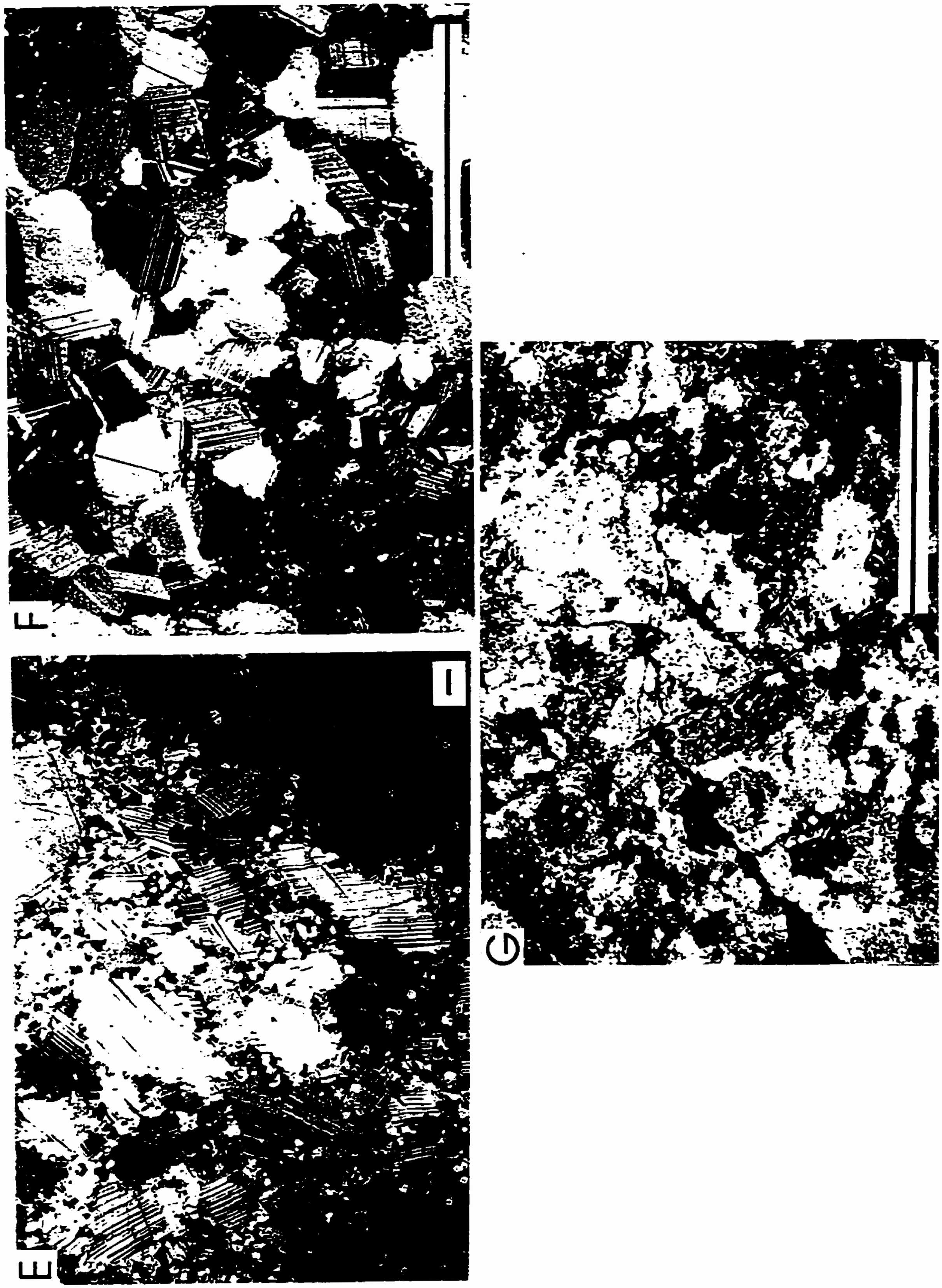

Figure 2.7

broadly parallel to the Wilkie Brook fault zone. Altered massive anorthosite locally contains streaky-green, polymineralic clots of chloritized mafic minerals. The mafic clots are oblate, defining a weak gneissic foliation that is broadly parallel to the Wilkie Brook fault zone. Unaltered and undeformed massive anorthosite is a rare, but distinctive, white-weathering rock with pink, blue, or purple spots of partly recrystallized labradorite are the least deformed anorthosite observed. The spots are large (0.5-1 cm diameter) grains of iridescent-blue labradorite in a matrix of sugar-texture, pearl-white, medium to fine-grained recrystallized plagioclase (Figure 2.7b). Some less deformed anorthosite samples contain either large (up to 2-5 cm) partly recrystallised megacrysts, augen, or polymineralic clusters of orthopyroxene that are recognisable in hand sample by their bronze lustre (Figure 2.7c).

Centimetre-scale flattened orthopyroxene megacrysts are only preserved in the least deformed, least altered, and most plagioclase-rich central portions of the Red River Anorthosite Suite. Larger (decimetre-scale) orthopyroxene megacrysts, like those commonly reported in other massif-type anorthosite bodies (e.g., Ashwal, 1993; Owens and Dymek, 1995), were not observed in the suite. If they were ever present, large megacrysts and their host rocks would probably be deformed and altered beyond recognition due to the lower competency and higher degree of alteration and metamorphism that have affected the more mafic rocks in the suite.

In the field it is difficult to distinguish weathered Qtz+Pl±Mc, here termed "white rock" (leucotonalite?, meta-anorthosite?) from anorthosite. "White rock" is fine-grained (~0.25-0.5 mm) and equigranular, composed of highly sericitized plagioclase ($An_{\sim 22}$) and quartz (generally 10-25% but up to ~50%; one sample contains more SiO_2 than normal igneous rocks) and minor microcline

(<10%). It commonly occurs together with massive anorthosite, and in particular near metagabbro. Some of the quartz may have been produced from either metamorphism accompanied by alteration of primary pyroxene (e.g., see layered unit description below; and Rousell, 1981), or contamination by country rocks during intrusion (Ashwal, 1993). Myrmekitic plagioclase is only rarely observed in the Red River Anorthosite Suite and, therefore, recrystallization of myrmekitic feldspar seems an unlikely source of quartz. Some samples of highly altered massive anorthosite also contain appreciable quartz (<5%) but are otherwise identical to "white rock". Therefore, quartz-bearing leucocratic rocks are provisionally included in the massive anorthosite unit. These ambiguous rocks, along with indisputable anorthosite, were mapped by early workers as quartzite of the George River Group (Nova Scotia Department of Mines and Energy Open File Map, 1965).

Dupuy et al. (1986) reported size-sorted plagioclase grains aligned parallel to the (implied primary) layering in anorthosite. In the present study, similar textures were not recognised in the field, in hand samples, or in thin sections. Very few samples of massive anorthosite preserve primary igneous textures of any type. Most samples are either highly altered or show incipient granulation at plagioclase grain boundaries and lack any obvious alignment of twin planes or of long dimensions of grains.

Massive anorthosite in the Red River Anorthosite Suite contains 90-97% plagioclase at the outcrop scale. Due to coarse grain size, hand samples and thin sections range up to 100% plagioclase. The least altered anorthosite samples contain calcic andesine (An_{43-50}) and rarely labradorite (An_{50-56}). Plagioclase grades to An_{88} in reaction zones with Fe-Mg silicate minerals.

Where plagioclase compositions could be determined from intensely altered samples, none were lower than An_{29}.

Mafic minerals are a minor constituent of anorthosite. Mafic clots or augen comprise biotite, chlorite, epidote and opaque oxide minerals and some preserve relict pyroxene cores. Some augen are recrystallized orthopyroxene draped by rims of hornblende, quartz, and calcic plagioclase (An_{75-88}). Clinopyroxene is extensively altered to zoned amphibole aggregates that range from tschermakitic to magnesio-hornblende. Altered samples contain actinolite and chlorite. Orange-brown biotite occurs only in association with altered pyroxene where it forms either acicular rims around Fe-Ti oxide minerals or separate unoriented grains. Rutile grains in quartz-bearing altered anorthosite resemble, in size and distribution, Fe-Ti oxide minerals in other anorthosite samples and some rutile grains have a titanite rim separating them from epidote and sericite.

Four types of massive anorthosite are recognised based mainly on differing textures:

Type 1) *Randomly oriented massive* - Type 1 anorthosite contains coarse-grained unzoned, subequigranular and semi-tabular plagioclase grains locally with straight 120°, grain boundaries (Figure 2.7d). Plagioclase in these samples is An_{45-50}. Some samples are sericitized either thoroughly, or in patches, but the texture can be recognised through the alteration. Plagioclase grains range in size from 1 mm to 4 mm (long dimension) and are broadly elongate or blocky, but grain boundaries are irrational or are rarely tabular parallel to twin lamellae. Both the lack of zoning and subhedral grain shapes are characteristic of undisturbed primary textures in massive adcumulate anorthosite, but this texture is also very similar to published examples of partly recrystallized anorthosite (Ashwal, 1993; Kehlenbeck, 1972). Regardless, the coarse grain size and lack of recrystallization to clearly metamorphic textures (see below) suggest that these samples represent the least recrystallized and deformed anorthosite in the Red River Anorthosite Suite.

Type 2) *Porphyroclastic granular* - This type of anorthosite ranges from incipient granulation of Type 1 to well developed mortar-texture of large (2 mm to 4 mm), rounded, primary(?) porphyroclasts (An_{45-55}) in a finer-grained (0.25 mm) matrix of polygonal plagioclase (An_{40-50}) aggregates (Figure 2.7d). Kehlenbeck (1972) demonstrated that further recrystallization produces augen textures and gneissic anorthosite. No plagioclase augen were noted in the Red River Anorthosite Suite, although large (1-4 cm) mafic mineral clusters associated with Type 2 samples are lensoid. Ashwal (1993) interpreted this texture as suggestive of deformation by magmatic ascent as a crystal mush or by later intrusion of surrounding plutons (charnockitic rocks?); recrystallization associated with metamorphism is plausible as well.

Type 3) *Granular* - This anorthosite is finer grained (~0.3 mm) throughout and is almost perfectly equigranular with straight 120° grain boundaries (Figure 2.7e). Granular anorthosite may be the end product of complete recrystallization from Type 2, or a perfect adcumulate. The two are indistinguishable except where adcumulate plagioclase preserves igneous zoning patterns (as in the Delaneys Brook body - see below). Only two samples preserve granular textures in the Red River Anorthosite Suite and both are partially altered.

Type 4) *Highly altered* - These rocks are so thoroughly sericitized and saussuritized that pre-alteration textures cannot be recognised in thin section (Figure 2.7f). Fine-grained muscovite (sericite) is distributed uniformly throughout the rock, but chlorite and epidote-group minerals are confined to intergranular aggregates, where they appear to have replaced mafic minerals, and in veins. Quartz blebs, within or between plagioclase grains, are a minor constituent, but are more prevalent than quartz in Types 1-3. Carbonate with or without quartz fills small fractures. Varying degrees of cataclasis are common in these rocks. Highly altered rocks comprise the bulk of the anorthosite unit in the Red River Anorthosite Suite.

Gabbro

Dupuy et al. (1986, p. 139) noted that on a north-flowing tributary of Red River, "...the transition from anorthositic gabbro through gabbroic anorthosite to anorthosite is generally gradual, although the contact between neighbouring units is often sharp". Examination of the same area during field mapping for this study confirmed that anorthosite does locally grade into leucogabbro and gabbro over a distance of a few to tens of metres, and that the lithology changes abruptly at faults. Lithologies in the gabbro unit include compositions from leucogabbronorite to gabbro and also pyroxene-hornblende gabbronorite. These rock types are locally intermixed and could not be separated into subunits at the present scale of mapping.

In contrast to the large isolated clusters or megacrysts of mafic minerals in anorthosite, mafic minerals in gabbro and leucogabbro contain smaller (0.5-1 mm) individual grains (or alteration aggregates) and are either massive or gneissic. Massive gabbro is coarse-grained and preserves relict subophitic texture, but hornblende and actinolite have replaced pyroxene. Gneissic gabbroic rocks are foliated, compositionally banded, and commonly highly altered to amphibole-biotite-chlorite assemblages (Figure 2.8a,b).

Typical gabbro contains granular plagioclase (~20-50%, An_{45} in less altered, and An_{32} in highly altered samples), partly or entirely altered pyroxenes (<10% preserved), brown (ferroan- to

Figure 2.8 - Examples of leucogabbro and layered rocks in the Red River Anorthosite Suite.

(a) hand samples of massive gabbro and leucogabbro (BVM90-056, RB91-012, RB91-030)

(b) hand samples of gneissic and massive gabbro and leucogabbro (RB91-074, BVM90-114, RR85-2017, BVM91-621)

(c) outcrop of layered leucogabbro.

(d) slab sample of layered gabbro with deformed and metamorphosed rhythmic-type layering defined by ambiguously graded mafic bands and quartz-rich felsic bands (BVM91-774).

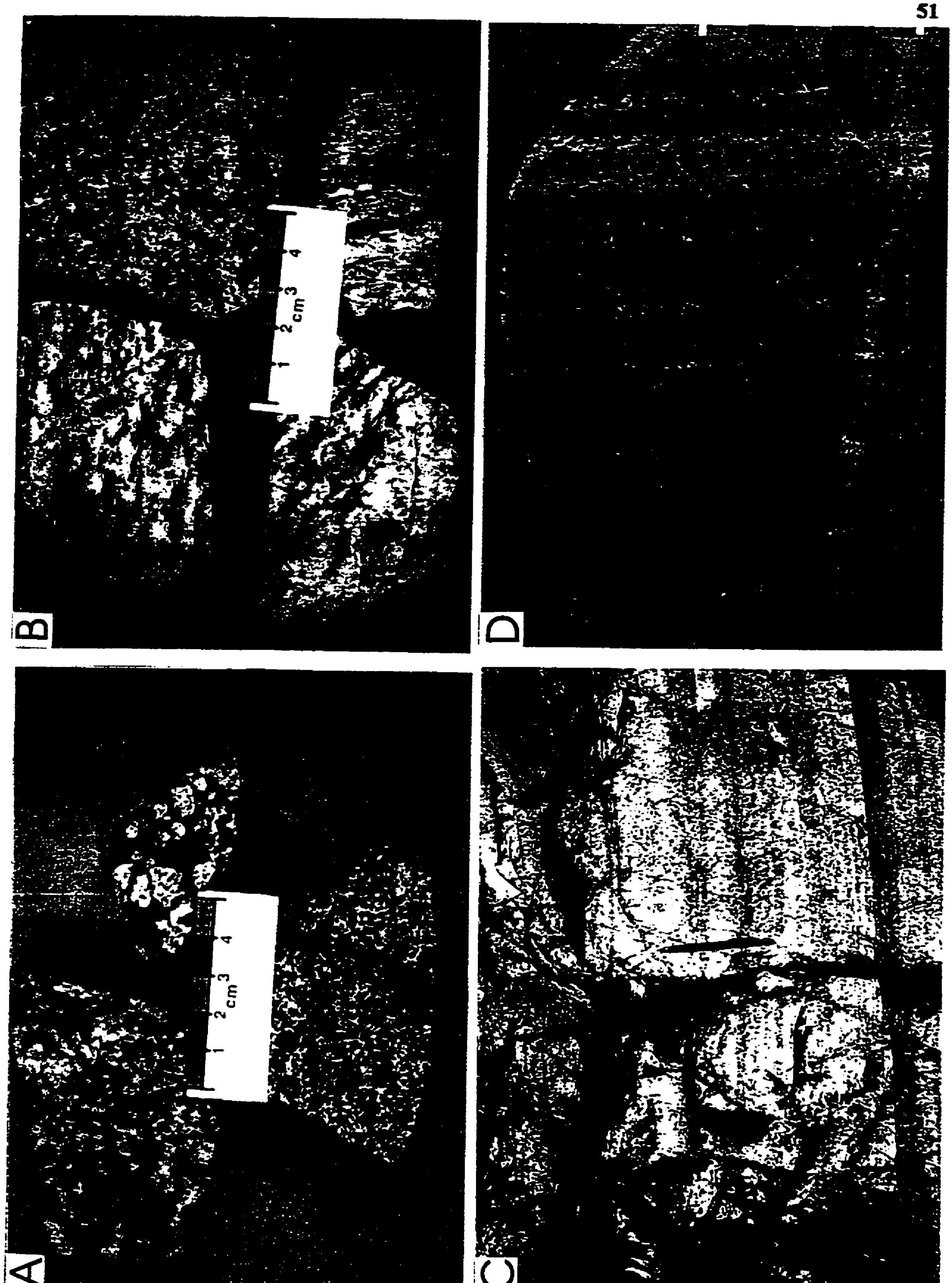

Figure 2.8

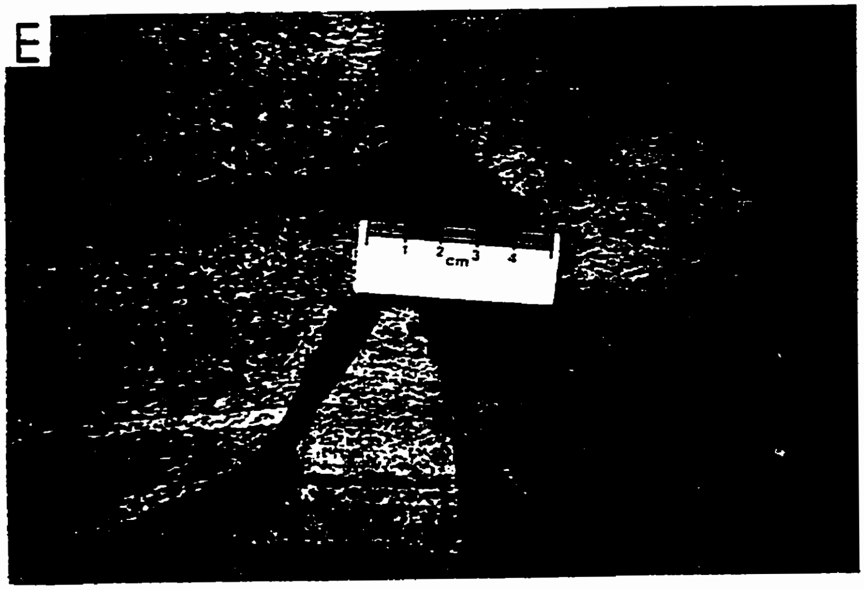

Figure 2.8 (continued)

(e) hand samples of layered unit (RB91-041, BVM91-651, RB91-047).

magnesio-) hornblende (~15-75%), biotite (~5-15%), Fe-Ti oxide minerals (2-5%) and accessory apatite. Highly altered gabbro contains significant (~5%) quartz relative to fresh varieties. Leucogabbronorite contains the same minerals, textures, and variable degrees of alteration, but has a lower percentage of mafic minerals than does gabbro.

Gabbronorite is distinguished from gabbro by the distinctive alteration textures of orthopyroxene (schillerized) and clinopyroxene (uralitized) and by amphibole-plagioclase-quartz mosaics. Several of the more mafic samples preserve macroscopic gabbroic texture, but pyroxenes are almost completely recrystallized to brown hornblende aggregates. Only rare clinopyroxene and orthopyroxene fragments preserved in the aggregates allow these to be recognised as metagabbros. Otherwise, the well formed textures and fresh-looking hornblende and plagioclase might be mistaken for granular amphibolite or anorthositic diorite. More commonly, pyroxenes are highly altered to fine-grained acicular actinolite and chlorite. Brown or green granular hornblende is preserved within or as partial rims around altered pyroxene. In these cases, granular hornblende appears to be a relict from an earlier alteration episode rather than part of the low-grade alteration assemblage.

One sample located near the boundary with the charnockite has a (presumed) oxide-rich gabbronorite protolith and contains large (up to 5 cm) metamorphic garnets that are now highly corroded, relict orthopyroxene, both igneous and granular recrystallized metamorphic clinopyroxene, Fe-Ti oxides, and large apatite grains. This is the only sample that may be an oxide-apatite gabbronorite (jotunite), a rock type commonly associated with the latest-crystallising portions of massif-type anorthosite complexes (e.g., Owens et al., 1993; McLelland et al., 1994).

Layered Rocks

Massive gabbroic rocks either change abruptly across faults, or grade, through various scales of layering and degrees of compositional segregation, into the layered unit. The layered unit is characterised by sharply defined, black and white, centimetre-scale rhythmic layering. More cryptic layering in some anorthosite and leuconorite is defined by bands, tens of centimetres thick, of Type 1 anorthosite with centimetre-scale bands of up to ~10% unoriented mafic minerals.

Rhythmical layers are commonly 3-6 centimetres thick, but locally up to 1 m thick, and are laterally extensive. Individual centimetre-scale layers can be traced across entire outcrops (up to 30 m) without pinching out (Figure 2.8c). The layers are generally flat-lying and are locally gently folded. Some samples contain a mineral lineation that is oblique to the layering. In places, alteration has produced a pink-red staining that, in the field, makes these rocks very difficult to distinguish from layered or deformed parts of the charnockite unit.

Boundaries between centimetre-scale layers are commonly marked by a sharp thin (~3-5 mm) black rind on one or both sides of a mafic layer. Mafic layers with black rinds on both sides show grain-size and modal gradation from both rinds toward the centre of the band (Figure 2.8d). Those with black rinds on only one side show grain-size and modal grading away from the black rind. In the same hand sample, however, other mafic bands grade in the opposite direction. Where bounded by two black rinds, felsic bands grade from being relatively rich in mafic minerals and feldspars at both edges to quartz-rich at the centre. In some cases, a thin (~5 mm) band almost entirely of quartz divides the felsic layer in half. Where bounded by only one black rind, felsic bands grade progressively into the next mafic band and quartz is disseminated throughout. In other, unmetamorphosed and better exposed, layered gabbro complexes (e.g., Skaergaard; Conrad and Naslund, 1989) cumulate layers are marked by an orthopyroxene-rich basal lithology grading upward into anorthosite. Such cumulate criteria (i.e., modal grading direction) to determine "way up" are ambiguous when applied to the layered unit in the Red River Anorthosite Suite.

An oblique mineral lineation is defined in mafic bands by elliptical black granules (amphibole-quartz mosaics in thin section) inclined at an angle of <10-30° to the layering (Figure 2.8e). The mineral lineation in felsic bands is defined by elongate quartz blebs with an angle of ~25° to the layering. Metamorphic and deformational overprints have obscured trough cross bed-type criteria for determining "way up". In the black rind, mafic mineral clusters and shape preferred orientations are parallel to the layering.

Mafic layers consist of relict pyroxene (up to 50% but gradational depending on position in the layer and degree of alteration), light-green and olive-green amphibole (up to 75% in highly altered samples), biotite (~10-20%), plagioclase (An_{30-35}), and minor quartz, epidote, and chlorite. Clinopyroxene appears to have been the predominant primary mafic mineral in the layered unit, but it is now preserved only as skeletal and relict grains or recognisable by its distinctive alteration textures. In mafic layers, clinopyroxene is altered along cleavage planes to green (magnesio-) hornblende and has a reaction rim of actinolitic hornblende that is, in turn, rimmed by fine-grained epidote-group minerals. Quartz blebs are present between the actinolite and epidote alteration rims. Taken to further stages, pyroxene alters completely to mosaics of granular amphibole-quartz±plagioclase. Individual amphibole granules are compositionally zoned with actinolitic compositions in the centres of the granule, grading outward to more tschermakitic compositions. Radial acicular brown biotite is common toward the centres of mafic bands and is associated with Fe-Mg oxide minerals. The black rinds that separate some mafic layers from felsic layers are devoid of biotite although Fe-Mg oxide minerals are present. Amphibole mosaics in the rinds are either monomineralic granular aggregates or they contain minor quartz. Quartz is concentrated outside of the amphibole aggregates adjacent to or within the felsic band. These textures appear to record the progressive production of quartz during pyroxene alteration (cf., Rousell, 1981), its expulsion from amphibole mosaics, and concentration in felsic bands.

Felsic layers are composed predominantly of plagioclase (An_{28-32}, 60-70%), quartz (30-40%) and rare relict clinopyroxene or monomineralic amphibole aggregates. Plagioclase is xenoblastic with scalloped or embayed grain boundaries against quartz and has straight or partly recrystallized grain boundaries against, or a granular texture with, other plagioclase grains.

In the field, the scale and general style of layering is similar to that in layered gabbro commonly associated with massif-type anorthosite or layered mafic intrusions (e.g., Morse, 1968; 1982; Woussen et al., 1988). However, the layering is distinctly different in detail. Common cumulate layering in massif-type anorthosite is consistently asymmetric (i.e., has a "way up") in mode and grain-size gradation and is generally at a larger scale (0.5 m or greater). Rhythmic layering is common in massif-type anorthosite, but centimetre-scale layers do not have great lateral extent (Wiebe, 1988; 1990; Ashwal, 1993). Lamination due to flow, cumulation in a convecting magma chamber, or crystal compaction can produce centimetre-scale sharply defined layers and a preferred orientation of crystals (e.g., Higgins, 1991), but does not explain the edge-centre symmetrical distribution of mafic minerals in some mafic bands or the concentration of quartz in the centres of felsic bands. Quartz is concentrated in the centres of felsic bands and may have been remobilzed from the mafic bands during metamorphism/deformation. A combination of igneous layering, enhanced by deformation and metamorphism is a possible explanation for the observed details of the layering.

Pyroxenites are rare but distinctive massive and dark green to black, rusty-weathering rocks Figure 2.9. They occur as 0.5-1 m thick, sharply bounded layers associated with centimetre-scale anorthosite-leuconorite layers. They are mostly concordant with the finer layering, but one well exposed example of a pyroxenite dike clearly cross-cuts the anorthosite-leuconorite layering. Pyroxenite consists mainly of coarse-grained (up to 4 mm) schillerized orthopyroxene, less abundant and less altered clinopyroxene, Fe-Ti oxide minerals with rims of dark brown biotite, and granular plagioclase. Two samples contain about 10% Fe-Ti oxides and thus may be considered oxide-rich gabbro (e.g., McLelland et al., 1994). The freshest orthopyroxene contains many small rutile inclusions giving it the brown sheen characteristic of bronzite, but more commonly it is altered to amphibole and opaque oxide minerals. Plagioclase compositions in pyroxenite are more closely comparable to metamorphic compositions in the layered rocks at $An_{\sim 35}$ than that of the freshest massive anorthosite, which is generally $An_{\sim 45-50}$.

Other anorthosite bodies

The Blair River inlier contains many small bodies of anorthosite apart from the Red River Anorthosite Suite; four of the larger bodies are shown on Figure 2.1. Raeside et al. (1986) recognised the Delaneys Brook and Salmon River anorthosite units, and two additional bodies, the High Capes and Polletts Cove River anorthosite units are named here. All four of these bodies are poorly exposed and sparsely sampled. Their boundaries are inferred from outcrops in rivers and brooks, sparse outcrops on the highlands plateau, the presence of locally derived boulders on steep hillsides, and large boulders in ponds and barrens.

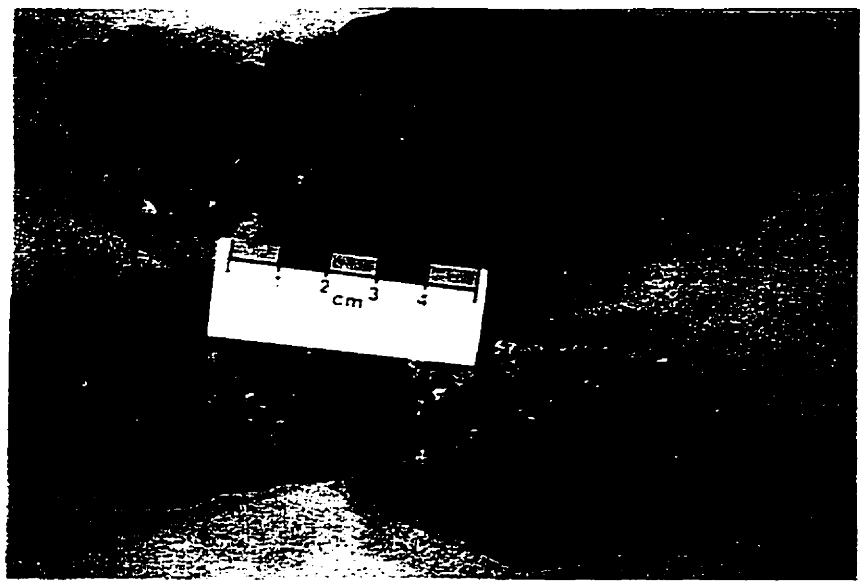

Figure 2.9 - Hand samples of pyroxenite from the Red River Anorthosite Suite (BVM91-733, BVM91-756, BVM91-757, RR85-2062b).

The Delaneys Brook body comprises almost entirely massive fine- to medium-grained buff white anorthosite and minor leuconorite. Raeside and Barr (1992) described a clearly intrusive relationship where thin sheets of anorthosite intruded adjacent mafic gneiss (Sailor Brook gneiss). They also reported gneissic xenoliths in the anorthosite. In several localities, for example in the small tip of the body north of Delaneys Brook (Map A) fine- to medium-grained (~0.2-0.5 mm) equigranular polygonal plagioclase (~An_{50}) grains show diffuse normal igneous zoning patterns (Figure 2.11a). The fine grain size and sharply defined zoning patterns suggests rapid cooling similar to anorthosite dikes from other massif-type bodies (Wiebe, 1979) and this is supported by reports of chilled margins on the thin anorthosite sheets (S. Barr, pers. comm., 1991).

In the centre of the body, medium-grained granular anorthosite contains blocky or tabular plagioclase grains with rational grain boundaries and irregularly shaped patches of poikilitic plagioclase (Figure 2.11b). The patches contain numerous inclusions of quartz and Fe-Ti oxide minerals. Each plagioclase patch is a single crystal but is bounded by the rational grain boundaries of adjacent grains. Albite-law twin lamellae are wider and extinction angles higher at the edges of the patch, suggesting reverse zoning. These poikilitic plagioclase patches may represent trapped intercumulus liquid in an otherwise nearly perfect adcumulate. Rare orthopyroxene megacrysts (1.5 cm diameter) have highly schillerized bronzite cores rimmed by clinopyroxene and hornblende (Figure 2.11c).

The Polletts Cove River anorthosite contains a straight or swirled gneissic foliation defined by wispy blue-grey bands of chlorite and epidote. Judging from the proportions of white (altered plagioclase) and blue-grey (epidote and chlorite) bands, the Polletts Cove River gneissic anorthosite was probably a leucogabbro prior to deformation and intense alteration. The High

Capes anorthosite forms white ridges and sea cliffs in the west-central Blair River inlier. It is composed primarily of highly altered massive anorthosite. The Salmon River anorthosite is located in the most remote region of the Blair River inlier. Its shape is poorly constrained due to poor exposure and limited mapping, and all samples from this body are very highly sericitized. Less altered patches contain granular zoned plagioclase ($An_{\sim 50}$) grains.

Charnockite

Charnockitic rocks[3], as mapped here, crop out discontinuously from Red River to Wilkie Brook as a thin band adjacent to the Red River Anorthosite Suite and as sheared lenses in the Wilkie Brook fault zone. Charnockite rocks are not associated with the smaller anorthosite bodies, although there are some altered two-pyroxene granitoid rocks in the Polletts Cove River gneiss which may have been charnockite. In the field, charnockite displays a greasy green lustre (a common characteristic of fresh charnockite in other areas) in only the freshest outcrops in areas of least alteration. More commonly, the charnockitic rocks are tan or pink, moderately to highly altered, and either weakly layered or foliated (Figure 2.10). Varieties lacking pyroxene (monzonite and granodiorite) are considered part of the charnockite unit because they can be traced into, and are texturally similar to, charnockite. Highly altered rocks of intermediate composition that, based

---

[3] By definition (Streckeisen, 1976) charnockitic rocks contain >5% hypersthene, but the usage is not rigorous and two-pyroxene rocks with <5% hypersthene, rocks with no pyroxene, and high-grade granitic metamorphic rocks are described as "charnockite". The term "charnockite" as used here includes lithologies that range in composition from (charnockite terms in parentheses) diorite (norite), monzodiorite (jotunite; this term is also used, incorrectly according to Ashwal, 1993, to describe oxide-apatite gabbronorite), granodiorite (opdalite), monzonite and monzogranite (mangerite), and granite (charnockite).

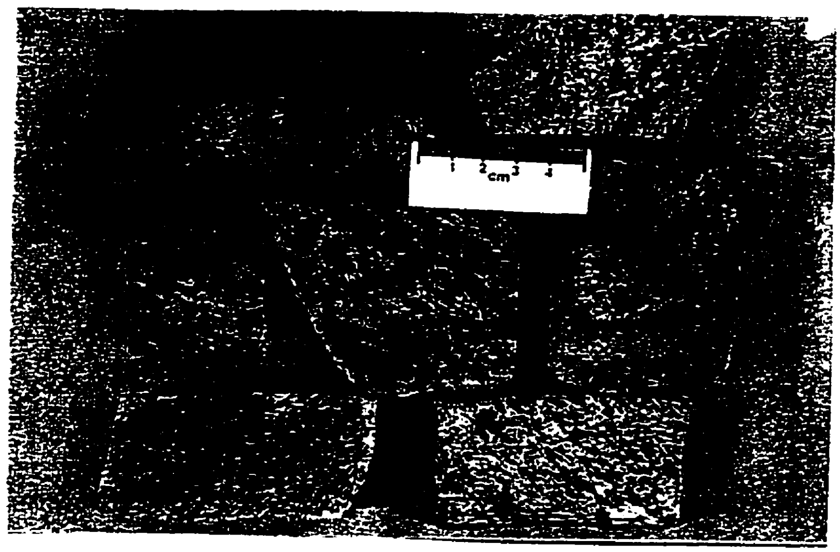

Figure 2.10 - Hand samples of charnockite (BVM91-602, BVM91-614, BVM90-073, BVM91-610, BVM91-057, BVM91-600, CW85-057).

Figure 2.11 - Examples of textures and minerals in the Delaneys Brook Anorthosite.

(a) normal zoning in equigranular plagioclase grains (SB85-1070; scale bar = 1 mm).

(b) zoned, inclusion-rich, plagioclase patch bounded by crystal faces of surrounding grains. This may represent a pocket of trapped intercumulus liquid (CW85-117; scale bar = 1 mm).

(c) orthopyroxene megacryst (highly schillerized and partly plucked from slide) rimmed consecutively by clinopyroxene, hornblende, and biotite (RB91-018; scale bar = 1 mm).

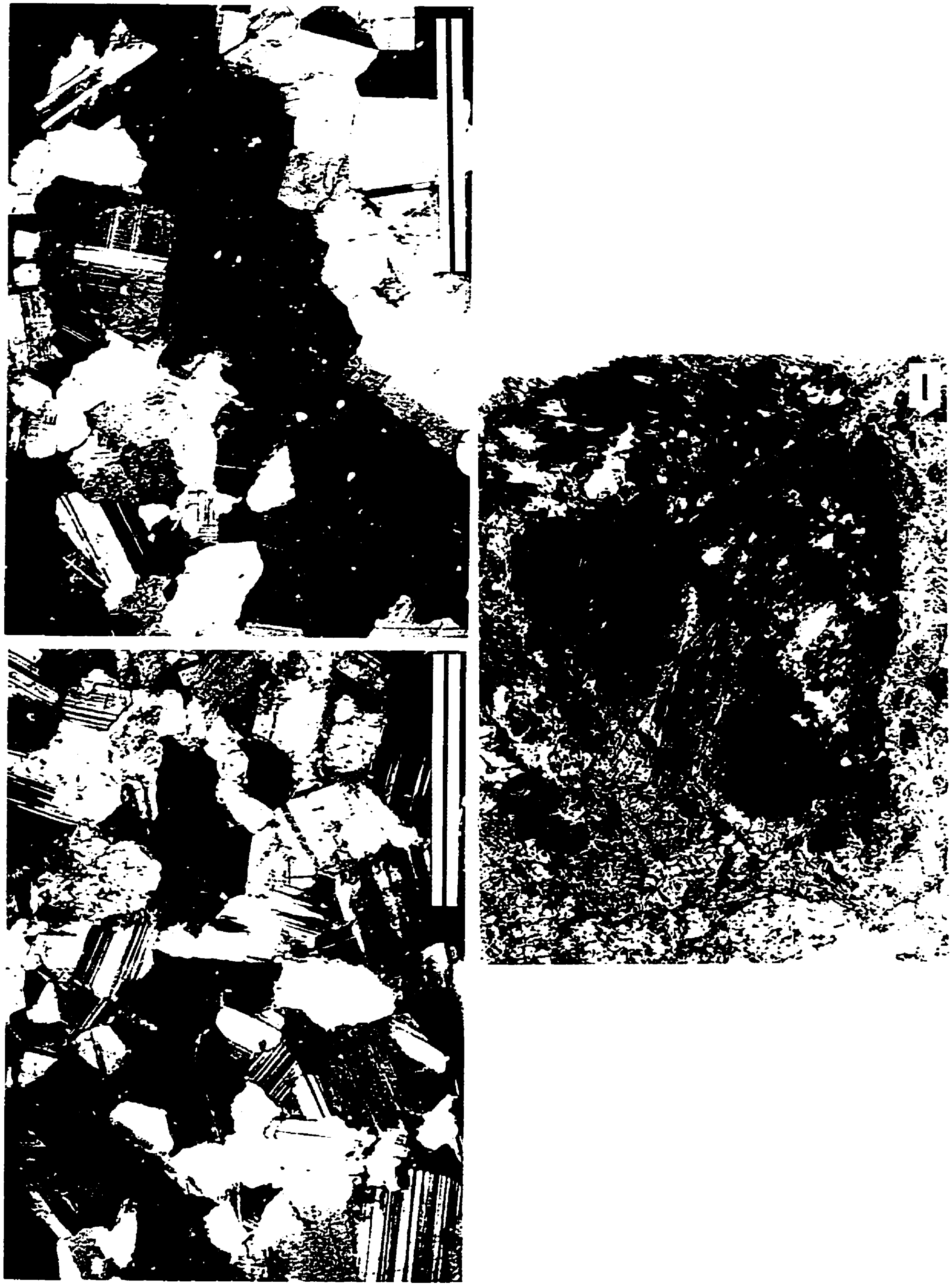

Figure 2.11

on relict mineral textures, are thought to have once contained pyroxene are also included in the charnockite unit.

Charnockite occurs adjacent to and appears to be gradational with the layered unit, although rocks in the transition zone are commonly altered and it is, in places, difficult to distinguish the two in the field. Rocks in both units have a red or pink tint where altered along late fractures and deformation of the charnockite enhances the layered appearance to very similar to that of the layered unit (Figure 2.10). Ashwal (1993) noted that the apparent lithological gradation between charnockite and anorthosite suites can, in some cases, be attributed to the smearing of contacts during high-grade metamorphism, and this appears to be the case in the Blair River inlier. The relationship is obscured further by the additional effects of a second, amphibolite-facies, metamorphic event and by low-grade alteration associated with faulting.

Charnockite contains large (up to 12 mm) plagioclase (An_{30-40}) grains, some of which have myrmekitic exsolution and are partly recrystallized into granular domains along grain boundaries, and coarsely perthitic K-feldspar. Both orthopyroxene and clinopyroxene are present, the former being dominant. Orthopyroxene is commonly severely schillerized and contains clinopyroxene exsolution lamellae. Separate clinopyroxene grains are partly to completely altered to light-brown to green poikiloblastic or mosaic texture hornblende. Brown to olive green, coarse-grained hornblende is distributed throughout the rock, and appears to be stable with both pyroxenes. Medium- to coarse-grained dark-brown biotite is present as inclusions in orthopyroxene and as separate matrix grains. Fine-grained tan biotite is associated with hornblende in alteration patches.

Recrystallized and deformed charnockite rocks contain the best preserved high-grade metamorphic mineral assemblages of any unit in the Blair River inlier. They commonly have a gneissic foliation defined by highly elongate hypersthene (2-7%, individual grains are 1x5 mm or longer), more equidimensional or slightly ovoid clinopyroxene (salite, 0-5%), preferentially oriented biotite (<5%), annealed quartz ribbons (14-20%), perthitic K-feldspar (~30%) and plagioclase ($An_{\sim 35}$, ~30%), all in a fine-grained recrystallized feldspathic matrix. Some samples contain granular magnesio- to ferroan pargastic hornblende and others lack Fe-Mg silicate minerals entirely. Fe-Ti oxides (rimmed by titanite only in metamorphosed samples), zircon, and apatite are ubiquitous accessory minerals.

Lowland Brook Syenite

The Lowland Brook Syenite (Figure 2.1) is a large crescent-shaped body of syenite in the northwestern part of the Blair River inlier. It is typically brick red, medium to coarse grained, and most commonly contains an anastomosing gneissic foliation. Layers of mafic minerals and zones of fine-grained recrystallized feldspars wrap around coarsely perthitic feldspar clasts or augen in gneissic syenite. In several low-strain zones on the order of tens of metres wide, relatively undeformed syenite is massive, equigranular, and dark red. Mafic enclaves, xenoliths, and intrusion breccia of granular and migmatitic gneiss are preserved in massive syenite in the low-strain zones.

Compared to massive syenite, gneissic syenite (Figure 2.12b) contains a higher proportion of mafic minerals (up to ~25%), quartz (up to ~10%), large plagioclase phenocrysts (1 cm; up to ~20%), and large and abundant (up to 0.4 mm diameter and 1.5 mm long) subhedral zircon. In gneissic samples, large (0.8-5 mm) perthitic feldspar porphyroclasts are wrapped by mafic layers

Figure 2.12 - Field occurrence and hand samples of the Lowland Brook Syenite.

(a) marble in highly sheared and faulted syenite in sea cliffs near Sailor Brook.

(b) gneissic syenite from the Lowland Brook Syenite, yellow slabs are stained for K-feldspar (Hutchinson, 1974).

(c) gneissic syenite; white (unstained) spots are recrystallized plagioclase porphyroclasts.

(d) massive syenite from the Lowland Brook Syenite; slab on the right is stained for K-feldspar

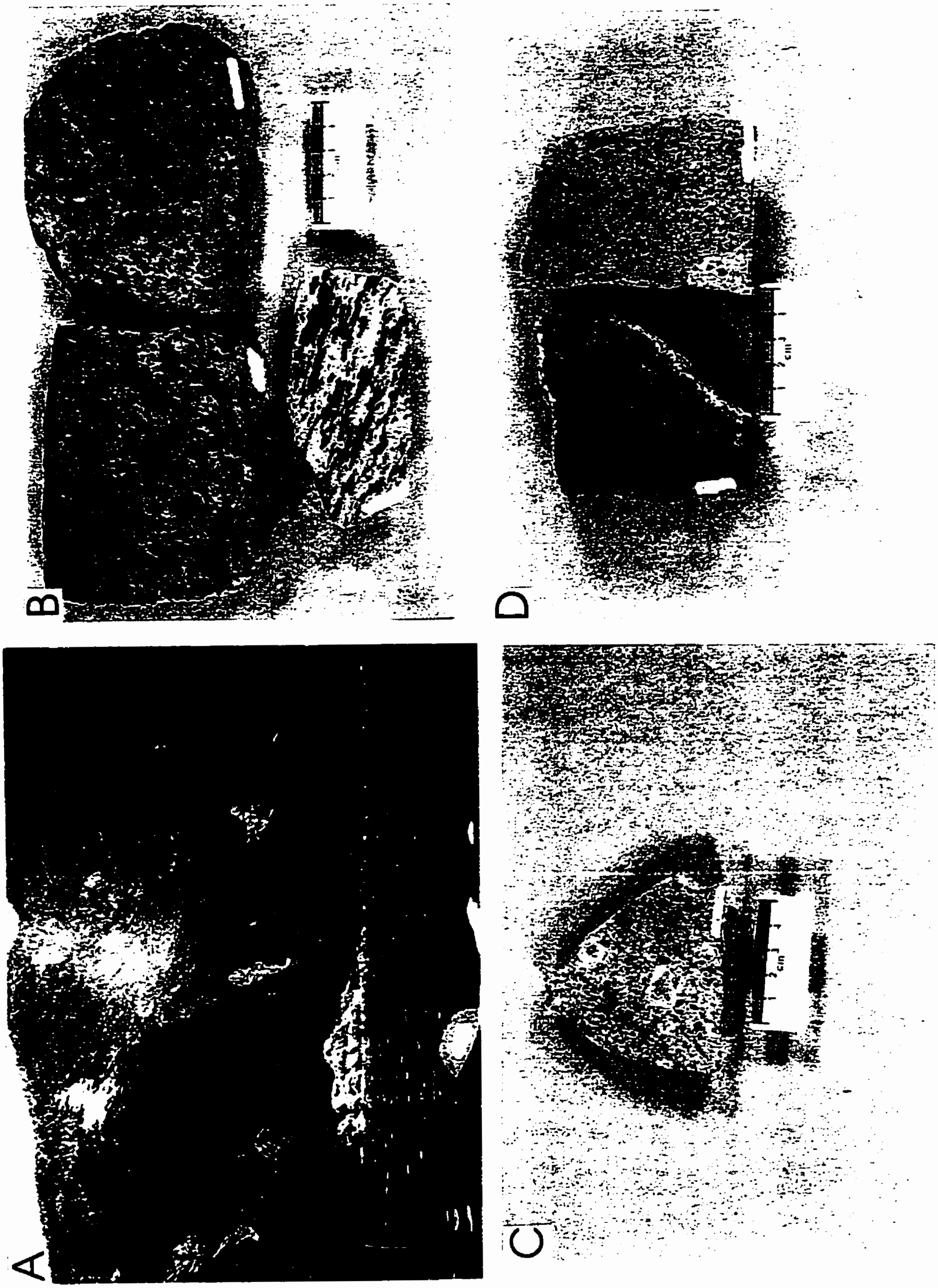

Figure 2.12

rich in green magnesio- to actinolitic hornblende and blocky brown ferro-edenitic hornblende in flattened elongate mosaics, preferentially oriented biotite partly altered to Chl+Kfs, and Fe-Ti oxide minerals rimmed by titanite. Titanite is also present as separate spindle-shaped grains.

Coarse perthitic and antiperthitic feldspar porphyroclasts (1-5 mm) in gneissic syenite samples are highly recrystallized to an equigranular matrix of separate feldspars and comprise about 40-60% of the rock. Perthitic feldspars contain lamellae of orthoclase (rarely microcline) and oligoclase (An_{15-22}). Recrystallized matrix grains are orthoclase and andesine ($An_{\sim 38}$). All feldspars are moderately to highly sericitized but plagioclase is more highly altered than K-feldspar. Rare large (2.5 mm to 1 cm), probably normally zoned, plagioclase phenocrysts are recrystallized into ~2.5-4 mm subgrain aggregates. A central patch of calcic plagioclase (An_{40}) subgrains is highly sericitized and surrounded by a rim of unaltered, less calcic (An_{20}) subgrains. In stained hand samples these aggregates appear to be large plagioclase porphyroclasts, but they are recrystallized plagioclase aggregates in thin section (Figure 2.12c).

Massive syenite (Figure 2.12d) comprises mostly coarse-grained (1-5 mm), anhedral, orthoclase microperthite (~80-95%). Zircon grains are relatively abundant, but smaller (~0.25 mm diameter, ~0.5 mm long) than in the deformed syenite. Plagioclase lamellae in microperthite are albite (An_{8-10}). Perthitic feldspars are recrystallized at grain edges into mortar-texture mantles or fine-grained (0.1-0.3 mm) granular aggregates of separate K-feldspar (orthoclase and, rarely, microcline) and plagioclase ($An_{\sim 35}$). Plagioclase grains and lamellae are commonly more highly sericitized than K-feldspars. Quartz is a minor constituent (<2%) and is most common in mafic patches with altered clinopyroxene.

Sparse mafic patches make up less than 8% of massive syenite. They are interstitial to large perthitic feldspars and contain relatively fresh (salite) or partly altered (ferroaugite) clinopyroxene, Fe-Ti oxide minerals that lack titanite rims, biotite partly altered to chlorite, and large (0.1-0.25 mm) zircon grains. Titanite is not present in these samples, but rutile is common as exsolution lamellae in pyroxene. Olive-green to brown (ferro-edenitic) hornblende grains are blocky with well defined crystal faces and cleavages. Pale-green (actinolitic) hornblende occurs in fibrous or irregularly zoned amphibole patches replacing clinopyroxene. The olive-green to brown hornblende appears to have been stable with (now mostly altered) clinopyroxene, and may have been a primary igneous mineral.

One of the low-strain lenses preserves undeformed irregular syenitic pegmatoid patches of cryptoperthite or microperthite megacrysts (1-6 cm) with straight, rational grain boundaries. Interstitial to the feldspar grains are coarsely crystalline quartz, large (2 mm) apatite grains, mafic patches with Fe-Ti oxide minerals, and chlorite and epidote pseudomorphous after clinopyroxene.

The northern and eastern portions of the Lowland Brook Syenite are flanked by Carboniferous sedimentary rocks, the Fisset Brook Formation and marble, calc-silicate, and skarn of the Meat Cove marble (described below). At a few well exposed localities, the contacts are complex zones of sinuous cataclastic to mylonitic fault zones that interleave syenite, basalt, rhyolite, granite, conglomerate, sandstone, and skarn. On Lowland Brook, the contact between the Lowland Brook Syenite and the Fisset Brook Formation is a 1.5 m wide fracture zone between relatively undeformed rhyolite and syenite. This zone may be a slightly sheared nonconformity.

Near a tributary of French Brook, an exploration trench in the Meat Cove Zn occurrence (Sangster et al., 1990) exposes brecciated rhyolite and syenite, mylonitic syenite, and highly foliated marble in the area of the contact with the Fisset Brook Formation. In sea cliffs near Sailor Brook, marble blocks occur in highly sheared, faulted, and mylonitic syenite (Figure 2.12a). These marbles may be related to the Meat Cove marble (described below), but they cannot be demonstrated to be xenoliths in the syenite. On a tributary of Lower Delaneys Brook, a coarse-grained metagabbroic dike separates the Lowland Brook Syenite and Sailor Brook gneiss. On Lower Delaneys Brook, the same (or a similar) dike is sheared along both contacts, yet preserves relict igneous textures toward the centre. On Sailor Brook the contact between the Lowland Brook Syenite and Sailor Brook gneiss is interpreted to be a faulted intrusive contact (as described above).

Otter Brook gneiss

The Otter Brook gneiss (Figure 2.1) is a heterogeneous unit of predominantly intermediate quartzofeldspathic to mafic gneiss. The dominant lithology (~80%) is a tan to brown, biotite-rich, locally garnet-bearing quartzofeldspathic augen to flaser gneiss (Figure 2.13a). More mafic variants include foliated amphibolite (~15%) and metagabbroic amphibolite (~8%), the latter recognised by a relict subophitic texture. Several small (<2 m wide) highly foliated lenses of calc-silicate rock in the Otter Brook gneiss crop out in shear zones and adjacent to faults. Boulders of anorthosite are present in several stream beds, along the steep banks of brooks, and in a narrow zone of the upland plateau between brooks. The boulders are likely derived from a local undiscovered outcrop source. In a tributary of Otter Brook, one small outcrop of brecciated and highly altered anorthosite (first recognised by Neale, 1964) coincides with the upstream limit of anorthosite boulders. The distribution of calc-silicate and anorthosite lenses is shown on Map A.

Figure 2.13 - Representative hand samples and mineral textures from the Otter Brook gneiss.

(a) slabbed hand samples; clockwise from upper left - intermediate quartzofeldspathic biotite-rich garnet-bearing flaser gneiss (BVM91-695), biotite-hornblende quartzofeldspathic gneiss (BVM91-714), intermediate biotite-hornblende quartzofeldspathic augen gneiss, and hornblende-garnet amphibolite intruded by small pegmatite.

(b) garnet porphyroclast separated from matrix Fe-Mg silicate minerals by a Kfs+Pl+Ms reaction zone, draped by the amphibolite-facies foliation, and with relict clinopyroxene grains in the strain shadow. The large black inclusion is biotite that also is separated from garnet by a reaction zone, but smaller biotite inclusions that are not connected to the matrix lack the reaction zone. (scale bar = 1 mm)

(c) thin mafic band of broken up clinopyroxene, partly altered to a green hornblende mosaic. These alteration minerals enclose a blocky brown hornblende grain, presumably of an earlier generation. (scale bar = 1 mm)

(d) calc-silicate from a sheared lens in the Otter Brook gneiss. Phlogopite defines the foliation and wraps around augen of diopside and tremolite. (scale bar = 1 mm)

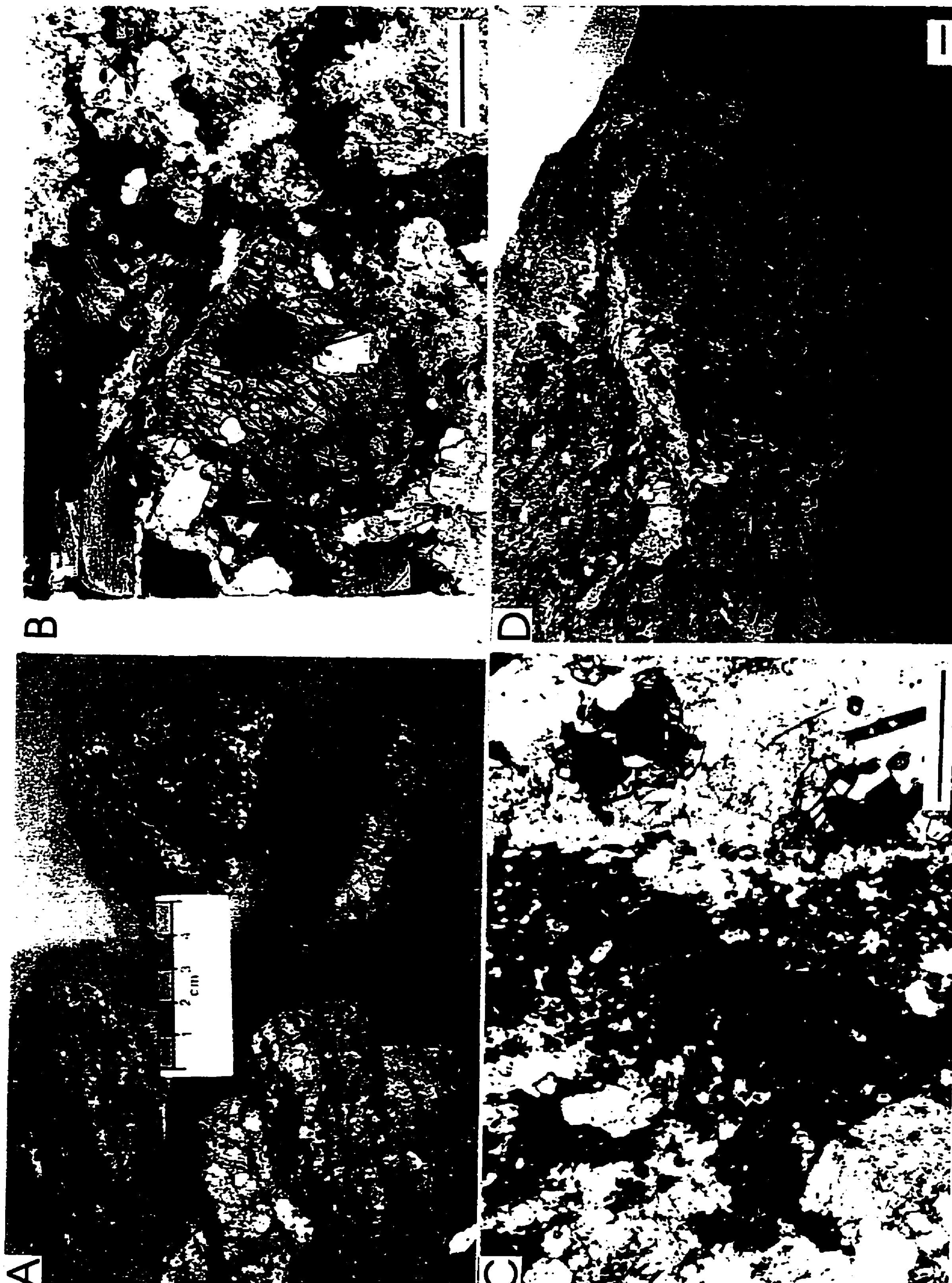

Figure 2.13

Granite pegmatite dikes are common in the biotite-garnet quartzofeldspathic gneiss and foliated amphibolite lithologies, but are absent from the metagabbro and calc-silicates. The pegmatites range from ~2 centimetres up to ~0.5 m wide and both cross-cut and are transposed parallel to the gneissic foliation. In several localities, a garnet-rich rind is developed in the foliated amphibolite adjacent to granitic pegmatites (Figure 2.13a).

Within the limits imposed by the generally poor exposure, the lithological variants in the Otter Brook gneiss are not recognisably layered at the unit or outcrop scale. At the scale of stream bed or small gorge-wall outcrops (up to about 10 m), the quartzofeldspathic gneiss is homogeneous. No compositional banding or layering occurs at scales greater than the 0.5-1 centimetre scale of the gneissic foliation as defined by the preferred shape orientation of amphibole and biotite. The Otter Brook gneiss is here considered to be a complexly deformed, intermediate quartzofeldspathic to mafic orthogneiss interleaved along fault zones with the various other minor lithologies. Rock types similar to the Otter Brook gneiss are also present in the Polletts Cove River gneiss, but could not be separated at the present map scale.

A narrow but highly foliated shear zone separates the eastern side of the Otter Brook gneiss from the Polletts Cove River gneiss. To the north the two units are separated by a brittle fault (Map A). Minor brittle faults, perhaps a faulted unconformity, separate the Otter Brook gneiss from Carboniferous conglomerate and rhyolite to the west. The contact between the Otter Brook gneiss and the Fox Back Ridge diorite/granodiorite is interpreted to be the extension of a late fault that cuts, and forms a distinctive gorge in, the nearby Carboniferous units.

Intermediate to mafic portions of the Otter Brook gneiss most commonly contain Kfs+Hbd+Bt+Pl+Ox+Ttn±Grt. In more felsic samples, K-feldspar and plagioclase (An_{23-30}) porphyroclasts are large (1.5-3 cm) and grain boundaries are recrystallized into mortar-texture subgrain mantles. K-feldspar grains contain irregular exsolved plagioclase in coarse patches (as opposed to spindle-lamellae perthite in many other igneous units in the Blair River inlier) and some plagioclase grains are myrmekitic. Recrystallized matrix plagioclase is generally fresh, but where plagioclase is in contact with amphibole, compositional zoning is recognised by concentric extinction and by the concentration of sericitic alteration.

Garnet grains are xenoblastic and many contain inclusions of plagioclase, quartz, biotite, zircon, and Fe-Ti oxides without titanite rims. K-feldspar, hornblende, and titanite are part of the amphibolite-facies matrix assemblage and help to define the foliation, but do not occur as inclusions in garnet. The amphibolite-facies foliation drapes around garnet porphyroblasts, and Fe-Ti oxide minerals commonly have titanite rims. Garnet grain boundaries are corroded and separated from amphibolite-facies Fe-Mg silicate matrix minerals (biotite and hornblende) by a reaction zone comprising primarily K-feldspar, but with small amounts of plagioclase and muscovite.

Amphibole (10-22%) in mafic layers of intermediate gneissic samples is mostly pale- to olive-green (pargasitic) hornblende (hereafter "green hornblende"), has ragged grain boundaries, erratic compositional zoning, numerous tiny dusty inclusions, and poorly developed cleavage except where enhanced by shearing, and is commonly intergrown with biotite. Green hornblende in less sheared portions of the mafic layers preserves poikiloblastic or mosaic textures that are typical of altered pyroxene. Rare (generally <2%) grains of dark-green to brown (hastingsitic) hornblende (hereafter "brown hornblende") are partly altered to biotite but appear to have once been clean, blocky grains with sharp, well defined cleavages. In foliated amphibolite samples, green hornblende is the only amphibole present and contains volumetrically significant (up to about 35-40%) inclusions of epidote and distinctive spindle-shaped K-feldspar. Dark brown biotite grains in these rocks show similar textures, with the same distinctive spindle-shaped K-feldspar, but with chlorite as inclusions.

Biotite is a common constituent (15-20%) of intermediate gneiss. Large dark brown grains help to define the foliation and smaller biotite grains are pleochroic in shades of green and tan to brown. Green hornblende appears to be stable with biotite but biotite appears to have replaced brown hornblende. Many garnet porphyroblasts contain inclusions of biotite, but the two minerals are separated by a reaction zone of Ms+Pl+Kfs. In many altered samples of the Otter Brook gneiss, biotite is partly broken down into Chl+Kfs. K-feldspar grains forms lozenges completely enclosed by biotite that is partly altered to chlorite. A few samples contain large (~8 mm) mafic mineral clusters in which the alteration of brown hornblende to biotite is associated with significant amounts (~25% of the biotite-hornblende cluster) of a carbonate mineral. Carbonate is not present in the felsic layers or in association with resorbed garnet but appears to be associated with alteration in the mafic mineral clusters.

Felsic layers of the intermediate gneiss comprise coarse-grained K-feldspar (~5-20%, 0.5-2 mm, Or_{93-95}) with serrated grain boundaries, plagioclase (~10-30%, 0.45-1.5 mm, An_{23-30}), and recrystallized quartz (~4-8%, aggregates of 0.3-1.5 mm). Both types of feldspar are partly recrystallized along grain boundaries and in irregular internal patches into mortar-texture subgrains (0.1-0.5 mm). Plagioclase and K-feldspar are both altered to fine-grained micas (sericite) and saussurite. Plagioclase is locally myrmekitic and is zoned adjacent to Fe-Mg silicate minerals. K-feldspar occurs as separate grains and as irregular exsolved patches in plagioclase (coarse-patch antiperthite, distinct from the spindle or lamellar perthite in the Lowland Brook Syenite and charnockite). The feldspar alteration, recrystallization, and exsolution textures are typical of most Otter Brook gneiss samples and complicate recognition of primary textures. Rarely preserved in the centres of polycrystalline augen are large (0.75-1.5 mm) blocky feldspar grains with interstitial biotite laths that are less altered and recrystallized and have straight and rational grain boundaries. These may be relict igneous textures.

Clusters of xenoblastic almandine-rich garnet grains (<2% in intermediate gneiss and up to ~7% in mafic gneiss) are concentrated in mafic layers, but smaller individual grains are also present in felsic layers. Garnet grains in mafic layers are large (0.5-1.2 mm), generally occur in clusters, and are ubiquitously corroded adjacent to, and separated by a Kfs+Pl+Ms reaction zone from, Fe-Mg silicate minerals. Large garnet grains contain inclusions of quartz, plagioclase, biotite, zircon, apatite, and Fe-Ti oxide minerals without titanite overgrowths. Inclusion minerals do not preserve pre-metamorphic textural relationships and there is no core-edge variation in inclusion concentration. Garnet grains in the felsic layers are <0.4 mm, and occur mostly along feldspar grain boundaries and rarely as inclusions in plagioclase, perthitic K-feldspar, and polycrystalline quartz. The foliation defined by amphibole and biotite is slightly draped around garnet grains. In foliated amphibolite samples, large (up to 3.5 mm) garnet porphyroblasts are commonly broken apart and the assemblage Pl+Kfs+Hbl±Ox fills the fractures. Garnet grains are more abundant in foliated amphibolite, but show the same reaction textures and also lack inclusion/matrix mineral relationships.

Rare relict clinopyroxene (ferrosilite) are broken into small fragments in felsic layers and are highly altered to green hornblende in mafic layers. Uralitized and relict clinopyroxene fragments are also present in mosaic-textured patches of green hornblende and quartz and in strain shadows provided by garnet porphyroblasts (Figure 2.13b,c).

One of the more conspicuous petrographic features of the Otter Brook gneiss is the presence of large and abundant (up to ~2% combined) accessory minerals. Zircon grains are large and abundant up to 1 mm in diameter, but most are between 0.25-0.4 mm. Zircon grains appear ovoid in thin section due to their orientation in the section, but those separated for geochronology were dominantly semi-prismatic with slightly rounded corners and tips and lacked obvious abrasion, frosting, or rounding typical of detrital zircon grains in metasedimentary units (e.g., van Breemen et al, 1990; Heaman and Parrish, 1991). Clusters of spindle-shaped titanite grains are also abundant (~0.5%), commonly strung out parallel to the foliation, and are restricted to mafic layers in association with Fe-Ti oxide minerals, biotite, and green hornblende. Titanite also occurs as rims around Fe-Ti oxide minerals in mafic layers. Medium to large (0.3-0.8 mm) apatite grains are distributed throughout the rock and occur as inclusions in all other minerals. Small grains (~0.1 mm) of allanite and other epidote-group minerals are the least abundant accessory mineral and are distributed throughout the rock.

Several calc-silicate lenses are present in the Otter Brook gneiss, but are associated with internal faults or shear zones and one lens is in the boundary shear zone. These rocks consist almost entirely of diopside, tremolite, and phlogopite with minor amounts of calcic plagioclase (Figure 2.13d).

It is uncertain whether the intermediate and mafic gneisses have a plutonic, volcanic, or sedimentary protolith. The calc-silicate samples may be metasedimentary or metasomatic, but they are tectonically interleaved lenses near late fault zones, and do not necessarily imply a supercrustal origin for the remainder of the unit any more than the presence of anorthosite (presumably tectonically interleaved lenses) would confirm an igneous protolith. Furthermore, small outcrops of marble and calc-silicate rocks occur throughout the Blair River inlier, but are everywhere associated with shear zones, and most commonly in faulted boundary zones between major units. No major metasedimentary source occurs in the Blair River inlier for these calc-silicate rocks and marbles. Within the intermediate augen to flaser gneiss, there are no sharply bounded compositional layers that might represent bedding, such as are common in metasedimentary units. Accessory minerals are consistently abundant in many samples from a wide area and are distributed throughout the gneissic compositional layers in individual samples. Dense detrital minerals might be expected to be concentrated in discrete layers or zones in sedimentary rocks. The igneous-type zircon morphology and lack of scatter in U-Pb systematics are consistent with an igneous protolith for the dated intermediate gneissic sample (Chapter 4). The coarse-grained, blocky feldspar and biotite textures preserved in the centres of augen in samples of intermediate composition are also consistent with an igneous protolith. Based on these observations, at least the intermediate flaser to augen quartzofeldspathic gneiss is here interpreted to have a plutonic protolith of approximately hornblende granodiorite composition.

Fox Back Ridge diorite/granodiorite

The Fox Back Ridge diorite/granodiorite forms much of the southern part of the map area between the Red River fault zone and the Red River Anorthosite Suite (Figure 2.1). The Fox Back Ridge unit consists of mixed porphyritic diorite and granodiorite to monzodiorite. It lacks a pervasive gneissic foliation, but is deformed by numerous brittle faults and small anastomosing shear zones. The unit is intruded dikes and small bodies of diabase, rhyolite, syenite, pegmatite, and medium-grained granite. The granite is similar, and probably related, to the Sammys Barren granite (Figure 2.14a).

The northern boundary of the Fox Back Ridge unit is constrained only by widely separated outcrops of the Polletts Cove River gneiss and the diorite/granodiorite. To the south, deformation increases progressively to form chlorite-epidote schist and phyllonite, and locally massive black mylonite and ultramylonite in the Red River fault zone. The lack of outcrop in the area of Sammys Barren obscures contact relations with the Red River Anorthosite Suite, but in one tributary of Red River, the contact is marked by a large, well exposed brittle fault. Highly deformed equivalents of the two units are intimately interleaved along anastomosing faults in the southernmost Blair River inlier.

Porphyritic diorite in the Fox Back Ridge unit contains actinolitic to magnesio-hornblende (60%) as small (0.1-0.25 mm) anhedral matrix grains with ragged edges and as recrystallized subgranular aggregates that are pseudomorphous after primary phenocrysts (0.1-0.25 mm each grain, 1-3 mm aggregates). Also present are plagioclase ($An_{\sim 30}$, 20%), orthoclase or microcline (15%), and quartz (5%). Where the unit grades to more granodioritic lithologies, the textures and minerals are the same, but with less hornblende (~40%) and more quartz (up to ~15%). Titanite is an abundant accessory mineral in some samples, and most samples contain minor amounts of Fe-Ti oxide minerals. Near late brittle fault zones and along individual fractures, amphiboles are highly altered to epidote and chlorite and feldspars are highly sericitized. Near the Red River fault zone, these same rocks become progressively more deformed with foliations defined by chlorite bands

Figure 2.14 - Field occurrences of, and textures in, late granite and syenite.

(a) dike of Sammys Barren granite intruded into Fox Back Ridge diorite/granodiorite.

(b) large yellow igneous titanite grains in coarse-grained, relatively undeformed Sammys Barren granite (CW85-034; scale bar = 1 mm)

(c) dike of undeformed granite intruded into the Sailor Brook gneiss and both are cut by a diabase dike, probably related to the Fisset Brook Formation.

(d) thin section of sample from the Red Ravine syenite showing microcline, and large yellow igneous titanite that is very similar to those of the Sammys Barren granite (BVM90-121; scale bar = 1 mm)

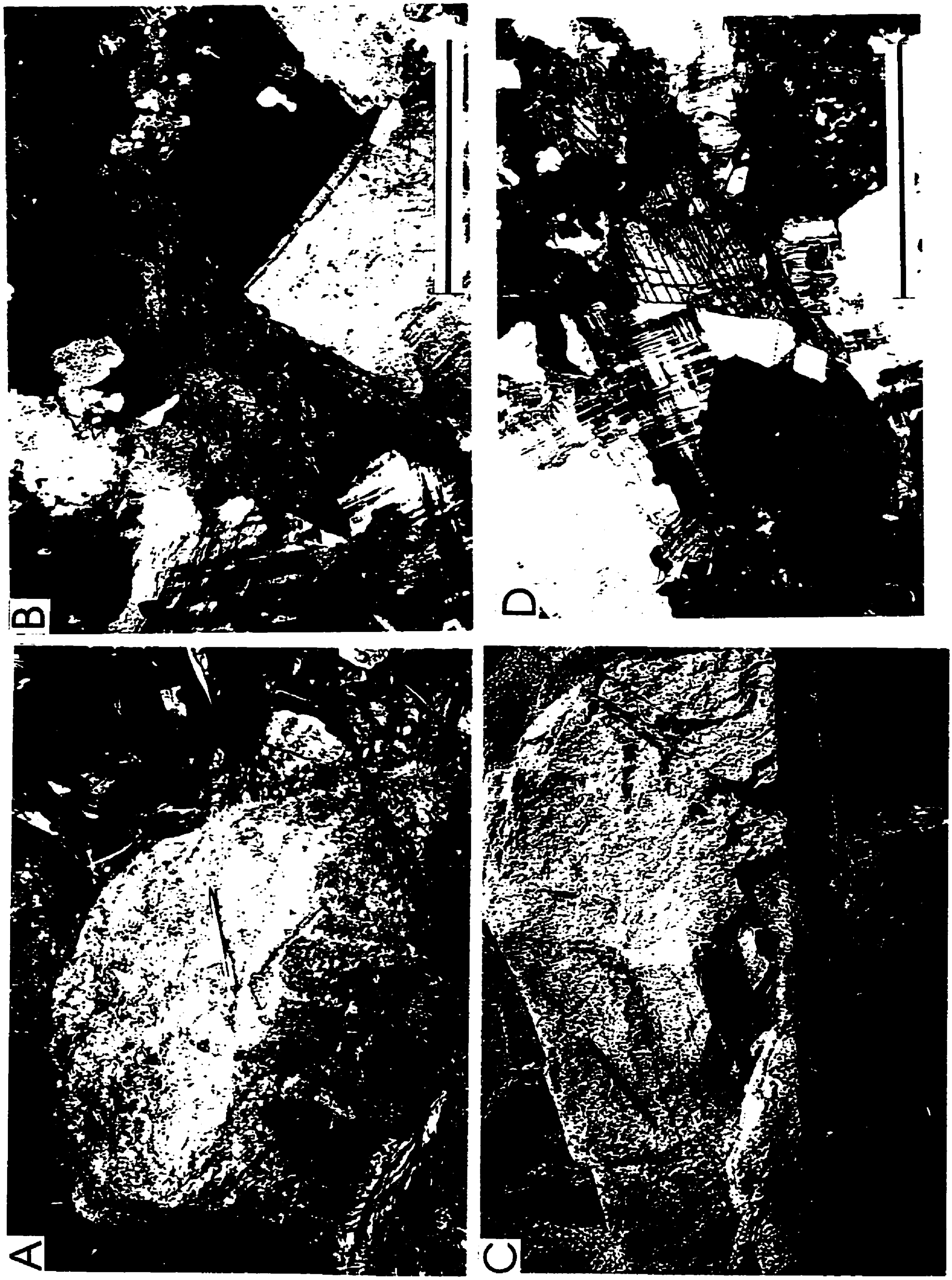

Figure 2.14

replacing amphibole, and by disaggregated epidote bands; quartz shows incipient ribbon formation and feldspars are fractured and highly altered. Significant structures in the Fox Back Ridge diorite/granodiorite are related to deformation along the Red River fault zone and are discussed in section 2.2.4.

Sammys Barren granite

The Sammys Barren granite (Figure 2.1) is an undeformed, medium- to coarse-grained, red or pink granite. The main granite body is located on Red River, and a tributary system. Similar granite also occurs as dikes and small bodies intruded into the Fox Back Ridge diorite/granodiorite. All of these granites contain subhedral microcline (generally non-perthitic) as the dominant K-feldspar (~50%), subhedral to euhedral plagioclase (An_{25}, ~25%), quartz (25%), and distinctive large (up to 2 mm) yellow, euhedral igneous titanite (Figure 2.14b). The only mafic minerals (<10%) are chlorite and epidote, which are pseudomorphous after biotite. These features contrast with the typically gneissic syenitic rocks of the Lowland Brook Syenite and charnockites, which commonly contain perthitic K-feldspar, amphibole or pyroxene, spindle-shaped (metamorphic) titanite or titanite as rims around Fe-Mg oxide minerals.

The boundaries of the Sammys Barren granite are poorly constrained. On Red River the boundary is marked by a highly fractured zone where granite dikes and pods in the Fox Back Ridge diorite/granodiorite gradually become more abundant than diorite and granodiorite. Granite, diorite, and granodiorite are intimately mixed on a tributary system of Red River, and the contact is placed somewhat arbitrarily where granite becomes the dominant lithology.

Small bodies or dikes of similar granite are also present in the Otter Brook gneiss, the Sailor Brook gneiss, and the Polletts Cove River gneiss. A granitic dike in the Sailor Brook gneiss is, in turn, cut by a mafic dike, probably related to the Fisset Brook Formation (Figure 2.14c).

Red Ravine syenite

The Red Ravine syenite (Figure 2.1) is medium to coarse grained, brick-red to pink, and commonly lacks a pervasive gneissic foliation. It crops out west of the Red River Anorthosite Suite and adjacent to charnockite unit. Although few contacts are exposed, no obvious textural or compositional gradation was observed from the charnockite to more K-feldspar-rich lithologies toward the syenite. The only observed contact between the Red Ravine syenite and the charnockite unit is a brittle (normal?) fault (Map A). On Red River, the contact between the syenite and the Fox Back Ridge diorite/granodiorite is a 15 metre-wide brittle fault zone. Dikes and veins of syenite and syenogranite intruded the Fox Back Ridge diorite/granodiorite and are mineralogically and texturally similar to the Sammys Barren granite (Figure 2.14d).

The dominant feldspars in the Red Ravine syenite are subhedral microcline (up to 70%), and anhedral plagioclase (An_{32}, 15%). Quartz is a constituent (up to 15%) in some samples, but most contain very little quartz. Rare mafic minerals are predominantly chlorite and epidote. Titanite grains are large yellow blades with well developed crystal faces and cleavages, and zircon grains are small and prismatic with sharp corners and flat crystal faces; both minerals appear to be magmatic in origin with no subsequent alteration of crystal habit. These minerals and textures are similar to those of the Sammys Barren granite but differ from those in the Lowland Brook Syenite.

Gabbro and Diabase

At least two generations of gabbroic dikes or small bodies are recognised in the Blair River inlier. An early set intruded the Sailor Brook gneiss, Lowland Brook Syenite, Otter Brook gneiss, Red River Anorthosite Suite, and Polletts Cove River gneiss. These gabbroic rocks are coarse grained and metamorphosed, and are distinctive in that they are only locally deformed, preserving subophitic textures, yet are commonly altered to amphibolite-facies mineral assemblages; aggregates of amphibole replace pyroxene and plagioclase is sericitized andesine or oligoclase.

A later generation of gabbro or diabase dikes intruded nearly all units. These mafic rocks are typically fresher and finer grained than the metagabbros, are only slightly altered, and not pervasively metamorphosed. They are most abundant near the boundaries of the Blair River inlier. Adjacent to the Blair River inlier in Lowland Cove, they are related to the Fisset Brook Formation (Smith and Macdonald, 1981). Similar dikes within the Blair River inlier are also interpreted to be part of the Fisset Brook Formation.

Rhyolite

Two distinct types of rhyolite occur in the Blair River inlier. Dikes of orange-brown, locally flow-banded, porphyritic rhyolite with phenocrysts of quartz and K-feldspar are concentrated near the edges of the Blair River inlier. This type of rhyolite is distinctive in that it is coarse-grained and more easily weathered compared to the aphanitic rhyolite. These dikes are probably related to the Fisset Brook Formation. The formation near Lowland Cove was assigned to the Late Devonian on the basis of poorly preserved trilete spores (reported in Smith and Macdonald, 1981). A more precise age of 373 ± 4 Ma was obtained by Barr et al. (1995) from a probable correlative unit in west-central Cape Breton Island.

In contrast, the second type of rhyolite is a hard, pink aphanitic rhyolite. It contains a very fine grained groundmass of quartz and feldspar and rare large (up to ~5 mm) phenocrysts of unstrained, euhedral quartz and concentrically zoned plagioclase. Other samples are foliated with rounded porphyroclasts of plagioclase and quartz in a fine-grained sheared matrix. Some dikes of this rhyolite either cut, or are concordant to the foliation in, the bounding fault zones of the Blair River inlier. Aphanitic rhyolite dikes locally separate the lithologies of the Red River Anorthosite Suite, and appear to have intruded along brittle faults. In the southern parts of the Red River and Wilkie Brook fault zones, these rhyolite dikes are difficult to distinguish in the field from altered pink anorthosite.

Marble and calc-silicate rocks

Marble and calc-silicate rocks are rare lithologies in the Blair River inlier. The largest outcrops are the mineralised skarn of the Meat Cove marbles (Chatterjee, 1979; Sangster et al., 1990a; 1990b) at the northern boundary of the Blair River inlier near the Lowland Brook Syenite. Other small outcrops of marble and calc-silicate rocks are located in the faulted boundary zones between major units or in shear zones.

Two types of marble and calc-silicate rocks are present in the Blair River inlier. One type is a marble composed of carbonate, forsterite, spinel, diopside, and muscovite with or without phlogopite; the other is a calc-silicate schist composed of diopside, tremolite, and phlogopite, with or without plagioclase and carbonate. The former is typical of the Meat Cove marble located in faulted boundaries of the Lowland Brook Syenite. The marble is commonly banded, with bands defined by concentrations of granular diopside and randomly oriented phlogopite. Forsterite is commonly partly serpentinized but most other minerals are relatively fresh. Patches of sphalerite overgrow both carbonate bands and bands rich in silicate minerals. These mineralised patches locally replace all minerals except muscovite, which is the only mineral present as inclusions in sphalerite. Thus the Zn-sulphide mineralization has overprinted (i.e., is later than) the calc-silicate metamorphic assemblage.

The calc-silicate schist is dark green to black and is more common in internal shear zones within units and at sheared boundaries between units. This type of calc-silicate rock is typified by polymineralic augen of recrystallized diopside, tremolite, and phlogopite. Phlogopite grains within the augen are small (<0.25 mm long), interstitial, and randomly oriented whereas phlogopite grains wrapped around augen are larger (0.3-0.5 mm long) grains that define the foliation. Some of these rocks may be deformed equivalents of silicate mineral-rich portions of the Meat Cove marble.

Chatterjee (1979) and Barr et al. (1987b) interpreted the Meat Cove marble to be xenoliths in the Lowland Brook Syenite. However, the marbles are located in the highly sheared and poorly exposed boundary region between the syenite and Carboniferous clastic rocks and only sheared contacts were observed during this study. No syenite dikes, fingers, apophyses, intrusion breccia, or other definitive indicators of an intrusive relationship were observed. At several localities, intense sulphide mineralization is associated with mafic dikes. Sheared marble lenses are spectacularly exposed in strongly gneissic to mylonitic syenite in sea cliffs near the mouth of Sailor Brook (Figure 2.12a). These lack sulphide mineralization, but contain metamorphic phlogopite, diopside, grossular, and serpentine pseudomorphous after forsterite.

2.3 Structure and foliation orientations

Sailor Brook gneiss

The Sailor Brook gneiss is divided into three structural subdivisions based on the distribution of fabric styles. The subdivisions are areas of (i) predominantly amphibolite-facies gneissic foliations, which affect the majority of the outcrop area, (ii) the best preserved relict high-grade granular banding, which is preserved adjacent to the Lowland Brook Syenite and in the centre of the unit on the southern branch of Sailor Brook, and (iii) the gneissic, mylonitic, and schistose foliations around the northern tip of the Delaneys Brook anorthosite. Amphibolite-facies foliations are gneissic to augen-gneissic foliations defined by the shape-prefered orientation of hornblende and biotite. These foliations wrap around rare, 1-2 mm, granular pyroxene-bearing lenses. High-grade banding is defined by the concentration of orthopyroxene, clinopyroxene, biotite and Fe-Ti oxide minerals relative to quartz and plagioclase. Fault zone foliations around the Delaneys Brook anorthosite are commonly defined by chlorite and muscovite anastomosing around lensese of quartz and feldspar.

Poles to the predominant amphibolite-facies gneissic foliation scatter widely about a NW-trending, steeply to moderately NE-dipping cluster (Map B, stereonet A) with a mean orientation of 339/78[4]. There are few data for the orientation of the relict high-grade granular compositional layering, but their orientation is parallel to the crescent-shaped contact with the Lowland Brook Syenite (Map B). Poles to the granular layers lie on a well defined girdle with a best fit orientation of 008/56 (Map B, stereonet B). Whether these orientations reflect that of the intrusive contact or a large-scale fold is uncertain, but no minor folds were observed in the granoblastic gneiss. Near the

[4] All planar orientation data are in right-hand-rule format. Stereoplots were made and contoured, and mean orientations and best fit great circles were calculated, using the computer program Rockworks (v. 6.13) by RockWare Inc.

Delaneys Brook anorthosite, where the High Capes and McEvoys Barren shear zones converge, gneissic foliations trend NNW and dip steeply WSW; they progressively rotate to E-W and south-dipping around the tip of the anorthosite, and west of it trend N-S and dip moderately W (Map B). Foliation data form a broad girdle on the stereonet (Map B, stereonet C), with a best fit orientation of 307/35.

Polletts Cove River gneiss

Foliation data from the Polletts Cove River gneiss west of the High Capes shear zone (Map B, stereonet D) scatter about a girdle that results from progressive rotation of foliation orientations into parallelism with the High Capes shear zone (Map B). The sense of foliation rotation is clockwise. Stereonet E on Map B shows foliation data from the segment of the unit between the two internal shear zones. The data are scattered, but are steeply to moderately dipping with a mean orientation of 318/81. No systematic foliation orientation is apparent in the southeastern segment of the unit west of the Red River Anorthosite Suite (Map B, stereonet F). In the eastern part of the unit north of McEvoys Barren (Map B, stereonet G), foliations trend NE near the Lowland Brook Syenite and NW near the Salmon River anorthosite, broadly parallel to the contacts with both bodies.

Red River Anorthosite Suite and charnockite unit

Bekkers (1993) recognised that the predominant foliation orientation in both the anorthosite and gabbro is NE-SW and that this orientation is broadly parallel to the trend of the Wilkie Brook fault zone. Foliations in the anorthosite are defined by wispy mafic streaks, flattened clusters of mafic minerals, or recrystallized cm-scale megacrysts. In deformed leucogabbro, a gneissic foliation is defined by the orientation of elongate pyroxene grains, or their alteration mosaics. The trends of the deformational foliations are generally parallel to the lensoid shape of the anorthosite body (Map B), but are also influenced by shearing on the Wilkie Brook fault zone and by late brittle faults and small shear zones. Thus, the foliation orientation data from the anorthosite and gabbroic units form no obvious pattern on the stereoplot (Map B, stereonet H). In layered units, compositional layering is the dominant fabric, an oblique mineral lineation is also rarely observed.

The orientation of the layering is also scattered, as shown in Map B, stereonet I, but the predominant orientation is 201/50, subparallel to the Wilkie Brook fault zone. Mineral lineations in the layered unit mostly plunge gently WNW, but are also scattered and fold axes plunge gently to the NNW or SSW (Map B, stereonet J). Although the data are too few for detailed analysis, minor faults and small shear zones in the Red River Anorthosite Suite appear to have no prevalent orientation, and mafic and felsic dikes trend generally NE (Map B, stereonet K). These faults locally deflect the predominant fabric of the anorthosite, gabbroic rocks, and the Wilkie Brook fault zone (see below) and are probably partly responsible for the wide scatter of data on the stereoplots.

Map B, stereonet L, and Map A show the orientation of layering and gneissic foliation in charnockite. These data form a broad cluster with NNE to ENE trends, steep to moderate northwest or west dips and a mean orientation of 022/81. Layering and foliation in the charnockite are generally subparallel to that of the layered unit, but with opposite dips.

Lowland Brook Syenite

The orientations of gneissic foliations in and adjacent to the Lowland Brook Syenite are shown on Map A. Foliation data are more abundant in the northern lobe of the syenite because of better access and better exposure. The gneissic foliations defined by amphibolite-facies minerals in both the northern lobe and the southern flange are subparallel, with a mean trend of 316/89 (Map B, stereonet M). The curved contact with the Sailor Brook gneiss, which may be folded, has no obvious effect on the orientation of foliations in the syenite. The orientation of the foliation in the syenite is similar to that of the deformational foliation in the Sailor Brook gneiss but differs significantly from that of the granular compositional layering (compare with Map B, stereonet A and contrast with Map B, stereonet B).

Otter Brook gneiss

In intermediate quartzofeldspathic gneiss, wispy (~0.5-1 cm wide) hornblende- and biotite-rich mafic bands and lensoid or augen bands of mostly quartz and feldspar define the gneissic foliation. Foliated amphibolite gneiss contains a foliation defined by the preferred orientation of hornblende and biotite. The gneissic foliation planes are consistent throughout the unit, trending NNE and dipping moderately to gently WNW (Map B). Foliation data form a broad cluster on the stereoplot (Map B, stereonet N) with a mean orientation of 012/74. Toward the boundary with the Polletts Cove River gneiss, the gneissic foliation progressively rotates to parallel to the ENE-trending boundary shear zone (Map A). Foliation data from the boundary shear zone cluster tightly with a mean orientation of 238/83 (Map B, stereonet O). The sense of rotation of the gneissic foliation into the boundary shear zone is clockwise and suggests dextral shear.

2.3 Boundary fault zones

The Blair River inlier is bounded on the east by the Wilkie Brook fault zone and on the southwest by the Red River fault zone. The two fault zones nearly merge to the south, but late brittle faults and granite intrusions obscure cross-cutting relationships. However, the Wilkie Brook fault zone appears to be the dominant structure, truncating and deflecting the Red River fault zone (Maps A, B).

2.3.1 Red River and Wilkie Brook fault zones

Red River fault zone

The Red River fault zone extends from near the village of Red River to near Grand Anse River at the foot of North Mountain. The fault zone trends NW-SE along much of its length but trends N-S at its southeastern extension where it converges with the Wilkie Brook fault zone. The Red River fault zone separates the bulk of Devonian or Carboniferous granitic plutons (Andrews Mountain, Grande Anse and Margaree plutons), Silurian metadiabase, pelitic and psammitic schist, and orthogneiss of the Aspy terrane from orthogneiss, diorite, granodiorite, granite, and syenogranite (Fox Back Ridge diorite/granodiorite and Sammys Barren granite) of the Blair River inlier.

Along much of its length, the Red River fault zone is a distinctive black mylonite or ultramylonite with a poorly developed foliation and weak compositional layering. The layering is defined by thin (generally <1 cm) felsic mylonite layers. In several locations, rocks grade from black ultramylonite to diorite with granitic veins and pods that resembles the Fox Back Ridge diorite/granodiorite. Therefore, the Fox Back Ridge diorite/granodiorite is considered the protolith of the mafic mylonite.

Where it is exposed in road cuts on the Cabot Trail, the Red River fault zone is a zone of anastomosing layers of locally intense deformation. Granite and syenogranite clasts in a mylonitic to schistose mafic (chlorite-biotite-epidote) matrix resemble the Sammys Barren granite and Red Ravine syenite. Highly sheared anorthosite clasts and lenses are present in the fault zone along the

Cabot Trail, but are not found elsewhere in the fault zone (Map A). At its northwestern extremity, the Red River fault zone is offset by brittle faults that juxtapose slivers of granite correlated with the nearby Andrews Mountain pluton (Raeside and Barr, 1992), rhyolite of the Fisset Brook Formation, and Carboniferous clastic rocks. Although all contacts observed in this study are faults, the rhyolite and clastic rocks were probably deposited unconformably over the Red River fault zone. At its southeastern end, the fault zone is truncated by late brittle faults that juxtapose sheared mafic rocks and protomylonitic coarse-grained granite with the relatively undeformed Grande Anse and Margaree granite plutons. Both plutons are locally sheared near the fault zone, indicating some post-intrusion movement.

Mylonitic foliations in the Red River fault zone strike generally NNE, or N-S, in accordance with its curved trace (Map B, stereonet P), and dip gently to moderately E or NE. Mineral lineation data scatter, but in general those associated with NW-SE trending foliations plunge moderately N, and those associated with N-S trending foliations plunge E or SE. Because the mafic ultramylonite and mylonite are very fine grained, they do not provide good macro-scale evidence for the sense of shear. However less deformed rocks in the anastomosing lenses along the Cabot Trail contain rigid felsic clasts in a fine-grained, foliated mafic matrix, the asymmetry of which suggests top-to-the-SW shear sense. Because foliation planes dip at low to moderate angles, the lineation is commonly down-dip, and sense-of-shear indicators suggest that the hanging wall moved up the lineation, the Red River fault zone is interpreted to be a predominantly NW-SE trending, moderately NE dipping, reverse fault.

Wilkie Brook fault zone

The Wilkie Brook fault zone extends from the Cape North peninsula, through the valleys of Wilkie Brook and Greys Hollow Brook, to the headwaters of North Aspy River. Exposure is poor on the North Mountain plateau and absent in the area of several large bogs and lakes (Red River Lakes). The position of the fault zone in this region is inferred from the first occurrence of large (up to 1 m^3) anorthosite boulders in bogs and lakes and on steep hillsides. On contoured orthophoto maps, the fault is marked by a prominent lineament across the North Mountain plateau, and by the trend of several small brooks. The Wilkie Brook fault zone is truncated by the Aspy fault at its southernmost extent, (Figure 2.1). The style of deformation in the fault zone is heterogeneous, both along and across strike, and consists of a system of anastomosing granitic mylonite, mafic phyllonite and schist, and cataclasite rocks.

The northern portion of the fault zone is characterised by a relatively narrow (<0.5 km) band of Chl+Ep+Bt±Ab schist and phyllonite with rare granitic mylonite. Within the fault zone, rocks recognisable as derived from both the Blair River inlier and Aspy terrane are interleaved and variably deformed and altered. Lenses of charnockite, anorthosite, marble, and calc-silicate rock preserve fresh anhydrous mineral assemblages even though the lenses are contained within a chloritic schist. In some of the larger lenses (2 m wide by about 10 m long), deformation is intense within a few tens of centimetres of the edge of the lens, but the centre of the lens is relatively undeformed. One marble lens preserves spinel, randomly oriented phlogopite, and partly serpentenised forsterite in the centre of the lens. Clasts and lenses of anorthosite that range from several tens of centimetres to tens of meters wide are present along the length of the fault zone.

In the northern segment of the Wilkie Brook fault zone, foliation planes strike predominantly NE-SW, and are steeply dipping, with a mean orientation of 047/82 (Map B, stereonet Q). The chloritic schist and phyllonite that typify this segment of the fault zone are fine-grained and easily weathered, therefore, mineral lineations are difficult to see in outcrop. Although the data are few, mineral lineations plunge gently to moderately NNE, W, or SE (Map B, stereonet Q). In the field, the NNE-plunging lineations are the most strongly developed and are from areas least likely to be complicated by rotation due to late faulting.

The southern segment of the Wilkie Brook fault zone is characterised by more abundant (compared to the northern segment) granitic mylonite or granitic augen gneiss along with cataclasite, mafic schist and phyllonite. Road cuts along the Cabot Trail expose medium to coarse grained porphyroclastic granitic mylonite (Figure 2.15a). Anorthosite clasts and lenses (perhaps originally xenoliths in the granite?) are present in the mylonite (Figure 2.15b). The abrupt along-strike discontinuity between mylonite on the Cabot Trail and anorthosite on Red River (Map A, B) implies that a fault that cuts the mylonite and is parallel to diabase dikes that also cut the mylonite (Figure 2.15 c). The late fault is not exposed, but its inferred trace follows a prominent gully and its probable along-strike continuation on Red River is marked by an intense breccia zone. Exposure is poor in the segment of the Wilkie Brook fault zone from North Mountain to the headwaters of Polletts Cove River. However, granitic mylonite foliation planes are steeply dipping with a mean orientation of 087/81 and mineral lineations plunge gently to moderately W or WSW (Map B, stereonet R). The granitic mylonite strikes nearly perpendicular to the overall trend of the fault zone and was probably rotated by the late brittle faulting.

Figure 2.15 - Samples and outcrops of mylonite and other sheared rocks in the Wilkie Brook fault zone along the Cabot Trail.

(a) slabbed hand samples of granitic mylonite from the southern segment of the Wilkie Brook fault zone (BVM91-557, BVM91-568).

(b) sheared anorthosite clast in granitic mylonite exposed along the Cabot Trail.

(c) mafic dikes (offset slightly by late minor faults) that cross-cut granitic mylonite.

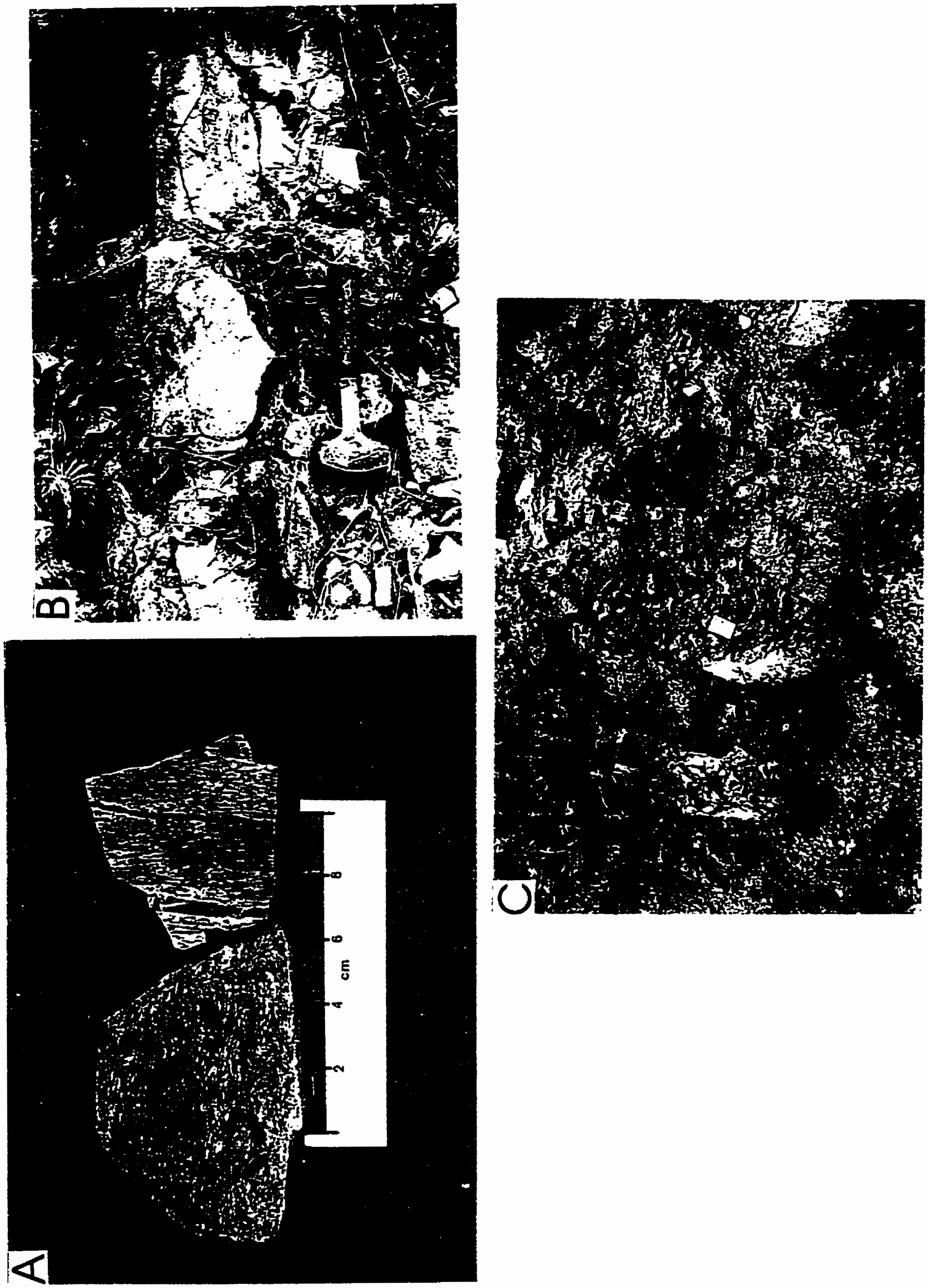

Figure 2.15

At the southernmost tip of the Blair River inlier, where the two bounding faults nearly merge, the Wilkie Brook fault zone trends nearly N-S and is the dominant structure. The fault zone in this area is characterised by lenses and clasts of anorthosite (ranging from several centimetres to tens of meters wide) in mafic schist, phyllonite and deformed granite. The eastern margin of the Margaree Pluton grades through various stages of brecciation and shearing toward the Wilkie Brook fault zone. A distinctive lithology in the southernmost portion of the fault zone is hornblende-biotite gneiss with a fine-grained quartzofeldspathic groundmass and large radiating acicular or bow-tie texture hornblende porphyroblasts (Wunapeera, 1992). The texture is distinctive and, in cross-strike traverses, this rock type marks the first identifiable outcrops of the Aspy terrane. In the more intensely deformed rocks adjacent to the fault zone, hornblende porphyroblasts are synkinematic with respect to shear under amphibolite-facies conditions. In this southernmost portion of the Wilkie Brook fault zone, foliation planes have a mean orientation of 342/77 and mineral lineations have no consistent orientation (Map B, stereonet S).

The orientation of deformational foliations is interpreted to indicate that the Wilkie Brook fault zone is a NNE to N trending, steeply SE dipping structure. Mineral lineation data are highly scattered and are insufficient to allow for interpretation of a vector of movement. Microstructural evidence for the sense of shear is indistinct, but larger scale features, such as the asymmetry of chlorite-schist foliation around anorthosite lenses (Figure 2.15b), the local sense of rotation of foliation in proximity to the shear zone (Map B), and the sense of deflection of the Red River fault zone suggest dextral shear.

By contrast, deformation attributed to shear on the Wilkie Brook fault zone (Raeside, 1989; Wunapeera, 1992) affects rocks in the Aspy terrane in a wide zone (up to 2.5 km) of highly foliated and layered rocks that contain mid- to upper-amphibolite facies metamorphic minerals. These rocks include foliated amphibolite, biotite-hornblende gneiss, pelitic schist and gneiss, quartzofeldspathic gneiss with large acicular hornblende, and granitic mylonite. Foliation planes in this zone strike consistently NE-SW and are nearly vertical (Wunapeera, 1992). Mineral lineations are well developed and plunge NE or SW at low to moderate angles (Wunapeera, 1992). Raeside (1989) interpreted the kinematic data (intrafolial minor folds, asymmetric boudins, and rotated clasts) from the Aspy terrane adjacent to the Wilkie Brook fault zone to indicate transcurrent sinistral movement.

2.3.2 Constraints on the timing of fault zone movement and terrane juxtaposition

Synkinematic hornblende in rocks of the Aspy terrane that were affected by shearing along the Wilkie Brook fault zone yielded $^{40}Ar/^{39}Ar$ ages of ca. 390-380 Ma (this study and Wunapeera, 1992). One pluton from a suite of undeformed granites in the Aspy terrane adjacent to the Wilkie Brook fault zone yielded an $^{40}Ar/^{39}Ar$ age on biotite of 370 ± 5 Ma (Reynolds et al., 1989) and related dikes and small pods of granite intrude the chlorite schist adjacent to the Blair River inlier, but are themseves sheared. The Fisset Brook Formation is assigned to the Late Devonian or early Carboniferous in this area (Smith and Macdonald, 1981). This is the oldest unit that can be correlated across the bounding fault zones, but it does not overstep either fault zone. Both the Wilkie Brook and Red River fault zones are locally overlain by the Horton, Windsor, and Canso groups, the oldest strata of which are Tournaisian in this area (Hamblin and Rust, 1989), but tilting and relatively minor faulting of these units indicate that relatively minor movements continued well into the Carboniferous.

Therefore, amphibolite-facies sinistral shear along the Wilkie Brook fault zone, as it affected the wide band of the Aspy terrane, had ceased and the area had cooled through hornblende closure temperatures (~$450 \pm 50°C$) by ca. 370 Ma. Lower-grade and higher level shear along the Wilkie Brook fault zone continued into the Carboniferous in a narrow zone adjacent to the Blair River inlier, and interleaved units from both sides of the fault zone. The later stage of shear probably represents the final juxtaposition of the Blair River inlier and Aspy terrane at a high structural level in the Late Devonian or Early Carboniferous.

2.4 Summary

The Blair River inlier is here defined as the pre-Devonian units in northernmost Cape Breton Island in the area bounded by the Red River and Wilkie Brook fault zones to the south and east and by Devonian to Carboniferous cover rocks to the north. The map and unit nomenclature of Barr and Raeside (1992) was updated as part of this study. Changes from their mapping include the recognition of the Sailor Brook gneiss and Otter Brook gneiss as separate gneissic units and combination of other undivided gneissic and plutonic rocks into a unit named the Polletts Cove River gneiss. Also newly recognised are the Fox Back Ridge diorite/granodiorite and Sammys Barren granite, which are known or assumed to be mid-Paleozoic in age based on the absence of penetrative deformational fabrics. The Red River Anorthosite Suite consists of a central massive anorthosite unit that grades to the west into leucogabbro, massive gabbro, and layered gabbro. Pyroxenite dikes or layers occur in the layered gabbro unit. A charnockite unit is locally gradational with the layered unit. The Lowland Brook Syenite intruded the Sailor Brook gneiss and is locally undeformed, but most of the body contains a gneissic foliation defined by amphibolite-facies metamorphic mineral assemblages. Minor units include several small anorthosite bodies, gabbroic and rhyolitic dikes, and small occurrences of marble, including the

Meat Cove Marble. The marbles are ubiquitously located in faulted zones between major units. The majority of movement on the Wilkie Brook and Red River fault zones had ceased by the Late Devonian on the basis of correlations of cross-cutting granitic dikes with Late Devonian granites in the Aspy Terrane and on the basis of the age of the overstepping Fisset Brook Formation.

CHAPTER 3 - Geochemistry

3.1 Introduction

Previous geochemical studies of the Blair River inlier have focused on the Red River Anorthosite Suite (Dupuy et al., 1986; Bekkers, 1993), the Lowland Brook Syenite (Deveau, 1988), and the Fisset Brook Formation (Smith and Macdonald, 1981). No systematic attempts have been made to characterise the chemistry of all of the major units, and to describe possible relationships between them and minor units. The primary purpose of this chapter, therefore, is a chemical characterisation of the major gneissic and plutonic units and the minor igneous units in the Blair River inlier.

As part of this study, forty samples were analysed for whole-rock major and trace element concentrations, including representative samples from most of the major and minor units. Additional data are compiled from Mitchell (1979), Smith and Macdonald (1981), Dupuy et al. (1986), Deveau (1988), Bekkers (1993), and unpublished data from S. Barr. Analytical techniques are described and the previously unpublished data are tabulated in Appendix A3.1. Sample locations are shown on Map C.

3.2 Gneissic units

Four samples from the Otter Brook gneiss and eight samples from the Sailor Brook gneiss were analysed in an attempt to define their geochemical character and investigate the nature of their protoliths. Also included are data from Deveau (1988) for two samples that are chemically and lithologically anomalous compared to the remainder of the syenite samples, and are here considered Sailor Brook gneiss. Samples from the main body of the Sailor Brook gneiss include those with modal compositions of tonalite, diorite, quartz monzodiorite, and granodiorite. The two samples from Deveau (1988) have modal compositions of monzogranite. Granoblastic mafic xenoliths in the Lowland Brook Syenite are of quartz diorite and granodiorite compositions. Samples from the Otter Brook gneiss have modal compositions of granodiorite, monzodiorite, and monzogabbro.

Harker variation diagrams for the gneissic units are shown in Figure 3.1. With the exception of the xenoliths, the data from the Sailor Brook gneiss show weakly defined trends, with respect to Al_2O_3, MgO, CaO, K_2O, and P_2O_5. The SiO_2 contents of mafic xenoliths are 47% and 55%, 54-62% in tonalitic and dioritic gneiss, and 61-65% in granodioritic and monzodioritic gneiss. The analyses from the Otter Brook gneiss form a general trend with respect to all elements, with the exception of the monzogabbro sample. The monzogabbro is consistently anomalous compared with the other three samples (e.g., 24% Al_2O_3), but is chemically similar to gabbroic rocks in the Red River Anorthosite Suite. Clusters or trends on Harker diagrams may be used to argue for derivation of a gneissic unit from a differentiated igneous suite (e.g., McLelland and Chiarenzelli, 1990a). However, the sparse data from the Sailor Brook gneiss and Otter Brook gneiss are insufficient to warrant such an interpretation based on major elements.

On plots using elements that are generally considered immobile during metamorphism and alteration (e.g., Ti, Zr, Y, Nb, Ga; Winchester and Floyd, 1976), the tonalite, diorite, and one xenolith from the Sailor Brook gneiss form a broad cluster (Figure 3.2a) that is as tight as many published examples of metamorphosed and altered mafic igneous suites (e.g., <1/2 log unit of scatter; cf., Atkin and Brewer, 1990; Floyd and Winchester, 1977). The three more potassic samples and the other xenolith fall outside of this cluster, and this may indicate that they have unrelated protoliths. Immobile element data from the Otter Brook gneiss samples scatter widely (Figure 3.2a-d) and more analyses are necessary to assess the significance of the data. Immobile elements in combination with other elements and element ratios (Figure 3.2e-g) corroborate, but do

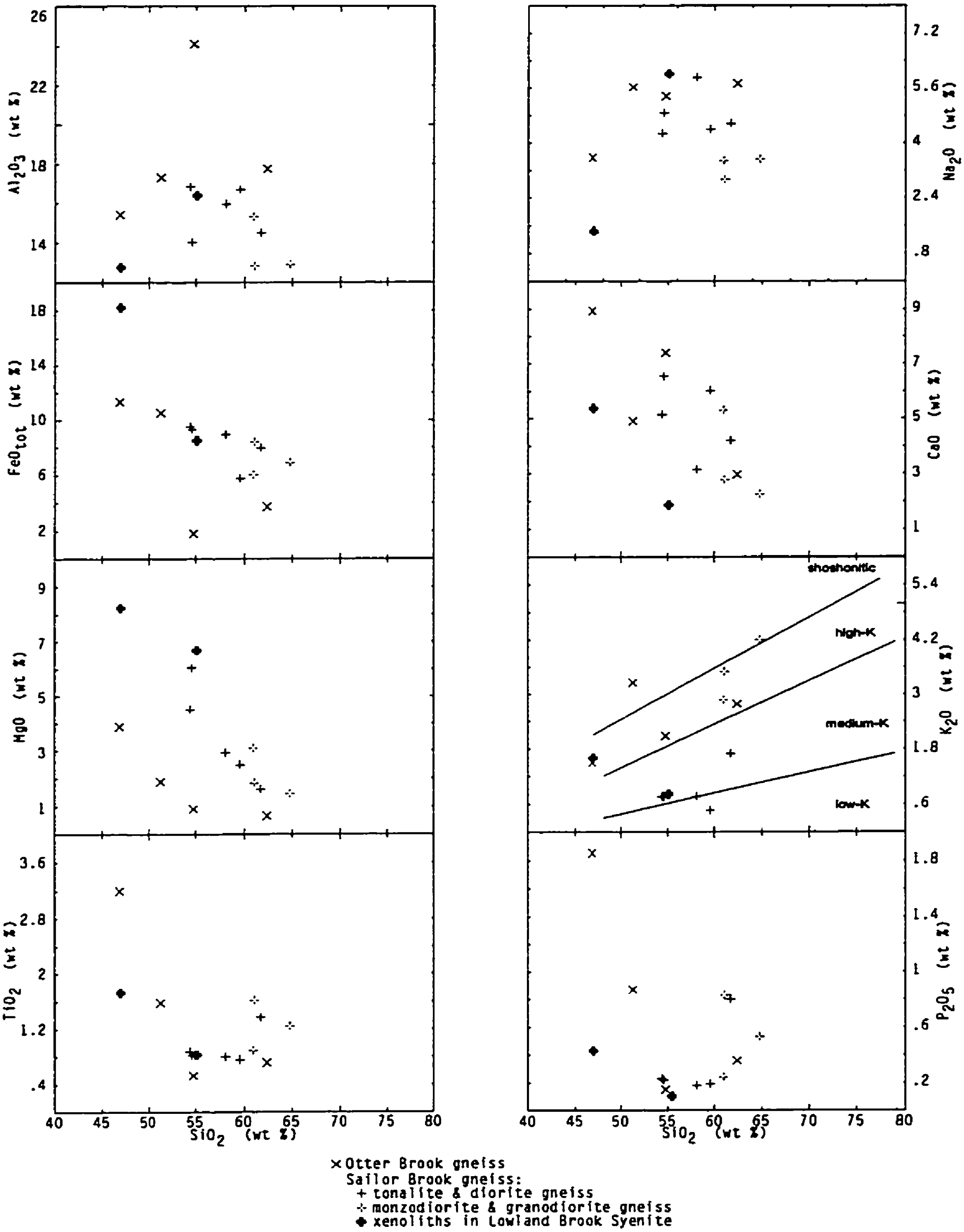

Figure 3.1 - Harker diagrams for major elements from gneissic units. Potassic divisions are after LeMaitre (1989)

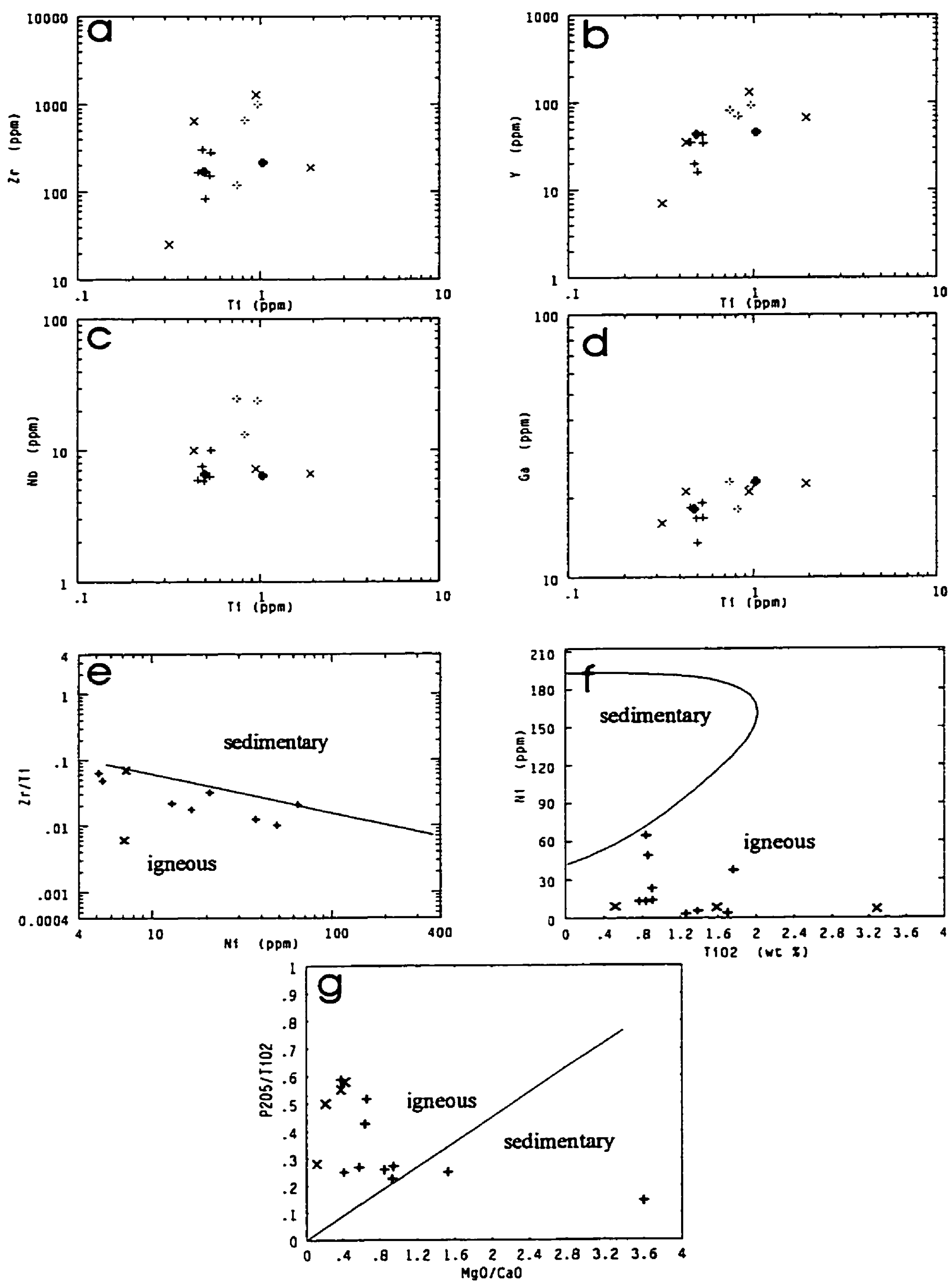

Figure 3.2 - (a-d) Immobile element concentrations in the Sailor Brook gneiss and Otter Brook gneiss. (e-g) Igneous vs. sedimentary geochemical discrimination diagrams for intermediate to felsic gneisses. Diagrams are after Winchester et al. (1980), Leake (1964), and Werner (1987) clockwise from top left. Symbols as in Figure 3.1.

not confirm, the interpretation of an igneous protolith as described in Chapter 2 based on field observations.

3.3 Lowland Brook Syenite

Whole-rock geochemical data from the Lowland Brook Syenite include one new analysis of undeformed massive syenite and thirteen analyses, mostly of gneissic syenite, from Deveau (1988).

On Harker diagrams (Figure 3.3), the Lowland Brook Syenite data form tight clusters or well-defined trends with SiO_2 between 56-62%. The six samples that consistently cluster at the high-SiO_2 end of the trend (e.g., highest K_2O; Figure 3.3) are relatively undeformed massive syenite with low mafic-mineral content, no plagioclase phenocrysts, and little or no titanite. The other samples are typically more mafic, titanite- and calcic plagioclase-bearing, gneissic syenite and that mineralogy is reflected in their higher MgO, FeO_{tot}, TiO_2, CaO, and lower K_2O contents. The Lowland Brook body is alkaline (Figure 3.4a), shoshonitic with K_2O above 3.6% and with K_20/Na_2O between 0.7-1.4. Al_20_3 contents are 16-18% and most samples are metaluminous (Figure 3.4b). Variation diagrams for selected trace elements are shown in Figure 3.4c-f. The syenite contains relatively high concentrations of Ti, Y, and Ga, and low concentrations of Nb (<30 ppm). On plots of important indicators of differentiation and fractionation, for example Zr vs. Ti (Figure 3.4c), the Lowland Brook Syenite data define an incompatible-element enrichment trend.

Foley et al. (1987) divided potassium-rich igneous rocks into three groups with distinct petrogeneses and implications for tectonic settings. Group I is composed mostly of mafic (44-55% SiO_2) lamproites (K_20/Na_2O>5) in stabilised orogenic areas following subduction-related

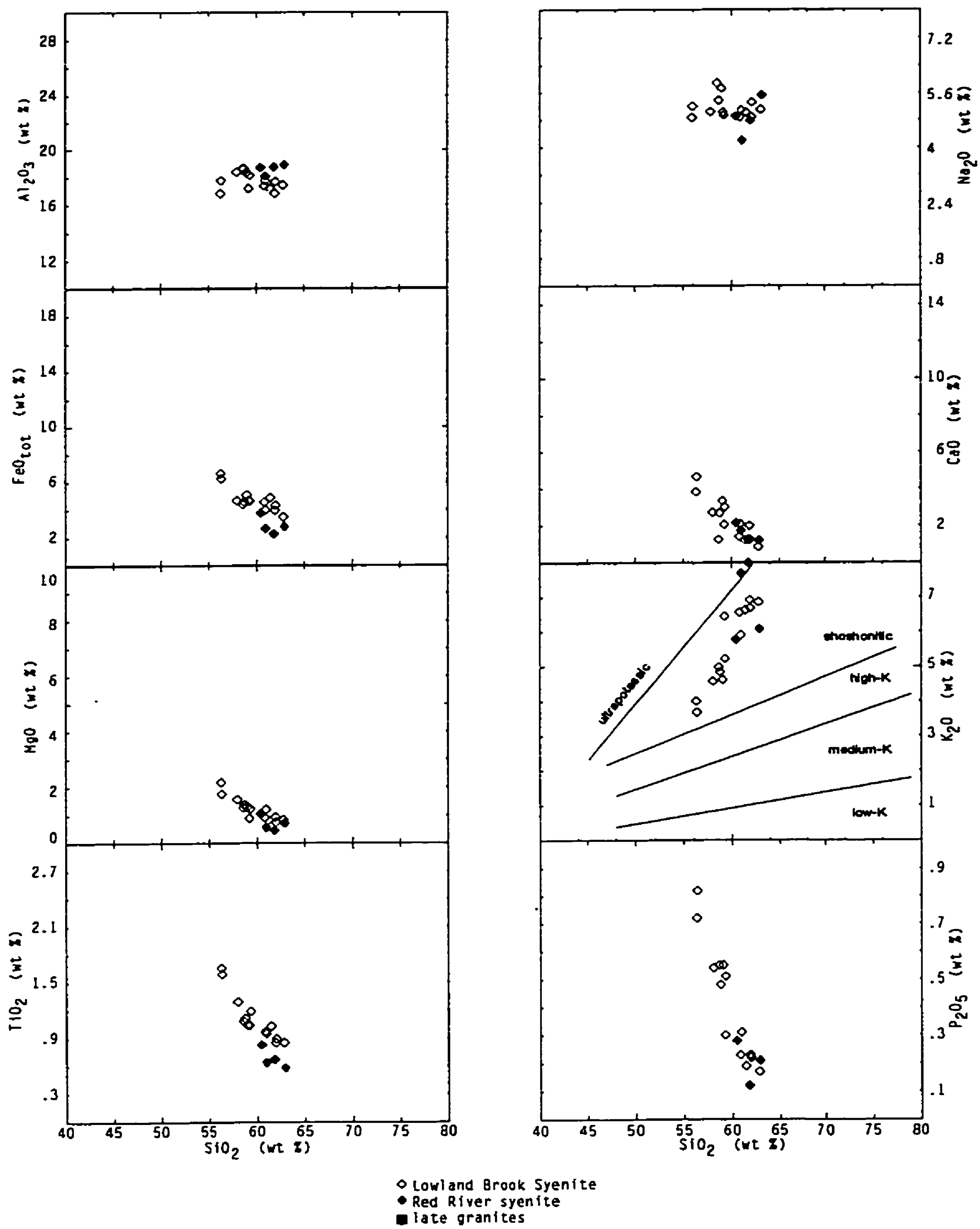

Figure 3.3 - Harker diagrams for major elements from the Lowland Brook and Red Ravine syenite bodies. Potassic divisions are after LeMaitre (1989) and Peccerillo and Taylor (1976).

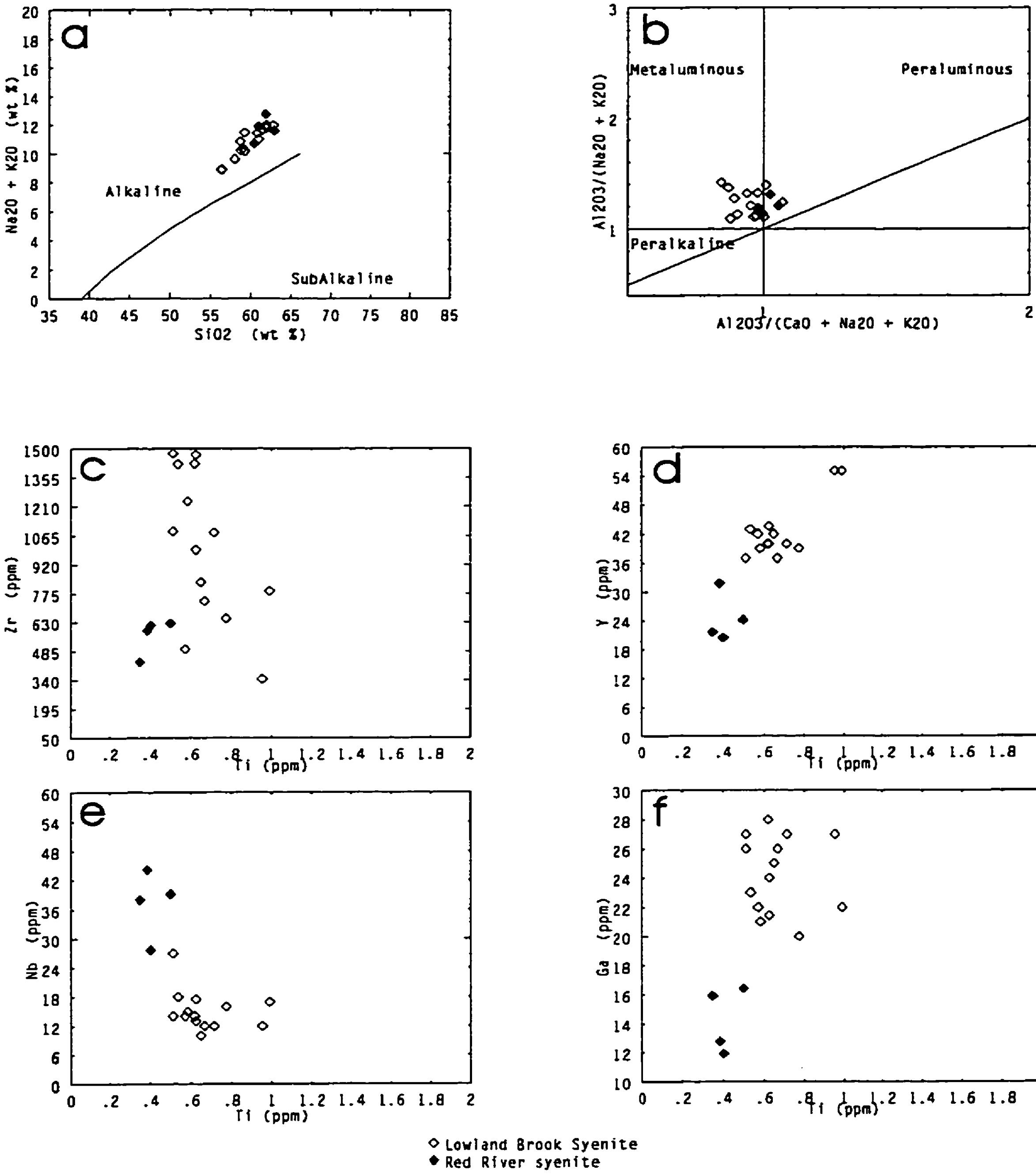

Figure 3.4 - Selected major and trace element variation diagrams for syenite bodies. (a-b) Alkaline vs. subalkaline and aluminum saturation classification diagrams of Maniar & Piccoli (1989), (c-f) selected trace element plots.

magmatism and Group II includes ultrapotassic mafic rocks of continental rift zones (Wilson, 1989). By contrast, Group III contains a wider variety of rock types, including more felsic (trachy-basalt to trachyte and intrusive equivalents) varieties associated with active subduction-related, orogenic zones. Low-pressure fractional crystallisation and crustal contamination in Group III help to produce the characteristically more silica-rich magmas and the extreme enrichments in incompatible elements. This group is also characteristically high in Al_2O_3 (>11%) compared to other K-rich igneous suites. Consistently low Nb (<50 ppm) concentrations over a wide range of Zr concentrations (100-1100 ppm) are typical of Group III K-rich magmatism and are distinct from the higher Nb (>100 ppm) concentrations of intraplate potassic plutonism (Thompson and Fowler, 1986). The Lowland Brook Syenite shows all of these characteristics and is here classified as a Group III shoshonitic pluton.

Corriveau and Gorton (1993) recognised a belt of Group III, ultrapotassic, potassic alkaline, and shoshonitic igneous suites that were emplaced into the Central Metasedimentary Belt of the Grenville Province between 1074 and 1089 Ma. The magmatic belt consists of two suites, a felsic, critically silica-saturated (quartz to slightly nepheline normative) shoshonitic suite and a felsic to ultramafic, silica-undersaturated potassic to ultrapotassic suite. The Kensington, Cameron, and Loranger plutons of the Mont-Laurier area of Quebec typify the shoshonitic suite (Corriveau and Gorton, 1993). The shoshonitic suite contains very little magmatic biotite with amphibole or clinopyroxene being the dominant Fe-Mg silicate mineral. The suite is alkaline, with K_2O/Na_2O between 0.8 and 1.2, has high Al_2O_3 (16-19%), and low (13-51 ppm) Nb concentrations. These were considered to be plutons related to subduction in a Middle Proterozoic island arc by Corriveau (1990). Associated mafic suites in the Central Metasedimentary Belt are thought to be related to subduction at an active continental margin (Pehrsson et al., 1996), and this interpretation is consistent with the chemistry (e.g., Thompson and Fowler, 1986; Foley et al., 1987; Wilson, 1989) of the Grenvillian syenites and the Lowland Brook Syenite. The shoshonitic, critically silica-saturated plutons in the Central Metasedimentary Belt are strikingly similar in age, size, rock type, mineralogy, mineral textures, and geochemical characteristics to the Lowland Brook Syenite.

3.4 Anorthosite and charnockite

Whole-rock geochemical data from subunits of the Red River Anorthosite Suite, several of the smaller anorthosite bodies and charnockitic rocks are compiled from Mitchell (1979), Smith and Macdonald (1981), Dupuy et al. (1986), Bekkers (1993), and unpublished data from S. Barr. The data are grouped into the lithological subunits defined in Chapter 2: massive anorthosite, leucogabbro, layered rocks, and pyroxenite. Highly altered samples of massive anorthosite and leucogabbro as well as quartz-rich (metasomatised?) "white rock" are separated as sub-types. In the field, the lithologic sequence in the Red River Anorthosite Suite is a gradation outward from the centre of the body from massive anorthosite into leucogabbro and gabbro, and layered rocks. Pyroxenite dikes intruded the layered rocks. The charnockite occurs around the periphery of the anorthosite suite.

The lithologic sequence recognised in the field is also evident in trends defined by major-element geochemistry. Fractionation trends of anorthosite suites typically show decreasing SiO_2, opposite to normal fractionation trends including those of charnockitic suites (Buddington, 1972; Ashwal, 1978). The disparate trends are apparent on the Harker diagrams (Figure 3.5) and are most pronounced with respect to Al_2O_3 concentrations. Anorthosite samples have the highest Al_2O_3 (27-29%) and the concentration decreases through leucogabbro, layered rocks and

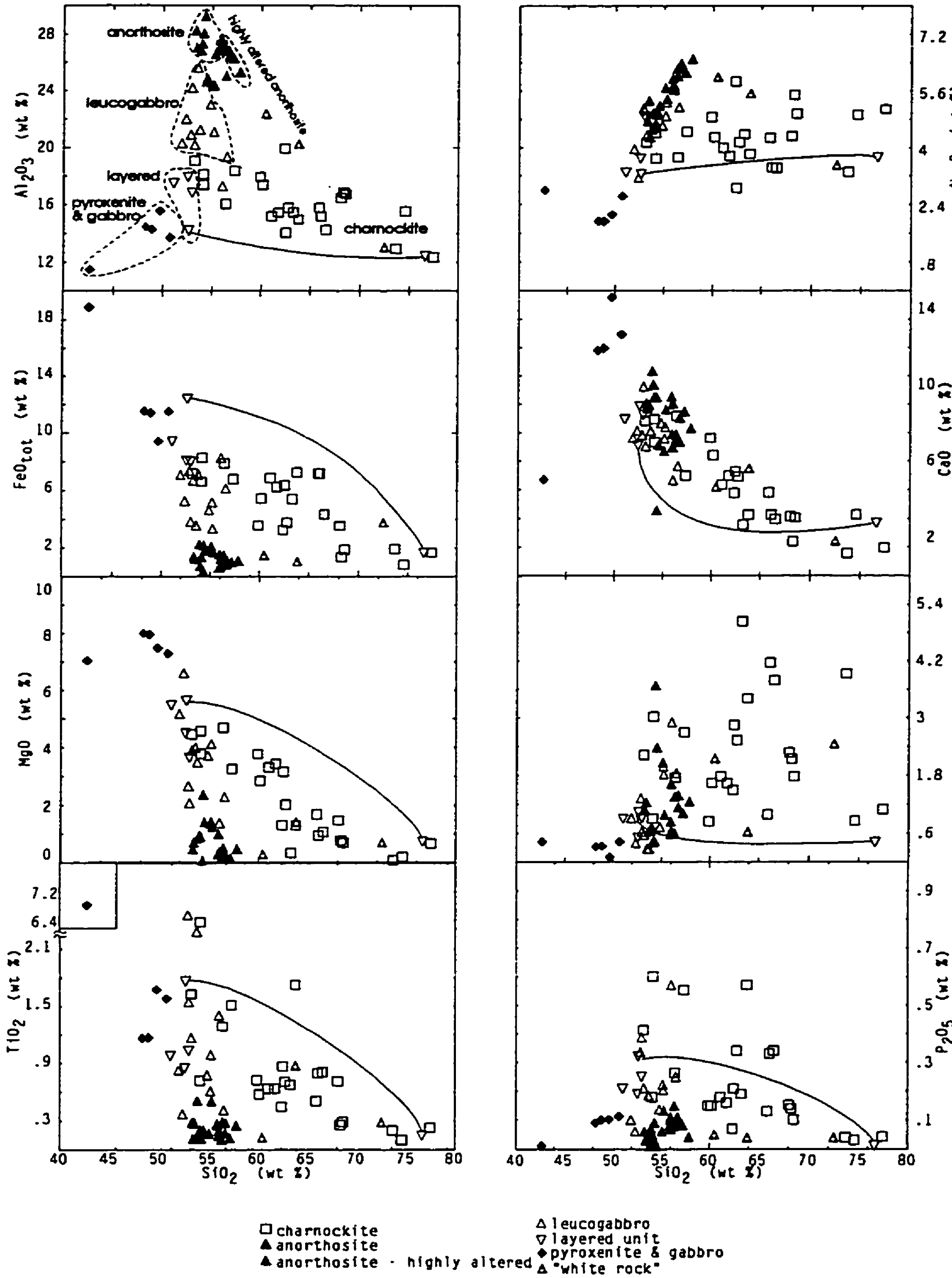

Figure 3.5 - Harker diagrams for major elements from the Red River Anorthosite Suite, charnockite, and "white rock". The separate analyses from mafic (low SiO_2) and felsic (high SiO_2) bands in the layered unit are connected by the solid line.

pyroxenite. A small gap in the trend occurs between the leucogabbro and the layered rocks, and the low-SiO_2 part of the charnockite trend falls into the gap (Figure 3.5). The decreasing Al_2O_3 trend occurs at fairly constant, or slightly decreasing, SiO_2 contents from the anorthosite to the layered rocks but an abrupt change of trend occurs in the pyroxenite samples. Similar, though less clearly defined, gradational relationships and trends are distinguishable in plots of the other major elements as well.

With increasing degree of alteration, Al_2O_3 in the anorthosite decreases slightly and SiO_2 increases slightly. The highly altered anorthosite samples are higher in Na_2O and K_2O and lower in CaO compared to the relatively fresh massive anorthosite. The "white rock" samples and a quartz-rich felsic layer separated from the layered unit form a diagonal trend from Al_2O_3 and SiO_2 concentrations comparable to the anorthosite samples to low Al_2O_3 and high SiO_2 comparable to the most siliceous charnockite samples. The trend of slightly higher Al_2O_3 and slightly lower SiO_2 concentrations also occurs in a highly altered leucogabbro sample that is displaced from the main cluster (Figure 3.5). The mafic and felsic layers from the layered unit that were analysed separately are joined with the solid line in Figure 3.5 (the mafic layer is the low-SiO_2 analysis). The mafic layer is higher in FeO_{tot}, MgO, TiO_2, and CaO, as reflected in the higher mafic mineral content but there is little difference in Al_2O_3, Na_2O, and K_2O.

Data from charnockite samples span a wide range in SiO_2 (54-74%), but form fairly tight trends on some Harker diagrams (Figure 3.5). On most diagrams the trend begins with the more mafic samples (lowest SiO_2) at values between the leucogabbro and layered unit. If this is a fractionation or differentiation trend, then the charnockitic rocks were derived from a magma with a major-element composition intermediate between the leucogabbro and the bulk layered unit, although the low-SiO_2 part of the trend may be blurred due to "smearing" of the contact during metamorphism or due to contamination of the charnockite by the anorthosite during emplacement.

In terms of their chemical constituents, the anorthosite data plot in the tonalite field on an An-Ab-Or diagram and in the gabbro (anorthosite) field on the QAP diagram (Figure 3.6). The highly altered samples are offset slightly toward the sodic and alkali apices, respectively. The trend toward less-calcic anorthosite compositions is consistent with the observed decrease in An content in the highly altered samples. Leucogabbro data plot in the monzogabbro, gabbro (anorthosite), and quartz diorite fields. Whole-rock samples of the layered unit plot in the gabbro (anorthosite) and quartz diorite fields. The felsic layer separated from the layered unit plots above the tonalite field and a mafic layer from the same sample is indistinguishable from the leucogabbro, despite an abundance of modal quartz associated with retrograded pyroxenes (Chapter 2 and Figure 3.6). Pyroxenite samples do not plot accurately on these diagrams due to their low SiO_2, Na_2O, and K_2O and high CaO contents. Data from charnockite samples scatter widely on nomenclature diagrams and include (charnockitic terms in parentheses) monzodiorite and quartz monzonite (mangerite), quartz diorite (norite), tonalite (enderbite), granodiorite (opdalite), and monzogranite or granite (charnockite).

The anorthosite and related rocks also have trend-forming relationships in terms of their trace elements, but the most informative is a plot of Sr vs. Zr (Figure 3.7a). Strontium is generally concentrated in anorthosite (600-1000 ppm) due to the abundance of calcic plagioclase but

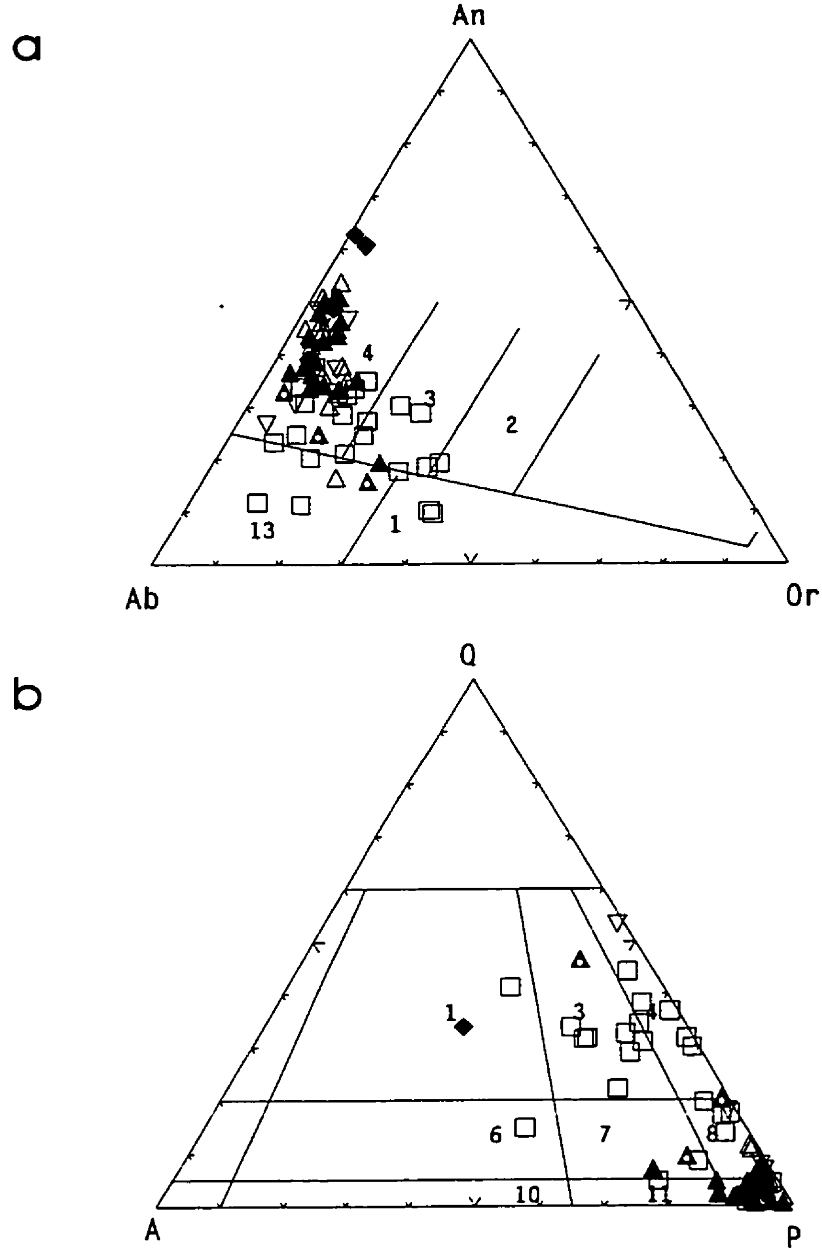

1 : granite
3 : granodiorite
4 : tonalite
6 : quartz monzonite
7 : quartz monzodiorite
8 : quartz diorite
10 : monzonite (monzodiorite)
11 : monzogabbro
12 : gabbro (diorite, anorthosite)
13 :

Figure 3.6 - Geochemical nomenclature diagrams for the Red River Anorthosite Suite, charnockite, and "white rock". (a) An-Ab-Or diagram, (b) QAP diagram after LeMaitre (1989). Symbols as in Figure 3.5.

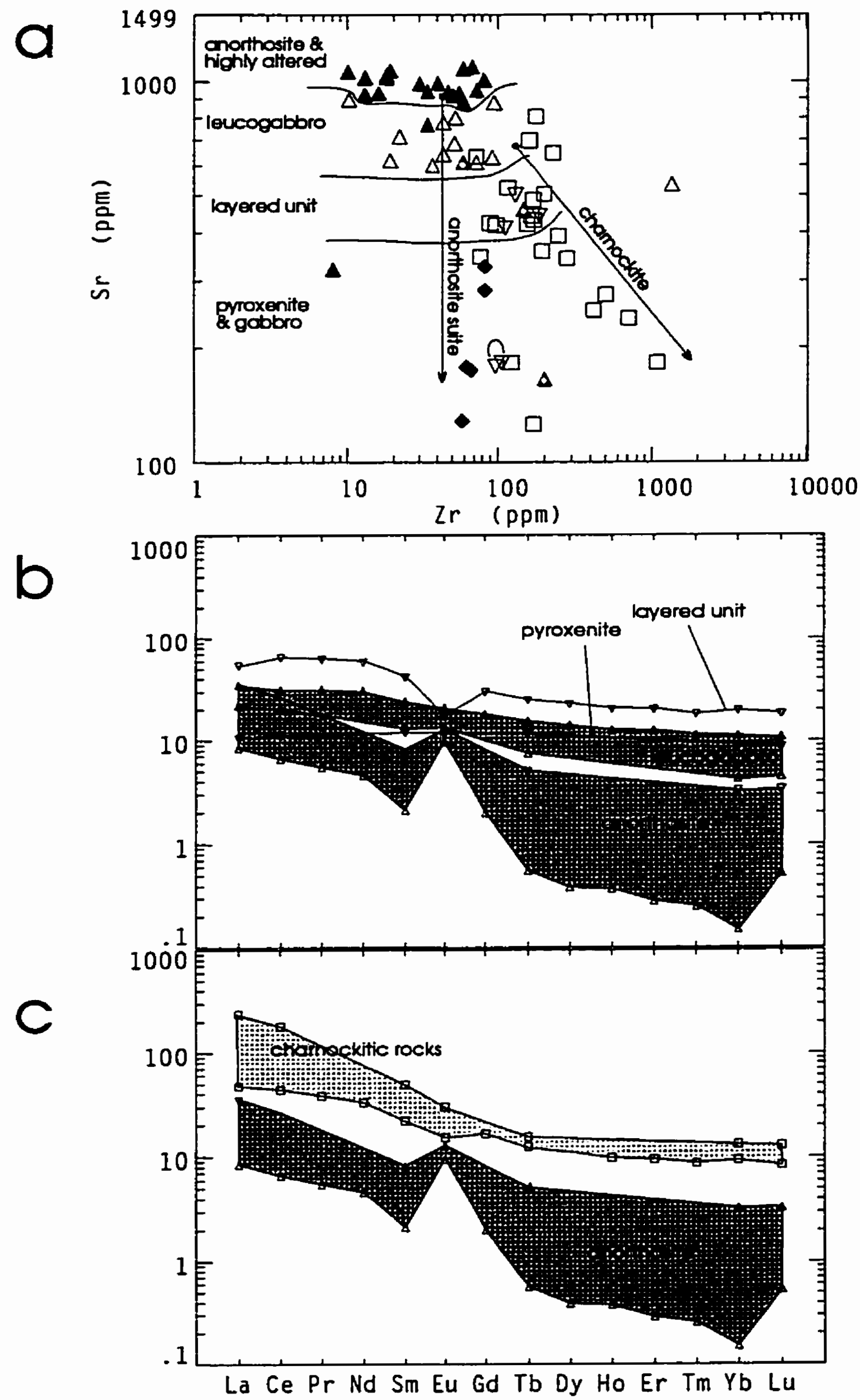

Figure 3.7 - (a) selected trace element concentrations showing differing fractionation trends between the anorthosite suite and charnockite. (b,c) chondrite-normalised REE diagrams for the Red River Anorthosite Suite, related rocks, and charnockite.

incompatible elements, for example Zr, are depleted in all lithologies of the anorthosite suite (e.g., Emslie, 1985; Ashwal, 1993). A plot of Sr vs. Zr, therefore, shows the involvement of plagioclase fractionation over the course of crystallisation (with Zr as a differentiation index). In the Red River Anorthosite Suite, Sr decreases progressively from anorthosite to pyroxenite and gabbro, at low (10-37 ppm) Zr concentrations with the exception of the layered unit (Figure 3.7a). The layered unit has higher Zr and overlaps with the beginning of the charnockite trend which may indicate contamination by charnockite. The charnockite samples, however, show a Zr-enrichment trend (100-1100 ppm). The separated mafic and felsic layers from the layered unit have nearly identical Sr and Zr concentrations and these are more similar to the concentrations in pyroxenite and gabbro samples than in the bulk samples of the layered unit.

Rare earth element (REE) profiles (Figure 3.7b) show that anorthosite samples have light REE enrichment, a moderate to highly negative slope, and large positive Eu anomaly, which are typical indicators of high degrees of plagioclase fractionation and are common characteristics of massif-type anorthosite (Ashwal, 1993). Leucogabbro samples have higher REE concentrations, and a flatter, but still slightly negative slope and no Eu anomaly. The one analysed layered sample is further enriched but with a slight depletion of light REE and a negative Eu anomaly. One sample of pyroxenite has a flat REE pattern with no Eu anomaly. Charnockite samples have the highest light REE enrichment of all units, flat heavy REE, and no, or a very small negative, Eu anomaly (Figure 3.7c). Some evidence for contamination of the charnockite may be present in the sample with the lowest REE concentrations; the data show a similar pattern and concentration as in the layered unit but with a smaller negative Eu anomaly.

Because anorthosite is almost entirely plagioclase, the An-Ab join on Figure 3.6a approximates the bulk plagioclase composition of the sample. This may be a better measure of bulk plagioclase composition for the anorthosite than individual plagioclase analyses because of variable An contents in zoned grains and in different textural types of plagioclase (see Chapter 2). Furthermore, in some highly altered samples, it is impossible to determine plagioclase compositions optically. Table 3.1 compares the bulk-rock plagioclase composition to that of individual plagioclase grains. In general, the optical and microprobe analyses are close to the bulk-rock An content, except in samples with more than one composition of plagioclase where estimating the bulk plagioclase composition is complicated by the widely varying plagioclase compositions and by highly zoned plagioclase grains. The bulk-rock plagioclase composition is highest in the massive anorthosite and is mostly calcic andesine but approaches labradorite (An_{42-50}). An content decreases in the highly altered rocks, including the High Capes sample, to $An_{\sim 35}$ (andesine) and as low as An_{16} (oligoclase) in the "white rock" (although the latter values may be low due to significant modal quartz).

The Red River Anorthosite Suite comprises rock types that show a progression, both lithologically and geochemically, from massive anorthosite, to leucogabbro, to layered rocks and ending with pyroxenites and massive gabbro. Charnockitic rocks partly envelop the anorthosite suite and these show a geochemical progression from monzogabbro (mangerite and jotunite) to tonalite (enderbite) and granodiorite (opdalite). Both the anorthosite and charnockite suites show typical (for their respective rock types) fractionation trends on appropriate geochemical diagrams and the lowest-silica portions of the charnockitic unit have compositions intermediate between or overlapping with the leucogabbro and layered unit of the anorthosite suite.

The chemical composition of the highly altered samples does not appear to have been

Table 3.1 - Bulk-rock An content of anorthosite as determined from An-Ab-Or diagram compared to plagioclase compositions determined optically or by microprobe analysis

Sample#	Rock Type	Bulk An	Plag[1]	Plag[2]	Plag[3]
SB85-1070	DB-an	51	50		
BVM91-584	RRAS-an	49	55	49-57	78-88
RB91-076	RRAS-an	48	50		
RB91-063	RRAS-an	46	42		
RR85-2092	RRAS-an	42	45		
BVM90-067	RRAS-an	38	45	50	
RB91-025	RRAS-ha	37	nd		
SB85-1097	HC-an	35	38		
CW86-3721	RRAS-ha	34	nd		
RB91-060	RRAS-ha	34	nd		
RR85-2138	RRAS-ha	34	nd		
RB91-057	wht rx	33	29	36	
SB85-1113	RRAS-ha	32	nd		
BVM91-774	RRAS-lay	26	29-32		
RR85-2130	wht rx	24	28		
CW85-136	SR-an	19	22		
SB86-3136	wht rx	16	25		

Abbreviations: DB - Delaneys Brook anorthosite, RRAS - Red River Anorthosite Suite, HC - High Capes anorthosite, SR - Salmon River anorthosite, an - anorthosite, ha - highly altered, lay - layered unit, wht rx - "white rock", nd - not determined. Plag columns are the compositions of different textural types of plagioclase in the same sample; 1 - average of microprobe analyses, 2 - composition of centres of large plagioclase grains, 3 - composition of plagioclase in metamorphic reaction zones.

affected greatly by alteration except for an increase in SiO_2 and accompanying decrease in Al_2O_3 and CaO. Geochemical data from "white rock" samples (including the silica-rich felsic layer) from trends opposite to the fractionation trends of the anorthosite suite, but which are continuations of the trends defined by highly altered anorthosite samples. With the exception of significantly decreased Sr concentrations, trace elements in white rock samples are broadly comparable to those in the anorthosite samples. Concentrations of Ba, Sr, and Zr in the silica-rich felsic layer from the layered unit are nearly identical to those in the mafic layer (Figure 3.7a), but concentrations of Cr, Ni, Cu, and Zn are lower (Bekkers, 1993). During metamorphism and alteration, Ba and Sr are typically considered mobile elements and Zr is an indicator of magma differentiation; Cr, Ni, Cu, and Zn are indicators of mafic-mineral fractionation during magma crystallisation. The lower values of Cr, Ni, Cu, and Zn are consistent with a cumulate layered origin, but the Sr and Ba concentrations are not, and would seem to require secondary (metamorphic) processes, as first suggested by Dupuy et al. (1986). Because they have an affinity for feldspars, Sr and Ba are expected to be higher in the felsic layer than the mafic layer, if the layering were solely of igneous origin. These relations help to support the inferences, based on field and petrographic observations (Chapter 2), that the "white rock" samples are relatively enriched in SiO_2 (or depleted in other major elements) and that the origin of the layering in the layered unit is a combination of cumulate and metamorphic/deformational processes. However, the details of the processes responsible are as yet unclear.

REE patterns and abundance are consistent with plagioclase accumulation in anorthosite samples and fractionation from layered unit samples. Leucogabbro samples have REE concentrations intermediate between the two and Ashwal (1993) attributed this typical feature of massif anorthosite complexes to progressive crystallisation from anorthosite to leucogabbro and leuconorite with "varying" (presumably meaning increasing) amounts of trapped residual liquid. The pyroxenite has a REE pattern and concentrations similar to MORB at 10x chondrite. The charnockite samples lack a significant negative Eu anomaly and therefore do not appear to be derived from residual liquids at the end of the anorthosite suite fractional crystallisation. The lack of these complimentary REE features is typical of charnockite suites associated with massif-type anorthosite (e.g., Ashwal and Seifert, 1980).

Based on REE modelling Mitchell (1979) concluded that the anorthosite parent magma was probably a tholeiitic basalt. This is in agreement with Owens et al. (1993) who determined that andesine-type anorthosite suites are derived from fractionation of a dioritic parent magma and labradorite-type suites from a basaltic parent magma. Dupuy et al. (1986) considered texture, mineralogy, major-element concentrations (high Al_2O_3, Sr, CaO/Na_2O, Na_2O/K_2O, and Sr/Ba), low REE abundance and chondrite-normalised REE patterns (LREE enrichment, large positive Eu anomaly) as indicative of plagioclase accumulation and effective expulsion of intercumulus liquid. Their trace-element modelling also showed that the anorthosite, leuconorite, and pyroxenite could have been derived from similar, or the same, basaltic parent magma and that the inferred parent magma characteristics (pg. 145), "resemble the composition of parental magmas of several large anorthositic massifs in the Grenville and Nain provinces." Dupuy et al. (1986) also note (pg. 146) that, "the lack of associated mangerites and voluminous granulite facies country rocks indicates that they were probably higher level intrusions than those of the Grenville Province which represent lower crust." Both granulite-facies gneisses (probably, but nowhere demonstrably, country rock) and charnockitic rocks associated with the anorthosite suite are now recognised in the Blair River inlier. Therefore, any implications of significant contrasts between the Red River Anorthosite

Suite and Proterozoic massif-type anorthosites are unfounded, at least in terms of the grounds described by Dupuy et al. (1986).

3.5 Fox Back Ridge diorite/granodiorite

Only two samples from the Fox Back Ridge diorite/granodiorite were analysed for whole-rock geochemistry. They contain 52% and 57% SiO_2 (Figure 3.8), and plot as subalkalic basalt and andesite on a diagram of SiO_2 vs. Zr/TiO_2 (Figure 3.9a). They plot on both sides of the alkaline/subalkaline and tholeiite/calc-alkaline boundary lines on alkali-silica and FeO/MgO-SiO_2 diagrams (Figure 3.9b,c). On a tectonic setting discrimination diagram for mafic rocks (Figure 3.9d), they plot toward the bottom of the within-plate field.

3.6 Sammys Barren granite and other undeformed granite

Four samples of undeformed granite were analysed, including one sample from the Sammys Barren granite and three samples from small bodies or dikes in the undivided unit, the Otter Brook gneiss and the Sailor Brook gneiss. The latter three samples are medium- to coarse-grained, undeformed and petrographically similar to the Sammys Barren granite. Harker diagrams (Figure 3.8) show a slight range in Al_2O_3, Na_2O, and K_2O, which corresponds to their proportion of plagioclase vs. K-feldspar (e.g., the lowest K sample has high-Ca and Na and has higher modal plagioclase which is mostly albite). The samples are subalkaline and peraluminous (Figure 3.9b,d) and plot in, or near, the volcanic-arc granite field on a Rb vs. Y+Nb diagram (Figure 3.9f). The major and trace-element characteristics are distinct from larger potassic plutons like the Lowland Brook and Red Ravine syenite bodies (Figure 3.3 and 3.4).

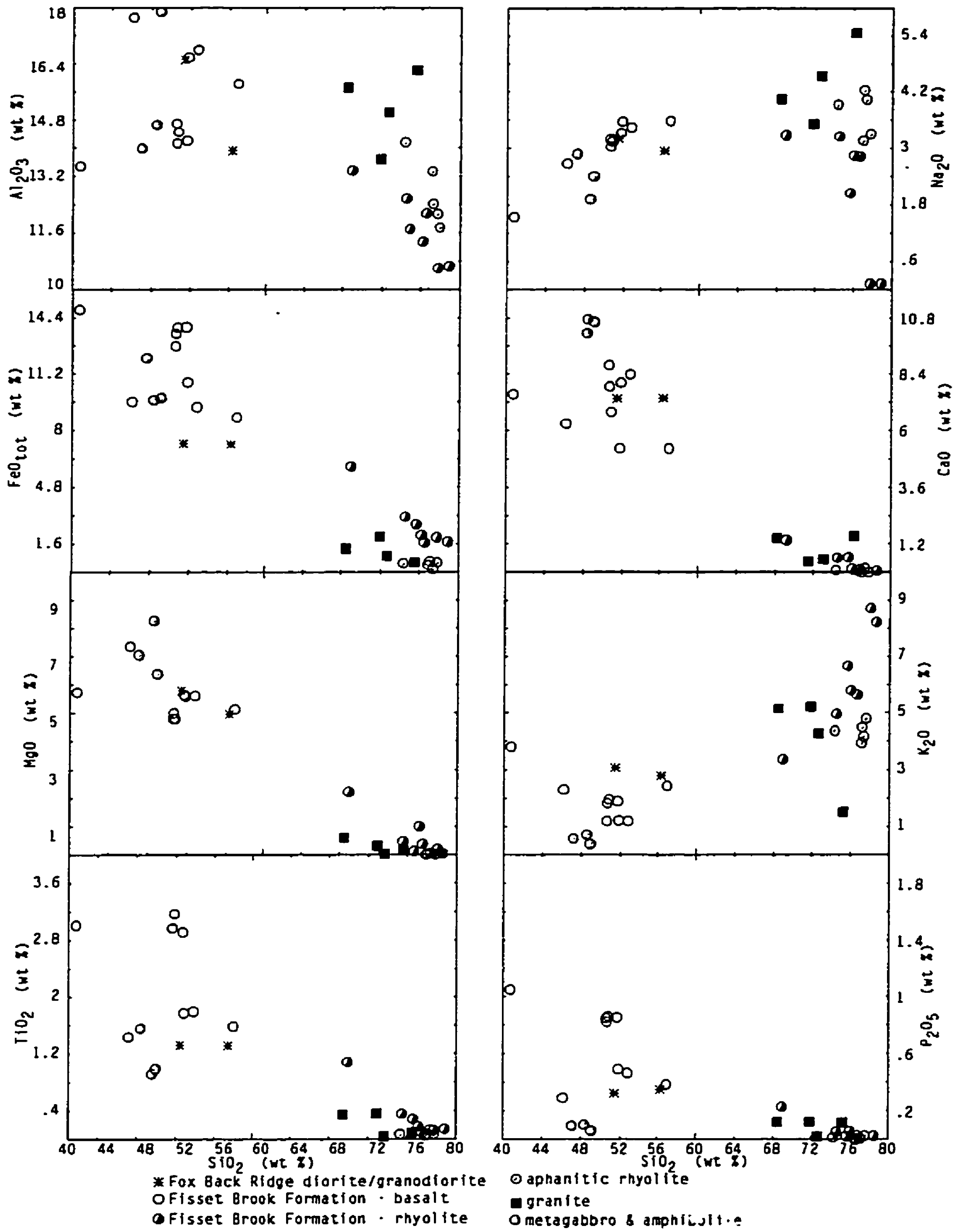

Figure 3.8 - Harker diagrams for the minor igneous units in the Blair River inlier.

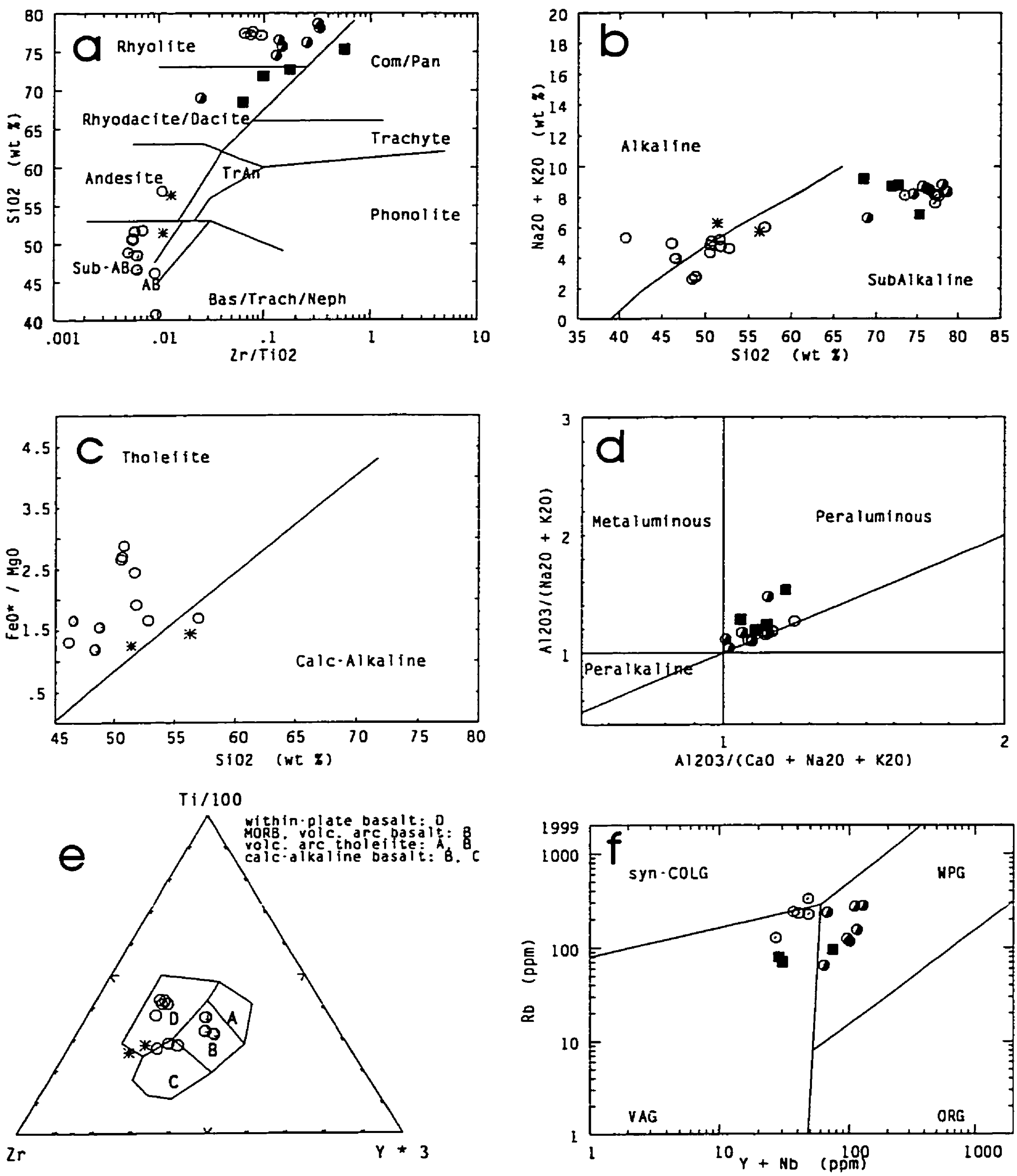

Figure 3.9 - (a) immobile element classification diagram of Winchester and Floyd (1977), (b) alkalinity diagram of Irvine and Baragar, 1971), (c) tholeiitic vs. calc-alkaline plot for mafic rocks (dividing line after Miyashiro, 1974), (d) ternary tectonic discrimination diagram for mafic rocks (Pearce and Cann, 1973), (e) tectonic discrimination diagram for felsic rocks (Pearce et al., 1984). Symbols as in Figure 3.9.

3.7 Red Ravine syenite

As noted in Chapter 2, the Red Ravine syenite has some distinctive petrographic features similar to those in the Sammys Barren granite and these features contrast with those of the Lowland Brook Syenite. For example, both the Red Ravine syenite and the Sammys Barren granite are undeformed, contain non-perthitic microcline, have separate subhedral plagioclase grains, large euhedral yellow titanite, medium-sized, sharply prismatic, zircon grains. In contrast the Lowland Brook Syenite is commonly gneissic, contains coarse perthite and antiperthite, anhedral titanite or titanite rims around opaque minerals, and zircon grains are resorbed at their corners and tips.

On Harker diagrams, the Red Ravine syenite data plot at the high end of the SiO_2 range (61-63%) and along the same trends as the Lowland Brook Syenite data (Figure 3.3). Like the Lowland Brook Syenite, the Red Ravine syenite is shoshonitic, with K_2O above 3.6%. Two of the Red Ravine syenite samples have high K_2O at ~8% and plot just into the ultrapotassic field. However, the syenite body is not ultrapotassic (e.g., $K_20/Na_2O > 2.0$ and $MgO > 3\%$) according to the definition of Foley et al. (1987) with K_20/Na_2O values of 1.1-1.8 and $MgO < 3\%$. Also like the Lowland Brook Syenite, the Red River body is alkaline, but straddles the boundary between metaluminous and peraluminous fields (Figure 3.4a,b).

In terms of major-element geochemistry, the Red Ravine syenite is indistinguishable from the SiO_2-rich portions of the Lowland Brook Syenite. However, chemical distinction between the Red Ravine syenite and the Lowland Brook Syenite is more apparent in their trace element concentrations, especially in incompatible elements like Ti, Zr, Nb, and Y (Figure 3.4c-f). The Red Ravine syenite contains lower concentrations of Ti, Y, and Ga, and distinctly higher concentrations of Nb (<30 ppm) compared to the Lowland Brook Syenite. On plots involving important indicators of differentiation and fractionation, for example Zr vs. Ti, the Red Ravine syenite data clearly plot off the enrichment trend defined by the Lowland Brook Syenite. These data suggest different magma sources and different fractional crystallisation processes for the two bodies.

Similar Paleozoic-age syenite bodies are known from other Proterozoic terranes. For example, in the Scottish Caledonides, ca. 456-415 Ma syenite plutons intruded through Grenville-age basement and have the characteristics of Group III subduction-related plutons at active continental margins (Thompson and Fowler, 1986). Therefore, there is a precedent for considering the undeformed syenite to be unrelated to the Proterozoic magmatic event that resulted in intrusion of the Lowland Brook Syenite.

3.8 Fisset Brook Formation, mafic and felsic dikes, and small gabbro bodies

Dikes and small bodies in the Blair River inlier include deformed and metamorphosed gabbro and amphibolite, aphanitic rhyolite that is deformed only in the boundary fault zones, and relatively undeformed mafic and felsic rocks of the Fisset Brook Formation. Geochemical data from the Fisset Brook Formation in the area of Lowland Cove are from Smith and Macdonald (1981) and are combined with several new analyses of brown porphyritic, Fisset Brook-type rhyolite dikes from several other areas on the margins of the Blair River inlier.

On Harker variation diagrams (Figure 3.8), the aphanitic rhyolite samples have higher Al_2O_3 and Na_2O contents and lower concentrations of other major elements compared to felsic rocks in the Fisset Brook Formation. Major element data from samples of Sammys Barren and other granites lie along the same general trend as those of aphanitic rhyolite. On the SiO_2 vs. Zr/TiO_2 nomenclature diagram, both the aphanitic and Fisset Brook felsic rocks plot as rhyolite (Figure 3.9a). Both are subalkaline and peraluminous (Figure 3.9b,d), but the aphanitic rhyolite samples and two granite samples plot near the apex of the volcanic-arc granite field whereas the Fisset Brook Formation and one the Sammys Barren granite samples plot in the within-plate field (Figure 3.9f).

The data from the mafic rocks scatter widely on Harker diagrams (Figure 3.8). The mafic rocks from the Fisset Brook Formation are slightly alkaline and transitional to tholeiitic subalkalic basalt (Figure 3.9b,c and Smith and Macdonald, 1983). The bimodal nature of the Fisset Brook Formation is clear on Harker variation diagrams (Figure 3.8) and on a trace-element classification diagram (Figure 3.9a). The aphanitic rhyolite and metagabbro and amphibolite have bimodal chemical characteristics comparable to those of the Fisset Brook Formation. However, the metagabbro, amphibolite, and aphanitic rhyolite are chemically distinct from the Paleozoic bimodal volcanic activity represented by the Fisset Brook Formation. The distinction lies mainly in their diagnostic trace-element characteristics. As plotted on standard tectonic discrimination diagrams, most of the Fisset Brook Formation data plot in within-plate fields; however the metagabbro samples, the aphanitic rhyolite, and three of the granite samples plot in volcanic-arc fields (Figure 3.9e,f).

3.9 Summary

Immobile-element geochemical characteristics of the Sailor Brook gneiss and Otter Brook gneiss are consistent with the interpretation that both units have igneous protoliths. The Lowland Brook Syenite is an alkaline shoshonite with high concentrations of Ti, Y, and Ga, and low concentrations of Nb. These characteristics are typical of the Group III potassic suite, which Foley et al. (1987) considered to be related to active subduction-related orogenic zones. Similar Group III syenite bodies occur in the Elzevir Terrane of the Central Metasedimentary Belt in the Grenville Province and are thought to be related to an island arc (Corriveau, 1990) or a continental-margin arc (Pehrsson, 1996). The petrographic distinction (lack of penetrative deformational fabrics, non-perthitic microcline instead of perthitic feldspars) between the Lowland Brook Syenite and the Red Ravine syenite is corroborated further by differing trace-element characteristics. The two syenite units appear to be unrelated petrogenetically. The lithological gradation sequence of the Red River Anorthosite Suite from massive anorthosite to layered gabbro recognized in the field is also recorded in major-element and trace-element concentrations. Spider diagrams of REE concentrations are consistent with fractionation of the Red River Anorthosite Suite from the same source material. Charnockitic rocks form distinct differentiation trends on appropriate diagrams, but the major-element and trace-element concentrations of the least-fractionated components are similar to those of the layered unit. Trace-element characteristics, for example the lack of a negative Eu anomaly, imply that the charnockite could not be derived from simple fractionation of the same magma that formed the anorthositic rocks. Geochemical discrimination plots using Zr, Ti, Y, and Nb distinguish two texturally distinct types of rhyolite and coarse-grained from the fine-grained gabbroic dikes. One set of rhyolitic and gabbroic rocks is correlated with the Fisset Brook Formation and the other is of uncertain affinity.

CHAPTER 4 - Geochronology

4.1 Introduction

Precise geochronologic data provide an important means for potential correlation of similar lithologies and lithotectonic zones along the strike of the orogen and for defining the age and extent of thermal events that have affected the Laurentian margin of ancient North America. Difficulties may arise in understanding the tectonic significance of a region and in justifying terrane correlations due to imprecise or inadequate age data. For example, Currie et al. (1991) suggested that the Steel Mountain Subzone in southwestern Newfoundland is correlative with the Long Range Inlier and therefore the Grenville Province, but noted (p. 155) that, "No comparisons between this subzone and nearby Precambrian crystalline terranes such as the Indian Head Complex, the northern Long Range, or northern Cape Breton Island could be attempted because of lack of chronologic data." The purpose of this chapter is to report the results of U-Pb and $^{40}Ar/^{39}Ar$ analyses from the Blair River inlier in an attempt to corroborate the previously inferred Grenvillian affinity of the Blair River inlier with precise geochronological evidence and to determine the timing, extent, and nature of the Appalachian thermal overprint.

Samples from the four major meta-igneous units, the Sailor Brook gneiss, Lowland Brook Syenite, Red River Anorthosite Suite, and Otter Brook gneiss, and from the undeformed Sammys Barren granite were selected for U-Pb zircon analysis in an attempt to determine the crystallisation age of the pluton or the protolith age of the gneiss. Titanite from two of these same samples and from other units throughout the Blair River inlier was analysed in order to determine the age of, and to determine the rate of cooling following, the metamorphic overprinting that is evident from petrographic observations. Hornblende and mica $^{40}Ar/^{39}Ar$ analyses were conducted to further constrain the cooling history at temperatures lower than the closure temperature of titanite (Table 4.1).

The locations of samples selected for geochronology are shown on Figure 4.1 and are located more precisely on Map C. Analytical techniques and notes on the interpretation of geochronologic data, zircon morphology, and images that expose the internal structure of zircon grains are described in Appendix A4.1. Geochronological data are presented below in the form of standard concordia (U-Pb), spectral, and isotope correlation ($^{40}Ar/^{39}Ar$) diagrams. The U-Pb data are tabulated in Table A4.1 and the $^{40}Ar/^{39}Ar$ data in Table A4.2.

Sailor Brook gneiss

The Sailor Brook gneiss was selected for geochronologic study because it is country rock to the Lowland Brook Syenite and, therefore, may be the oldest unit in the Blair River inlier. The gneiss locally preserves granulite-facies metamorphic mineral assemblages and granoblastic textures, and is correlated with mafic xenoliths in the Middle Proterozoic (e.g., Barr et al., 1987b) Lowland Brook Syenite. Therefore, the Sailor Brook gneiss has the potential for preserving a protracted history including crystallisation of its (presumed igneous - Chapters 2 and 3) Precambrian protolith, high-grade metamorphism, and retrograde overprinting metamorphism. The sample selected for U-Pb analysis and dated zircon fractions are illustrated and described in Figure 4.2.

Stubby semi-prismatic grains with rounded corners and tips were rare among the mostly spheroidal population of zircon grains. Because prismatic morphologies are commonly interpreted to indicate zircon crystallisation from a melt (see discussion of zircon morphology in Appendix A4.2), four fractions of semi-prismatic grains were analysed in an attempt to obtain an igneous age

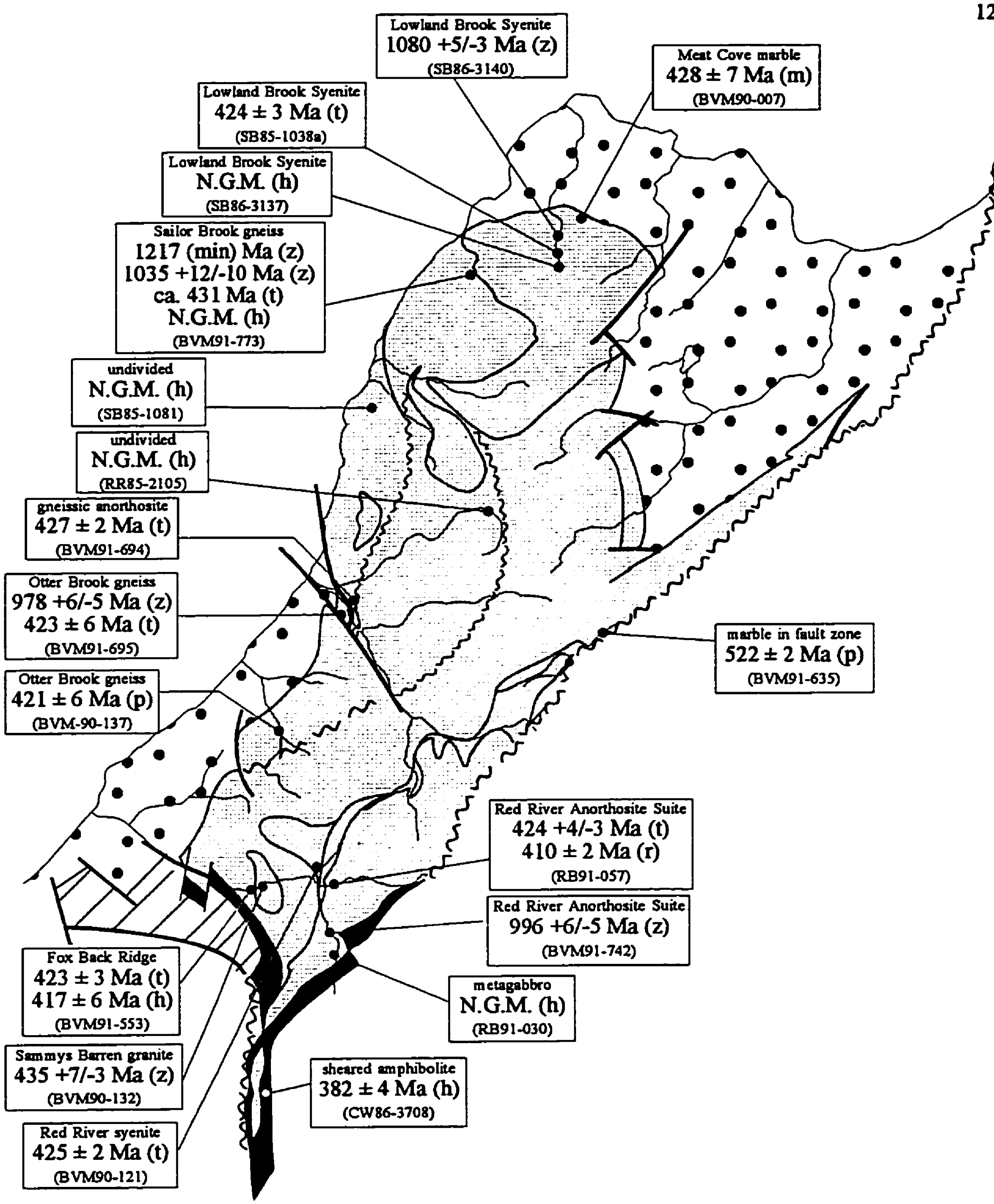

Figure 4.1 - Locations of geochronology samples. See Fig. 2.1 for units and Map B for more precise locations. Abbreviations: z = zircon, t = titanite, h = hornblende, p = phlogopite, m = muscovite, N.G.M. = no geologically meaningful age.

Table 4.1 - Closure temperatures of dated metamorphic minerals. See Appendix A4.3 for discussion.

Mineral	**Closure Temperature**	**Reference**
Titanite	550 ± 50°C	Tucker et al., 1987; Heaman and Parrish, 1991
Titanite	525 ± 25°C	Mezger et al., 1991
Rutile	405 ± 25°C	Mezger et al., 1991
Hornblende	450 ± 50°C	Harrison, 1981; Onstott and Peacock, 1987
Muscovite	350 ● 50°C	Purdy and Jäger, 1976; Snee et al., 1988
Phlogopite (Ann_{-12})	410 ± 50°C	Calculated - see Appendix A4.3
Phlogopite (Ann_{-5})	449 ● 51°C	Calculated - see Appendix A4.3

Figure 4.2 - Hand sample and analysed zircon fractions from the Sailor Brook gneiss.

(a) Slabbed hand sample of BVM91-773. This sample shows a faint compositional banding defined by the concentration of granular mafic minerals and granite migmatitic segregations. The mafic minerals are polycrystalline hornblende and/or hornblende + quartz mosaics. Leucosome and mesosome were impossible to separate, to allow minerals from each to be separately analysed, because of their diffuse and irregular boundaries.

(b) Semi-prismatic zircon grains from the Sailor Brook gneiss. The bulk fraction was divided according to morphology, size and colour. Fractions 1 and 2 were small, clear grains with slightly resorbed corners and tips. Fraction 2 comprised the highest-quality zircons with the best prismatic crystal shapes. Fraction 3 zircons were also prismatic, about the same size and shape as fractions 1 and 2, but were light brown and turbid with many cracks. Fraction 4 contains four grains that were much larger and more highly resorbed than fractions 1-3. (scale bar = 1mm)

(c) Spheroidal zircon fractions from the Sailor Brook gneiss. This bulk sample was divided arbitrarily into two fractions of large grains (fractions 5 and 7) and one of small grains (fraction 6). (scale bar = 1mm)

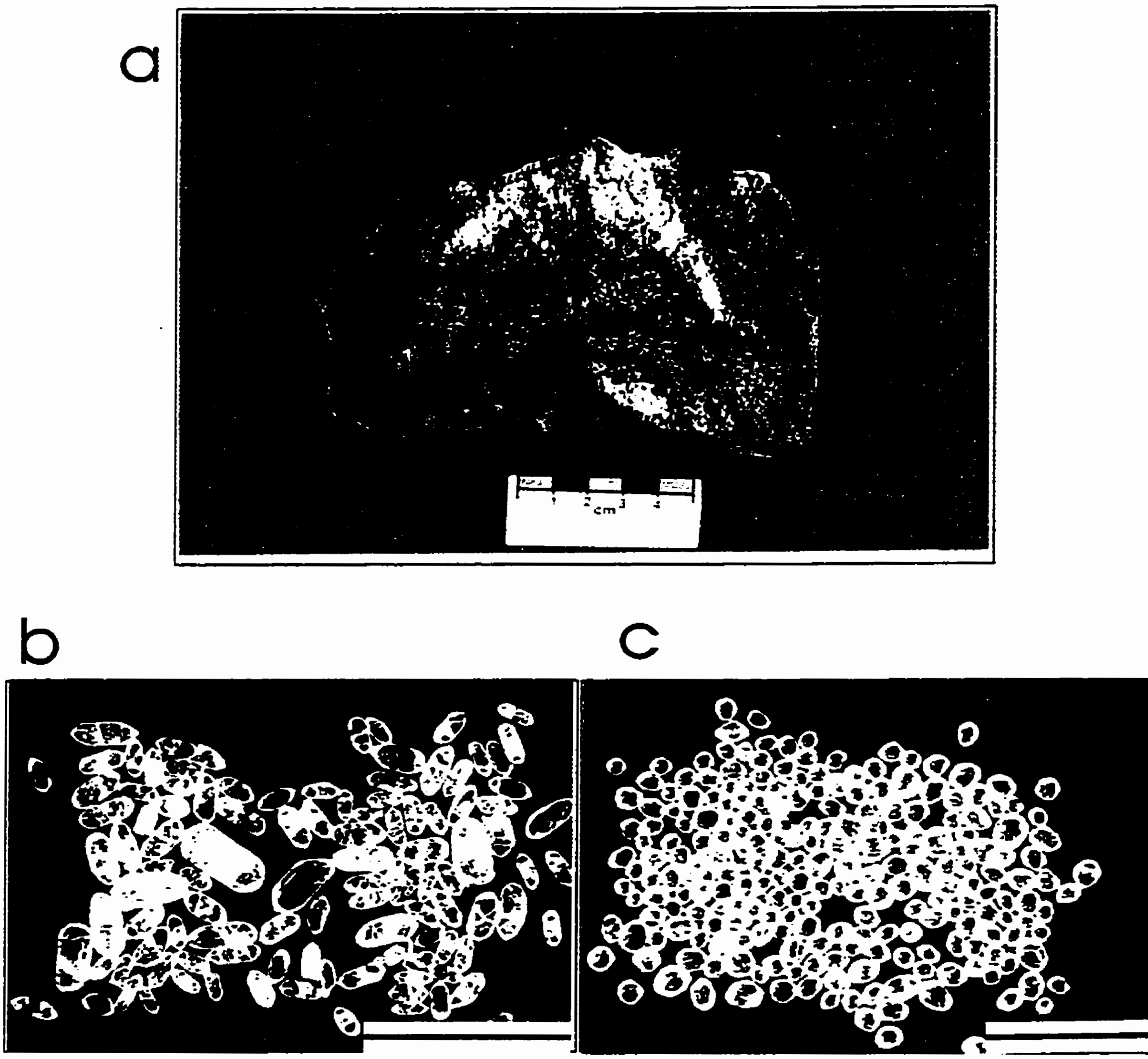

Figure 4.2

for the protolith of the Sailor Brook gneiss. In contrast, spheroidal morphologies are generally interpreted as indicative of metamorphic zircon, and three such fractions were analysed in order to try to constrain the age of metamorphism in the Sailor Brook gneiss.

Internal zoning can provide important evidence for interpreting the crystallisation history of a morphological population of zircon grains and, thus, help to interpret the geological relevance of the U-Pb data (e.g., van Breemen et al., 1986; Paterson et al., 1989; Hancahar and Miller, 1993). The internal zoning of the semi-prismatic grains, as revealed by back-scattered electron (BSE) and cathodoluminescence (CL) images (Figure 4.3), shows a central core of high mean atomic number (bright in BSE, dark in CL) surrounded by a faintly zoned, semi-prismatic rim. This type of distinct core/rim contrast in BSE images likely indicates a core enriched in high-atomic number (relative to Zr) elements, the most important in this context being U, but probably including La, Hf, and Th. Radiation-induced crystal structure damage can result in up to 5% volume expansion at the metamict state (Heaman and Parrish, 1991). Volume expansion of high-U cores can explain the numerous fractures (e.g., Williams, 1992) in the light brown (the colour is also an indication of radiation damage), semi-prismatic grains of fraction 3.

The bright in BSE (Figure 4.3a,b) core is truncated and contained within another ovoid core. The ovoid core is itself truncated and surrounded by increasingly better-defined rims of zoned, semi-prismatic zircon (best seen in CL, Figure 4.3a). These types of truncated zones are characteristic of igneous zircons with multi-stage growth histories that result from partial resorption during crystallisation from a melt (Paterson et al., 1989; 1992). The small central core (bright in BSE) may also be a small inherited (xenocrystic) component. Therefore, the semi-prismatic morphology and internal zoning of the grains shown in Figure 4.2a are interpreted to

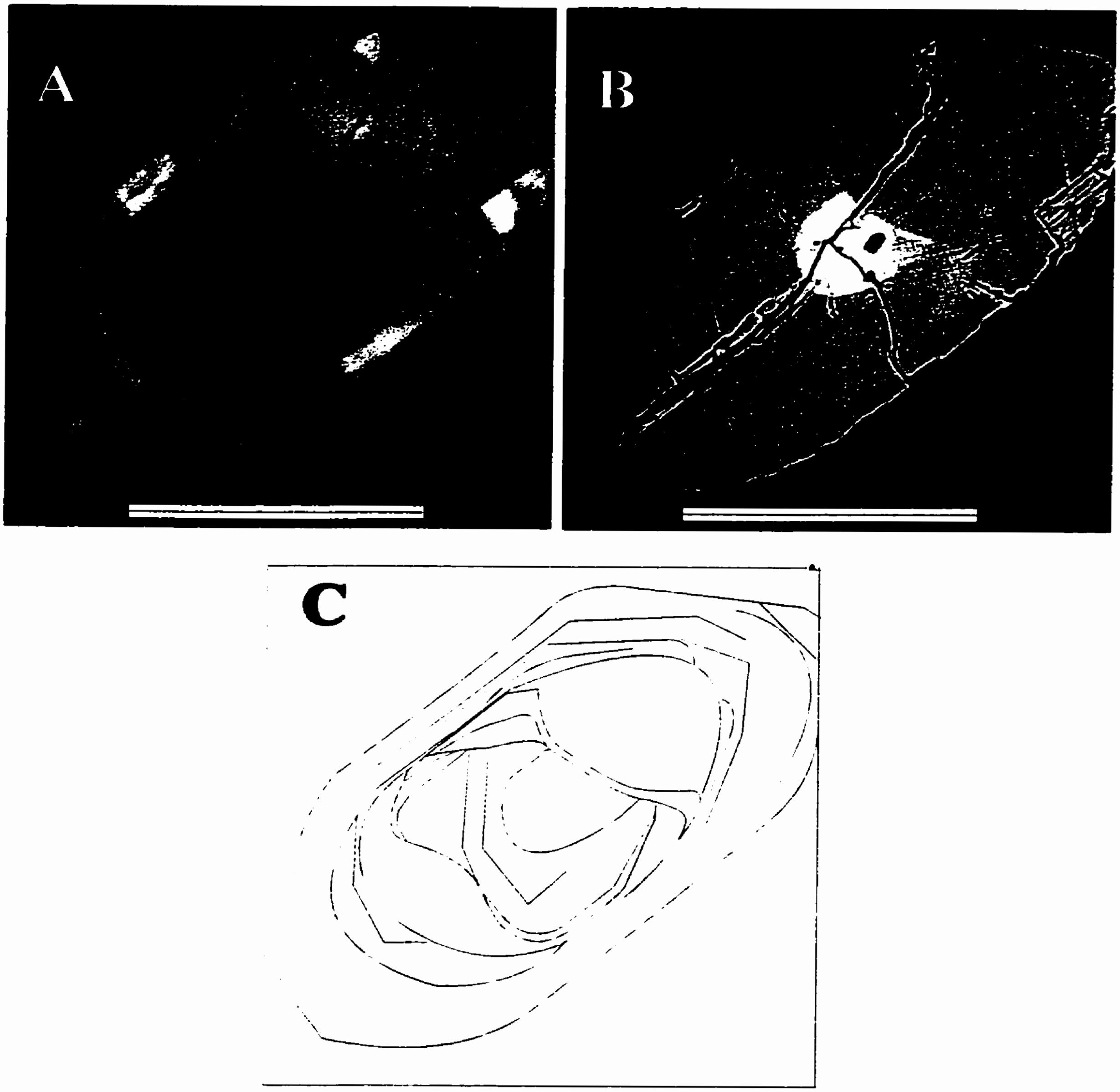

Figure 4.3 - (a) CL and (b) BSE images and (c) line drawing of internal zoning in a semi-prismatic zircon grain from the Sailor Brook gneiss (sample BVM91-773; scale bar = 0.1 mm). Note the appearance of several resorption/precipitation surfaces suggesting a complex growth and dissolution history for the semi-prismatic zircon grains. The style of the zoning is consistent with crystallisation from a melt. See text for discussion of the implications for the disruption of U-Pb systematics.

indicate that the semi-prismatic grains are of igneous origin and the rounded external corners and tips indicate subsequent resorption during a thermal or fluid-flux event. By contrast, BSE and CL images of spheroidal zircon grains (Figure 4.5) show no internal zoning patterns. The slight concentric increase in CL intensity is a lens effect due to internal reflections from the back of the zircon grain.

U-Pb data from the four highly abraded fractions of semi-prismatic zircon grains are plotted as elongate polygons on Figure 4.4a. The analysed fractions show complex discordance in a right-stepping array. Other geochronological evidence (see below) indicates that the Sailor Brook gneiss was metamorphosed at ca. 1035 Ma and in the Silurian. The simplest explanation for the complex discordance that is consistent with the U-Pb data, zircon morphology, and internal zoning patterns is that the two metamorphic episodes resulted in two stages of zircon resorption accompanied by Pb loss. Because the degree of Pb loss from each event cannot be determined, these data can only constrain the minimum age of the protolith by projection to concordia from the later event.

Projected from the 423 Ma age of regional metamorphism, as indicated by titanite analyses (see below), the four fractions yield concordia intercepts up to 1217 Ma (Figure 4.4a). Line-fit confidence is not applicable to a two-point chord, and no errors are reported as they reflect only the arbitrary error associated with the 423 Ma projection point. The 1217 Ma intercept is interpreted as the minimum age for the protolith of the Sailor Brook gneiss. Inheritance does not appear to be a significant factor because all four fractions plot in an array to the right of concordia rather than on a reverse discordance trend. Reverse discordance from 1035 Ma would imply an unreasonably old age of 3500 Ma or more. Furthermore, the U concentration, the radiogenic Pb concentration, and the common Pb composition of the three fractions of smaller semi-prismatic grains (fractions

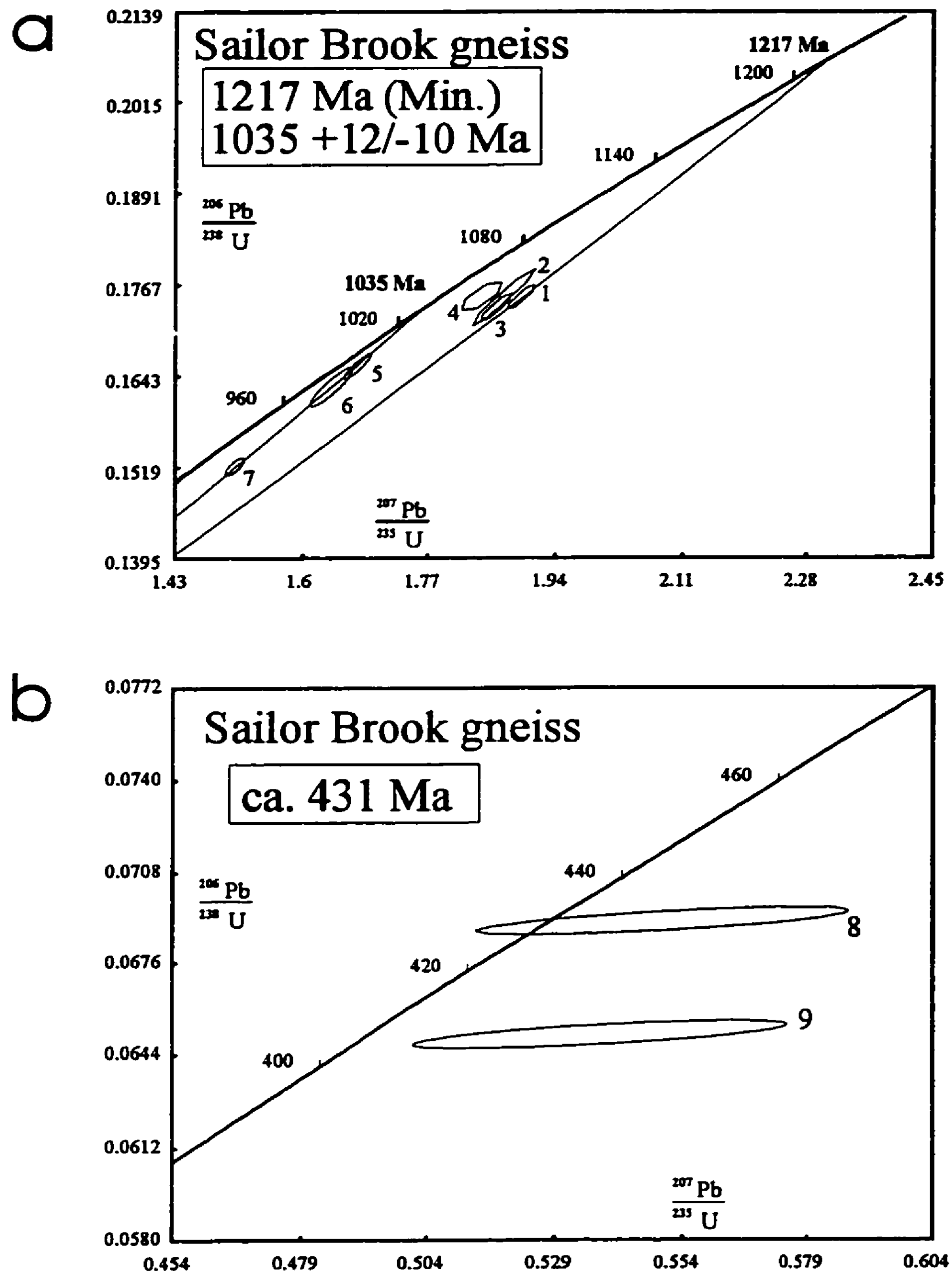

Figure 4.4 - Concordia diagrams for zircon and titanite from the Sailor Brook gneiss (sample BVM91-773). (a) U-Pb data from zircon. Ellipses are the 2σ errors for spheroidal fractions and elongate polygons are the 2σ errors for semi-prismatic fractions. Fraction numbers correspond to those in Table A4.1 and as described in Figure 4.2b,c. (b) Concordia diagram for titanite (also sample BVM91-773); the indicated age is based on the $^{206}Pb/^{238}U$ age of fraction 8 only.

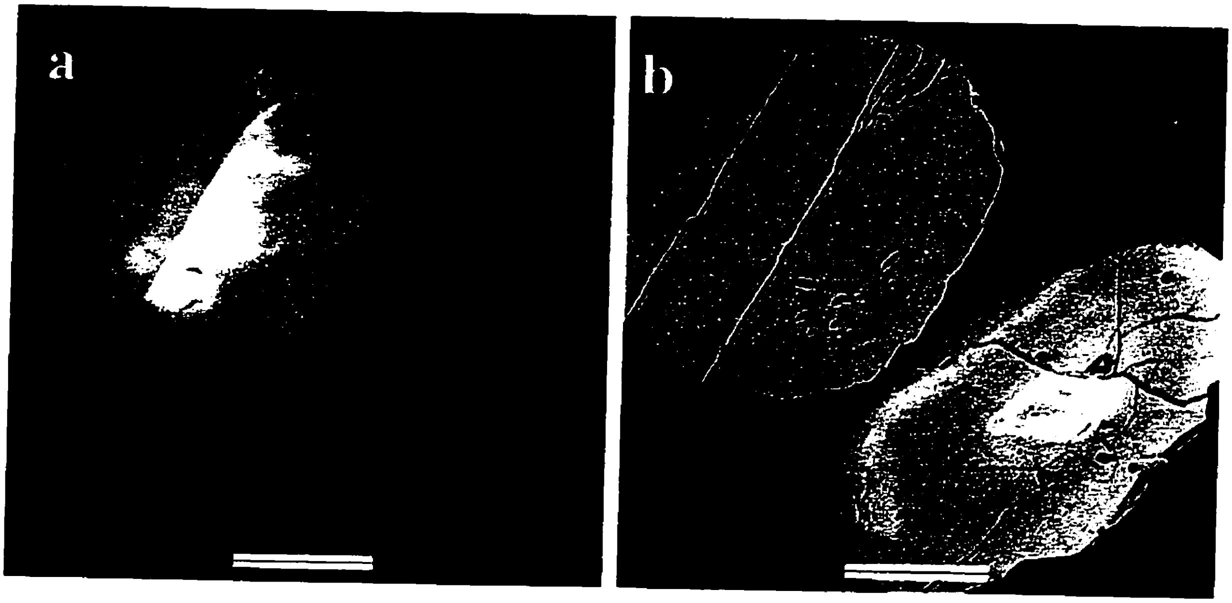

Figure 4.5 - CL and BSE images comparing spheroidal (top left) and semi-prismatic (bottom right) zircon grains from the Sailor Brook gneiss (sample BVM91-773; scale bar = 0.1 mm). The apparent centre-intense zoning in the CL image (a) of the spheroidal grain is the result of a lens-effect on internal reflections from the back of the grain. Note the absence of any zoning in the BSE (b) image of the spheroidal grain. The lack of internal growth zoning in the spheroidal grain is consistent with crystallisation during metamorphism.

1,2,and 3) are very similar to one another, an unlikely occurrence if they contained a significant amount of foreign zircon with differing isotopic compositions.

Data from three highly abraded fractions of spheroidal zircon grains lie on a single discordia line (ellipses on Figure 4.4b) at 8-21% discordant toward the fixed lower intercept of 423 ± 20 Ma. The discordia has a probability of fit of 79% and an upper intercept of 1035 +12/-10 Ma. This is interpreted to be the age of high-grade metamorphism because of the good fit of the discordia line, the morphology of the grains, the lack of internal growth zoning (Figure 4.5), and the presence of granulite-facies metamorphic mineral assemblages in this unit.

A comparison of the nature of the discordance between the spheroidal and semi-prismatic grains also supports the interpretation of two stages of Pb loss. Higher-U zircon grains are typically more discordant than low-U grains from the same sample because radioactivity-induced structural-site defects promote the diffusion of Pb (Silver and Deutsch, 1963; Ellsworth et al., 1994). Therefore, it is unlikely that the higher-U, semi-prismatic fractions would be less discordant (e.g., fraction 4; 13% discordant toward 423 Ma) than the lower-U spheroidal fractions (e.g., fraction 7; 21% discordant towards 423 Ma). Pb-loss from a prior event, such as the ca. 1035 Ma metamorphic event, explains why the higher-U prismatic fractions are more discordant than the lower-U spheroidal fractions.

Titanite and hornblende separates were analysed from the same sample as described above (Figure 4.2a). The titanite grains separated from this sample are clear, small, and shard-shaped. One large sample was highly abraded and arbitrarily divided into the two analysed fractions. Hornblende grains from this sample are nearly equidimensional (0.2 mm - 0.4 mm) and were selected for their lack of inclusions or grain-boundary alteration. Only grains that were of uniform colour and translucence throughout were selected.

The two titanite fractions from the Sailor Brook gneiss are significantly discordant and their ages are not consistent (Figure 4.4b). Fractions 8 and 9 yield $^{206}Pb/^{238}U$ ages (see Appendix A4.2 for justification of the use of $^{206}Pb/^{238}U$ ages) of ca. 431 Ma and ca. 389 Ma, respectively. The high common Pb and low U concentrations (Table A4.1) reduce the reliability of both ages. The ca. 389 Ma age is not duplicated (within error) in titanite analyses from other units and is, therefore, considered to have no geological significance. The ca. 431 Ma age is interpreted as an imprecise estimate of the age of post-metamorphic cooling through the titanite closure temperature (ca. 550°C; Table 4.1).

An $^{40}Ar/^{39}Ar$ spectral diagram for hornblende from the Sailor Brook gneiss is shown in Figure 4.6. The accompanying $^{37}Ar/^{39}Ar$ spectrum shows that the apparent Ca/K ratio of steps 4-14 are within the microprobe-determined range. The peak at step 9 (1175°C) is characteristic of non-systematic outgassing resulting from a mineralogical phase transition during the heating experiment (e.g., Harrison, 1981; Harrison et al., 1985; Foland, 1983) and is accompanied by a slight anomaly in the $^{37}Ar/^{39}Ar$ ratio. Steps 4-8 and 10-13 produce near-plateau, shallow saddle-shaped spectral segments with weighted mean apparent ages of 464 Ma and 487 Ma respectively. The saddle-shaped spectra probably result from excess ^{40}Ar. The centres of the saddles do not approach meaningful cooling ages because the $^{40}Ar/^{39}Ar$ apparent ages are older than the ages of coexisting titanite.

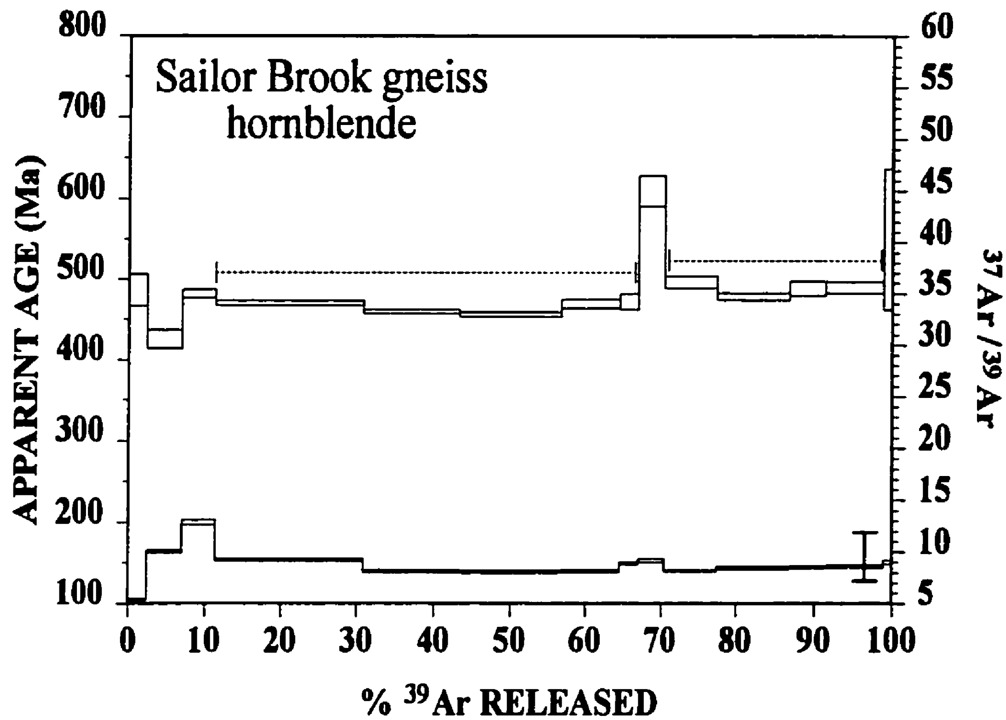

Figure 4.6 - ^{40}Ar/^{39}Ar spectral diagram for hornblende (sample BVM-91-773) from the Sailor Brook gneiss. The two saddle-shaped segments of the spectrum result from excess ^{40}Ar and the weighted mean apparent ages from each saddle (464 Ma and 487 Ma) are not geologically meaningful ages. The lower spectrum is ^{37}Ar/^{39}Ar and bar at lower right indicates the ^{37}Ar/^{39}Ar range calculated from microprobe Ca/K analyses.

Lowland Brook Syenite

A sample of massive, brick red syenite from one of the low-strain lenses in the Lowland Brook Syenite was selected for U-Pb analysis in an attempt to obtain zircon grains of igneous origin, least affected by metamorphism. The sample (Figure 4.7a) is undeformed and contains mostly perthitic K-feldspar, with minor clinopyroxene and Fe-Ti oxide minerals, and lacks titanite. The analysed sample contrasts with the gneissic syenite analysed by Barr et al. (1987b) that contains coarsely perthitic K-feldspar, recrystallised plagioclase phenocrysts, hornblende pseudomorphous after clinopyroxene and with titanite as independent grains and as rims around Fe-Ti oxide minerals. The analysed zircon grains are shown in Figure 4.7b,c.

Despite the lack of obvious metamorphic minerals and textures, this sample contained a significant quantity of spheroidal and multi-faceted ovoid (the latter were not analysed) zircon grains, as well as large semi-prismatic grains. In an attempt to determine the relationship between the morphological classes, and in particular if the spheroidal grains show the characteristics of metamorphic zircon grains, BSE and CL images were obtained from both morphologies. The images shown in Figure 4.8 are from in-situ zircon grains in a polished thin section. The large semi-prismatic zircon grain contains a euhedral core with no apparent resorption at the outer edge and thin, sharply defined growth zones. The core is bordered by a rim of wider, diffuse growth zones. The spheroidal zircon grains also show diffuse zoning of approximately the same style and image intensity as zones in the prismatic zircon rim.

Detailed CL and BSE studies have shown that interpretations of an igneous vs. metamorphic origin based on external morphologies alone can be misleading (Paterson et al., 1989; Hancahar and Miller, 1993; Lanzirotti and Hanson, 1995). This also appears to be the case with spheroidal grains in the Lowland Brook Syenite. Whereas nearly all spheroidal zircon grains in other samples

Figure 4.7 - Hand sample and analysed zircon fractions from the Lowland Brook Syenite.

(a) Slabbed hand sample of SB86-3140. This sample is a massive, undeformed syenite from a low-strain zone in the Lowland Brook body. The sample comprises mostly microperthite with minor amounts of clinopyroxene and Fe-Ti oxide minerals; titanite is absent from this sample.

(b) Large, elongate, semi-prismatic zircon grains and semi-prismatic fragments with slightly rounded corners and tips (scale bar = 1mm). Fractions 1 and 4 were separated from this bulk fraction.

(c) Large spheroidal zircon grains (scale bar = 1mm). Fractions 2 and 3 were separated from this bulk fraction.

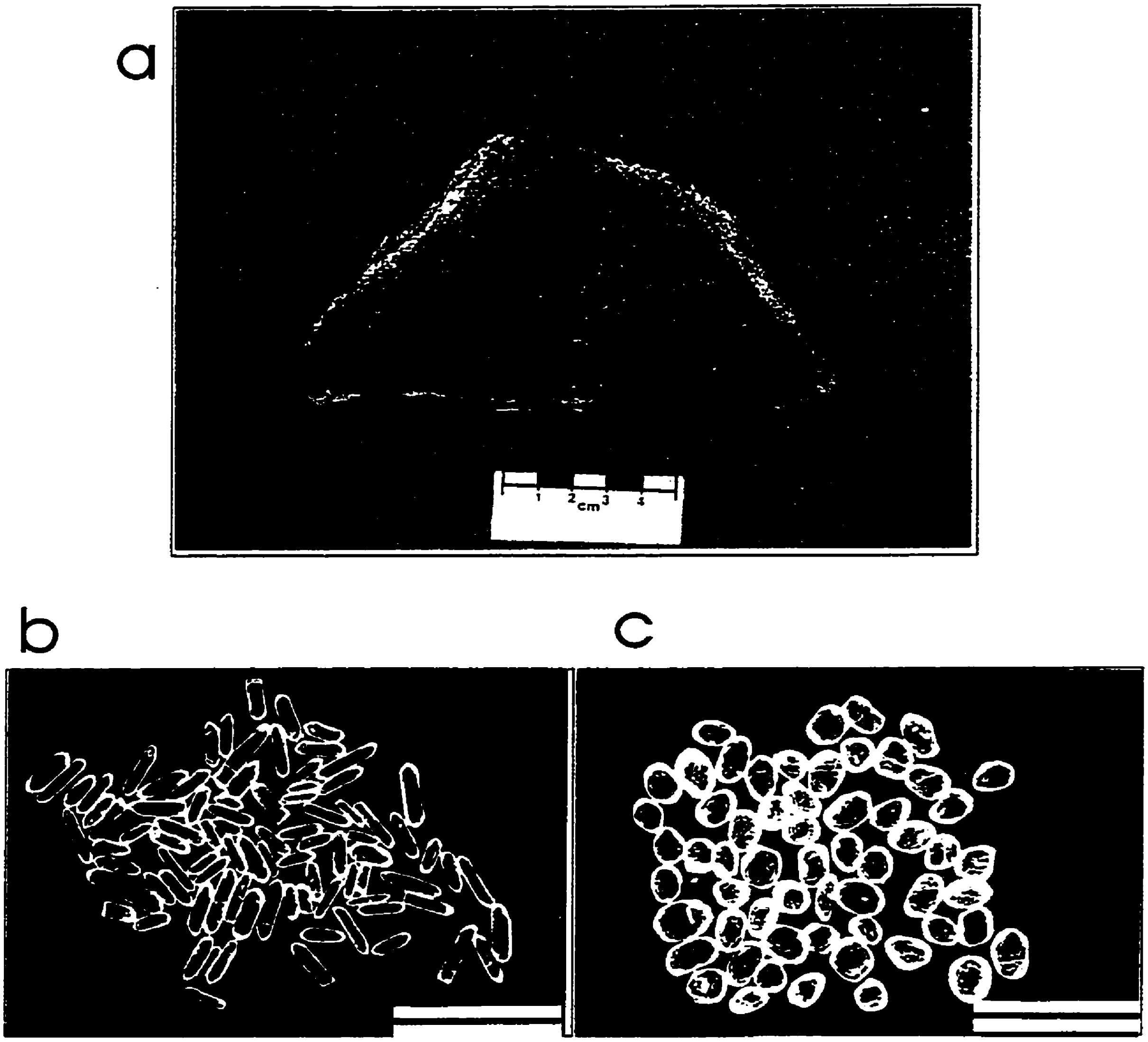

Figure 4.7

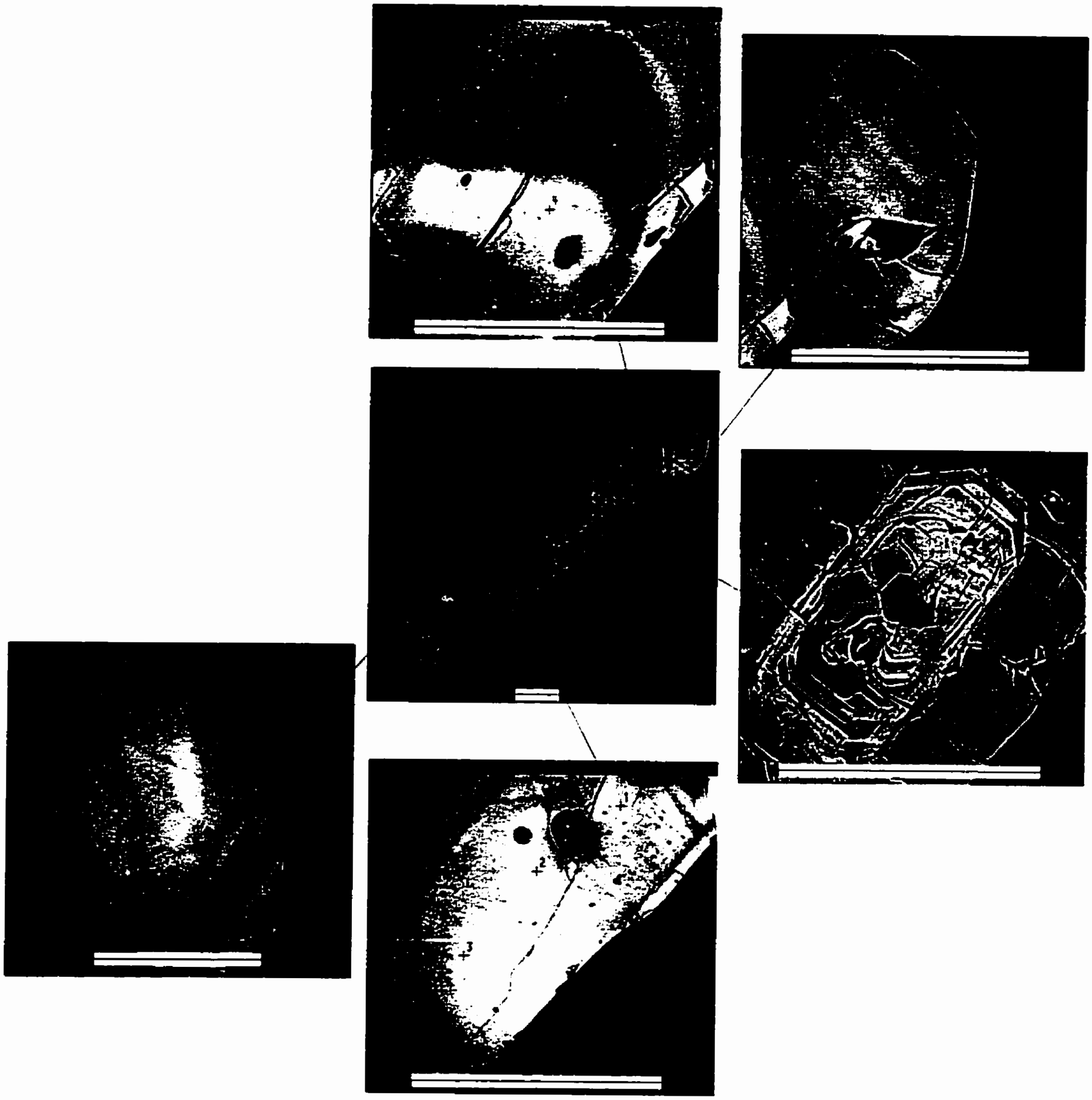

Figure 4.8 - In-situ CL images of semi-prismatic and spheroidal zircon grains from a thin section of the dated Lowland Brook Syenite sample (SB86-3140). The grains are surrounded by perthitic K-feldspar which appears solid black in CL images. Spheroidal grains have concentric growth zones similar to the zones around the core of the prismatic grain; this contrasts with lack of internal zoning in typical metamorphic spheroidal zircon grains, and suggests an igneous origin for zircon grains of both morphologies from the Lowland Brook Syenite. (scale bars = 0.1 mm)

lack internal zoning (suggestive of a metamorphic origin), the zones in spheroidal grains from the Lowland Brook Syenite are similar in width and BSE intensity to growth zones in the semi-prismatic and suggest an igneous origin for both morphologies. Zirconium saturation models of Watson and Harrison (1983) predict high Zr solubility for high-temperature, alkali-rich magmas, and changes in late-stage fluid chemistry, for example fO_2, and Si-activity may account for rapid growth of zircon crystals (Watson, 1979; Jones and Peckett, 1980), and thus the large size, poorly developed crystal faces, and diffuse growth zones as seen in BSE images (Figure 4.8). Based on the evidence from internal zoning patterns, both the spheroidal (including multi-faceted ovoid) and semi-prismatic grains are interpreted to be of igneous origin.

Four highly abraded zircon fractions were analysed from the massive syenite sample and the results are plotted on the concordia diagram in Figure 4.9. Fractions 1 and 4 are large semi-prismatic grains and grain fragments with slightly rounded corners and tips. Fractions 2 and 3 consist of large spheroidal zircon grains. Fractions 2, 3 and 4 have nearly identical $^{207}Pb/^{206}Pb$ ages and define a discordia line with a 72% probability of fit, an upper intercept age of 1080 +5/-3 Ma and a lower intercept of 100 ± 90 Ma, suggesting recent Pb loss. Fraction 1 has a greater $^{207}Pb/^{206}Pb$ age of 1102 Ma and does not fall on the chord defined by fractions 2-4.

The upper intercept age of 1080 +5/-3 Ma is here taken to represent the age of intrusion of the Lowland Brook Syenite and data for fraction 1 are interpreted to indicate a small degree of inheritance. The coincidence of the $^{207}Pb/^{206}Pb$ ages of semi-prismatic and spheroidal fractions 2-4 suggests that both morphologies crystallised from the melt, as inferred above based on internal igneous growth zoning patterns.

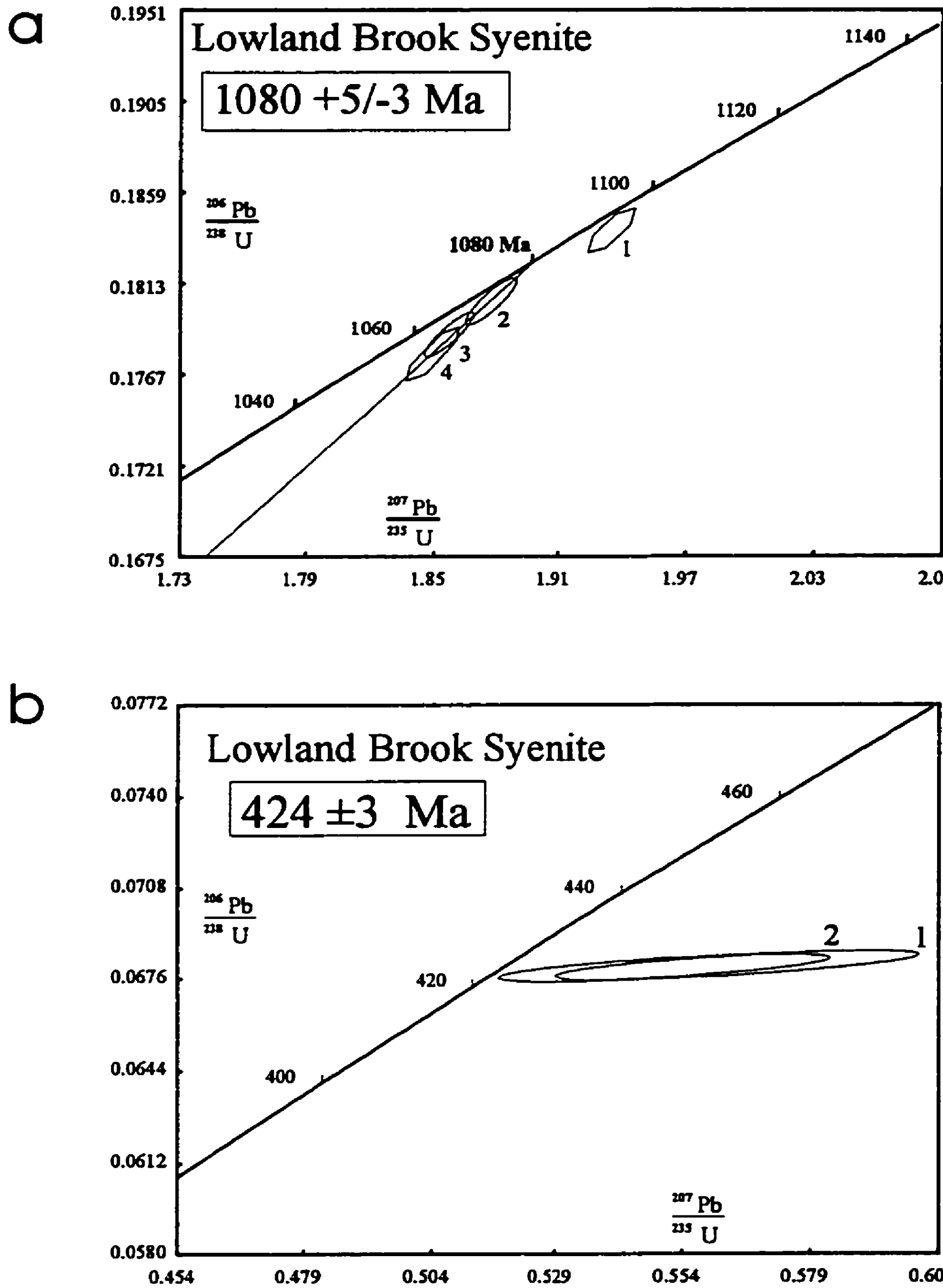

Figure 4.9 - Concordia diagrams for zircon and titanite from the Lowland Brook Syenite. (a) Zircon U-Pb data from sample SB86-3140; elongate polygons are the 2σ errors on the data from semi-prismatic grains and ellipses are the 2σ errors on the data from spheroidal grains. (b) U-Pb data for titanite from sample SB85-1038a. The indicated age is based on $^{206}Pb/^{238}U$ and is interpreted to indicate the time of post-metamorphic cooling through the titanite closure temperature.

Titanite grains were analysed from a gneissic syenite sample (Figure 4.10) because the massive sample described above lacked titanite. Hornblende was obtained from a separate gneissic sample with hornblende + quartz mosaics, pseudomorphous after clinopyroxene, and larger grains altered at their edges to chlorite and biotite. The hornblende separate was finely sieved and carefully hand-picked in an attempt to obtain a pure fraction of the small (0.25 mm) clean mosaic grains and to avoid the larger altered grains.

The titanite shown in Figure 4.10 was highly abraded and divided arbitrarily into two fractions. Both have low U concentrations and require large common Pb corrections which produce large uncertainties in the $^{207}Pb/^{235}U$ and $^{207}Pb/^{206}Pb$ ages. However, they yielded nearly identical $^{206}Pb/^{238}U$ ages of 425 +2/-3 Ma and 423 ± 2 Ma (Figure 4.9, Table A4.1). The $^{206}Pb/^{238}U$ ages of the titanite are taken to indicate amphibolite-facies post-metamorphic cooling through the titanite closure temperature (Table 4.1) at 424 ±3 Ma.

The $^{40}Ar/^{39}Ar$ spectrum (Figure 4.11) is internally discordant. Approximately 70% of the gas was released in two steps and these form the bottom of a saddle-shaped spectrum that is interpreted to indicate excess ^{40}Ar. With the exception of the first step, the $^{37}Ar/^{39}Ar$ spectrum is within the range of apparent Ca/K as calculated from microprobe data, indicating a relatively homogeneous sample. A high apparent age spike in the $^{40}Ar/^{39}Ar$ spectrum occurs at the 1100°C temperature step and is probably the result of a mineralogical phase transition during heating. No geologically meaningful age can be inferred from these $^{40}Ar/^{39}Ar$ data.

Figure 4.10 - Hand samples from which titanite and rutile were separated and photomicrographs of analysed titanite and rutile fractions.

(a) Hand samples of (clockwise from top left) Fox Back Ridge diorite/granodiorite (BVM91-553), gneissic anorthosite in the Polletts Cove River gneiss (BVM91-694), Red River Anorthosite Suite (RB91-057), Sailor Brook gneiss (BVM91-773), Red Ravine syenite (BVM90-121), Lowland Brook Syenite (SB85-1038a), and (centre) Otter Brook gneiss (BVM91-695).

(b) Yellow titanite from the Lowland Brook Syenite (scale bar = 1mm).

(c) Tan titanite shards from the Red River Anorthosite Suite (scale bar = 1mm).

(d) Brown cylindrical rutile from the Red River Anorthosite Suite (scale bar = 1mm).

(e) Brown rutile rimmed by tan titanite from the same sample as the fractions shown in (c) and (d); these polymineralic grains were not analysed separately (scale bar = 1mm).

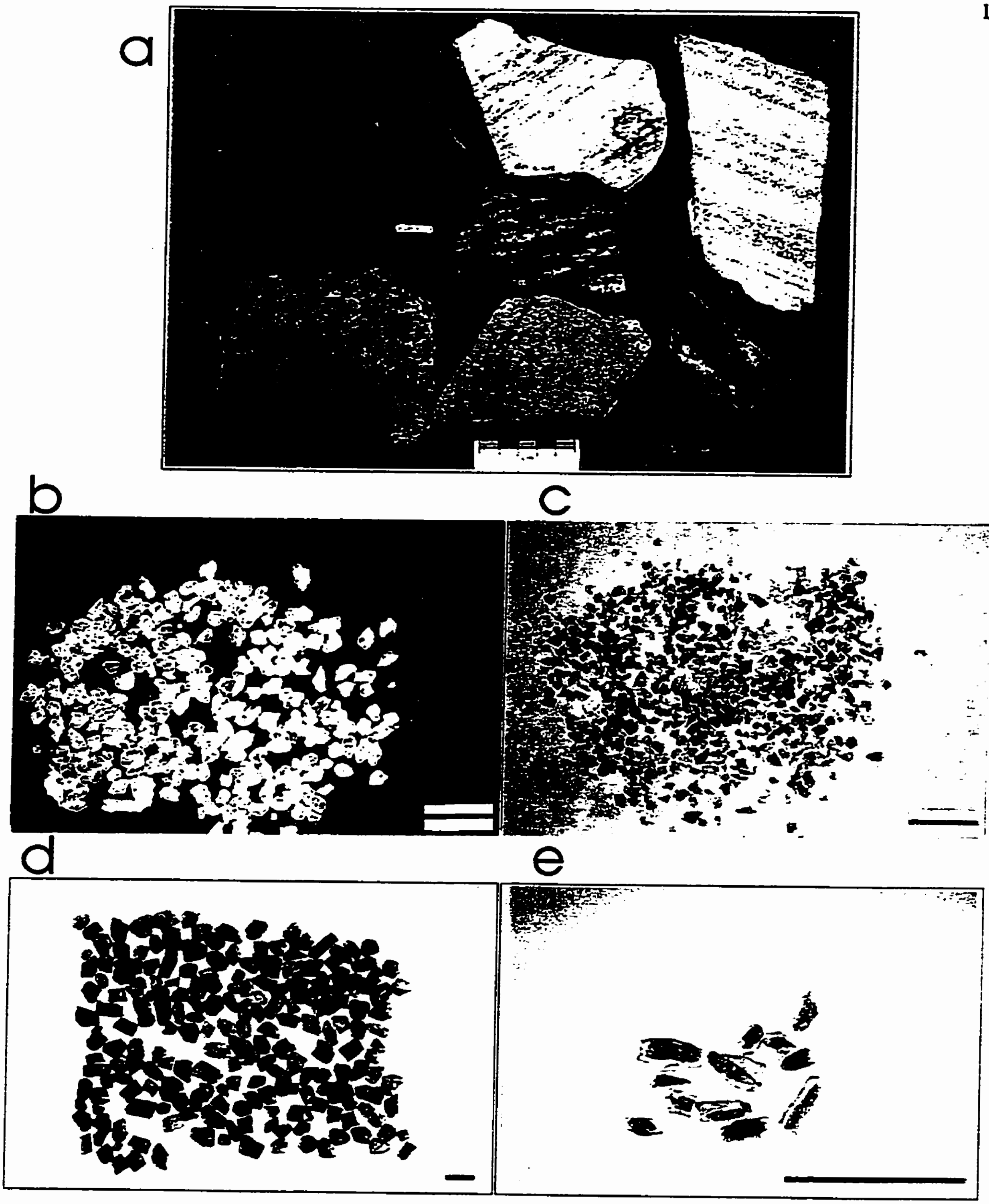

Figure 4.10

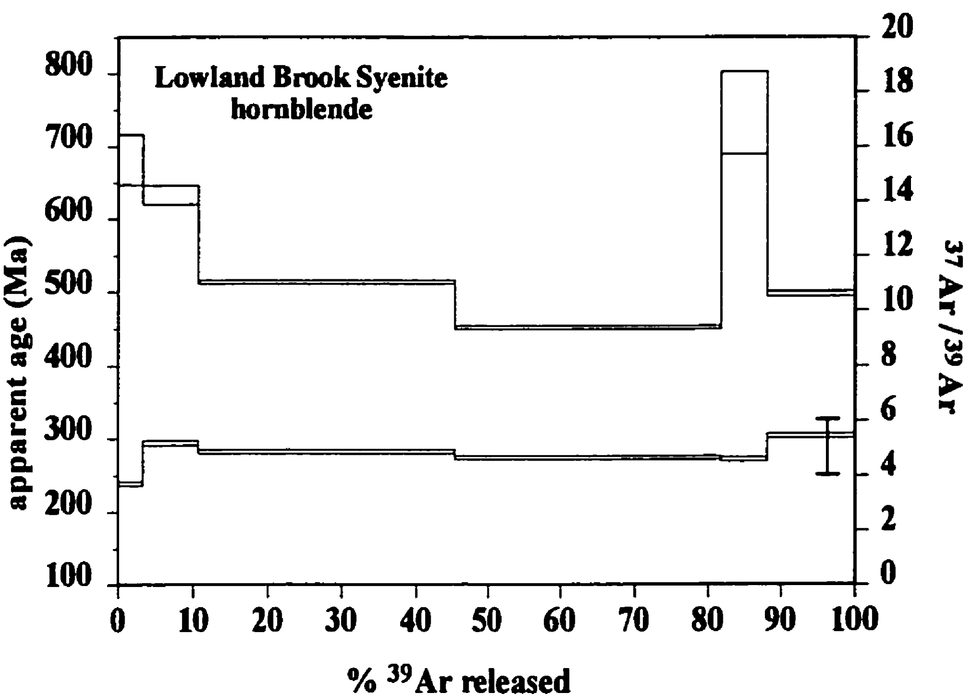

Figure 4.11 - $^{40}Ar/^{39}Ar$ spectral diagram for hornblende (sample SB-3137) from the Lowland Brook Syenite. The saddle-shaped spectrum indicates excess ^{40}Ar and approximately 70% of the gas was released in two steps. The lowest step has an apparent age of ca. 451 Ma which is older than the titanite ages from this unit. Therefore, the $^{40}Ar/^{39}Ar$ data are interpreted to provide no geologically meaningful age. The lower spectrum is $^{37}Ar/^{39}Ar$ and bar at lower right indicates the $^{37}Ar/^{39}Ar$ range calculated from microprobe Ca/K analyses.

Red River Anorthosite Suite

The age of intrusion of very few anorthosite bodies has been directly dated using U-Pb methods because anorthosite is notorious for lacking zircon of igneous origin (e.g., McLelland and Chiarenzelli, 1989; Emslie and Hunt, 1990; Doig, 1991; Owens and Dymek, 1992; Ashwal, 1993). Mineral separates from the least deformed and metamorphosed anorthosite sample observed in this study confirm the scarcity of zircon in massive anorthosite of the Red River Anorthosite Suite. The sample from the layered unit was selected for U-Pb analysis because prismatic zircon was observed in thin section. The origin of the layering and the excess quartz in this sample are uncertain but both are probably at least partly metamorphic (Chapter 2). The dated sample and the separated zircon fractions are shown in Figure 4.12.

CL and BSE images of semi-prismatic zircon grains (Figure 4.14) show faint, non-rational zoning in CL and no zoning in BSE images. This is in contrast to most of the known or presumed igneous prismatic and semi-prismatic zircons in this study that show face-parallel concentric zoning in CL images. Lanzirotti and Hanson (1995) showed that elongate acicular zircon grains with a similar style of zoning are of hydrothermal origin associated with metamorphism and crystallised in mm-scale quartz veins. The prismatic, highly elongate grains from the Red River Anorthosite Suite may have a similar origin because the sample contains silica-rich bands interpreted to be of metamorphic origin (Chapters 2 & 3). Spheroidal zircon grains show no internal zoning, which is consistent with crystallisation during metamorphism.

U-Pb data from prismatic fractions 2, 5, and 6 are shown as elongate polygons on Figure 4.13a and data from spheroidal fractions 1, 3, and 4 are shown as ellipses. Regressed through points 1-4 and 6, with a fixed lower intercept at 423 ± 20 Ma, the discordia line has a probability of fit of 49% and yields an upper intercept age of 996 +6/-5 Ma. Fraction 5 plots to the left of the

Figure 4.12 - Hand sample and analysed zircon from the Red River Anorthosite Suite.

(a) The dated sample (BVM91-742) is from the layered unit of the Red River Anorthosite Suite. The sample is compositionally layered with layers defined by relative proportions of quartz and feldspar, and to a lesser extent biotite and altered pyroxene. This sample contains porphyroclasts of plagioclase and uralitized clinopyroxene, in a recrystallised matrix of plagioclase, microcline, orthopyroxene, biotite, and Fe-Ti oxide minerals. The centimetre-wide quartz- and K-feldspar-rich layers are probably related to recrystallisation and metamorphism (Chapter 2).

(b) Elongate prismatic zircon grains (scale bar = 1mm). These grains were very rare among the total zircon population and the pictured grains were divided into three fractions based on similarities in size and development of crystal faces. Fractions 2 and 5 consisted of clear, thin needle-shaped prismatic zircon grains and grain fragments. The very elongate needle-shaped grains were broken into two or more fragments to facilitate abrasion. Zircon grains in fraction 6 were small, doubly-terminated, clear, semi-prismatic grains with lower aspect ratios than those of fractions 2 and 5.

(c) This bulk fraction of spheroidal grains (scale bar = 1mm) was divided arbitrarily into the analysed fractions 1, 3 and 4.

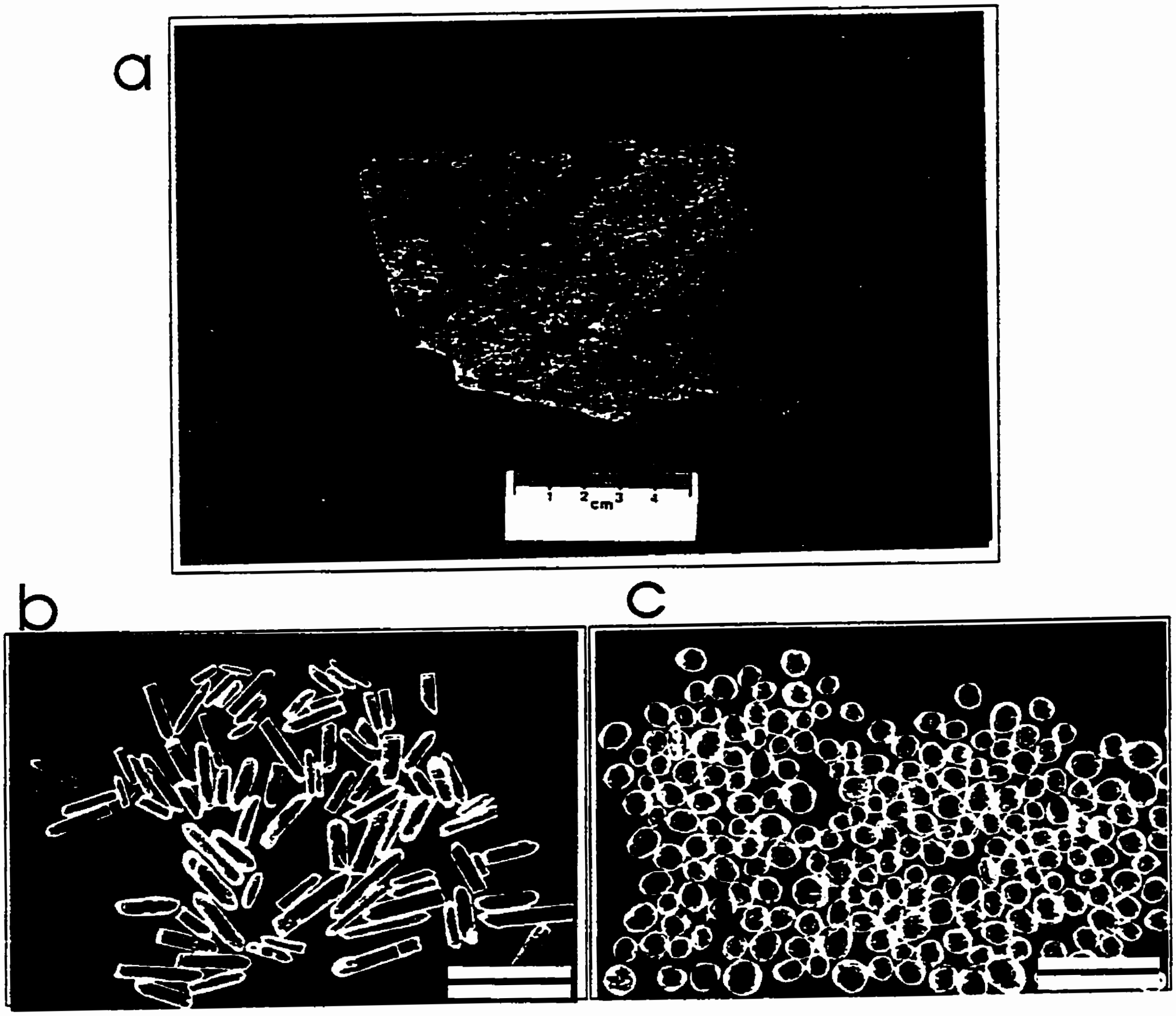

Figure 4.12

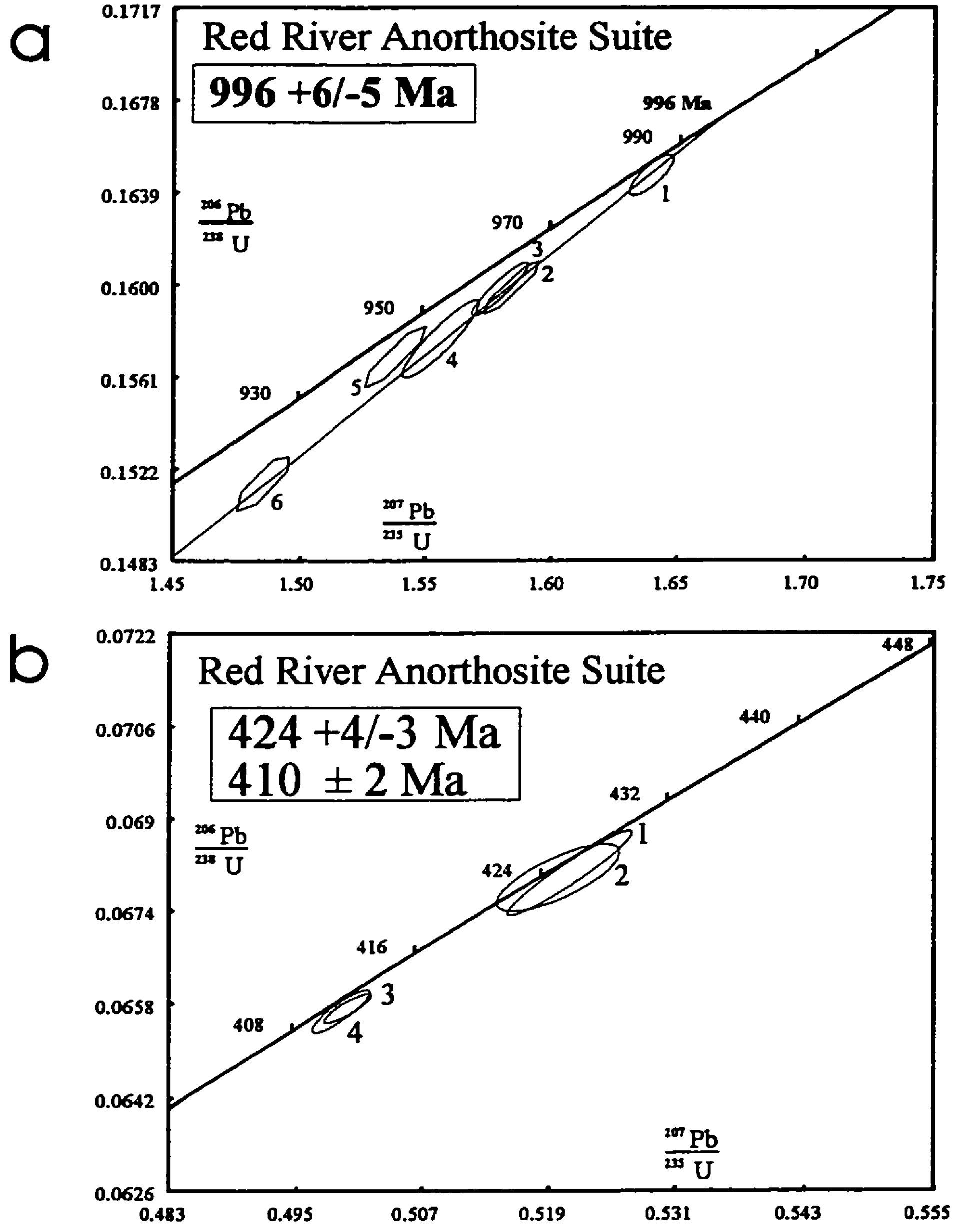

Figure 4.13 - Concordia diagrams for zircon, titanite, and rutile from the Red River Anorthosite Suite. (a) Zircon U-Pb data from sample BVM91-742. Elongate polygons are the 2σ errors on the data from prismatic grains and ellipses are the 2σ errors on the data from spheroidal grains. (b) U-Pb data for titanite (fractions 1&2) and rutile (fractions 3&4) from sample RB91-057. The indicated ages are based on $^{206}Pb/^{238}U$ and are interpreted to indicate the time of post-metamorphic cooling through titanite and rutile closure temperatures.

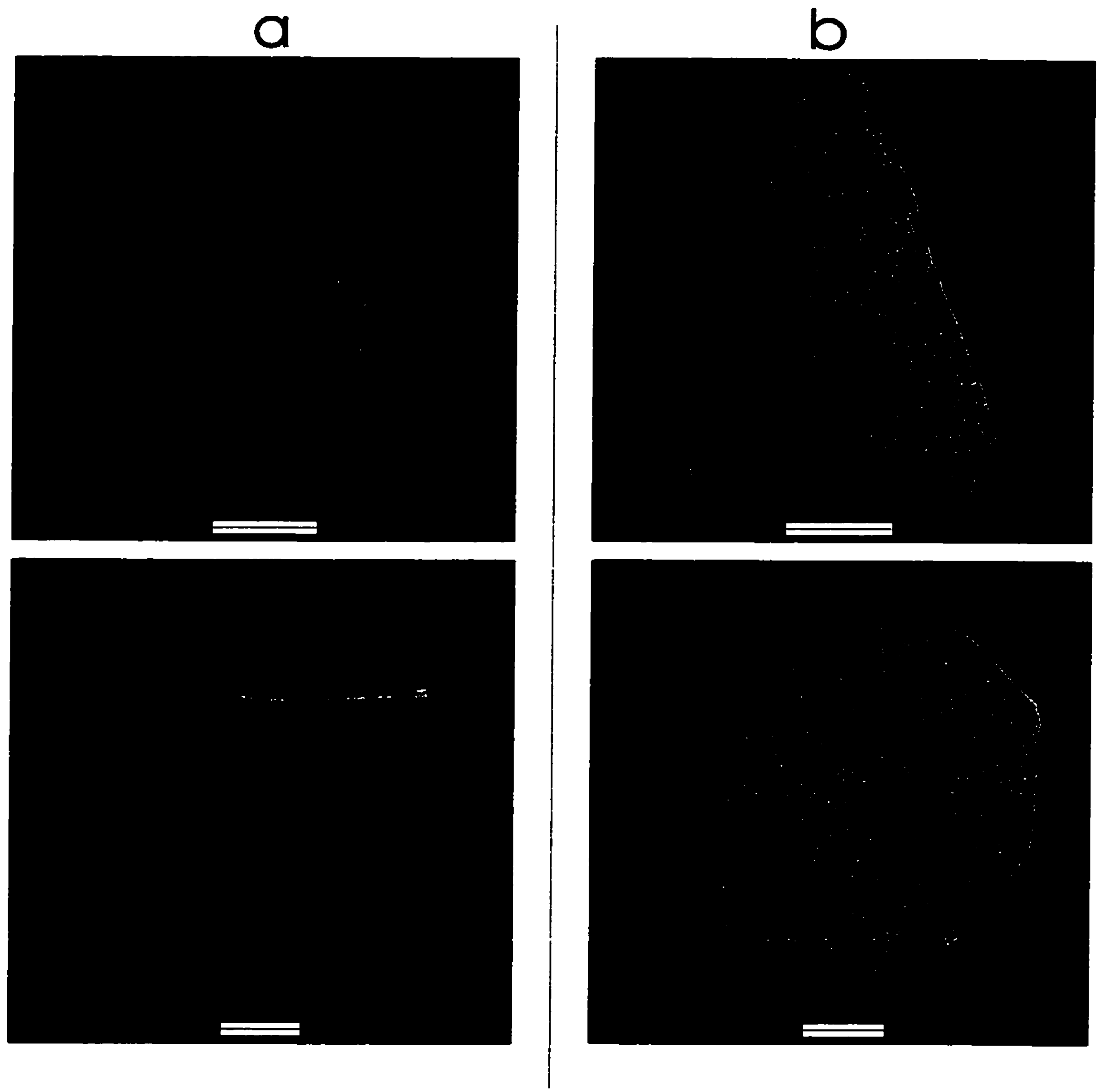

Figure 4.14 - (a) CL and (b) BSE images of semi-prismatic and spheroidal zircon grains from the Red River Anorthosite Suite (BVM91-742; scale bars = 0.1 mm). A thin elongate prism like those of fractions 2 and 5 (top) is weakly and non-rationally zoned and has a thin overgrowth around one end. The spheroidal grain (bottom) lacks clear growth zoning. These relations suggest multiple generations of zircon growth that complicate the interpretation of U-Pb results (see discussion in text).

line defined by the other fractions for unknown reasons and is not included in the regression. The upper intercept is here considered a metamorphic age, based on the spheroidal morphology of some zircon fractions in this sample, including the least discordant fraction, and the observation that the least deformed and metamorphosed anorthosite contains no igneous zircon.

Another sample from the layered unit of the Red River Anorthosite Suite was selected for U-Pb analysis because it contains both titanite and rutile, and some grains of rutile have overgrowths of titanite. It contains a significant quantity of quartz, but quartz is disseminated throughout the sample instead of concentrated in layers. The weak layering is defined by the relative proportions and alignment of mafic minerals and the elongation of recrystallised quartz aggregates. The sample contains plagioclase, quartz, pale brown amphibole, and accessory minerals including titanite, rutile, and apatite. Plagioclase grains are recrystallised into a polygonal mosaic texture. Plagioclase is roughly equidimensional (~0.4 mm) and altered to white mica along fractures and in patches. Quartz subgrains are also roughly equidimensional (~0.4 mm-0.6 mm), but the aggregates are elongate parallel to the layering. Amphibole is present mainly as recrystallised aggregates, but rare large grains have a zoned core that preserves skeletal clinopyroxene.

The sample and mineral separates are shown in Figure 4.10e. The bulk titanite and rutile fractions were each abraded and separated arbitrarily into two fractions. The U-Pb concordia diagram for both minerals is presented in Figure 4.13b. The two fractions of titanite from the Red River Anorthosite Suite overlap one another and fraction 2 overlaps concordia (Figure 4.13b). The titanite data indicate a $^{206}Pb/^{238}U$ age of 424 +4/-3 Ma whereas the two rutile fractions yielded a $^{206}Pb/^{238}U$ age of 410 ±2 Ma (Figure 4.13b). The ages are interpreted to indicate post-metamorphic cooling through the respective closure temperatures for titanite and rutile (Table 4.1).

A metagabbro sample was selected for $^{40}Ar/^{39}Ar$ analysis because it contains relict gabbroic textures in which pyroxene is nearly completely altered to recrystallised aggregates of hornblende. Hornblende is slightly altered to chlorite and epidote along fractures. The analysed hornblende grains were large, dark green or black, and blocky with well-developed cleavage.

The $^{40}Ar/^{39}Ar$ spectrum (Figure 4.15) is internally discordant with old apparent ages from the low-temperature steps. The overall shape of the spectrum is similar to that of a mixed-phase spectrum (Hanes, 1991), but measured $^{37}Ar/^{39}Ar$ ratios are in the range of microprobe-determined apparent Ca/K for all but the first two steps and one step in an anomalous low-age spike, suggesting mostly single-phase sample outgassing. A large percentage (~40%) of gas was released in one temperature step which, if broken down into more steps, would probably reveal a saddle-shaped spectrum typical of excess ^{40}Ar. Thus, the $^{40}Ar/^{39}Ar$ spectrum is here considered to provide no geologically meaningful age data.

Otter Brook gneiss

The Otter Brook gneiss was selected for U-Pb analysis because it is a distinctive (inferred) meta-igneous unit that is spatially separated from the major Proterozoic meta-igneous units. The analysed sample is shown in Figure 4.16, along with the bulk fraction of zircon grains.

Mineral separates from the Otter Brook gneiss sample yielded a large quantity of zircon, most of which were large semi-prismatic grains with slightly rounded corners and tips. Spheroidal zircon was relatively rare and equant grains were mostly multi-faceted ovoid grains of probable igneous origin. No frosted and pitted zircon grains, typical of detrital zircon grains in paragneiss, were observed. A CL image of a typical semi-prismatic zircon from the Otter Brook gneiss

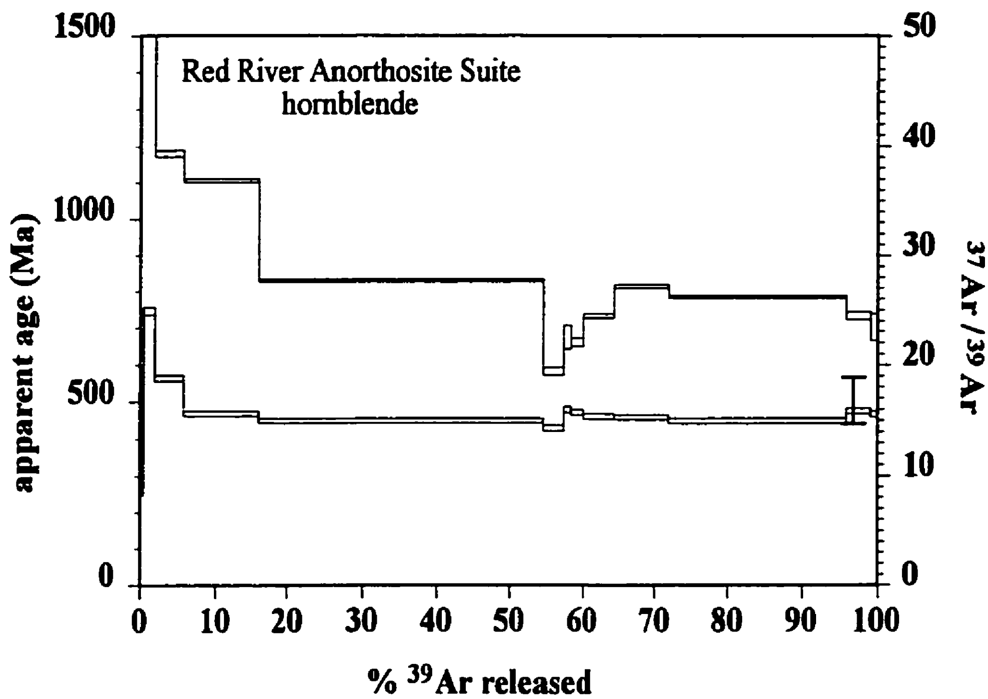

Figure 4.15 - $^{40}Ar/^{39}Ar$ spectral diagram for hornblende (sample RB91-030) from the Red River Anorthosite Suite. With better resolution in the intermediate-temperature steps, the spectrum would probably resolve into a saddle shape typical of excess ^{40}Ar. Therefore, the spectrum does not yield any geologically meaningful age data. The lower spectrum is $^{37}Ar/^{39}Ar$ and bar at lower right indicates the $^{37}Ar/^{39}Ar$ range calculated from microprobe Ca/K analyses.

Figure 4.16 - Hand sample and analysed zircon grains from the Otter Brook gneiss.

(a) The dated sample (BVM91-695) is a quartzofeldspathic flaser gneiss typical of this unit. It contains coarse-patch perthite, plagioclase, biotite, hornblende resorbed garnet, relict clinopyroxene, and titanite. The latter mineral is present as spindle-shaped grains in the amphibolite-facies foliation.

(b) Large semi-prismatic zircon grains (scale bar = 1mm). This bulk fraction was highly abraded and divided arbitrarily into the three analysed fractions.

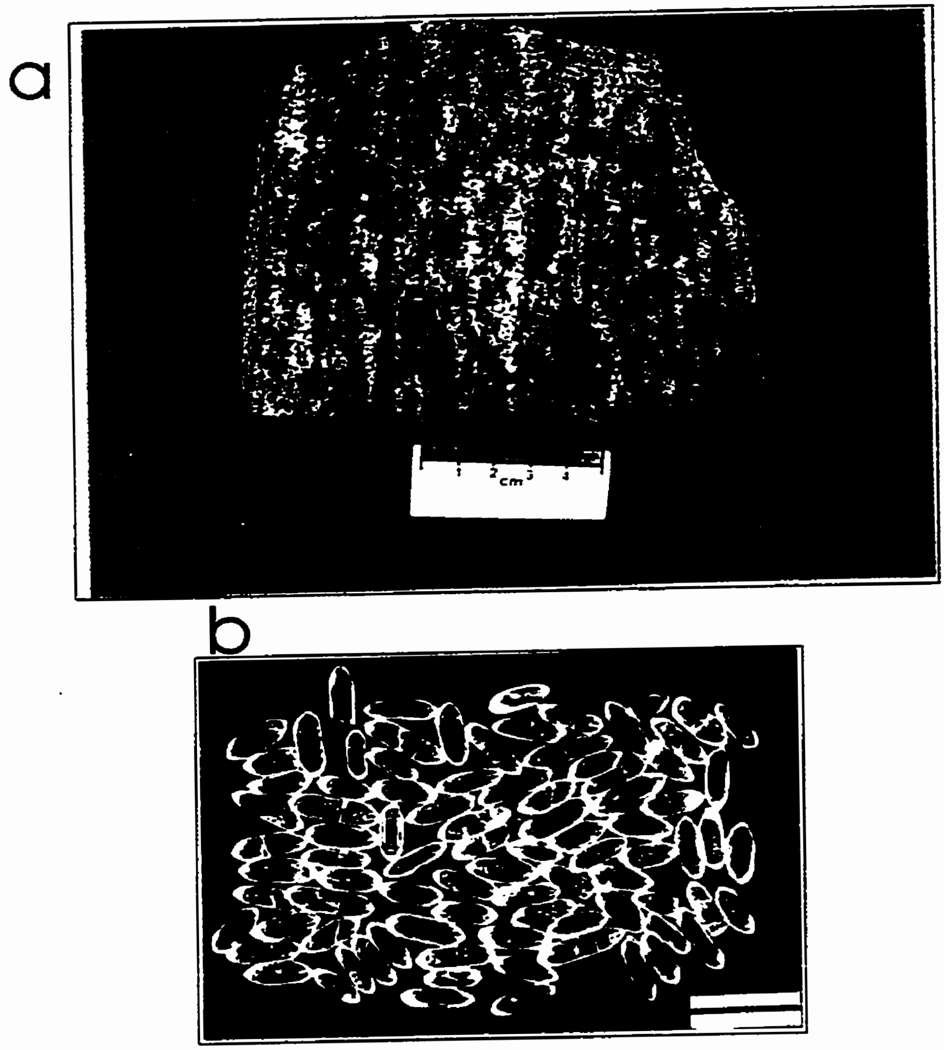

Figure 4.16

(Figure 4.17) shows rational internal growth zoning and some resorption surfaces and is typical of zircon grains of igneous origin. The consistency of U-Pb systematics (Table A4.1) between different fractions would not be expected from a detrital zircon population and also supports the interpretation of an igneous protolith.

All three zircon fractions from the Otter Brook gneiss lie on a chord regressed from 423 ● 20 Ma, with a probability of fit of 64% (Figure 4.18a). The similarity in $^{207}Pb/^{206}Pb$ ages (964-967 Ma; Table A4.1) is unlikely to indicate only recent Pb-loss because this sample was affected by amphibolite-facies metamorphism at ca. 423 Ma (see below). A line regressed through the three data points without a pinned lower intercept yielded upper and lower intercepts of 981 Ma and 482 Ma with large errors, which also suggests that the data are not discordant toward a recent Pb-loss age. The known metamorphic age, therefore, provides a more precise constraint on the lower intercept age. The upper intercept age of 978 +6/-5 Ma is interpreted to be the igneous crystallisation age of the protolith.

Two fractions of clear titanite were separated from the same sample of the Otter Brook gneiss used in the zircon analysis(Figure 4.19a). The analysed titanite grains are shown in Figure 4.19b. Phlogopite was separated from a sample of sheared calc-silicate in the Otter Brook gneiss that contains phlogopite, diopside, and tremolite. Phlogopite defines the foliation, and wraps around augen of diopside and tremolite. The latter two minerals are highly fractured, but are not pervasively altered.

The concordia diagram for titanite data is shown in Figure 4.18b. Titanite in fraction 4 yields a $^{206}Pb/^{238}U$ age of 423 ± 6 Ma. Fraction 5 contains an extremely high common Pb component (Table A4.1), probably due to an unnoticed inclusion of a high-Pb mineral such as

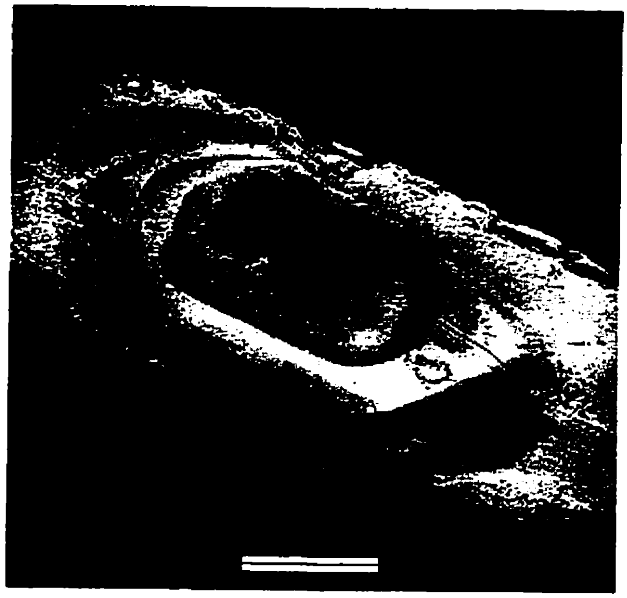

Figure 4.17 - CL image of a typical semi-prismatic zircon grain from the Otter Brook gneiss (BVM91-695; scale bar = 0.1 mm). The rational internal growth zoning and localised resorption surfaces are typical of zircon grains of igneous origin.

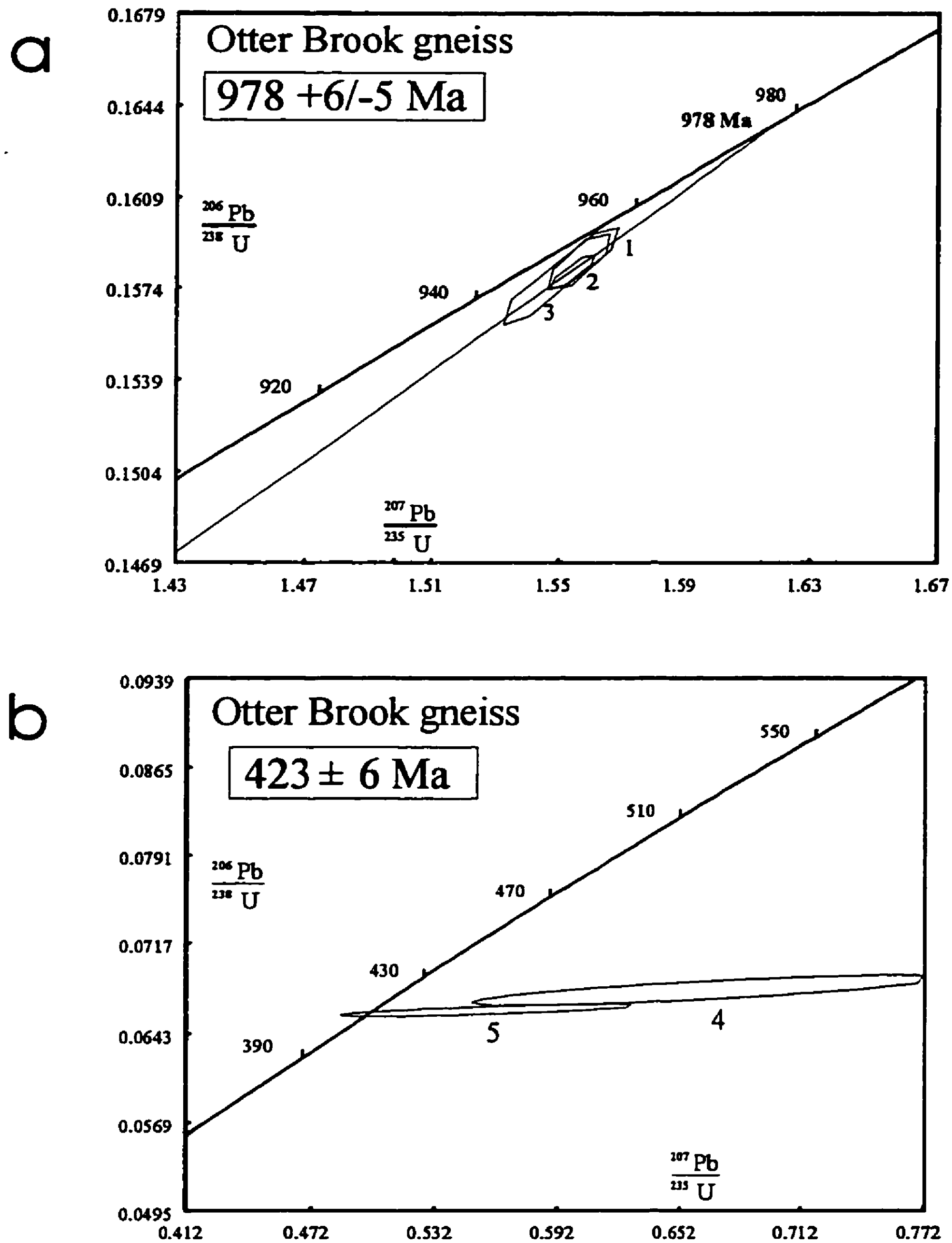

Figure 4.18 - Concordia diagrams for zircon and titanite data from the Otter Brook gneiss (sample BVM91-695). (a) U-Pb data for zircon; elongate polygons are the 2σ errors on analyses from semi-prismatic grains. (b) Titanite data (same sample); the indicated preferred age is based on the $^{206}Pb/^{238}U$ age of fraction 4.

Figure 4.19 - Slabbed hand samples collected for titanite analyses and photomicrographs of analysed titanite fractions.

(a) Hand samples of (clockwise from top right) Fox Back Ridge diorite/granodiorite (BVM91-553, gneissic anorthosite in the Polletts Cove River gneiss (BVM91-694), Red River Anorthosite Suite (RB91-057), Sailor Brook gneiss (BVM91-773), Red Ravine syenite (BVM90-121), Lowland Brook Syenite (SB85-1038a), and (centre) Otter Brook gneiss (BVM91-695).

(b) Clear titanite from the Otter Brook gneiss (scale bar = 1mm).

(c) Tan (left) and brown (right) titanite from a sample of gneissic anorthosite in the Polletts Cove River gneiss (scale bar = 1mm).

(d) Yellow titanite blades from the Red Ravine syenite (scale bar = 1mm).

(e) Brown titanite from the Fox Back Ridge diorite/granodiorite (scale bar = 1mm).

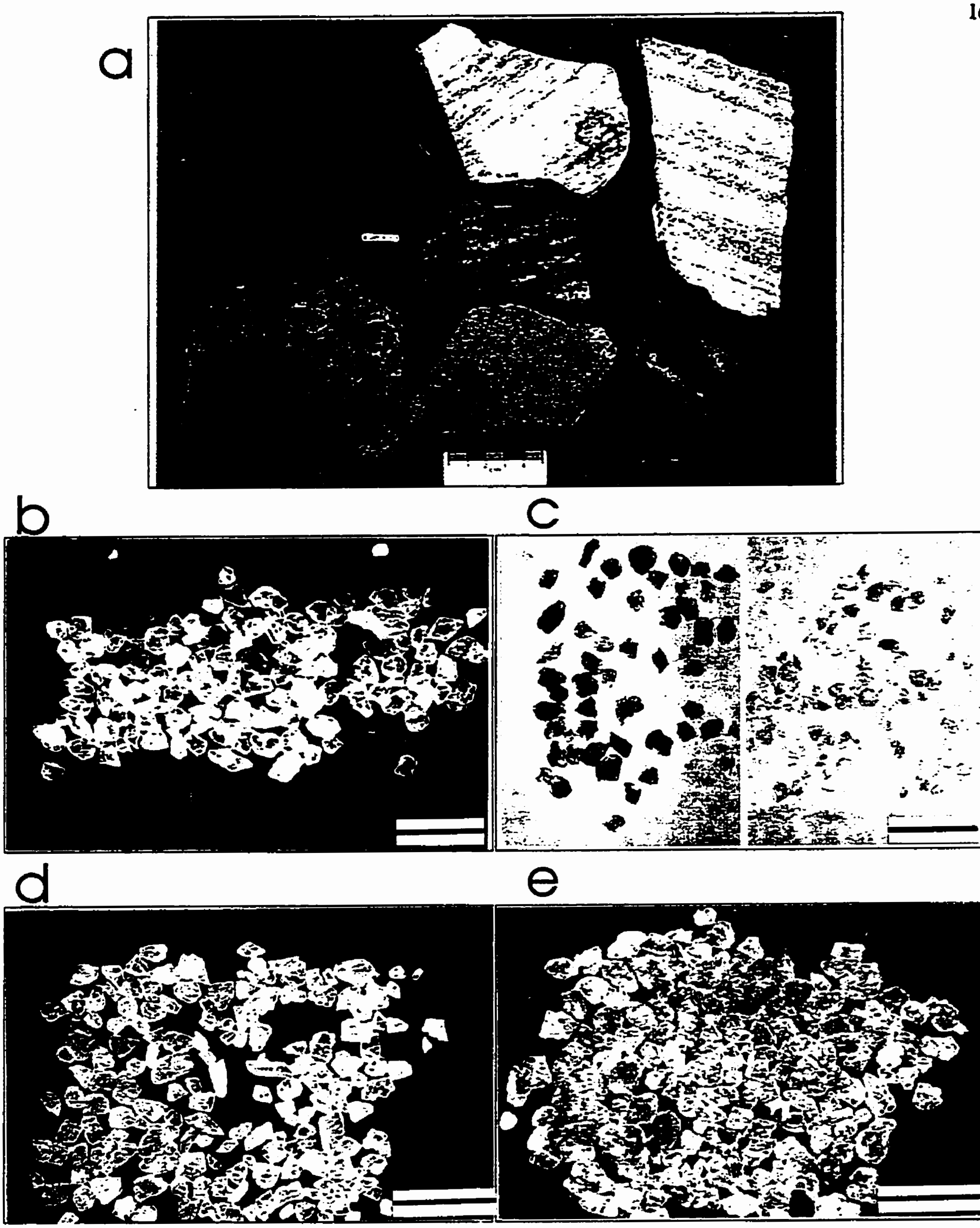

Figure 4.19

apatite or an opaque-oxide mineral. The age of fraction 5 is thus rendered inaccurate and unreliable because, despite being a more precise analysis than fraction 4, the low U concentration makes the age almost totally dependent on the common-Pb correction. The age of fraction 4 is considered the age of post-metamorphic cooling of the Otter Brook gneiss through the closure temperature for titanite (Table 4.1).

The $^{40}Ar/^{39}Ar$ spectrum of phlogopite (Figure 4.20a) from a calc-silicate lens in the Otter Brook gneiss defines a plateau over steps 10-13, and yields an age of 421 ± 6 Ma. This is within error of the total gas age (Table A3.2) of 420 ± 2 Ma. The data fit a line well ($\Sigma S = 8.3$, $n = 7$) on the isotope correlation diagram (Figure 4.20b), with an inverse ordinate intercept apparent age of 423 ± 4 Ma and an $^{40}Ar/^{36}Ar$ ratio of ~165. The $^{40}Ar/^{36}Ar$ ratio is lower than the present-day atmospheric value; however, the cluster of points near the lower portion of this diagram makes for a large uncertainty in the Y-intercept. The 421 ± 6 Ma plateau age is taken to represent the age of post-metamorphic cooling of this sample through the phlogopite closure temperature (Table 4.1; Appendix A4.3).

Sammys Barren granite

The Sammys Barren granite was selected for zircon U-Pb analysis because it is a relatively undeformed, unmetamorphosed granite which, based on field relations (Chapter 2), is thought to be the youngest plutonic unit in the Blair River inlier. The selected sample (Figure 4.21a) is coarse-grained and comprises approximately equal amounts of oligoclase and microcline, subordinate quartz, and minor amounts of yellow titanite with well-defined cleavage planes, and epidote and chlorite pseudomorphs after biotite. The least magnetic fraction of zircons consisted mostly of small, stubby, doubly terminated grains with sharp tips and corners on both the prismatic and

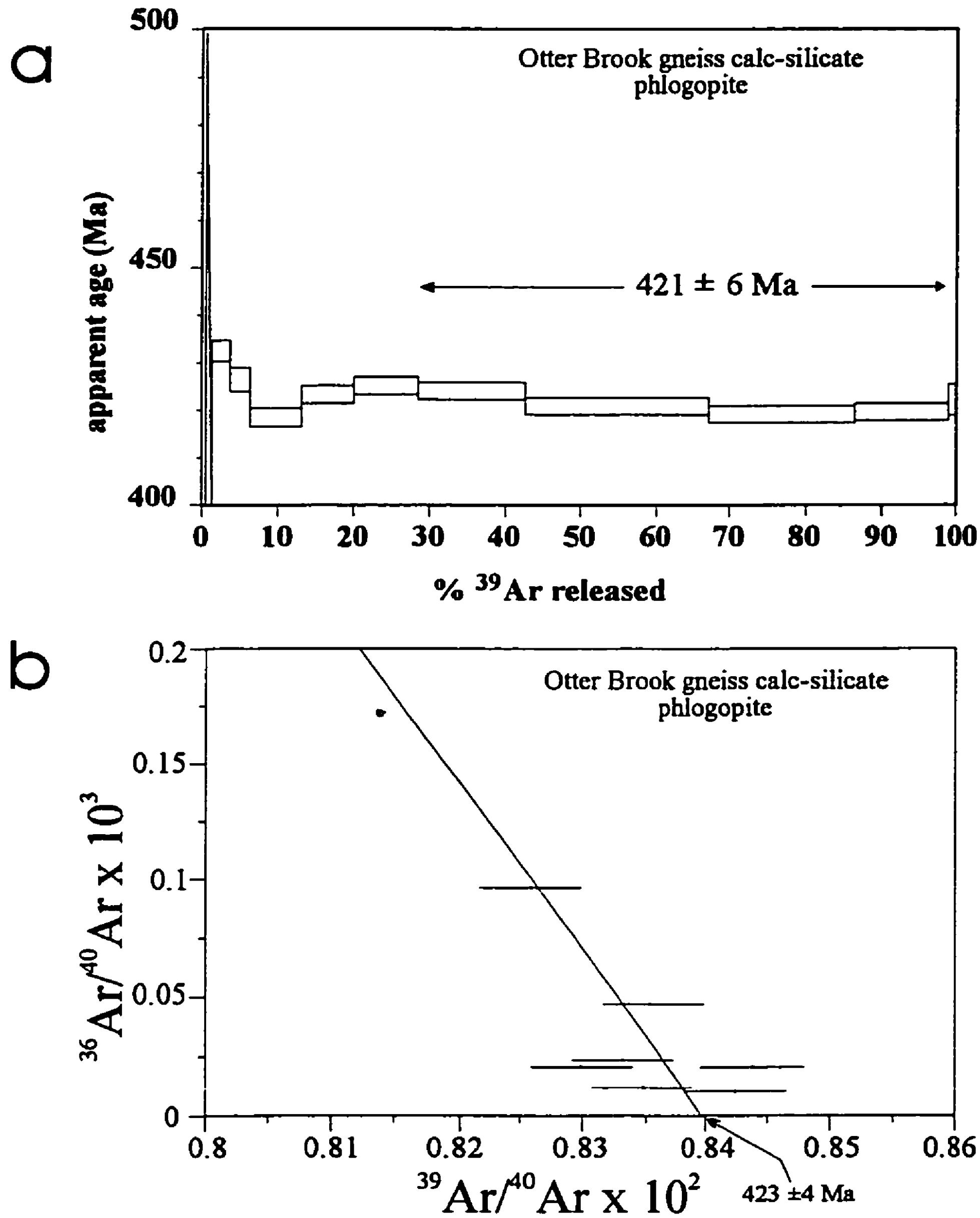

Figure 4.20 - (a) $^{40}Ar/^{39}Ar$ spectral diagram for phlogopite data from a calc-silicate lens in the Otter Brook gneiss (sample BVM-90-137). (b) Isotope correlation diagram for argon data. The indicated plateau age (steps 10-13; Table A4.2) is interpreted to indicate the time of post-metamorphic cooling through the closure temperature for phlogopite of this composition (Ann_{12}, $T_c = 410 \pm 50°C$).

a

b

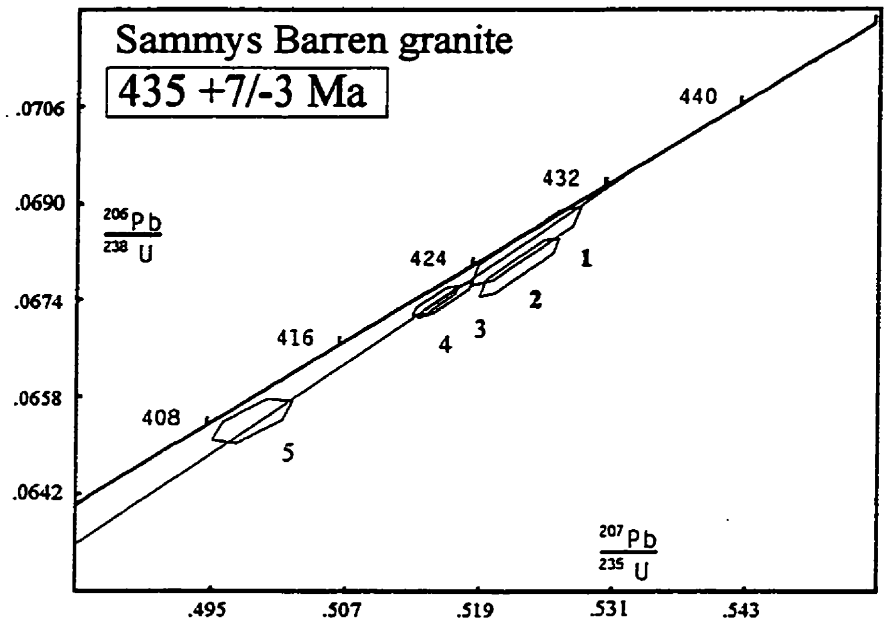

Figure 4.21 - Outcrop photograph and U-Pb concordia diagram for zircon data from the Sammys Barren granite.

(a) Sampled outcrop of Sammys Barren granite (BVM90-132). The dated sample is in direct intrusive contact with the Fox Back Ridge diorite/granodiorite. The sample is undeformed, and contains non-perthitic microcline and large euhedral titanite with well-developed cleavages.

(b) Concordia diagram for U-Pb data of prismatic zircon grains (photomicrograph of dated fractions is not available) from the Sammys Barren granite (sample BVM90-132).

pyramidal faces. This morphology contrasts with that of most of the other prismatic zircons analysed in this study in that they had rounded edges and tips. The selected sample and U-Pb concordia diagram are shown in Figure 4.21.

Five fractions of zircon were analysed from the Sammys Barren granite and all are discordant (Figure 4.21b). Abraded fractions 1-4 cluster close to concordia and do not constrain precisely a discordia line. Therefore, fraction 5 was purposely not abraded in order to provide a more discordant point and thus enable more precise regression through the other four points. Fraction 2 plots to the right of the trend of the other four fractions, perhaps because of a small amount of inheritance. Fractions 1, 3, 4, and 5 lie on a discordia line with a 18.4% probability of fit and an upper intercept age of 435 +7/-3 Ma. The upper intercept is interpreted to represent the approximate age of intrusion of the Sammys Barren granite because of the prismatic zircon morphology.

Gneissic anorthosite

Two fractions of titanite were separated from a highly deformed and altered sample from a small outcrop of gneissic anorthosite on Polletts Cove River. This sample contains a swirled gneissic foliation defined by wispy green layers of chlorite and epidote. It contains plagioclase, biotite, epidote, chlorite, quartz, and titanite. Plagioclase is extensively altered to white mica. Epidote and chlorite are alteration products and fracture-filling minerals. Titanite occurs throughout the rock in 0.5 mm to 2 mm clusters of small (0.1 mm) spindle-shaped grains, a morphology typical of metamorphic titanite.

Two titanite fractions were analysed from this sample. Fraction 1 contained dark brown grains which were relatively rare in the total population. Fraction 2 consisted of the more abundant tan titanite. Titanite from fraction 2 overlaps concordia within error (Figure 4.22b), but fraction 1 contains a higher U and lower common Pb concentration (Table A4.1). Both fractions yield $^{206}Pb/^{238}U$ ages of 427 ± 2 Ma, indicating the time of post-metamorphic cooling through the titanite closure temperature (Table 4.1).

Red Ravine syenite

The Red Ravine syenite shares some important textural similarities with the Sammys Barren granite and contrasts with the Lowland Brook Syenite (Chapter 2), but the chemistry of the syenite differs significantly from most of the late granites (Chapter 3). The sample selected for U-Pb analysis (Figure 4.19) is an undeformed, coarse-grained, subequigranular, red syenite that contains microcline, plagioclase, chlorite, titanite, Fe-Mg oxide minerals, and accessory epidote, apatite, and zircon. Zircon grains are small and prismatic with sharp corners and tips and are morphologically similar to those in the Sammys Barren granite.

Titanite occurs as large yellow grains with well-defined cleavages and crystal faces. The titanite habit suggests a magmatic origin and contrasts with titanite of metamorphic origin from other samples which are commonly spindle-shaped grains or rims around Fe-Ti oxide minerals. Three fractions of titanite were separated for U-Pb analysis. Fractions 1 and 3 were large grains bounded by crystal faces or fractured along cleavage planes and fraction 2 comprised small irregularly shaped grain fragments. The bulk sample from which these fractions were separated is shown in Figure 4.19.

The titanite analyses are discordant, and their ages do not overlap. Fraction 3 contains a very high component of common Pb which could not be corrected for by the model of Stacey and Kramers (1975) and hence the age of this fraction is unreliable. It plots far to the right of

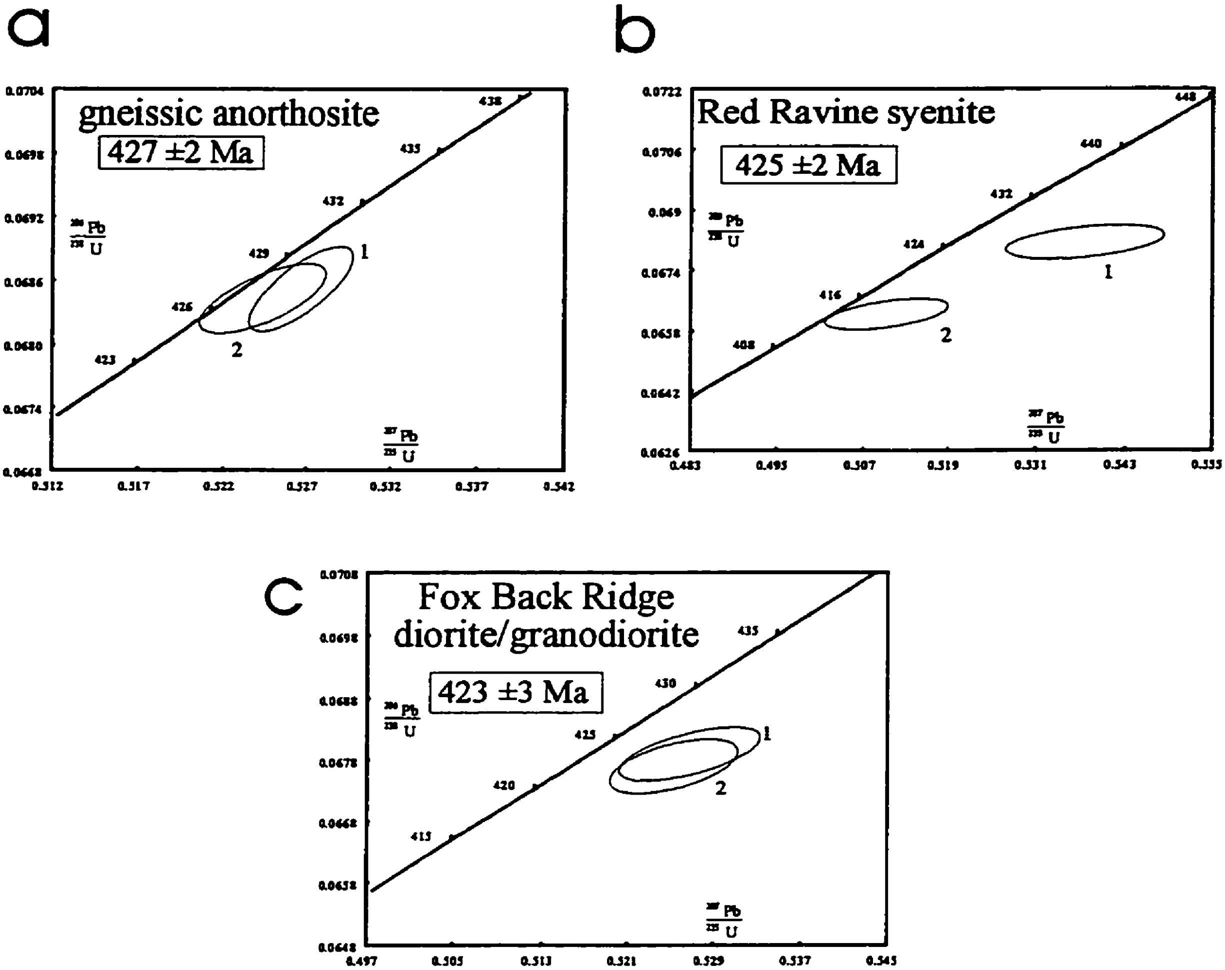

Figure 4.22 - U-Pb concordia diagrams for titanite data from minor units. (a) Data from gneissic anorthosite in the Polletts Cove River gneiss (BVM91-694). Fractions 1 and 2 are the brown and tan titanite fractions, respectively. (b) Data from the bladed yellow titanite in the Red Ravine syenite (BVM90-121). (c) Data from brown titanite in the Fox Back Ridge diorite/granodiorite (BVM91-553). All indicated ages are $^{206}Pb/^{238}U$ ages and are considered the time of post-crystallisation or post-metamorphic cooling through the closure temperature for titanite.

concordia with very large errors and is not included on the concordia diagram to allow clearer representation of the other two fractions. Fractions 1 and 2 plot nearer to concordia with $^{206}Pb/^{238}U$ ages of 425 ± 2 Ma and 414 +1/-3 Ma respectively (Figure 4.22). An igneous origin for the titanite is inferred from morphology and this is supported by the $^{208}Pb/^{206}Pb$ ratio which is an order of magnitude higher than that of metamorphic grains. Because ^{208}Pb is a stable daughter of ^{232}Th, and Th is generally more mobile in a melt than during metamorphism, $^{208}Pb/^{206}Pb$ ratios are generally higher in titanite of igneous origin. The $^{206}Pb/^{238}U$ age of fraction 1 is taken to represent the time of post-crystallisation cooling through the titanite closure temperature (Table 4.1).

Fox Back Ridge diorite/granodiorite

Both titanite and hornblende were separated from a sample of the Fox Back Ridge diorite/granodiorite (Figure 4.19a). The sample is a granodiorite that is deformed by brittle fractures, but lacks a pervasive deformational foliation. It contains hornblende as both recrystallised phenocrysts and as small, more highly altered groundmass grains, plagioclase, K-feldspar, epidote, and titanite. Hornblende phenocrysts are ~2.5 mm to ~4 mm in diameter and retain pseudomorphic amphibole outlines, but are recrystallised into small aggregates. The individual grains in the aggregates are relatively unaltered but are compositionally zoned with actinolitic compositions near the centres grading into magnesio-hornblende toward the edge. Feldspar phenocrysts are also partly recrystallised to ~0.5 mm equidimensional aggregates around grain edges. Groundmass hornblende is anhedral, contains numerous dusty inclusions, and is commonly partially altered to biotite and chlorite along fractures. Plagioclase is present only in the groundmass as small (~0.6mm) subhedral laths and is highly sericitized. K-feldspar grains are also highly altered. Epidote is associated with zones of intense alteration. Some titanite grains are euhedral with well-defined cleavage planes, but most grains are subhedral to anhedral with inclusions of groundmass minerals. None of the grains have the spindle-shaped morphology typical of metamorphic titanite and, therefore, are considered to be of igneous origin.

The sample and bulk titanite fraction are shown in Figure 4.19. Two fractions of brown titanite from the Fox Back Ridge unit overlap within error and have $^{206}Pb/^{238}U$ ages of 423 ± 3 Ma. This age is taken to indicate the time of post-crystallisation cooling through the closure temperature of titanite (Table 4.1). The igneous origin of the analysed titanite is also indicated by the high $^{208}Pb/^{206}Pb$ ratios.

In order to avoid the altered groundmass hornblende, only large clean, translucent hornblende grains were selected from this sample. Two hornblende separates were picked from the same coarse concentrate and irradiated in different batches.

Age spectra and an isochron plot are shown in Figure 4.23. Both $^{40}Ar/^{39}Ar$ spectra show broadly similar patterns, but fraction 2 was analysed with smaller temperature increments, and thus its spectrum has higher resolution over the low temperature steps. The spectra have a typical multi-phase pattern (e.g., Hanes, 1991), and this is supported by the anomalous $^{37}Ar/^{39}Ar$ spectra over the first 30% of the gas released. Over the latter part of the gas release, there is good agreement between the two analyses, and the microprobe-determined apparent Ca/K ratio agrees closely with the measured $^{37}Ar/^{39}Ar$.

The weighted mean ages of the latter portion of the spectra are 419 ± 4 Ma for fraction 1 and 422 ● 3 Ma for fraction 2. Only the data from fraction 2 produce an acceptable isotope

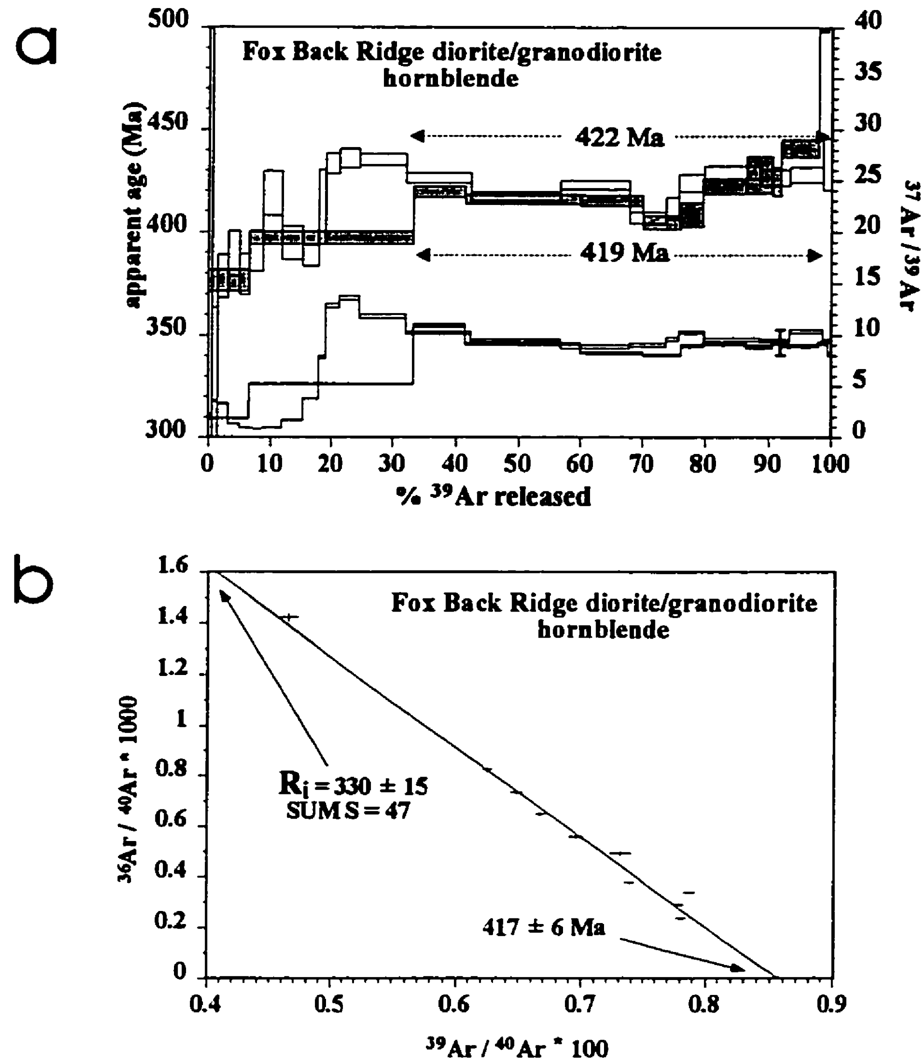

Figure 4.23 - (a) $^{40}Ar/^{39}Ar$ spectral diagram and (b) isotope correlation diagram for hornblende from the Fox Back Ridge diorite/granodiorite (sample BVM91-553). The ages indicated on the spectral diagram are weighted-mean ages over the indicated temperature steps, not plateaux. Fraction 1 is shaded and fraction 2 is white. The best estimate for the time of post-metamorphic cooling through the hornblende closure temperature is considered to be that indicated by the isotope correlation diagram. The lower spectra are $^{37}Ar/^{39}Ar$ and bar at lower right indicates the $^{37}Ar/^{39}Ar$ range calculated from microprobe Ca/K analyses.

correlation diagram (Figure 4.23b). These data indicate an inverse ordinate intercept apparent age of 417 ± 6 Ma and an apparent $^{40}Ar/^{36}Ar$ ratios of 330 ● 15. The ΣS of the line is 47 (n = 10) which indicates excess scatter in the data, a result that is consistent with the relatively discordant nature of the age spectrum. The age obtained from the isochron plot is here considered more satisfactory than ages derived from the age spectra because the age spectra do not form plateaux. Therefore, 417 ● 6 Ma is interpreted to indicate the time of post-metamorphic cooling through the hornblende closure temperature (Table 4.1).

Amphibolite and metagabbro

Two samples of amphibolite and one sample of metagabbro from widely separated areas in the Blair River inlier were selected for $^{40}Ar/^{39}Ar$ analysis of hornblende. A sheared amphibolite sample from adjacent to the Wilkie Brook fault zone contains hornblende, plagioclase, biotite, quartz, and Fe-Ti oxide minerals. The hornblende grains form large elongate (up to 2mm long, ~0.2mm wide) poikiloblastic blades aligned within the foliation. These grains overgrew finely recrystallised groundmass minerals including quartz and opaque minerals but the foliation as defined by feldspars and matrix biotite wraps around the larger porphyroblasts. At the time it was selected for analysis, the outcrop from which this sample was obtained was mapped as part of the Blair River inlier in the Wilkie Brook fault zone. Subsequent mapping revealed that it is in the Wilkie Brook fault zone adjacent to the Aspy terrane. This type of unaltered fresh, well-foliated, biotite-amphibolite is rare in the Blair River inlier, but common in the Cape North Group of the Aspy terrane near the Wilkie Brook fault zone (Wunapeera, 1992). Hornblende from this sample was analysed in an attempt to constrain the age of fault zone movement because the textures suggests recrystallisation as a result of shear on the Wilkie Brook fault zone.

A massive amphibolite sample from the Polletts Cove River gneiss in the High Capes area consists almost entirely of actinolitic hornblende and minor amounts of opaque minerals. Chloritic alteration occurs along fractures. The actinolitic hornblende is coarse grained (up to 3 mm) and grains are subhedral and blocky. A metagabbro sample from within the Polletts Cove River gneiss contains hornblende, plagioclase, and minor opaque minerals. It retains relict subophitic texture, and pyroxene is altered to aggregates of hornblende. The recrystallised hornblende aggregates are about 2 mm across and comprise individual grains on the order of 0.3 mm in diameter.

Hornblende from the sheared quartzofeldspathic amphibolite produced a discordant $^{40}Ar/^{39}Ar$ spectrum (Figure 4.24a) which provides no meaningful age data. The data plot on an isotope correlation diagram (Figure 4.24b) with an inverse ordinate intercept apparent age of 382 ± 4 Ma, and an apparent $^{40}Ar/^{36}Ar$ ratio of ~345. The fit of the line is poor ($\Sigma S = 94.9$, $n = 9$). The age is comparable to the $^{40}Ar/^{39}Ar$ hornblende ages from amphibolite and metabasite in the Aspy terrane near the Wilkie Brook fault zone which are ca. 371-384 Ma (Wunapeera, 1992; Keppie et al., 1992). Therefore, the isotope correlation age is interpreted as the age of final cooling through the hornblende closure temperature for Aspy terrane rocks in this higher grade segment of the Wilkie Brook fault zone (see Chapter 2).

Hornblende from the amphibolite sample in the High Capes area produced a discordant, saddle-shaped $^{40}Ar/^{39}Ar$ spectrum (Figure 4.24c) that provides no geologically meaningful age information. An isotope correlation diagram (not shown) provides no additional insight.

The $^{40}Ar/^{39}Ar$ spectrum of hornblende from the metagabbro sample from Polletts Cove River gneiss (Figure 4.24d) is also discordant, but the shape of the $^{37}Ar/^{39}Ar$ spectrum suggests

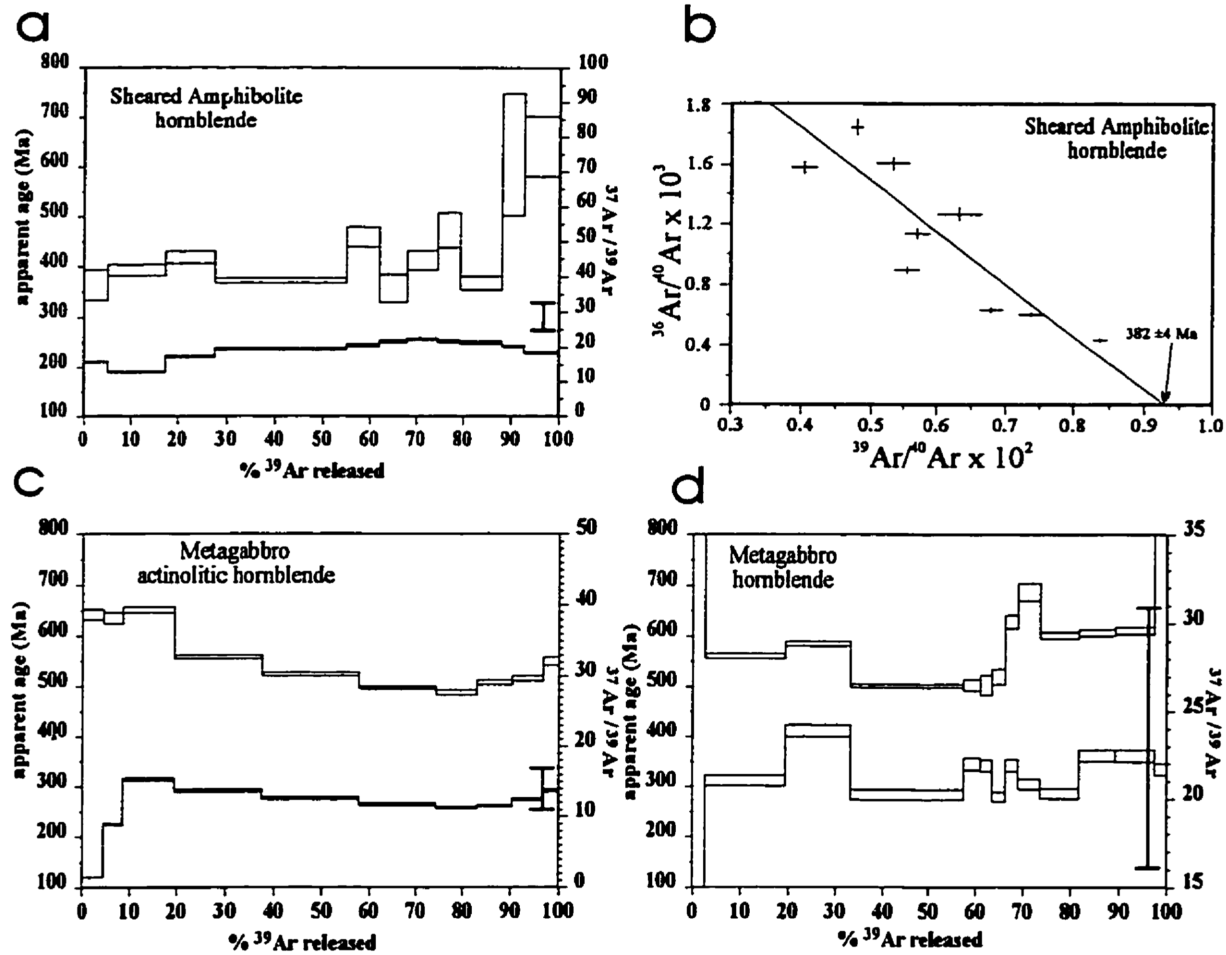

Figure 4.24 - ^{40}Ar/^{39}Ar spectral diagrams and isotope correlation diagram for hornblende from amphibolite and metagabbro samples. (a) Spectral diagram and (b) isotope correlation diagram for sheared amphibolite (CW86-3708). (c) Spectral diagram for metagabbro with actinolitic hornblende (SB85-1081). (d) Spectral diagram for metagabbro in the Polletts Cove River gneiss (RR85-2105). Spectra (a) and (c) show excess-argon type patterns and spectrum (d) appears to be affected by contamination by another phase. None of the spectra indicate geologically meaningful ages but the isotope correlation diagram in (c) suggests an age that is comparable to amphibolites in the Aspy terrane (see text). The lower spectrum is ^{37}Ar/^{39}Ar and bar at lower right indicates the ^{37}Ar/^{39}Ar range calculated from microprobe Ca/K analyses.

multiphase contamination. The contaminant phase could be fine chlorite formed by alteration at grain edges, but the wide range in microprobe-determined Ca/K for hornblende in the sample suggests that more than one composition of hornblende is present. Because of the internal discordance of the spectrum and fluctuations in the apparent Ca/K ratios, the $^{40}Ar/^{39}Ar$ data from this sample provide no meaningful age information.

Meat Cove and unnamed marble

Two samples of marble were selected for $^{40}Ar/^{39}Ar$ analysis. A sample of Meat Cove marble was selected from near the faulted boundary zone with the Lowland Brook Syenite. This sample is compositionally layered and extensively altered along fractures. Where less altered, the sample consists almost entirely of diopside, with thin layers rich in muscovite. Muscovite grains were separated from the least altered portions of the sample. The other sample is from a marble lens within the Wilkie Brook fault zone. The lens is ~1 m wide and highly sheared along the edges, but is relatively undeformed near the centre. The sample contains carbonate, diopside, partially serpentinized olivine, phlogopite, and spinel.

The $^{40}Ar/^{39}Ar$ spectra (Figure 4.25a) for two fractions of muscovite from the Meat Cove marble have internally discordant spectra with shallow saddle-shapes and erratic spectra over the initial 10% of gas released. Data for the final 90% of ^{39}Ar released from fraction 2 are plotted on the isotope correlation diagram in Figure 4.25b. The inverse ordinate intercept age is 428 ± 7 Ma with a good line fit ($\Sigma S = 15$, $n = 11$) and an $^{40}Ar/^{36}Ar$ ratio of 670. The ca. 428 Ma age is interpreted to represent the time of post-metamorphic cooling through the closure temperature for muscovite (Table 4.1).

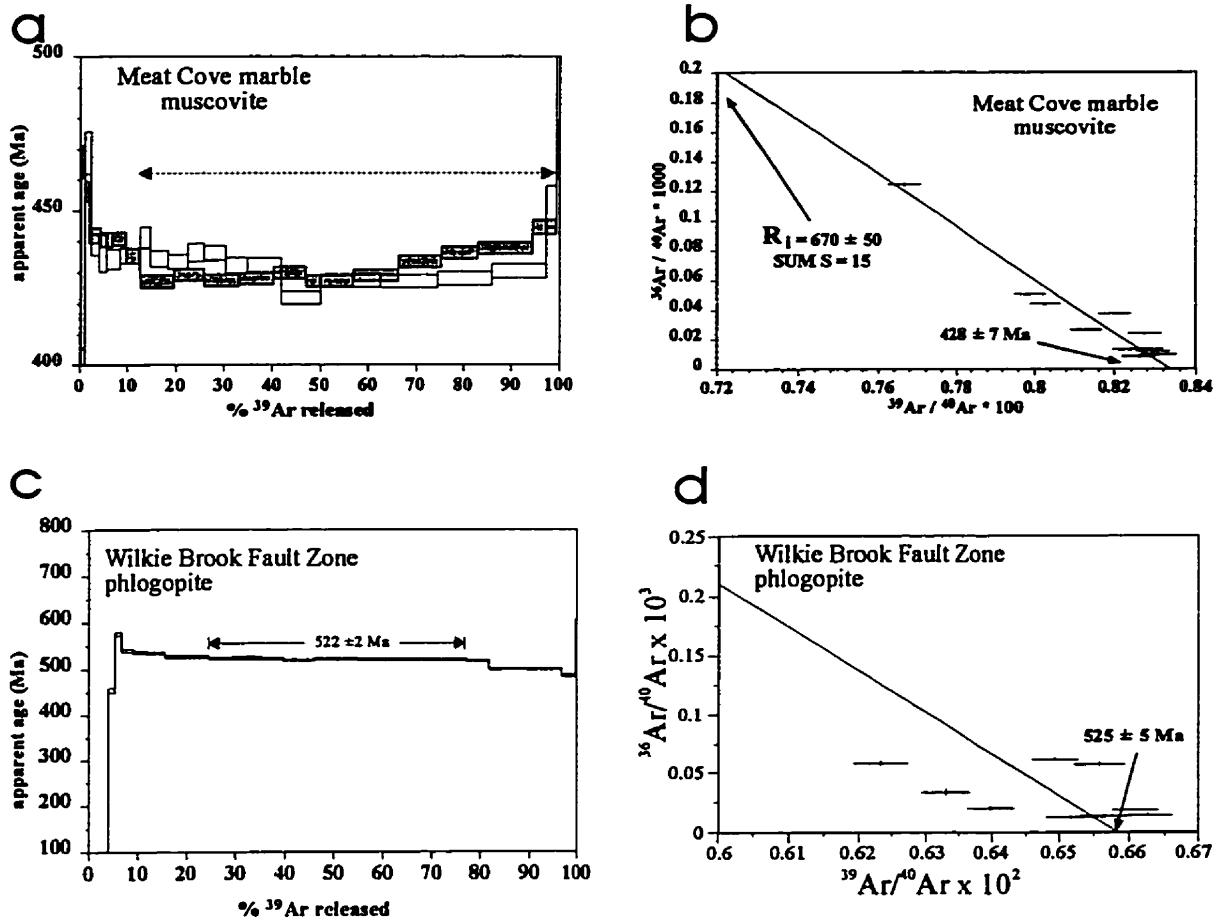

Figure 4.25 - $^{40}Ar/^{39}Ar$ spectral and isotope correlation diagrams for marble samples. (a) Data for Meat Cove marble; fraction 1 is shaded and fraction 2 is white. The segments indicated by the dashed line are the segments used in the isotope correlation diagram in (b). The age indicated on the isotope correlation diagram is interpreted to be the time of cooling of this unit through the closure temperature for muscovite. (c) Spectral diagram and (d) isotope correlation diagram for a marble lens in the Wilkie Brook fault zone. The near-plateau age is taken to indicate the time of cooling through the closure temperature of this composition of phlogopite ($Ann_{.5}$ = 449 ± 51°C).

Phlogopite from marble in the Wilkie Brook fault zone yielded an $^{40}Ar/^{39}Ar$ spectrum that nearly defines a plateau (Figure 4.25c) with an apparent age of 522 ± 2 Ma. The data fit poorly ($\Sigma S = 86$, $n = 10$) a line on the isotope correlation diagram (Figure 4.25d) but the best-fit line indicates an inverse ordinate intercept age of 525 ± 5 Ma. The 522 ● 2 Ma near-plateau age is here taken to represent the time of cooling through the phlogopite closure temperature (Table 4.1). This probably records the time of cooling of this foreign block because the block is located within a younger (see Chapter 2) chlorite-grade shear zone and contains spinel augen wrapped by sheared phlogopite and serpentine after forsterite along the edges of the lens, but the centre of the lens (where the sample was obtained) contains relatively fresh forsterite and unfoliated phlogopite.

4.3 Summary and discussion

A minimum protolith age of 1217 Ma and a metamorphic age of 1035 Ma were obtained from U-Pb analyses of igneous zircon grains in the Sailor Brook gneiss. The crystallisation age of the Lowland Brook Syenite is ca. 1080 Ma based on U-Pb analysis of igneous zircon grains. Metamorphic zircon grains from the Red River Anorthosite Suite yielded an age of ca. 996 Ma. Igneous zircon grains from the Otter Brook gneiss yielded a protolith age of ca. 978 Ma. The Sammys Barren granite crystallised at ca. 435 Ma. Titanite $^{206}Pb/^{238}U$ ages are remarkably consistent in the widely separated metamorphic and igneous rock samples (weighted mean of 425 ● 1 Ma for the seven ages in Table 4.2). These include titanite grains of different sizes, habits, morphologies, origins, and isotopic compositions. Given the many factors that may affect closure temperature (e.g., diffusion domain size which may be related to grain size, cooling rate, mineral composition, fluid composition, fluid activity, and strain rate; Dodson, 1973; Mezger et al., 1991; Cherniak, 1993) and the wide variety of analysed titanite, it is noteworthy that all of the precise titanite analyses fall in such a narrow age range. Relatively rapid cooling, on the order of 9°C/m.y. (e.g., Figure 4.26; contrast with a rate of ~0.6-1.2°C/m.y. for slow cooling according to Scott and St-Onge, 1995), through the closure temperature could explain the similarity in ages among the types of titanite (e.g., Heaman and Parrish, 1991). The consistency of the ages is interpreted to indicate that the Blair River inlier, including Paleozoic igneous and metamorphosed Proterozoic rocks, cooled rapidly through the titanite closure temperature (550 ± 50°C).

Along with the units from which titanite was analysed, other integral parts of the Blair River inlier are the Sammys Barren granite, the Fox Back Ridge diorite/granodiorite, and the anorthosite suite. As described in Chapter 2, the Meat Cove marble unit, the calc-silicate rock in the Otter Brook gneiss, and the two fault zone rocks have uncertain relationships to the remainder of the inlier. Therefore, further constraints are placed on Paleozoic cooling by the assigned crystallisation temperature of 670 ± 50°C (ternary minimum of liquid + Qtz + Kfs at PH_2O = 3 kbar; Luth et al., 1964) for the Sammys Barren granite, closure temperature of 450 ± 50°C for hornblende from the Fox Back Ridge unit, and closure temperature of 405 ± 25°C for rutile from the anorthosite suite. The Blair River inlier was at the surface by the time the Fisset Brook Formation was deposited.

Plotted on a diagram of temperature vs. time (Figure 4.26), these constraints imply a linear cooling path with a slope of approximately 9°C per m.y. However, it should be noted that this excludes data from the two fault zone samples, the Meat Cove marble, and the Otter Brook gneiss calc-silicate, and that the high-temperature constraint provided by the Sammys Barren granite is only a crude estimate. The two fault zone samples are anomalous and were not affected by the metamorphic event that reset or disturbed the radioisotope systematics of the rest of the Blair

Table 4.2 - Summary of geochronology results.

Unit and Mineral	U-Pb	$^{40}Ar/^{39}Ar$	Interpretation
Sailor Brook gneiss			
prismatic zircon	ca. 1217		minimum age of protolith
spheroidal zircon	1035 +12/-10		high-grade metam.
metamorphic titanite	ca. 431*		amphibolite facies metam cooling
hornblende		N.G.M	no interpretation
Lowland Brook Syenite			
prismatic & sph zircon	1080 +5-3		igneous crystallisation
metamorphic titanite	424 ± 3*		amphibolite facies metam cooling
hornblende		N.G.M	no interpretation
Red River Anorthosite Suite			
prismatic & sph zircon	996 +6/-5		contact(?) metamorphism w/charnockite
metamorphic titanite	424 +4/-3*		amphibolite facies metam cooling
metamorphic rutile	410 ± 2*		amphibolite facies metam cooling
hornblende		N.G.M	no interpretation
Otter Brook gneiss			
prismatic zircon	978 +6/-5		igneous crystallisation of protolith
metamorphic titanite	423 ± 6*		amphibolite facies metam cooling
phlogopite		421 ± 6	amphibolite facies metam cooling
Sammys Barren granite			
prismatic zircon	435 +7/-3		igneous crystallisation
Red Ravine syenite			
igneous titanite	425 ± 2*		post-igneous cooling
Fox Back Ridge diorite/granodiorite			
igneous titanite	423 ± 3*		post-igneous cooling
hornblende		417 ± 6	amphibolite facies metam cooling
Gneissic Anorthosite			
metamorphic titanite	427 ± 2*		amphibolite facies metam cooling
Amphibolite and Metagabbro			
actinolitic hornblende (PCRg)		N.G.M	no interpretation
hornblende (WBF)		382 ± 4	post-amphibolite-facies shear on WBF
Other Marbles and Calc-silicates			
muscovite (Meat Cove)		428 ± 2	amphibolite-facies metam cooling
phlogopite (WBF)		522 ± 2	post-metam. cooling (of foreign block?)

Abbreviations: sph = spheroidal, WBF = Wilkie Brook fault zone, N.G.M. = no geologically meaningful age, * = $^{206}Pb/^{238}U$ age,

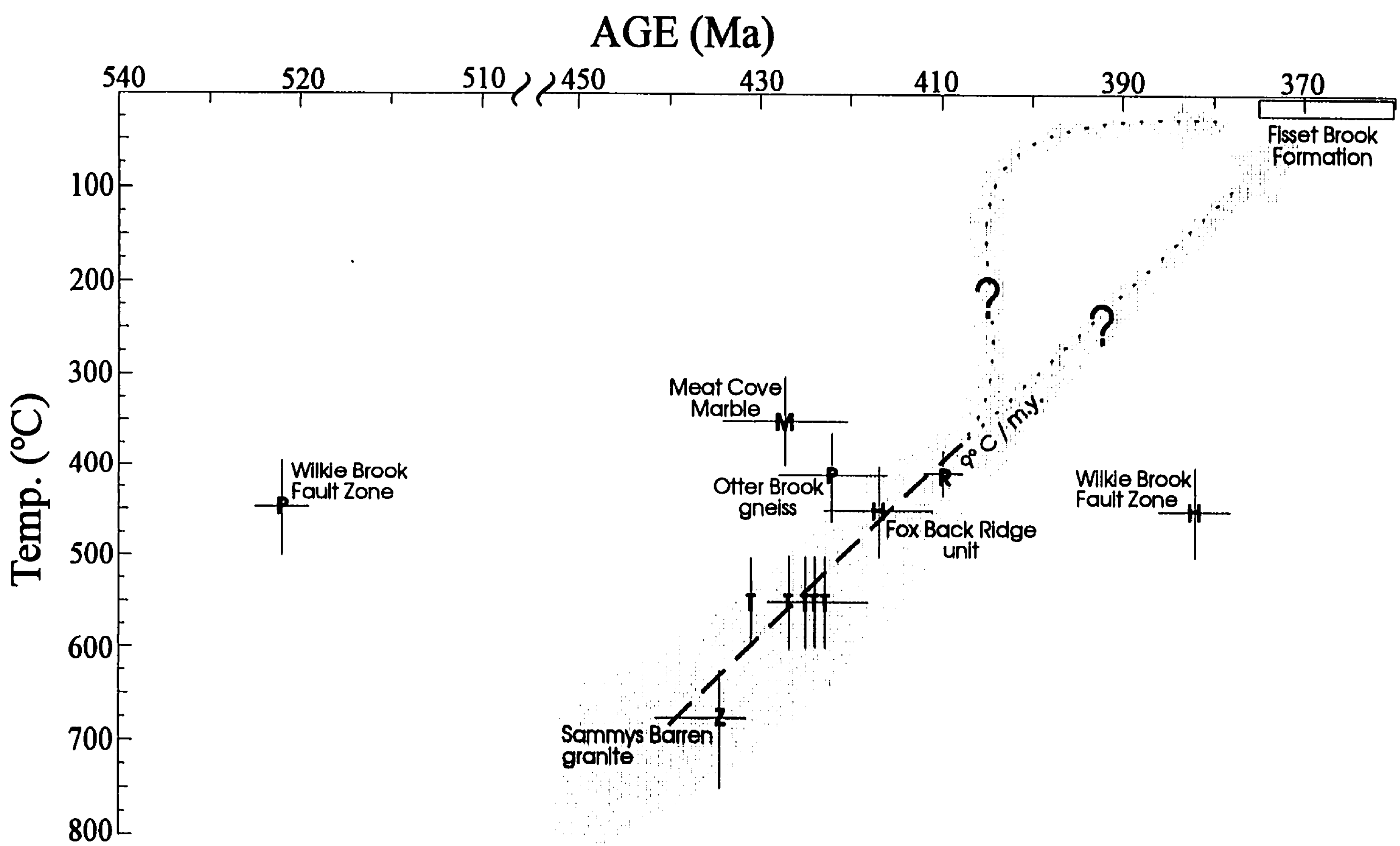

Figure 4.26 - Temperature vs. time path for the Blair River inlier. The indicated rate of ~9°C/m.y. is based on an estimate of the crystallisation temperature of the Sammys Barren granite, and inferred closure temperature for all analysed titanite, hornblende from the Fox Back Ridge unit, and rutile from the Red River Anorthosite Suite. P = phlogopite, M = muscovite, T = titanite, R = rutile, Z = zircon, H = hornblende.

River inlier, perhaps from a once-overlying (or underlying?) metacarbonate unit that is now preserved only in shear zones. The data from the Meat Cove marble and Otter Brook gneiss calc silicate are also off the inferred cooling curve. If all the assumptions involved in construction of the curve are correct (e.g., closure temperatures, crystallisation temperature of the granite), then the Meat Cove marble and calc silicate rock in the Otter Brook gneiss may have been late additions to the the Blair River inlier.

Low temperature data, for example $^{40}Ar/^{39}Ar$ K-feldspar and fission track analyses, are needed to constrain better the cooling history of the Blair River inlier. Two possible low-temperature cooling paths are shown on Figure 4.26.

CHAPTER 5 - Metamorphism

5.1 Introduction

Previous metamorphic studies of the Blair River inlier have been of a reconnaissance nature (Raeside and Barr, 1992) and few attempts have been made to estimate the conditions of metamorphism (Mitchell, 1979; Bekkers, 1993). Documentation of metamorphic mineral assemblages and any potential P-T constraints are therefore important as part of the first systematic account of polymetamorphism in the Blair River inlier.

Metamorphic mineral assemblages in the Blair River inlier can be divided into three generations on the basis of mineralogy and overprinting relations. Proterozoic gneissic and metaplutonic rocks rarely preserve pyroxene-bearing metamorphic mineral assemblages. In most units, however, amphibolite facies metamorphic mineral assemblages predominate and some of these samples contain vestiges of an earlier, higher-grade metamorphic mineral assemblage in low-strain zones and in samples that have a mineralogical, but not a strong deformational, overprint. More highly deformed, foliated amphibolites and schists rarely contain indications of prior metamorphic assemblages. Low-grade rocks are mostly Chl-Ab-Ep schists associated with late shear zones and these overprint all other metamorphic and igneous mineral assemblages. The generalised categories of "high-grade", "amphibolite-facies", and "low-grade" metamorphism, therefore, provide a convenient context for further discussion.

Because high-grade mineral assemblages are poorly preserved and microstructures that are indicative of reactions and textural equilibrium are almost completely obliterated by a secondary metamorphic overprint, the data needed to construct a detailed P-T-t path are not available and the insights they may provide into Grenvillian (e.g., Wodicka, 1994; Jamieson et al., 1994; 1995) or Appalachian (e.g., Burgess et al., 1995) tectonic processes based on comparisons with numerical models of orogens (e.g., England and Thompson, 1984) remain obscure. The section below on high-grade metamorphism, therefore, concentrates on an attempt to derive qualitative and quantitative P-T information from the Sailor Brook gneiss, Red River Anorthosite Suite, charnockitic rocks, and the Otter Brook gneiss in order to document the presence, extent, and general conditions of high-grade metamorphism.

Nearly all samples from the Blair River inlier were affected, to some degree, by one or more amphibolite-facies or lower-grade metamorphic event(s). High-grade, pyroxene-bearing assemblages are commonly partly altered to amphibole-biotite-oligoclase assemblages. In some samples, distinctive alteration textures and relict minerals allow for identification of a high-grade precursor and in other samples metamorphism accompanied by deformation has largely erased any possibility of recognising the pre-existing mineralogy. However, not all amphibolite-facies assemblages were necessarily produced during a single metamorphic event. Other possibilities include retrogression to amphibolite facies conditions following granulite-facies metamorphism and one or more subsequent amphibolite-facies overprinting events.

In Chapter 4 metamorphic titanite grains analysed for U-Pb geochronology were attributed to amphibolite-facies metamorphism and the Silurian titanite ages were interpreted to record the age of post-metamorphic cooling through 550 ± 50°C. However, some important details leading to these inferences were not documented fully. Part of the aim of the section below on amphibolite-facies metamorphism, therefore, is to document the evidence that titanite is part of the amphibolite-facies metamorphic mineral assemblage. Additionally, evidence for the temperature of amphibolite-facies metamorphism is evaluated in an attempt to distinguish between the possibilities of regional post-metamorphic cooling of the Blair River inlier through ca. 550°C after crystallisation of titanite (the preferred interpretation of Chapter 4) versus synchronous widespread growth of titanite below its closure temperature.

Documenting the extent, and constraining the conditions, of metamorphism in the Blair River inlier also has implications for understanding the role of the Blair River inlier in Appalachian orogenesis. For example, Currie (1987b) included the Blair River inlier in the Pleasant Bay Complex (part of the Aspy terrane) based, in part, on what he considered to be evidence for a shared high-grade metamorphic history. Keppie (1990) considered the (presumed) shared metamorphic history to be evidence of a Precambrian linkage between the Blair River inlier, the Pleasant Bay Complex, and the Avalon terrane. Barr and Raeside (1990), however, refuted the correlation based on important differences in metamorphic mineral assemblages.

5.2 Approach to derivation of quantitative P-T data

Quantitative geothermobarometry is difficult in the Blair River inlier due to polymetamorphism and lack of metapelitic or well-equilibrated metabasic rocks. Important metamorphic minerals, such as aluminosilicates, are absent and pyroxenes in almost all samples are exsolved and/or highly altered to hydrous amphibolite- or greenschist-facies minerals. Rare metamorphic garnet is ubiquitously resorbed adjacent to a later generation of Fe-Mg silicate minerals.

Despite the textural disequilibrium of many samples, an attempt is made here to evaluate the potential for preservation of equilibrium assemblages within sub-domains among texturally related sub-assemblages, relict mineral fragments, and reaction-texture assemblages and to provide quantitative constraints on metamorphic conditions using the TWQ multi-equilibrium approach of

Berman (1991), with the amphibole thermodynamic properties of Mader and Berman (1992). Intersections of at least three independent equilibria constitute a P-T estimate if they lie within ±1 kbar and ±50°C after one iteration of exclusion analysis to remove problematic end-member components and intersections more than 1.5 σ from the mean. Intersections that satisfy these criteria are suggestive, but not proof, of an equilibrium assemblage if they comprise two or more independently calibrated equilibria and if the thermodynamic data of included end-member components are reliable. Calibrated and high-confidence reactions are listed in Table 5.1 and are highlighted in the discussion of TWQ diagrams.

Component exclusion analyses and intersection statistics were evaluated by the program INTERSX, an accessory program distributed with TWQ. The standard deviation quoted on TWQ diagrams is a measure of the "tightness" of the cluster of intersections and is not an error on the P-T estimate because it does not include uncertainties in microprobe analyses, thermodynamic properties, and solution models. Calculated P-T estimates are presented accurately on TWQ diagrams, but are rounded to the nearest 0.5 kbar and 10°C in the text in order to avoid false precision. Errors in this technique are assumed to be on the order of ±1 kbar and ±50°C (e.g., Berman, 1991; Jamieson et al., 1995; Burgess et al., 1995). Errors arising from uncertainties in solution models can be large (e.g., Holland and Powell, 1985; Kohn and Spear, 1989) and represent the largest source of error in TWQ results (Berman, 1991).

Compositional data were selected from subsets of 40-120 microprobe analyses per thin section and 10-30 analyses of each mineral. Analyses were concentrated in 2-4 areas per thin section and, where possible, minerals in grain-boundary contact or close proximity were analysed. Matrix grains were analysed as well as porphyroblasts, porphyroclasts, and minerals with reaction textures. Both grain edges and centres were commonly analysed, using BSE images and

Table 5.1 - Selected (calibrated or high-confidence) equilibria used in TWQ analyses and in conventional thermobarometers. Numbered reactions correspond to numbered equilibria on TWQ diagrams, abbreviations correspond to conventional thermobarometers in Table 5.4

Geobarometers		Equilibria			Reference
	Grt-Pl-Cpx-Qtz				
1)		Pyp+12Grs+3Qtz	=	3An+3Di	1,2,3
2)		Alm+Grs+Qtz	=	An+Hd	1,2,4
	Pl-Cpx-Qtz				
3)		Cpx+Qtz	=	An	5,6,7
	Amph-Grt-Cpx-Pl				
4)		3Tr+5Prp+10Grs+3Ab	=	3Prg+18Di+12An	8,9
	Amph-Grt-Pl-Qtz				
5) KS(90)		3Ts+2Prp+4Grs+12Qtz	=	3Tr+12An	10,11,12,13,14,15
6) KS(90)		3Fts+2Alm+4Grs+12Qtz	=	3Ftr+12An	10,11,12,13,14,15
7) KS(89)		3Prg+Prp+2Grs+18Qtz	=	3Tr+6An+3Ab	10,11,12,13,14,15
8) KS(89)		3Fprg+Alm+2Grs+18Qtz	=	3Ftr+6An+3Ab	10,11,12,13,14,15
	Amph-Cpx-Pl-Qtz				
9)		Ts+2Di+2Qtz	=	Tr+2An	10,11,12,13,16,17
10)		Fts+2Hd+2Qtz	=	Ftr+2An	10,11,12,13,16,17
11)		Prg+Di+5Qtz	=	Tr+Ab+An	10,11,12,13,16,17,18
12)		Fprg+Hd+5Qtz	=	Ftr+Ab+An	10,11,12,13,16,17
	Bt-Pl-Ms-Grt				
13)		Phl+3An	=	Ms+Prp+Grs	19

Geothermometers		Equilibria			Reference
	Grt-Cpx				
14) EG(79),GS(87)		Alm+3Di	=	Prp+3Hd	20
	Grt-Bt				
15) FS(78),IM(85)		Ann+Prp	=	Phl+Alm	21,22
	Amph-Grt-Cpx-Pl-Qtz				
16)		3Tr+5Prp+10Grs+3Ab	=	3Prg+12An+18Di	8,9
GP(84)	*Grt-Amph*				23
17)		3Tr+5Alm	=	3Ftr+5Prp	10,11,12,13,14
18)		Ts+Alm	=	Fts+Prp	10,11,12,13,14
19)		3Prg+4Alm	=	3Fprg+4Prp	10,11,12,13,14
	Amph-Pl-Qtz				
20) HBa(94)		Edenite+4Qtz	=	Tr+Ab	24
21) HBb(94)		Edenite+Ab	=	Richterite+An	24
	Opx-Cpx				
22) K(82)nt,L(83)		low-Ca Pyx	=	high-Ca Pyx	25,26
23) K(82)ex,L(83)		En+Hd	=	Fs+Di	25,26

References; (1) Newton and Perkins, 1982; (2) Moecher et al., 1988; (3) Powell and Holland, 1988; (4) Mukhopadhyay et al., 1992; (5) Wood, 1979; (6) Holland, 1981; (7) Gasparik, 1984; (8) Mader and Berman, 1992; (9) Mader et al., 1994; (10) Percival, 1983; (11) Coolen, 1980; (12) Glassley and Sorensen, 1980; (13) Leger and Ferry, 1991; (14) Labotka, 1987; (15) Kohn and Spear, 1989 and 1990; (16) Ferry, 1988; (17) Sharma and Jenkins, (18) Jenkins, 1991; 1994; (19) Ghent and Stout, 1981; (20) Ellis and Green, 1979; (21) Ferry and Spear, 1978; (22) Perchuk and Laurent'eva, 1983; (23) Graham and Powell, 1984; (24) Holland and Blundy (1994); (25) Lindsley, 1983; (26) Kretz (1982) microprobe traverses across some minerals (e.g., garnet) to check for compositional zoning. An average of 2 to 6 analyses from texturally related and compositionally similar grains were used in order to minimise the effects of random analytical error.

Mineral compositions were determined by electron microprobe analysis using standard operating conditions as described in Appendix A5.1. Mineral classification and nomenclature diagrams are presented with tabulated microprobe data as weight% oxides, normalised cations, and end-member components in Appendix A5.2.

5.3 High grade metamorphism

5.3.1 Petrography, mineral chemistry, and textural relations

Samples that contain metamorphic clinopyroxene with or without metamorphic garnet and orthopyroxene occur in the Sailor Brook gneiss, parts of the Red River Anorthosite Suite, the charnockite unit and the Otter Brook gneiss. However, nearly all samples are altered or show retrograde re-equilibration textures which have largely obliterated fine microstructures, for example reaction textures (coronas, symplectites, relict grains, porphyroblast/fabric relations) and equilibrium textures (multigranular aggregates, unexsolved solid solution minerals, compatible minerals with unaltered grain boundaries) that are commonly used to infer metamorphic reactions and evaluate potential equilibrium mineral assemblages (Vernon, 1996). Pyroxene grains in even the best-preserved samples show alteration textures like exsolution of fine-grained Fe-Mg oxide minerals (schillerite in orthopyroxene) or are replaced by fiberous pale green amphibole (uralite in clinopyroxene), exsolution lamellae of plagioclase, and amphibole or biotite rims. In some cases the high-grade metamorphic mineral assemblage may be inferred from relict minerals and distinctive alteration textures. The metamorphic mineral assemblages (observed or inferred) of representative samples from these four units are summarised in (Table 5.3) and compositional and textural relations are discussed below along with an attempt to derive P-T information using qualitative inferences and quantitative geothermobarometry techniques.

Sailor Brook gneiss

Petrography and mineral chemistry

Four samples from the centre of the Sailor Brook gneiss (i.e., samples that are not xenoliths or near the contact zone with the Lowland Brook Syenite), contain hypersthene, diopside, plagioclase (An_{40}), K-feldspar, quartz, and Fe-Ti oxide minerals in a medium-grained (0.3-0.5 mm) granoblastic texture. Thin (~0.5 cm wide) pyroxene-rich layers define a faint metamorphic layering. Hypersthene in all samples is highly altered with fine Fe-Mg oxide mineral inclusions. Diopside is altered to fine-grained amphibole or granular hornblende around grain edges, in fractures and preferentially along exsolution lamellae (Figure 5.1a). Fe-Ti oxide minerals are commonly rimmed by either granular hornblende or acicular radiating biotite. The high-grade assemblage in samples of intermediate composition is interpreted to have been Pl + Hyp + Di + Ox ± Kfs ● Qtz (mineral abbreviations as in Table 5.2) and in more mafic compositions it is Pl + Hyp ● Di + Bt + Ox. The poor preservation of pyroxene and the lack of mineral assemblages that constrain pressure (e.g., garnet) make these samples inappropriate for quantitative geothermobarometry.

Xenoliths in the Lowland Brook Syenite are some of the freshest granoblastic granulite samples (Figure 5.1b). One particularly well-preserved sample contains hypersthene (En_{54-57}), plagioclase (An_{55}), K-feldspar, and Fe-Ti oxide minerals ubiquitously rimmed by orange-brown

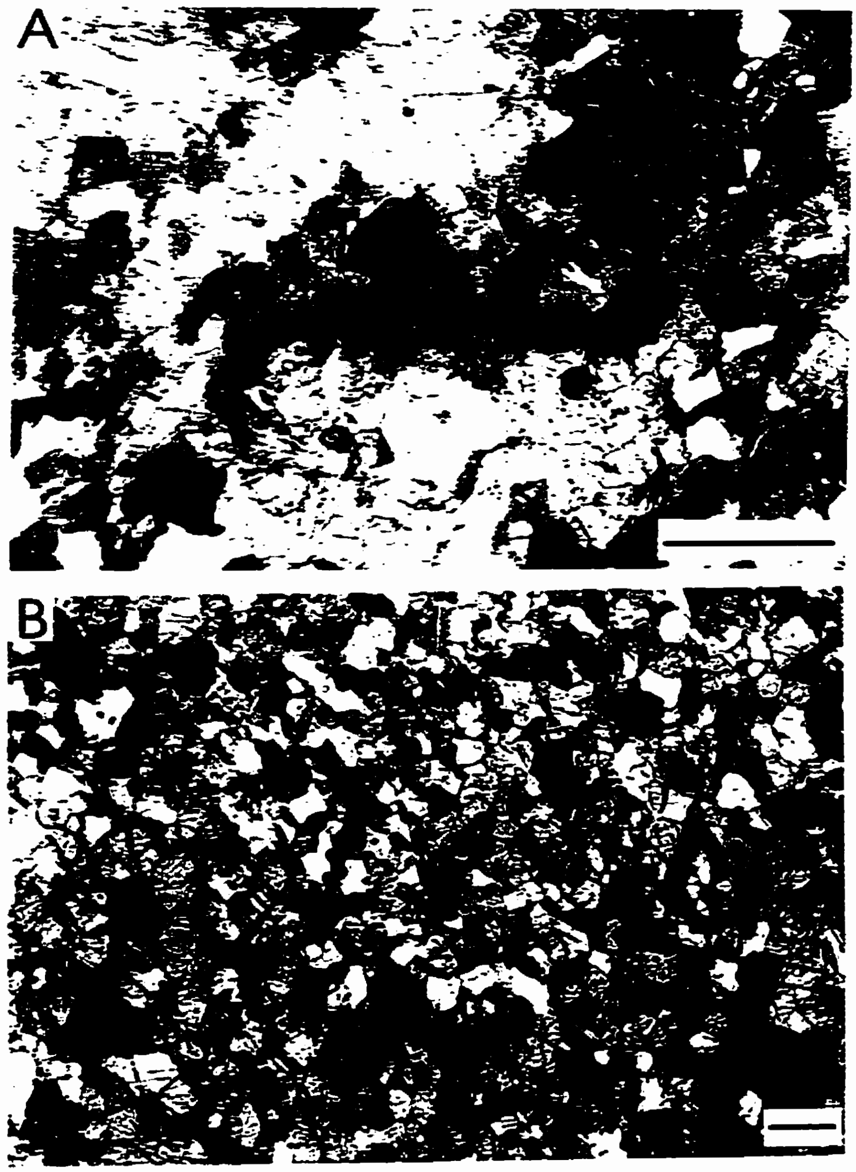

Figure 5.1 - Photomicrographs of granulite samples from the Sailor Brook gneiss.

(a) Highly altered orthopyroxene (brown mass of fine-grained minerals in cluster in upper right) and clinopyroxene altered to uralite (green minerals along left and right edges of the photomicrograph). [BVM91-527; plane-polarized (PP) light; scale bar = 1mm].

(b) Fresh Opx + Pl + Ox + Bt granoblastic mafic granulite [SB85-1048, crossed-polarized light (XP); scale bar = 1 mm].

Table 5.2- Mineral Abbreviations after Kretz (1983).

Act	Actinolite	Ep	Epidote	Ol	Olivine
Agt	Aegirine-augite	Fa	Fayalite	Opx	Orthopyroxene
Ab	Albite	Fs	Ferrosilite	Or	Orthoclase
Aln	Allanite	Fo	Forsterite	Pg	Paragonite
Alm	Almandine	Fprg	Ferropargasite	Phl	Phlogopite
And	Andalusite	Ftr	Ferrotremolite	Pl	Plagioclase
Adr	Andradite	Fts	Ferrotschermakite	Prg	Pargasite
Ann	Annite	Grs	Grossular	Prp	Pyrope
An	Anorthite	Grt	Garnet	Qtz	Quartz
Ath	Anthophyllite	Hbl	Hornblende	Rt	Rutile
Ap	Apatite	Hd	Hedenburgite	Sa	Sanadine
Aug	Augite	Hm	Hematite	Scp	Scapolite
Bt	Biotite	Hyp	Hypersthene	Ser	Sericite
Chl	Chlorite	Ilm	Ilmenite	Sil	Sillimanite
Cpx	Clinopyroxene	Kfs	K-feldspar	Sps	Spessartine
Cal	Calcite	Ky	Kyanite	Sp	Sphalerite
Cum	Cummingtonite	Mag	Magnetite	Tr	Tremolite
Czo	Clinozoisite	Mc	Microcline	Ts	Tschermakite
Di	Diopside	Ms	Muscovite	Ttn	Titanite
En	Enstatite	Ox	Fe-Ti oxide	Zrn	Zircon

Table 5.3 - Metamorphic mineral assemblages of analysed and selected representative samples.

Unit/Sample	High-grade	Amphibolite Facies	Low-grade
Sailor Brook gneiss			
SB85-1048	An$_{55}$+En$_{53}$+Kfs+Ox+Bt$_r$	n/a	n/a
BVM91-527	Kfs$_p$+An$_{40}$+Qtz+Aug+Hyp$_r$+Ox+Bt$_r$	n/a	n/a
CW85-103	An$_{40}$+Qtz+Aug+Hyp$_r$+Qtz+Ox	Pl+Hbl$_r$+Qtz$_r$	Chl$_s$
BVM91-753	Pl+Opx$_R$+Cpx$_R$+Ox+Bt$_r$	uralite,schiller	Chl$_s$
BVM91-534	An$_{35}$+Aug+Hyp$_R$+Ox	Hbl$_r$+Qtz$_r$,schiller	Chl$_s$+Ser$_s$
BVM91-535	Pl+Cpx$_R$+Ox	Hbl+An$_{\sim 20}$+Chl+Bt+Ttn+Qtz	Chl+Ser+Ep
BVM91-773	Pyx$_R$+Pl	Act+Tsc+Pl+Qtz+Ttn	Chl$_s$+Ser$_s$+Ep$_s$
Red River Anorthosite Suite			
BVM91-584 (An)	En$_{70r}$+Di$_{75r}$+An$_{85r}$+Tsc$_r$+Bt$_r$	(?)Mg-Hbl+Pl+Ox	n/a
BVM91-774 (Lay)	Cpx$_R$+Pl (igneous?)	Act-Tsc+Qtz(mosaic)+An$_{30}$+Ox+Bt$_r$	n/a
SB86-3139c (Gab)	Cpx$_R$+Pl (igneous?)	Hbl+Qtz(mosaic)+Ox+Ttn$_r$	Act+Ep+Ser
charnockite			
BVM91-144	An$_{40}$+Pl+Kfsp+Qtz+En$_{60}$+Di$_{70}$+Bt$_r$+Ox	n/a	n/a
BVM91-608	Kfsp+Pl+Qtz+Cpx$_R$+Opx$_R$+Bt$_r$	Hbl+Qtz(mosaic)+Ttn$_r$+Ox	Chl+Kfs+Ep
BVM91-739	An$_{34}$+Kfs+Fprg+Grt+Di$_{70}$+Opx$_R$+Hast	n/a	Ab+Bt+Chl+Ms+Ep
BVM90-057	An$_{45}$+En$_{64}$+Hast+Bt	n/a	Chl$_s$+Ser$_s$
Otter Brook Gneiss			
BVM91-714	An$_{35}$+Kfs+Hast+Grt+Bt+Di$_{40}$	Pl+Kfs+Prg+Qtz+Bt+Ttn	Ab+Chl+Ser
BVM91-717	An$_{40}$+Hast+Grt+Bt	An$_{20}$+Prg+Qtz+Bt+Ttn	Ab+Chl$_r$+Kfs$_r$+Ser
BVM90-137	n/a	Di$_{90}$+Tr+Phl+An$_{3-20}$+Cal+Qtz	n/a

Mineral abbreviations as in Table 5.2. Subscripts and abbreviations: P = perthitic, R = relict, r = rim-forming mineral, s = spotty or localised, n/a = not applicable, An = anorthosite, Lay = layered unit, Gab = leucogabbro, Hast = hastingsite and hastingsitic hornblende biotite (Ann_{40-44}). Hypersthene is not highly exsolved and there is no significant compositional variation within or between grains, but many grains near Fe-Ti oxide minerals have a thin overgrowth of biotite, fine-grained green hornblende, and/or Mg-rich chlorite. Several other xenoliths are very similar to the high-grade samples from the centre of the Sailor Brook gneiss in mineralogy, grain size and texture, but pyroxenes are completely altered and larger (up to 1.5 mm) orange-brown biotite grains surround Fe-Ti oxide minerals.

Other granular, layered but poorly foliated, one- and two-pyroxene gneissic rocks are present in the undivided unit. Several samples contain highly altered orthopyroxene with only slightly altered clinopyroxene. These rocks were probably once part of a larger granulite-facies gneissic complex that included the Sailor Brook gneiss. However, a large granulite terrane cannot be mapped as a single unit because of extensive subsequent amphibolite-facies metamorphism and late displacements along fault zones.

The widespread presence of preserved, relict, or inferred granulite-facies metamorphic mineral assemblages in the Sailor Brook gneiss, and in similar samples throughout the undivided unit, suggests that a large portion of the Blair River inlier underwent regional high-grade metamorphism. The preservation and enhancement of granular textures and two-pyroxene mineral assemblages in gneissic xenoliths in the Lowland Brook Syenite suggests that the syenite intruded the Sailor Brook gneiss at granulite-facies conditions.

P-T constraints

Widely applicable and well-calibrated geobarometric equilibria for granulite-facies rocks require aluminosilicate, garnet, and/or olivine (cf., Essene, 1982; 1989) and Fe-Mg exchange geothermometers are known to be very sensitive to retrograde re-equilibration in even the best of cases (e.g., Pattison and Newton, 1988). Therefore, no samples from the Sailor Brook gneiss were considered adequate for quantitative geothermobarometric analysis. However, the two-pyroxene metamorphic mineral assemblages imply granulite-facies conditions in the general range of 700-1000°C and 4-12 kbar (Turner, 1968; Anovitz and Essene, 1989). At relatively higher pressures in mafic and ultramafic granulite, orthopyroxene reacts with plagioclase to produce garnet and defines a high-P granulite subfacies characterised by Grt + Cpx ± Opx assemblages in metabasite (Green and Ringwood, 1967). The lack of garnet in the most mafic, least siliceous, Opx + Pl ± Qtz samples from the Sailor Brook gneiss, xenoliths in the syenite, and in the undivided unit suggests fairly typical, moderate pressure, granulite-facies regional metamorphic conditions of about 6-8 kbar and 700-850°C (e.g., Newton, 1983; Bohlen, 1987; Harley, 1989; Essene, 1989).

Red River Anorthosite Suite

Petrography and mineral chemistry

Preserved or relict pyroxene-bearing metamorphic mineral assemblages are rare in the interior portions of the Red River Anorthosite Suite. Metamorphic minerals are commonly associated with a weak apparent flattening fabric defined in some anorthosite samples by symmetric augen and clusters of mafic minerals and by 3.5-8 mm plagioclase porphyroclasts that are recrystallised along grain boundaries into elongate lenticular zones of 0.5-0.7 mm diameter granular aggregates. The zones of recrystallised plagioclase lack internal or external asymmetry and also appear to be flattening fabrics. In many of the metamorphosed samples that are least affected by subsequent lower-grade alteration, some mineral relicts are preserved from the igneous precursor, but these are commonly partly recrystallised to a texturally and compositionally distinct metamorphic assemblage. As a whole, however, the Red River Anorthosite Suite does not preserve good mineralogical evidence of high-grade metamorphism because mafic rocks of suitable composition are concentrated around the edges of the suite where the amphibolite-facies overprint is most intense.

Orthopyroxene in the Red River Anorthosite Suite is mostly bronzite (En_{70-78}) and hypersthene (En_{59-70}). Bronzite is probably of igneous origin because these grains are large (0.4-1 mm) with fine {100} exsolution lamellae of clinopyroxene. Bronzite has well-defined cleavages along which plagioclase, and Fe-Ti oxide minerals are exsolved. By contrast, metamorphic hypersthene grains are small (0.1-0.25 mm) and lack significant exsolution textures. Hypersthene grains have poorly developed cleavage, and occur as zones of granular aggregates with plagioclase and Fe-Ti oxide minerals around igneous grains.

The most common plagioclase composition in the best preserved samples is calcic andesine and labradorite (An_{45-68}). Unaltered, but partly or completely recrystallised granular-texture plagioclase is also labradorite in plagioclase-rich samples and zones, but these recrystallised grains lose their iridescent-blue hue in hand sample. In anorthosite samples that contain primary pyroxenes, both large igneous and smaller recrystallised plagioclase grains are progressively more calcic (An_{79-88}) in proximity to metamorphic reaction zones with Fe-Mg silicate minerals. Andesine is the most common plagioclase composition in more mafic samples (leucogabbro) from the Red River Anorthosite Suite that preserve high-grade metamorphic textures and minerals. Highly altered plagioclase grains in the Red River Anorthosite Suite are albite or oligoclase and the An content generally varies inversely with the degree of sericitic alteration. In gabbroic samples, clusters of orange-brown biotite rim Fe-Ti oxide minerals and in some deformed samples the biotite rims help define the foliation.

Anorthosite sample BVM91-584 was selected for detailed study because it is one of the very few samples that preserves delicate reaction textures. The sample contains large augen-shaped clusters (0.5-2 cm long dimension) of orthopyroxene that are optically only slightly offset from one another and appear to have once been a single crystal. Subgrains (2-5 mm each) are common in strained and exsolved orthopyroxene megacrysts in other anorthosite bodies including the Labrieville and St-Urbain anorthosite bodies in Quebec (Dymek and Gromet, 1984; Owens and Dymek, 1995). The orthopyroxene subgrains have exsolved plagioclase blebs and lamellae and high Al_{tot} (3-3.75% of total cations) compared to nearby recrystallised metamorphic orthopyroxene (1-2.25% of total cations). No attempt was made to re-integrate plagioclase and pyroxene compositions, but Al_2O_3 is up to 3.5 weight% in the centres of the largest grains. By comparison, the re-integrated or bulk Al_2O_3 of high-Al megacrysts from other anorthosite massifs ranges from 4-12 weight%, but most are in the range 4.5-6 weight% (Ashwal, 1993; Owens and Dymek, 1995). The orthopyroxene clusters in sample BVM91-584 are, therefore, considered to be partly recrystallised high-Al orthopyroxene megacrysts.

The largest orthopyroxene augen are draped by metamorphic reaction rims and smaller augen are altered completely to hornblende (Figure 5.2). On one side of a large auge the reaction zone comprises granoblastic hornblende with remnant fragments of orthopyroxene and rare relict clinopyroxene lamellae. On the other side of the orthopyroxene cluster is an Opx + Pl + Bt symplectite with localised patches of granoblastic hornblende. Orthopyroxene grains in the

Figure 5.2 - Partly recrystallised high-Al orthopyroxene megacryst draped by reaction rims; from the Red River Anorthosite Suite.

(a) Recrystallised orthopyroxene megacryst (BVM91-584; XP; scale bar = 1 mm)

(b) Photomicrograph in plane polarized light shows hornblende reaction around the top of the auge and symplectite with local granoblastic zones around the bottom of auge (BVM91-584; PP; scale bar = 1 mm).

(c) Close-up of symplectite and granoblastic reaction zones (BVM91-584; PP: scale bar = 1 mm).

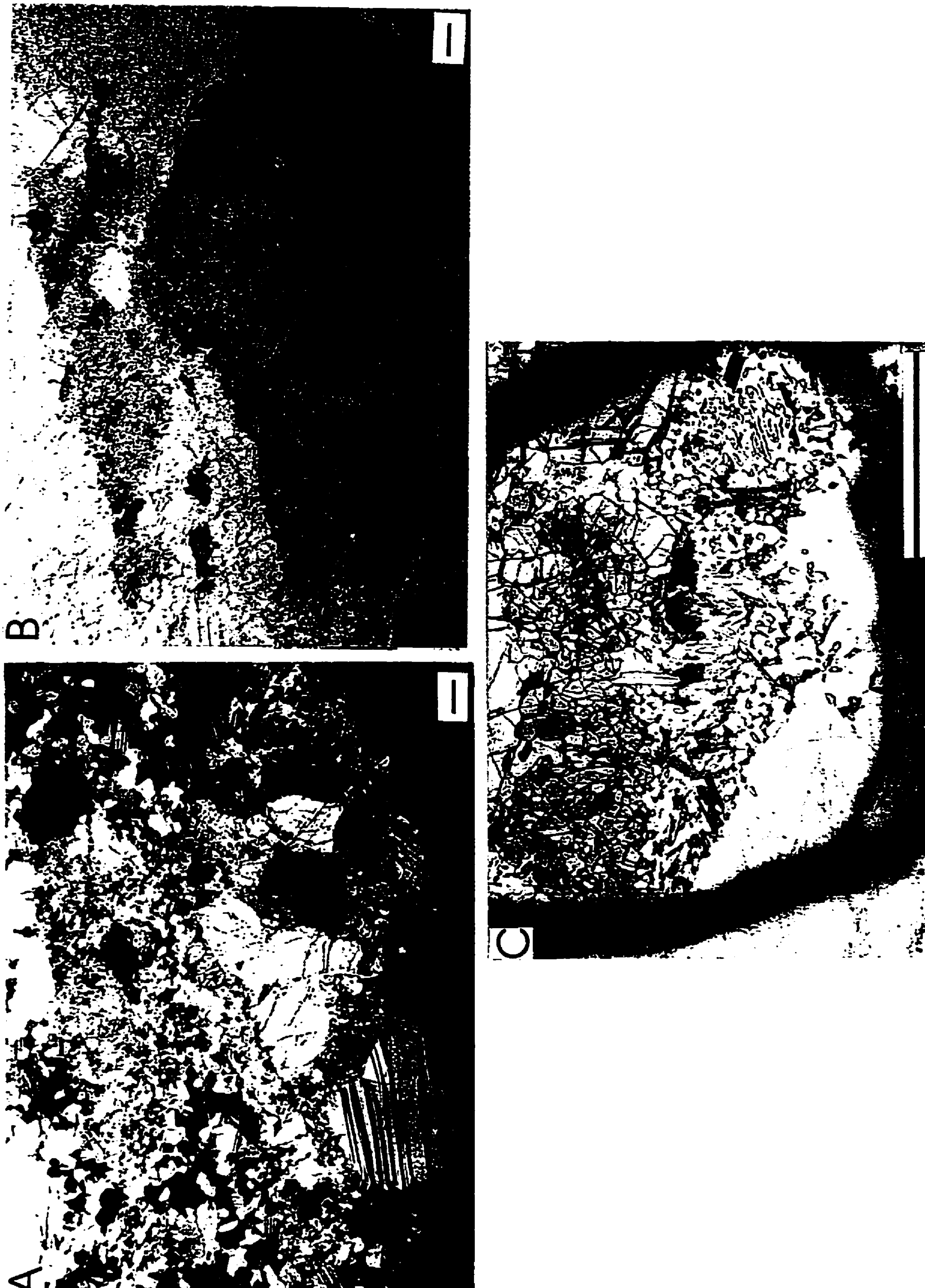

Figure 5.2

symplectite are either granoblastic aggregates adjacent to and recrystallised directly from orthopyroxene in the auge or are fine intergrowths in a reaction-zone symplectite with plagioclase and biotite.

BSE intensities of orthopyroxene grade from darker in grain centres to brighter at grain edges and in the symplectite (Figure 5.3) and this corresponds to decreasing Al_{tot} increasing Fe/Mg. The BSE intensity gradations correspond to compositions that range from En_{70} and Al_{tot} = 0.5-1.3 (centres) to $En_{66\text{-}69}$ and Al_{tot} = .06-.09 (symplectite). The variation in BSE intensity is less pronounced adjacent to the hornblende rim in which the composition of orthopyroxene fragments grade from En_{68} to En_{66} and Al_{tot} from 0.06 to 0.03. Although total Al contents are variable throughout the auge and reaction zones, they are generally much higher in the recrystallised orthopyroxene megacryst, much lower in the hornblende rim and intermediate in the symplectite (Figure 5.4). Most other compositional parameters do not vary significantly.

Large (0.5-2cm) plagioclase grains around the auge are $An_{\sim 50}$ and are compositionally zoned adjacent to the reaction rims to $An_{\sim 80}$ near the symplectite. The zoning in plagioclase is apparent both optically and in BSE images (Figure 5.5a). Plagioclase compositions in the symplectite, in exsolution lamellae within orthopyroxene grains, and in the hornblende rim are also $An_{\sim 80}$ (Figure 5.4).

Clinopyroxene is rare in this sample and all grains are small fragments or relict lamellae associated with granular hornblende aggregates and in hornblende-rich reaction rims adjacent to orthopyroxene (Figure 5.3). Small augen of granular hornblende in the matrix (Figure 5.6) contain

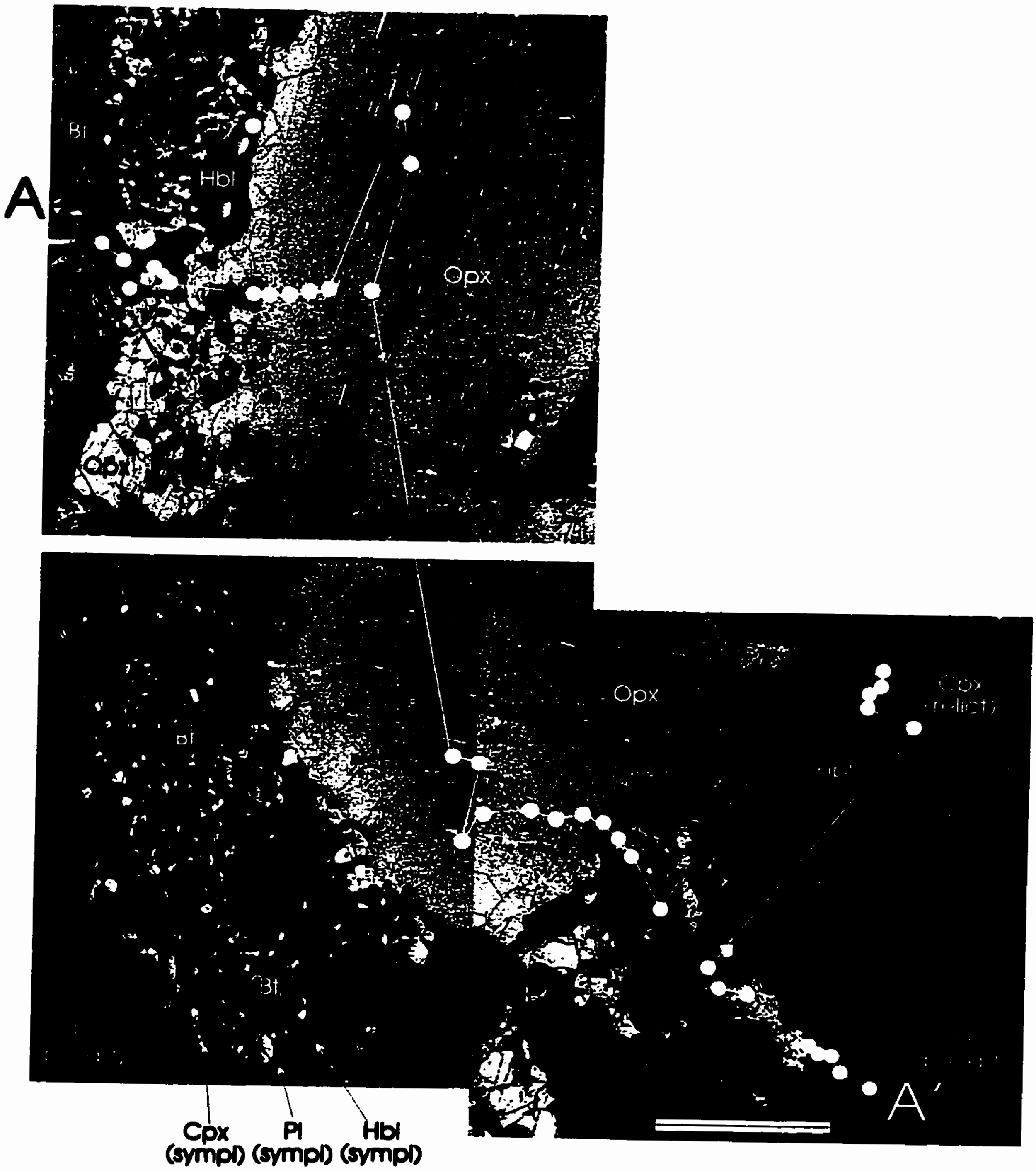

Figure 5.3 - BSE image mosaic of orthopyroxene auge in anorthosite sample BVM91-584 (pictured in Figure 5.2) from the Red River Anorthosite Suite. Microprobe traverse A-A' is shown and corresponds to the selected compositional parameters in Figure 5.4. Scale bar = 1 mm

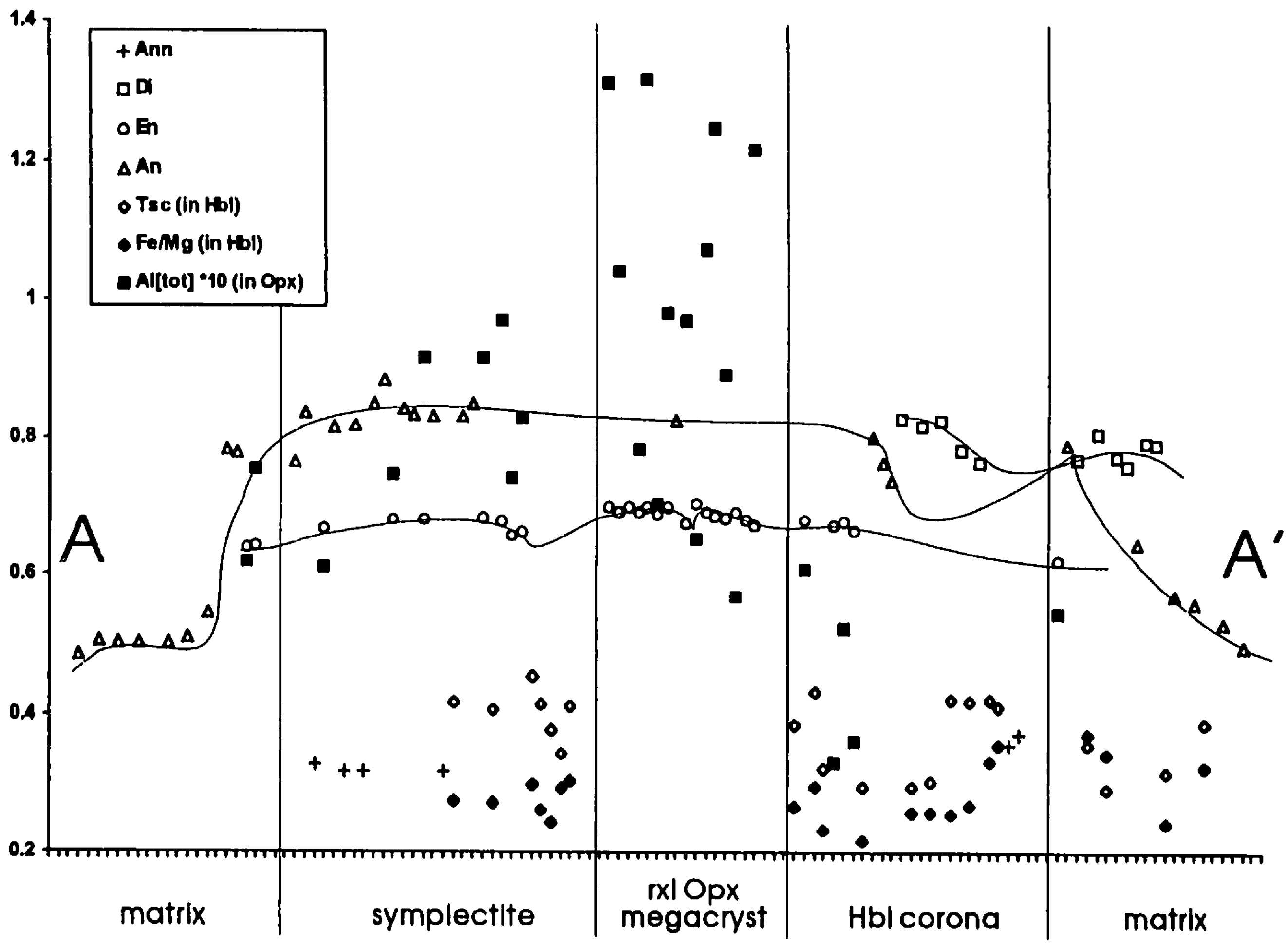

Figure 5.4 - Mineral compositions in traverse (A - A' in Figure 5.3) across orthopyroxene megacryst with reaction rims. End-member abbreviations as in Table 5.2; Fe/Mg is $[Fe^{2+}/(Fe^{2+}+Mg)]^{C}$ in Hbl. Vertical scale is end-member percent for all but cations of Al_{tot}. Solid lines show variations in An (triangles), En (open circles), and Di (squares) contents.

Figure 5.5 - (a) BSE image mosaic of transitional zone between large igeous plagioclase grain (bottom right) and symplectite (top left), note plagioclase zoning adjacent to the symplectite (scale bar = 1mm). (b) Granoblastic orthopyroxene and relatively unzoned hornblende (compare with that of hornblende rim, Figure 5.3) in the symplectite (scale bar = 1mm). (c) Swallow-tail biotite grains in the symplectic rim (scale bar = 0.5 mm). All are from sample BVM91-584 of the Red River Anorthosite Suite.

Figure 5.6 - Small auge of granular hornblende with relict lamellae of clinopyroxene (BMV91-584; XP; scale bar = 1 mm).

relict salite (Di_{77-81}) lamellae and clinopyroxene lamellae within the hornblende reaction rim around orthopyroxene preserves a systematic gradation from Di_{77} to Di_{83}, with the more magnesian compositions nearer to the orthopyroxene megacryst (Figure 5.4). A few clinopyroxene analyses yielded compositions of pigeonite or subcalcic augite but these are from areas with very fine lamellae of orthopyroxene, hornblende, and perhaps plagioclase, and probably do not represent the composition of any single phase.

Hornblende grains in the reaction rims are individually zoned (Figure 5.3 and Figure 5.5b) with compositions ranging from tschermakitic hornblende at grain centres to magnesio-hornblende at grain edges. Hornblende grains in the smaller augen that contain relict clinopyroxene lamellae are magnesio-hornblende. Both the tschermakite content and the Fe/Mg ratio appear to be controlled more by the zoning within individual grains than by the proximity of the grain to the recrystallised orthopyroxene megacryst (Figure 5.4).

Swallow-tail biotite grains are present in the Opx + Pl + Bt symplectic reaction rim surrounding recrystallised megacrysts (Figure 5.5c) and rare blocky biotite grains are present in the hornblende reaction rim and in granular hornblende aggregates in the symplectic rim. Several biotite grains extend into orthopyroxene grains along lamellae that are otherwise occupied by plagioclase and Fe-Ti oxides. Biotite grains in the symplectite are $Ann_{\sim 32}$ and in the hornblende reaction rim are $Ann_{\sim 37}$.

In many samples it is difficult to determine whether reaction rims around anhydrous igneous minerals (e.g., partly recrystallised orthopyroxene megacrysts) result from subsolidous late-stage igneous processes (including alteration from late-magmatic fluids and re-equilibration during postemplacement cooling) or a subsequent metamorphic episode (e.g., Buddington, 1939; Whitney and McLelland, 1973; Johnson and Essene, 1982; Rivers and Mengel, 1988). The preservation of the symplectite, however, suggests a metamorphic origin because the fine textures and high surface energy grains would not be expected to survive the high-grade thermal event that is known to have affected the enveloping charnockitic rocks (see below) and probably coincided with late Middle Proterozoic metamorphic zircon growth (Chapter 4). By comparison, orthopyroxene megacrysts in other massif-type anorthosite bodies are commonly large (several to tens of centimetres), blocky grains with internal exsolution textures and grain-boundary reaction rims that have a wide variety of mineral assemblages and textures (e.g., Emslie, 1975; Dymek and Gromet, 1984; Owens and Dymek, 1995). Although few authors speculate on the origin of the secondary minerals, the general implication is that they result from late-stage igneous processes (Bhattacharya and Mukherjee, 1987; Ashwal, 1993; Owens and Dymek, 1995). Wodicka (1994) inferred flattened polycrystalline aggregates of hornblende and plagioclase in the highly recrystallised margins of the Parry Island anorthosite to be metamorphosed orthopyroxene megacrysts.

Some hornblende rims around orthopyroxene megacrysts may result from secondary hydration of a late-igneous clinopyroxene corona. Owens and Dymek (1995) reported that red-brown biotite and green hornblende are present around orthopyroxene megacrysts in the Labrieville anorthosite and that some of the secondary minerals have grown into the megacryst along plagioclase lamellae. They attributed all of the megacryst re-equilibration, exsolution, and reaction textures to late-stage igneous processes. The opposite case, multiple stages of reaction that produce anhydrous silicate minerals at the expense of early-formed amphibole and biotite, has been reported in coronitic gabbro from western Labrador (Rivers and Mengel, 1988). The hornblende reaction rim in sample BVM91-584 may have replaced a clinopyroxene corona rather than directly replacing orthopyroxene. This would explain the lack of zoning in orthopyroxene adjacent to the hornblende rim and the presence of relict clinopyroxene.

All of these lines of evidence and the comparisons with similar textures in other anorthosite and mafic rocks support the interpretation of metamorphism, accompanied by deformation, as the origin for the reaction-rim mineral assemblages in sample BVM91-584 and the apparent flattening fabric they help to define.

P-T constraints

Bekkers (1993) attempted two-pyroxene thermometry on one sample each from the anorthosite, charnockite, and the layered unit but obtained unreasonably high temperatures of 1119-1930°C. Mitchell (1979) also attempted two-pyroxene thermometry on a "banded gneiss" (perhaps layered unit or charnockite?) and obtained high, but more reasonable, metamorphic temperature estimates of 860-932°C. Neither study was of sufficient detail to assess the effects of polymetamorphism and disequilibrium.

The Red River Anorthosite Suite is interpreted to have been subjected to high-grade metamorphism based on recrystallisation textures and relict mineral assemblages. However, most of the anorthosite suite is of inappropriate bulk composition to have formed mineral assemblages appropriate for precise P-T constraints or the rocks have been subsequently overprinted by amphibolite-facies assemblages. Therefore, the focus is here on an attempt to determine the conditions of metamorphism implied by the reaction rims in sample BVM91-584.

For TWQ analyses, closely associated minerals in small (<3mm) areas were analysed from the symplectite, a small patch of granoblastic minerals in the symplectic rim, and minerals in the hornblende rim. Mineral compositions in the granoblastic patch were obtained from averages of four plagioclase analyses, three orthopyroxene analyses, two hornblende analyses, and three biotite analyses. It was deemed necessary to exclude biotite from TWQ analysis because Fe-Mg equilibria involving biotite plot at about 250°C and other equilibria are clearly outliers. Although this sample contains magnesio-hornblende to tschermakitic hornblende, all six amphibole end members (Tr, Tsc, Prg, and Fe-equivalents) were included in the TWQ analyses and, with the exception of the highly sensitive two-amphibole Fe-Mg equilibria, other equilibria involving amphibole are remarkably consistent, especially considering that uncertainties in the appropriate (equilibrium) amphibole composition commonly caused difficulties in other samples.

In the resulting TWQ diagram (Figure 5.7a), Fe-Mg exchange reactions between orthopyroxene and hornblende plot at about 760°C. Although these are not high-confidence equilibria, TWQ analyses using other combinations of orthopyroxene, hornblende, and including relict clinopyroxene from the hornblende reaction (e.g., Figure 5.7b,c), all produced Amph-Pyx and Cpx-Opx Fe-Mg exchange equilibria between 700-800°C, but with widely varying pressure-constraining equilibria (not reproduced here). There is also fair agreement with the hornblende end-member Schreinemakers bundle which, in many analyses of other samples, does not even plot within the P-T limits of the diagram, and is more reliable in this case because hornblende is Tr- and Tsc-rich (i.e., more reliable thermodynamic properties - Mader et al., 1994; Jenkins, 1994). Applicable conventional thermometers are limited by the lack of quartz, but the HBb(94) thermometer yielded a high temperature of 830°C (Table 5.4).

Mineral compositions in the symplectite were averaged from two orthopyroxene analyses, three analyses of adjacent plagioclase ($An_{\sim 84}$), two analyses of granular hornblende. In contrast to

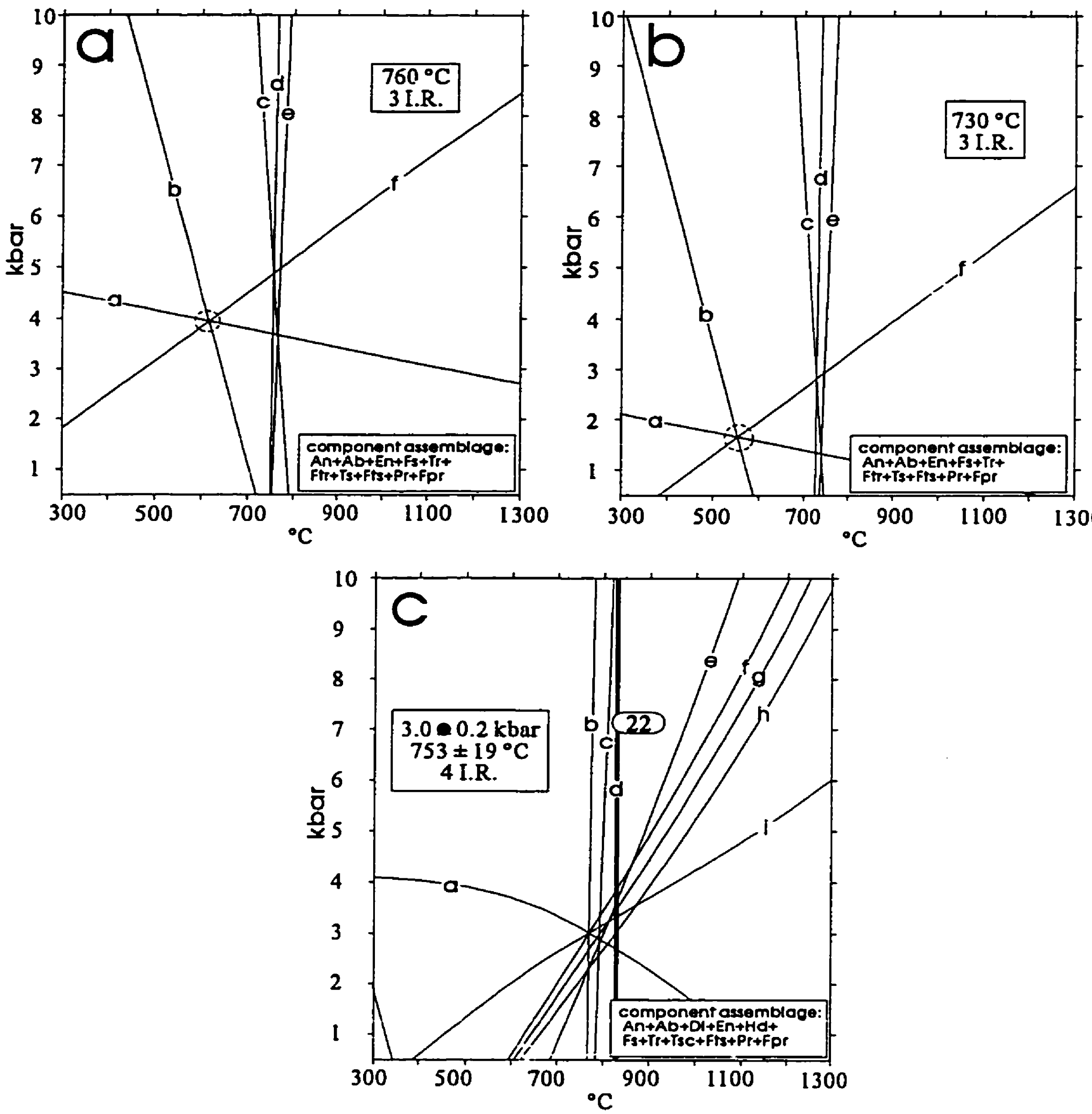

Figure 5.7 - TWQ diagrams from assemblages in reaction rims around a partly recrystallized orthopyroxene megacryst from the Red River Anorthosite Suite. Assemblages are from (a) granular aggregates, (b) symplectite, (c) hornblende reaction rim. Quoted errors are the 1.5σ standard deviation on the cluster of intersections and not the accuracy of the P-T estimate. Numbered heavy equilibria are calibrated or high-confidence reactions and correspond to Table 5.1. Circled Schreinemakers bundle is the Fe-Mg exchange equilibria between amphibole end-members. Lettered equilibria are listed in Appendix A5.3.

Table 5.4 - Comparison between P-T results from TWQ analyses and conventional thermobarometry (T in °C and P in kbar).

Sample	584	584	584	144	739	739	057	714	714	717
TWQ Figure	5.7a	5.7b	5.7c	5.13a	5.13b	5.13c	5.13d	5.17a	5.17b	5.17c
P-TWQ			3.0		10.0	8.0			9.5	11.9
T-TWQ	760	730	753	~671	791	745	~755	~800	726	825
Grt-Bt										
T-FS(78)					(1176)	(1213)		(710)	(738)	(829)
T-IM(85)					(1032)	(1103)		(753)	(782)	(848)
Grt-Hbl-Pl-Qtz										
T-GP(84)					687	721		730	730	715
T-HBa(94)	990*	878*	980*		982*	905*	774*		931*	943*
T-HBb(94)	833	739	826		788	757	771		703	762
P-KS(89)					8.6	8.6		8.2	8.2	8.2
P-KS(90)					10.3	9.9			11.9	10.4
Grt-Cpx										
T-EG(79)					796	778		755	755	
T-GS(87)					691	647		939	939	
Opx-Cpx										
T-K(82)nt			888	746						
T-K(82)ex			733	747						
T-L(83)			(620)	(620)						

Errors on P and T are estimated to be on the order of ±1 kbar and ±50°C as explained in text, *-quartz not present in assemblage, parentheses indicate mineral composition outside range suggested by author of calibration. To facilitate P-T comparisons within units, thermometric calculations assume P = 3.5 kbar for BVM91-584 (except L(83) at 5 kbar), P = 9 kbar for BVM90-144 (except L(83) at 10 kbar), BVM91-739, BVM90-057, P = 10 kbar for BVM91-714, BVM91-717; barometric calculations assume T = 750°C for BVM91-584, T = 775°C for BVM90-144, BVM91-739, BVM90-057, T = 700°C for BVM91-714, BVM91-717. Holland and Blundy (1994) reaction A (edenite-tremolite) is HBa(94), and reaction B (edenite-richterite) is HBb(94). K(82)nt K(82)ex are the calibrations of Kretz (1982) for the Ca-Mg net-transfer and Fe-Mg exchange reactions respectively. Other calibration abbreviations as in Table 5.1.

granular hornblende grains in the hornblende reaction rim, these hornblende grains do not show significant zoning in BSE images are texturally stable. The equilibria yield Opx-Hbl exchange equilibria that suggest a temperature of about 730°C (Figure 5.7b). The HBb(94) conventional thermometer yielded a temperature of 740°C (Table 5.4). Mineral compositions in the hornblende reaction rim were combined from the average of six granular, zoned hornblende grain centres, four relict fragments of orthopyroxene, the average of three clinopyroxene in relict lamellae, and three granular plagioclase grains within the reaction rim. The best set of intersections was obtained by excluding FeTr. Although the orthopyroxene, amphibole and plagioclase compositions differ from the two preceding analyses, the positions of equilibria are remarkably similar and indicate a pressure of 3 kbar and 750°C (Figure 5.7c). In this analysis, the two-pyroxene Fe-Mg exchange equilibrium plots within the diagram limits at about 800°C. The temperatures produced by conventional thermometers are higher than TWQ for K(82)nt and HBb(94) at 890°C and 930°C respectively, but the K(82)ex temperature is 747°C (Table 5.4).

Charnockite

Petrography and mineral chemistry

Metamorphosed charnockite samples contain the best preserved high-grade mineral assemblages in the Blair River inlier. Some samples contain clearly metamorphic two-pyroxene assemblages, but others preserve grains of igneous origin that are partly recrystallised to a texturally distinct generation of pyroxene. Partly resorbed garnet and clinopyroxene are present in some samples, but no samples preserve texturally equilibrated Pyx + Grt assemblages. The least-altered samples are from competent lenses surrounded by chloritic schist in the Wilkie Brook fault zone. The high-grade metamorphosed charnockite differs from the Sailor Brook granulite gneiss in that the charnockite is more felsic, many samples contain quartz, the high-grade assemblage is commonly oriented in a weak shape-preferred fabric, and igneous precursor grains are locally recognisable.

Igneous orthopyroxene grains are recognised by being generally large (1-4 mm), equigranular bronzite with exsolved Fe-Ti oxides, clinopyroxene, and/or plagioclase. They are commonly bordered by recrystallised granular aggregates of homogeneous (i.e., unexsolved and unzoned) metamorphic hypersthene. Igneous pyroxene grains are also recognised by their association with large (up to ~1 mm) perthitic K-feldspars, both of which are commonly porphyroclasts in a finer-grained recrystallised matrix that defines a weak foliation and includes granular metamorphic orthopyroxene and two feldspars. Other metamorphic orthopyroxene (En_{59-63}) grains are large (up to 7mm) and elongate, defining a macroscopic foliation along with layers of recrystallised equigranular and granoblastic feldspars and mosaic-quartz ribbons. Metamorphic clinopyroxene (Di_{60-76}) grains are ellipsoidal or round, the former being aligned with the macroscopic foliation. In more highly altered samples, orthopyroxene is partly or completely altered whereas clinopyroxene is commonly unaltered, or rimmed by Hbl + Pl + Qtz aggregates.

In the least-altered two-pyroxene charnockite sample (BVM90-144), large elongate metamorphic hypersthene grains contain dusty inclusions of an Fe-oxide mineral along fractures and cleavage planes. Individual cleavage- or fracture-bounded fragments show a slight but systematic compositional variation from $En_{62.7}$ in the centres of large fragments, $En_{61.5-60}$ in smaller fragments, to En_{59} near zones of dusty inclusions. However, this compositional gradation is not resolved by BSE images which are of uniform intensity within fragments (Figure 5.8a). Clinopyroxene grains have optically continuous rims of granular augite, diopside, and salite that

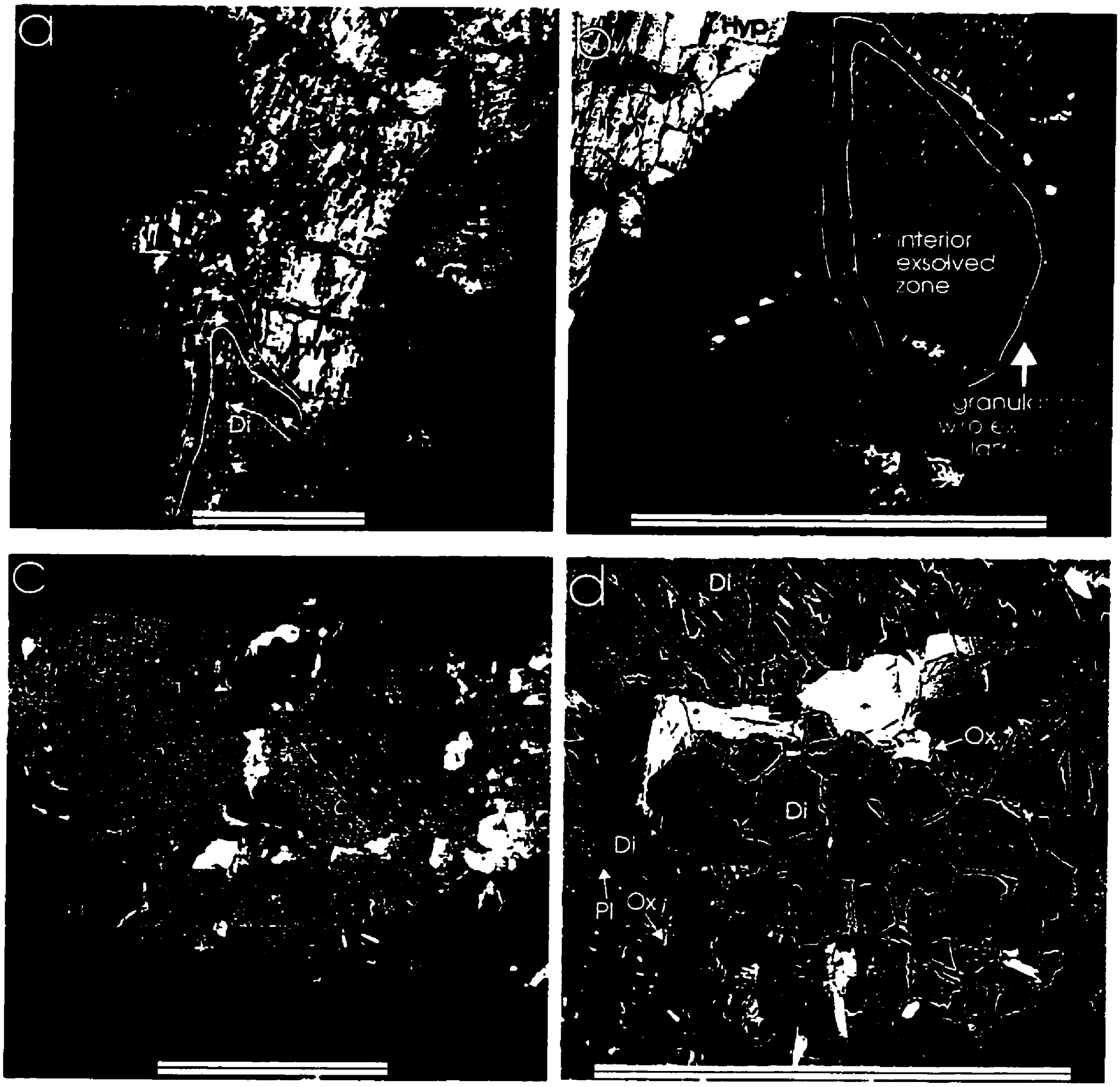

Figure 5.8 - BSE images of pyroxene textures in charnockites. (a) Exsolved orthopyroxene that shows little variation in BSE intensity within cleavage-bounded fragments (BVM90-144; scale bar = 1mm). (a) and (b) Exsolved clinopyroxene grains recrystallized along grain edges to granoblastic aggregates without exsolution lamellae (BVM90-144; scale bar = 1mm). (c) Larger relict igneous clinopyroxene grains recrystallized around grain edges to separate granoblastic Cpx+Pl+Ox±Hbl assemblage (BVM91-739; scale bar = 1mm). (d) Close-up of granoblastic recrystallized minerals (scale bar = 0.5mm).

lack exsolution textures surrounding larger cores with exsolution lamellae of plagioclase, quartz, and Fe-Ti oxide minerals (Figure 5.8b). The granular rims are slightly Di-rich relative to the cores ($Di_{72.8}$ vs. $Di_{71.4}$ respectively).

Orange-brown biotite occurs as rims around Fe-Ti oxide minerals in association with pyroxene clusters, but oxide minerals in the quartzofeldspathic matrix largely lack biotite rims. Large tabular biotite grains help define the foliation along with elongate pyroxenes and amphiboles, recrystallised quartz ribbons, and zones of granular recrystallised feldspars (Figure 5.9).

Large (up to 2.5 mm) grains of both K-feldspar with fine-bead perthite and relict igneous plagioclase with deformed twin lamellae occur in a fine-grained (0.2 mm) granular recrystallised matrix. Centres of large igneous plagioclase grains are An_{34-37}, plagioclase grains near pyroxenes are An_{31-34} and plagioclase exsolution lamellae and blebs in clinopyroxene are more calcic ($An_{\sim 42}$).

Although textural disequilibrium is evident in charnockite sample BVM91-739, this sample is the only garnet-bearing granulite observed from the Blair River inlier. Large (0.75 mm) clinopyroxene grains contain cores with exsolved lamellae of Pl + Ox and rims that lack (or have expelled) exsolved minerals within about 0.1 mm of their edges. These grains are more magnesian towards their edges (Di_{70-72}) compared to their centres ($Di_{\sim 68}$). Many large clinopyroxene grains are mantled by finer-grained (0.1-0.3 mm) granoblastic aggregates of Cpx + Pl + Hbl + Ox that

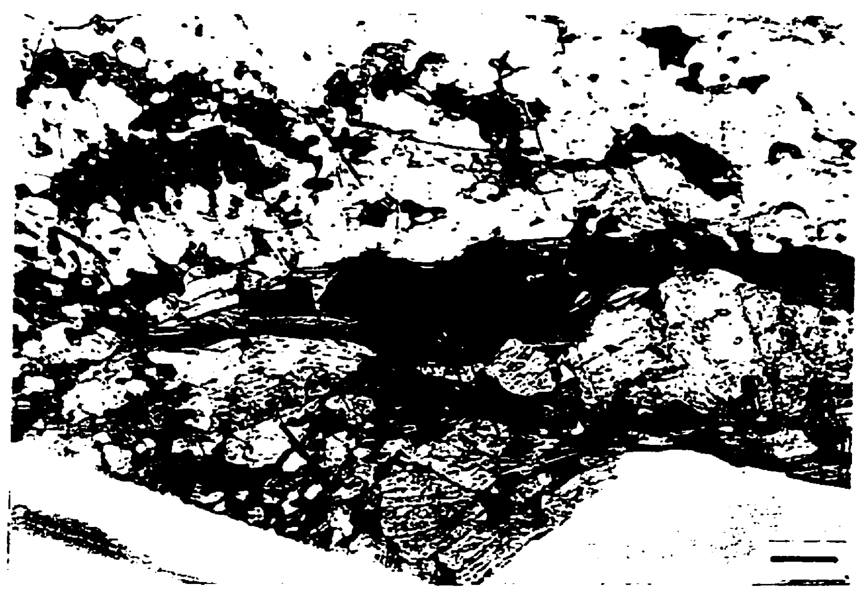

Figure 5.9 - Biotite grains and Fe-Ti oxide mineral that help to define a folation with elongate pyroxene, granular hornblende aggregates and recrystallized feldspars in charnockite sample BVM90-057 (PP; scale bar = 1 mm).

help to define a weak foliation. The compositions of clinopyroxene grains in the granoblastic aggregates are comparable to large grain edges (Di_{70-72}).

Garnet (Alm > Prp > Grs) is highly resorbed along grain edges and in fractures to a locally symplectitic, very fine-grained group of minerals that includes chlorite, muscovite, biotite, hornblende, plagioclase, and Fe-Ti oxide minerals (Figure 5.10). Microprobe traverses across remnant garnet fragments show that almandine and spessartine components increase dramatically, whereas pyrope and grossular components decrease adjacent to the zone of fine-grained alteration minerals (Figure 5.11). This appears to be the result of partitioning during retrogression and may indicate that the garnet composition of the high-grade assemblage is preserved in the centre of larger grains.

Hornblende is present as large (0.5 mm) brown blocky grains associated with clusters of igneous clinopyroxene and Fe-Ti oxide minerals where they are not significantly recrystallised. Green-brown magnesian hastingsitic hornblende occurs as part of the granular recrystallised aggregates around large clinopyroxene grains.

The centres of large (igneous?) plagioclase grains are $An_{\sim 40}$ and grain edges adjacent to clinopyroxene are An_{46-51}, plagioclase in granoblastic aggregates associated with recrystallised pyroxene is An_{43-45}, and plagioclase exsolution lamellae in large igneous clinopyroxene grains are $An_{\sim 50}$. Albite (An_{3-4}) is the dominant plagioclase composition among the fine-grained minerals around resorbed garnet.

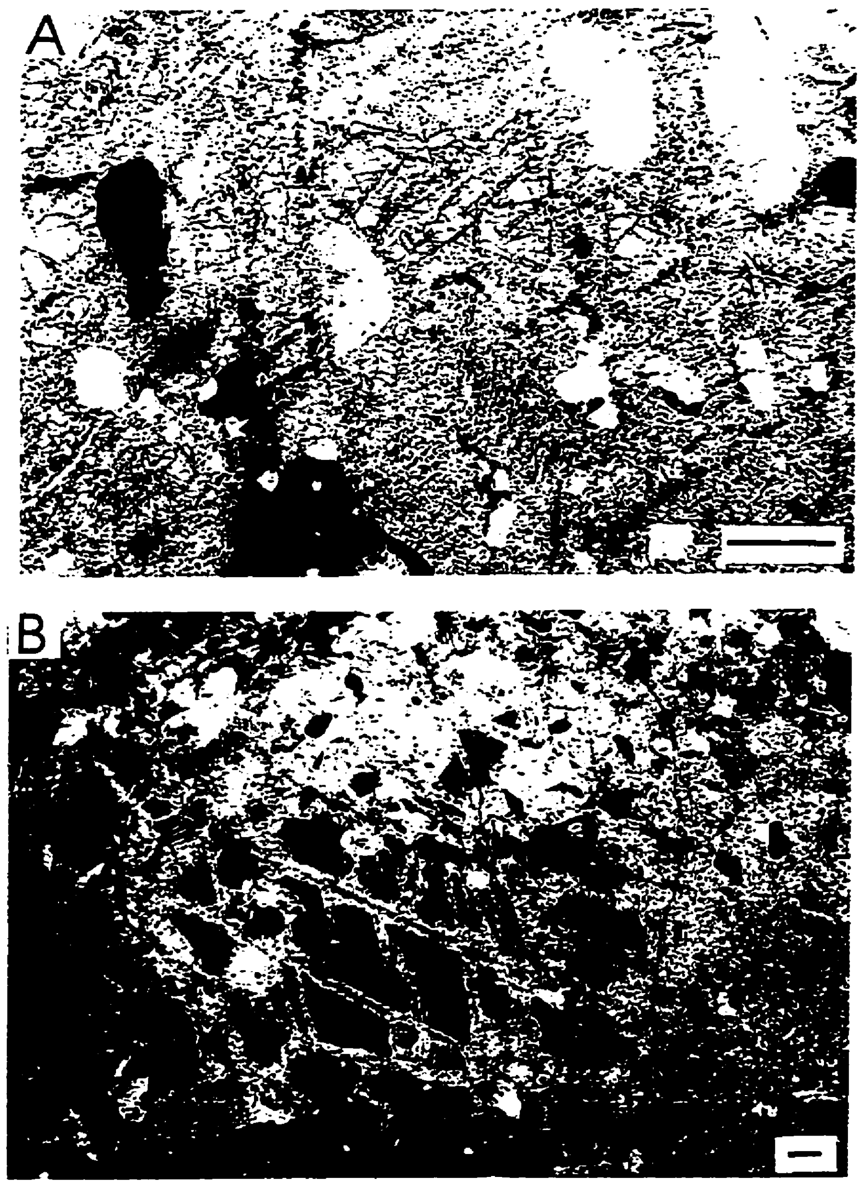

Figure 5.10 - Highly resorbed garnet in charnockite.

(a) garnet (centre-top, high-relief mineral) and altered orthopyroxene (fibrous brown spot beneath garnet) with oxide minerals that mimic pyroxene cleavage in charnockite sample BVM91-739. Garnet is replaced by a very fine-grained, locally symplectic, group of minerals that includes chlorite, muscovite, biotite, hornblende, plagioclase, and Fe-Ti oxide minerals (PP; scale bar = 1 mm).

(b) garnet from another spot in same sample (crossed polars) shows alteration along fractures (XP; scale bar = 1 mm).

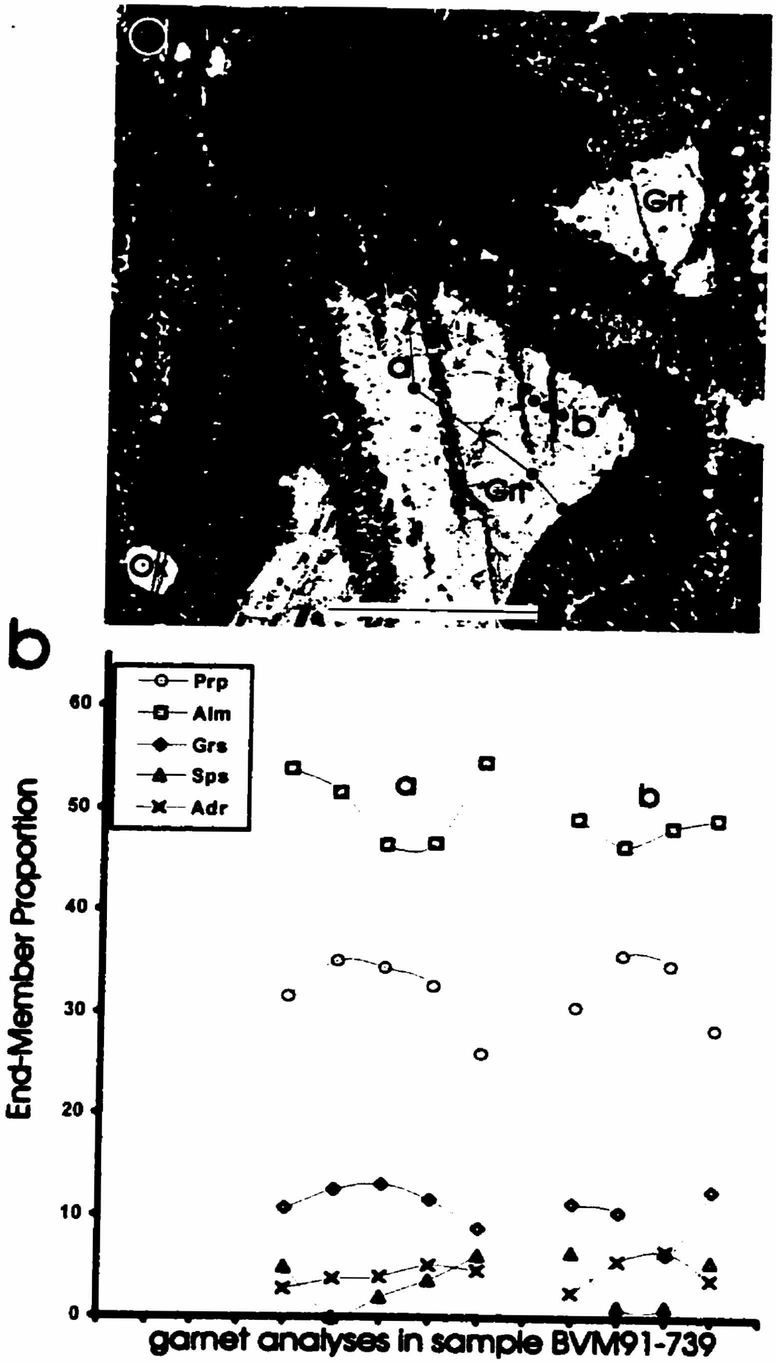

Figure 5.11 - (a) BSE image of highly resorbed garnet from charnockite (BVM91-739; scale bar = 1mm). (b) End-member proportions in microprobe traverse across two garnet fragments indicated as a and b on BSE image.

Clusters of (~0.3 mm) biotite grains rim Fe-Ti oxide minerals adjacent to, or within, resorbed garnet. Biotite (Ann_{25-29}) is part of the fine-grained garnet alteration assemblage, is associated with partly altered or relict igneous clinopyroxene (Ann_{34-36}), and forms small (Ann_{43-46}) grains in granoblastic recrystallisation zones around clinopyroxene.

In the best preserved hornblende-bearing granulite sample (BVM90-057), elongate, foliation-defining mafic-mineral clusters consist of metamorphic hypersthene (En_{61-65}), dark green to brown pleochroic magnesio-hastingsitic hornblende and orange-brown biotite. Orthopyroxene grains are large and elongate and contain inclusions of, or are associated with granular hornblende grains and granular, tabular, or highly elongate biotite grains. Where orthopyroxene grains show the least exsolution of fine oxide minerals, all three Fe-Mg silicate minerals have sharp, clean grain boundaries and are in textural equilibrium (Figure 5.12).

Orange-brown matrix biotite grains commonly rim Fe-Ti oxide minerals and are flattened into the foliation. Biotite grains in mafic-mineral clusters are randomly oriented. Biotite in both occurrences is Ann_{34-37}. The matrix around mafic mineral clusters consists of coarse-grained plagioclase (An_{43-48}), granular hornblende aggregates aligned parallel to the foliation and well-oriented orange-brown biotite. Quartz is absent from this sample.

P-T constraints

For charnockite sample BVM90-144, averages of analyses were used for TWQ from a cluster of mafic minerals including the centres of three orthopyroxene cleavage-bounded fragments, five plagioclase grain edges or small recrystallised grains adjacent to orthopyroxene, three granular

Figure 5.12 - Elongate orthopyroxene grain (centre nearly at extinction) in charnockite (BVM90-057; XP; scale bar = 1 mm) with texturally stable inclusions of biotite and hornblende.

clinopyroxene granules or grain edges lack exsolution textures, and two small biotite grains adjacent to the Opx-Cpx cluster. From this assemblage, only two-pyroxene and Cpx-Bt Fe-Mg exchange reactions plot within the P-T limits of the TWQ diagram (Figure 5.13a). The two-pyroxene thermometer indicates a temperature of about 670°C. Applicable conventional two-pyroxene thermometers yielded temperatures of 750°C (Table 5.4).

In sample BVM91-739, an attempt was made to distinguish and analyse separately the compositions of relict igneous grains from the recrystallised mantle grains. In order to assess an assumption that the relict igneous assemblage re-equilibrated (as indicated by exsolution textures) but did not totally recrystallise during metamorphism, a combination of the average of four grain-centre analyses from the highly resorbed garnet fragments, three grain centre analyses from the large exsolved clinopyroxene grains, five plagioclase grain centre analyses, and two analyses from large dark brown hornblende grains, were used in TWQ analysis. Quartz is not a part of this assemblage and biotite produced problematic equilibria. The TWQ results provide three independent reactions, including the Grt-Cpx thermometer and the Amph-Grt-Cpx-Pl barometer, and an excellent set of intersections at 10 kbar and 790°C (Figure 5.13b). The disequilibrium between biotite and garnet is also evident in the conventional thermobarometry, both Grt-Bt thermometers produced unreasonably high temperatures but the minerals are of inappropriate compositions. Conventional thermobarometry produced consistent results (790-800°C) for the HBb(94), and EG(79) thermometers and a pressure of 10 kbar is indicated by the GS(87) barometer (Table 5.4).

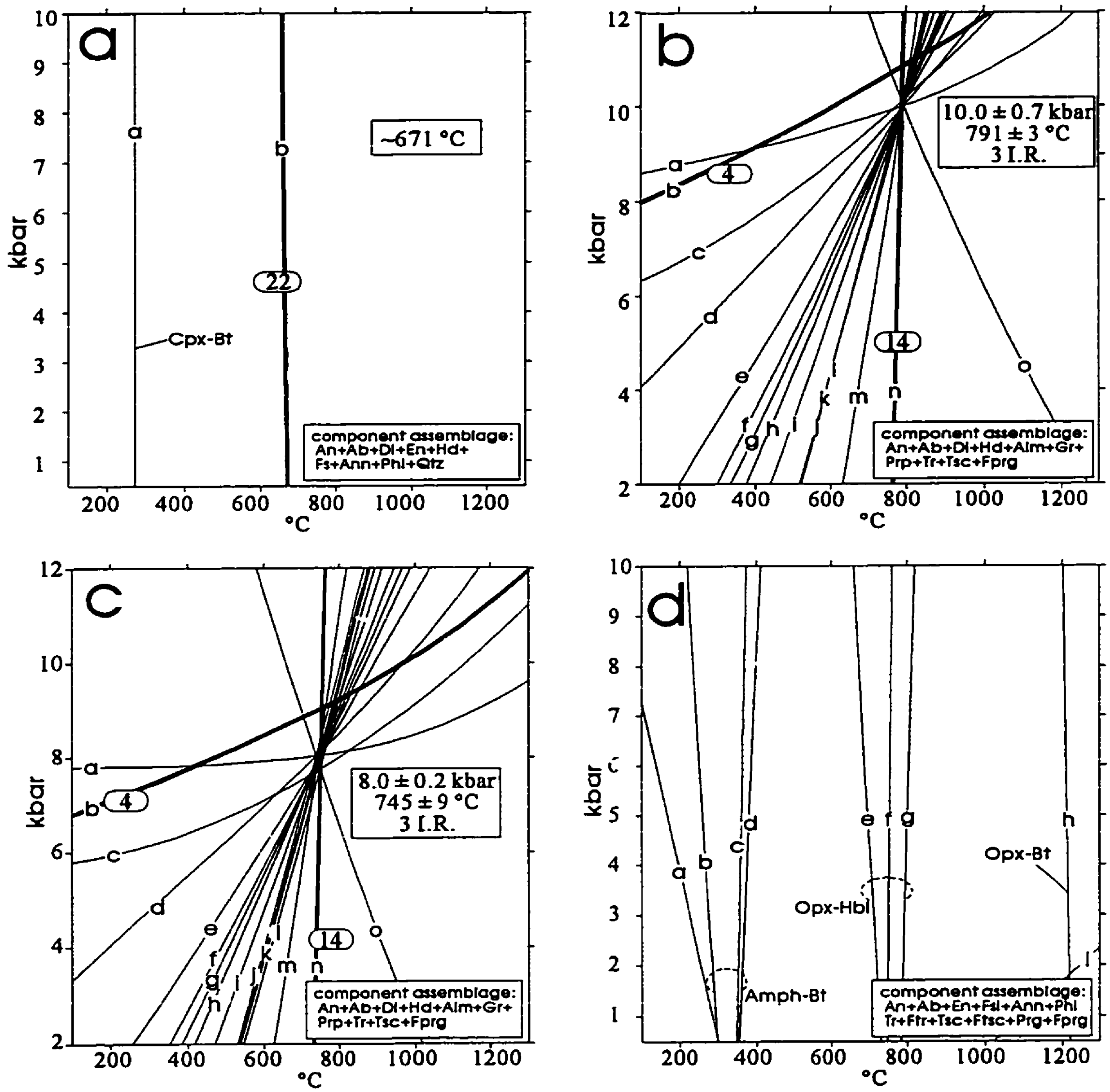

Figure 5.13 - TWQ diagrams for charnockite. Samples; (a) BVM90-144, (b) and (c) BVM91-739, (d) BVM90-057. Quoted errors are the 1.5σ standard deviation on the cluster of intersections and not the accuracy of the P-T estimate. Numbered heavy equilibria are calibrated or high-confidence reactions and correspond to Table 5.1. Lettered equilibria are listed in Appendix A5.3.

In the recrystallised assemblage, analyses were averaged from the centres of four highly resorbed garnet fragments, seven recrystallised granular clinopyroxene grains, three each of biotite and hornblende grains, and six plagioclase analyses, three from small granular grains in recrystallisation zones and three from large grain edges adjacent to recrystallisation. Quartz is present only in highly altered areas and therefore is not included in the phase assemblage. Biotite equilibria were widely scattered (but, again, Fe-Mg exchange equilibria were at about 200°C) and this mineral was also excluded from the TWQ phase assemblage. Remaining equilibria, including the Grt-Cpx thermometer and the Amph-Grt-Cpx-Pl barometer, provide a good cluster of intersections (Figure 5.13c) at 8 kbar and 745°C based on three independent reactions. Biotite is problematic in TWQ and in conventional thermometry, but other calibrated reactions indicate temperatures in the range of 650-720°C and pressures of 9-10 kbar (Table 5.4).

Compositions used for TWQ analysis from sample BVM90-057, were averages of three amphibole, four orthopyroxene, three plagioclase, and two biotite analyses from the freshest mafic mineral cluster. From this assemblage, only Fe-Mg exchange reactions are available for use in TWQ analysis. Equilibria involving biotite are clearly out of equilibrium with the rest of the assemblage. Equilibria involving Fe-Mg exchange between orthopyroxene and amphibole end-members plot between about 720-790°C (Figure 5.13d). Only the HBb(94) thermometer is applicable with this assemblage and it yielded a temperature of 770°C (Table 5.4).

Otter Brook gneiss

Petrography and mineral chemistry

In some samples from the Otter Brook gneiss, rare relicts of a high-grade precursor assemblage can be distinguished through a dominant amphibolite-facies mineralogical and deformational overprint. Sample BVM91-714 was selected for detailed study because it contains garnet, clinopyroxene relicts, and reaction zones with the amphibolite-facies fabric. Another, sample (BVM91-717) lacks relict pyroxene but contains hornblende and garnet (Figure 5.14). Garnet grains are separated and resorbed along fractures and amphibolite-facies mineral assemblages fill the separated fractures. Although these samples clearly contain disequilibrium mineral assemblages, they are two of the best samples from the Otter Brook gneiss in terms of preservation of relict high-grade minerals and reaction textures.

Sample BVM91-714 contains large (1-4 mm), highly resorbed garnet (Alm > Grs > Sps > Prp) grains that are corroded around their edges and are separated from Fe-Mg silicate minerals by a reaction zone of Pl + Kfs ± Ms. One garnet grain is resorbed and is draped by minerals that define the amphibolite-facies fabric. Clinopyroxene fragments are preserved in the strain shadows. A microprobe traverse of this garnet grain (shown on the BSE image; Figure 5.15) reveals that the almandine component decreases slightly and the spessartine component increases near reaction zones with biotite, but levels off in the centre of the grain. Grossular components do not vary greatly from grain edge to centre, but are slightly lower adjacent to reaction zones with biotite and are dramatically decreased in garnet relicts within reaction zones. The pyrope component decreases from about 8% in the centre of the grain to near zero at a reaction zone with one of the biotite inclusions, but to only slightly less than grain-centre values near the other two biotite inclusions. The spessartine component is relatively uniform across the grain at about 10% but increases to about 18% near the biotite grains with reaction zones. Garnet compositions adjacent to a small biotite inclusion that lacks a reaction zone are not significantly different from the relatively uniform grain centre compositions (Figure 5.15b).

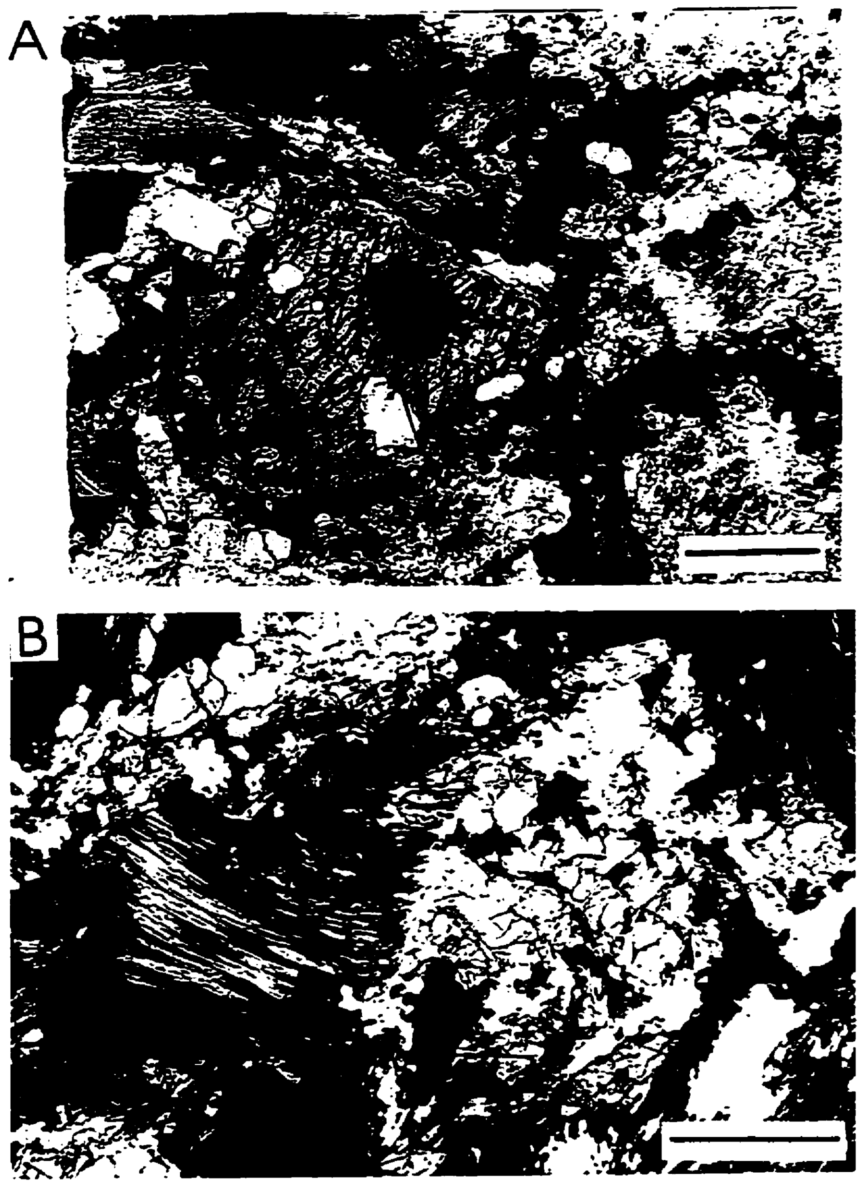

Figure 5.14 - (a) Augen-shaped garnet in Otter Brook gneiss sample BVM91-714 wrapped by, and separated from foliation-defining amphibolite-facies minerals by a Kfs + Pl + Ms reaction rim. Note small clinopyroxene fragments (light green) at tip of auge in a pressure-shadow position (PP; scale bar = 1mm). (b) Fractured and resorbed garnet grain (BVM91-717) with Hbl + Pl + Kfs filling the separated fractures (PP; scale bar = 1mm).

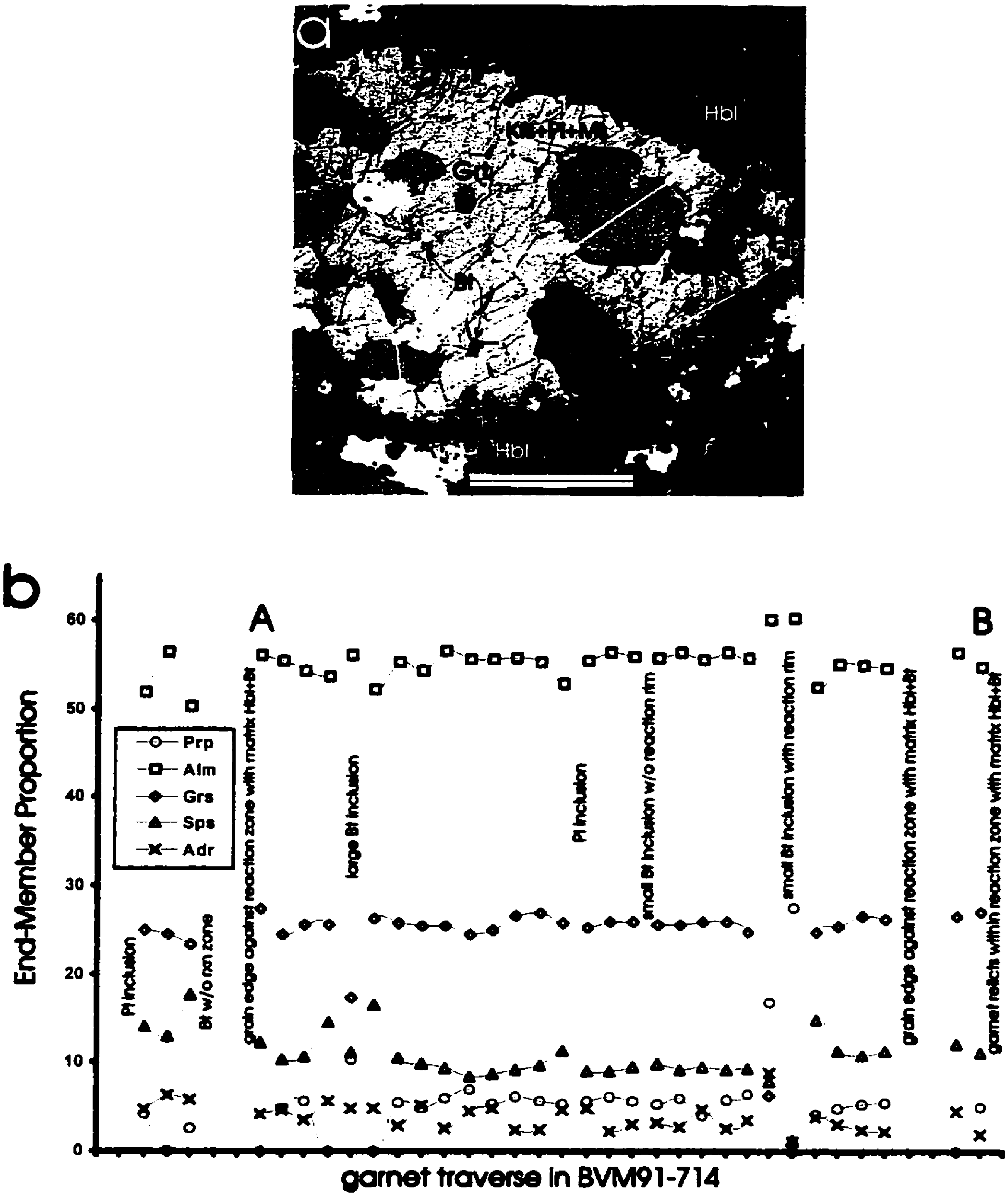

Figure 5.15 - (a) BSE image of same garnet grain shown in Figure 5.14a, showing microprobe traverse (scale bar = 1mm). (b) End-member proportions from microprobe traverse indicated on BSE image. Analyses in grey bars are from small relict garnet fragments within reaction zones.

Small (<0.2 mm) highly altered clinopyroxene (Di_{37-44}) fragments are poorly preserved in the feldspathic layers of the gneiss and are rarely present where the amphibolite-facies fabric has draped around garnet. Clinopyroxene can be attributed to a pre-amphibolite-facies mineral assemblage based on textural relations but whether it was ever in equilibrium with garnet cannot be determined.

Biotite, plagioclase, quartz, zircon, and apatite grains are inclusions in garnet but cannot be assigned definitively to a prior metamorphic generation because they do not define an internal foliation and they are also present in the external amphibolite-facies fabric. These are features that Vernon (1996) considered to be unreliable microstructural evidence for identifying relict metamorphic mineral assemblages. Large partly enclosed biotite inclusions have a reaction zone separating them from garnet, but smaller completely enclosed biotite grains do not, suggesting that the garnet resorption reaction is not isochemical and that a connection to the matrix allowed for fluid access and/or exchange with matrix phases. Matrix biotite and biotite inclusions with reaction zones in garnet are uniform at Ann_{67-69}, but the small, completely enclosed biotite grains without reaction zones are more variable at Ann_{65-76}.

Two generations of hornblende are recognised based on colour, texture, association with other minerals, and composition. Brown to olive-green pleochroic hastingsitic hornblende ("brown hornblende") is commonly associated with, but not an obvious alteration product of, clinopyroxene. In felsic layers, where clinopyroxene fragments are largest and least altered, brown hornblende is also least altered, shows a well-defined amphibole cleavage, and rarely preserves granular grain shapes. In mafic layers the brown hornblende is altered to biotite and a second generation of olive-green to blue-green pleochroic ferro-pargasitic hornblende ("green hornblende"). Green hornblende is common in fine grained mosaics with plagioclase and quartz, and takes the form of more elongate and fibrous grains that help to define the amphibolite-facies foliation. The brown hastingsitic hornblende is considered part of the pre-amphibolite facies assemblage.

Matrix K-feldspars (i.e., those away from Fe-Mg minerals and reaction zones) are large (1.5-3 mm) irregularly shaped grains with sutured boundaries and coarse patches of exsolved plagioclase. The plagioclase compositions are oligoclase (An_{21-27}) but rare small (<0.3 mm) separate plagioclase grains in the matrix are $An_{\sim 14}$ and this is similar to the composition of plagioclase inclusions in garnet (An_{10-16}). Most plagioclase grains adjacent to Fe-Mg silicate minerals show compositional zoning from cores of $An_{\sim 25}$ to edges of $An_{\sim 13}$. K-feldspar in reaction zones between garnet and Fe-Mg silicate minerals is Or_{71-88} and plagioclase in these zones is albite (An_5).

In sample BVM91-717, garnet grains are separated from amphibole and biotite by a fine-grained reaction rim that locally includes plagioclase, K-feldspar, muscovite, and chlorite. Most garnet grains are separated and/or resorbed along fractures which are filled with the amphibolite-facies assemblage Hbl+Pl+Kfs (Figure 5.14b and Figure 5.16a). The centres of garnet fragments range up to about 60% almandine component and this decreases to about 50% adjacent to the reaction zones with matrix hornblende (Figure 5.16b). The almandine component decreases to a lesser extent adjacent to the fractures filled with Hbl + Pl + Kfs. Grossular and pyrope contents show a slight variability in the fragments and the spessartine component increases dramatically at

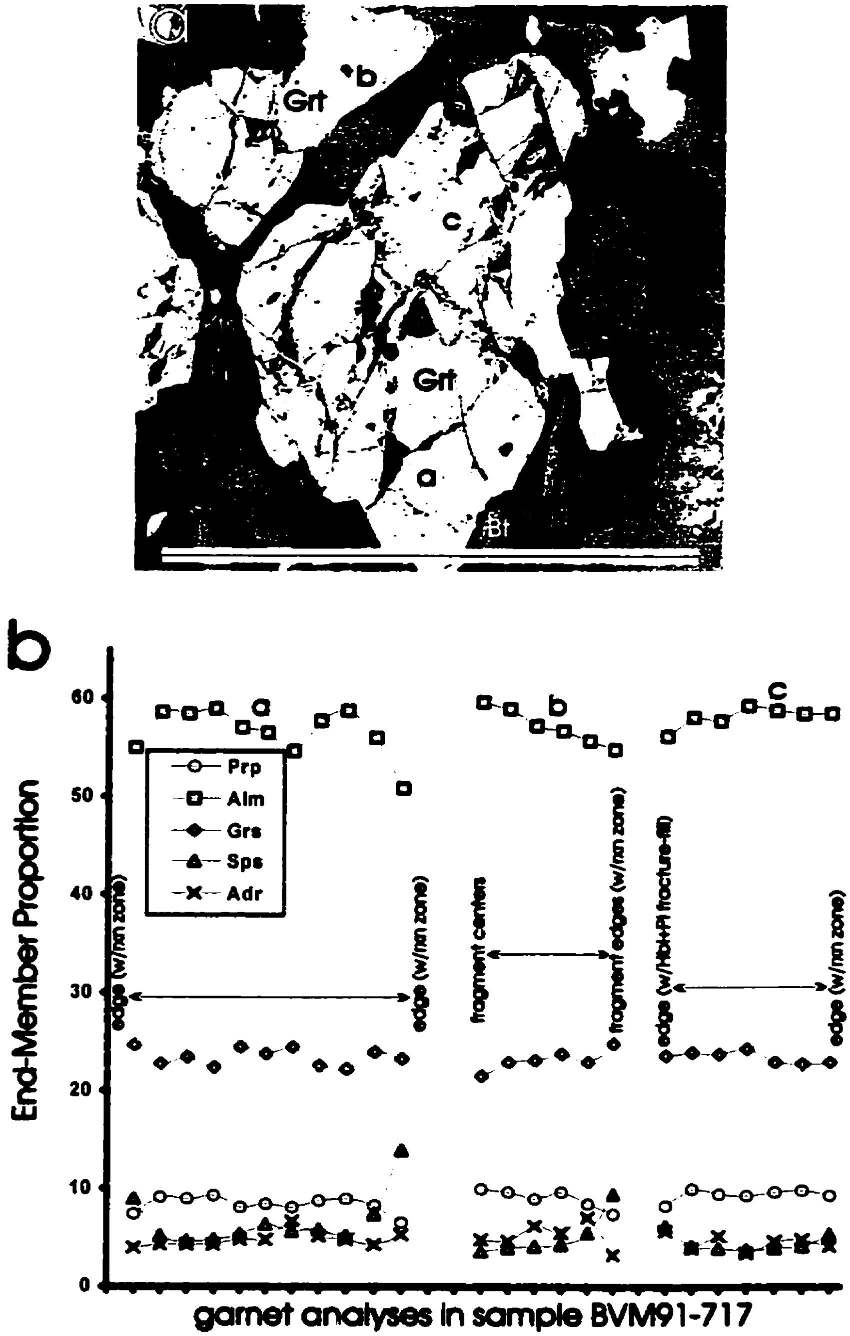

Figure 5.16 - (a) BSE image of right two fragments of same fractured garnet grain from the Otter Brook gneiss (same as shown in Figure 5.14b; scale bar = 1mm). (b) End-member proportions from traverses across several garnet fragments.

grain edges adjacent to reaction zones with the matrix compared to fragment centres (Figure 5.16b).

Hornblende in this sample is olive-green ferroan pargasitic to magnesian hastingsitic hornblende but cannot be separated into distinct generations based on textures as was possible in BVM91-714. Hornblende grains are locally fractured and altered to biotite and the extinction and pleochroism of these grains suggests that they have complex compositional zoning. Biotite occurs as both large grains in the matrix and as alteration zones in hornblende and both have lenticular inclusions of K-feldspar (e.g., Figure 5.14b) and are partly altered to chlorite. Biotite is not present in the separated fractures in garnet grains. Plagioclase in the matrix is $An_{\sim 41}$, in the separated fractures in garnet is An_{34-38} and is $An_{\sim 49}$ in the reaction zones separating garnet from matrix Fe-Mg silicate minerals. Quartz is present in the matrix, in association with altered biotite and hornblende, and in the separated fractures in garnet.

P-T constraints

There is no evidence that orthopyroxene was ever present in any sample from the Otter Brook gneiss. Therefore, the assemblage that pre-dates the amphibolite-facies fabric is interpreted to have been Pl + Kfs + Hbl + Cpx + Grt + Bt for sample BVM91-714 and Pl + Kfs + Hbl + Grt + Bt for BVM91-717. These assemblages are characteristic of upper amphibolite facies or hornblende-granulite facies and may persist to the granulite facies at high PH_2O. The presence of relict Pl + Hbl + Grt ± Cpx assemblages in samples of differing bulk composition, however, suggests that upper amphibolite facies is most likely. The P-T range qualitatively assigned to, or quantitatively derived from, upper-amphibolite transitional to granulite-facies assemblages is generally regarded as about 600-700°C and 4-10 kbar (Turner, 1981; Essene, 1989).

For quantitative thermobarometry, mineral compositions in sample BVM91-714 were averaged from four clinopyroxene fragments in feldspathic layers, three grains of brown hastingsitic hornblende, five grain-centre analyses away from inclusions in the largest garnet grain, and three analyses from two small biotite grains that are completely enclosed by, and that lack reaction rims adjacent to, garnet. These data were selected because the compositions are relatively consistent and are distinct from those of the overprint assemblage or, in the case of garnet, distinct from the compositions adjacent to reaction zones. The minerals from which the selected compositions were obtained are thought to represent the best estimate of the pre-overprint, higher-grade mineral assemblage based on the textural relations described above. However, there is no *a priori* basis for assuming that these represent equilibrium mineral compositions.

Feldspars were excluded from TWQ analysis because most grains are highly exsolved to coarse-patch perthite and antiperthite and could not be re-integrated to a bulk composition. Quartz is excluded from the phase assemblage because it is not present in the feldspathic matrix in this sample, and is associated mainly with mafic layers and Hbl-Qtz aggregates where it appears to be a product of pyroxene alteration. Both Mg and Fe end members were included in the component assemblage for clinopyroxene and biotite, and Grs, Alm, and Prp were included for garnet. Only FePrg and Prg amphibole end members were included in TWQ analysis because inclusion of the other four amphibole end members are dilute in these grains and thus produced spurious equilibria.

Remaining equilibria after exclusion of problematic components are Fe-Mg exchange reactions, and provide only temperature estimates. Equilibria involving Fe-Mg exchange with garnet and the Cpx-Bt, Fe-Mg exchange equilibrium cluster tightly at about 800°C (Figure 5.17a). The Cpx-Hbl equilibrium intersects the other equilibria, but at a low angle and the vertical position of this equilibrium is very sensitive to small variations in hornblende composition, thus the intersections do not constrain pressure estimates. The steeply sloping segment of this equilibrium generally agrees with the ca. 800°C temperature estimates of the other Fe-Mg exchange equilibria. Four conventional thermometers produced temperatures of 710-750°C and the GS(87) thermometer was higher at 940°C (Table 5.4).

Many more equilibria are made possible by including a plagioclase composition (An_{22}) that is the average of matrix grains, the average garnet core composition, the average of four clinopyroxene analyses from within the strain shadow, and the average composition of two brown hornblende grains. These compositions were selected in order to assess the quality and position of equilibria intersections derived from grains that are located as near as possible to one another. The resulting TWQ diagram displays a relatively good cluster of intersections at about 650°C and 12 kbar and the Fe-Mg exchange equilibria indicate temperatures closer to 750°C (Figure 5.17b). Conventional thermometers yielded temperatures of between 700-780°C (Table 5.4), which are within error of the TWQ temperature. Pressures estimated from conventional barometers (Table 5.4) are both higher and lower than the TWQ result at 8 kbar and 12 kbar.

In sample BVM91-717, it is not possible to ascribe the different compositions of plagioclase, garnet, biotite, and hornblende to discrete metamorphic generations based on textural evidence. Nevertheless, for a first approximation, average garnet grain centre compositions were combined with the average compositions of hastingsitic hornblende grain centres, matrix plagioclase grain centres and the least-altered biotite grains. Quartz is present in the matrix, and in association with

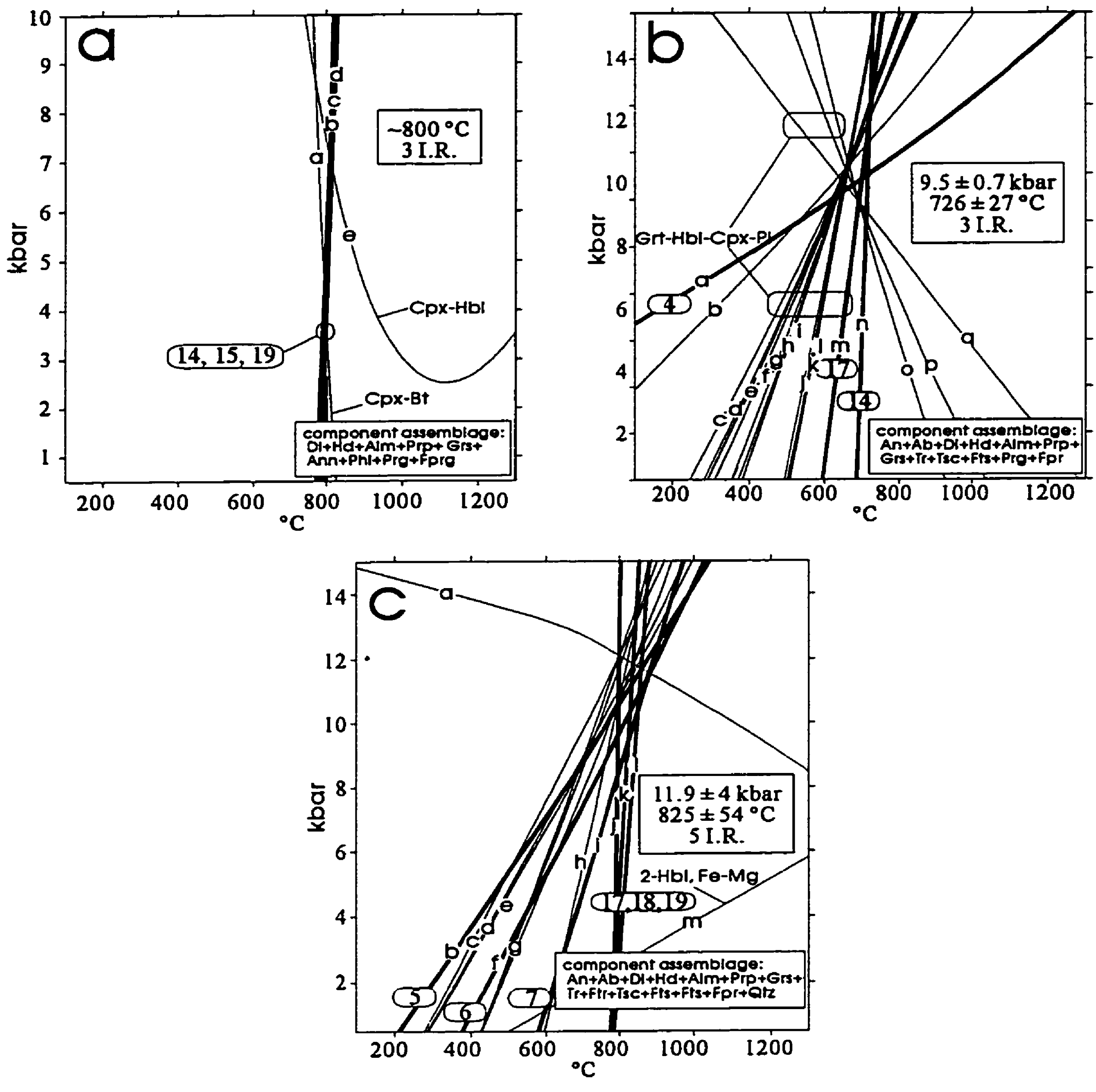

Figure 5.17 - TWQ diagrams from the Otter Brook gneiss. (a) and (b) Analyses from quartz-absent garnet-clinopyroxene-amphibole assemblages in sample BVM91-714 with different selected component assemblages and compositions as described in text. (c) Analysis from quartz-present garnet-amphibole assemblage in sample BVM91-717. Quoted errors are the 1.5σ standard deviation on the cluster of intersections and not the accuracy of the P-T estimate. Numbered heavy equilibria are calibrated or high-confidence reactions and correspond to Table 5.1. Lettered equilibria are listed in Appendix A5.3.

all alteration and retrogression textures and, therefore, quartz is included in the phase assemblage. Equilibria involving biotite were clearly outliers in the preliminary diagrams and were, therefore, excluded subsequently.

The resulting TWQ diagram provides a reasonable clustering of intersections at about 12 kbar and 825°C (Figure 5.17c), but the Fe-Mg exchange equilibria plot at about 800°C. With the same mineral compositions, including the questionable biotite composition, most of the conventional thermometers indicate temperatures of around 700-800°C and the KS(90) geobarometer yielded a pressure of 10 kbar (Table 5.4).

5.4 Amphibolite facies metamorphism

Based on the widespread presence of altered granulite, the Blair River inlier appears to have been a granulite-facies terrane that was subsequently affected by one or more metamorphic and deformational episodes at amphibolite facies and lower grades. Amphibolite samples commonly contain deformational fabrics of variable intensity and preserve different types of retrogression or overprinting textures. In foliated amphibolites, the presence of rare pyroxene relicts and varying degrees of replacement by amphibole, reflects heterogeneous deformation and fluid infiltration. Rare samples show static (i.e., non-deformational) amphibolite-facies overprint of high-grade metamorphic assemblages or anhydrous igneous minerals. Samples that display static overprint textures preserve fabrics attributable to their granulite gneiss or igneous rock predecessor but are composed mainly of amphibolite-facies metamorphic mineral assemblages.

Regional overprinting of high-grade assemblages during a prograde event requires large-scale fluid infiltration and this is most likely to occur in regions undergoing deformation (Brodie and Rutter, 1985). Distinguishing between prograde and retrograde metamorphism, therefore, requires preservation of differing types, or a sequence of overprinting textural relations.The two texturally distinct types (static overprint vs. foliated) of amphibolites in the Blair River inlier are discussed below along with their textural relationships with metamorphic titanite, and the implications for the timing of amphibolite-facies metamorphism.

5.4.1 Static overprint of high-grade or anhydrous igneous assemblages

In the Blair River inlier, progressive static overprinting of anhydrous (metamorphic or igneous) mineral assemblages by amphibolite-facies assemblages can be identified in some metamorphosed mafic rocks. Igneous and metamorphic pyroxene-bearing samples provide the best examples of these textures.

Figure 5.18 shows an example from the Lowland Brook Syenite of progressive stages of static overprinting. Igneous clinopyroxene grains in the freshest syenite samples commonly have a hornblende rim (Figure 5.18a) that may be of late magmatic (deuteric) origin and feldspars are microperthite. In samples with increasing amounts of recrystallised matrix and coarsely exsolved feldspar, coarse grains of dark-green or brown hornblende replace pyroxene to increasingly greater degrees and hornblende rims are progressively wider (Figure 5.18b). At further stages, the central core of clinopyroxene is altered completely to a mosaic-texture aggregate of Hbl+Qtz. In many samples titanite rims begin to develop around Fe-Ti oxide minerals at this stage, especially in samples that also have some Chl±Ep replacing hornblende and biotite. The mosaics comprise light-green actinolitic hornblende and are rimmed by coarse darker-green or brown magnesio-hornblende (Figure 5.18c). Samples that are completely altered to amphibolite-facies assemblages commonly contain significant amounts of titanite, both as rims around Fe-Ti oxide minerals and as spindle-shaped matrix grains. In samples within or near shear zones or highly fractured areas,

Figure 5.18 - Example of progressive igneous pyroxene alteration to amphibolite-facies assemblages from the Lowland Brook Syenite.

(a) igneous clinopyroxene inclusion in microperthite from an undeformed sample (SB86-3140; XP; scale bar = 1mm). The clinopyroxene grain has an igneous (deuteric?) hornblende reaction rim.

(b) initial stage of metamorphic alteration of clinopyroxene grain, with the growth of coarse green-brown hornblende and exsolution of Fe-Ti oxide minerals (SB85-1030; PP; scale bar = 1mm).

(c) mosaics of Hbl+Qtz replacing what was once a core of clinopyroxene that was rimmed by coarser-grained hornblende. Note that there is no fine-grained exsolved Fe-Ti oxide mineral present in the mosaic, that titanite rims large Fe-Ti oxide minerals, and that there is a small degree of Chl+Ep alteration. (SB85-1047; PP; scale bar = 1mm)

(d) Chl+Ep pseudomorphous after clinopyroxene in a sample that was affected only by late, low-grade alteration associated with a fracture that cuts the thin section. Note lack of titanite around Fe-Ti oxide minerals (SB85-1049; PP; scale bar = 1mm).

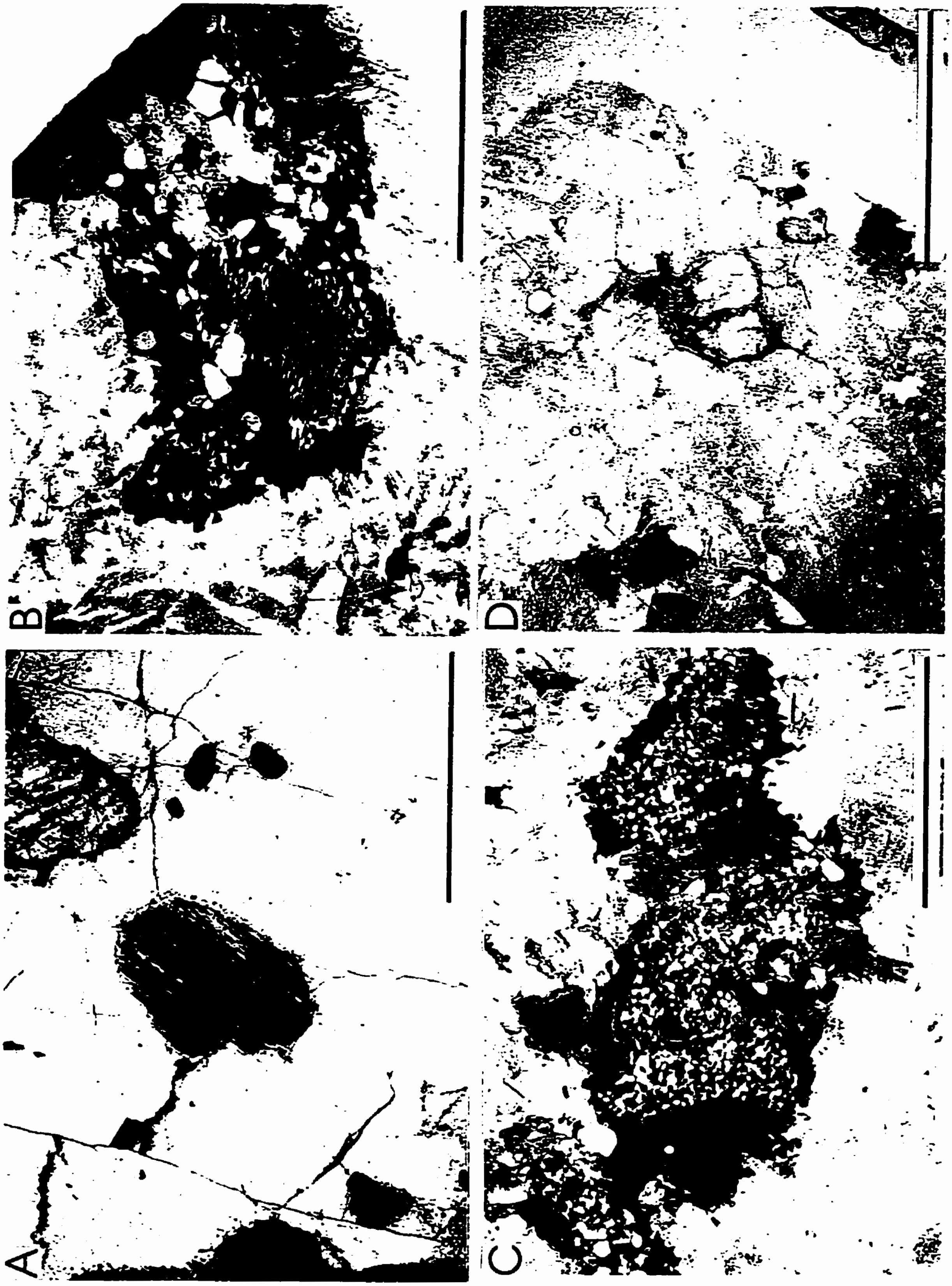

Figure 5.18

clinopyroxene is replaced directly by chlorite and Fe-Ti oxide minerals are rimmed by biotite or chlorite instead of titanite (Figure 5.18d).

Mafic units in the Red River Anorthosite Suite also show progressive alteration textures. Some samples of leucogabbro have a granular rim of brown hornblende around clinopyroxene (Figure 5.19a) and, at further stages the granular hornblende is highly zoned and clinopyroxene is replaced by Hbl+Qtz mosaics (Figure 5.19b). The layered unit also shows progressive alteration textures. Amphibole-quartz mosaics contain relict clinopyroxene cores and clinopyroxene is progressively altered to hornblende or Act+Chl with rims of fine-grained epidote (Figure 5.19c, d). The relationship between progressive pyroxene alteration and titanite growth in the Red River Anorthosite Suite is unclear. Samples that contain either titanite rims around Fe-Ti oxide minerals, or separate titanite grains, most commonly contain Chl+Ep assemblages, but whether titanite grew during a previous stage of development of the amphibolite-facies overprint is uncertain.

In the Sailor Brook gneiss and the undivided unit, mafic and intermediate gneiss samples shows progressive alteration from pyroxene-bearing to pyroxene-bearing assemblages to Hbl+Pl or Chl+Ep±Ab assemblages. In some cases, the entire progression is contained within the area of a single thin section (Figure 5.20a). Figure 5.20b shows an example from the Sailor Brook gneiss of static amphibolite-facies overprint of a pyroxene-granulite with well-preserved relict pyroxene cleavage in hornblende. A gneiss of intermediate (granodioritic) composition from the undivided unit shows incipient development of Hbl+Qtz mosaics and preserves Fe-Ti oxide inclusions that mimic pyroxene cleavage (Figure 5.20c).

Figure 5.19 - Progressive alteration textures in the Red River Anorthosite Suite.

(a) primary pyroxene and Fe-Ti oxide grains are rimmed by granular green-brown hornblende. The green-brown hornblende is altered around grain edges to a pale-green amphibole and clinopyroxene grains are further altered to actinolite and chlorite, but retain Fe-Ti oxide inclusions that mimic original pyroxene cleavage. (leucogabbro, RB91-009b; PP; scale bar = 1mm)

(b) at further stages of alteration, pyroxene is replaced completely by amphibole aggregates. Each grain of the aggregate is zoned from tremolite-rich at the centre to tschermakite-rich at the edge and the aggregate as a whole also shows compositional zoning, with generally darker green aggregates around the edge. The adjacent grains retain part of a previous mosaic texture, but appear to have locally expelled quartz to form multi-granular aggregates. (leucogabbro, SB86-3139c; PP; scale bar = 1mm)

(c) textures like those of (a) grade into Hbl+Qtz mosaics with hints of prior pyroxene cleavage surrounded by granular hornblende (layered unit, BVM91-774; PP; scale bar = 1mm)

(d) at further stages of retrogression, mafic mineral clusters develop a rim of very fine-grained Ep+Chl between hornblende and plagioclase (layered unit, BVM90-065; PP; scale bar = 1mm).

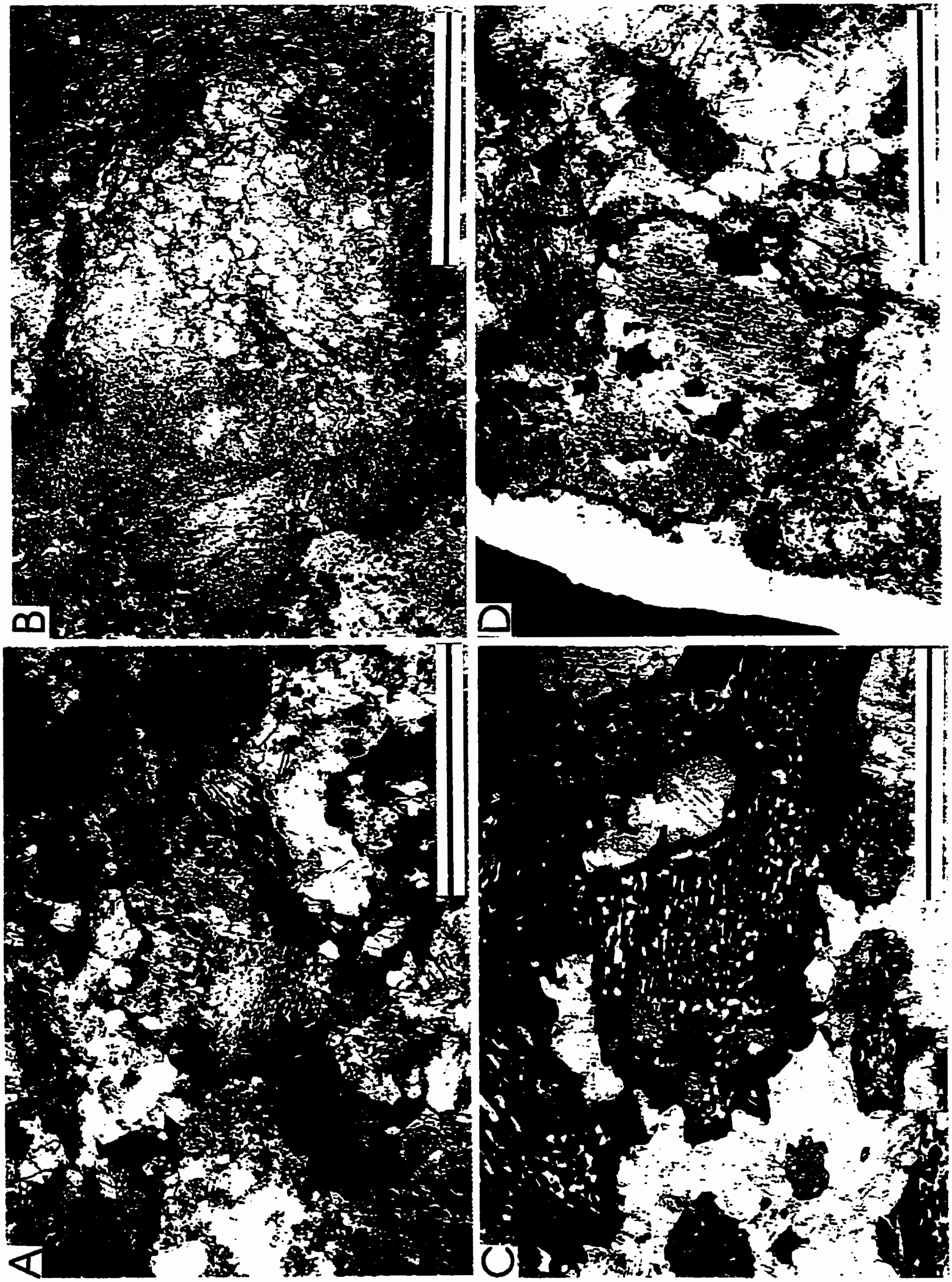

Figure 5.19

Figure 5.20 - Examples of retrogression textures in the Sailor Brook gneiss and undivided unit.

(a) cores of exsolved clinopyroxene surrounded by fine grained Hbl+Qtz mosaics (RR2047a; PP; scale bar = 1mm).

(b) medium-grained granular amphibolite with relict pyroxene cleavage in hornblende (BVM91-526; PP; scale bar = 1mm).

(c) retrograded granulite with greater degree of amphibole recrystallisation, but that still retains relict pyroxene cleavage defined by opaque inclusions (BVM91-773; PP; scale bar = 1mm).

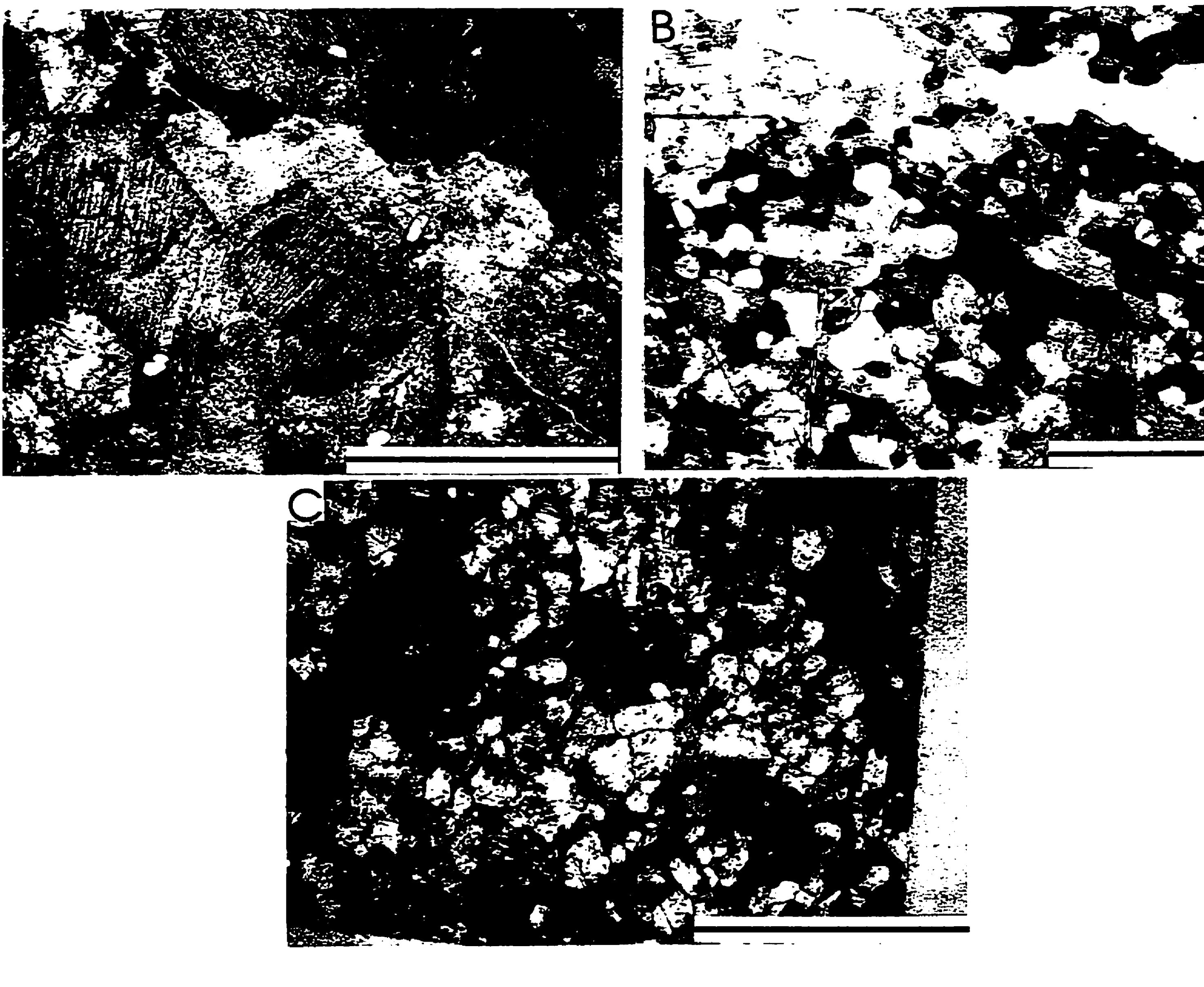

Figure 5.20

In the samples that show a static amphibolite-facies overprint, lower grade mineral assemblages progressively overgrow or replace minerals from a higher grade or anhydrous assemblage. Alteration of pyroxene to hornblende appears to be sequentially followed by alteration of hornblende and biotite to chlorite and epidote. The static amphibolite-facies overprint is, therefore, interpreted to result from retrograde metamorphism of a granulite-facies or anhydrous igneous assemblage. At least some titanite growth, particularly as rims around Fe-Ti oxide minerals, is associated with retrogression. Samples that show a static overprint directly to Chl+Ep±Ab assemblages generally lack titanite and are associated with late shear zones.

5.4.2 Foliated amphibolites

By contrast with static retrogression, foliated amphibolites are commonly hornblende-chlorite-epidote-plagioclase gneiss, or chlorite-biotite-amphibole schist. These rocks generally lack textures or relict minerals from a higher-grade precursor, or they rarely contain textures that are the deformed equivalents of the retrogression textures described above.

In gneissic samples from the Lowland Brook Syenite, Hbl+Qtz mosaics are deformed and help define the foliation. Biotite replaces hornblende around the edges of the sheared mosaics, and biotite is locally altered to Chl±Ep±Kfs. Titanite rims around Fe-Ti oxide minerals are common in the gneissic syenite and the rims are most commonly associated with Chl+Ep alteration of hornblende and biotite (Figure 5.21a).

The predominant mineral assemblage in foliated amphibolite samples from the gneissic units is Hbl±Act±Bt+$An_{\sim 21-33}$±Kfs+Chl+Ep±Ab+Ttn. Some samples preserve rare indications of a prior anhydrous mineral assemblage, for example, the samples from the Otter Brook gneiss

Figure 5.21 - Textures of foliated amphibolites.

(a) sheared Hbl+Qtz mosaic from gneissic syenite (FD85-548; PP; scale bar = 1mm). Biotite has partly replaced hornblende around the edges of the mosaic, but the biotite is itself altered to chlorite and epidote. Titanite rims around Fe-Ti oxides occur adjacent to chlorite.

(b) clinopyroxene porphyroclast mantled by feldspar and wrapped by amphibolite-facies fabric including coarse rhomboid titanite (Otter Brook gneiss, BVM90-138; PP; scale bar = 1mm).

(c) fine-grained, highly foliated epidote-amphibolite gneiss (Act+Chl+Pl+Ep+Ab) with abundant titanite both as rims around Fe-Ti oxide minerals and as separate spindle-shaped grains within the deformational fabric (undivided unit; BVM90-094; PP; scale bar = 1mm).

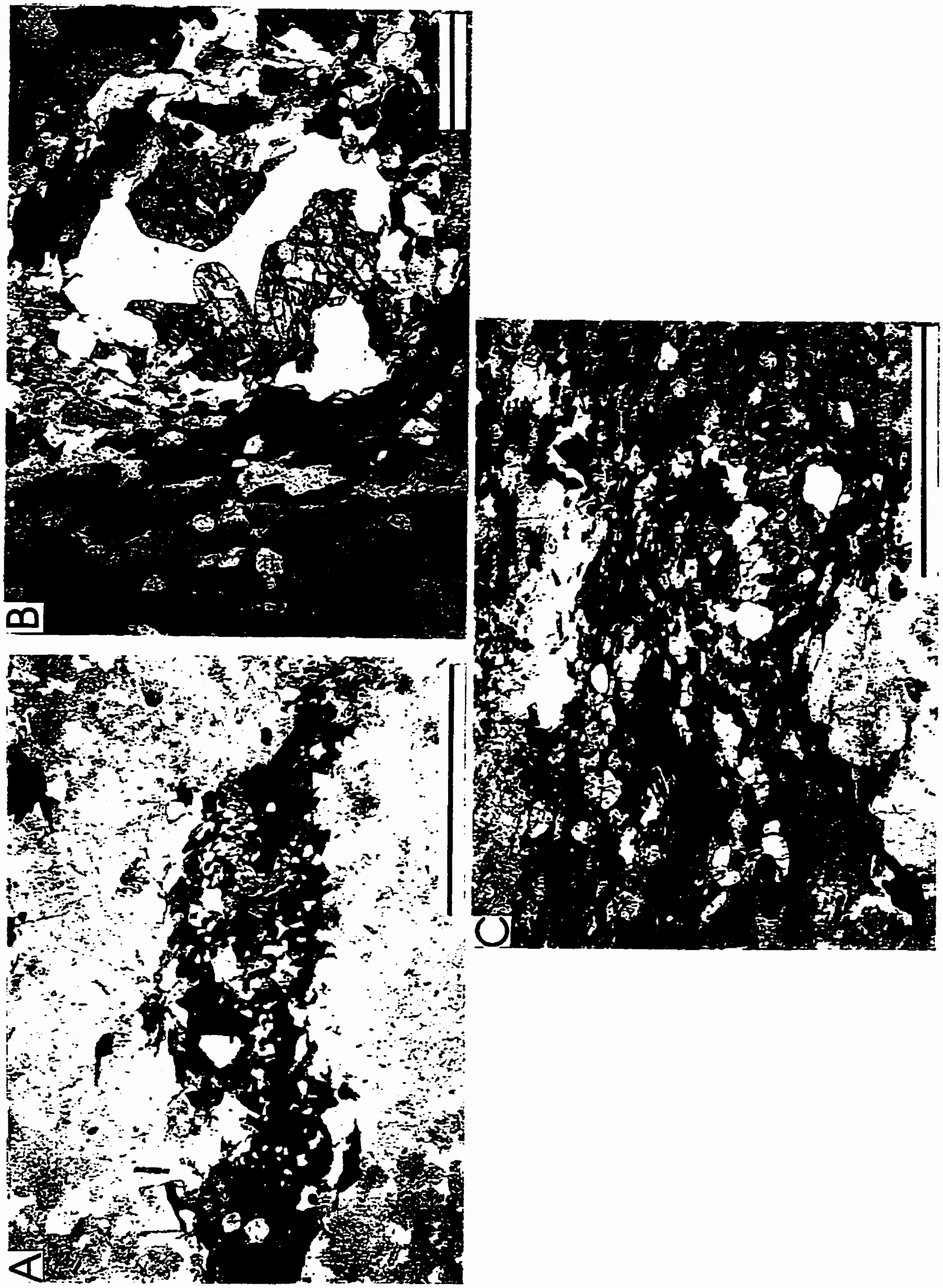

Figure 5.21

described in Section 5.3.1. However, in all cases, the high-grade minerals are relicts. There is no indication in any foliated amphibolite-facies sample of the incipient development of clinopyroxene or garnet. A foliated amphibolite from the Otter Brook gneiss contains a fabric-defining assemblage of Hbl+An_{24}+Bt+Ep+Chl+Ttn. Clinopyroxene grains in this sample are preserved only where mantled by feldspar and the foliation wraps around the mantled clinopyroxene augen (Figure 5.21b). The amphibolite-facies fabric includes large titanite grains with the coarse rhomboid habit of those of igneous origin. In the undivided unit, many foliated amphibolites contain the assemblage Hbl+Ep±Act+Bt+Chl+Ab (Figure 5.21c). Other coarse-grained amphibolites in the undivided unit contain Hbl+Pl with Chl+Ep alteration along fractures.

5.4.3 Textural and mineralogical relations and P-T constraints

The amphibolite-facies rocks in the Blair River inlier are poor candidates for quantitative thermobarometry. There is no newly-grown garnet in the amphibolite-facies assemblages and pre-existing garnet is resorbed adjacent to biotite and amphibole, amphibole grains are commonly zoned, multiple generations of amphibole may be present in one sample, and amphiboles of retrograde origin are incompletely altered pyroxene and are themselves partly altered to chlorite and epidote. Other solid solution minerals, for example plagioclase, are also zoned, altered, or of variable composition throughout the sample. Given these difficulties, equilibrium mineral compositions are ambiguous and therefore most amphibolite samples were not analysed in detail.

Microprobe analyses were, however, conducted on several samples that show static retrogression textures and the compositional/textural relationships could not be deciphered. For example, a sample from the layered unit (BVM91-774) contains hornblende aggregates pseudomorphous after pyroxene. Individual hornblende grains are optically zoned (Figure 5.19c), varying in composition from actinolitic hornblende to tschermakitic hornblende and plagioclase compositions vary from An_{29} to An_{32}. However, there is no texturally justifiable criteria with which to select combinations of compositions. Using combinations of hornblende and plagioclase compositions, the Holland and Blundy (1994) thermometers yielded temperatures of 630°C to 1032°C. The lowest temperatures imply that retrogression occurred above 600°C, but there is no basis on which to assess whether any of the mineral compositions are valid equilibrium pairs.

A necessarily more general approach is taken here to constrain P-T conditions of amphibolite-facies metamorphism based on mineral paragenesis, inferences from reaction limits, and assemblage stability fields. There are two distinct textural and mineralogical types of amphibolite in the Blair River inlier (Table 5.5), and both lack any evidence for the incipient crystallisation, or stable coexistence, of pyroxene or garnet. Therefore, the amphibolites did not reach uppermost amphibolite facies conditions. The upper-amphibolite transition to hornblende-granulite or pyroxene-granulite assemblages in mafic and ultramafic rocks is generally considered to be at about 650-700°C and 8 kbar (Green and Ringwood, 1967: 1972; Turner, 1981; Essene, 1989). Cummingtonite is an intermediary retrogression product (i.e., Opx→Cum→Ca-amphibole) during the amphibolitisation of mafic granulite at low pressure (<3 kbar; e.g., Mongkoltip and Ashworth, 1986; Turner, 1981). However, cummingtonite was not recognised in any thin section of either type of amphibolite; all analyses are Ca-amphiboles and, where optically determinable, all colourless or very pale green amphiboles (including the centres of zoned grains, e.g., Figure 5.19c) are tremolite or actinolite. Both types of amphibolite in the Blair River inlier are therefore constrained to less than about 675°C and between 3-8 kbar on the basis of phases absent from their parageneses.

Table 5.5 - Summary of distinctions between styles of amphibolite-facies metamorphism.

	Static Retrograde Amphibolite	Foliated Prograde Amphibolite
Characteristic textures	relict Pyx partly alted to Hbl common, Hbl+Qtz mosaics, zoned Hbl, little deformation, preservation of some high-grade metamorphic reaction textures by subsequent overprint	little evidence for relict high-grade minerals, sheared or flattened Hbl+Qtz mosaics, shape-preferred alignment of coarse amphibole and bioite, quartz ribbons, little evidence preserved of prior lower grade reactions
Characteristic mineral assemblage	zoned green-brown Hbl, $An_{22\text{-}30}$, Qtz, ±Bt, ±Chl, ±Ep	unzoned blue-green or green Hbl, $An_{20\text{-}25}$, ±Chl, Ep, Bt, ± Act, ±Ab, ±Qtz
Metamorpic facies	amphibolite facies	epidote-amphibolite subfacies
Inferred P-T range	550-650°C 3-5.5 kbar	375-600°C 5-7 kbar
Relationship to titanite	rare Ttn with Hbl+Pl assemblages, some may have crystallized prior to retrogression (e.g., igneous) Ttn rims common around Ox in local areas retrogressed to Chl+Ep	Ttn rims on Ox common abundant separate spindle-shaped grains in coarse foliated samples igneous Ttn of same age in intrusive units
Interpretation	retrograde metamorphism during cooling following high-grade metamorphic event	prograde metamorphism associated with petentrative deformation during a discrete thermal pulse
Age of metamorphism	any time between ca. 1000 Ma and final cooling at ca. 425 Ma	immediately preceding final cooling at ca. 425 Ma

Unfoliated amphibolites contain mostly magnesio-hornblende or tschermakitic-hornblende, plagioclase (An_{21-33}), with or without significant biotite. Actinolite, chlorite, and epidote are minor phases concentrated along late fractures. Several lines of evidence suggest that these amphibolites formed during a retrogression event. Relatively fresh granulite and pyroxene-bearing igneous rocks have a patchy distribution throughout the outcrop area (i.e., in the Lowland Brook Syenite, Sailor Brook gneiss, and undivided unit), the amphibolites lack a pervasive foliation, and commonly preserve relict high-grade minerals that are successively overgrown by lower-grade minerals where sequential reaction textures are recognisable. Because static retrograde textures are locally deformed and overprinted by a second generation of fabric-defining amphibolite-facies minerals (e.g., see description of Otter Brook gneiss), the static retrogression is interpreted to have occurred during cooling from granulite-facies conditions. Retrograde re-equilibration at amphibolite-facies conditions is a common occurrence in moderately or slowly cooled granulite terranes (e.g., Harley, 1989; Martingole, 1992; Lucassen and Franz, 1996). Most of the static-texture amphibolites were not retrograded to epidote-amphibolite facies assemblages and, therefore, they are interpreted to have formed at conditions within the stability field of common Hbl+Pl amphibolites. Apted and Liou (1983) and Liou et al. (1985) determined experimentally the positions of epidote-out reactions (i.e., reactions that separate epidote-amphibolite-subfacies from amphibolite-facies assemblages) for metabasaltic rocks and placed the reactions in the range of 550-625°C at 5.5 kbar. With increasing fO_2, these reactions move to higher temperature and lower pressure, therefore, the retrograde amphibolites are constrained to 550-650°C and 3-5.5 kbar.

The foliated amphibolites that form the bulk of the Blair River inlier are characterised by actinolitic or magnesio-hornblende and plagioclase (An_{20-28}) but contain significant quantities of epidote, actinolite, and patches of chlorite and albite. The presence of deformed relicts of static retrogression textures within the foliated amphibolites, and the otherwise very rare evidence for prior high-grade assemblages suggests that the foliated amphibolites represent a discrete prograde thermal and deformational episode that achieved epidote-amphibolite subfacies conditions. This contrasts with the static overprint which produced Hbl+Pl amphibolites; the characteristic textural and mineralogical distinctions between the two are summarised in Table 5.5. Liou et al. (1985) constrained the chlorite-out reactions that separate greenschist facies assemblages from epidote-amphibolite-subfacies assemblages to a minimum of about 375° (independent of pressure), thus the field for epidote-amphibolite-subfacies assemblages is at higher pressure (>5 kbar at 500°C) over the same temperature range as Hbl+Pl±Chl amphibolites. Therefore, the epidote-amphibolite-subfacies event occurred at temperatures above 375°C to perhaps as high as 600°C at higher pressure (5-7 kbar) and/or higher fO_2 than the static retrograde overprint.

Metamorphic titanite rims around Fe-Ti oxide minerals are very rare in retrograde amphibolite, but are common in foliated amphibolite. Spindle-shaped titanite grains, some of which may have been igneous grains, are present in both types of amphibolite, but are more common in foliated amphibolite. The bulk of the metamorphic titanite is associated with samples affected by prograde epidote-amphibolite-subfacies metamorphism accompanied by deformation and in retrograde amphibolite samples that have some degree of localised alteration to chlorite and epidote. Titanite is well documented as part of lower amphibolite- or greenschist-facies assemblages. For example, in prograde metamorphism to mid- or upper-amphibolite-facies, decreasing amounts of titanite accompany chlorite- and epidote-out reactions, increasingly calcic plagioclase, increasingly titaniferous amphibole, and ilmenite-in reactions (Spear, 1981; Apted and Liou, 1983; Liou et al., 1974).

The inferred temperatures of amphibolite-facies metamorphic events (550-650°C and 375-600°C) are close to the inferred U-Pb systematics closure temperature for titanite (500-600°C). Metamorphic temperatures are not constrained sufficiently to distinguish between the possibilities of regional cooling and synchronous crystallisation to account for the close correlation between the U-Pb titanite ages (Chapter 4). However, synchronous crystallisation is unlikely given the varying sizes, types (thin rims around rutile and opaque oxide minerals, spindle-shaped matrix grains, coarse crystalline igneous grains), origins (two different metamorphic parageneses and ca. 435 Ma igneous units) and wide varyations in rock composition. It is much more likely that the ubiquitous ca. 425 Ma titanite ages were produced by regional cooling of the Blair River inlier, including the Paleozoic igneous units (i.e., Sammys Barren granite, Red River syenite, and Fox Back Ridge diorite/granodiorite), through the closure temperature for titanite.

5.5 Low grade metamorphism

In the Blair River inlier, greenschist-facies retrogression is most common along high-level brittle faults. Some samples near high-level faults are not highly deformed but contain the assemblage Ep+Chl+Ab±Act which overprints both high-grade and amphibolite-facies precursors. Most of these samples also contain relicts of blue-green hornblende coexisting with actinolite. Carbonate is present in a few samples in association with small highly retrogressed zones or pockets near fractures. Greenschist-facies mineral assemblages also predominate in highly sheared rocks in the Wilkie Brook fault zone, in internal shear zones, and along zones of highly fractured rocks, most commonly forming Chl+Ep+Ab+Ms±Cal schists. These low-temperature assemblages probably formed when the Blair River inlier was at a high structural level. In the case of the Wilkie Brook fault zone, these assemblages probably formed in response to deformation associated with the docking of the Aspy terrane (Chapter 2).

The reactions that separate sub-greenschist, greenschist, and amphibolite facies assemblages occur over a small temperature range and no sub-greenschist minerals (e.g., prehnite, pumpellyite, lawsonite) were observed in any sample, including in low-grade metamorphosed and altered gabbro and diabase dikes. The parageneses of greenschist-facies assemblages suggest conditions in the P-T range of about 4-7 kbar and 250-350°C (Liou et al., 1985; Apted and Liou, 1983).

5.5 Summary

The Blair River inlier lacks metapelites, and most metabasites are partly retrograded and have disequillibrium textures. Few samples preserve metamorphic garnet, which is necessary for many geobarometers, and garnet grains are partly resorbed (suggesting compositional disequilibrium) in all samples that contain garnet. Quantitative thermobarometry is, therefore, difficult in these rocks. Nevertheless, the few samples that preserve equilibrium or reaction textures provide some insight into metamorphic conditions, and known or inferred mineral assemblages provide for further constraints. Granulite-facies metamorphic conditions in the range of 6-8 kbar and 700-850°C are inferred, based on the two-pyroxene, garnet-absent mineral assemblages of the Sailor Brook gneiss. In the Red River Anorthosite Suite, the combination of the TWQ approach (Berman, 1991) and conventional thermobarometers indicates temperatures of about 700-800°C and about 3 kbar for the reaction rims around high-Al orthopyroxene megacrysts. These conditions may record decompression following either igneous crystallization or high-grade metamorphism, as is consistent with the symplectitic reaction zone textures (e.g., Harley, 1989; Clarke and Powell, 1991). Two-pyroxene metamorphic mineral assemblages are best preserved in the charnockite unit. TWQ and conventional analysis of recrystallized granular clinopyroxene-bearing assemblages indicate temperatures of about 700-800°C and pressures of 8-10 kbar. Rare relicts of a clinopyroxene + garnet assemblage are preserved in the Otter Brook gneiss. Geothermobarometric analyses of these rocks indicate metamorphic conditions of about 700-850°C and higher pressures than the other units at about 10-12 kbar. However, it should be noted that the Otter Brook gneiss results are less reliable due to the uncertainty of recovered mineral compositions as a result of the strong affects of retrograde and/or overprinting metamorphic events. Both static and dynamic amphibolite-facies overprint metamorphic events are recognized based on metamorphic mineral textures. The latter event is interpreted to have occured after the former based on overprinting relations of progressive deformation and new amphibolite-facies mineral growth over the static retrogression textures. Metamorphic titanite grains are associated with the dynamic, foliation-forming amphibolite-facies event. Conditions of metamorphism could not be constraind precisely enough to determine if the grains grew simultaneously below their closure temperature or whether they cooled through their closure temperature together. The latter interpretation is prefered for the reasons presented in Chapter 5. Based on paragenetic inferences and calibrated greenschist-facies reactions, the low-grade metamorphism that is concentrated along late fault zones, and that overprints both high-grade and amphibolite-facies assemblages, is inferred to have occurred in the P-T range of 4-7 kbar and 250-350°C.

CHAPTER 6 - Summary and Discussion

6.1 Introduction

The Proterozoic history of the Blair River inlier is preserved in major gneissic and plutonic units. Comparisons of rock types, chemical characteristics, ages, and the timing and conditions of metamorphism provide a specific basis for the general correlation of the Blair River inlier with the Grenville Province as inferred by previous workers using various lines of evidence (Brown 1973; Currie, 1975; Macdonald and Smith 1979; Raeside et al., 1986; Barr et al., 1987a; 1987b; Dickin and Raeside, 1990; Barr and Hegner, 1992; Ayuso and Barr, 1991; 1993). Defining the basis for correlation between the Blair River inlier and the Grenville Province is critical to understanding the role of the inlier in Paleozoic tectonic events along the Laurentian continental margin.

6.2 Correlation with the Grenville Province and alternative interpretations

An important part of the present study has been acquisition of data to test the hypothesis that the Blair River inlier is an exposure of Laurentian basement rocks, and thus helps to constrain the geometry and style of Appalachian terrane interactions. Alternative interpretations for the origin of the inlier are that it is an exotic piece in, or basement to, Gondwanan terranes (eg., Murphy et al., 1989; Keppie et al., 1990; Keppie and Dostal, 1991, Keppie, 1992), and that the inlier could be Grenville-age but not derived from Laurentia. These alternative interpretations are part of recent tectonic models proposed by Keppie et al., (1996) and Lynch (1996). Keppie et al., (1996), suggest that the Blair River inlier could have been derived from a broadly "Grenville-age" orogenic belt along the Amazon Craton (western South America) and was accreted to North America in the Ordovician Taconian orogeny. Lynch (1996) considered the Blair River inlier to be part of the "Cabot nappe" of Gondwanan affinity in the Central Mobile Belt. In his model the nappe was accreted during Silurian and Devonian thick-skinned, thrust-related accretionary events prior to Late Devonian to Carboniferous extensional exhumation.

In the model proposed by Lynch (1996), the inclusion of the Blair River inlier in the Cabot nappe is based on two lines of evidence. The first is the correlation of metasedimentary units ("George River Group") throughout Cape Breton Island. The Meat Cove Marble (at that time considered to be part of the Polletts Cove Brook Group) in the Blair River inlier was correlated with the "George River Group" by early workers (e.g., Milligan, 1970) at a time when all crystalline rocks on the island was considered a single lithotectonic block. Parts of the "George River Group" in southern Cape Breton Island are interpreted to be Proterozoic carbonate and detrital-clastic shelf sequences that formed on the margin of Gondwana (e.g., Keppie, 1989; 1992). Therefore, the correlation of the group across the four lithotectonic zones proposed by Barr and Raeside (1989) is critical to defining the Gondwanan affinity of the Blair River inlier. The second line of evidence for inclusion of the Blair River inlier in the Cabot nappe is the continuity of thrust-related deformational fabrics between the main décollement beneath the Cabot nappe (Highlands Shear Zone) and the Wilkie Brook fault zone.

The idea of a single Cape Breton Island-wide, Proterozoic-age, "George River Group" must be abandoned, as has been suggested by many other workers (e.g., Jamieson and Doucet, 1983; Currie, 1987a; Hill, 1988; Raeside and Barr, 1990; Lexicon of Canadian Stratigraphy, Vol. VI, pg. 137). The correlation is overly simplistic and does not take into account the likelihood that the units that make up the "group" are of very different ages, and are parts of disparate tectonic blocks. Furthermore, Sangster et al., (1990a; 1990b) showed that the isotopic characteristics of the Meat Cove marble in the Blair River inlier are dissimilar to those in the remainder of Cape Breton Island with the exception of the Lime Hill gneissic complex. They clearly stated that an island-wide correlation cannot be made on the basis of isotopic characteristics, despite the claim by Lynch (1996; p. 95) to the contrary. Sangster et al., (1990b; p. 31) further stated that, "Marble-hosted zinc occurrences at Lime Hill and Meat Cove on Cape Breton Island are geologically, geochemically, and isotopically (S and Pb) similar to a distinctive group of zinc occurrences hosted by Grenville Supergroup marble in Ontario, Quebec, and New York". Major and trace-element geochemical characterisation of units once thought to be part of the "George River Group" led Hill (1988; p. 173) to conclude, "Carbonates underlying the Cape Breton Highlands are a third type. These metalliferous marble units are unrelated to carbonates of southern Cape Breton Island". The obsolete notion of a single island-wide metasedimentary unit is an inadequate basis for a correlation with the important implications proposed by Lynch (1996).

Despite the depiction of the Wilkie Brook fault zone as a northwest-dipping thrust fault (Lynch, 1996; his figure 3), he presents no structural data to support such a claim. Structural data presented in this study, by Raeside (1989), and by Raeside and Barr (1992) have demonstrated that the Wilkie Brook fault zone is a steeply-dipping, predominantly strike-slip fault. Thus, when considered in detail, both arguments fail and the inclusion of the Blair River inlier in the Cabot nappe cannot be substantiated on the grounds proposed by Lynch (1996). If the Blair River inlier cannot be demonstrated to be part of the Cabot nappe, then there is no basis for including the inlier in the Central Mobile Belt or in the Gondwanan terranes.

The terrane transfer model of Keppie et al., (1996) proposes the possibility that the Blair River "terrane" is exotic to North America and was accreted during Taconian collision between Laurentia and western Gondwana (i.e., Amazonian craton of South America). They do not propose a specific tectonic model for terrane transfer involving the Blair River inlier. Instead, Keppie et al., (1996) consider the possibility of a South American origin because basement terranes with Laurentian ages are found in the central Andes (e.g., the Precordillera terrane; Ramos et al., 1986) and the Grenville-age Goochland Terrane in the Appalachian orogen may be exotic to North America (Hibbard and Samson, 1995). Furthermore, early Paleozoic tectonic reconstructions (e.g., Dalziel 1991) place Laurentia adjacent to western South America where ca. 1000-1200 Ma orogens and allochthonous terranes exist (e.g., Tosdal, 1996). Therefore, the present location of basement terranes does not uniquely identify their origin. Keppie et al., (1996) proposed that it may be possible for portions of cratonic South American to have been accreted to Laurentia in the same manner as the Laurentian Precordillera terrane was accreted to South America ("terrane transfer").

The terrane transfer model, while possible (and plausible in the case of the Precordillera) is not applied in a specific manner to the Blair River inlier, but is instead based on its generalised identity as a "Middle Proterozoic basement terrane". Because few high-precision radiometric ages are available from potential South American source regions, there are insufficient data with which to compare and contrast tectonothermal histories. However, the Blair River inlier lacks any indication of typical Gondwanan thermal events (e.g., ca. 600 Ma) that would be expected in South American basement rocks. Furthermore, the terrane transfer model Keppie et al (1996) fails to explain the continuity of the Blair River inlier with the Laurentian side of the orogen as suggested by gravity and magnetic data, and fails to explain the continuity of events recorded in other parts of the Laurentian margin.

In the absence of unambiguous criteria to link the Blair River inlier to either Laurentia or Gondwana, the simplest explanation that can account for all the known characteristics of the inlier must be the preferred interpretation. As explained in more detail below, every Proterozoic unit in the Blair River inlier has a lithologic and temporal counterpart in the Grenville Province.

Furthermore, isotopic characteristics of the Blair River inlier are consistent with a Laurentian origin and these data contrast with the Gondwanan and peri-Gondwanan outboard terranes in Cape Breton Island (Barr and Hegner, 1992; Ayuso et al., 1996). The implications of possible massif-type anorthosite recovered from drill cores in Gondwanan rocks in New Brunswick (Boyle and Stirling, 1994) cannot be evaluated at present due to the scarcity of material, the lack of observable field and structural relations, and conflicting reports of the significance of associated "charnockitic" rocks, which yielded a ca. 390 Ma crystallisation age (S. Barr, pers. comm., 1996).

6.2.1 Comparison of Proterozoic rocks of the Blair River inlier with the Grenville Province

The Sailor Brook gneiss is lithologically similar to pre-Grenvillian (i.e., older than about 1200 Ma) trondjhemitic, tonalitic, dioritic, and granodioritic gneisses in the Adirondack Mountains, the Central Metasedimentary Belt, and in basement inliers in Vermont and New York (Figure 6.1; Pride and Moore, 1983; Lumbers et al., 1990; McLelland and Chiarenzelli, 1990a; Ratcliffe et al., 1988, 1991). These suites belong to either an older (ca. 1350-1310 Ma) or younger (ca. 1285-1230 Ma) period of igneous activity, but both generations are described as part of the "Elzevirian orogenic event" (e.g., Moore and Thompson, 1980; Gower et al., 1990; McLelland and Chiarenzelli, 1990a) or "Elzevirian phase of the Grenville orogeny" (e.g., Ratcliffe et al., 1991). Rocks of the older phase are present in Vermont, the Adirondack Highlands, and along the northwestern margin (Bancroft terrane) of the Central Metasedimentary Belt. Rocks of the younger phase are widely distributed throughout the Central Metasedimentary Belt, including in the Elzevir terrane and the Adirondack Lowlands, and potassic plutons of this age are also present in Vermont. The Sailor Brook gneiss, however, is not trondjhemite in the sense of Streckeisen (1976; tonalitic rock with <10% mafic minerals) or Lumbers et al., (1990; oligoclase-bearing tonalite with <15% biotite and amphibole).

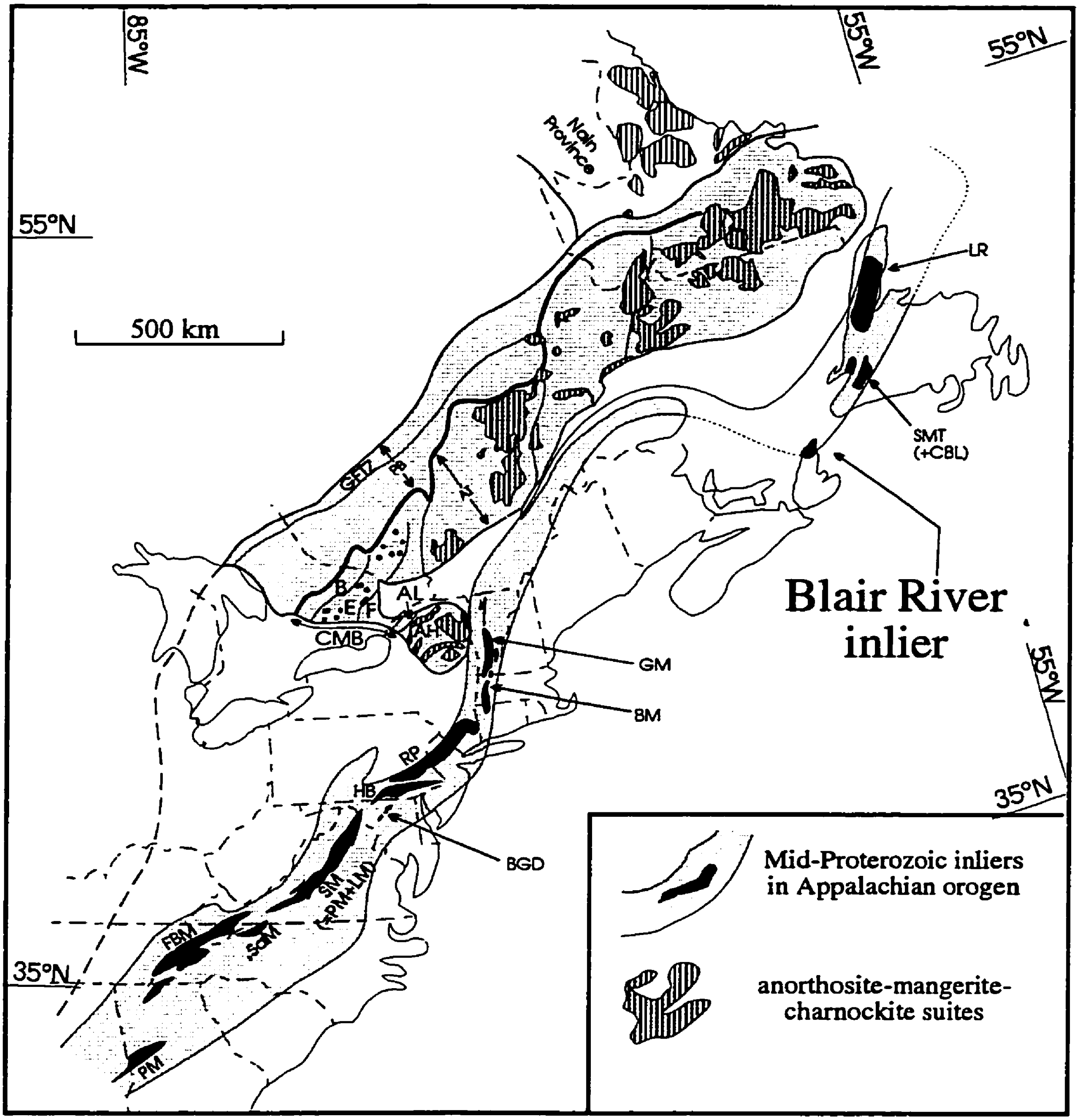

Figure 6.1 - Grenvillian inliers in the Appalachian Orogen (solid black) and tectonic subdivisions of the Grenville Province (modified after Rankin et al., 1993 and Rivers et al., 1989). Black dots in the Elzevir terrane are K-rich plutons (after Corriveau and Gorton, 1993). AH = Adirondack Highlands, AL = Adirondack Lowlands, AT = allochthonous terranes, B = Bancroft terrane, BGD = Baltimore Gneiss Domes, BM = Berkshire Massif, CMB = Central Metasedimentary Belt, E = Elzevir terrane, F = Frontenac terrane, FBM = French Broad Massif, GFTZ = Grenville front tectonic zone, GM = Green Mountain Massif, HB = Honey Brook Upland, LR = Long Range Inlier, PB = parautochthonous belt, PM = Pine Mountain Belt, RP = Reading Prong, SaM = Sauratown Mountain Massif, SM = Shenandoah Massif (Pedlar and Lovingston massifs), SMT = Steel Mountain Terrane (Corner Brook Lake).

The Vermont tonalite-trondjhemite suite was metamorphosed to granulite facies in the Middle Proterozoic and was retrograded, altered, and locally deformed in the mid-Paleozoic (Ratcliffe et al., 1991). The late trondjhemite-tonalite suite in the Central Metasedimentary Belt is variably deformed and metamorphosed from greenschist facies in the Hastings metamorphic low to sporadically distributed granulite facies. The Sailor Brook gneiss, like the Vermont and Adirondack suites, lacks interlayered pelite, psammite, calc-silicate or other unequivocal metasedimentary rocks, and lacks a recognisable stratigraphy among lithologic variants. However, unlike the Vermont and Adirondack suites, the Sailor Brook gneiss also lacks recognisable relict primary volcanic or igneous textures.

The ca. 1035 Ma age of metamorphic zircon in the Sailor Brook gneiss is similar to metamorphic mineral ages of the Ottawan phase (1100-1000 Ma; Moore and Thompson, 1980) of Grenvillian orogenesis. Metamorphism of this age is widespread throughout the Grenville Province (Easton, 1986; van Breemen et al., 1986; Schärer et al., 1986), including in the Central Gneiss Belt in Ontario and Quebec (Corrigan, 1990; Jamieson et al., 1992; Culshaw et al., 1990; Culshaw et al., in press) and along the Central Metasedimentary Belt Boundary Zone (ca. 1065-1029 Ma; van Breemen and Hanmer, 1986; Cosca and Essene, 1988). The peak of the Grenvillian Orogeny in the Adirondacks region of New York also occurred during the Ottawan phase (Rawnsley, 1987; Mezger et al., 1988; McLelland et al., 1988; McLelland and Chiarenzelli, 1990a; 1990b). Other Ottawan-age events in the Central Metasedimentary Belt appear to be restricted to plutonism without significant deformation (Lumbers et al., 1990; Corriveau et al., 1990).

The Otter Brook gneiss is comparable in age and in general lithology to a band of ca. 956 to 966 Ma granite, monzonite, and quartz syenite bodies in eastern Labrador. The units in Labrador are part of a more extensive belt of late-Grenvillian plutons that extend into eastern Quebec, as inferred by Gower et al. (1991), based on map patterns, general lithologic similarities, and geophysical evidence. Potentially related plutonic and gneissic units in the age range of 980-950 Ma are present in basement inliers of western Newfoundland, Vermont, and Virginia (Baadsgaard et al., reported in Owen and Erdmer, 1990; Karabinos, 1988; Karabinos and Aleinikoff, 1988; 1990; Herz, 1984; Herz and Force, 1984).

The Lowland Brook Syenite is closely comparable in field relations, chemistry, and age to ca. 1089-1076 Ma K-rich plutons in the Elsevir terrane of the Central Metasedimentary Belt (Figure 6.1; Corriveau et al., 1990; Corriveau and Gorton, 1993). Like the Lowland Brook Syenite, the Grenvillian syenite plutons have the characteristics of Group III ultrapotassic rocks (Chapter 3; Corriveau and Gorton, 1993; Foley et al., 1987) and are interpreted to have intruded a high-grade gneissic terrane during the waning stages of Grenvillian deformation and high-grade metamorphism. Unlike the Grenvillian plutons, however, the Lowland Brook Syenite experienced subsequent Paleozoic metamorphism and deformation.

Bekkers (1993) concluded that the major, trace, and rare-earth element chemistry of the Red River Anorthosite Suite, although altered due to Paleozoic metamorphism and low-grade alteration, is similar to those of well-characterised anorthosite suites in the Nain Province and are typical of Proterozoic massif-type anorthosite bodies in the Grenville Province. Charnockitic rocks in the Blair River inlier envelop the northwestern margin of the Red River Anorthosite Suite and appear to be gradational with the layered unit of the suite. The paragenetic association of massive anorthosite, massive gabbro and leuconorite-leucotroctolite, layered anorthosite/gabbro/ leuconorite, and rocks of charnockitic affinity (AMCG suite; Emslie and Hunt, 1990) is well documented in the Grenville Province (Figure 6.1; McLelland and Chiarenzelli, 1990b; Easton, 1990; Emslie, 1991) and in other Precambrian terranes (Wiebe, 1978; 1990; Giest et al., 1990). Phanerozoic anorthositic complexes (ca. 560 Ma; Higgins and Doig, 1981) in eastern North America are part of layered mafic bodies with a small volume of massive anorthosite compared to the large intrusions in Quebec and Labrador. The Paleozoic age of the Arden Pluton in Delaware (Foland and Muessig, 1978) is based on Rb/Sr whole-rock data and has not been confirmed by U-Pb geochronology.

Proterozoic massif-type anorthosite bodies are, in general, large in areal extent and include anorthosite, leuconorite, leucogabbro, and/or leucotroctolite, minor volumes of more mafic rocks and rare ultramafic rocks. These anorthosite suites contain calcic andesine or labradorite, high-Al orthopyroxene megacrysts, and are commonly associated with charnockitic rocks (Ashwal, 1993). The Red River Anorthosite Suite shares all of these features. Most anorthosite bodies in the Grenville Province are either massif-type or are associated with layered mafic intrusions (Easton, 1990). However, no rigorous criteria discriminate between the two types and most bodies show some characteristics of both (Frost et al., 1989). Large, relatively undeformed Proterozoic massif-type anorthosite is common in the allochthonous terranes of the Grenville Province (Figure 6.1) but is less abundant and commonly deformed in the parautochonous belt (Emslie, 1978; Rivers et al., 1989; Easton, 1990; Gower et al., 1990).

Older anorthosite suites in the Grenville Province intruded between ca. 1600 and 1400 Ma during periods of apparent crustal stability (Gower et al., 1990) and were overprinted to varying degrees by Grenvillian metamorphism and deformation (e.g., Easton, 1990). A younger period of broadly Grenville-age or slightly older anorthosite magmatism includes some of the best-studied Grenvillian anorthosite bodies, for example the Morin, Lac St.-Jean, and Havre-Saint-Pierre, and Marcy bodies (ca. 1160-1125 Ma; Higgins and van Breemen, 1989; Doig, 1991; van Breemen and

Higgins, 1993 McLelland and Chiarenzelli, 1990b). Some of these may have been emplaced either during ca. 1200-1090 Ma extension (Gower et al., 1990) or during the main phase of Grenvillian orogenesis itself (e.g., Emslie and Hunt, 1989; McLelland et al., 1988; McLelland and Chiarenzelli, 1990a).

The traditional view of the relationship between members of the AMCG suite is one of bimodal, cogenetic but not comagmatic, magmatism resulting from ponding of enriched mantle-derived basalt. Plagioclase accumulation produces anorthosite and country rock anatexis produces the charnockitic rocks (e.g., Emslie, 1978; 1985; 1991, Morse, 1982, McLelland and Whitney, 1990; Whitney, 1992). However, Owens et al. (1993) pointed out that this interpretation is based mainly on comparisons between the alkali-granite and anorthosite end-members and largely excludes the role of the intermediary mangerite and jotunite. In the case of the Morin anorthosite, the AMCG suite crystallisation process took ~20 m.y. Doig (1991) obtained ages of ca. 1155 Ma, 1146 Ma, and 1135 Ma from Morin anorthosite, jotunite, and mangerite respectively. McLelland and Chiarenzelli (1989; 1990b) used a similar time lag to argue against comagmatism for the Marcy Massif.

If the differentiation scheme proposed by Owens et al. (1993) and the relative age differences obtained by Doig (1991) and McLelland and Chiarenzelli (1989; 1990b) are characteristic of AMCG suites, then ages obtained from charnockitic end-members would be minimum ages for the suite, and may be significantly younger than the anorthosite. The time for crystallisation of the sequence from anorthosite to charnockite might require long periods (e.g., ~20 m.y.; e.g., Doig, 1991) of tectonic quiescence, and the charnockitic rocks could intrude, metasomatise, and metamorphose the anorthosite. In the case of the Red River Anorthosite Suite, contact metamorphism and metasomatisation related to the intrusion/crystallisation of the charnockitic border phases could explain the blurring of the contact and the production of metamorphic zircon in nearby anorthosite. This could also explain why other dated Grenvillian units in the Blair River inlier show no indication in their U-Pb systematics of the ca. 996 Ma metamorphism.

Regardless of magmatic models, the important field and geochemical relationships between anorthosite and related charnockitic rocks as outlined by Duchesne (1984), Whitney (1992), Ashwal (1993), and Owens et al. (1993) from a variety of Grenvillian AMCG suites corresponds closely with those of the Red River Anorthosite Suite and charnockite. This characterisation further demonstrates that these distinctive rock types in the Blair River inlier are in no significant way (age, petrogenetic relationships, or tectonic relationships) anomalous compared to those of the Grenville Province.

Sm/Nd data for the Blair River inlier were provided by Dickin and Raeside (1990), Barr and Hegner (1992), and unpublished data from R. Raeside and S. Barr. Depleted mantle model ages (DePaolo, 1981) are 1690-1500 Ma for the gneisses, 1660-1470 Ma for the syenite, 1224 Ma for the anorthosite, 1380 and 961 Ma for the granites and 1000 Ma for the rhyolite. The model age of the anorthosite is close to its inferred crystallisation age (between ca. 1217 and ca. 1080 Ma), an indication of the mantle-derived nature of the magma. The other model ages reflect the mean mantle separation ages of the source rocks involved in their petrogenesis. Initial ε_{Nd} values (Figure 6.2) plot within the "envelope for Grenville age rocks" of Patchet and Ruiz (1989) with the exception of the late granites and rhyolite. Barr and Hegner (1992) interpreted the latter data as an indication of a mixture of juvenile magma and Grenvillian crustal sources.

Pb-isotope data were presented by Ayuso et al. (1996) for the Lowland Brook Syenite, Delaney Brook Anorthosite, and the Sammys Barren granite. The syenite and anorthosite samples

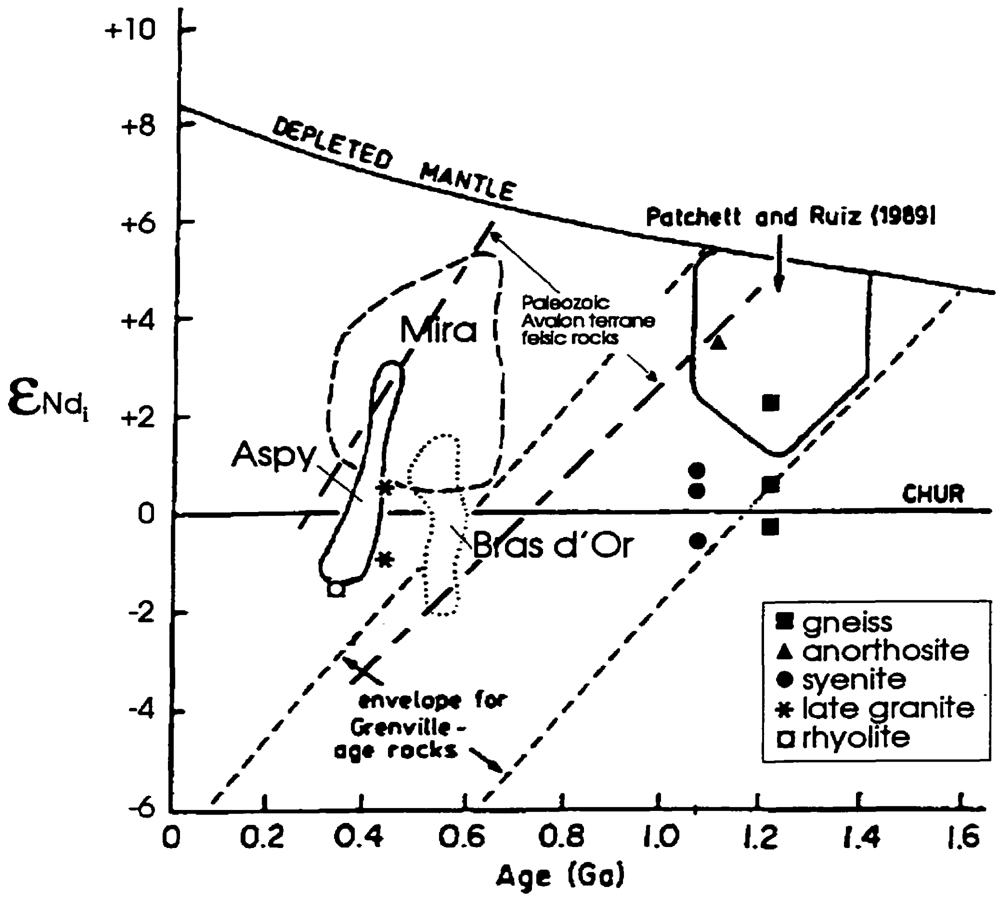

Figure 6.2 - Initial εNd plotted against age (modified from Barr and Hegner, 1992) for samples from the Blair River inlier. Also plotted are fields for the Mira, Aspy, and Bras d'Or terranes in Cape Breton Island, isotopic evolution envelope for Grenvillian rocks (after Patchett and Ruiz, 1989; Dickin and McNutt, 1989). The envelope for Avalonian rocks (after Murphy et al., 1995; Dostal et al., 1996) includes data from New Brunswick (Whalen et al., 1994), Newfoundland (Fryer et al., 1992), and Cape Breton Island (Barr and Hegner, 1992).

are characterised by nonradiogenic Pb-compositions, which Ayuso et al. (1996) interpreted as an indication of an old (i.e., Grenville-age) source region of mantle-derived material with minor crustal contamination. The Sammys Barren granite data are consistent with derivation of the magma from a source with Pb-isotopic compositions similar to the Proterozoic rocks of the Blair River inlier, but the data are distinctly less radiogenic than other granites in Cape Breton Island.

Sangster et al. (1990a) presented Pb and S isotope data from the Meat Cove marble and Sangster et al. (1990b) showed that the Pb compositions are distinctly non-radiogenic compared to other mineralised metasedimentary units in Cape Breton Island. Sangster et al. (1990b) concluded that the isotopic characteristics from the Meat Cove marbles are comparable to those of the Grenville Supergroup. The isotopic characteristics of rocks of the Blair River inlier are distinct from those elsewhere in Cape Breton Island, including those thought to characterise Avalonian basement, but are consistent with a North American Grenvillian affinity (Barr and Hegner, 1992; Murphy et al., 1993: Dostal et al., 1996; Ayuso et al., 1996).

In summary, the major Proterozoic gneissic (Sailor Brook gneiss and Otter Brook gneiss) and igneous (Lowland Brook Syenite Red River Anorthosite Suite) units in the Blair River inlier have close lithological and temporal counterparts in the Grenville Province. These counterparts are located widely throughout the southeastern Grenville Province, and provide a basis for general correlation with the Blair River inlier. A specific correlation with a single terrane, domain, or subdivision of the province is not warranted at present due to the lack of data at the same level of detail from the allochthonous terranes in western Quebec and southern Labrador, the nearest exposed portions of the Grenville Province. Furthermore, because lithotectonic subdomains are generally subparallel to the strike of the orogen, there may be no directly correlative subdomain exposed in the Grenville Province.

6.3 The Blair River inlier as part of the Laurentian continental margin

Remnants of the Laurentian continental margin in the northern Appalachian orogen constitute the Humber Zone (Williams, 1979). The zone is characterized by Middle Proterozoic basement units overlain by Cambrian to Ordovician passive margin sedimentary sequences that were deformed and metamorphosed during Appalachian orogenesis (Williams and Stevens, 1974). If the Blair River inlier is part of the Laurentian continental margin, then the inlier should share a general lithostratigraphy and thermal history, with the established parts of the Humber Zone in the northern Appalachian orogen. Other along-strike comparisons between the Blair River inlier and, for example, the Blue Ridge Province are unwarranted at present because of the paucity of detailed petrologic and geochronologic studies in other basement inliers and because large-scale lithotectonic variation in Laurentian basement is to be expected over large distances. The following discussion concentrates instead on the nearest Laurentian basement and cover units, those in western Newfoundland. The key lithological features and the timing of Paleozoic thermal events in the northern Appalachian Humber Zone are outlined below for the purpose of comparisons with those of the Blair River inlier. The body of geophysical data that suggests that the Blair River inlier lies on the western side of the Appalachian orogen is also reviewed.

Laurentian basement exposures in western Newfoundland occur in the Long Range Inlier, the Indian Head Range, and the Steel Mountain terrane . In the Long Range Inlier, basement comprises granoblastic granulite-facies and amphibolite-facies granitic, granodioritic, and tonalitic orthogneiss and minor paragneissic units along with marble and calc-silicate rocks (Owen and Erdmer, 1990). Preliminary U-Pb zircon ages of ca. 1503 Ma and ca. 1020 Ma have been obtained from granulite and amphibolite gneissic units, respectively, in the basement gneiss complex (Heaman et al., 1996). The gneiss complex was intruded by plutons at ca. 1080-960 Ma (reported in Owen and Erdmer, 1990), and Heaman et al. (1996) obtained preliminary ages of 1025-998 Ma for 6 granitoid plutons. The Indian Head Range contains mainly orthogneissic rocks with compositions of anorthosite, gabbro, norite, diorite, and charnockite along with minor screens of metapelitic rocks. Basement is unconformably overlain by platformal Cambrian to Ordovician carbonate and clastic units (Riley, 1962; Williams, 1975). The Steel Mountain terrane consists of allochthonous thrust slices that include granulite-facies gneiss, massif-type anorthosite and associated gabbroic rocks, and their retrograded equivalents (Currie, 1987c; Currie et al, 1991). Granulite gneiss yielded a U-Pb zircon age of ca. 1498 Ma and a late granite, with unclear stratigraphic and contact relations to older units, gave an age of ca. 608 Ma. Basement units in the Steel Mountain terrane are locally overlain by metasedimentary units of the Fleur de Lys Supergroup (Hibbard, 1983; Currie, 1987c). These three major basement blocks in the Humber Zone of western Newfoundland have long been accepted as exposures of Laurentian basement and as correlatives of the Grenville Province (Williams and Stevens, 1974; Erdmer, 1984; Owen and Erdmer, 1989; Rodgers, 1995).

The Fleur de Lys Supergroup comprises metamorphosed continental margin deposits including medium- to high-grade metapelitic and metapsammitic schists, amphibolites and eclogite pods (de Wit, 1980; Hibbard, 1982; Hibbard, 1983; Jamieson 1990). The supergroup is interpreted to be unconformable on Laurentian basement units (Cawood and van Gool, 1992). Correlative deformed and metamorphosed cover units are tectonically interleaved with basement near Corner Brook Lake (Figure 6.1; Cawood and Van Gool, 1992; Cawood et al., 1996).

Until recently, Paleozoic metamorphism in the basement complex in the Long Range Inlier was thought to be confined to a 15-km-wide zone of epidote-amphibolite and greenschist facies assemblages at its southern margin (Owen and Erdmer, 1989). However, the recent surprising discovery that the Taylor Brook Gabbro complex, which has a significant aureole and was thought to have contributed substantially to the thermal budget of Grenvillian metamorphism in the inlier (Owen and Erdmer, 1989), is actually Silurian (ca. 429 Ma; Heaman et al., 1996) indicates that the true extent of Paleozoic metamorphism is not known. Similarly, very little is known about the possibility of a Paleozoic thermal overprint in the Indian Head and Steel Mountain basement exposures. However, Dallmeyer (1978) obtained $^{40}Ar/^{39}Ar$ ages of ca. 880 Ma from hornblende and ca. 825 Ma from biotite in granitoid gneisses from the Indian Head Range and interpreted the ages to reflect slow cooling following a Grenville-age metamorphic episode.

The Fleur de Lys Supergroup and related rocks in the Baie Verte Peninsula and near Corner Brook Lake, have clearly been affected by Paleozoic metamorphism and plutonism, and the ages of these events are well constrained. In the Baie Verte region, Cawood and Dunning (1993) obtained U-Pb monazite, zircon, and titanite ages of ca. 427-423 Ma from syntectonic melts in, and plutons associated with, the Fleur de Lys Supergroup. Dallmeyer (1977) obtained $^{40}Ar/^{39}Ar$ hornblende and muscovite ages of ca. 429 to ca. 421 Ma from rocks in the Fleur de Lys Supergroup west of the Baie Verte Line. In the Corner Brook Lake region, Cawood et al (1994) obtained a U-Pb zircon age of ca. 434 Ma from a pegmatite that intrudes both basement and cover and a garnet-kyanite schist yielded similar metamorphic ages from monazite (ca. 430 Ma) and rutile (ca. 437 Ma). Cawood et al., (1994) also report $^{40}Ar/^{39}Ar$ ages of ca. 427-424 Ma on hornblende and ca. 429-413 Ma on muscovite.

The Blair River inlier is similar in general lithologic makeup to Proterozoic basement in the Humber Zone of western Newfoundland. Both the Blair River inlier and the Humber basement are dominated by orthogneissic units including granulite-facies gneisses that were intruded by ca. 1100-960 Ma plutons. Some details differ, for example, the largest basement exposure, the Long Range Inlier, does not contain massif-type anorthosite and the oldest known unit in the Blair River inlier, the granulite-facies Sailor Brook gneiss, may be significantly younger (minimum of 1217 Ma) than the oldest known granulite-facies gneisses in western Newfoundland (ca. 1500 Ma). The differences and similarities between these Middle Proterozoic inliers are explained most easily by along-strike variation in Laurentian basement. Analogous along-strike variation, at a larger scale, is seen in the Grenville Province between, for example, eastern Labrador and Ontario-New York.

The Blair River inlier lacks the passive-margin and related cover units. Rare small lenses of marble and calc-silicate rocks in fault zones and along the faulted contacts of several major units may be remnants of cover, tectonically interleaved with basement units along late high-level fault zones. The lack of an overlying continental margin sequence may be the result of tectonic removal of sedimentary cover, or of exhumation of the Blair River inlier from middle to lower crustal depths, below the basement-cover unconformity. Furthermore, Cambrian to Ordovician cover along the entire length of the Laurentian margin was thinner on the promontories than in the re-entrants (Rankin, 1976; Thomas, 1977; Read, 1989), thus, the St. Lawrence promontory may have had only a thin cover sequence. Because the Blair River inlier is small relative to other Laurentian basement-cover exposures, Cambrian to Ordovician passive margin units may be present, but perhaps buried beneath Carboniferous clastic units.

Although the Blair River inlier lacks pre-Carboniferous cover successions, the basement units record amphibolite-facies metamorphism and associated minor granitoid plutonism at the same time as similar events in basement and cover units in western Newfoundland. The timing of both the plutonism (ca. 435 Ma) and post-metamorphic cooling (ca. 425 Ma) are remarkably consistent in this segment of the northern Appalachian Humber Zone. Silurian tectonothermal events, including widespread metamorphism, deformation, plutonism, volcanism and sedimentation, are documented in the Humber Zone as well as parts of the Central Mobile Belt in Newfoundland and in New Brunswick (Bevier and Whalen, 1990; Dunning et al., 1990a; O'Brien et al., 1991; Dubé et al, 1993, 1996; Cawood et al., 1994; Lin et al., 1994). Displacement along the boundary between the Central Mobile Belt and the Avalon Zone has been correlated with Silurian events in southern Newfoundland (O'Brien et al., 1991; Holdsworth, 1991), thus documenting the orogen-wide nature of a Silurian peak of orogenesis. In detail, however, the Silurian thermal record in the Blair River inlier is more closely comparable to that of the Humber Zone than the events recorded in the Central Mobile Belt of the Aspy terrane and southwestern Newfoundland (Figure 6.3). The mid-Paleozoic Sammys Barren granite (ca. 435 Ma) is the same age as plutonism in western Newfoundland (ca. 434-423 Ma; Cawood et al., 1994), and is similar in age to the older of the two pulses of plutonism in the Central Mobile Belt (ca. 435-430 Ma and ca. 420-414; Dunning et al., 1990a; 1990b; van Staal et al., 1994). Silurian metamorphism and post-metamorphic cooling (Figure 6.3) through ca. 550-300°C in the Blair River inlier (ca. 425 Ma) predates by about 10-14 m.y. that of the Aspy terrane and Central Mobile Belt of southern Newfoundland (ca. 415-411 Ma; Jamieson et al., 1986; Dunning et al., 1990b; Barr and Jamieson, 1991; Dubé et al., 1996; Reynolds et al., 1989; Keppie et al., 1992; Wunapeera, 1992; Dallmeyer and Keppie, 1993; Dubé et al., 1994). The timing of Silurian metamorphism and magmatism in the Blair River inlier suggests continuity with Silurian events documented along the northwestern margin of the Appalachian orogen.

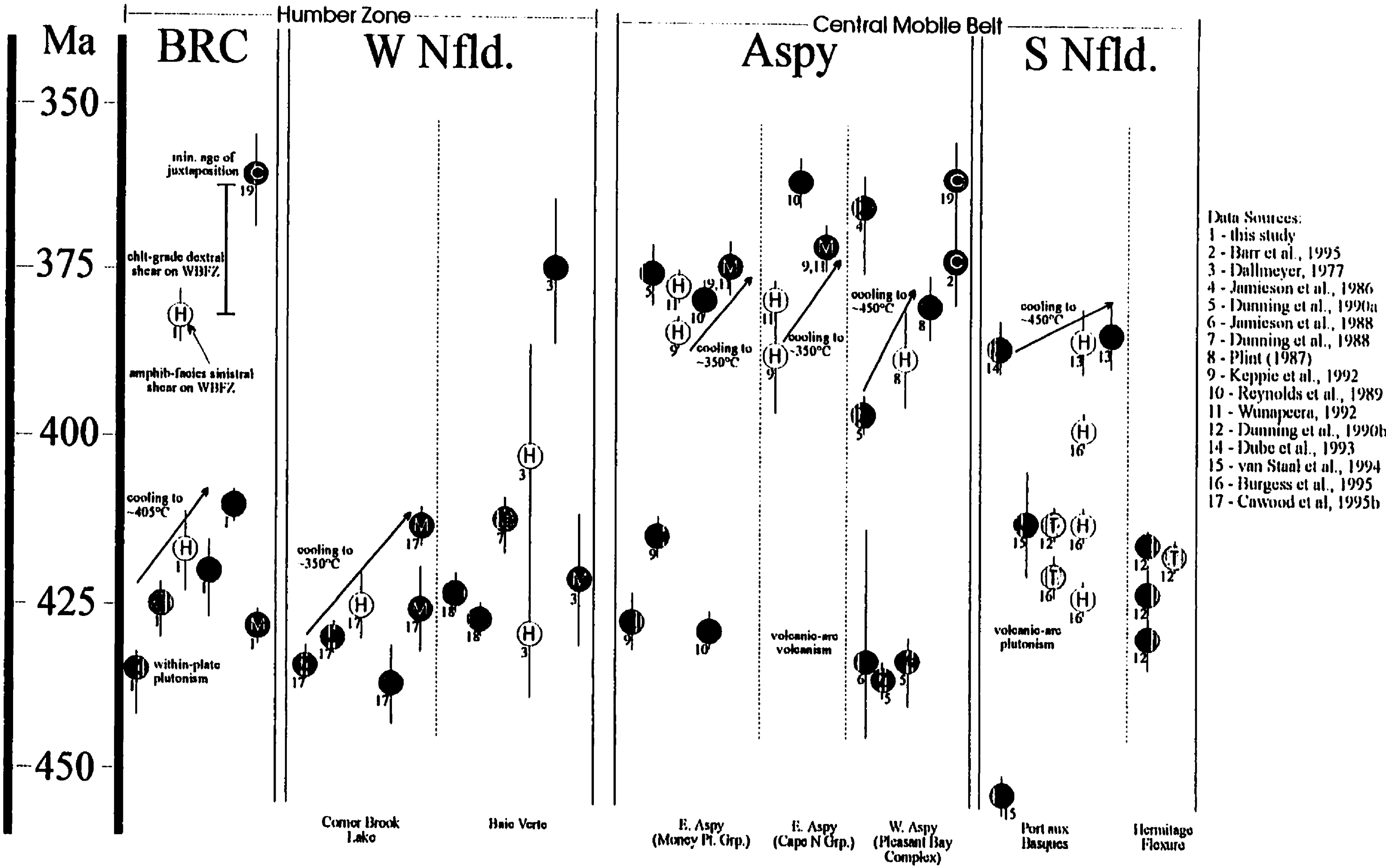

Figure 6.3 - Summary of mid Paleozoic age data from the Blair River inlier, western Newfoundland and the Central Mobile Belt adjacent to each area (Aspy terrane and southern Newfoundland). Z = U-Pb zircon, T = U-Pb titanite, Mz = U-Pb monazite, R = U-Pb rutile, H = $^{40}Ar/^{39}Ar$ hornblende, P = $^{40}Ar/^{39}Ar$ phlogopite, B = $^{40}Ar/^{39}Ar$ biotite, M = $^{40}Ar/^{39}Ar$ muscovite, C = sedimentary or volcanic cover rocks.

The contemporaneity of Silurian events between the Blair River inlier and the Humber Zone in western Newfoundland does not conclusively identify the Laurentian parentage of the Blair River inlier because events of similar age are also recorded in the Appalachian outboard terranes. Other lines of evidence must be considered in order to demonstrate that the structural zonation of the orogen is consistent with the Blair River inlier forming part of the along-strike extension of the Humber Zone (i.e., major structures must strike into, rather than around Cape Breton Island, as earlier models predicted). A variety of geophysical data provide this additional evidence.

Bougeur gravity anomaly and magnet maps (Figure 1.4; Loncarevic et al., 1989) show that the structural grain of the orogen trends into Cape Breton Island and that the Blair River inlier is north of (on the Laurentian side of) the along-strike extension of the Cabot Fault, the southeastern boundary of the Humber Zone in southwestern Newfoundland. Langdon and Hall (1994) traced upper crustal, Paleozoic, structures using a dense network of shallow seismic data and also concluded that the offshore extension of the Cabot Fault system trends into northern Cape Breton Island and links, in part, with the Wilkie Brook Fault Zone. Durling and Marillier (1990) and Marillier et al., (1989) interpreted deep seismic lines (LITHOPROBE East profiles 86-2 and 86-4) on either side of Cape Breton Island as showing that Grenvillian basement dips gently south and southeast, from near the surface to near the Moho, at about 10 seconds two-way travel time. The top of this Grenville block would be at considerable depth if projected below the Blair River inlier. However, Marillier et al., (1989) interpreted LITHOPROBE East line 86-5a, which is nearer to Cape Breton Island, to show a steeply dipping boundary for the Laurentian basement block extending to near the surface. Keppie (1990) disputed this boundary, claiming that this fault is not clear on the profile. Because of poor resolution toward the top of the seismic section, LITHOPROBE East line 86-5a provides no real constraints on the degree to which the Blair River inlier may be allochthonous. However, Marillier et al., (1989), Durling and Marillier (1990), and Loncarevic et al., (1989) all agree that the geophysical data are consistent with Laurentian lower crust extending into the Gulf of St. Lawrence to at least as far as northern Cape Breton Island.

The geophysical evidence alone does not constitute conclusive proof of a Laurentian origin for the Blair River inlier. However, the combination of the geophysical data that suggest the Blair River inlier lies on the western margin of the orogen, the presence of basement units that are, in every aspect, compatible with Laurentian basement and correlative with the Grenville Province, and a Paleozoic thermal history that is nearly identical to that of Laurentian margin rocks in western Newfoundland and that has some important contrasts with the thermal history of Appalachian outboard terranes, argues strongly that this is the simplest and currently most credible explanation explanation for the observations and data. Furthermore, this interpretation is consistent with evolving, detailed tectonic models for the northern Appalachian orogen as described in the next section.

6.4 The Blair River inlier in northern Appalachian tectonic models

Silurian sinistral transpression between the Laurentian and Gondwanan margins resulting in metamorphism, deformation, plutonism, and sedimentation, marked the culmination of orogenesis in the northern Appalachian orogen (e.g., Dunning et al, 1990a; Doig et al., 1990; Bevier and Whalen, 1990; Soper et al., 1992; Dubé et al., 1993; 1996; Cawood et al., 1994; Lin et al., 1994; van Staal, 1994). The Taconian (Ordovician) orogeny is recorded by overthrusts of oceanic fragments, including ophiolites, onto the Laurentian margin. In the northern Appalachians, Devonian (classic Acadian) tectonic events include high-level faulting and thrusting and large-scale, right-lateral shear systems (Waldron and Milne, 1991; Barr et al., 1995; Malo et al., 1995) developed during continued convergence between Laurentia and Gondwana. Alleghanian (Carboniferous) strike-slip faulting resulted in the development of large sedimentary basins.

It is now widely recognised that the inherited geometry of continental margins, notably the pattern of promontories and re-entrants, must be considered in models and reconstructions of the style and timing of tectonism in the Appalachian orogen (Hatcher, 1983; Stockmal et al., 1987; 1990; Keppie and Dostal, 1994; Cawood et al., 1994; Lin et al., 1994; Malo et al., 1992; 1996). For example, in the central and southern Appalachian orogen, the (Devonian) Acadian orogeny is typically interpreted to have resulted from continent-continent collision (Glover et al., 1983; Rankin et al., 1993). Cawood et al., (1994) attributed the difference in the style and timing of peak orogenesis between the northern and central-southern segments to initiation of continent-continent collision in the northern Appalachians at promontories in either one, or both, of the continental margins. Lin et al., (1994), adapted the tectonic model of Stockmal et al., (1987; 1990) to include the possibility of promontory-promontory collision in the northern Appalachian orogen. Malo et al., (1995) modified the Stockmal et al., (1987; 1990) model to take into account the tectonothermal evolution of the Quebec re-entrant and proposed that the St. Lawrence promontory acted as a rigid indentor, with thrust-dominated tectonics in the re-entrant and dextral transcurrent faulting along the southern flank of the promontory. These structures resulted in the nearly 200 km offset in Appalachian structural trends between the promontory and the Quebec re-entrant.

Detailed tectonostratigraphic correlations of terranes between Cape Breton Island and Newfoundland require that orogen-scale tectonic models developed for Newfoundland and Quebec be applicable also to Cape Breton Island (e.g., Barr et al., 1995). The close correspondence between the Humber Zone of western Newfoundland and the Blair River inlier, in terms of their position within the orogen and their Paleozoic thermal histories, suggests that some of the details of more specific models for the structural and thermal history of the Humber Zone in western Newfoundland (most notably basement-involved thrusting; Waldron and Stockmal, 1994) may apply as well to northern Cape Breton Island.

The tectonic model of Stockmal et al., (1987; 1990) postulates that the large-scale structure of the northern Appalachian orogen resulted from suborthogonal collision between the St. Lawrence promontory and either a linear or curvilinear combined Gondwanan margin/peri-Gondwanan arc complex. They reconstructed lower-crustal blocks from the present terrane configuration by palinspastic restoration along major fault systems. Their model, with modifications after Lin et al., (1994), Malo et al., (1995), and with refinements in timing of events to account for a Silurian thermal peak in Cape Breton Island and Newfoundland (e.g., Cawood et al., 1994; this work), is used here to describe the role of the Blair River inlier in constraining the geometry, timing, and style of northern Appalachian orogenesis. The proposed tectonic model is shown schematically in Figure 6.4.

There is no evidence to suggest that the Blair River inlier was near to the surface at any time prior to the mid-Paleozoic. The inlier lacks Middle and Late Proterozoic sedimentary successions, the major high-grade gneissic units are interpreted to have had plutonic protoliths, and granulite-facies metamorphic mineral assemblages (6-8kbar, 700-850°C; Chapter 5) and a hypersolvus pyroxene-syenite body (>700°C ; cf., Morse, 1970) indicate deep crustal conditions. Some degree of post-orogenic exhumation, perhaps during rifting to form the Iapetus Ocean, probably brought the Blair River inlier nearer to the surface and may have resulted in partial retrogression of the high-grade assemblages. Therefore, the model presented here begins following Iapetan rifting with the Blair River inlier located near the tip of the St. Lawrence promontory at mid- to lower-crustal levels (Figure 6.4a).

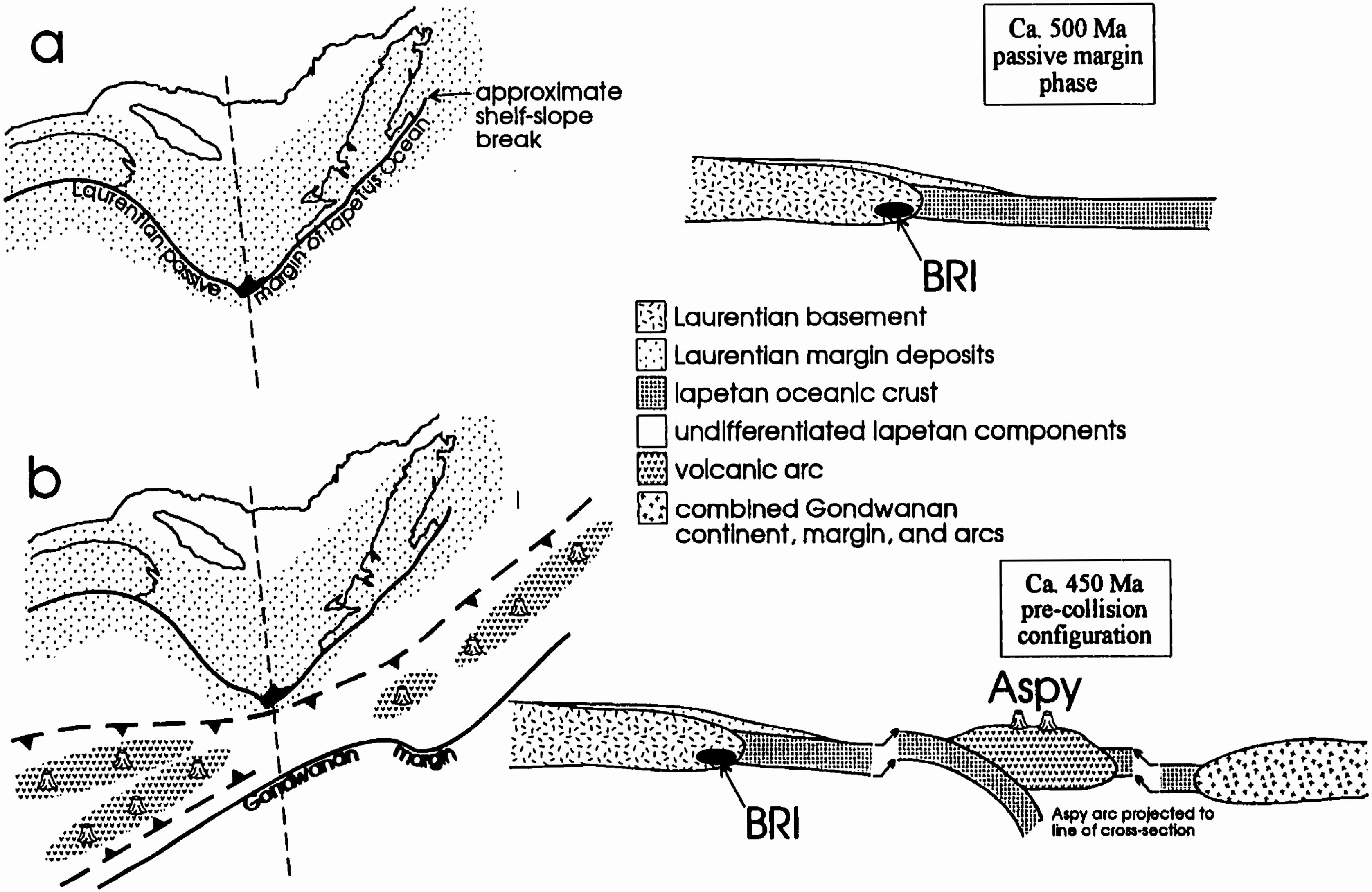

Figure 6.4 - a) Post-rift, passive margin configuration of the Laurentian continental margin. Plan-view geometry is based on interpretation of gravity and magnetic data (after Loncarevic et al., 1989; Miller, 1990). Blair River inlier (BRI) is inferred to have been located in the middle- to lower-crust near the tip of the promontory. b) Configuration prior to onset of Appalachian orogenesis. Incipient Aspy arc is projected onto the cross-section. Relative positions of Gondwanan margin and Iapetan volcanic arcs is diagrammatic.

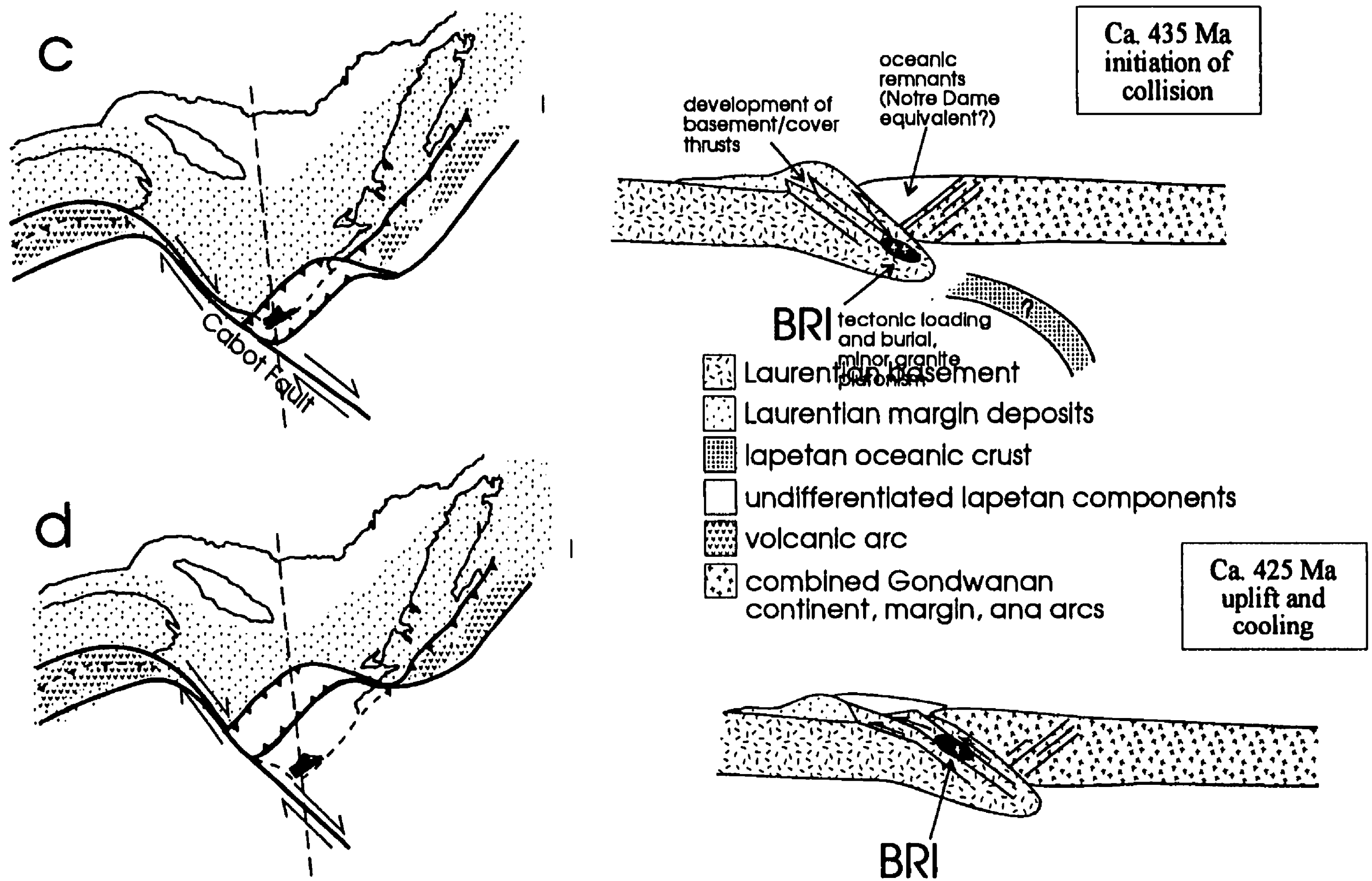

Figure 6.4 (continued) - c) Proposed position of the Blair River inlier at the initiation of continent-continent collision. Overthrusting by the Gondwanan margin depressed the Laurentian crust, the tectonic loading and heating resulting in minor plutonism (i.e., Sammys Barren granite), amphibolite-facies metamorphism accompanied by localized deformation, new growth and/or Pb-loss in titanite and rutile. d) Continued convergence to about 425 Ma thrust the Blair River inlier to higher crustal levels, resulting in cooling through the titanite closure temperature. Both Laurentian passive margin sequences and peri-Laurentian remnants of Iapetus (equivalent of Notre Dame terrane in Newfoundland), if ever present, may have been thrust over the Blair River inlier at this time.

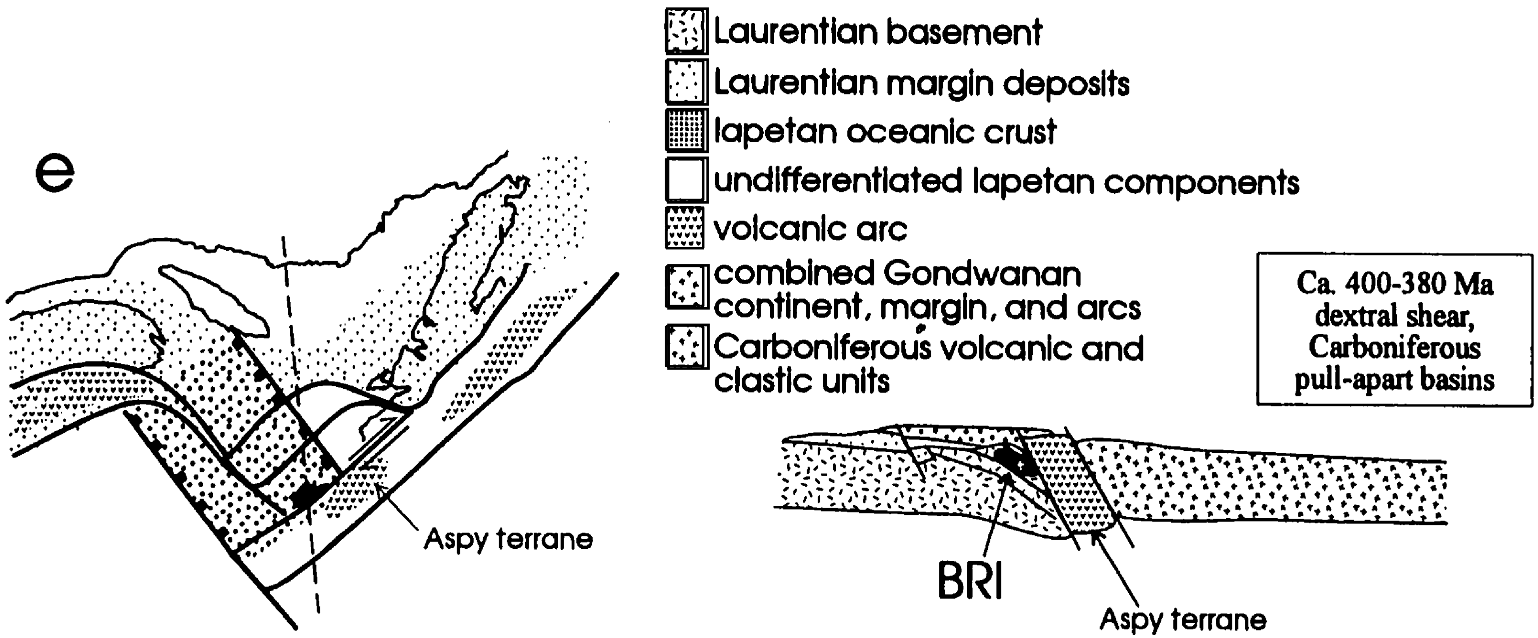

Figure 6.4 (continued) - e) Dextral strike-slip along the Laurentian margin juxtaposed the Blair River inlier and Aspy terrane at a high enough structural level to preclude widespread resetting of mineral ages in the Laurentian basement rocks. Carboniferous pull-apart basins (e.g., Magdalin Basin is shown schematically) also began to form accompanied by deposition of clastic sequences over Blair River inlier, and (if present) remnants of passive margin sequences and Iapetus oceanic fragments. Final uplift and exhumation of the Blair River inlier, through the Carboniferous cover, to the surface occurred subsequently, perhaps in the Mesozoic, due to reactivation of thrust and/or strike-slip faults.

The Gondwanan continental margin and Iapetan volcanic arc terranes approached Laurentia (Figure 6.4b) in the Ordovician, prior to the (Silurian) thermal peak. In Newfoundland thrusting resulted in obduction of ophiolites and thrusting of peri-Laurentian fragments of Iapetus (Notre Dame terrane) over the Laurentian continental margin. No Ordovician events are recorded in the Blair River inlier. Collision of the continental margin occurred between the St. Lawrence promontory and Gondwanan margin/arc terranes (Figure 6.4c) in the Late Ordovician (J. Waldron, 1996, pers. comm.). This resulted in downwarping of the proximal Laurentian margin, and in the initial development of fault systems (thrusts in Newfoundland) that interleaved basement and Laurentian margin sedimentary sequences. At this time the Blair River inlier experienced amphibolite-facies metamorphism, localised deformation, minor granitic melt generation (i.e., Sammys Barren granite), at conditions above the closure temperature for titanite and rutile. Any remnants of Iapetus near the St. Lawrence promontory may have overthrust the tip of promontory by this time and the thin cover of Laurentian margin sequences may have been peeled back off the promontory. Tear-faulting in the Gondwanan margin occurred along the inferred Cabot Fault system providing for the ca. 200 km of dextral offset of the Central Mobile belt (Iapetan components and arc terranes) between the St. Lawrence promontory and the Quebec re-entrant.

Continued Silurian convergence and continent-continent collision resulted in tectonic exhumation of the Blair River inlier, perhaps along previously developed fault systems (Figure 6.4d). Exhumation and denudation allowed for cooling of the Blair River inlier through the closure temperature for titanite, soon followed by hornblende and rutile. By this time, any cover sequences or Iapetan remnants were thrust well over the tip of the St. Lawrence promontory. Continued movement on the Cabot Fault system enhanced the offset at the southern flank of the promontory.

In the early Carboniferous, the overall tectonic style changed from suborthogonal convergence to a large-scale, dextral strike-slip regime (e.g., Hibbard, 1994; Dubé and Lauziére, 1996; Figure 6.4e). This movement assembled most of the tectonostratigraphic components of Cape Breton Island to near their present-day positions. The Aspy terrane was juxtaposed with the Laurentian margin at the tip of the promontory. However, Devonian hornblende cooling ages in rocks deformed by an early stage of movement along Wilkie Brook fault zone (Wunapeera, 1992), and the lack of widespread complete resetting of $^{40}Ar/^{39}Ar$ systematics in the Blair River inlier, suggest that the inlier was at a high structural level relative to the present-day level of the neighbouring Aspy terrane during this stage of movement. The Carboniferous strike-slip regime also resulted in the opening of sedimentary basins, for example the Magdalin Basin (e.g., Langdon and Hall, 1994). Thick Carboniferous clastic deposits blanketed much of the northern Appalachian orogen at this time. Final juxtaposition of the Blair River inlier with the Aspy terrane and exhumation of both through the Carboniferous cover units occurred along late, high-level brittle faults (e.g., the Wilkie Brook fault zone adjacent to the Blair River inlier). Fission track data (e.g., Ryan and Zentilli, 1993) record Mesozoic uplift and erosion of Carboniferous rocks in the Maritimes Basin and is associated with reactivation of older fault systems (Langdon and Hall, 1994).

6.5 Conclusions

Middle Proterozoic units in the Blair River inlier have close lithological and temporal counterparts in the Grenville Province that provide for a general correlation between the two areas. Tectonic models that consider the Blair River inlier to be Gondwanan basement or a Proterozoic fragment in the Central Mobile belt are based on either incomplete information or inaccurate and out-of-date interpretations. These models do not take into account the many specific details (e.g., gravity, magnetic, and seismic data, lithologic and tectonostratigraphic correlations, isotopic contrasts with Appalachian outboard terranes and similarities with Grenvillian rocks, continuity of ages of plutonism and metamorphism along the Laurentian margin) that, when taken together, are explained easily if the Blair River inlier is interpreted as a fragment of Laurentian basement derived from the St. Lawrence promontory. Models developed for the northern Appalachian orogen to explain the tectonics of collision at an irregular margin (e.g., Stockmal et al., 1987; 1990), modified slightly to account for recent recognition of Silurian interaction between the Laurentian and Gondwanan margins (e.g., Dunning et al, 1990a; Dubé et al, 1996; Cawood et al., 1994; Cawood and Dunning, 1993; this work) are consistent with the style of tectonism from Quebec (e.g., Malo et al., 1995) to Newfoundland (e.g., Waldron and Stockmal, 1994, Cawood, 1993).

CHAPTER 7 - Conclusions

1. The Blair River inlier consists of the pre-Devonian rocks that form the crystalline core of the northwestern Cape Breton Highlands in northern Cape Breton Island, Nova Scotia. The complex is bounded to the southwest by the Red River fault zone, to the east by the Wilkie Brook fault zone, and elsewhere by Late Devonian and Carboniferous volcanic and clastic sedimentary cover rocks.

2. The inlier comprises seven Proterozoic units, the Sailor Brook gneiss, Polletts Cove River gneiss, Otter Brook gneiss, Lowland Brook Syenite, Red River Anorthosite Suite, charnockitic rocks, several smaller anorthosite bodies (Delaneys Brook, Salmon River, High Capes, and Polletts Cove River anorthosites). The Fox Back Ridge diorite/granodiorite, Sammys Barren granite, and Red River syenite are Silurian units. Various small bodies and dikes of gabbro, diabase, and rhyolite, as well as marble and calc-silicate rocks were metamorphosed or deformed in the Silurian, but their ages are otherwise unconstrained.

3. The tonalitic to dioritic Sailor Brook gneiss is the oldest unit in the Blair River inlier; the plutonic protolith crystallised prior to 1217 Ma based on U-Pb (zircon) data. The gneiss has a granular texture, weak compositional banding, migmatitic leucosomes, and locally preserves granulite-facies metamorphic mineral assemblages that indicate conditions of about 6-8 kbar and 700-850°C. Metamorphic zircon associated with the granulite-facies metamorphism crystallised at 1035 +12/-10 Ma and titanite associated with the amphibolite-facies overprint fabric cooled through titanite closure temperature at ca. 431 Ma. High-grade

metamorphic mineral assemblages are largely overprinted by amphibolite-facies metamorphic assemblages that locally define a deformational fabric.

4. The Otter Brook gneiss is characterised by biotite- and hornblende-rich, garnet-bearing, augen to flaser quartzofeldspathic to amphibolitic orthogneiss, but locally contains sheared calc-silicate rocks. A quartzofeldspathic orthogneiss component of the gneiss crystallised at 978 +6/-5 Ma. It was subsequently metamorphosed at upper-amphibolite transitional to granulite-facies conditions in the range of 600-700°C and 4-10 kbar. Cooling ages following amphibolite-facies metamorphism are recorded by metamorphic mineral ages of 423 ± 6 Ma (titanite) and 421 ± 6 Ma (phlogopite).

5. The Lowland Brook Syenite is coarse-grained with perthitic and antiperthitic feldspars and contains a gneissic foliation defined by biotite and hornblende, but in low-strain zones contains microperthitic feldspars and clinopyroxene. The syenite is alkaline, shoshonitic, and metaluminous. It intruded the Sailor Brook gneiss at 1080 +5/-3 Ma, was deformed an metamorphosed at amphibolite-facies conditions, and subsequently cooled through the titanite closure temperature range at 424 ± 3 Ma.

6. The Red River Anorthosite Suite consists of a gradational sequence of massive anorthosite, leucogabbro, and layered gabbroic rocks. The suite has lithological and chemical characteristics typical of Proterozoic massif-type anorthosite bodies. Metamorphism of the anorthosite occurred at 996 ±5 Ma (U-Pb ages of metamorphic zircon). Metamorphic minerals associated with this event suggest a relatively low pressure of about 3 kbar and temperatures of 730-760°C. Titanite and rutile from samples affected by amphibolite-facies

metamorphism cooled through their closure temperatures at 424 +4/-2 Ma and 410 ± 2 Ma, respectively.

7. The Sammys Barren granite is undeformed, medium- to coarse-grained and, based on geochemical contrasts, does not appear to be related to post-tectonic granite and rhyolite in the neighbouring Aspy terrane. The Sammys Barren granite intruded the Fox Back Ridge diorite/granodiorite at 435 +7/-3 Ma (U-Pb zircon crystallisation age of the granite).

8. A cooling rate of about 7-12°C/m.y. followed a widespread Silurian thermal episode in the Blair River inlier. The rate is constrained by the Sammys Barren granite, which is interpreted to have crystallised at about 670 ● 50°C, and by the ages and inferred U-Pb closure temperature of titanite and rutile. The titanite grains differ in origin, paragenesis, and size, and are from units throughout the Blair River inlier. However, all record near-synchronous cooling ages of about 425 Ma. Hornblende from the Fox Back Ridge unit cooled through 450 ± 50°C at 417 ± Ma and rutile from the anorthosite suite cooled through 405 ● 25°C at ca. 410 Ma.

9. The chronologic, geochemical, and petrologic characteristics of the Proterozoic units in the Blair River inlier are consistent with a general correlation with the Grenville Province. Deep seismic data in the Gulf of St. Lawrence indicate that Laurentian basement extends, at depth, to at least as far as northern Cape Breton Island. Gravity, magnetic, and shallow seismic data in the northern Appalachian orogen indicate that major tectonostratigraphic boundaries trend from southern Newfoundland into, rather than around, Cape Breton Island. These data also indicate the Blair River inlier occupies a position within the Appalachian orogen in Cape Breton Island that is the along-strike equivalent of the Humber Zone (deformed Laurentian margin) in Newfoundland. The Blair River inlier records Silurian metamorphism

and minor plutonism that are nearly identical in age to thermal events in the Humber Zone of western Newfoundland. The Blair River inlier, therefore, is interpreted to be an exposed fragment of Laurentian basement rocks and to provide a surficial constraint on the minimum southeasterward extension of the Humber Zone in the northern Appalachian orogen.

APPENDICES

A3 - Appendix to Chapter 3

A3.1 Whole-rock geochemistry analytical techniques

40 samples were selected for whole-rock geochemical analysis. Major and trace element contents were measured on a Philips PW-1400 sequential X-ray fluorescence spectrometer with a Rh-anode X-ray tube at St. Mary's University XRF laboratory. Major element oxides (SiO_2, TiO_2, Al_2O_3, MgO, Fe_2O_{3tot}, CaO, Na_2O, K_2O, and P_2O_5) and trace elements (Ba, Rb, Sr, Y, Zr, Nb, Th, Pb, Ga, Zn, Cu, Ni, V, and Cr) were analysed, with 5% and 5-10% precision respectively, from fused glass disks and pressed powder pellets respectively, using in-house standards for calibration. Samples were heated in an electric furnace for 1.5 hrs at 1050°C to determine loss on ignition (LOI). Iron is reported from the XRF laboratory and in Table A3.1 as ferric, but is recalculated as ferrous as required in some diagrams assuming the relationship:

$$FeO_{tot} = Fe_2O_{3tot}*0.89981$$

which is a default recalculation method of the geochemical plotting program NewPet v. 93.02.16 (D. Clarke, Memorial University of Newfoundland).

Table A3.1 Major and Trace Element Data

Sample	BVM90-135*	BVM91-670*	BVM91-673*	RB91-003*	RB91-044*	BVM90-057[2]	BVM90-073[2]	BVM90-128*	BVM90-144[2]	BVM91-504[2]
Lithology	aph-rhy	aph-rhy	aph-rhy	aph-rhy	aph-rhy	charn	charn	charn	charn	charn
SiO_2	74.35	77.19	77.58	77.12	77.34	51.93	60.18	62.77	54.10	62.52
TiO_2	0.07	0.08	0.08	0.07	0.11	0.83	0.58	0.71	0.72	0.87
Al_2O_3	14.16	11.84	12.21	13.34	12.35	20.31	17.38	15.75	18.11	14.04
Fe_2O_3	0.54	0.52	0.49	0.41	0.28	7.87	6.05	4.16	7.34	7.07
MgO	0.00	0.02	0.01	0.01	0.04	5.17	2.83	2.02	4.57	3.16
MnO	0.01	0.02	0.03	0.01	0.02	0.11	0.11	0.05	0.09	0.11
CaO	0.08	0.03	0.03	0.09	0.12	6.73	5.88	4.84	7.65	5.10
Na_2O	3.93	3.20	3.27	4.24	4.04	3.97	4.30	4.16	4.41	2.88
K_2O	4.37	4.43	4.81	3.94	4.17	0.92	1.64	2.53	0.91	2.85
P_2O_5	0.02	0.02	0.02	0.01	0.01	0.10	0.15	0.34	0.18	0.21
L.O.I.	0.80	0.60	0.10	0.40	0.40	1.00	0.40	1.60	0.80	1.10
Total	98.33	97.95	98.63	99.64	98.88	98.94	99.50	98.93	98.88	99.89
Ba	56	186	131	71	136	422	537	891	438	589
Rb	327	232	240	226	128	6	20	30	5	54
Sr	10	30	56	28	32	617	419	392	633	343
Y	18	19	14	15	10	7	32	39	23	26
Zr	61	59	63	66	72	19	98	247	73	282
Nb	30	22	23	33	17			7		7
Th	32	29	30	28	39			<10		
Pb	11	<10	<10	10	9			<10		
Ga	22	17	13	19	12	13	17	16	18	15
Zn	19	12	9	9	6	67	66	27	43	66
Cu	<5	<5	<5	4	4		28	16	30	22
Ni	<5	<5	<5	4	4	66	13	28	50	21
Cr	9	6	6	6	4	226	25	30	88	37
V	<5	6	6	4	4	99	112	94	170	162

Major elements in wt.% oxides. All iron determined as Fe_2O_3
Trace elements in parts per million
See end of table for explanation of abbreviations

Table A3.1 (continued)

Sample	BVM91-608*	BVM91-614[2]	BVM91-625[2]	BVM91-626[2]	BVM91-736*	BVM91-738*	CW85-057*	RR85-2042*	RR85-2061[2]	RR85-2075[2]
Lithology	charn	charn	charn	charn	charn	charn	charn	charn	charn	charn
SiO_2	66.57	62.39	61.08	65.91	61.74	68.31	63.31	73.66	66.11	68.57
TiO_2	0.81	0.45	0.64	0.51	0.64	0.26	0.68	0.20	0.80	0.29
Al_2O_3	14.25	19.94	15.19	15.76	15.44	16.85	15.45	12.94	15.19	16.74
Fe_2O_3	4.84	3.62	7.65	7.96	6.92	1.51	6.00	2.14	7.96	2.09
MgO	1.08	1.31	3.32	1.68	3.43	0.77	0.35	0.10	0.96	0.70
MnO	0.09	0.04	0.17	0.07	0.17	0.04	0.12	0.02	0.07	0.04
CaO	2.78	4.04	4.47	4.07	4.90	1.69	2.51	1.12	3.00	2.86
Na_2O	3.43	5.86	3.99	4.28	3.75	5.48	4.38	3.32	3.45	4.95
K_2O	3.79	1.49	1.78	0.99	1.63	2.14	5.04	3.93	4.17	1.78
P_2O_5	0.34	0.07	0.18	0.13	0.16	0.14	0.19	0.04	0.33	0.10
L.O.I.	0.70	0.60	1.70	0.90	2.50	1.40	0.30	0.60	0.40	0.90
Total	98.68	99.81	100.17	102.26	101.28	98.59	98.33	98.07	102.44	99.02
Ba	1071	507	529	324	639	544	2024	791	1161	422
Rb	54	12	48		33	26	77	86	56	25
Sr	251	526	421	505	432	347	183	126	276	425
Y	65	11	25	9	22	5	80	8	67	<5
Zr	423	116	154	200	172	77	1096	170	509	90
Nb	13				5	<5	29	<5	12	<5
Th	<10				<10	<10	<10	<10		<10
Pb	10	12			<10	<10	25	10		11
Ga	18	19	17	19	14	15	24	14	17	18
Zn	51	22	71	60	91	27	123	29	53	38
Cu	37	26	91	8	21	6	12	6	21	<5
Ni	8	10	26	11	23	6	<5	5	6	<5
Cr	12	11	42	38	45	9	<5	11	8	6
V	50	39	146	71	164	29	6	<5	41	25

Major elements in wt.% oxides. All iron determined as Fe_2O_3
Trace elements in parts per million
See end of table for explanation of abbreviations

Table A3.1 (continued)

Sample	BVM90-153*	BVM91-553*	RR85-2033[3]	RR85-2037[3]	CW85-096[3]	RR85-2044[3]	SB85-1016[3]	SB85-1022[3]	CW85-158*	BVM90-159*
Lithology	FBR	FBR	Fiss-bas	Fiss-bas	Fiss-rhy	Fiss-rhy	Fiss-rhy	Fiss-rhy	OBg-granite	SBg-granite
SiO_2	56.33	51.42	40.75	46.15	76.18	78.62	76.49	78.04	72.64	75.28
TiO_2	1.31	1.32	3.01	1.43	0.18	0.14	0.11	0.13	0.04	0.05
Al_2O_3	13.92	16.51	13.47	17.71	11.35	10.65	12.04	10.62	15.01	16.19
Fe_2O_3	8.01	8.05	16.50	10.69	2.32	1.96	1.84	2.10	1.00	0.63
MgO	4.96	5.78	5.72	7.35	1.00	0.04	0.37	0.20	0.02	0.08
MnO	0.13	0.15	0.35	0.90	0.03	0.03	0.02	0.04	0.04	0.02
CaO	7.37	7.35	7.54	6.29	0.13	0.05	0.09		0.53	1.52
Na_2O	2.94	3.20	1.54	2.67	2.84	0.13	2.83	0.13	4.54	5.50
K_2O	2.80	3.08	3.81	2.31	5.75	8.23	5.68	8.72	4.27	1.39
P_2O_5	0.35	0.32	1.05	0.29	0.04		0.01	0.02	0.02	0.03
L.O.I.	1.60	2.20	7.00	3.92	0.42	0.49	0.60	0.37	0.60	0.80
Total	99.72	99.38	100.74	99.71	100.24	100.34	100.08	100.37	98.71	101.49
Ba	869	916	877	301	392	193	206	233	118	391
Rb	79	99	125	70	155	274	236	280	71	22
Sr	462	421	190	582	75	41	26	44	79	327
Y	17	19	54	29	69	62	43	79	27	<5
Zr	176	148	289	134	454	454	151	434	70	285
Nb	42	27	13	6	46	49	25	49	<5	<5
Th	10	<10	2		26	26	44	23	<10	<10
Pb	10	<10	9	10	18	11	13	10	16	<10
Ga	15	15	25	23	13	13	24	14	24	12
Zn	71	77	133	771	26	45	30	48	22	15
Cu	17	22	48	10	6	13	5	16	6	5
Ni	58	28	42	70	30	37	28	39	<5	<5
Cr	130	53	25	23	21	24	22	20	11	10
V	246	229	328	231	1	1	7	9	6	7

Major elements in wt.% oxides. All iron determined as Fe_2O_3
Trace elements in parts per million
See end of table for explanation of abbreviations

Table A3.1 (continued)

Sample Lithology	BVM90-132* SmsBr-grani	FD85-577* Undiv-granite	CW85-085[1] LBS	CW85-087[1] LBS	CW85-091[1] LBS	RR85-2045[1] LBS	SB85-1023[1] LBS	SB85-1024[1] LBS	SB85-1030[1] LBS	SB85-1034[1] LBS
SiO_2	68.47	71.86	56.38	59.27	60.93	58.61	61.92	60.81	59.02	58.76
TiO_2	0.35	0.36	1.59	1.19	0.95	1.08	0.85	0.97	1.04	1.11
Al_2O_3	15.72	13.68	17.77	18.15	17.76	18.62	16.86	17.38	18.34	18.61
Fe_2O_3	1.47	2.22	6.97	5.17	4.48	4.91	4.42	5.08	5.65	5.12
MgO	0.60	0.32	1.76	1.22	1.21	1.27	0.93	0.92	1.29	1.38
MnO	0.03	0.07	0.25	0.14	0.24	0.21	0.14	0.19	0.19	0.21
CaO	1.43	0.48	4.66	3.03	2.11	1.27	2.00	1.42	3.36	2.70
Na_2O	4.05	3.52	5.20	4.94	5.09	5.88	4.89	4.88	5.73	5.38
K_2O	5.16	5.23	3.68	5.23	5.90	4.98	6.91	6.55	4.62	4.85
P_2O_5	0.12	0.12	0.82	0.51	0.31	0.55	0.23	0.23	0.55	0.48
L.O.I.	1.10	0.40	0.81	1.00	0.82	1.60	0.48	0.40	0.51	1.10
Total	98.50	98.26	99.89	99.85	99.80	98.98	99.63	98.83	100.30	99.70
Ba	1126	715	2177	2541	2073	2156	1093	888	2098	2360
Rb	96	79	32	53	85	70	101	88	43	54
Sr	292	147	492	426	366	412	140	108	442	409
Y	20	18	55	40	42	42	37	39	40	37
Zr	220	352	346	1080	496	834	1474	1237	995	738
Nb	54	11	12	12	14	10	14	15	13	12
Th	<10	<10			5					
Pb	14	13	15	19	19	16	10	20	11	16
Ga	15	15	27	27	22	25	26	21	24	26
Zn	20	165	172	127	201	175	149	95	121	127
Cu	<5	<5	19	16	14	13	19		16	20
Ni	5	<5	13	14	18	18	17	15	11	14
Cr	7	6	6	13	9	9	11	15	6	8
V	33	10	24	6	9	27	13	3	16	20

Major elements in wt.% oxides. All iron determined as Fe_2O_3

Trace elements in parts per million

See end of table for explanation of abbreviations

Table A3.1 (continued)

Sample	SB85-1038[1]	SB85-1043[1]	SB85-1112[1]	SB86-3140*	SD87-01[1]	SD87-02[1]	BVM91-545*	RR85-2105*	BVM91-574*	BVM91-696*
Lithology	LBS	LBS	LBS	LBS	LBS	LBS	metagabbro	metagabbro	Undiv-amphi	OBg
SiO_2	61.97	62.80	61.42	59.20	57.99	56.30	48.53	48.88	46.63	54.74
TiO_2	0.89	0.85	1.03	1.04	1.29	1.65	0.92	0.99	1.47	0.53
Al_2O_3	17.67	17.43	17.21	17.20	18.39	16.85	14.66	17.88	13.61	24.10
Fe_2O_3	4.80	3.89	5.43	5.22	5.20	7.39	10.82	10.88	13.34	2.04
MgO	0.75	0.84	0.59	0.89	1.57	2.18	8.27	6.37	7.28	0.90
MnO	0.11	0.21	0.16	0.16	0.21	0.23	0.20	0.17	0.22	0.10
CaO	1.27	0.87	1.23	2.08	2.73	3.84	10.71	10.65	9.87	7.40
Na_2O	5.32	5.11	5.02	5.03	5.04	4.87	1.92	2.40	2.90	5.37
K_2O	6.68	6.85	6.61	6.44	4.58	4.00	0.71	0.37	1.09	2.09
P_2O_5	0.22	0.17	0.19	0.30	0.54	0.72	0.09	0.07	0.14	0.15
L.O.I.	5.80	0.52	0.59	0.60	1.30	0.90	2.70	1.00	1.90	2.70
Total	105.48	99.54	99.48	98.16	98.84	98.93	99.53	99.66	98.45	100.12
Ba	1672	549	791	941	2276	2116	111	78	460	490
Rb	92	86	84	95	51	35	17	11	17	58
Sr	114	68	99	117	414	413	177	202	129	282
Y	43	37	40	44	39	55	19	17	32	7
Zr	1420	1085	1423	1468	650	789	59	52	93	25
Nb	18	27	14	18	16	17	<5	<5	7	
Th		1		<10			<10	<10	<10	
Pb	22	13	19	16	18	2	<10	<10	51	10
Ga	23	27	28	21	20	22	14	17	18	16
Zn	68	62	121	90	132	74	83	75	353	594
Cu	15	8	11	10	8	9	17	137	141	
Ni	20	17	16	5		5	128	94	99	9
Cr	11	12	10	<5		2	265	47	241	15
V	2	8	5	<5	17	23	300	286	380	25

Major elements in wt.% oxides. All iron determined as Fe_2O_3
Trace elements in parts per million
See end of table for explanation of abbreviations

Table A3.1 (continued)

Sample	BVM91-714*	BVM91-724*	CW85-159*	BVM90-121*	BVM91-740*	SB85-1090*	SB85-1092*	BVM90-067[a]	BVM91-584[a]	RB91-063[a]
Lithology	OBg	OBg	OBg	RR syn	RR syn	RR syn	RR syn	RRAS-an	RRAS-an	RRAS-an
SiO_2	51.27	46.84	62.35	61.78	60.96	60.43	62.87	55.94	54.08	53.32
TiO_2	1.58	3.20	0.72	0.67	0.64	0.83	0.58	0.26	0.21	0.28
Al_2O_3	17.31	15.41	17.74	18.73	18.09	18.71	18.90	26.91	28.04	28.23
Fe_2O_3	11.71	12.61	4.13	2.54	2.96	4.18	3.12	1.70	1.50	1.55
MgO	1.88	3.89	0.65	0.45	0.57	1.06	0.71	1.01	0.92	0.49
MnO	0.25	0.21	0.10	0.04	0.06	0.08	0.05	0.02	0.02	0.03
CaO	4.91	8.93	2.96	1.25	1.75	2.16	1.22	6.92	8.73	8.43
Na_2O	5.63	3.58	5.73	4.78	4.21	4.91	5.53	5.76	4.66	4.74
K_2O	3.25	1.50	2.78	7.99	7.69	5.78	6.07	0.85	0.41	1.08
P_2O_5	0.87	1.85	0.36	0.12	0.14	0.28	0.21	0.10	0.05	0.06
L.O.I.	1.10	1.00	0.70	0.90	1.00	1.30	1.10	1.10	0.40	1.60
Total	99.76	99.02	98.22	99.25	98.07	99.72	100.36	100.57	99.02	99.81
Ba	2522	899	1951	347	1936	2092	1454	346	185	270
Rb	42	17	21	76	88	65	75	9		42
Sr	951	700	644	84	345	388	264	1024	1041	1068
Y	131	67	35	20	32	24	22			
Zr	1286	188	644	615	589	625	431	13	18	19
Nb	7	7	10	28	44	39	38			
Th	<10	<10	<10	12	<10	<10	<10			
Pb	19	12	12	11	10	10	10			
Ga	21	23	21	12	13	16	16	16	17	16
Zn	253	193	71	19	39	46	37	17	15	15
Cu	21	21	8	7	10	10	6			8
Ni	7	7	<5	<5	<5	<5	7	17	13	10
Cr	<5	<5	7	<5	<5	<5	<5	19	11	8
V	21	161	9	23	40	45	44	18	23	35

Major elements in wt.% oxides. All iron determined as Fe_2O_3
Trace elements in parts per million
See end of table for explanation of abbreviations

Table A3.1 (continued)

Sample	RB91-076[2]	RR85-2092[2]	SB85-1070[3]	SB85-1097[2]	CW85-136[2]	CW86-3721[2]	RB91-025[2]	RB91-060[2]	SB85-1113[2]	RR85-2138[2]
Lithology	RRAS-an	RRAS-an	DB-an	HC-an	SR-an	RRAS-ha	RRAS-ha	RRAS-ha	RRAS-ha	RRAS-ha
SiO_2	54.27	53.42	53.96	56.39	54.34	56.74	56.36	56.02	55.11	54.50
TiO_2	0.12	0.12	0.16	0.29	0.18	0.18	0.11	0.15	0.17	0.21
Al_2O_3	29.27	27.03	27.32	25.07	24.63	26.84	26.96	27.37	24.38	24.85
Fe_2O_3	0.41	1.38	0.83	1.65	2.41	1.19	0.88	0.74	2.35	2.02
MgO	0.09	0.71	0.97	0.53	2.37	0.25	0.20	0.37	1.37	1.43
MnO	0.01	0.04	0.02	0.04	0.11	0.02	0.01	0.04	0.09	0.04
CaO	8.73	8.19	9.34	6.70	3.21	6.53	6.90	6.27	6.11	6.38
Na_2O	4.99	5.33	4.57	6.01	4.93	6.23	6.24	5.63	5.69	5.18
K_2O	0.43	1.24	0.72	1.36	3.68	1.38	0.60	1.62	2.06	2.37
P_2O_5	0.03	0.03	0.07	0.15	0.09	0.09	0.08	0.07	0.06	0.01
L.O.I.	0.70	1.95	1.00	1.25	3.90	1.50	1.10	1.90	2.22	2.52
Total	99.05	99.44	98.96	99.44	99.85	100.95	99.44	100.18	99.61	99.51
Ba	161	225	230	470	437	298	239	400	429	558
Rb		26	6	18	132	30		36	38	91
Sr	1059	940	989	938	321	1023	932	923	766	987
Y		5	4	8	5	8		6	6	5
Zr	10	34	40	47	8	18	16	13	34	30
Nb		2	3	3					2	3
Th										
Pb				4					6	
Ga	17	19	16	23	12	16	20	15	20	22
Zn	8	21	24	72	81	17	13	54	62	21
Cu		17	2	16		87			11	16
Ni		7	8		18	4			5	6
Cr		21	13	32	37	5			61	12
V	5	15	10	16	18	10	11	9	18	6

Major elements in wt.% oxides. All iron determined as Fe_2O_3
Trace elements in parts per million
See end of table for explanation of abbreviations

Table A3.1 (continued)

Sample	BVM90-114[2]	BVM91-733*	BVM91-774a	BVM91-774b	RB91-043[2]	RB91-009[2]	BVM90-056[2]	BVM91-610[2]	RB91-050[2]	BVM91-695a
Lithology	RRAS-lay	RRAS-lay	RRAS-lay, w	RRAS-lay,ga	RRAS-lay	RRAS-leucog	RRAS-leucg	RRAS-leucg	RRAS-leucg	PCR-leuco,h
SiO_2	52.57	52.98	76.62	52.63	59.90	51.07	53.23	56.54	52.36	56.06
TiO_2	0.85	1.03	0.15	1.76	0.73	0.98	1.17	0.41	0.37	1.40
Al_2O_3	17.93	16.84	12.42	14.09	17.93	17.50	20.20	19.39	21.99	17.28
Fe_2O_3	8.99	8.68	1.82	13.77	3.97	10.45	7.43	6.83	5.88	9.20
MgO	4.48	3.64	0.73	5.63	3.77	5.47	3.89	2.29	6.61	1.38
MnO	0.15	0.15	0.03	0.24	0.07	0.18	0.12	0.15	0.09	0.20
CaO	8.30	7.86	2.60	6.62	6.73	7.66	6.33	5.37	7.10	4.67
Na_2O	3.70	4.87	3.73	3.25	4.86	3.31	4.35	5.14	3.15	5.67
K_2O	0.51	0.92	0.41	1.04	0.85	0.90	0.57	1.84	0.39	2.91
P_2O_5	0.19	0.25	0.01	0.32	0.15	0.21	0.21	0.25	0.06	0.57
L.O.I.	1.60	1.10	0.40	1.10	0.70	1.70	2.10	1.30	2.10	0.70
Total	99.27	98.52	98.92	100.45	99.66	99.43	99.60	99.51	100.10	100.04
Ba	218	418	212	368	273	293	315	1092	146	2203
Rb	7	11		15	10	13	8	27	9	30
Sr	503	412	183	179	443	443	602	775	715	535
Y	25	46		36	48	46	6	19	6	77
Zr	130	111	107	97	166	186	37	44	22	1358
Nb		<5			5					38
Th		<10								<10
Pb		<10								11
Ga	17	22	11	21	19	24	21	18	15	24
Zn	76	67	20	126	23	92	66	69	48	170
Cu	15	21	5	86		25	31	15		14
Ni	26	18	6	64	15	29	37	8	81	5
Cr	63	25	9	117	53	247	66	6	117	6
V	195	262	22	322	124	205	98	91	83	19

Major elements in wt.% oxides. All iron determined as Fe_2O_3

Trace elements in parts per million

See end of table for explanation of abbreviations

Table A3.1 (continued)

Sample Lithology	BVM91-518[2] RRAS-pyxite	BVM91-757[*] RRAS-pyxite	RB91-030[*] RRAS-pyxite	BVM91-526[*] SBg	BVM91-527[*] SBg	BVM91-753[*] SBg	BVM91-773[*] SBg	CW85-103[*] SBg	CW85-110[1] SBg	CW85-118a[*] SBg
SiO_2	48.22	42.66	48.87	58.13	60.94	55.13	54.56	59.56	61.07	61.71
TiO_2	1.16	6.78	1.17	0.80	0.89	0.83	0.82	0.76	1.61	1.37
Al_2O_3	14.45	11.51	14.29	15.95	15.30	16.37	14.03	16.67	12.83	14.50
Fe_2O_3	12.81	20.97	12.67	9.94	6.72	9.46	10.36	6.40	9.35	8.86
MgO	8.01	7.05	7.97	2.94	3.09	6.67	6.04	2.49	1.83	1.60
MnO	0.20	0.20	0.19	0.12	0.14	0.31	0.21	0.16	0.23	0.17
CaO	11.05	4.71	11.16	3.14	5.30	1.85	6.54	6.03	2.77	4.19
Na_2O	1.94	2.80	1.94	5.90	3.49	6.01	4.87	4.40	2.92	4.57
K_2O	0.32	0.42	0.33	0.77	2.87	0.81	0.75	0.47	3.49	1.69
P_2O_5	0.09	0.01	0.10	0.18	0.24	0.12	0.22	0.19	0.83	0.80
L.O.I.	1.00	2.10	1.00	1.50	1.40	2.90	1.40	2.10	1.80	1.10
Total	99.25	99.21	99.69	99.37	100.38	100.46	99.80	99.23	98.73	100.56
Ba	70	214	67	180	749	68	165	362	1625	1359
Rb	9	13	8	19	55	9	9	<5	38	14
Sr	178	283	175	272	375	67	85	381	300	481
Y	22	<5	25	20	34	16	43	35	93	70
Zr	62	83	67	299	278	82	167	164	995	653
Nb		6	<5	7	10	6	6	6	24	13
Th		<10	<10	<10	<10	<10	<10	<10		<10
Pb	16	<10	21	15	12	26	<10	15		13
Ga	16	17	17	18	17	14	17	18	22	18
Zn	104	113	102	100	102	231	37	141	145	113
Cu	152	108	175	39	11	9	10	11	11	26
Ni	106	105	111	12	21	47	63	13	5	5
Cr	271	69	312	57	58	177	271	29	1	11
V	340	721	334	152	146	243	209	142	40	80

Major elements in wt.% oxides. All iron determined as Fe_2O_3

Trace elements in parts per million

See end of table for explanation of abbreviations

Table A3.1 (continued)

Sample Lithology	RR85-2047a SBg	SB85-1048[*] SBg	SB85-1074[1] SBg	RB91-057[2] wht rx	RR85-2130[3] wht rx	SB86-3136[*] wht rx
SiO_2	54.40	46.98	64.75	63.86	60.48	72.50
TiO_2	0.88	1.72	1.24	0.88	0.13	0.29
Al_2O_3	16.82	12.76	12.90	20.29	22.35	13.07
Fe_2O_3	10.58	20.22	7.69	1.18	1.63	4.22
MgO	4.51	8.22	1.45	1.42	0.31	0.71
MnO	0.17	0.34	0.23	0.02	0.03	0.11
CaO	5.14	5.37	2.25	5.25	4.35	1.72
Na_2O	4.28	1.43	3.53	5.53	6.00	3.51
K_2O	0.77	1.60	4.19	0.63	2.15	2.45
P_2O_5	0.23	0.43	0.53	0.04	0.05	0.04
L.O.I.	1.80	0.70	0.80	0.80	1.95	0.50
Total	99.58	99.77	99.56	99.90	99.43	99.12
Ba	284	306	1731	127	842	724
Rb	14	31	54	8	37	40
Sr	384	114	253	461	611	165
Y	42	46	82	31	7	63
Zr	151	213	118	147	59	200
Nb	6	6	25		12	5
Th	<10	<10			1	<10
Pb	<10	<10	3		5	20
Ga	19	23	23	17	19	17
Zn	82	233	107	16	13	98
Cu	30	348	11		9	27
Ni	16	36	3	5		<5
Cr	27	11	2	41	15	10
V	202	495	12	75	5	35

Major elements in wt.% oxides. All iron determined as Fe_2O_3
Trace elements in parts per million
See end of table for explanation of abbreviations

Unit and Lithology Abbreviations:

DB = Delaneys Brook anorthosite
FBR = Fox Back Ridge diorite/granodiorite
Fiss = Fisset Brook Formation
HC = High Cape anorthosite
LBS = Lowland Brook Syenite
OBg = Otter Brook gneiss
PCR = Polletts Cove River anorthosite
RR syn = Red River syenite
RRAS = Red River Anorthosite Suite
SBg = Sailor Brook gneiss
SmsBr = Sammys Barren granite
SR = Salmon River anorthosite
Undiv = undivided unit
amphib = amphibolite
an = anorthosite
aph = aphanitic
bas = basalt
charn = charnockite
ha = highly altered
lay = layered
leucgb = leucogabbro
pyxite = pyroxenite & gabbro
wht rx = "white rock"
rhy = rhyolite

Data Sources:
[*] This study
[1] Deveau, 1988
[2] Bekkers, 1993
[3] S. Barr, unpublished

Table A3.2 Rare Earth Element Data

Sample Lithology	CW85-085[1] LBS	SB85-1024[1] LBS	SB85-1030[1] LBS	BVM91-584[2] RRAS-an	RB91-025[2] RRAS-ha	RB91-043[2] RRAS-lay	RB91-009[2] RRAS-leucgb	BVM91-057[2] RRAS-leucg	BVM90-144[2] charn	BVM91-625[2] charn
La	72	82	54	2.787	3.552	17.42	15.44	8.836	17.88	15.61
Ce	115	68	87	5.76	6.817	55.3	39.99	27.13	39.98	38
Pr				0.715	0.782	8.017	5.705	4.139	5.008	5.093
Nd	69	39	54	3.07	2.917	36.45	26.48	19.56	20.75	21.89
Sm	14.90	8.23	11.00	0.622	0.429	8.36	6.681	4.905	4.444	4.823
Eu	6.23	2.20	4.58	0.756	0.836	1.556	1.765	1.36	1.217	1.175
Gd				0.763	0.553	8.181	7.044	5.04	4.586	4.734
Tb	1.50	1.10	1.30	0.064	0.028	1.235	1.087	0.771	0.621	0.649
Dy				0.385	0.134	7.758	7.046	4.835	3.847	4.1
Ho				0.078	0.029	1.559	1.452	0.985	0.747	0.826
Er				0.205	0.065	4.508	4.395	2.84	2.129	2.411
Tm				0.029	0.009	0.647	0.631	0.402	0.306	0.337
Yb	4.75	4.18	4.18	0.199	0.033	4.413	4.264	2.484	2.061	2.35
Lu	0.74	0.80	0.73	0.039	0.018	0.624	0.611	0.366	0.283	0.35

All values in parts per million

All values in parts per million

Unit and Lithology Abbreviations:

DB = Delaneys Brook anorthosite
FBR = Fox Back Ridge diorite/granodiorite
Fiss = Fisset Brook Formation
HC = High Cape anorthosite
LBS = Lowland Brook Syenite
OBg = Otter Brook gniess
PCR = Polletts Cove River anorthosite
RR syn = Red River syenite
RRAS = Red River Anorthosite Suite
SBg = Sailor Brook gneiss
SmsBr = Sammys Barren granite
SR = Salmon River anorthosit
Undiv = undivided unit

amphib = amphibolite
an = anorthosite
aph = aphanitic
bas = basalt
charn = charnockite
ha = highly altered
lay = layered
leucgb = leucogabbro
pyxite = pyroxenite & gabbro
wht rx = "white rock"
rhy = rhyolite

Data Source
* This study
[1] Deveau, 1988
[2] Bekkers, 1993
[3] S. Barr, unpublished

A4 - Appendix to Chapter 4

A4.1 Analytical methods

U-Pb

U-Pb dating was conducted at the Memorial University geochronology laboratory. Zircon, titanite, and rutile were separated from bulk crushed rock using a Wilfley table and a combination of heavy liquids and Frantz magnetic separation. Mineral separates were sieved to size fractions and hand-picked under a microscope to obtain high-quality, inclusion-free, morphologically similar grains. All fractions were abraded, using the technique of Krogh (1982), to remove outer surfaces of the crystal which are more likely affected by Pb loss. Sieve-size fractions and abrasion times are shown in Table A3.1. Following abrasion, grains were washed in distilled HNO_3, H_2O, and acetone, spiked with a mixed $^{205}Pb/^{235}U$ tracer and dissolved with HF and HNO_3 in Teflon pressure-dissolution capsules at 220°C for 5 days (zircon and rutile) or in Savillex capsules at 90°C for 3-5 days (titanite). U and Pb were collected using ion-exchange chemistry, modified after Krogh (1973), and loaded on a single Re filament using phosphoric acid and silica gel. Isotopic ratios were measured in the temperature range 1400°C-1550°C (Pb) and 1500°C-1600°C (U) on a Finnigan MAT 262 mass spectrometer using multiple Faraday detectors in static-collection mode. Samples with small U or Pb concentrations were measured by peak jumping on a secondary electron multiplier-ion counter.

Measured isotopic ratios were corrected for fractionation within the mass spectrometer and procedural blank (in the range 5-15 picograms when these analyses were carried out). Further corrections were made for the isotopic composition of initial common Pb in excess of procedural blank using the model of Stacey and Kramers (1975). Uncertainties in the isotopic ratios, reported at 2σ in Table 1, include propagated uncertainties in U and Pb fractionation and blank composition, spike weight, and measurement precision of $^{238}U/^{235}U$, $^{207}Pb/^{206}Pb$, $^{207}Pb/^{205}Pb$, $^{207}Pb/^{208}Pb$, $^{207}Pb/^{204}Pb$ ratios. The fitting of regression lines is after Davis (1982). Uncertainties in the ages are reported at the 95% confidence level. Analytical data are presented in Table A4.1.

$^{40}Ar/^{39}Ar$

Dating of hornblende and mica using $^{40}Ar/^{39}Ar$ techniques was conducted at the Dalhousie University geochronology laboratory. Bulk crushed rock was sieved to fractions between 0.25mm > 0.5mm. Hornblende and micas of this size interval were concentrated using a Frantz magnetic separator, and hand picked under a microscope to include only the least altered inclusion-free grains. Mineral concentrates of ~10 mg, or less, were irradiated and analysed in a VG 3600 mass spectrometer coupled to and internal tantalum resistance furnace of the double-vacuum type. The standard flux monitor is hornblende MMhb-1 with an accepted age of 519 ● 3 Ma (Alexander et al., 1978). J-parameter values determined using this standard were plotted against position in the can to determine sample J-values (Table A4.2). Random analytical uncertainty in J-values are the major source of error in the final age calculation. Other laboratory methods are described in Muecke et al. (1988).

Analytical data are presented in Table A4.2. Errors on individual steps are reported at the 1σ level based on the uncertainties in the correction for atmospheric argon composition and measured ^{40}Ar and ^{39}Ar. Apparent Ca/K ratios are calculated from microprobe analyses by:

$(Ca/K_{probe})/ß = 37/39_{measured}$ Where: $Ca = CaO_{wt\%}/56.08$;

$K = (K_2O_{wt\%}/94.2)*2$; $ß= 1.9$

The value of ß was calibrated over time using the laboratory standard and has remained fairly constant. Significant discrepancies between the microprobe-determined apparent $^{37}Ar/^{39}Ar$ and the measured $^{37}Ar/^{39}Ar$ (e.g., Fig. 3.8a) may indicate that the correction factor ß does not apply to this sample, perhaps because of significant compositional differences between the sample and standard.

A4.2 Interpreting geochronologic results

Cathodoluminescence and Backscatter Electron Imaging

Backscattered scanning electron microscopy images and cathodoluminescence microscopy images of zircon grains were obtained at the Dalhousie University electron microprobe laboratory using standard operating conditions. Zircon grains were mounted on a glass slide using standard thin section epoxy and ground and polished to approximately half their original width in order to expose a cross-section of their internal structure.

Zircon grains with euhedral morphologies (prismatic and pyramidal grains with sharp terminations and corners and flat crystal faces) are commonly considered to have crystallised from melts, whereas spheroidal, or multi-faceted ovoid grains are typically considered to have crystallised during metamorphism (e.g., van Breemen et al., 1986). This interpretation is not universally true, but it provides a starting point for interpreting the geologic significance of age data. A wide variety of irregular grain shapes is present in most of the samples from the Blair River Complex between the prismatic and spheroidal end members, but only the best examples of similar morphologic classes were selected for analysis.

Cathodoluminescence (CL) and backscatter electron (BSE) imaging techniques reveal a cross-section of the internal morphology of a zircon grain. These images allow for evaluation of the growth and/or resorption history of zircon grains with similar external morphologies, thereby helping to interpret the geological significance of the age data (Hanchar and Miller, 1993). CL images reveal minor differences in the relative concentrations of trace constituents substituting or trapped in the zircon crystal structure (Smith and Stenstrom, 1965; Yang et al., 1992), and variations in the brightness of BSE images are directly related to the variation in mean atomic number (Krinsley and Manley, 1989; Paterson et al., 1989). BSE an CL images may reveal semi-concentric zoning patterns that can result from either crystallographic preferential inclusion of trace constituents, or inclusion of varying amounts of trace constituents during growth stages (Vavra, 1990; Benisek and Finger, 1993). The latter essentially records the growth history of the mineral.

Zircon resorption is possible as a result of changes in magma temperature, pressure, or chemistry during crystallisation of an igneous body, or in metamorphic rocks as a result of reactions during thermal or fluid-flux events. Resorption causes disruption of the zoning patterns and, if overgrown by a subsequent generation of zircon, an unconformity is produced between zoning patterns in the core and overgrowth. Unconformable zoning relationships may also result from overgrowths on a xenocrystic zircon. Although these images must be interpreted with some degree of caution (e.g., Paterson et al., 1992), the empirical observations of relationships between growth zones, resorption, and overgrowth can be useful in interpreting isotopic data.

Since the intensity of the BSE image is related to mean atomic number, which is controlled largely by the substitutions of large-ion lithophile elements (U, Th, Hf, La being the most abundant), the relative intensity of BSE images gives a qualitative measure of trace-element chemistry. An empirical observation made during the acquisition of BSE images in this study was that images of spheroidal zircons commonly required increasing BSE gain and contrast, suggesting significantly lower concentrations of high-atomic number (relative to Zr) elements. This is confirmed by the measured U concentrations of spheroidal zircons for all fractions except those from the Lowland Brook Syenite (Table A4.1), which are interpreted to be of igneous origin.

U-Pb data

All zircon U-Pb data presented in Chapter 4 are discordant. The assumption that discordance is the result of only Pb-loss during a single metamorphic event may yield unreliable lower intercept ages if independent constraints on the age of metamorphism are lacking. The data presented below, however, fit well on regression lines and have geologically reasonable upper intercept ages. Discordia lines regressed through zircon data points alone have lower intercepts that either suggest recent Pb-loss or have lower intercepts within error (albeit large, because points cluster near the upper intercept) of independent metamorphic titanite. The metamorphic mineral control provides a reasonable estimate for a lower intercept "pin" (a more precise constraint on the lower intercept) and, in turn, produces a better refinement of the upper intercept age. Pinning the lower intercept does not significantly affect the quality-of-fit statistics for these discordia lines.

The assessment of discordant data from titanite and rutile must include a discussion of the effects of non-radiogenic Pb that is incorporated into a mineral at the time of its growth or closure with respect to the diffusion of Pb (initial common Pb). Many factors may contribute to the isotopic composition of initial common Pb and Pb-evolution models cannot accommodate all of these factors. Therefore, corrections of U-Pb data for the amount of common Pb cannot always be accurate. The effects of uncertainties in initial common Pb compositions are most important for minerals such as titanite and rutile which may contain large amounts of common Pb of an uncertain isotopic composition.

Due to the high proportion of common Pb in many of the titanite and rutile analyses presented below, the composition of the initial common Pb used in the correction is critical. The model of Stacey and Kramers (1975) requires nearly equal ^{206}Pb and ^{207}Pb corrections for minerals of mid-Paleozoic age, yet titanite of this study commonly contain an order of magnitude less total ^{207}Pb. Thus, ^{206}Pb is, by an order of magnitude, less affected by the common Pb correction, and the ^{206}Pb/^{238}U age is therefore less affected by inaccuracies in the model initial common Pb composition.

The ^{206}Pb/^{238}U ages presented in Chapter 4 are consistent between widely separated samples, separate fractions from the same sample, and analyses with widely varying proportions of common Pb. These relationships suggest that discordance on the concordia diagrams is the result of data points displaced to the right along the ^{207}Pb/^{235}U axis due to an incorrect model common Pb value for ^{207}Pb/^{204}Pb, rather than displaced down a ^{207}Pb/^{206}Pb discordia line due to Pb-loss. Therefore, the ^{206}Pb/^{238}U age from titanite and rutile analyses are here considered to represent the best approximation for the age of mineral growth, or of post-metamorphic cooling through the closure temperature of the mineral.

^{40}Ar/^{39}Ar

Data from ^{40}Ar/^{39}Ar step-heating analyses produce a spectral plot of the apparent age (calculated from the ^{40}Ar/^{39}Ar ratio of the gas released at each temperature step) versus cumulative percent ^{39}Ar released. A "plateau age" is defined by the age (within analytical uncertainty) of two or more contiguous gas fractions, each representing >4%, and together totalling >50% of the ^{39}Ar released (Fleck et al., 1977).

In the case where no plateau is defined, an isotope correlation diagram can help to elucidate meaningful geochronologic information as well as to assess the reliability of the data and the accuracy of some assumptions. These diagrams plot $^{39}Ar/^{40}Ar$ against $^{36}Ar/^{40}Ar$; the resulting (inverted) isochron plot is analogous to that of the Rb/Sr method. The use of this diagram assumes that sample argon is a combination of pure radiogenic and pure atmospheric argon incorporated into the sample at the time of formation. If all assumptions hold (McDougal and Harrison, 1988), the inverse of the X-axis intercept of a line regressed through the data is proportional to the age and the Y-axis intercept is the inverse of the atmospheric argon composition. The critical assumption is that the data points represent degrees of mixing of pure atmospheric and pure radiogenic gas components. The inverse Y-intercept provides a test for the assumption that trapped argon is of atmospheric ($^{40}Ar/^{36}Ar = 295.5$) composition. The fit of the line provides a test of the assumption that the sample argon is a mixture of only trapped and radiogenic source reservoirs. Significant scatter (i.e., ΣS values much greater than n-1; York, 1969) indicates that this condition is not met, and may suggest a component of excess ^{40}Ar, or disruption of $^{40}Ar/^{39}Ar$ systematics.

Excess argon commonly results in a "saddle-shaped" spectrum with old apparent ages in both the low-temperature and high-temperature gas release increments. An age cannot be inferred from this type of spectrum, even if a plateau is defined in the bottom of the saddle, because the ages are often older than the known age of the mineral (e.g. Harrison and MacDougal, 1981;

Roddick et al., 1980; Foland, 1983). The bottom of the saddle can, in some cases, approach the true age but this cannot be known without independent age control.

Hornblende spectral diagrams include a plot of the $^{37}Ar/^{39}Ar$ ratio of each temperature step. Because ^{37}Ar is produced by irradiation of Ca, the $^{37}Ar/^{39}Ar$ ratio is a proportional to the Ca/K ratio in the mineral. Significant changes in the $^{37}Ar/^{39}Ar$ (apparent Ca/K) ratio during step-heating could indicate the presence of more than one mineral phase. In the low-temperature steps this is generally thought to be the result of compositional heterogeneity or a non-monomineralic sample (e.g., multiple generations of the mineral, exsolution phases, small biotite or chlorite inclusions in, or alteration of, hornblende, etc.). At higher temperatures, phase transitions (for example, dehydration reactions) may account for disruptions of the apparent Ca/K ratio. These high-temperature disruptions are commonly associated with anomalous $^{40}Ar/^{39}Ar$ apparent ages. Electron microprobe analyses provide an independent measure of Ca/K ratio and can be compared to the $^{37}Ar/^{39}Ar$ ratio in order to assess the purity of the analysed mineral separate and the temperature steps over which the mineral(s) release most of their gas.

A4.3 Mineral Closure Temperatures

The closure temperature of a mineral dated by the $^{40}Ar/^{39}Ar$ technique, as defined by Faure (1986, p. 82), is "the temperature at which the loss of ^{40}Ar by diffusion out of a particular mineral becomes negligible compared to its rate of accumulation". An analogous definition applies to the U-Pb system. Closure temperatures are specific to the mineral under investigation and the radioactive parent and radiogenic daughter elements used in the geochronometer. Table 4.1 lists the assumed closure temperatures of relevant minerals in U-Pb and $^{40}Ar/^{39}Ar$ isotopic systems.

Harrison et al. (1985), Norwood (1974), and Giletti (1974) demonstrated the dependence of the activation energy on the composition and grain-size for annite and phlogopite. Their experimental calibrations show that decreasing mole percent annite compositions have an inverse (apparently linear) relationship to the activation energy of Ar, which is related to closure temperature via the well-known Dodson equation. Quantifiable uncertainties in this method are accommodated by errors calculated in both the activation energy and the frequency factors derived from Arrhenius plots. Non-quantifiable uncertainties include the reliability with which experimental conditions can be extrapolated to geologic conditions, and parameters of the Dodson equation which require assumptions, such as the geometric factor and the effective diffusion radius. Harrison et al. (1985) noted that biotite diffusion parameters from natural geologic settings are nearly identical to the parameters of their experimental studies and that the effective diffusion radius of 150-200 µm is common to all micas. The actual radius of micas analysed in this study are an order of magnitude larger (0.25mm - 0.5mm) than this range of radii, thus implying that the effective diffusion radius used by Harrison et al. (1985) also applies to the micas of this study.

Using the Dodson equation and the method described by Harrison et al. (1985), closure temperatures for the two phlogopite analyses were calculated assuming an infinite cylinder diffusion and a log-linear extrapolation of D_0 from Ann_3 (Giletti, 1974b) to Ann_{56} (Harrison et al., 1985). The respective closure temperatures were found to be:

- calc-silicate in Otter Brook gneiss (BVM-90-137) $Ann_{\sim 12}$ = 410 ±50°C
- Marble in Wilkie Brook fault zone(BVM-91-635) $Ann_{\sim 5}$ = 449 ±51°C

Table A4.1 - Blair River Complex : U-Pb data

Unit Name (Sample #, UTM Coordinates) Fraction Description	Sieve Size [mesh]	Weight [mg]	Concentrations U [ppm]	Pb rad [ppm]	Total common Pb	Atomic Ratios* 206Pb/204Pb	208Pb/206Pb	206Pb/238U	±	207Pb/235U	±	207Pb/206Pb	±	Age (Ma) 206Pb/238U	207Pb/235U	207Pb/206Pb
Sailor Brook Gneiss (BVM-91-773, 20T-PH 799076)																
1 Clear Prsm Zircon	>100	0.026	78	15.7	16	1444	0.2453	0.1751	124	1.8947	136	0.0785	16	1040	1079	1159
2 Best Prsm Zircon	>100	0.075	69	14.4	12	4647	0.3147	0.1751	304	1.8718	320	0.0776	24	1040	1071	1135
3 Turbid Prsm Zircon	>100	0.062	81	16	15	3740	0.237	0.1737	138	1.862	144	0.0778	22	1032	1068	1141
4 Four Lrg Prsm Zircon	>100	0.015	29	6.3	12	419	0.3337	0.1753	160	1.8428	218	0.0763	64	1041	1061	1102
5 Large Sph Zircon	>100	0.078	10	2.1	7	1282	0.4095	0.1657	144	1.6725	158	0.0732	26	988	998	1020
6 Small Sph Zircon	100>200	0.039	13	2.9	9	613	0.5308	0.1628	218	1.6369	232	0.0729	42	973	985	1011
7 Large Sph Zircon	>100	0.32	10	1.8	30	1010	0.3584	0.1521	96	1.5088	102	0.0719	32	913	934	984
8 Clear Titanite	>100	0.152	4	0.4	72	61	0.5572	0.0691	40	0.5507	300	0.0578	292	431	445	523
9 Clear Titanite	>100	0.175	4	0.5	142	42	0.8584	0.0622	42	0.5242	336	0.0611	362	389	428	644
Lowland Brook Syenite (SB-86-3140, 20T-PH 823084)																
1 Large Prsm Zircon	>100	0.076	68	12.9	30	1982	0.1194	0.184	96	1.9359	96	0.0763	20	1089	1094	1103
2 Large Sph Zircon	>100	0.153	75	14	5	24749	0.1203	0.1804	102	1.8768	100	0.0754	18	1069	1073	1080
3 Large Sph Zircon	>100	0.066	78	14.3	28	2046	0.117	0.1787	90	1.8565	94	0.0754	16	1060	1066	1078
4 Large Prsm Zircon	>100	0.123	80	14.6	16	6790	0.1223	0.1777	114	1.8493	108	0.0755	24	1055	1063	1081
—(SB-85-1038a, 20T-PH 821081)—																
1 Clear Titanite	>100	0.155	21	1.7	645	40	0.3465	0.0681	48	0.5695	330	0.0607	326	425	458	627
2 Clear Titanite	>100	0.171	21	1.8	708	40	0.3476	0.0678	36	0.5468	236	0.0585	234	423	443	548
Red River Anorthosite Suite (BVM-91-742, 20T-PG 766874)																
1 Large Sph Zircon	>100	0.031	93	16.4	11	2689	0.1764	0.1647	70	1.6396	72	0.0722	18	983	986	992
2 Small Prsm Zircon	100>200	0.155	100	16.1	28	5465	0.0954	0.1599	90	1.5843	90	0.0719	12	956	964	982
3 Large Sph Zircon	>100	0.05	80	12.7	6	6191	0.0821	0.1598	92	1.5797	92	0.0717	16	956	962	977
4 Large Sph Zircon	>100	0.165	81	12.7	29	4608	0.0893	0.1577	134	1.556	124	0.0716	24	944	953	973
5 Small Prsm Zircon	100>200	0.041	172	27.6	8	9150	0.1201	0.157	106	1.5381	100	0.0711	18	940	946	959
6 Small Prsm Zircon	100>200	0.015	19	5 30	4	6483	0.1078	0.1516	94	1.4852	84	0.0711	22	910	924	959

Abbreviations: Sph=spheroidal, Prsm=prismatic, Med=medium, nd=not determined
Field sample number and UTM coordinates are in brackets following unit name

* Atomic Ratios corrected for fractionation and spike, 5 to 10 pg Pb laboratory blank, and initial common lead calculated from the model of Stacey and Kramers (1975) for the age of the sample and 2 pg U blank. 2s uncertainties on the isotopic ratios calculated with an error propagation program, as discussed in Analytical Techniques section, are reported after the ratios and refer to the final digits.

Table A4.1 - Blair River Complex : U-Pb data

Unit Name (Sample #, UTM Coordinates) Fraction Description	Sieve Size [mesh]	Weight [mg]	U [ppm]	Pb rad [ppm]	Total common Pb	206Pb/204Pb	208Pb/206Pb	206Pb/238U	±	207Pb/235U	±	207Pb/206Pb	±	Age (Ma) 206Pb/238U	Age (Ma) 207Pb/235U	Age (Ma) 207Pb/206Pb
	Concentrations					Atomic Ratios*										
(RB-91-057, 20T-PG 767887)																
1 Tan Titanite	>100	0.274	94	8.9	160	704	0.5504	0.068	48	0.5199	48	0.0555	34	424	425	431
2 Tan Titanite	>100	0.329	91	8.7	177	736	0.57	0.0681	60	0.521	48	0.0555	14	424	426	434
3 Dark Brown Rutile	>100	0.4	79	4.7	87	1508	0.0019	0.0657	20	0.5	18	0.0552	10	410	412	419
4 Dark Brown Rutile	>100	0.441	76	4.5	56	2461	0.0013	0.0657	30	0.4993	22	0.0552	12	410	411	418
Gneissic Anorthosite (BVM-91-694, 20T-PG 778963)																
1 Brown Titanite	>100	0.109	311	19.5	151	977	0.0093	0.0685	32	0.5266	26	0.0557	18	427	430	442
2 Tan Titanite	>100	0.447	63	4.1	315	399	0.0706	0.0684	26	0.5244	32	0.0556	24	427	428	435
Otter Brook Gneiss (BVM-91-695, 20T-PG 767966)																
1 Large Prsm Zircon	>100	0.15	47	7.4	8	9221	0.0792	0.1584	92	1.556	80	0.0713	22	948	953	965
2 Large Prsm Zircon	>100	0.485	43	6.7	75	2757	0.0731	0.158	50	1.554	54	0.0713	10	946	952	967
3 Large Prsm Zircon	>100	0.371	60	9.3	29	7452	0.0808	0.1579	156	1.5505	148	0.0712	20	945	951	964
4 Clear Titanite	>100	0.111	7	0.4	416	27	nd	0.0679	100	0.6646	934	0.071	918	423	517	959
5 Clear Titanite	>100	1.499	6	0.3	6134	24	nd	0.0657	54	0.5414	700	0.0597	724	410	439	594
Fox Back Ridge diorite/granodiorite (BVM-91-553, 20T-PG 738884)																
1 Brown Titanite	>100	0.221	79	10.2	422	193	1.1577	0.0679	36	0.5267	54	0.0563	44	423	430	463
2 Brown Titanite	>100	0.231	78	9.8	426	197	1.0948	0.0677	36	0.5252	48	0.0563	44	422	429	463
Sammys Barren granite (BVM-90-132, 20T-PG 742885)																
1 Med Prsm Zircon	>100	0.082	522	42.1	50	3672	0.316	0.0683	56	0.5231	42	0.0556	16	426	427	435
2 Best Euhedral Prsm Zircon	>100	0.07	619	50.4	51	3677	0.3364	0.0679	38	0.5225	30	0.0558	12	424	427	443
3 Best Small Prsm Zircon	>100	0.13	628	50.2	89	3894	0.3231	0.0674	26	0.5157	20	0.0555	8	420	422	433
4 Prsm Zircon	>100	0.107	566	45.9	21	12206	0.3403	0.0674	20	0.5148	16	0.0554	6	420	422	429
5 Non-abraded Prsm Zircon	>100	0.083	600	45.5	150	1373	0.2905	0.0654	30	0.4984	30	0.0553	20	408	411	423
Red River syenite (BVM-90-121, 20T-PG 758889)																
1 Yellow Titanite	>100	0.247	32	5.5	433	97	1.8959	0.0681	36	0.5375	88	0.0572	86	425	437	500
2 Yellow Titanite	100>200	0.088	31	nd	144	97	nd	0.0663	34	0.5102	72	0.0559	68	414	419	447
3 Yellow Titanite	>100	0.224	32	6.6	3692	28	1.8959	0.0787	46	0.9927	468	0.0914	392	489	700	1456

Abbreviations: Sph=spheroidal, Prsm=prismatic, Med=medium, nd=not determined

Field sample number and UTM coordinates are in brackets following unit name

* Atomic Ratios corrected for fractionation and spike, 5 to 10 pg Pb laboratory blank, and initial common lead calculated from the model of Stacey and Kramers (1975) for the age of the sample and 2 pg U blank. 2-sigma uncertainties on the isotopic ratios calculated with an error propagation program, as discussed in Analytical Techniques section, are reported after the ratios and refer to the final digits.

Table A4.2 - Blair River Complex - Argon Isotopic Data

Step	°C	mV 39	% 39	AGE (Ma	(±)	% ATM	37/39	36/40	39/40	% IIC
	Sailor Brook Gneiss - (BVM-91-773) hornblende									
1	750	6.50	2.40	485.9	19.9	48.90	5.38	.001657	.003654	0.64
2	950	12.30	4.50	425.3	11.4	33.70	10.09	.001140	.005521	1.29
3	1000	11.50	4.20	481.6	5.1	15.90	12.88	.000538	.006084	1.54
4	1050	52.40	19.40	469.7	2.5	7.70	9.27	.000263	.006866	1.12
5	1075	33.80	12.50	459.3	2.7	7.60	8.15	.000259	.007050	1.00
6	1100	35.90	13.30	455.9	2.7	8.00	8.11	.000273	.007078	1.00
7	1125	21.00	7.80	468.6	5.6	12.10	8.18	.000412	.006555	0.99
8	1150	6.30	2.30	471.5	9.5	14.30	8.93	.000485	.006351	1.08
9	1175	9.30	3.40	609.1	19.1	13.20	9.18	.000448	.004783	0.98
10	1225	19.00	7.00	495.6	7.4	12.40	8.20	.000420	.006133	0.96
11	1275	25.10	9.30	477.7	4.1	14.30	8.46	.000485	.006256	1.01
12	1325	12.20	4.50	488.1	9.1	23.10	8.56	.000783	.005476	1.01
13	1375	20.10	7.40	488.9	7	36.60	8.61	.001238	.004509	1.02
14	1425	3.30	1.20	549.4	87.6	72.30	9.06	.002449	.001718	1.01
		Total Gas Age = 476.4			J = 0.002215					
	Lowland Brook Syenite - (SB-87-3137) hornblende									
1	750	4.50	3.20	681.9	34	23.20	3.71	.000786	.003679	0.37
2	950	10.40	7.30	633.1	13	9.80	5.19	.000333	.004722	0.54
3	1000	49.00	34.60	513.7	2.4	2.30	4.87	.000079	.006529	0.56
4	1050	51.40	36.30	452.1	2.2	1.90	4.66	.000066	.007580	0.57
5	1100	9.10	6.40	745.9	57.3	4.30	4.60	.000146	.004114	0.44
6	1150	16.90	11.90	497.7	3.6	7.20	5.45	.000243	.006433	0.64
		Total Gas Age = 520.5			J = 0.002203					
	Red River Anorthosite Suite metagabbro - (RB-91-030) hornblende									
1	750	2.20	0.40	4786.8	58.6	4.50	8.43	.000155	.000158	0.56
2	950	7.70	1.40	2206.5	32.6	5.50	24.89	.000187	.000865	1.79
3	1000	19.20	3.70	1179.9	8.6	6.40	18.81	.000217	.002227	1.56
4	1025	53.40	10.30	1106.4	5	4.10	15.59	.000139	.002489	1.32
5	1050	198.40	38.40	831.8	3.4	2.90	14.95	.000099	.003641	1.39
6	1065	14.50	2.80	583.2	10	15.20	14.25	.000516	.004879	1.54
7	1080	5.20	1.00	676.1	31	20.10	15.96	.000683	.003857	1.62
8	1100	9.00	1.70	662.3	11	14.70	15.67	.000499	.004223	1.60
9	1125	23.00	4.40	734.9	5	9.20	15.35	.000311	.003967	1.50
10	1150	38.00	7.30	815.3	4.4	5.20	15.24	.000177	.003644	1.43
11	1200	124.00	24.00	785.6	3.3	3.80	14.93	.000128	.003873	1.42
12	1300	16.10	3.10	734	11.2	19.50	15.82	.000661	.003521	1.55
13	1350	5.30	1.00	703.1	35	35.80	15.54	.001213	.002957	1.55
		Total Gas Age = 936.8			J = 0.002198					

Table A4.2 - Blair River Complex - Argon Isotopic Data

Step	°C	mV 39	% 39	AGE (Ma	(±)	% ATM	37/39	36/40	39/40	% IIC
	Calc-silicate in Otter Brook gneiss - (BVM-90-137) phlogopite									
1	550	2.00	0.00	246.9	50.1	60.70	0.08	.002055	.005946	0.01
2	600	13.80	0.40	138.4	3.6	35.30	0.06	.001196	.017997	0.01
3	650	24.70	0.70	290.8	2.9	16.10	0.03	.000547	.010644	0.00
4	750	77.50	2.40	432.4	2.1	5.60	0.00	.000189	.007740	0.00
5	800	84.00	2.60	426.4	2.4	10.50	0.00	.000355	.007455	0.00
6	850	205.50	6.50	418.4	1.9	3.10	0.00	.000106	.008242	0.00
7	900	216.30	6.90	423.2	1.8	0.90	0.00	.000033	.008317	0.00
8	950	265.00	8.40	425.1	1.8	0.80	0.00	.000028	.008287	0.00
9	1000	440.80	14.10	424	1.8	0.50	0.00	.000017	.008341	0.00
10	1050	766.80	24.50	420.8	1.8	0.40	0.00	.000013	.008421	0.00
11	1100	598.00	19.10	419.1	1.8	0.70	0.00	.000024	.008432	0.00
12	1150	387.90	12.40	419.6	1.8	1.50	0.01	.000052	.008349	0.00
13	1200	34.50	1.10	422.1	3.2	16.30	0.15	.000553	.007048	0.01
14	1300	5.10	0.10	627.7	33.9	61.90	1.42	.002095	.002032	0.15
		Total Gas Age = 419.7			J = 0.002222					
	Fox Back Ridge diorite/granodiorite - (BVM91-553) hornblende fraction 1									
1	750	36.50	6.40	376.4	5.3	31.10	1.86	.001054	.006554	0.25
2	950	152.10	26.70	397.1	3.1	26.20	5.28	.000887	.006618	0.70
3	975	46.80	8.20	419.4	2.8	12.20	10.93	.000415	.007405	1.41
4	1025	104.90	18.40	415.7	2.2	8.50	9.17	.000288	.007798	1.19
5	1050	57.00	10.00	415.2	2.7	7.40	8.31	.000252	.007900	1.07
6	1075	36.00	6.30	404.6	3.1	10.90	8.09	.000371	.007821	1.06
7	1125	19.10	3.30	408.3	5.6	18.20	8.98	.000617	.007110	1.17
8	1175	39.40	6.90	422.1	3.6	18.60	9.18	.000630	.006820	1.18
9	1200	21.80	3.80	427.7	9	30.20	8.90	.001022	.005763	1.13
10	1225	8.60	1.50	424.3	6.8	25.60	9.26	.000869	.006192	1.18
11	1300	33.60	5.90	440.7	4.1	22.60	9.01	.000766	.006174	1.13
12	1350	8.60	1.50	517.2	19.1	53.90	9.27	.001825	.003064	1.07
13	1400	4.00	0.70	1494.7	114	40.70	8.14	.001379	.001014	0.63
		Total Gas Age = 422.2			J = 0.002210					

Table A4.2 - Blair River Complex - Argon Isotopic Data

Step	°C	mV 39	% 39	AGE (Ma	(±)	% ATM	37/39	36/40	39/40	% IIC
	Fox Back Ridge diorite/granodiorite - (BVM91-553) hornblende fraction 2									
1	600	4.10	0.50	7950.6	4880	2.00	2.24	.000069	.000026	0.14
2	650	5.80	0.80	329.1	34.3	66.50	3.60	.002252	.003713	0.53
3	720	11.80	1.60	378.6	10.4	39.90	3.32	.001352	.005714	0.45
4	760	12.70	1.70	389.6	10.8	38.40	1.30	.001300	.005677	0.17
5	800	11.80	1.60	379.5	9.7	44.40	0.95	.001503	.005275	0.13
6	840	15.10	2.10	390.6	9.8	38.60	0.84	.001309	.005636	0.13
7	880	22.10	3.10	418.8	10.8	52.80	0.94	.001789	.004007	0.11
8	920	24.70	3.40	394.4	8	48.60	1.66	.001646	.004670	0.12
9	950	18.60	2.60	388.6	5	27.60	3.82	.000934	.006692	0.22
10	970	8.20	1.10	412.1	18.2	31.90	7.88	.001082	.005888	0.51
11	990	16.40	2.30	433.3	4.8	26.70	12.90	.000904	.005998	1.03
12	1010	22.70	3.10	435.8	4.6	19.70	13.64	.000668	.006527	1.72
13	1030	52.70	7.40	435.1	2.7	14.20	11.85	.000481	.006987	1.50
14	1050	73.50	10.30	426.3	2.4	11.80	10.24	.000399	.007352	1.31
15	1070	101.30	14.20	417.3	2.1	9.00	9.50	.000307	.007764	1.23
16	1090	78.20	11.00	422.9	2.1	7.60	8.90	.000259	.007769	1.14
17	1110	43.60	6.10	406.8	2.5	11.10	9.08	.000376	.007809	1.19
18	1130	14.70	2.00	411.6	5.3	17.50	9.65	.000592	.007151	1.26
19	1180	28.50	4.00	423.7	4.2	17.90	10.29	.000606	.006889	1.32
20	1250	63.00	8.80	429	3	19.70	9.59	.000669	.006641	1.22
21	1300	32.00	4.50	426.3	3.9	22.80	9.48	.000775	.006428	1.21
22	1350	38.10	5.30	427.8	3.7	25.20	10.37	.000854	.006208	1.32
23	1400	10.20	1.40	432.9	12.5	43.90	9.49	.001489	.004588	1.20

Total Gas Age = 987.0 J = 0.002223

Step	°C	mV 39	% 39	AGE (Ma	(±)	% ATM	37/39	36/40	39/40	% IIC
	Sheared amphibolite in Wilkie Brook Shear Zone - (CW86-3708) hornblende									
1	750	3.80	5.00	364.1	30.2	48.00	15.89	.001627	.005091	2.21
2	950	9.30	12.20	393.2	10.7	20.60	12.97	.000699	.007146	1.72
3	1000	7.80	10.30	418.9	12.5	21.60	17.44	.000733	.006573	2.24
4	1050	20.70	27.10	372.5	4.4	13.90	19.67	.000471	.008233	2.70
5	1100	5.50	7.30	460.3	19.4	28.90	20.58	.000981	.005358	2.51
6	1150	4.40	5.80	357.7	27.7	40.10	21.72	.001358	.005987	3.05
7	1200	4.90	6.50	412.9	19.4	35.80	22.43	.001214	.005469	2.90
8	1250	3.60	4.70	472.9	34.7	46.40	21.74	.001570	.003922	2.62
9	1300	6.60	8.70	367.3	13.9	51.60	21.36	.001748	.004695	2.96
10	1350	3.60	4.80	625.2	122	58.70	20.37	.001987	.002185	2.14
11	1450	5.40	7.10	640.9	60.9	65.30	18.59	.002212	.001781	1.93

Total Gas Age = 425.4 J = 0.002194

Table A4.2 - Blair River Complex - Argon Isotopic Data

Step	°C	mV 39	% 39	AGE (Ma	(±)	% ATM	37/39	36/40	39/40	% IIC
	Amphibolite in undivided unit - (SB85-1081) hornblende									
1	750	12.60	4.30	641.6	9.9	19.60	1.43	.000664	.004147	0.14
2	950	11.60	4.00	634.3	10.6	20.10	8.87	.000683	.004175	0.92
3	1000	31.70	10.90	651.4	5.1	7.30	15.31	.000247	.004698	1.58
4	1025	52.10	18.00	559.3	2.8	4.80	13.73	.000163	.005772	1.52
5	1050	58.50	20.20	524.6	2.9	4.00	12.65	.000136	.006269	1.44
6	1075	48.10	16.60	498.1	2.7	3.80	11.74	.000129	.006667	1.38
7	1125	24.80	8.50	488.6	3.9	4.90	11.24	.000167	.006737	1.33
8	1175	21.40	7.40	508.6	4.2	7.30	11.50	.000247	.006272	1.33
9	1225	18.30	6.30	516.8	4.9	9.10	12.40	.000310	.006036	1.43
10	1275	9.60	3.30	550.4	8.3	14.00	13.68	.000475	.005310	1.53
		Total Gas Age = 546.8			J = 0.002205					
	Metagabbro in undivided unit - (RR85-2105) hornblende									
1	750	6.20	2.60	1097.4	34.7	46.20	10.62	.001566	.001423	0.90
2	950	38.90	16.60	560.9	4.3	20.00	21.04	.000678	.004864	2.33
3	1000	32.20	13.80	584.8	4	13.90	23.91	.000471	.004986	2.60
4	1050	56.40	24.20	502	2.9	10.00	20.26	.000342	.006216	2.37
5	1075	8.30	3.50	503.3	11.4	19.80	21.99	.000673	.005522	2.58
6	1100	5.50	2.40	503.5	19.5	21.00	21.90	.000712	.005439	2.56
7	1125	6.40	2.70	520.4	15.2	23.50	20.12	.000796	.005073	2.32
8	1150	6.20	2.60	628.7	12.5	26.80	21.92	.000907	.003893	2.31
9	1200	11.00	4.70	687	17.4	15.90	20.86	.000538	.004024	2.11
10	1250	18.80	8.10	601.9	6	19.20	20.33	.000652	.004521	2.18
11	1300	17.30	7.40	607.4	6.2	20.40	22.49	.000691	.004409	2.40
12	1350	19.10	8.20	611.7	7.2	26.80	22.47	.000909	.004019	2.39
13	1375	6.00	2.50	5206.2	1184	4.00	21.68	.000138	.000125	1.43
		Total Gas Age = 1070.4			J = 0.002219					

Table A4.2 - Blair River Complex - Argon Isotopic Data

Step	°C	mV 39	% 39	AGE (Ma	(±)	% ATM	37/39	36/40	39/40	% IIC
	Meat Cove Marble - (BVM90-007) muscovite Fraction 1									
1	650	6.30	0.30	270.6	5.1	6.30	0.23	.000213	.012897	0.04
2	750	15.30	0.70	466.1	5.1	5.20	0.87	.000176	.007164	0.10
3	800	17.80	0.80	456.4	3.2	1.90	0.30	.000065	.007591	0.03
4	850	50.40	2.40	442.1	2.4	1.20	0.07	.000043	.007922	0.00
5	875	51.90	2.40	440.6	2.3	1.10	0.02	.000037	.007966	0.00
6	900	61.10	2.90	440.9	2.1	0.80	0.01	.000029	.007979	0.00
7	925	56.60	2.70	435.4	2.3	0.90	0.01	.000030	.008089	0.00
8	950	0.80	0.00	4565.8	2173	1.10	0.42	.000039	.000190	0.02
9	975	150.10	7.10	427.1	2	0.60	0.01	.000023	.008284	0.00
10	1000	130.90	6.20	429.3	2	0.60	0.00	.000023	.008236	0.00
11	1025	150.50	7.20	427.4	1	0.70	0.00	.000024	.008273	0.00
12	1050	149.60	7.10	428	1.9	0.70	0.01	.000026	.008257	0.00
13	1075	142.30	6.80	429.9	1	0.70	0.01	.000027	.008214	0.00
14	1100	202.50	9.60	427.1	1	1.00	0.01	.000034	.008257	0.00
15	1125	196.30	9.30	429	1.9	1.40	0.01	.000047	.008183	0.00
16	1150	191.00	9.10	433.5	1	1.10	0.02	.000037	.008113	0.00
17	1200	159.80	7.60	436.3	1	1.60	0.03	.000056	.008007	0.00
18	1250	239.20	11.40	437.7	1	1.70	0.07	.000058	.007974	0.00
19	1300	102.90	4.90	444.5	2	4.20	0.15	.000142	.007639	0.01
20	1350	13.10	0.60	469.8	9	37.50	0.11	.001269	.004682	0.01
		Total Gas Age = 439			J = 0.002229					
	Meat Cove Marble - (BVM90-007) muscovite fraction 2									
1	650	3.80	0.30	91.6	25.5	73.50	0.22	.002489	.011267	0.08
2	750	7.80	0.70	390.5	15	21.00	0.35	.000713	.007253	0.04
3	800	13.40	1.20	468.7	6	7.30	0.71	.000247	.006938	0.08
4	850	19.00	1.70	439	3.3	5.30	0.18	.000179	.007634	0.02
5	870	16.60	1.50	436.3	6	10.80	0.04	.000367	.007238	0.00
6	900	30.30	2.70	434.2	3	3.70	0.02	.000126	.007857	0.00
7	925	44.20	4.00	435.4	2	2.60	0.01	.000091	.007918	0.00
8	945	24.80	2.20	441.3	3	3.10	0.01	.000105	.007765	0.00
9	970	39.80	3.60	434.5	2	2.60	0.01	.000090	.007938	0.00
10	995	44.70	4.10	433.4	2	2.40	0.00	.000083	.007978	0.00
11	1015	36.30	3.30	436.4	2	2.70	0.00	.000094	.007891	0.00
12	1035	48.90	4.40	436.2	2	2.70	0.00	.000093	.007897	0.00
13	1060	49.30	4.50	432.2	2	2.40	0.00	.000082	.008005	0.00
14	1090	74.40	6.80	432.2	2	2.30	0.00	.000077	.008016	0.00
15	1150	89.50	8.20	421.9	2	5.60	0.01	.000190	.007956	0.00
16	1180	136.00	12.50	427.4	2	5.30	0.01	.000181	.007864	0.00
17	1210	130.00	11.90	427.2	2	5.80	0.01	.000196	.007830	0.00
18	1250	124.00	11.40	428	2.1	7.10	0.03	.000242	.007701	0.00
19	1300	121.00	11.20	430.5	2	10.40	0.07	.000354	.007378	0.00
20	1350	23.20	2.10	451.2	6	42.90	0.23	.001453	.004460	0.02
21	1400	7.00	0.60	499.6	30	68.10	0.08	.002306	.002216	0.00
		Total Gas Age = 430.4			J = 0.002222					

Table A4.2 - Blair River Complex - Argon Isotopic Data

Step	°C	mV 39	% 39	AGE (Ma	(±)	% ATM	37/39	36/40	39/40	% IIC
	Marble in Wilkie Brook Fault Zone - (BVM91-635) phlogopite									
1	650	35.20	2.00	84.6	1	34.90	0.94	.001184	.030099	0.39
2	750	25.70	1.40	454.4	4.4	7.90	0.22	.000268	.007151	0.02
3	800	21.70	1.20	575.5	3.4	3.90	0.09	.000134	.005687	0.01
4	850	43.00	2.40	540.2	3	2.70	0.05	.000092	.006200	0.00
5	875	48.80	2.80	536.7	2.6	1.90	0.01	.000064	.006299	0.00
6	900	62.30	3.50	533.9	2.5	1.30	0.00	.000044	.006375	0.00
7	925	76.30	4.40	526.7	2.5	0.90	0.00	.000033	.006498	0.00
8	950	84.40	4.80	523.3	2.5	0.90	0.00	.000032	.006548	0.00
9	975	91.60	5.20	523.8	2.3	0.80	0.00	.000030	.006546	0.00
10	1000	112.00	6.50	519.2	2.2	0.80	0.00	.000029	.006615	0.00
11	1050	162.00	9.30	522.3	2.3	2.10	0.00	.000071	.006486	0.00
12	1100	380.00	21.90	520.6	2.2	0.60	0.00	.000023	.006605	0.00
13	1150	78.90	4.50	517.9	2.5	2.30	0.00	.000078	.006537	0.00
14	1200	256.00	14.70	500.1	2.1	1.90	0.01	.000064	.006833	0.00
15	1250	53.00	3.00	486	2.7	7.90	0.02	.000267	.006628	0.00
16	1350	5.40	0.30	572.5	33	55.50	0.35	.001878	.002651	0.03

Total Gas Age = 503 J = 0.002226

Error estimates at 1-sigma level
37/39, 36/40, and 39/40 Ar ratios are corrected
for interfering isotopes
% IIC = Interfering isotopes correction

Steps in brackets are those from which age data are derived as shown on figures and discussed in text

Appendix to Chapter 5

A5.1 Microprobe analytical methods

Minerals were analyzed on a JEOL 733 electron microprobe equipped with four wavelength dispersive spectrometers and an Oxford Link eXL energy dispersive system; all element analyses used the latter system. Resolution of the energy dispersive detector is 137eV at 5.9 KeV. Acquisition of each spectrum lasted 40 seconds with an accelerating voltage of 15 Kv and a beam current of 15nA. Probe spot size is approximately 1μm. Raw data are corrected by the Link ZAF matrix correction program. Cobalt metal was used for instrument calibration. Instrument precision on cobalt metal (x=10) was ±0.5% at 1σ. Accuracy for major elements was ±1.5 to 2.0% relative (R. MacKay, written comm). The following standard minerals were used as controls: 12442 garnet (Si,Al,Fe), sanadine (Si, Al, K), KK amphibole (Ca, Mg, Ti), and jadeite (Na). Mineral compositions used in geothermobarometry are presented in Tables A5.2.1 to A5.2.5. The complete set of microprobe data are available on diskette from the author or from the Department of Earth Sciences, Dalhousie University.

A5.2 Anion normalization, cation-site distribution, and Fe^{3+} recalculation

Biotite

For the purposes of biotite classification and discrimination diagrams, microprobe data are recalculated to total cations based on 22 oxygen and all iron is assumed to be Fe^{2+}. All biotite and phlogopite compositions are displayed in Figure A5.1 and the data used in thermobarometry in Chapter 5 are presented in Table A5.2.1. Although the total Fe^{3+} content and the extent of its substitution into tetrahedral sites may significantly alter the activity of end-member phases, many

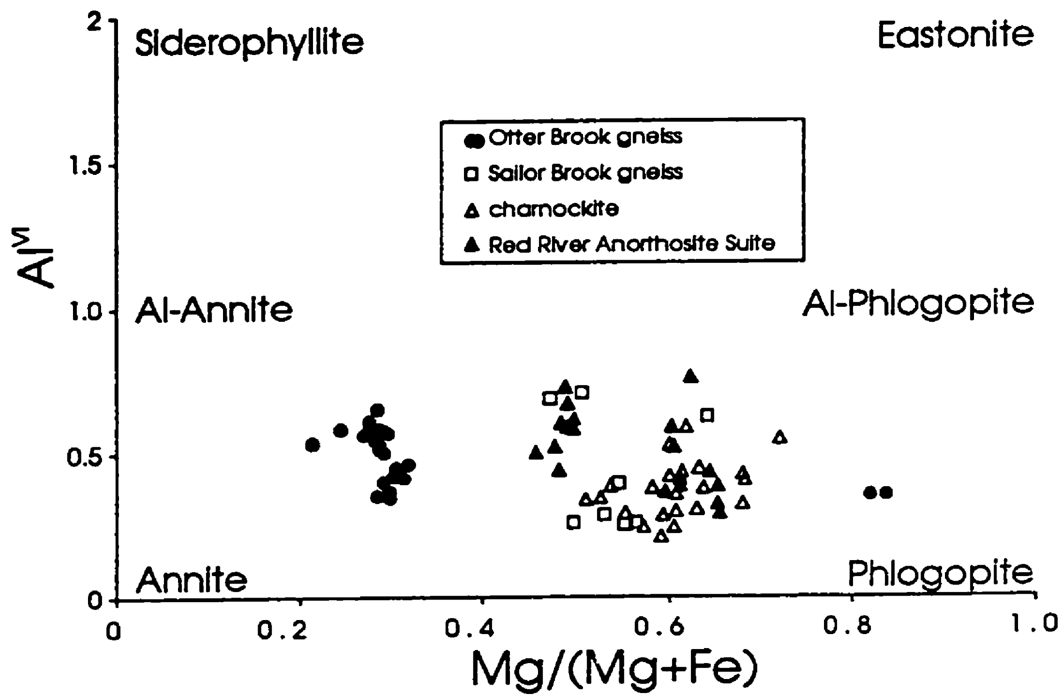

Figure A5.1 - Biotite and phlogopite compositions plotted on the "ideal biotite plane" of Guidotti (1984).

Table A5.2.1 - Biotite compositions used in TWQ analysis and in conventional thermobarometers

Sample	BVM90-057	BVM90-144	BVM91-584	BVM91-584	BVM91-584	BVM91-714	BVM91-714	BVM91-717	BVM91-739	BVM91-739
TWQ Fig.	Fig 5.13d	Fig 5.13a	Fig 5.7a	Fig 5.7b	Fig 5.7c	Fig 5.17a	Fig 5.17b	Fig 5.17c	Fig 5.13b	Fig 5.13c
Avg. of	2	3	3	2	3	3	2	1	3	3
SiO2	36.92	37.28	36.58	36.52	36.35	36.35	33.84	33.66	35.13	35.13
TiO2	2.87	3.82	2.92	3.63	2.74	2.74	3.63	4.41	4.41	4.41
Al2O3	15.05	13.96	15.78	15.59	15.85	15.85	14.38	14.26	14.64	14.64
FeO	15.18	18.05	14.93	14.91	15.23	15.23	25.68	25.55	16.06	16.06
MnO	0.09	0.07	0.14	0.13	0.14	0.14	0.49	0.33	0.10	0.10
MgO	14.84	13.09	15.47	15.80	15.67	15.67	6.02	6.56	12.75	12.75
CaO			0.03	0.09	0.03	0.03	0.07	0.06	0.07	0.07
Na2O	0.38	0.41	0.29	0.36	0.29	0.29	0.33	0.20	0.26	0.26
K2O	8.70	9.51	9.05	8.86	8.80	8.80	8.98	8.58	8.72	8.72
Cations per 0= 22										
Si	5.579	5.613	5.468	5.418	5.441	5.441	5.492	5.432	5.474	5.474
Ti	0.326	0.433	0.328	0.405	0.308	0.308	0.443	0.535	0.516	0.516
Al [iv]	2.421	2.387	2.532	2.582	2.559	2.559	2.508	2.568	2.526	2.526
Al [vi]	0.260	0.090	0.247	0.144	0.237	0.237	0.243	0.145	0.163	0.163
Fe	1.918	2.272	1.866	1.850	1.906	1.906	3.485	3.448	2.092	2.092
Mn	0.011	0.009	0.018	0.016	0.018	0.018	0.067	0.046	0.013	0.013
Mg	3.343	2.939	3.447	3.494	3.497	3.497	1.457	1.577	2.962	2.962
Ca	0.000	0.000	0.004	0.014	0.005	0.005	0.011	0.011	0.013	0.013
Na	0.112	0.119	0.085	0.104	0.083	0.083	0.105	0.063	0.078	0.078
K	1.678	1.827	1.725	1.677	1.680	1.680	1.859	1.766	1.734	1.734
total	15.650	15.689	15.719	15.705	15.734	15.734	15.671	15.591	15.571	15.571

studies evaluated thermodynamic properties for Fe-Mg exchange reactions assuming $Fe^{2+}=Fe_{tot}$ (e.g. McMulllin et al, 1991; Ferry and Spear, 1978; Dasgputa et al., 1991), an assumption necessary in order to simplify models and derivation techniques. For the purposes of TWQ, biotite cation-distribution and end-member models are calculated using the program CMP2.EXE, which recalculates microprobe data in accordance with McMullin et al. (1991) and assumes $Fe^{2+}=Fe_{tot}$.

Pyroxene

Pyroxene microprobe data are recalculated to total cations based on 6 oxygen. All data are plotted on the quadrilateal in Figure A5.2 and the data used in thermobarometry in Chapter 5 are presented in Table A5.2.2. For the purpose of TWQ, Fe^{2+}/Fe^{3+} cation-site distribution and end-member composition models were calculated using the program CMP2.EXE in which all Fe is Fe^{2+} in order to conform to the derivation of thermodynamic data (Berman, 1991). For the purposes of classification and discrimination diagrams, Fe^{2+}/Fe^{3+} in both clinopyroxene and orthopyroxene follows the charge-ballance recalculation procedure of Papike (1974), which follows from Kretz (1981) in which $Fe^{3+} = (Al^{[iv]}+ Na)-(Al^{[vi]}+2Ti+Cr)$. For clinopyroxene, Mg and Fe^{2+} are distributed between M-sites according to the relations:

$$Mg^{[M1]} = Mg_{rat}*(1-Al^{[vi]}-Ti-Fe^{3+})$$

$$Mg^{[M2]} = Mg_{rat}*(1-Ca-Mn-Na)$$

$$Fe^{[M1]} = (1-Mg_{rat})*(1-Al^{[vi]}-Ti-Fe^{3+})$$

$$Fe^{[M2]} = (1-Mg_{rat})* (1-Ca-Mn-Na)$$

Where : $Mg_{rat} = Mg/(Mg+Fe)$

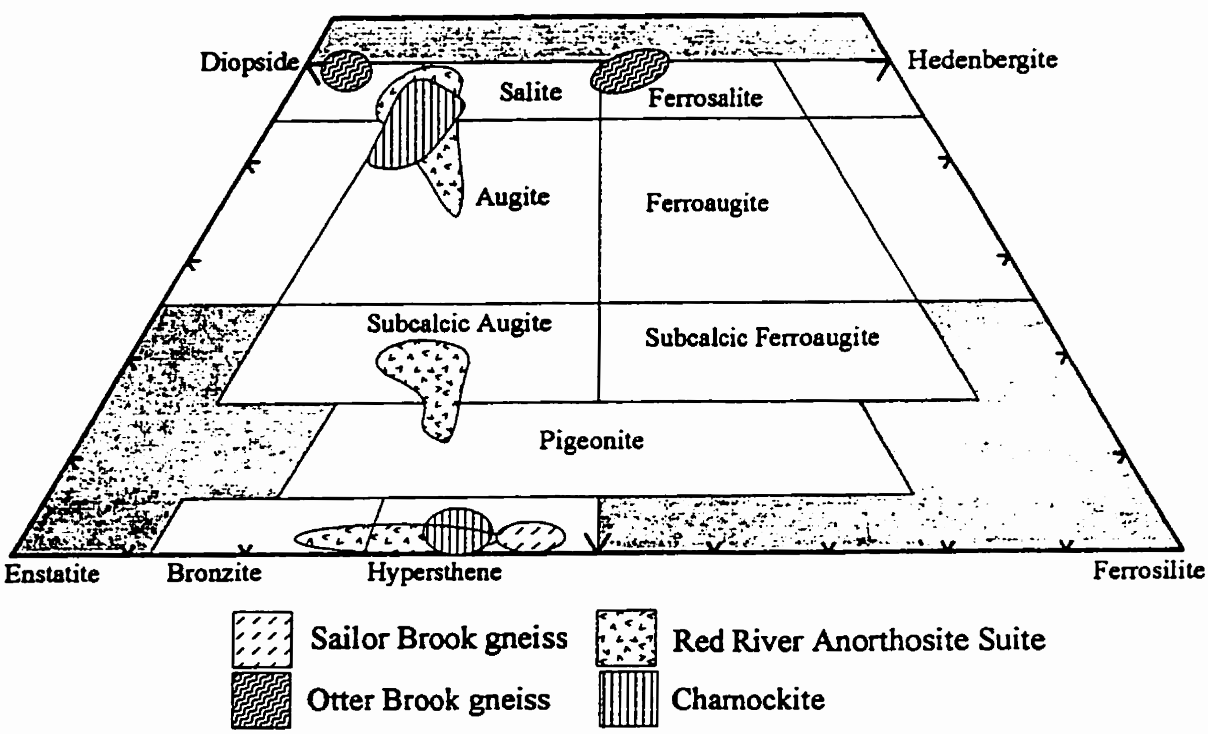

Figure A5.2 - Quadrilateral clinopyroxene compositions. Orthopyroxene composition are plotted on the clinoenstatite-clinoferrosilite join for convenience. Nomenclature after Poldervaart and Hess (1951), quadrilateral projection after Lindsely and Andersen (1983).

Table A5.2.2 - Pyroxene compositions used in TWQ analysis and in conventional thermobarometers

Sample	BVM90-057	BVM90-144	BVM90-144	BVM91-584	BVM91-584	BVM91-584	BVM91-584	BVM91-714	BVM91-714	BVM91-739	BVM91-739
TWQ Fig.	Fig 5.13d	Fig 5.13a	Fig 5.13a	Fig 5.7a	Fig 5.7b	Fig 5.7c	Fig 5.7c	Fig 5.17a	Fig 5.17b	Fig 5.13b	Fig 5.13c
Avg. of	4	2	2	3	4	3	4	4	4	3	7
SiO2	50.68	52.17	51.71	52.60	52.39	52.20	52.09	49.35	49.35	49.11	51.10
TiO2	0.12	0.22	0.12	0.07	0.11	0.34	0.08	0.09	0.09	0.79	0.15
Al2O3	1.29	1.49	0.71	1.42	1.68	2.50	2.15	0.90	0.90	5.42	2.32
FeO	23.86	9.56	25.22	21.55	22.23	8.57	21.81	17.52	17.52	9.52	9.70
MnO	0.52	0.19	0.40	0.34	0.41	0.19	0.35	1.10	1.10	0.46	0.43
MgO	21.10	13.69	20.83	23.80	22.98	14.05	23.44	6.75	6.75	12.21	13.39
CaO	0.40	22.44	0.56	0.28	0.34	20.74	0.37	22.67	22.67	21.98	21.68
Na2O	0.22	0.62	0.29	0.31	0.29	0.51	0.28	0.74	0.74	0.64	0.61
K2O	0.00		0.01	0.02	-0.01	0.12		0.00	0.00	0.00	0.02
Cations per 0= 6											
Si	1.945	1.950	1.961	1.945	1.943	1.953	1.926	1.960	1.960	1.845	1.931
Ti	0.003	0.006	0.003	0.002	0.003	0.010	0.002	0.003	0.003	0.022	0.004
Al [iv]	0.055	0.050	0.032	0.055	0.057	0.047	0.074	0.042	0.042	0.240	0.103
Al [vi]	0.004	0.016		0.007	0.017	0.063	0.020				
Fe	0.766	0.299	0.800	0.666	0.690	0.268	0.674	0.582	0.582	0.299	0.307
Mn	0.017	0.006	0.013	0.011	0.013	0.006	0.011	0.037	0.037	0.015	0.014
Mg	1.207	0.763	1.178	1.312	1.271	0.784	1.292	0.400	0.400	0.684	0.754
Ca	0.017	0.899	0.023	0.011	0.013	0.831	0.015	0.965	0.965	0.885	0.878
Na	0.017	0.045	0.021	0.022	0.021	0.037	0.020	0.057	0.057	0.046	0.044
K	0.000	0.000	0.001	0.001	-0.001	0.006	0.000	0.000	0.000	0.000	0.001
total	4.030	4.033	4.031	4.033	4.027	4.004	4.035	4.045	4.045	4.036	4.036
Fe [2+]	0.663	0.167	0.703	0.549	0.572	0.130	0.527	0.444	0.444	0.190	0.198
Fe [3+]	0.102	0.146	0.092	0.120	0.130	0.200	0.162	0.133	0.133	0.107	0.107

Fe [3+] = charge-balance with 4 cations and 6 oxygens.

For orthopyroxne, site distributions are calculated as in Newton (1983) and "ideal two-site mixing" activity-composition relations calculated as suggested by Berman (1991).

Garnet

Microprobe data from garnet are recalculated to total cations based on 12 oxygen. All data are plotted in terms of the major end-member components in Figure A5.3 and the data used in thermobarometry in Chapter 5 are presented in Table A5.2.3. For the purpose of TWQ, end-member proportions are computed with the program CMP2.EXE which considers all Fe as Fe^{2+} and calculates Prp-Alm-Grs-Sps end-members. The method (and BASIC computer program) described in Muhling and Griffin (1991) is used for classification and discrimination. Their method calculates all garnet end-members (except hydrogarnets) and estimates Fe^{3+} based on iterative calculations of site-occupancy constraints. For garnets in this study, the primary difference between the Muhling and Griffin (1991) and the CMP2.EXE methods is that the former allows for Fe^{3+} estimation and, therefore, definition of andradite and khorarite components (i.e., Fe^{3+} substitution for $Al^{[VI]}$ in grossular and pyrope respectively).

Although the andradite and khorarite components are generally very small (<1%), the total cation recalculation that they necessitate can significantly change the proportion of other end-members. For example, using the Muhling and Griffin (1991) method the pyrope component in sample BVM-714 goes to zero adjacent to biotite and hornblende, whereas the CMP2.EXE program calculates this component at about 5%. According to Deer et al. (1982) common garnets may contain up to 30 wt% Fe_2O_3, therefore, assuming all Fe as Fe^{2+} can lead to overestimation of

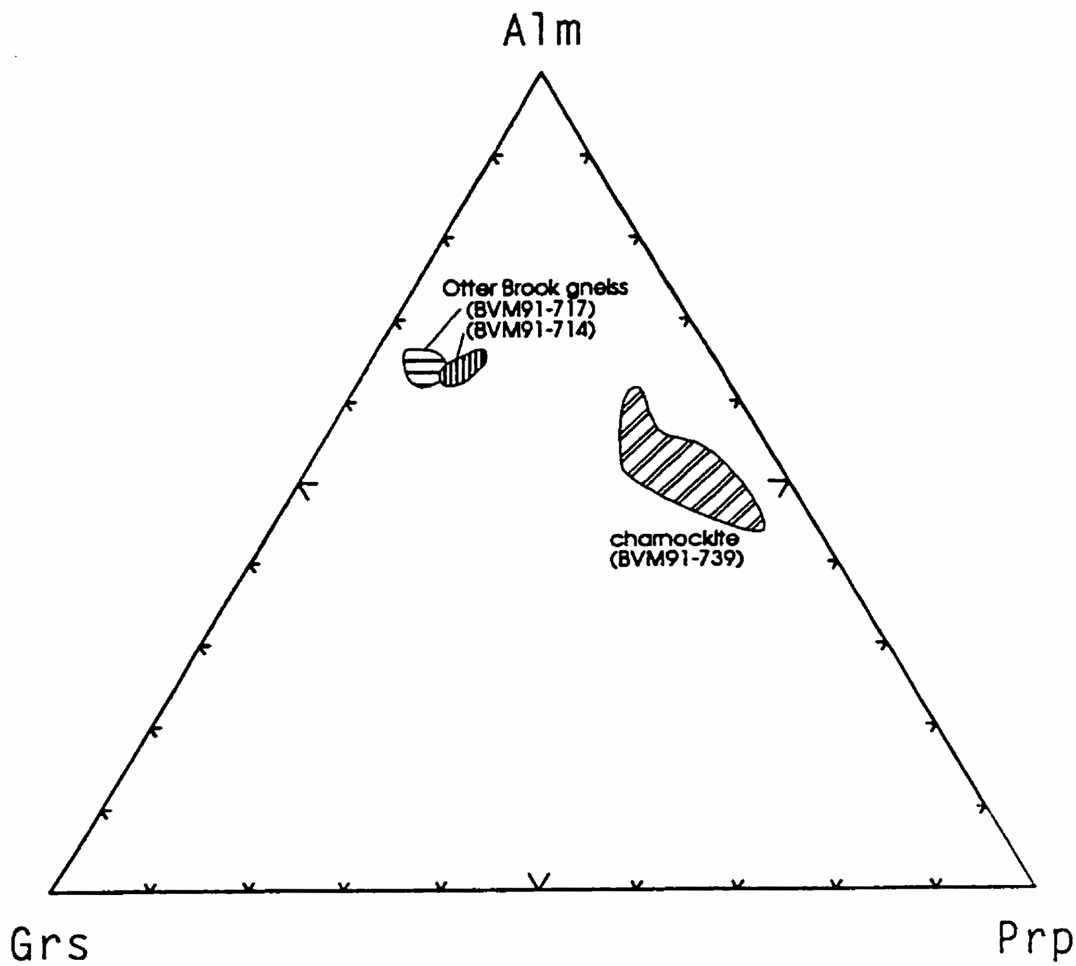

Figure A5.3 - Garnet compositions from the Otter Brook gneiss and charnockite.

Table A5.2.3 - Garnet compositions used in TWQ analysis and in conventional thermobarometers

Sample	BVM91-714	BVM91-714	BVM91-717	BVM91-739	BVM91-739
TWQ Fig.	Fig 5.17a	Fig 5.17b	Fig 5.17c	Fig 5.13b	Fig 5.13c
Avg. of	5	5	4	4	4
SiO2	37.60	37.60	36.36	38.59	38.59
TiO2	0.05	0.05	0.05	0.39	0.39
Al2O3	20.50	20.50	19.46	21.55	21.55
FeO	25.69	25.69	25.78	23.58	23.58
MnO	3.98	3.98	2.60	1.36	1.36
MgO	1.52	1.52	1.99	9.13	9.13
CaO	10.06	10.06	10.70	5.97	5.97
Na2O	0.20	0.20	0.15	0.21	0.21
K2O	0.00	0.00	-0.02	0.01	0.01
Cations per 0= 12					
Si	3.016	3.016	2.998	2.951	2.951
Ti	0.003	0.003	0.003	0.023	0.023
Al	1.938	1.938	1.891	1.942	1.942
Fe	1.723	1.723	1.777	1.508	1.508
Mn	0.270	0.270	0.182	0.088	0.088
Mg	0.182	0.182	0.245	1.040	1.040
Ca	0.864	0.864	0.945	0.489	0.489
Na	0.031	0.031	0.025	0.030	0.030
K	0.000	0.000	-0.002	0.001	0.001
total	8.028	8.028	8.064	8.072	8.072
Fe [2+]	1.634	1.634	1.574	1.284	1.284
Fe [3+]	0.083	0.083	0.191	0.213	0.213
Alm	0.567	0.567	0.564	0.482	0.482
Prp	0.060	0.060	0.078	0.333	0.333
Gr	0.284	0.284	0.300	0.157	0.157
Sps	0.089	0.089	0.058	0.028	0.028

Fe [3+] = charge-balance with 8 cations and 12 oxygens.

almandine end-member. Through total cation and site-occupancy constraints other end-member proportions may be affected as well.

Amphibole

For purposes of classification and discrimination diagrams, amphibole microprobe data are recalculated to cation-site distributions with the AMPHIBOL.EXE program of Richard and Clarke (1990) which follows the classification of Leake (1978). Amphibole data are presented in Figure A5.4 with cations normalized to a total of 13 exclusive of Ca, Na, and K ("13eCNK"), the charge-ballance restrictions of this cation normalization scheme apparently provide the most accurate Fe^{3+} recalculation when compared to complete chemical analyses (e.g., Cosca et al., 1991).

TWQ uses the Margules parameters of Mader et al. (1994) which were derived from amphiboles with the Fe3+ recalculation and cation distribution scheme described in Mader and Berman (1992). These authors provide a computer program (CMP2.EXE) which calculates formulae based on a modified version of "15eNK" normalization. The CMP2 program is used for the purpose of TWQ amphibole formulae in order to ensure consistency with the renormaliztion method from which thermodynamic properties were derived.

Feldspar

Feldspar microprobe data are recalculated to total cations based on 8 oxygen and end-members calculated based on proportions of Na-Ca-K for the purposes of classification, discrimination and thermobarometry (including TWQ). The compositions used in thermobarometric analyses are presented in Table A5.2.5.

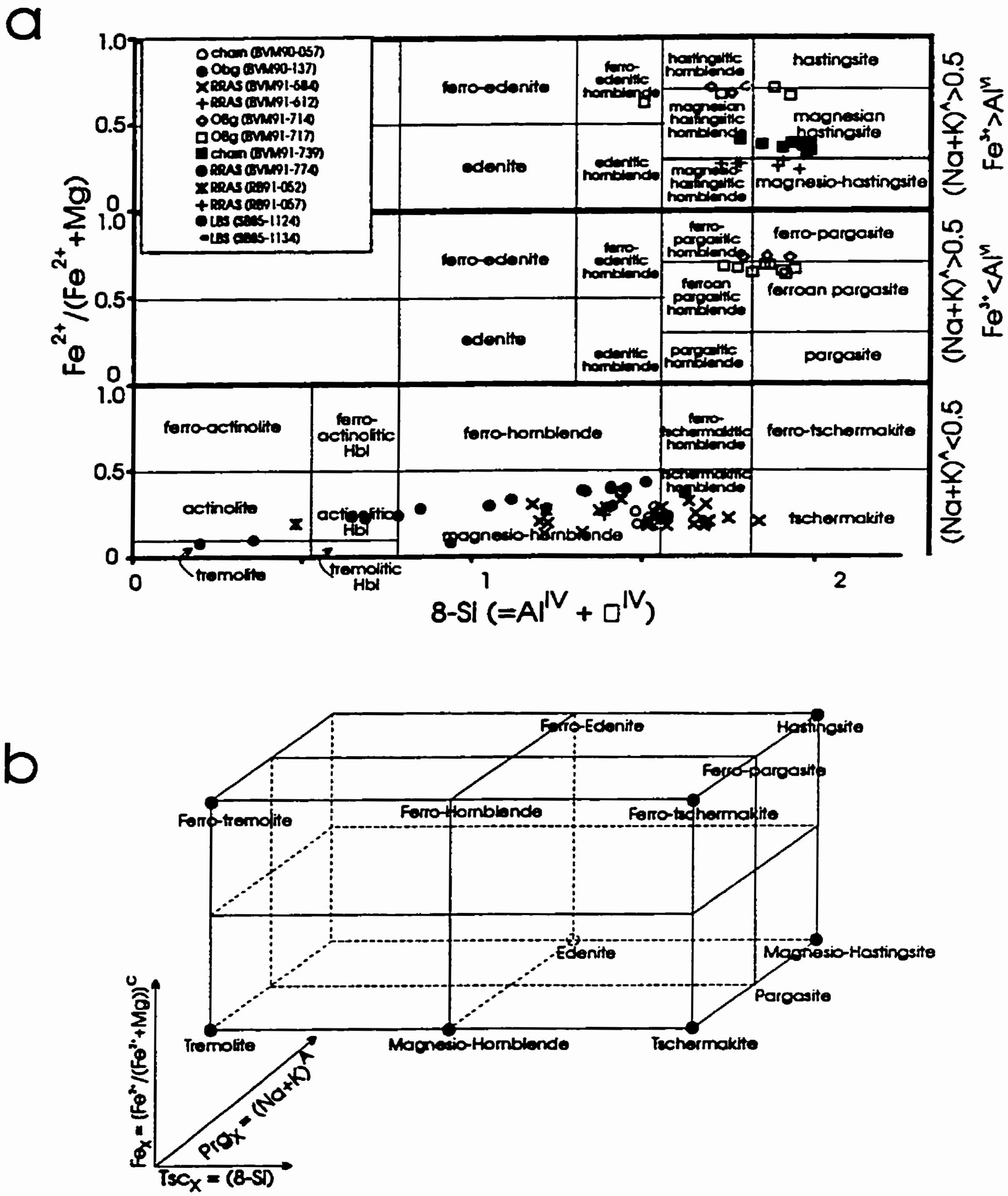

Figure A5.4 - (a) Amphibole classification and nomenclature modified after Hawthorne (1983) and Leake (1978). (b) Locations of end-members in quadrilateral planes which correspond to the three panels in (a).

Table A5.2.4 - Hornblende compositions used in TWQ analysis and in conventional thermobarometers

Sample	BVM90-057	BVM91-584	BVM91-584	BVM91-584	BVM91-714	BVM91-714	BVM91-717	BVM91-739	BVM91-739
TWQ Fig.	Fig 5.13d	Fig 5.7a	Fig 5.7b	Fig 5.7c	Fig 5.17a	Fig 5.17b	Fig 5.17c	Fig 5.13b	Fig 5.13c
Avg. of	3	2	2	6	4	2	3	2	4
SiO2	44.43	43.58	45.51	43.46	39.39	39.39	37.95	40.24	40.91
TiO2	0.94	1.65	1.07	1.25	1.49	1.49	1.12	2.51	1.87
Al2O3	10.36	12.02	10.03	11.90	11.45	11.45	12.27	12.57	12.50
FeO	14.47	12.59	13.15	12.50	24.09	24.09	22.30	14.66	15.84
MnO	0.11	0.12	0.14	0.01	0.72	0.72	0.43	0.21	0.26
MgO	13.09	13.75	13.36	13.60	4.88	4.88	5.33	11.16	10.49
CaO	11.21	11.68	12.48	11.60	11.25	11.25	11.70	11.67	11.67
Na2O	1.28	1.72	0.78	1.47	1.70	1.70	1.20	1.65	1.37
K2O	0.61	0.93	0.76	0.82	1.58	1.58	1.65	1.52	1.42
Cations per 0= 23									
Si	6.638	6.393	6.709	6.451	6.292	6.292	6.192	6.145	6.249
Ti	0.106	0.182	0.119	0.139	0.179	0.179	0.137	0.288	0.214
Al [iv]	1.362	1.607	1.291	1.549	1.708	1.708	1.808	1.855	1.751
Al [vi]	0.462	0.471	0.451	0.534	0.447	0.447	0.551	0.407	0.500
Fe	1.808	1.544	1.621	1.551	3.217	3.217	3.042	1.872	2.023
Mn	0.014	0.015	0.018	0.001	0.097	0.097	0.060	0.027	0.034
Mg	2.915	3.007	2.937	3.009	1.162	1.162	1.297	2.541	2.389
Ca	1.795	1.835	1.972	1.845	1.925	1.925	2.044	1.910	1.910
Na	0.372	0.490	0.222	0.423	0.526	0.526	0.379	0.489	0.406
K	0.116	0.174	0.143	0.154	0.322	0.322	0.342	0.295	0.277
total	15.588	15.718	15.483	15.657	15.876	15.876	15.852	15.828	15.753
Fe [2+]	0.955	0.905	1.011	0.849	2.819	2.819	2.216	1.394	1.463
Fe [3+]	0.852	0.639	0.609	0.702	0.398	0.398	0.826	0.478	0.560

Fe [3+] after Holland and Blundy (1994)

Table A5.2.5 - Plagioclase compositions used in TWQ analysis and in conventional thermobarometers

Sample	BVM90-057	BVM90-144	BVM91-584	BVM91-584	BVM91-584	BVM91-714	BVM91-717	BVM91-739	BVM91-739
TWQ Fig.	Fig 5.13d	Fig 5.13a	Fig 5.7a	Fig 5.7b	Fig 5.7c	Fig 5.17b	Fig 5.17c	Fig 5.13b	Fig 5.13c
Avg. of	3	5	4	3	3	4	5	5	6
SiO2	56.69	58.37	47.74	46.65	46.85	62.58	57.13	57.78	57.32
TiO2				0.03					0.09
Al2O3	27.16	23.77	33.32	34.86	34.79	22.85	25.95	26.89	27.18
FeO	0.39	0.78	0.25	0.24	0.26	0.23	0.12	0.08	0.08
MnO		0.01			0.04	0.00			
MgO		0.51		0.05	0.01	0.03		0.03	0.07
CaO	9.11	6.73	16.25	17.49	17.18	4.35	8.54	8.45	8.90
Na2O	6.31	6.99	2.45	1.75	1.85	8.43	6.52	6.88	6.50
K2O	0.07	0.50	0.02	0.01	0.03	0.08	0.11	0.13	0.21
Cations per O= 8									
Si	2.553	2.676	2.190	2.124	2.133	2.802	2.600	2.582	2.563
Ti	0.000	0.000	0.000	0.001	0.000	0.000	0.000	0.000	0.003
Al	1.441	1.284	1.801	1.871	1.867	1.206	1.392	1.416	1.432
Fe	0.015	0.030	0.010	0.009	0.010	0.009	0.005	0.003	0.003
Mn	0.000	0.000	0.000	0.000	0.001	0.000	0.000	0.000	0.000
Mg	0.000	0.035	0.000	0.003	0.001	0.002	0.000	0.002	0.005
Ca	0.439	0.331	0.799	0.853	0.838	0.209	0.416	0.405	0.426
Na	0.551	0.621	0.218	0.154	0.163	0.732	0.575	0.596	0.563
K	0.004	0.029	0.001	0.001	0.002	0.005	0.006	0.007	0.012
total	5.003	5.007	5.018	5.017	5.015	4.964	4.995	5.011	5.006
An	0.442	0.337	0.785	0.846	0.836	0.221	0.417	0.402	0.426
Ab	0.554	0.633	0.214	0.153	0.163	0.774	0.576	0.591	0.562
Or	0.004	0.030	0.001	0.001	0.002	0.005	0.006	0.007	0.012

A5.3 Reactions in TWQ analyses

The reactions labelled with letters in TWQ diagrams (Figures 5.7, 5.13, 5.17) are listed below:

Figure 5.7a,b

a) 3Tr+5FeTs=5Tsc+3FeTr
b) 5FePa+4Tr=4FeTr+5Parg
c) Phl+FeTs=Tsc+Ann
d) 5Ann+3Tr=3FeTr+5Phl
e) 3Parg+4Ann=4Phl+3FePa
f) 4FeTs+3Parg=3FePa+4Tsc

Figure 5.7c

a) 4Ab+16Di+15En+10FeTs=4Parg+6Tr+15Fsl+16An
b) 2FeTs+3En=3Fsl+2Tsc
c) 2Fsl+parg=FePa+2En
d) 2Hd+En=2Di+Fsl
e) 5Tsc+4Fsl+8Di+2Ab=8An+4En+3Tr+2FePa
f) 2Ab+8Di+5Tsc=2Parg+3Tr+8An
g) 8FeTs+7Tsc+24Di+6Ab=24An+9Tr+6FePa
h) 7Parg+20FeTs+32Di+8Ab=32An+12Tr+15FePa
i) 4Ab+16Di+7En+10FeTs=4FePa+6Tr+7Fsl+16An

Figure 5.13a

a) 3Di+Ann=3Hd+Phl
b) 2Hd+En=2Di+Fsl

Figure 5.13b,c

a) 2Alm+4Gr+3Tr=3Tsc+6Hd+6Di
b) 3Ab+10Gr+12Hd+5Py+3Tr=3FePa+30Di+12An
c) Tsc+Py+4Hd+2Gr+Ab=4An+6Di+FePa
d) 3Tr+Py+10Gr+4Alm+3Ab=12An+18Di+3FePa
e) 3Ab+5Alm+10Gr+3Tr=3FePa+3Hd+15Di+12An
f) 3Tsc+3Tr+16Gr+8Alm+6Ab=24An+24Di+6FePa
g) Tsc+Hd+2Gr+Alm+Ab=4An+3Di+FePa
h) 3Ab+10Alm+10Gr+3Tr=3FePa+5Py+18Hd+12An
I) 3Tsc+6Gr+4Alm+3Ab=12An+6Di+Py+3FePa
j) 5Tsc+8Hd+2Ab=8An+3Tr+2FePa
k) 4Alm+4Gr+3Tr=3Tsc+2Py+12Hd
l) Tsc+2Gr+2Alm+Ab=4An+2Hd+Py+FePa
m) 15Tsc+24Di+8Alm+6Ab=24An+8Py+9Tr+6FePa
n) Alm+3Di=Py+3Hd
o) 4Gr+2Py+3Tr=3Tsc+12Di

Figure 5.13d

a) 4Tr+5FePa=5Parg+4FeTr
b) Phl+FeTs=Tsc+Ann

c) 3Parg+4Ann=4Phl+3FePa
d) 5Ann+3Tr=3FeTr+5Phl
e) 2FeTs+3En=3Fsl+2Tsc
f) Parg+2Fsl=2En+FePa
g) 5Fsl+2Tr=2FeTr+5En
h) 3En+2Ann=3Fsl+2Phl
i) 3Parg+4FeTs=4Tsc+3FePa

Figure 5.17a

a) 3Hd+Phl=3Di+Ann
b) Alm+3Di=Py+3Hd
c) Phl+Alm=Ann+Py
d) 4Alm+3Parg=3FePa+4Py
e) Parg+4Hd=4Di+FePa

Figure 5.17b

a) 3Tr+5Py+10Gr+3Ab=12An+18Di+3Parg
b) 15Tsc+8Py+24Hd+6Ab=8Alm+24An+9Tr+6Parg
c) 2Alm+4Gr+3Tr=3Tsc+6Hd+6Di
d) Tsc+2Gr+Di+Alm+Ab=4An+3Hd+Parg
e) 3Tsc+3Tr+16Gr+8Alm+6Ab=24An+24Hd+6Parg
f) 3Tr+10Gr+5Alm+3Ab=12An+3Di+15Hd+3Parg
g) 9Tsc+4Py+8Gr+6Ab=24An+3Tr+6Parg
h) Tsc+Py+2Gr+Ab=4An+2Di+Parg
i) 3Tsc+Py+6Gr+2Alm+3Ab=12An+6Hd+3Parg
j) 3Tr+10Gr+6Alm+3Ab=12An+18Hd+Py+3Parg
m) 3Tr+5Alm=3FeTr+5Prp
n) Alm+3Di=Py+3Hd
o) 4Alm+4Gr+3Tr=3Tsc+2Py+12Hd
p) 5Tsc+8Di+2Ab=8An+3Tr+2Parg
q) 4Gr+2Py+3Tr=3Tsc+12Di

Figure 5.17b

a) 3Ab+2Gr+4Py+3FeTs=3Parg+6bQz+6An+3Alm
b) 3Ab+Alm+2Gr+4Tsc=3Parg+FeTs+6bQz+6An
c) 3Ab+2Gr+Py+3Tsc=3Parg+6bQz+6An
d) 12Ab+4Alm+8Gr+12Tsc=3FePa+9Parg+24bQz+24An
e) 3Ab+Alm+2Gr+3FeTs=3FePa+6bQz+6An
f) 12Ab+8Gr+4Py+12FeTs=9FePa+3Parg+24bQz+24An
g) 3Ab+2Gr+Py+4FeTs=3FePa+Tsc+6bQz+6An
h) 3Tsc+2Gr+4Alm+3Ab=6An+3Py+6bQz+3FePa
j) Alm+Tsc=FeTs+Py
k) 3Tr+5Alm=3FeTr+5Prp
l) 3Parg+4Alm=4Py+3FePa
m) 4FeTs+3Parg=3FePa+4Tsc

REFERENCES

Alexander, E.C., Michelson, G.M., and Lanphere, M.A., 1978, Mmhb-1: a new $^{40}Ar/^{39}Ar$ dating standard, in Short Paper, 4th International Conference on geochronology, cosmochronlogy, and isotope geology, U.S. Geological Survey Open File Report 78-701, 6-8.

Anderson, A.T., 1968, Massif-type anorthosite: a widespread Precambrian igneous rock, *in* Y.W. Isachensen (ed.), Origin of anorthosite and related rocks, 47-55, New York State Museum and Science Service, Memoir 18, Albany, New York.

Anovitz, L.M., and Essene, E.J., 1989, Phase equilibria in the system $CaCO^3$-$MgCO^3$-$FeCO^3$, Journal of Petrology, **28**, 389-414.

Apted, M.J., and Liou, J.G., 1983, Phase relations among greenschist, epidote amphibolite and amphibolite in a basaltic system, American Journal Science, **283a**, 328-354.

Ashwal, L.D., 1978, Petrogenesis of massif-type anorthosites: crystallization history and liquid line of descent of the Adirondack and Morin complexes, PhD dissertation, Princeton Univ.

Ashwal, L.D., 1993, Anorthosites, Springer-Verlag, Berlin, 422 p.

Ashwal, L.D., and Seifert, K., 1980, Rare earth element geochemistry of anorthosite and related rocks from the Adirondacks, New York, and other massif complexes, Geological Society of America Bulletin, **91**, 659-684.

Atkin, B.P., and Brewer, T.S., 1990, The tectonic setting of basaltic magmatism in the Kongsberg, Bamble and Telemark sectors, southern Norway, *in* Gower, C.F., Rivers, T., and Ryan, B. (eds.), Middle-Proterozoic Laurentia-Baltica, Geological Association of Canada Paper 38, 471-484.

Ayuso, R.A., and Barr, S.M., 1991, Lead isotopic compositions of feldspars from plutonic rocks of Cape Breton Island, Nova Scotia: Implications for sources and terranes, Geological Association of Canada-Mineralogical Association of Canada, Program with Abstracts, **16**, A5.

Ayuso, R.A., and Barr, S.M., 1993, Lead isotopic compositions of plutonic rocks in Cape Breton Island, Nova Scotia: Implications for petrogenesis and terrane correlation, Geological Society of America, Northeastern Section Meeting, Abstracts with Programs, **25**, 3.

Ayuso, R.A., Barr, S.M., and Longstaffe, F.J., 1996, Pb and O isotopic constraints on the source of granitic rocks from Cape Breton Island, Nova Scotia, American Journal Science, **296**, 789-817.

Barr, S.M., and Hegner, E., 1992, Nd isotopic compositions of felsic igneous rocks in Cape Breton Island, Nova Scotia, Canadian Journal of Earth Sciences, **29**, 650-657.

Barr, S.M., and Jamieson, R.A., 1991, Tectonic setting and regional correlation of Ordovician-Silurian rocks of the Aspy terrane, Cape Breton Island, Nova Scotia, Canadian Journal of Earth Sciences, **28**, 1769-1779.

Barr, S.M., and Raeside, R.P., 1986, Pre-Carboniferous tectonostratigraphic subdivisions of Cape Breton Island, Nova Scotia, Maritime Sediments and Atlantic Geology, **22**, 252-263.

Barr, S.M., and Raeside, R.P., 1989, Tectonostratigraphic terranes in Cape Breton Island, Nova Scotia: Implications for the configuration of the northern Appalachian Orogen, Geology, **17**, 822-825.

Barr, S.M., and Raeside, R.P., 1990, Comment and Reply on "Tectonostratigraphic terranes in Cape Breton Island, Nova Scotia: Implications for the configuration of the northern Appalachian orogen", Geology, **18**, 669-671.

Barr, S.M., Raeside, R.P., White, C.W., and Yaowanoiyothin, W., 1987a, Geology of the northeastern and central Cape Breton Highlands, Nova Scotia, Current Research, Part A, Geological Survey of Canada, Paper 87-1A, 199-207.

Barr, S.M., Raeside, R.P., and van Breemen, O., 1987b, Grenvillian basement in the northern Cape Breton Highlands, Nova Scotia, Canadian Journal of Earth Sciences, **24**, 992-997.

Barr, S.M., Mcdonald, A.S., Arnott, A.M., and Dunning, G.R., 1995a, Field relations, structure, and geochemistry of the Fisset Brook Formation in the Lake Ainslie-Gilanders Mt. area, central Cape Breton Island, Nova Scotia, Atlantic Geology, **31**, 127-139.

Barr, S.M., Raeside, R.P., Miller, B.V., and White, C.E., 1995b, Terrane evolution and accretion in Cape Breton Island, Nova Scotia, *in* Hibbard, J.P., van Staal, C.R., and Cawood, P.A., eds., Current Perspectives in the Appalachian-Caledonian orogen, Geological Association of Canada, Special Paper 41, 391-407.

Bartholomew, M.J., 1983, Palinspastic reconstruction of the Grenville terrane in the Blue Ridge Province, southern and central Appalachians, U.S.A., Geological Journal, **18**, 241-253.

Bartholomew, M.J., 1984 (ed.) The Grenville event in the Appalachians and related topics, Geological Society of America Special Paper 194, 287 p.

Bartholomew, M.J., and Lewis, S.E., 1988, Peregrination of Grenvillian massifs and terranes within the Appalachian orogen, eastern U.S.A., *in* Martinez-Garcia, E. (ed.), Geology of the Iberian Massif with communications presented at the International Conference on Iberian terranes and their regional correlation, Trabajos de Geologia, University of Oviedo (Spain), 17, 155-165.

Bartholomew, M.J., and Lewis, S.E., 1992, Appalachian Grenville massifs: pre-Appalachian translational tectonics, in R. Mason (ed.), Basement Tectonics, International Basement Tectonics Association Publication no. 7, Kluwer Academic Press, 363-374.

Bekkers, R., 1993, Petrology and petrogenesis of the anorthosite and associated rocks in the Blair River Complex, Northern Cape Breton Island, Nova Scotia, M.Sc. thesis, Acadia Univ., Nova Scotia, Canada.

Benisek, A., and Finger, F., 1993, Factors controlling the development of prism faces in granite zircons: a microprobe study, Contributions to Mineralogy and Petrology, **114**, 441-451.

Berman, R.G., 1991, Thermobarometry using multi-equilibrium calculations: a new technique, with petrological applications, Canadian Mineralogist, **29**, 833-855.

Bevier, M.L., and Whalen, J.B., 1990, Tectonic significance of Silurian magmatism in the Canadian Appalachians, Geology, **18**, 411-414.

Bhattacharya, P.K., and Mukherjee, S., 1987, Granulites in and around the Bengal anorthosite, eastern India; genesis of coronal garente, and evolution of the granulite-anorthosite complex. Geological Magazine, **124**, 21-32.

Bohlen, S.R., 1987, Pressure-temperature-time paths and a tectonic model fro the evolution of granuites, Journal of Geology, **95**, 617-623.

Boyle, D.R., and Stirling, J.A.R., 1994, Geochemistry, mineralogy, and possible origin of the Coverdale Ti-P-ferrogabbro complex, New Brunswick, in Nineteenth Annual Review of Activities, edited by S. Merlini, New Brunswick Department of Natural Resources and Energy, Minerals and Energy Division, Miscellaneous Report 14, 4.

Bradley, D.C., 1983, Tectonics of the Acadian orogeny in New England and adjacent Canada, Journal of Geology, **91**, 381-400.

Bradley, D.C., and Bradley, L.M., 1984, Age and development of structural relief between basement and Carboniferous, northern Cape Breton Island, Nova Scotia; Geological Society of America, Northeastern Section, Abstracts with Programs, **16**, 5.

Brodie, K.H., and Rutter, E.H., 1985, On the relationship between deformation and metamorphism, with special refreence to the behaviour of basic rocks, *in* Metamorphic reactions: kinetics, textures, and deformation, Thompson, A.B., Rubie, D.C. (eds.), Springer-Verlag, Heidelberg, Advances in Physical Geochemistry, **4**, 138-179.

Brown, P.A., 1973, Possible cryptic suture in southwest Newfoundland, Nature, **146**, 9-10.

Buddington, A.F., 1939, Adirondack igneous rocks and their metamorphism, Geological Society of America, Memoir 7, 343 p.

Buddington, A.F., 1972, Differentiation trends and parental magmas for anorthositic and quartz mangerite series, Adirondacks, New York, *in* Shagam, R. et al. (eds.), Studies in Earth and Space Sciences, Geological Society of America Memoir 132, 477-488.

Burgess, J.L., Brown, M., Dallmeyer, R.D., and van Staal, C.R., 1995, Microstructure, metamorphism, thermochronology and P-T-t-deformation history of the Port aux Basques gneisses, southwest Newfoundland, Canada, Journal of Metamorphic Geology, **13**, 751-776.

Burke, K., and Dewey, J.F., 1973, Plume-generated triple junctions; Key indicators in applying plate tectonics to old rocks, Journal of Geology, **81**, 406-433.

Cameron, H.L., 1966, The Cabot Fault Zone, *in* Royal Society of Canada, Special Publication No. 9, Garland, G.D. , (ed.), 129-140.

Cawood, P.A., 1993, Acadian orogeny in west Newfoundland: Definition, character, and significance, in Roy, D.C., and Skehan, J.W., eds., The Acadian Orogeny: Recent studies in New England, Maritime Canada, and the autochthonous foreland, Geological Society of America, Special Paper, 275, 135-152.

Cawood, P.A., and Dunning, G.R., 1993, Silurian age for movement on the Baie Verte Line: Implications for accretionary tectonics in the Northern Appalachians, Geological Society of America, Abstracts with Programs, **25**, no. 6, A422.

Cawood, P.A., Dunning, G.R., Lux, D., and van Gool, J.A.M., 1994, Timing of peak metamorphism and deformation along the Appalachian margin of Laurentia in Newfoundland: Silurian not Ordovician, Geology, **22**, 399-402.

Cawood, P.A., and van Gool, J.A.M., 1992, Stratigraphic, structural and metamorphic relations along the eastern margin of the Humber Zone, Corner Brook Lake region, western Newfoundland, *in* Current Research, Part E, Geological Survey of Canada paper 92-1E, 239-247.

Cawood, P.A., van Gool, J.A.M., and Dunning, G.R., 1996, Geological development of eastern Humber and western Dunnage zones: Corner Brook - Glover Island region, Newfoundland, Canadian Journal of Earth Science, **33**, 182-198.

Chatterjee, A.K., 1979, Geology of the Meat Cove zinc deposit, Cape Breton Island, Nova Scotia, Nova Scotia Department of Mines, Paper 79-3, 27 p.

Chen, Y.D., Lin, S., and van Staal, C., 1995, Detrital zircon geochronology of a conglomerate in the northeastern Cape Breton Highlands: implications for the relationships between terranes in Cape Breton Island, the Canadian Appalachians, Canadian Journal of Earth Sciences, **32**, 216-223.

Cherniak, D.J., 1993, Lead diffusion in titanite and preliminary results on the effects of radiation damage on Pb transport, Chemical Geology, **110**, 177-194.

Clarke, G.L., and Powell, R., 1991, Decompression coronas and symplectites in granulites of the Musgrave Complex, central Australia, Journal of Metamorphic Geology, **9**, 441-450.

Colman-Sadd, S.P., Dunning, G.R., and Dec, T., 1992, Dunnage-Gander relationships and Ordovician orogeny in central Newfoundland: A sediment provenance and U/Pb age study, American Journal of Science, **292**, 317-355.

Conrad, M.E., and Naslund, H.R., 1989, Modally-graded rhythmic layering in the Skaergaard intrusion, Journal of Petrology, **30**, 251-269.

Cook, F.A., and Oliver, J.E., 1981, The late Precambrian-early Paleozoic continental edge in the Appalachian orogen, American Journal Science, **281**, 993-1008.

Coolen, J.J.M., 1980, Chemical petrology of the Furua granulite complex, sourthern Tansania, GUA (Amsterdam) Paper 13, 1-258.

Corrigan, D., 1990, Geology and U-Pb geochronology of the Key Harbour area, Britt Domain, southwest Grenville Province, Unpublished MSc thesis, Dalhousie Univ, Halifax, NS.

Corriveau, L., 1990, Proterozoic subduction and terrane amalgamation in the southwestern Grenville Province, Canada: evidence from ultrpotassic to shoshonitic plutonism, Geology, **15**, 614-617.

Corriveau, L., Heaman, L.M., Marcantonio, F., and van Breemen, O., 1990, 1.1 Ga K-rich alkaline plutonism in the SW Grenville Province: U-Pb constraints for the timing of subduction-related magmatism. Contributions to Mineralogy and Petrology, **105**, 473-485.

Corriveau, L., and Gorton, M.P., 1993, Coexisting K-rich alkaline and shoshonitic magmatism of arc affinities in the Proterozoic: a reassessmento of syenitic stocks in the southwestern Grenville Province, Contributions to Mineralogy and Petrology, **113**, 262-279.

Cosca, M.A., and Essene, E.J., 1988, Application of $^{40}Ar/^{39}Ar$ thermochronometry to the post-metamorphic cooling and denudation history of the Ontario Grenville Terrane. Grenville Workshop, Gananoque, ON, Abstract, 4.

Cosca, M.A., Essene, E.J., Bowman, J.R., 1991, Complete chemical analyses of metamorphic hornblendes: Implications for normalizations, calculated H2O activities, and thermobarometry, Contributions to Mineralogy and Petrology, **108**, 472-484.

Culshaw, N.G., Corrigan, D., Ketchum, J.W.F., and Wallace, P., 1990, Georgian Bay geological synthesis III: Twelve Mile Bay to Port Severn, Grenville Province of Ontario, *in* Current Research, Part C, Geological Survey Canada, Paper 90-1c, 107-112.

Culshaw, N.G., Jamieson, R.A., Ketchum, J.W.F., Wodicka, N, Corrigan, D, and Reynolds, P.H., submitted, Transect across the northwestern Grenville orogen, Georgian Bay, Ontario: Polystage convergence and extension in the lower orogenic crust, Tectonics.

Currie, K.L., 1975, Studies of granitoid rocks in the Canadian Appalachians, Geological Survey of Canada, Paper 75-1A, 265-270.

Currie, K.L., 1987a, Contrasting metamorphic terranes near Cheticamp, Cape Breton Highlands, Nova Scotia, Canadian Journal of Earth Sciences, **24**, 2422-2435.

Currie, K.L., 1987b, Relations between metamorphism and magmatism near Cheticamp, Cape Breton Island, Nova Scotia, Geological Survey of Canada, Paper 85-23, 66 p.

Currie, K.L., 1987c, A preliminary account of the geology of the Harry's River map area, southern Long Range of Newfoundland, Geological Survey of Canada, Paper 87-1A, 653-662.

Currie, K.L., van Breemen, O., Hunt, P.A., and van Berkel, J.T., 1991, Age of high-grade gneisses south of Grand Lake, Newfoundland, Atlantic Geology, **28**, 153-161.

Dallmeyer, R.D., 1977, $^{40}Ar/^{39}Ar$ age spectra of mineral from the Fleur de Lys terrane in northwest Newfoundland: Their bearing on chronology of metamorphis within the Appalachian orthotectonic zone, Journal of Geology, **85**, 263-282.

Dallmeyer, R.D., 1978, $^{40}Ar/^{39}Ar$ incremental release ages of hornblende and biotite from Grenvillian basement rocks within the Indian Head complex southwestern Newfoundland: their bearing on Late Proterozoic-Early Paleozoic thermal history, Canadian Journal of Earth Sciences, **15**, 1374-1379.

Dallmeyer, R.D., and Keppie, J.D., 1993, $^{40}Ar/^{39}Ar$ Mineral Ages from the Southern Cape Breton Highlands and Creignish Hills, Cape Breton Island, Canada: Evidence for a polyphase tectonothermal evolution, Journal of Geology, **101**, 467-482.

Dalziel, I.W.D., 1991, Pacific margins of Laurentia and East Antarctica-Australia as a conjugate rift pair: Evidence and implications for an Eocambrian supercontinent, Geology, **19**, 598-601.

Dasgupta, S., Sengupta, P., Guha, D., and Fukuoka, M., 1991, A refined garnet-biotite Fe-Mg exchange geothermometer and its application in amphibolites and granulites, Contributions to Mineralogy and Petrology, **109**, 130-137.

Davis, D.W., 1982, Optimum linear regression and error estimation applied to U-Pb data, Canadian Journal of Earth Sciences, **19**, 2141-2149.

Deer, W.A., Howie, R.A., and Zussman, J., 1982, An introduction to the rock-forming minerals, Longmans, Green, and Company, London, 825p.

de Wit, M.J, 1980, Structural and metamorphic relationships of pre-Fleur de Lys and Fleur de Lys rocks of the Baie Verte Peninsula, Newfoundland, Canadian Journal Earth Science, **17**, 1559-1575.

DePaolo, D.J., 1981, Neodymium isotopes in the Colorado Front Range and crust-mantle evolution in the Proterozoic, Nature, **291**, 193-196.

Deveau, S.W., 1988, Petrography and geochemistry of the Lowland Brook Syenite and associated rocks, Cape Breton Island, Nova Scotia; B.Sc. thesis, Acadia University, Wolfville, Nova Scotia 119 p.

Dickin, A.P., and McNutt, R.H., 1990, Nd model-age mapping of Grenville lithotectonic domains: Mid-Proterozoic crustal evolution in Ontario, *in* Gower, C.F., Ryan, A.B., and Rivers, T., Mid-Proterozoic Laurentia-Baltica, Geological Association of Canada, Special Paper 38, 79-94.

Dickin, A.P., and Raeside, R.P., 1990, Sm-Nd analysis of Grenville gneisses from Cape Breton Island, Nova Scotia, Proceedings of the LITHOPROBE-EAST Transect Meeting, St. John's, Nfld., 1990, 37-38.

Dodson, M.H., 1973, Closure temperature in cooling geochronological and petrological systems, Contributions to Mineralogy and Petrology, **40**, 259-274.

Doig, R., 1991, U-Pb zircon dates of Morin anorthosite suite rocks, Grenville Province, Quebec, Journal of Geology, **99**, 729-738.

Doig, R., Nance, R.D., Murphy, J.B., and Casseday, R.P., 1990, Evidence for Early Silurian sinistral accretion of the Avalon composite terrane in Canada, Journal of the Geologic Society of London, **147**, 927-930.

Dostal, J, Keppie, J.D, Cousens, B.L., and Murphy, J.B., 1996, 550-580 Ma magmatism in Cape Breton Island (Nova Scotia, Canada): the product of NW-dipping subduction during the final stage of amalgamation of Gondwana, Precambrian Research, **76**, 93-113.

Drake, A.A., 1984, The Reading Prong of New Jersey and eastern Pennsylvania; An appraisal of rock relations and chemisty of a major Proterozoic terrane in the Appalachians, *in* Bartholomew, M.J., (ed.), The Grenville event in the Appalachians and related topics, Geological Society of America Special Paper 194, 75-109.

Dubé, B., Dunning, G., Lauziére, K., and Roddick, C., 1993, The Gondwanan - Laurentian suture: Timing of deformation on the Cape Ray Fault, Newfoundland Appalachians, Annual Meeting, Geological Society of America, Abstracts with Program, **25**, 421.

Dubé, B. and Lauziére, K., 1996, Structural evolution of a major fault zone: the Cape Ray Fault Zone, southwestern Newfoundland, Canada, Canadian Journal of Earth Science, **33**, 199-215.

Dubé, B., Dunning, G., Lauziére, K., and Roddick, C., 1996, New insights into the Appalachian orogen from geology and geochronology along the Cape Ray Fault, SW Newfoundland. Geological Society of America Bulletin, **108**, 101-116.

Duchesne, J.C., 1984, Massif anorthosites: another partisan review, *in* Brown, W.L., ed, Feldspars and feldspathoids, Reidel, Dordrecht, 411-433.

Dunning, G.R., O'Brien, S.J., Colman-Sadd, S.P., Blackwood, R.F., Dickson, W.L., O'Neill, P.P, and Krogh, T.E., 1990a, Silurian Orogeny in the Newfoundland Appalachians, Journal of Geology, **98**, 895-913.

Dunning, G.R., Barr, S.M., Raeside, R.P., and Jamieson, R.A., 1990b, U-Pb zircon, titanite, and monazite ages in the in the Bras d'Or and Aspy terranes of Cape Breton Island, Nova Scotia: Implications for igneous and metamorphic history, Geological Society of America Bulletin, **102**, 322-330.

Dupuy, C., Dostal, J., Smith, P.K., and Keppie, J.D., 1986, Anorthosites and gabbroic bodies in northern Cape Breton Island, Nova Scotia, Maritime Sediments and Atlantic Geology, **22**, 136-147.

Durling, P.W., and Marillier, F.J.Y., 1990, Structural trends and basement rock subdivisions in the western Gulf of St. Lawrence, northern Appalachians, Atlantic Geology, **26**, 79-95.

Dymek, R.F., and Gromet, L.P., 1984, Nature and origin of orthopyroxene megacrysts from the St-Urbain anorthosite massif, Quebec, Canadian Mineralogist, **22**, 297-326.

Easton, R.M., 1986, Geochronology of the Grenville Province: Part I, Compilation of data and Part II, Synthesis and interpretation, *in* Moore, J.M., Davidson, A., and Baer, A.J. (eds.), The Grenville Province, Geological Association of Canada, Special Paper 31, 127-173.

Easton, R.M., 1990, Meta-anorthosites in the Grenville Province. in Gower, C.F., Rivers, T., and Ryan, B. (eds.), Middle-Proterozoic Laurentia-Baltica, Geological Association of Canada Paper 38, 387-497.

Ellis, D.J., and Green, D.H., 1979, An experimental study of the effect of Ca upon garnet-clinopyroxene Fe-Mg exhange equilibria, Contributions to Mineralogy and Petrology, **71**, 13-22.

Ellsworth, S., Navrotsky, A., and Ewing, R., 1994, Energetics of radiation damage in natural zircon (ZrSiO4), Physics and Chemistry of Minerals, **21**, 140-149.

Emslie, R.F., 1975, Pyroxene megacrysts from anorthositic rocks: new clues to the source and evolution of the parent magmas, Canadian Mineralogist, **13**, 138-145.

Emslie, R.F., 1978, Anorthosite massifs, rapakivi granites, and late Proterozoic rifiting of North America, Precambrian Research, **7**, 61-98.

Emslie, R.F., 1985, Proterozoic anorthosite massifs, *in* Tobi, A. and Touret, L. (eds.), The Deep Proterozoic Crust of the North Atlantic provinces; Dordrecht D. Reidel, 39-60.

Emslie, R.F., 1991, Granitoids of rapakivi granite-anorthosite and related associations, Precambrian Research, **51**, 173-192.

Emslie, R.F., and Hunt, P.A., 1989, The Grenvillian event: magmatism and high-grade metamorphism, Current Research, Part C, Geological Survey of Canada, Paper 89-1C, 11-17.

Emslie, R.F., and Hunt, P.A., 1990, Ages and petrogenetic significance of igneous mangerite-charnockite suites associated with massif anorthosites, Grenville province, Journal of Geology, **98**, 213-231.

England, P.C., and Thompson, A.B., 1984, Pressure-temperature-time paths of regional metamorphism I. Heat transfer during the evolution of regions of thickened crust, Journal of Petrology, **25**, 894-928.

Erdmer, P., 1984, Summary of the fieldwork iln the northern Long Range Mountains, western Newfoundland, *in* Current Research, Part A, Geologic Survey of Canada, Paper 84-1A, 521-530.

Essene, E.J., 1982, Geologic thermometry and barometry, *in* Ferry, J.M. (ed.), Characterisation of metamorphism through mineral equilibria, Reviews in Mineralogy, **10**, 77-96.

Essene, E.J., 1989, The current status of thermobarometry in metamorphic rocks, *in* Evolution of metamorphic belts. Daly, J.S., Cliff, R.A., Yardley, B.W.D. (eds.), Geological Society of London, Special Publication 43, 1-44.

Farrar, S.S., 1984 The Goochland granulite terrane; remobilised Grenville basement inthe eastern Virginia Piedmont, Geological Society of America Special Paper 194, 215-227.

Faure, G., 1986, Principles of Isotope Geology, John Wiley and Sons, New York, 464 p.

Ferry, J.M., 1988, Constrasting mechanism of fluid flow through adjacent strigraphic units during regional metamorphism, south-central Maine, USA, Contributions to Mineralogy and Petrology, **98**, 1-12.

Ferry, J.M., and Spear, F.S., 1978, Experimental calibration of the partioning of Fe and Mg between biotite and garnet, Contributions to Mineralogy and Petrology, **66**, 113-117.

Floyd, P.A., and Winchester, J.A., 1977, Identification and discrimination of altered and metamorphosed volcanic rocks using immobile elements, Chemical Geology, **39**, 1-15.

Foland, K.A., 1983, $^{40}Ar/^{39}Ar$ incremental heating plateaus for biotites with excess argon, Isotope Geoscience, **1**, 3-21.

Foland, K.A., and Muessig, K.W., 1978, A Paleozoic age for some charnockitic-anorthositic rocks, Geology, **6**, 143-146.

Foley, S.F., Venturelli, G., Green, D.H., and Toscani, L., 1987, The ultrapotassic rocks: characteristics, classification and constraints from petrogenetic models, Earth Science Reviews, **24**, 81-134.

Frost, B.R., Lindsley, D.H., and Simmons, C., 1989, Penrose Conference Report: Origin and evolution of anorthosites and related rocks, Geology, 474-475.

Fryer, B.J., Kerr, A, Jenner, G.A., and Longstaffe, F.J., 1992, Probing the crust with plutons: regional isotopic geochemistry of granitoid intrusions across insular Newfoundland, Newfoundland Department Mines Energy, Geological Survey Branch Report, **92-1**, 1119-139.

Fullagar, P.D., and Odom A.L., 1973, Geochronology of Precambrian gneisses in the Blue Ridge province of northwestern North Carolina and adjacent parts of Virginia and Tennessee, Geological Society of America Bulletin, **84**, 3065-3080.

Gasparik, T., 1984, Two-pyroxene thermobarometry with new experimental data in the system $CaO\text{-}MgO\text{-}Al^2O^3\text{-}SiO^2$, Contributions to Mineralogy and Petrology, **87**, 87-97.

Ghent, E.D., and Stout, M.Z., 1981, Geobarometry and geothermometry of plagioclase-biotite-garnet-muscovite assemblages, Contributions to Mineralogy and Petrology, **76**, 92-97.

Giest, D.J., Frost, C.D., and Kolker, A., 1990, Sr and Nd isotopic constraints on the origin of the Laramie Anorthosite Complex, Wyoming, American Mineralogist, **75**, 13-20.

Glassley, W.E., and Sørensen, K., 1980, Constant P-T amphibolite to granulite facies transition in Agto (West Greenland) metadolerites, Journal of Petrology, **21**, 69-105.

Glover, L., Speer, J.A., Russel, G.S, and Farrarr, S.S., 1983, Ages of regional metamorphism and ductile deformation in the central and southern Appalachians, Lithos, **16**, 223-245.

Gower, C.F., 1990, Mid-Proterozoic evolution of the eastern Grenville Province, Canada, Geologiska Føreningens (Stockholm), **112**, 127-139.

Gower, C.F., Ryan, A.B., and Rivers, T., 1990, Mid-Proterozoic Laurentia-Baltica: An overview of its geological evolution and a summary of the contributions of this volume, *in* Gower, C.F., Ryan, A.B., and Rivers, T., Mid-Proterozoic Laurentia-Baltica, Geological Association of Canada, Special Paper 38, 1-20.

Gower, C.F., Heaman, L.M., Loveridge, W.D., Schärer, U., and Tucker, R.D., 1991, Grenvillian magmatism in the eastern Grenville Province, Canada, Precambrian Research, **51**, 315-33.

Graham, C.M., and Powell, R., 1984, A garnet-hornblende geothermometer: calibration, testing and application to the Pelona schist, Southern California, Journal of Metamorphic Geology, **2**, 13-31.

Green, D.H., and Ringwood, A.E., 1967, An experimental investigation of the gabbro to eclogite tranformation and its petrological applications, Geochimica et Cosmochimica Acta, **31**, 767-833.

Green, D.H., and Ringwood, A.E., 1972, A comparison of recent experimental data on the gabbro-garnet granulite-eclogite transition. Journal of Geology, **80**, 277-288.

Gross, S.O., 1968, Titaniferous ores of the Lake Sanford district, New York. in Ridge, J.D., (ed.), Ore Deposits of the United States, American Institute of Mining and Metallography, New York, 140-154.

Guidotti, C.V., 1984, Ferric iron in metamorphic biotite and its petrologic and crystallochemical implications, American Mineralogist, **76**, 161-175.

Hamblin, A.P., and Rust, B.R., 1989, Tectonosedimentary analysis of alternate-polarity half-graben basin-fill successions: Late Devonian Early Carboniferous Horton Group, Cape Breton Island, Nova Scotia, Basin Research, **2**, 239-255.

Hancahar, J.M., and Miller, C.F, 1993, Zircon zonation patterns as revealed by cathodoluminescence and backscattered electron images: Implications for interpretation of complex crustal histories, Chemical Geology, **110**, 1-13.

Hanes, J.A., 1991, K-Ar and $^{40}Ar/^{39}Ar$ geochronology: methods and applications, In Short course handbook on applications of radiogenic isotope systems to problems in geology, L. Heaman and J.N. Ludden (eds.), Mineralogical Association of Canada, **19**, 27-57.

Harley, S.L., 1989, The origins of granulites: a metamorphic perspective, Geological Magazine, **126**, 215-247.

Harrison, T.M., 1981, Diffusion of ^{40}Ar in hornblende, Contributions to Mineralogy and Petrology, **78**, 324-331.

Harrison, T.M., and McDougall, 1981, Excess ^{40}Ar in metamorphic rocks from Broken Hill, New South Wales: implications for $^{40}Ar/^{39}Ar$ age spectra and the thermal history of the region, Earth and Planetary Science Letters, **55**, 123-149.

Harrison, T.M., Duncan, I., and McDougall, I., 1985, Diffusion of ^{40}Ar in bioite: temperature pressure and compositional effects. Geochimica and Cosomochimica Acta, **50**, 247-253.

Hatcher, R.D., 1978, Tectonics of the western Piedmont and Blue Ridge, Southern Appalachians: Review and Speculation, American Journal of Science, **278**, 276-304.

Hatcher, R.D., 1983, Basement massifs in the Appalachians: their role in deformation during Appalachian orogenies, Geological Journal, **18**, 255-265.

Hatcher, R.D., 1984, Southern and central Appalachian basement massifs, *in* Bartholomew, M.J. (ed.), The Grenville event in the Appalachians and related topics, Geological Society of America Special Paper 194, 149-154.

Hatcher, R.D., and Zeitz I., 1980, Tectonic implication of regional aeromagnetic and gravity data from the southern Appalachians, *in* Wones, D.R. (ed.), Proceedings, The Caledonides in the U.S.A.; Blacksburg, Virginia Polytechnic Institute and State Uinversity Memoir 2, 235-244.

Haworth, R.T., Daniels, D.L., Williams, H., and Zietz, I., 1981, Gravity anomaly map of the Appalachian orogen, Memorial University of Newfoundland, map no. 3, scale 1/1,000,000.

Hawthorne, F.C., 1983, The crystal chemistry of the amphiboles, The Canadian Mineralogist, **21**, 173-480.

Heaman, L.M., and Parrish, R., 1991, U-Pb geochronology of accessory minerals, In Short course handbook on applications of radiogenic isotope systems to problems in geology, Edited by L. Heaman and J.N. Ludden, Mineralogical Association of Canada, **19**, 59-102.

Heaman, L.M., Erdmer, P., and Owen, J.V., 1996, Preliminary U-Pb results from the Long Range Inlier, Newfoundland, *in* Wardle, R.J. and Hall, J., compilers, Eastern Canadian Shield onshore-offshore transed (ECSOOT), Transect Meeting, March 14-15, 1996 Univeristy of British Columbia, Lithoprobe Secretariat, Report #57, 123-132

Helenek, H.L., and Mose, D.G., 1984, Geology and geochronology of Canada Hill Granite and its bearing on the timing of Grenvillian events in the Hudson Highlands, New York, *in* Bartholomew, M.J. (ed.), The Grenville event in the Appalachians and related topics, Geological Society of America Special Paper 194, 57-73.

Herz, N., 1984, Rock suites in Grenvillian terrane of the Roseland district, Virginia, Part 2 Igneous and metamorphic petrology, in Bartholomew, M.J. (ed.), The Grenville event in the Appalachians and related topics, Geological Society of America Special Paper 194, 200-214.

Herz, N, and Force, E.R., 1984, Rock suites in Grenvillian terrane of the Roseland district, Virginia, Part 1 Lithologic relations, in Bartholomew, M.J. (ed.), The Grenville event in the Appalachians and related topics, Geological Society of America Special Paper 194, 187-199.

Herz, N, and Force, E.R., 1987, Geology and mineral deposits of the Roseland district of central Virginia U.S. Geological Survey, Paper 1371, 56 p.

Hibbard, J., 1982, The significance of the Baie Verte Flexure, Newfoundland, Geological Society of America Bulletin, **93**, 790-797.

Hibbard, J., 1983, Geology of the Baie Verte Peninsula, Newfoundland, Newfoundland Department of Mines and Energy, Mineral Development Division, Memoir 2, 279 p.

Hibbard, J., 1994, Kinematics of Acadian Deformation in the Northern Appalachians, Journal of Geology, **102**, 215-228.

Hibbard, J., and Samson, S.D., 1995, Orogenesis exotic to the Iapetan cycle in the southern Appalachians, in, Hibbard, J.P., van Staal, C.R., and Cawood, P.A. (eds.), Current Perspectives in the Appalachian-Caledonian Orogen, Geological Association Canada, Special Paper 41, 191-205.

Higgins, M.D., 1991, The origin of laminated and massive anorthosite, Sept Iles layered intrusion, Quebec, Canada, Contributions to Mineralogy and Petrology, **106**, 340-354.

Higgins, M.D., and Doig, R., 1981, The Sept Iles anorthosite complex: field relationships, geochronology, and petrology, Canadian Journal of Earth Sciences, **18**, 561-573.

Higgins, M.D., and van Breemen, O., 1989, Age of the Lac-St-Jean anorthosite intrusion and associated mafic rocks, Geological Association Canada - Mineral Association Canada, Programs with Abstracts, **14**, A84.

Hill, J.R., 1988, Geochemical differentiation of Precambrian metacarbonate assemblages, Cape Breton Island, Nova Scotia, *in* Current Research, Part B, Geological Survey of Canada, Paper 88-b, p. 173-185.

Hoffman, P.F., 1991, Did the breakout of Laurentia turn Gondwanaland inside-out?, Science, 1409-1412.

Holdsworth, R.E., 1991, The geology and structure of the Gander-Avalon boundary zone in northeastern Newfoundland, Newfoundland Department of Mines and Energy, Paper 91-1, 109-126.

Holland, T.J.B., 1981, Thermodynamic analysis of simple systems, in Newton, R.L., Navrotsky, A., Wood, B.J. (eds.), Advances in physical geochemistry, **1**, 19-34.

Holland, T., and Blundy, J., 1994, Non-ideal interactions in calcic amphiboles and their bearing on amphibole-plagioclase thermometry, Contributions to Mineralogy and Petrology, **116**, 433-447.

Holland, T.J.B., and Powell, R.,1985, An internally consistent thermodynamic dataset with uncertainties and correlations. II. Data and results, Journal of Metamorphic Geology, 3, 343-370.

Horton, J.W., Drake, A.A. Jr, and Rankin, D.W., 1989, Tectonostrigraphic terranes and their boundaries in the central and southern Appalachians, *in* Dallmeyer, R.D. (ed.), Terranes in the Circum-Atlantic Paleozoic orogens, Geological Society of America Special Paper 230, 213-245.

Hutchinson, C.S., 1974, Labratory Handbook of Petrographic Techniques, Wiley, NY, 551 p.

Indares, A., and Martingole, J., 1985, Biotite-garnet geothermometry in the granulite facies: The influence of Ti and Al in biotite, American Mineralogist, **70**, 272-278.

Irvine, T.N., and Baragar, W.R.A., 1971, A guide to the chemical classification of common volcanic rocks, Canadian Journal of Earth Science, **8**, 523-548.

Jamieson, R.A., 1990, Metamorphism of an early Paleozoic continental margin, western Baie Verte Peninsula, Newfoundland, Journal of Metamorphic Geology, **8**, 269-288.

Jamieson, R.A., and Doucet, P., 1983, Reconnaissance mapping of the southern Cape Breton Highlands - A preliminary report, in Current Research, Part A, Geological Survey Canada, paper 83-1a, 263-268.

Jamieson, R.A., van Breemen, O., Sullivan, R.W., and Currie, K.L., 1986, The age of igneous and metamorphic events in the western Cape Breton Highlands, Nova Scotia, Canadian Journal of Earth Sciences, **23**, 1891-1901.

Jamieson, R.A., Culshaw, N.G., Wodicka, N., Corrigan, D., and Ketchum, J.W.F., 1992, Timing and tectonic setting of Grenvillian metamorphism - constraints from a transect along Georgian Bay, Ontario, Journal of Metamorphic Geology, **10**, 321-332.

Jamieson, R.A., Culshaw, N.G., and Corrigan, D., 1995, North-west propigantion of the Grenville orogen: Grenvillian structure and metamorphism near Key Harbour, Georgian Bay, Ontario, Canada, Journal of Metamorphic Geology, **13**, 185-207.

Jenkins, D.M., 1994, Experimental reversal of the aluminum content in tremolitic amphiboles in the system H2O-CaO-MgO-Al2O3-SiO3, American Journal of Science, **294**, 593-620.

Jenkins, D.M., Holland, T.J.B., and Clare, A.K., 1991, Experimental determination of the pressure-temperature stability field and themochemical properties of synthetic tremolite, American Mineralogist, **76**, 458-469.

Jenness, S.E., 1966, The anorthosite of northern Cape Breton Island, Nova Scotia, a petrological enigma, Geological Survey of Canada, Paper 66-21, 25 p.

Johnson, C.A., and Essene, E.J., 1982, The formation of garnet in olivine-bearing metagabbros from the Adirondacks, Contributions to Mineralogy and Petrology, **81**, 240-251.

Jones, A.P., and Peckett, A., 1980, Zirconium-bearing aegirines from Motzfeldt, South Greenland, Contributions to Mineralogy and Petrology, **75**, 251-255.

Karabinos, P., 1988, Tectonic significance of basement-cover relationships in the Green Mountain Massif, Vermont, Journal of Geology, **96**, 445-454.

Karabinos, P., and Aleinikoff, J.N., 1988, U-Pb zircon ages of augen gneisses in the Green Mountain and Chester dome, Vermont; Geological Society of America, Abstracts with Programs, **20**, 29-30.

Karabinos, P., and Aieinikoff, J.N., 1990, Evidence for a major middle Proterozoic post-Grenvillian igneous event in western New England, American Journal of Science, **290**, 959-974.

Kehlenbeck, M.M, 1972, Deformation textures in the Lac Rouvray anorthosite mass, Canadian Journal of Earth Science., **9**, 1087-1098.

Keppie, J.D., 1989, Northern Appalachian terranes and their accretionary history, *in* R.D. Dallmeyer (ed.), Terranes in the Circum-Atlantic Paleozoic Orogens, Geological Society of America Special Paper 230, 159-192.

Keppie, J.D., 1990, Tectono-stratigraphic terranes in Cape Breton Island, Nova Scotia - implications for the configuration of the northern Appalachian Orogen - comment, Geology, **18**, 669-670.

Keppie, J.D., 1992, North-south American trade in the Silurian: Annual Meeting - Geologic Association of Canada - Mineralogical Association of Canada, Abstracts Volume, **17**, A56.

Keppie, J.D., 1993, Synthesis of Paleozoic deformational events and terrane accretion in the Canadian Appalachians, Geologische Rundsch, **82**, 381-431.

Keppie, J.D., and Dallmeyer, R.D., 1989, Tectonic map of pre-Mesozoic terranes in circum-Atlantic phanerozoic orogens, Nova Scotia Department Mines Energy, Halifax, Nova Scotia, scale 1:5000000.

Keppie, J.D., Dallmeyer, R.D., and Murphy, J.B., 1990, Tectonic implications of $^{40}Ar/^{39}Ar$ hornblende ages from Late Proterozoic-Cambrian plutons in the Avalon Composite Terrane, Nova Scotia, Canada, Geological Society of America Bulletin, **102**, 516-528.

Keppie, J.D., Dallmeyer, R.D., and Krogh, T.E., 1992, U-Pb and $^{40}Ar/^{39}Ar$ mineral ages from Cape North, northern Cape Breton Island: implications for accretion of the Avalon Composite Terrane, Canadian Journal of Earth Sciences, **29**, 277-295.

Keppie, J.D., and Dostal, J., 1991, Late Proterozoic tectonic model for the Avalon Terrane in Maritime Canada, Tectonics, **10**, 842-85.

Keppie, J.D., and Dostal, J., 1994, Late Silurian-Early Devonian transpressional rift origin of the -Quebec Reentrant, northern Appalahcians: Constraints from geochemistry of volcanic rocks, Tectonics, **13**, 1183-1189.

Keppie, J.D., Dostal, J, Murphy, J.B., and Nance, R.D., 1996, Terrane transfer between eastern Laurentia and western Gondwana in the early Paleozoic: Constraints on global reconstructions, in Nance, R.D., and Thompson, M.D. (eds.), Avalonian and related peri-Gondwanan terranes of the circum-Atlantic, Boulder Colorado, Geological Society of America, Special Paper 304, 369-380.

Kohn, M.J., and Spear, F.S., 1989, Empirical calibration of geobarometers for the assemblage garnet + hornblende + plagioclase + quartz, American Mineralogist, **74**, 77-84.

Kohn, M.J., and Spear, F.S., 1990, Two new geobarometers for garnet amphibolites, with applications to southeastern Vermont, American Mineralogist, **75**, 89-96.

Kolker, A., 1982, Mineralogy and geochemistry of Fe-Ti oxide and apatite (nelsonite) deposits and evaluation of the liquid immiscibility hypothesis. Economic Geology, 77, 1146-1158.

Kretz, R., 1981, Site-occupancy interpretation of the distribution of Mg and Fe between orthopyroxene and clinopyroxene in metamorphic rocks, Canadian Mineralogist, **19**, 493-500.

Kretz, R., 1982, Transfer and exchange equilibria in a portion of the pyroxene quadrilateral as deduced from natural and experimental data, Geochimica et Cosomochimica Acta, **46**, 411-422.

Kretz, R., 1983, Symbols for rock-forming minerals. American Mineralogist, **68**, 277-279.

Krinsley, D.H., and Manley, C.R., 1989, Backscattered electron microscopy as an advanced technique in petrography, Journal of Geological Education, **37**, 202-209.

Krogh, T.E., 1973, A low contamination method for hydrothermal decomposition of zircon and extraction of U and Pb for isotopic age determinations, Geochimica et Cosmochimica Acta, **37**, 485-494.

Krogh, T.E., 1982, Improved accuracy of U-Pb zircon ages by the creation of more concordant systems using an air abrasion technique, Geochimica et Cosmochimica Acta, **46**, 637-649.

Labotka, T.C., 1987, The garnet-hornblende isograd in calcic schists from an andalusite-type regional metamorphic terraine, Panamint Mountains, California, Journal of Petrology, **28**, 232-254.

Langdon, G.S., and Hall, J., 1994, Devonian-Carboniferous tectonics and basin deformation in the Cabot Strait area, eastern Canada, AAPG Bulletin, **78**, 1748-1774.

Lanzirotti, A., and Hanson, G. N., 1995, U-Pb dating of major and accessory minerals formed during metamorphism and deformation of metapelites, Geochimica et Cosmochimica Acta, **59**, 2513-2526.

Le Maitre, R.W., 1989, A Classification of Igneous Rocks and Glossary of Terms, Blackwell, Oxford, 193 p.

Leake, B.E., 1964, The chemical distinction between ortho- and para-amphibolites, Journal of Petrology, **5** 238-254.

Leake, B.E., 1978, Nomenclature of Amphiboles, Canadian Mineralogist, **16**, 501-520.

Leger, A., and Ferry, J.M., 1991, Highly aluminous hornblende from low-pressure metacarbonates and a preliminary thermodynamic model for the Al-content of calcic amphibole, American Mineralogist, **76**, 1002-1017.

Lin, S., 1993, Relationship between the Aspy and Bras d'Or "terranes" in the northeastern Cape Breton Highlands, Nova Scotia, Canadian Journal of Earth Sciences, **30**, 1773-1781.

Lin, S., van Staal, C.R., and Dube, B., 1994, Promontory-promontory collision in the Canadian Appalachians, Geology, **22**, 897-900.

Lindsley, D.H., 1983, Pyroxene thermometry, American Mineralogist, **68**, 477-493.

Lindsley, D.H., and Andersen, D.J., 1983, A two-pyroxene thermometer, Proceedings of the thirteenth lunar and planetary science conference, Part 2, Journal of Geophysical Research, Supplement, **88**, A887-A906.

Liou, J.G., Kuniyoshi, S., and Ito, K., 1974, Experimental studies of the phase relations between greenschist and amphibolite in a basaltic system, American Journal Science, **274**, 613-632.

Liou, J.G., Maruyama, S., and Cho, M., 1985, Phase equilibria and mineral parageneses of metabasites in low-grade metamorphism, Mineralogical Magazine, **49**, 321-333.

Loncarevic, B.D., Barr, S.M., Raeside, R.P., Keen, C.E., and Marillier, F., 1989, Northeastern extension and crustal expression of terranes from Cape Breton Island, Nova Scotia, based on geophysical data, Canadian Journal of Earth Sciences, **26**, 2255-2267.

Lucassen, F., and Franz, G., 1996, Magmatic arc metamorphism: petrology and temperature history of metabasic rocks in the Coastal Cordillera of northern Chile, Journal of Metamorphic Geology, **14**, 249-265.

Lumbers, S.B., Heaman, L.M., Vertolli, V.M., and Wu, T.W., 1990, Nature and timing of middle Proterozoic magmatism in the Central Metasedimentary Belt, Grenville province, Ontario, in Gower, C.F., Rivers, T., and Ryan, A.B. (eds.), Mid-Proterozoic Laurentia-Baltica, Geological Association of Canada Paper 38, 243-276.

Luth, W.C, Jahns, R.H, and Tuttle, O.F., 1964, The granite system at pressures of 4 to 10 kilobars, Journal of Geophysical Research, **69**, 759-773.

Lynch, G., 1996, Tectonic burial, thrust emplacement, and extensional exhumation of the Cabot nappe in the Appalachian hinterland of Cape Breton Island, Canada, Tectonics, **15**, 94-105.

Macdonald, A.S., and Smith, P.K., 1979, Red River anorthosite complex, Nova Scotia Department of Mines and Energy, Paper 79-1, 103-104.

Mader, U.K., and Berman, R.G., 1992, Amphibole thermobarometry: A thermodynamic approach, in Current Research, Part E; Geological Survey of Canada, Paper 92-1E, 393-400.

Mader, U.K., Percival, J.A., and Berman, R.G., 1994, Thermobarometry of garnet-clinopyroxene-hornblende granulites from the Kapuskasking structural zone, Canadian Journal of Earth Sciences, **31**, 1134-1145.

Malo, M., Kirkwood, D., De Broucker, G., and St-Julien, P., 1992, A reevalution of the position of the Baie Verte-Brompton Line in Quebec Appalachians: the influence of Middle Devonian strike-slip faulting in the Gaspe Peninsula, Canadian Journal of Earth Sciences, **29**, 1265-1273.

Malo, M., Tremblay, A, and Kirkwood, D., 1995, Along-strike Acadian structural variations in the Quebec Appalachians: Consequences of a collision along an irregular margin, Tectonics, **14**, 1327-1338.

Maniar, P.D., and Piccoli, P.M, 1989, Tectonic discrimination of granitoids, Geological Society of Amer Bulletin, **101**, 635-643.

Marillier, F., and Verhoef, J., 1989, Crustal thickness under the Gulf of St. Lawrence, northern Appalachians, from gravity and deep seismic data, Canadian Journal of Earth Sciences, **26**, 1517-1532.

Marillier, F., Keen, C.E., Stockmal, G.S., Quinlan, G., Williams, H., and Colman-Sadd, S.P., and O'Brien, S.J., 1989, Crustal structure and surface zonation of the Canadian Appalachians: implications of deep seismic reflection data, Canadian Journal of Earth Sciences, **26**, 305-321.

Martingole, J., 1992, Exhumation of high-grade terranes - a review, Canadian Journal of Earth Sciences, **29**, 737-745.

McDougal, I., and Harrison, T.M., 1988, Geochronology and thermochronology by the $^{40}Ar/^{39}Ar$ method, Oxford University Press, London, 346 p.

McLelland, J.M., and Chairenzelli, J., 1989, Constraints on the emplacement age of Adirondack anorthosite, Geological Association Canada - Mineralogical Association Canada, Program with Abstracts, **14**, A52.

McLelland, J.M., and Chiarenzelli, J.R., 1990a, Geochronological studies in the Adirondack Mountains and the implications of a Middle Proterozoic tonalitic suite, in Gower, C.F., Rivers, T., and Ryan, B. (eds.), Middle-Proterozoic Laurentia-Baltica, Geological Association of Canada Paper 38, 175-194.

McLelland, J.M., and Chiarenzelli, J., 1990b, Isotopic constraints on emplacement age of anorthositic rocks of the Marcy Massif, Adirondack Mts., New York, Journal of Geology, **98**, 19-41.

McLelland, J.M., and Whitney, P.R., 1990, A generalized garnet-forming reaction for meta-igneous rocks in the Adirondacks, Contributions to Mineralogy and Petrology., **72**, 111-122.

McLelland, J.M., Chiarenzelli, J., Whitney, P., and Isachesen, Y., 1988, U-Pb zircon geochronology of the Adirondack Mountains and implications for their geologic evolution. Geology, **16**, 920-924.

McLelland, J., Ashwal, L., and Moore, L., 1994, Composition and petrogenesis of oxide-, apatite-rich gabbronorites associated with Proterozoic anorthosite massifs: examples from the Adirondack Mountains, New York, Contributions to Mineralogy and Petrology, **116**, 225-238.

McMullin, D.W.A., Berman, R.G., Greenwood, H.J., 1991, Calibration of the SGAM thermobarometer for pelitic rocks using data from phase-equilibrium experiments and natural assemblages, Canadian Mineralogist, **29**, 889-908.

Mezger, K., Bohlen, S., and Hanson, G., 1988, U-Pb garnet, monazite, and rutile ages; Implications for the duration of high grade metamorphism and cooling historyies, Adirondack Mountains, Geological Society of America, Abstracts with Programs, **20**, A100.

Mezger, K., Rawnsley, C.M., Bohlen, S.R., and Hanson, G.N., 1991, U-Pb garnet, sphene, monazite, and rutile ages: implications for the duration of high-grade metamorphism and cooling histories, Adirondack Mountains, New York, Journal of Geology, **99**, 415-428 .

Miller, H.G., 1990, A synthesis of the geophysical characteristics of terranes in eastern Canada, Tectonophysics, **177**, 171-191.

Milligan, G.C., 1970, Geology of the George River Series, Cape Breton; stratigraphy, structure, and economic geology, Nova Scotia Department of Mines and Energy, Memoir 7, 11p.

Mitchell, P.L., 1979, A study of the rare earth element geochemistry and mineral chemistry of the anorthosites and related rocks near Pleasant Bay, Cape Breton Island, Nova Scotia, B.Sc. thesis, Dalhousie University, Halifax, Nova Scotia.

Miyashiro, A., 1974, Volcanic rocks series in island arec and active continental margins, American Journal Science, **274**, 293-303.

Moecher, D.P., Anovitz, L.M., and Essene, E.J., 1988, Calculation of clinopyroxene-garnet-plagioclase-quartz geobarometers and application to high grade metamorphic rocks, Contributions to Mineralogy and Petrology, **100**, 92-106.

Mongkoltip, P., and Ashworth, J.R., 1986, Amphibolitization of metagabbros in the Scottish Highlands, Journal of Metamorphic Geology, **4**, 261-283.

Moore, J.M., 1986, Introduction; The "Grenville problem" then and now, *in* Moore, J.M., Davidson, A., and Baer, A.J. (eds.), The Grenville Province, Geological Association of Canada Special Paper 31, **348**, 1-11.

Moore, J.M., and Thompson, P.H., 1980, The Flinton Group: a late Precambrian metasedimentary succession in the Grenville Province of eastern Ontario, Canadian Journal Earth Science, **17**, 1685-1707.

Morse, S.A., 1968, Layered intrusions and anorthosite genesis, *in* Isachsen, Y.W. (ed.), Origin of Anorthosite and Related Rocks; New York State Museum and Science Service Memoir 18, 175-187.

Morse, S.A., 1970, Alkali feldspars with water at 5 kb pressure, Journal of Petrology, **11**, 221-251.

Morse, S.A., 1982, A partisan view of Proterozoic anorthosites, American Mineralogist, **67**, 1087-1100.

Mueck, G.K., Ellias, P., and Reynolds, P.H., 1988, Hercynian/Alleghanian overprinting of an Acadian terrane: $^{40}Ar/^{39}Ar$ studies in the Meguma zone, Nova Scotia, Canada, Chemical Geology (Isotopte Geoscience), **73**, 153-167

Muhling, J.R., Griffin, B.J., 1991, On recasting garnet analyses into end-member molecules-revisited, Computers & Geosciences, **17**, 161-170.

Mukhopadhyay, A., Bhattacharya, A., and Mohanty, L., 1992, Geobarometers involving clinopyroxene, garnet, plagioclase, ilmenite, rutile, sphene, and quartz: Estimation of pressure in quartz-absent assemblages, Contributions to Mineralogy and Petrology, **110**, 346-354.

Murphy, J.B., Keppie, J.D., Nance, R.D., and Dostal, J., 1989, Reassessment of terranes in the Avalon Composite Terrane of Atlantic Canada, Geological Society of America, Northeastern Section, Abstracts with Programs, **21**, 54.

Murphy, J.B., Keppie, J.D., and Krogh, T., 1993, Tectonic implications of Sm-Nd and U-Pb isotopic compositions of felsic volcanic rocks, Antigonish Highlands, Avalon Composite Terrane, Nova Scotia, Geological Society of America, Northeastern Section Annual Meeting, 25, no. 2, 67.

Murphy, J.B., Keppie, J.D., Dostal, J, and Cousens, B.L., 1995, Repeated lower crustal melting beneath the Antigonish Highlands, Avalon Composite terrane, Nova Scotia, Nd isotopic evidence and tectonic implications, Geological Society of America, Special Paper.

Nance, R.D., 1986, Precambrian evolution of the Avalon terrane in the northern Appalachians: a review, Maritime Sediments and Atlantic Geology, **22**, 214-238.

Neale, E.R.W., 1963, Geology, Pleasant Bay, Nova Scotia, Geological Survey of Canada, Map 1119a, scale 1:50,000.

Neale, E.R.W., 1964, Geology, Cape North, Cape Breton Island, Nova Scotia, Geological Survey of Canada, Map 1150a, scale 1:50,000.

Neale, E.R.W., and Kennedy, M.J., 1965, Basement and cover rocks at Cape North, Cape Breton Island, Nova Scotia, Maritime Sediments, **2**, 1-4.

Neale, E.R.W., and Kennedy, M.J., 1975, Basement and cover rocks at Cape North, Cape Breton Island, Nova Scotia, Maritime Sed Atlantic Geology, **11**, 1-4.

Newton, R.C., 1983, Geobarometry of high-grade metamorphic rocks, American Journal of Science, **283-A**, 1-28.

Newton, R.C., and Perkins, D.III., 1982, Thermodynamic calibration of geobarometers based on the assemblages garent-plagioclase-orthopyroxen-(clinopyroxene)-quartz, American Mineralogist, **67**, 203-222.

O'Brien, S.J., O'Brien, B.H., O'Driscoll, C.F., Dunning, G.R., Holdsworth, R.E., and Tucker, R., 1991, Silurian orogenesis and the northwestern limit of Avalonian rocks in the Hermitage Flexure, Newfoundland Appalachians, Geological Society of America, Joint Northeastern-Southeastern Sections Meeting, Abstracts with Programs, **23**, 109.

Onstott, T.C., and Peacock, M.W., 1987, Argon retentivity of hornblendes: A field experiment in a slowly cooled metamorphic terrane, Geochimica et Cosmochimica Acta, **51**, 2891-2903.

Owen, J.V., 1991, Cordierite+spinel paragenesis in pelitic gneiss from the contact aureoles of the Mistastin batholith (Quebec) and the Taylor Brook gabbro complex (Newfoundland), Canadian Journal of Earth Sciences, **28**, 372-381.

Owen, J.V., and Erdmer, P., 1989, Metamorphic geology and regional geothermobarometry of a Grenvillilan Massif: the Long Range Inlier, Newfoundland, Precambrian Research, **43**, 79-100.

Owen, J.V., and Erdmer, P., 1990, Middle Proterozoic geology of the Long Range Inlier, Newfoundland: regional significance and tectonic implications, *in* Gower, C.F., Rivers, T., and Ryan, B. (eds.)., Mid-Proterozoic Laurentia-Baltica, Geological Association of Canada, Special Paper 38, 215-231.

Owens, B.E., and Dymek, R.F., 1992, Fe-Ti-P-rich rocks and massif anorthosite from the Labrieville and St. Urban Plutons, Quebec, Canadian Mineralogist, **30**, 163-190.

Owens, B.E., and Dymek, R.F., 1995, Significance of pyroxene megacrysts for massif anorthosite petrogenesis: constraints from the Labrieville, Quebec, pluton, American Mineralogist, **80**, 144-161.

Owens, B.E., Rockow, M.W., and Dymek, R.F., 1993, Jotunites from the Grenville Province, Quebec: petrological characteristics and implications for massif anorthosite petrogenesis, Lithos, **30**, 57-80.

Patchett, P.J., and Ruiz, J., 1989, Nd isotopes and the origin of Grenville-age rocks in Texas; Implications for Proterozoic evolution of the U.S. mid-continent region, Journal Geology, **97**, 685-696.

Paterson, B.A., Stephens, W.E., and Herd, D.A., 1989, Zoning in granitoid accessory minerals as revealed by backscattered electron imagery, Mineralogical Magazine, **53**, 55-62.

Paterson, B.A., Stephens, W.E., Rogers, G., Williams, I.S., Hinton, R.W., and Herd, D.A., 1992, The nature of zircon inheritance in two granite plutons, Transactions of the Royal Society of Edinburgh, Earth Sciences, **83**, 459-471.

Pattison, D.R.M., and Newton, R.C., 1988, Reversed experimental calibration of the garnet-clinopyroxene K^D (Fe-Mg) exchange thermometer, Contributions to Mineralogy and Petrology, **85**, 85-97.

Pearce, J.A., and Cann, J.R., 1973, Tectonic setting of basic volcanic rocks determined using trace element analysis, Earth Planet Science Letters, **19**, 290-300.

Pearce, J.A., Harris, N.B.W, and Tindle, A.G., 1984, Trace element discrimination diagrams for the tectonic interpretation of granitic rocks, Journal of Petrology, **25**, 956-983.

Peccerillo, A., and Taylor, S.R., 1976, Geochemistry of Eocene calc-alkaline volcanic rocks from the Kastamonu area, northern Turkey, Contributions to Mineralogy and Petrology, **58**, 63-81.

Pehrsson, S., Hanmer, S., and van Breemen, O., 1996, U-Pb geochronology of the Raglan gabbro belt, Central Metasedimentary Belt, Ontario: implications for an ensialic marginal basin in the Grenville Province, Canadian Journal of Earth Science, **33**, 691-702.

Perchuk, L.L., and Lavrent'eva, I.V., 1983, Experimental investigation of exchange equilibria in the system cordierite-garnet-biotite, *in* Saxena, S.K. (ed), Kinetics and Equilibrium in Mineral Reactions, Advances in Physical Geochemistry, **3**, 199-239, Springer-Verlag, New York.

Percival, J.A., 1983, High-grade metamorphism in the Chaplau-Foleyet area, Ontario, American Mineralogist, **68**, 667-686.

Piasecki, M.A.J., 1991, Geology of the soutwest arem of Grand Lake, western Newfoundland, *in* Current Research, Part D, Geological Survey of Canada, Paper 91-1D, 1-8.

Poldervaart, A., Hess, H.H., 1951, Pyroxenes in the crystallization of basaltic magma, Journal of Geology, **59**, 472-489.

Powell, R., and Holland, T.J.B., 1988, An internally consistent dataset with uncertainties and correlations: 3. Applications to geobarometry, worked examples and a computer program, Journal of Metamorphic Geology, **6**, 173-204.

Pride, C., and Moore, J.M., 1983, Petrogenesis of the Elzevir batholith and related trondhjemitic intrusions in the Grenville Province of Ontario, Canada, Contributions to Mineralogy and Petrology, **82**, 187-194.

Purdy, J.W., and Jäger, E., 1976, K-Ar ages on rock-forming minerals from the Central Alps, Memoirs, Insititute of Geology and Mineralogy, University of Padova, **30**, 1-31

Raeside, R.P., 1989, Fault systems in the Cape Breton Highlands, Proceedings of the LITHOPROBE-East Transect Meeting, St. John's Newfoundland, 44-48.

Raeside, R.P., and Barr, S.M., 1990, Geology and tectonic development of the Bras d'Or suspect terrane, Cape Breton Island, Nova Scotia, Canadian Journal of Earth Sciences, **27**, 1371-1381.

Raeside, R.P., and Barr, S.M., 1992, Geology of the northern and eastern Cape Breton Highlands, Nova Scotia, Geological Survey of Canada Paper 89-13, 39 p.

Raeside, R.P., Barr, S.M., White, C.E., and Dennis, F.A.R., 1986, Geology of the northernmost Cape Breton Highlands, Nova Scotia; in Current Research, Part A, Geological Survey of Canada, Paper 86-1a, 291-296.

Ramos, V.A., Jordan, T.A., Allmendinger, R.W, Mpodozis, C. Kay, S.M., Cortes, J.M., and Plama, M., 1986, Paleozoic terranes of the central Argentine-Chilean Andes, Tectonics, 5, 855-880.

Rankin, D.W., 1976, Appalachian salients and recesses: Late Precambrian continental breakup and the opening of the Iapetus Ocean, Journal of Geophysical Research, **81**, 5505-5619.

Rankin, D.W., and 9 others, 1989, Proterozoic evolution of the rifted margin of Laurentia, *in* Hatcher, R.D., Thomas, W.A., Viele, G.W (eds.), The Appalachian-Ouachita orogen in the United States, Geological Society of Amer, The Geology of North America, **F-2**, 7-100.

Rankin, D.W., and 11 others, 1993, Proterozoic rocks east and southeast of the Grenville Front, *in* Reed, J.C et al. (eds.), Precambrian conterminous U.S., Geological Society of America, The Geology of North America, **C-2**, 355-461.

Ratcliffe, N.M, Burton, W.C. Sutter, J.F., and Mukasa, S.B., 1988, Stratigraphy, structural geology and thermochronology of the Northern Berkshire massif and southern Green Mountains, *in* Bothner, W.A. (ed.), Guidebook for fieldtrips in southwestern New Hampshire, New England Intercollegiate Geological Conference, Keene, New Hampshire, Durham Univ, 1-39.

Ratcliffe, N.M., Aleinikoff, J.N., Burton, W.C., and Karabinos, P., 1991, Trondhjemitic 1.35 to 1.31 Ga gneisses of the Mount Holly Complex of Vermont: Evidence for an Elzevirian event in the Grenville basement of the U.S. Appalachians, Canadian Journal Earth Science, **28**, 77-93.

Rawnsley, C., Bohlen, S., and Hanson, G, 1987, Constraints on the cooling history of the Adirondack Mts., U-Pb investigation of metamorphic sphene; EOS Trans American Geophysical Union, **68**, p1515.

Read, J.R., 1989, Controls on evolution of Cambro-Ordovician passive margin, U.S. Appalachians, *in* Crevello, P.D., and others (eds), Controls on Carbonate Platform and Basin Development, Tulsa Oklahoma, Society of Economic Paleontologists Mineralogists, Special Publication 44, 147-165.

Reynolds, P.H., Jamieson, R.A., Barr, S.M., and Raeside, R.P., 1989, An $^{40}Ar/^{39}Ar$ study of the Cape Breton Highlands, Nova Scotia: thermal histories and tectonic implications, Canadian Journal of Earth Sciences, **26**, 2081-2091.

Richard, L.R., and Clarke, D.B., 1990, AMPHIBOL: A program for calculating structural formulae and for classifying and plotting analyses of amphiboles, American Mineralogist, **75**, 421-423.

Riley, G.C., 1962, Stephenville map-area, Newfoundland, Geological Survey of Canda, Memoir 322.

Rivers, T., and Mengel, F.C., 1988, Contrasting assemblages and petrogenetic evolution of corona and noncorona gabbros in the Grenville Province of western Labrador, Canadian Journal of Earth Sciences, **25**, 1629-1648.

Rivers, T., Martingole, J., Gower, C.F., and Davidson, A., 1989, New tectonic divisions of the Grenville Province, southeast Canadian shield, Tectonics, **8**, 63-84.

Rodgers, J., 1970, The tectonics of the Appalachians, New York, Wiley Interscience, 271 p.

Rodgers, J., 1995, Lines of basement uplifts within the external parts of orogenic belts, American Journal of Science, **295**, 455-487.

Rousell, D.H., 1981, Fabric and origin of gneissic layering in anorthositic rocks of the St. Charles sill, Ontario, Canadian Journal Earth Science, **11**, 1681-1693.

Ryan, R.J., and Zentilli, M., 1993, Allocyclic and thermochronological constraints on the evolution of the Maritimes Basin of eastern Canada, Atlantic Geoscience Society, Annual Colloquium and Symposia, Halifax, Nova Scotia, Programs with Abstracts.

Sangster, A.L., Thorpe, R.I., and Chatterjee, A.K., 1990a, A reconnaissance lead isotopic study of mineral occurrences in pre-Carboniferous basement rocks of northern and central Cape Breton Island, Nova Scotia, *in* Mineral Deposit Studies in Nova Scotia, 1, Geological Survey Canada, Paper 90-8.

Sangster, A.L., Justino, M.F., and Thorpe, R.I., 1990b, Metallogeny of the Proterozoic marble-hosted zinc occurrences at Lime Hill and Meat Cove, Cape Breton Island, Nova Scotia, *in* Sangster, A.L. (ed.), Mineral Deposit Studies in Nova Scotia, (Volume 1), Geological Survey of Canada, Paper 90-8, 31-66.

Schärer, U., Krogh, T.E., and Gower, C.F., 1986, Age and evolution of the Grenville Province in eastern Labrador from U-Pb systematics in accessory minerals, Contributions to Mineralogy and Petrology, **94**, 438-451.

Scott, D.J, St-Onge, M.R., 1995, Constraints on Pb closure termperature in titanite based on rocks from the Ungava orogen, Canada: Implications for U-Pb geochronlogy and P-T-t path deteminations, Geology, **23**, 1123-1126.

Sevigny, J.H., and Hanson, G.N., 1993, Orogenic evolution of the New England Appalachians of soutwestern Connecticut, Geological Society of America Bulletin, **105**, 1591-1605.

Sharma, A., and Jenkins, D.M., 1991, Experimental reversals for the Al-content in pargasitic amphiboles coexisting with plagioclase, diopside, and quartz, Geological Society of America, Abstracts with Programs, **23**, 94.

Silver, L.T., and Deutsch, S., 1963, Isotopic investigations of zircons in Precambrian igneous rocks of the Adirondack Mountains, New York, Geological Society of America, Program with Abstracts, **76**, 150-151.

Smith, J.V., and Stenstrom, R.C., 1965, Electron-excited luminescence as a petrologic tool, Journal of Geology, **73**, 627-635

Smith, P.K., and Macdonald, A.S., 1981, The Fisset Brook Formation at Lowland Cove, Inverness County, Nova Scotia; Nova Scotia Department of Mines and Energy, Paper 81-1, 18 .

Smith, P.K., and Macdonald, A.S., 1983a, The geology of the Red River Anorthosite Complex, Inverness and Victoria Counties, Nova Scotia; Nova Scotia Department of Mines and Energy, Paper 83-1.

Smith, P.K., and Macdonald, A.S., 1983b, Geological map of the geology of the Red River anorthosite complex, Inverness and Victoria Counties, Nova Scotia, Nova Scotia Department of Mines and Energy, Map 83-4, scale 1:25,000.

Snee, L.W., Sutter, J.F., and Kelly, W.C., 1988, Thermochronology of economic mineral deposits: dating the stages of mineralisation at Panasquiera, Portugal, by high-prescision $^{40}Ar/^{39}Ar$ age spectrum techniques on muscovite, Economic Geology, **83**, 335-354.

Soper, N.J., Strachan, R.A., Holdsworth, R.E., Gayer, R.A., and Greiling, R.O., 1992, Sinistral transpression and the Silurian closure of Iapetus, Journal of the Geological Society, **149**, 871-880.

Stacey, J.S., and Kramers, J.D., 1975, Approximation of terrestrial lead isotope evolution by a two stage model, Earth and Planetary Science Letters, **26**, 207-221.

Stockmal, G.S., Colman-Sadd, S.P., Keen, C.E., O'Brien, S.J., and Quinlan, G., 1987, Collision along an irregular margin: a regional plate tectonic interpretation of the Canadian Appalachians, Canadian Journal of Earth Sciences, **24**, 1098-1107.

Stockmal, G.S., Colman-Sadd, S.P., Keen, C.E., Marillier, F., O'Brien, S.J., and Quinlan, G.M., 1990, Deep seismic structure and plate tectionic evolution of the Canadian Appalachians, Tectonics, **9**, pg.45-62.

Streckeisen, A., 1976, To each plutonic rock its proper name, Earth Science Reviews, **12**, 1-33.

Thomas, W.A., 1977, Evolution of Appalachian-Ouachita salients and recesses from reentrants and promontories in the continental margin, American Journal of Science, **277**, 1233-1278.

Thompson, R.N., and Fowler, M.B., 1986, Subduction-related shoshonitic and ultrapotassic magmatism: a study of Siluro-Ordovician syenites from the Scottish Caledonides, Contributions to Mineralogy and Petrology, **94**, 507-522.

Tosdal, R.M., 1996, The Amazon-Laurentian connection as viewed from the Middle Proterozoic rocks in the central Andes, western Bolivia and northern Chile, Tectonics, **15**, 827-842.

Tucker, R.D., Råheim, A., Krogh, T.E., and Corfu, F., 1987, Uranium-lead zircon and titanite ages from the northern portion of the Western Gneiss Region, south-central Norway, Earth and Planetary Science Letters, 81, 203-211.

Turner, F.J., 1968, Structural analysis of metamorphic tectonites, McGraw-Hill, New York 545 p.

Turner, F.J., 1981, Metamorphic petrology: Mineralogical, field and tectonic aspects, Second Edition, McGraw-Hill, NY.

Valières, A, Hubert, C., and Brooks, C., 1978, A slice of basement in the western margin of the Appalachian Orogen, Sainte-Malachie, Quebec, Canadian Journal Earth Science, **15**, 1242-1249.

van Breemen, O., and Davidson, A., 1990, U-Pb zircon and baddeleyite ages from the Central Gneiss Belt, Ontario, *in* Radiomentric age and isotopic studies, Report 3, Geological Survey Canada, Paper89-2, 85-92.

van Breemen, O., and Hanmer, S., 1986, Zircon morphology and U-Pb geochronology in active shear zones: Studies on syntectonic intrusions along the western boundary of the CMB, Grenville Province, Ontario, *in* Current Research, Part B, Geological Survey Canada, Paper 86-1b, 775-784.

van Breemen, O., Davidson, A., Loveridge, W.D., and Sullivan, R.D., 1986, U-Pb zircon chronology of Grenville tectonites, granulites, and igneous precursors, Parry Sound, Ontario, *in* Moore, J.M., Davidson, A., Baer, A.J. (eds.)., The Grenville Province, Geological Association Canada, Special Paper 31, 191-208.

van Breemen, O., and Higgins, M.D., 1993, U-Pb zircon age of the southwest lobe of the Havre-Saint-Pierre Anorthosite Complex, Grenville, Province, Canada, Canadian Journal of Earth Sciences, **30**, 1453-1457.

van Staal, C.R., 1994, Brunswick subduction complex in the Canadian Appalachians: Record of the Late Ordovician to Late Silurian collision between Laurentia and the Gander margin of Avalon, Tectonics, **13**, 946-962.

van Staal, C.R., and Fyffe, L.R., 1991, Dunnage and Gander Zones, New Brunswick, Canadian Appalachian Region , Geoscience Report, 91-2, **39**, New Brunswick Department of Natural Res, Fredricton .

Vavra, G., 1990, On the kinematics of zircon growth and its petrological significance: a cathodoluminescence study, Contributions to Mineralogy and Petrology, **106**, 90-99.

Vernon, R.H., 1996, Problems with inferring P-T-t paths in low-P granulite facies rocks, Journal of Metamorphic Geology, **14**, 143-153.

Waldron, J.W.F, Milne, J.V., 1991, Tectonic history of the central Humber Zone, western Newfoundland Appalachians: post-Taconian deformation in the Old Man's Pond area, Canadian Journal of Earth Sciences, **28**, 398-410.

Waldron, J.W.F., and Stockmal, G.S., 1994, Structural and tectonic evolution of the Humber Zone, western Newfoundland 2. A regional model for Acadian thrust tectonics, Tectonics, **13**, 1498-1513.

Watson, E.B., 1979, Zircon saturation in felsic liquids: experimental data and applications to trace element geochemistry, Contributions to Mineralogy and Petrology, **57**, 407-419.

Watson, E.B., and Harrison, T.M., 1983, Zircon saturation revisited: temperature and composition effects in a variety of crustal magma types, Earth and Planetary Science Letters, **64**, 295-304.

Whalen, J.B., Jenner, G.A., Hegner, E., and Longstaffe, F.J., 1994, Geochemical and isotopic (Nd, O, and Pb) constraints on granite sources in the Humber and Dunnage zones, Gaspesie, Quebec, and New Brunswick: implications for tectonics and crustal structure, Canadian Journal of Earth Sciences, **31**, 323-340.

Whitney, P.R., 1992, Charnockites and granites of the western Adirondacks, New York, USA, A differentiated A-type suite, Precambrian Research, **57**, 1-19.

Whitney, P.R., and McLelland, J.M., 1973, Origin of coronas in metagabbros of the Adirondack Mts., NY, Contributions to Mineralogy and Petrology, **39**, 81-98.

Wiebe, R.A., 1972, Igneous and tectonic events in northeastern Cape Breton Island, Nova Scotia, Canadian Journal of Earth Sciences, **9**, 1262-1277.

Wiebe, R.A., 1978, Anorthosite and related plutons, southern Nain complex, Labrador, Canadian Journal Earth Science, **15**, 1326-1340.

Wiebe, R.A., 1979, Anorthosite dikes, sourhtern Nain Complex, Labrador, American Journal Science, **279**, 394-410.

Wiebe, R.A., 1988, Replenishment and fractionation in a massive anorthosite pluton, Paul Island, Nain, Labrador, Geological Association Canada, Program with Abstracts, **13**, A134.

Wiebe, R.A., 1990, Evidence for unusually feldspathic liquids in the Nain complex, Labrador, American Mineralogist, **75**, 1-12.

Williams, H., 1975, Structural succession, nomenclature, and interpretation of transported rocks in western Newfoundland, Canadian Journal of Earth Sciences, **12**, 1874-1894.

Williams, H., 1978, Tectonic lithofacies map of the Canadian Appalachians, Memorial University of Newfoundland, St. John's Newfoundland, Map 1, scale 1:1000000.

Williams, H., 1979, Appalachian Orogen in Canada, Canadian Journal of Earth Sciences, **16**, 792-807.

Williams, H., and Hatcher, R.D., 1982, Suspect terranes and accretionary history of the Appalachian orogen, Geology, **10**, 530-536.

Williams, H., and Hatcher, R.D., 1983, Appalachian suspect terranes, *in* Contributions to the tectonics and geophysics of mountain chains, Hatcher, R.D., Williams, H., and Zietz, I., eds., Geological Society of America, Memoir **158**, 33-53.

Williams, H., Colman-Sadd, S.P., and Swinden, H.S., 1988, Tectonostratigraphic subdivisions of central Newfoundland, *in* Current Research, Part B, Geological Survey Canada, Paper 89-1b, 55-66.

Williams, H., and Stevens, R.K., 1974, The ancient continental margin of eastern North America, in Burk, C.A., and Drake, C.L., eds., The geology of continental margins, New York, Springer - Verlag, 781-796.

Williams, I.S., 1992, Some observations on the use of zircon U-Pb geochronology in the study of granitic rocks, Transactions of the Royal Society of Edinburgh, Earth Sciences, **83**, 447-458.

Wilson, M., 1989, Igneous petrogenesis: A global tectonic approach, Chapman and Hall, London, 466 p.

Winchester, J.A., and Floyd, P.A., 1976, Geochemical magma type discrimination: application to altered and metamorphosed basic igneous rocks, Earth Planet Science Letters, **28**, 459-469.

Winchester, J.A., and Floyd, P.A., 1977, Geochemical discrimination of different magma series and their differentiation products using immobile elements, Chemical Geology, **20**, 325-343.

Wintsch, R.P., Sutter, J.F., Kunk, M.J., Aleinikoff, J.N., and Boyd, J.L., 1993, Alleghanian assembly of Proterozoic and Paleozoic lithotectonic terranes in South Central New England: New Constraints from Geochronology and Petrology, *in* Cheney, J.T., and Hepburn, J.C. (eds.)., 1993 Geological Society of America Annual Meeting Field Trip Guidebook, Boston Massachussetts, Chapter H.

Wodicka, N., 1994, Middle Proterozoic evolution of the Parry Sound domain, southwestern Grenville orogen, Ontario, Structural, metamorphic, U-Pb, and $^{40}Ar/^{39}Ar$ constraints, Ph.D. thesis, Dalhousie Univ, Halifax, NS.

Wood, B.J., 1979, Activity-composition relations in CaO(Mg, Fe)Si2O6-CaAl2SiO6 clinopyroxene solid solutions, American Journal Science, **279**, 854-875.

Woussen, G., Martignole, J., and Nantel., S., 1988, The Lac-St-Jean Anorthosite in the St-Henri-de-Taillon Area (Grenville Province): A relic of a layered complex, Canadian Mineralogist, **26**, 1013-1025.

Wunapeera, A., 1992, Geology of the Cape North and Money Point Groups, northeastern Cape Breton Highlands, Nova Scotia, M.Sc. thesis, Acadia University, Wolfville, Nova Scotia, 293 p.

Yang, B., Luff, B.J., and Townsend, P.D., 1992, Cathodoluminescence of natural zircons, Journal of Physics of Condensed Matter, **4**, 5617-5624.

York, D., 1969, Least squares fitting on a straight line with correlated errors, Earth and Planetary Science Letters, **5**, 320-324.

NOTE TO USERS

Oversize maps and charts are microfilmed in sections in the following manner:

LEFT TO RIGHT, TOP TO BOTTOM, WITH SMALL OVERLAPS

The following map or chart has been microfilmed in its entirety at the end of this manuscript (not available on microfiche). A xerographic reproduction has been provided for paper copies and is inserted into the inside of the back cover.

Black and white photographic prints (17"x 23") are available for an additional charge.

UMI

47°05'00"
60°50'00"

LEGEND

Aspy Terrane and cover rocks

Carboniferous

CARB	undivided Carboniferous sedimentary units

Devonian to Carboniferous

DCF	Fisset Brook Formation - basalt, rhyolite
DCv	undifferentiated basalt, rhyolite
DCg	granite, syenogranite, syenite: Ag - Andrews Mountain granite GAg - Grande Anse granite MM - Margaree pluton
DM	shear zone rocks: mylonite, chlorite schist, breccia

Ordovician to Silurian

OSM	Money Point Group
OSBO	Belle Côte Road orthogneiss (Pleasant Bay Complex)

Hadrynian to Silurian

HSc	Cape North Group

Blair River Inlier

Carboniferous to Proterozoic (?)

CPsz	zones of intimately mixed sheared rocks 1 - foliated mafic schist: fissile chlorite-epidote schist and phyllonite 2 - black mylonite: weakly foliated, highly deformed mafic rocks with rare felsic ultramylonit 3 - mylonitized granitiod: pink to tan porphyroclastic to ultramylonitic granite and granoc

47°00'00"

Devonian to Silurian (?)

Ma
Geology of the
Northern Cape Breto

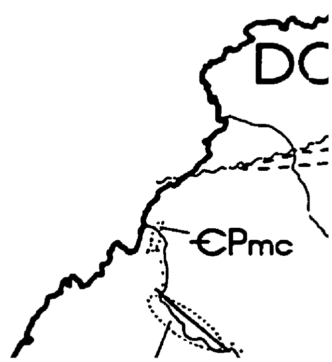

te

ap A
e Blair River inlier
ton Island, Nova Scotia

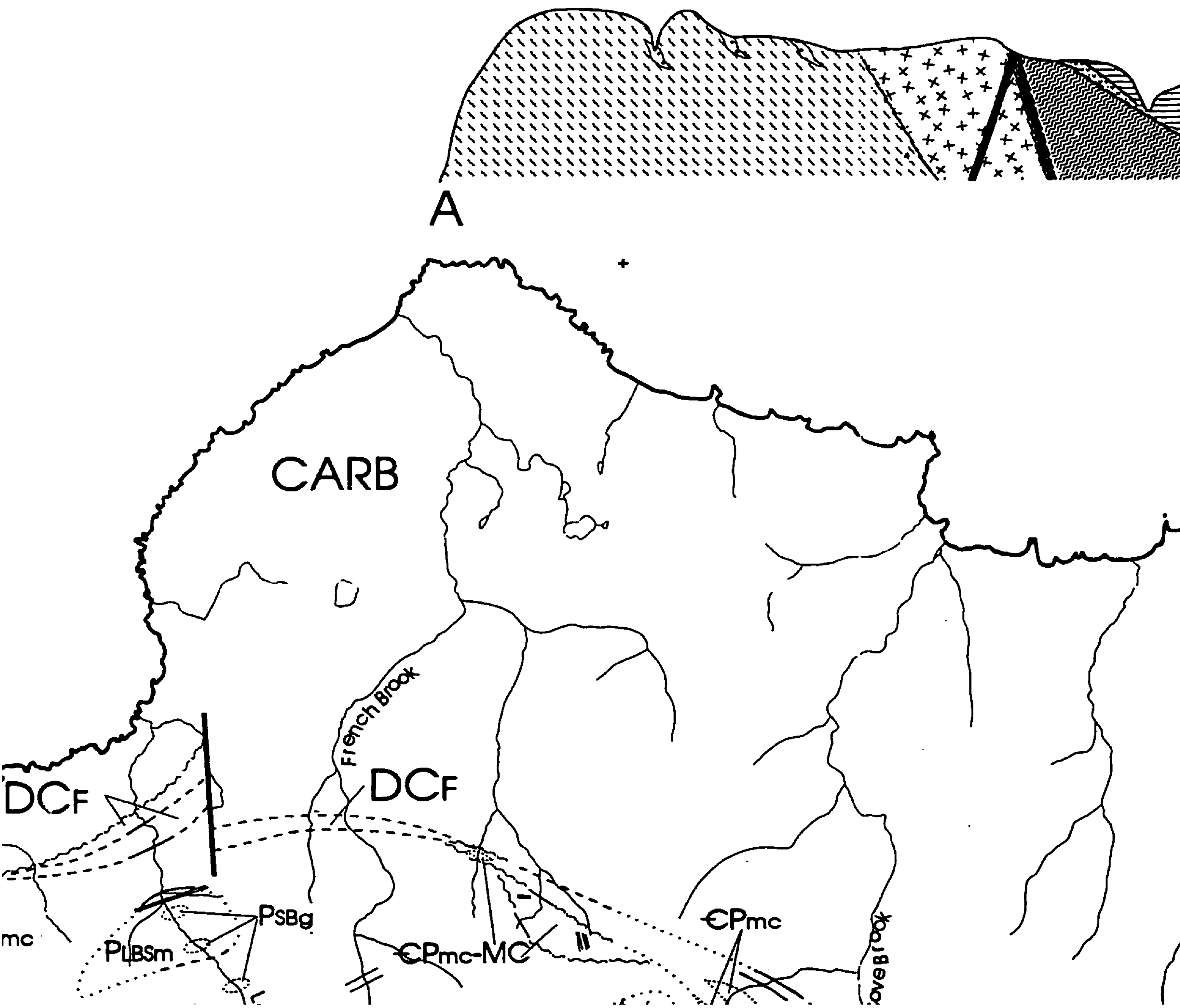

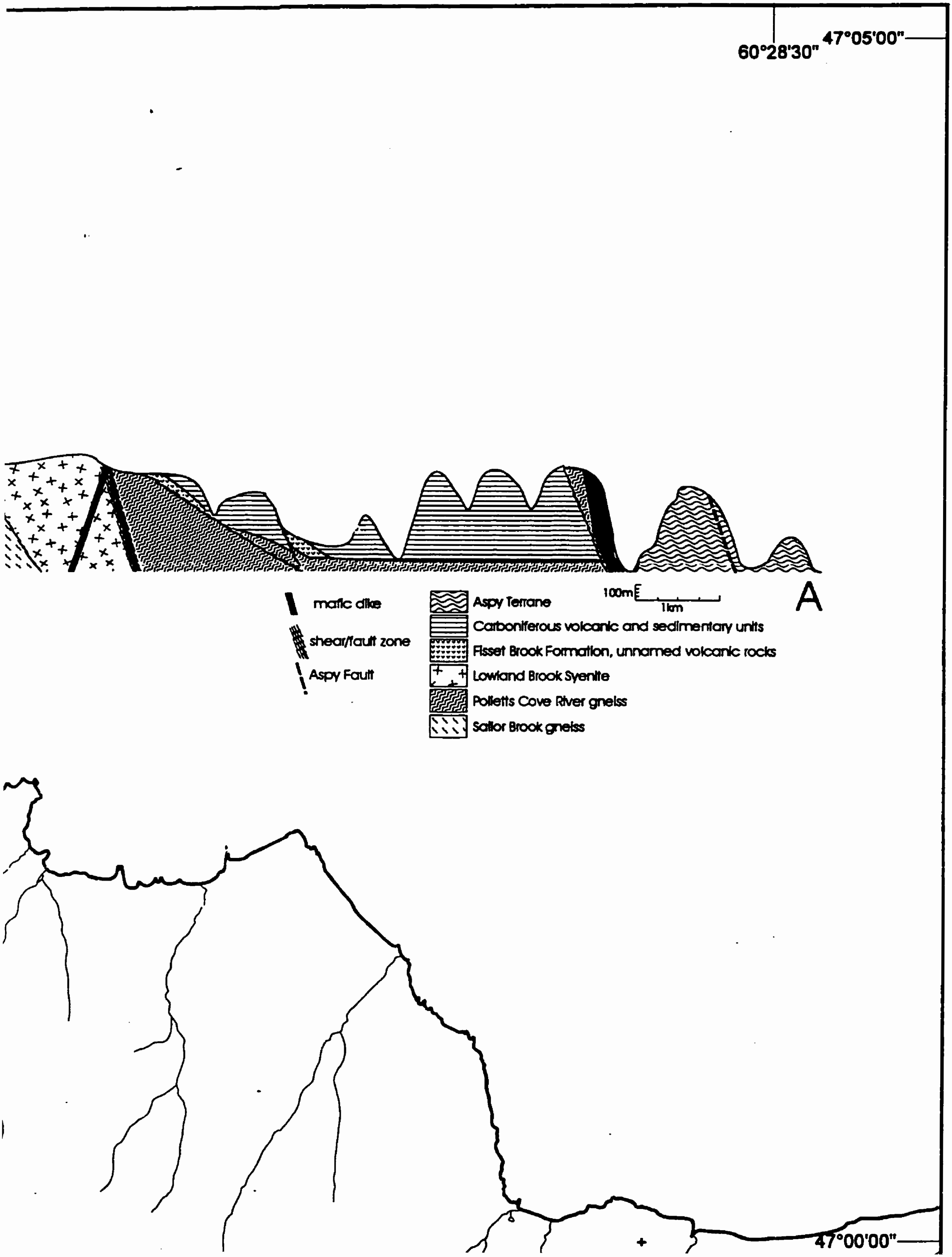
60°28'30"
47°05'00"
mafic dike
shear/fault zone
Aspy Fault
Aspy Terrane
Carboniferous volcanic and sedimentary units
Fisset Brook Formation, unnamed volcanic rocks
Lowland Brook Syenite
Polletts Cove River gneiss
Sailor Brook gneiss
100m
1km
A
47°00'00"

Carboniferous to Proterozoic (?)

CPsz zones of intimately mixed sheared rocks
1 - foliated mafic schist: fissile chlorite-epidote schist and phyllonite
2 - black mylonite: weakly foliated, highly deformed mafic rocks with rare felsic ultramy
3 - mylonitized granitiod: pink to tan porphyroclastic to ultramylonitic granite and gr

47°00'00"

Devonian to Silurian (?)

DSAr aphanitic rhyolite - fine-grained rhyolite with quartz phenocrysts

Silurian

Sg granite, syenogranite, syenite:
SB - Sammys Barren granite - pink medium-grained quart
RRs - Red Ravine syenite - red, medium-grained microcline-

SFBR Fox Back Ridge diorite and granodiorite - hornblende-p

Cambrian(?) to Proterozoic (?)

ЄPmc marble and calc-silicate rock - forsterite-spinel-phlogopite skar
MC - Meat Cove marble with or without sphalerite r

ЄPba biotite amphibolite - coarse-grained biotite+hornblende±garnet gne

Middle Proterozoic

Pmgb metagabbro - coarse grained, relict subophitic texture

POBg Otter Brook gneiss - medium- to coarse-grained, augen to flaser, biotit

PCh Charnockite - massive and layered granitoid rocks with fresh or relict hyp

PLBS Lowland Brook Syenite - brick red, coarse-grained gneissic hornble
of massive (LBSm), undeformed perthite a

PAn Anorthosite:
Red River Anorthosite Suite
1 - massive anorthosite - coarse- to medium-grained white, b
2 - leucogabbro - massive and foliated coarse-grained gabbro
3 - layered unit - cm-scale interlayered gabbro, leucogabbro, anor
4 - pyroxenite - pyroxene-apatite-ilmenite dikes and layers associate
DB - Delaneys Brook - mainly massive white anorthosite
HC - High Capes
SR - Salmon River
PCR - Pollets Cove River
} small bodies of highly deformed an

PPCR Pollets Cove River gneiss

PSBg Sailor Brook gneiss - foliated tonalitic to dioritic gneiss, foliated granit
gg - granular gneiss - unfoliated weakly layered mafic gneiss, locally

geological contact: defined, approximate, inferred

brittle fault

shear zone

ıe granite

diorite and granodiorite

>-silicate rock
ɔn

ıranitoid gneiss

salite, and diopside

ɜ with zones
thite pyroxene-bearing syenite

ɔnorthosite

red unit

ɔnorthosite

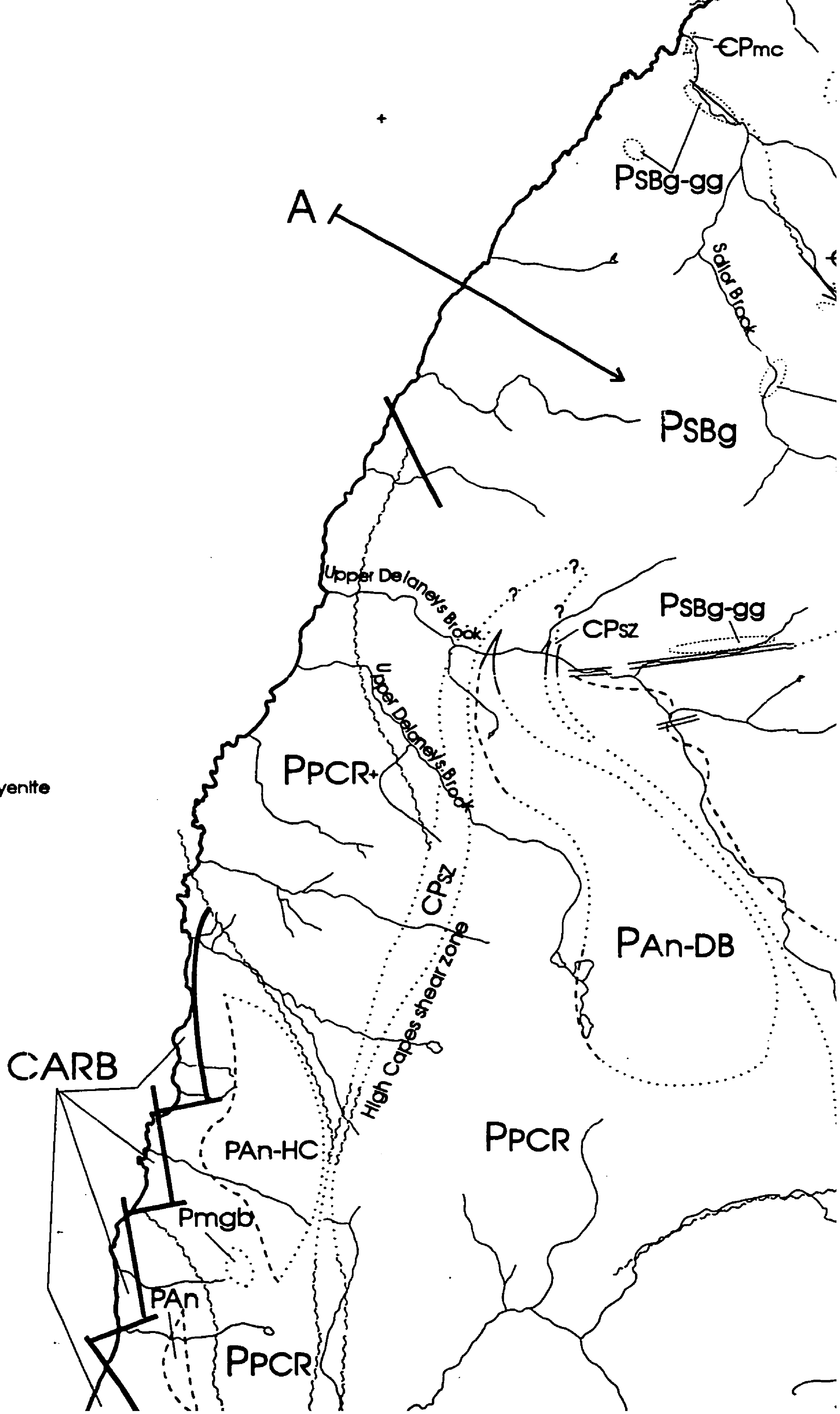

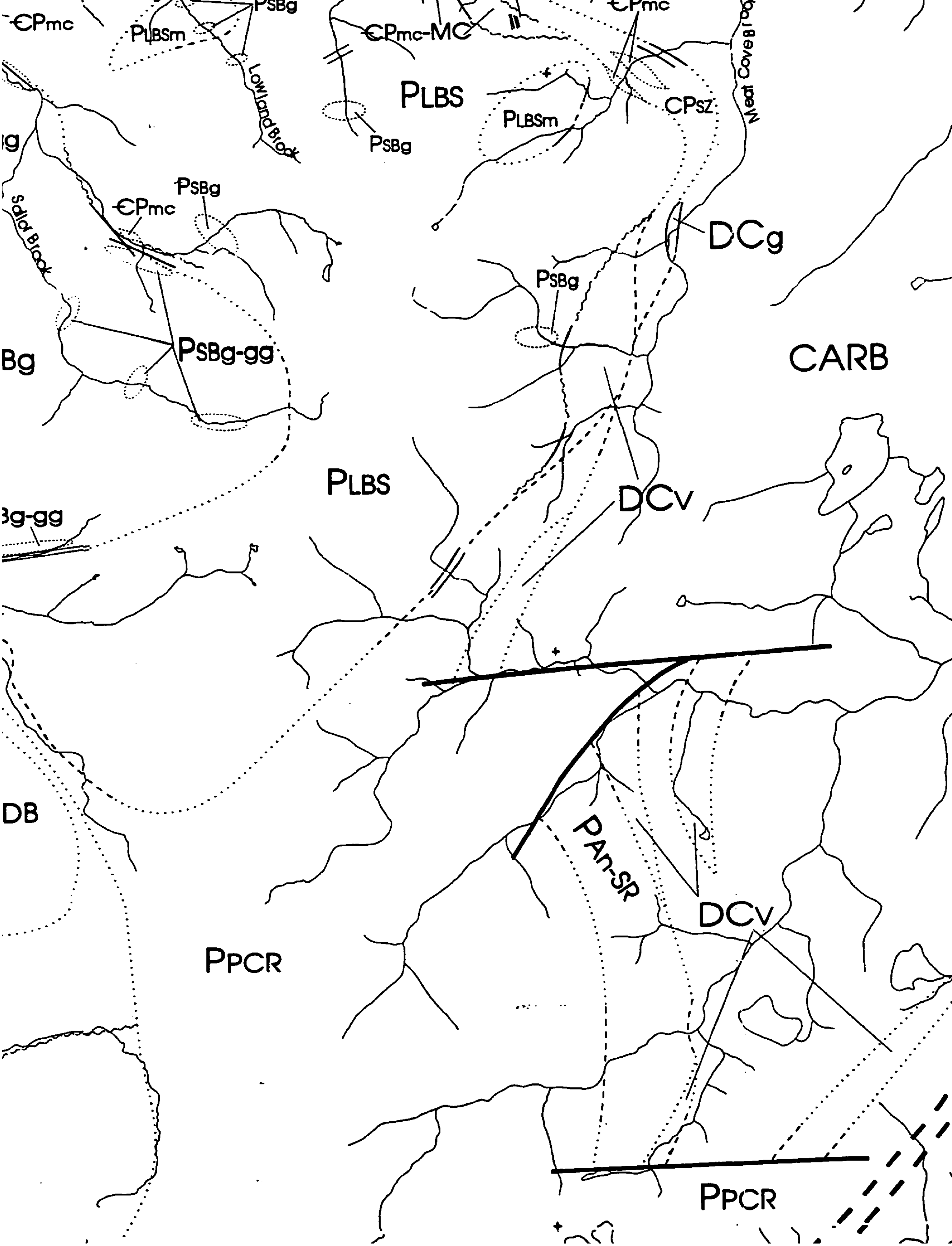

€Pmc
PSBg
PLBSm
€Pmc-MC
€Pmc
PLBS
Lowland Brook
PSBg
PLBSm
CPsz
Meat Cove Brook
Sailor Brook
€Pmc
PSBg
DCg
PSBg
PSBg-gg
Bg
CARB
PLBS
DCv
Bg-gg
DB
PAn-SR
DCv
PPCR
PPCR

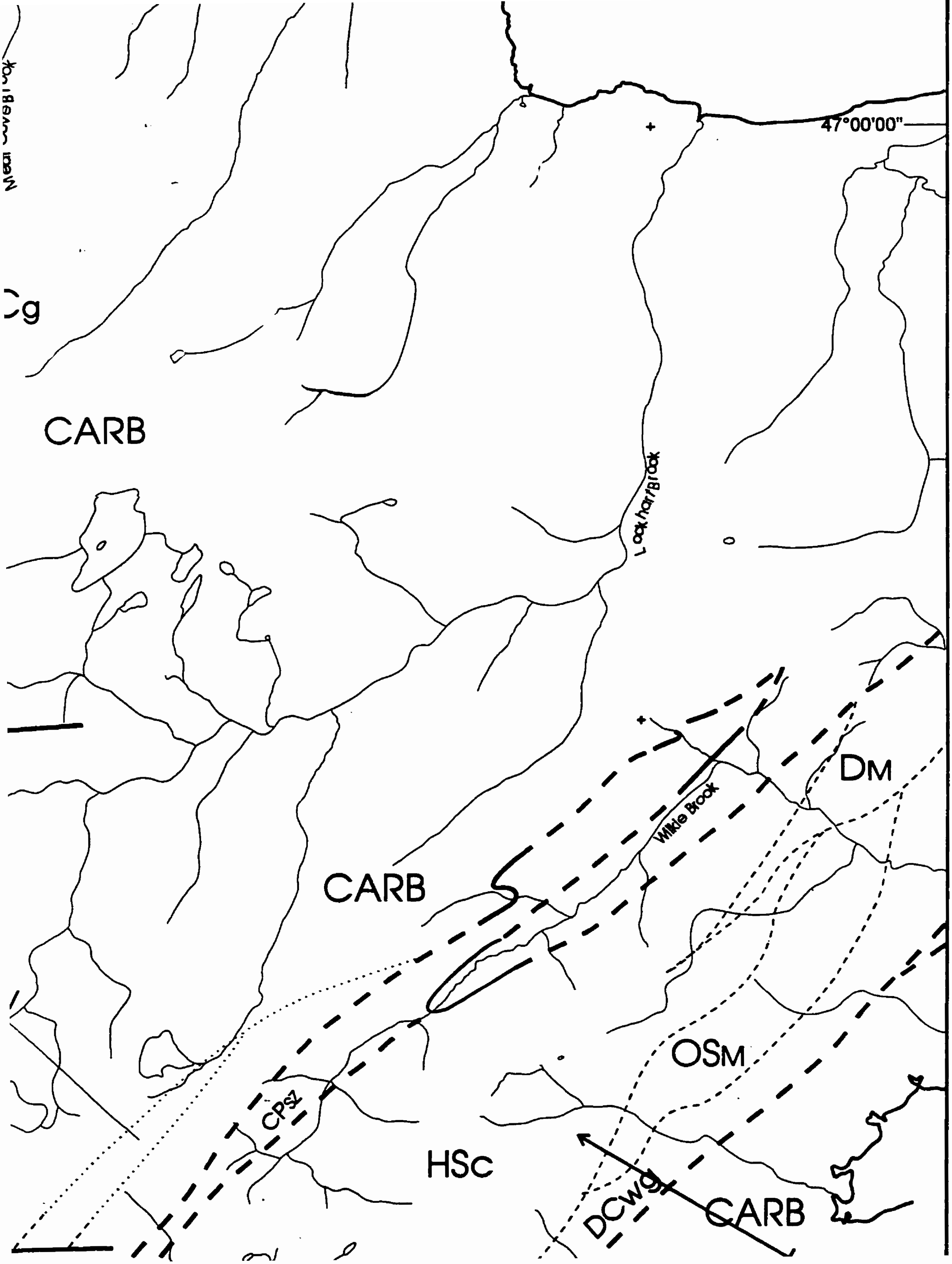
47°00'00"
Cg
CARB
Lockhart Brook
CARB
Wilkie Brook
DM
OSM
CPsz
HSc
DCWg
CARB

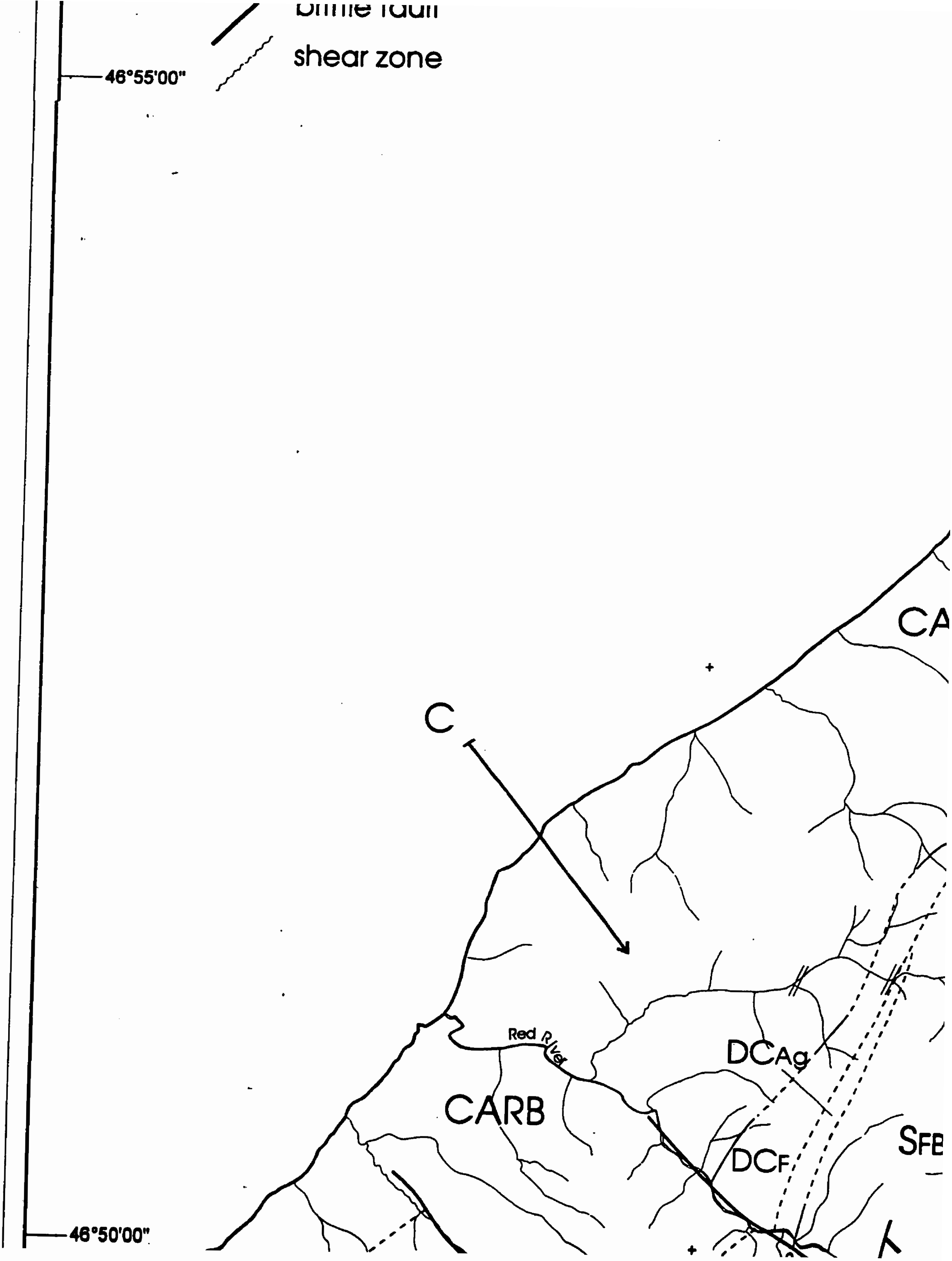
brittle fault
shear zone
46°55'00"
C
CA
Red River
DCAg
CARB
DCF
SFB
46°50'00"

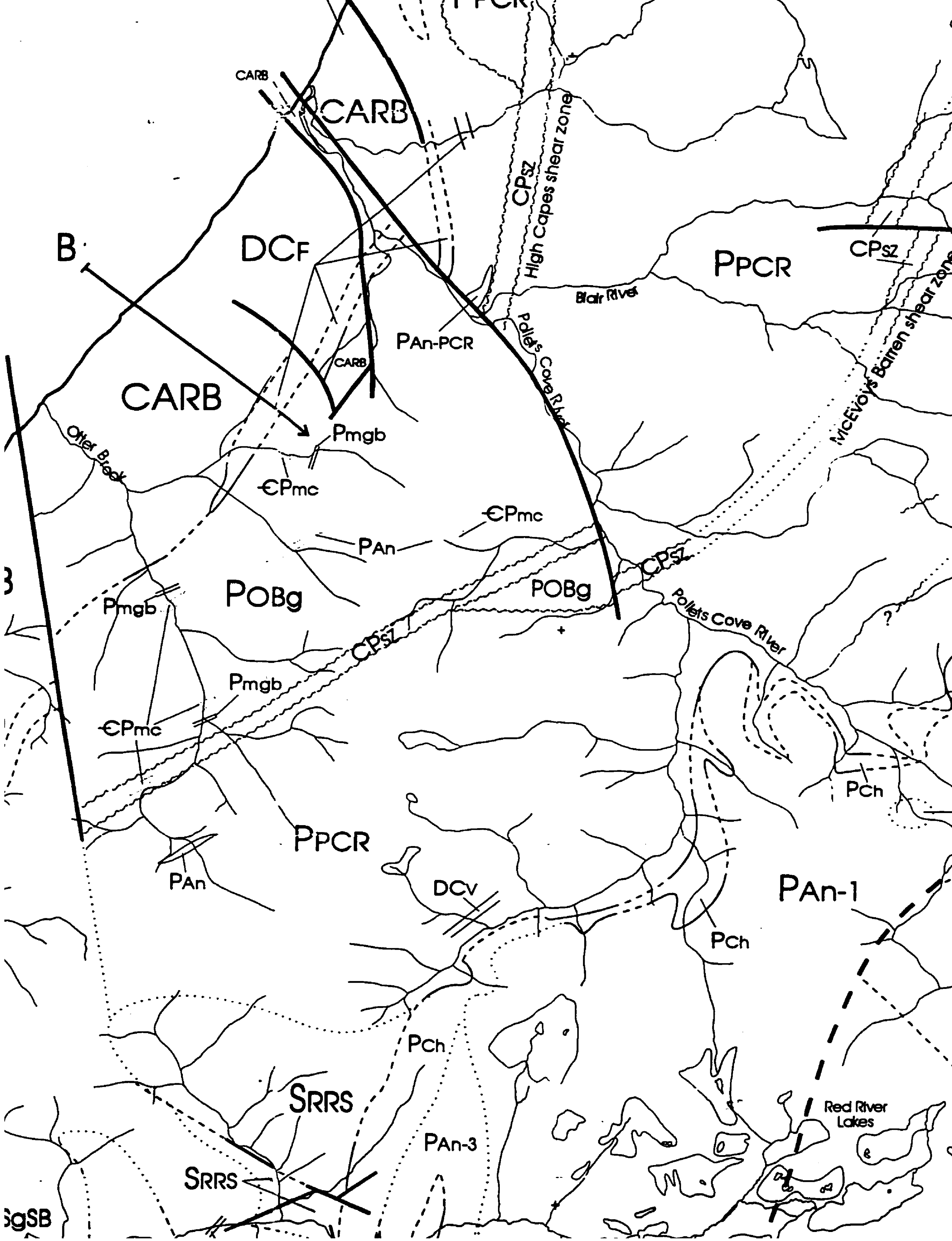

CARB
CARB
DCF
B
CARB
CARB
CPsz
High Capes shear zone
PPCR
CPsz
McEvoy's Barren shear zone
Blair River
PAn-PCR
Pollets Cove River
Pmgb
Otter Brook
€Pmc
€Pmc
PAn
POBg
POBg
CPsz
Pollets Cove River
Pmgb
CPsz
Pmgb
€Pmc
?
PCh
PPCR
PAn
DCv
PAn-1
PCh
PCh
SRRS
PAn-3
Red River Lakes
SRRS
SgSB

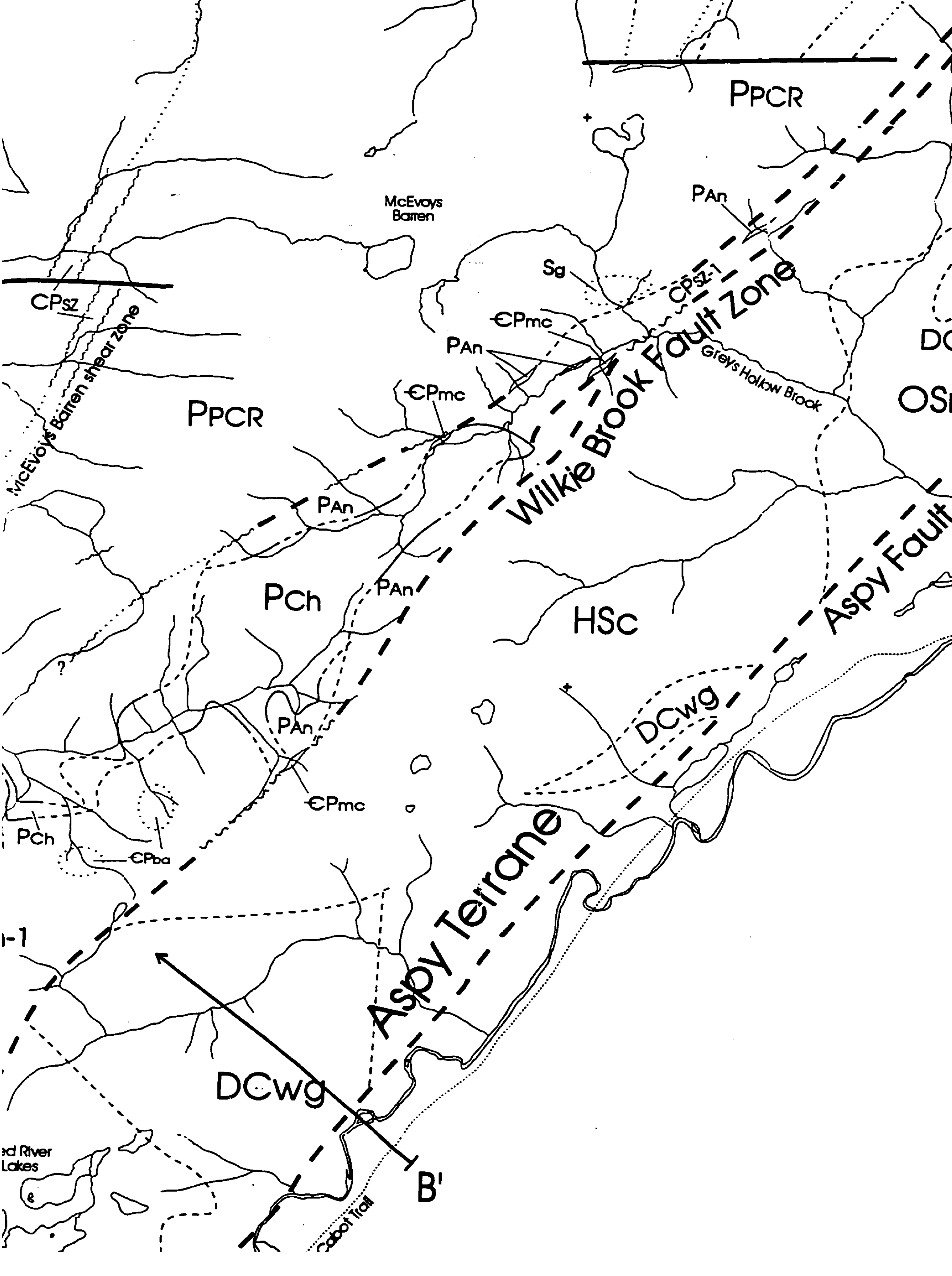

PPCR
PAn
McEvoys
Barren
Sg
CPsz-1
CPsz
McEvoys Barren shear zone
€Pmc
PAn
Wilkie Brook Fault Zone
Greys Hollow Brook
DC
OS
PPCR
€Pmc
PAn
Pch
PAn
HSc
Aspy Fault
?
DCwg
PAn
€Pmc
Pch
€Pba
Aspy Terrane
-1
DCwg
ed River
Lakes
B'
Cabot Trail

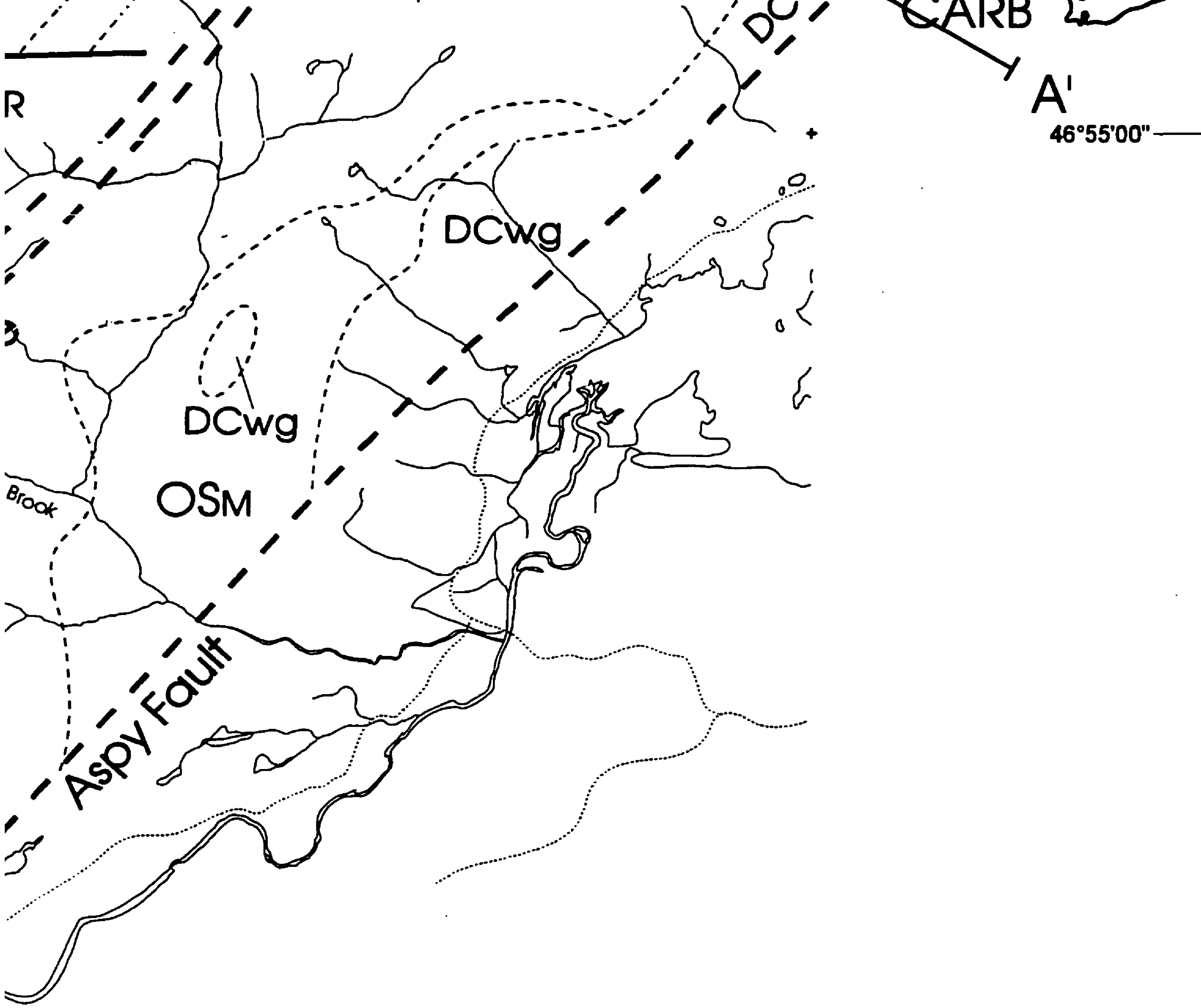

CARB
A'
46°55'00"
R
DC
DCwg
DCwg
OSM
Brook
Aspy Fault

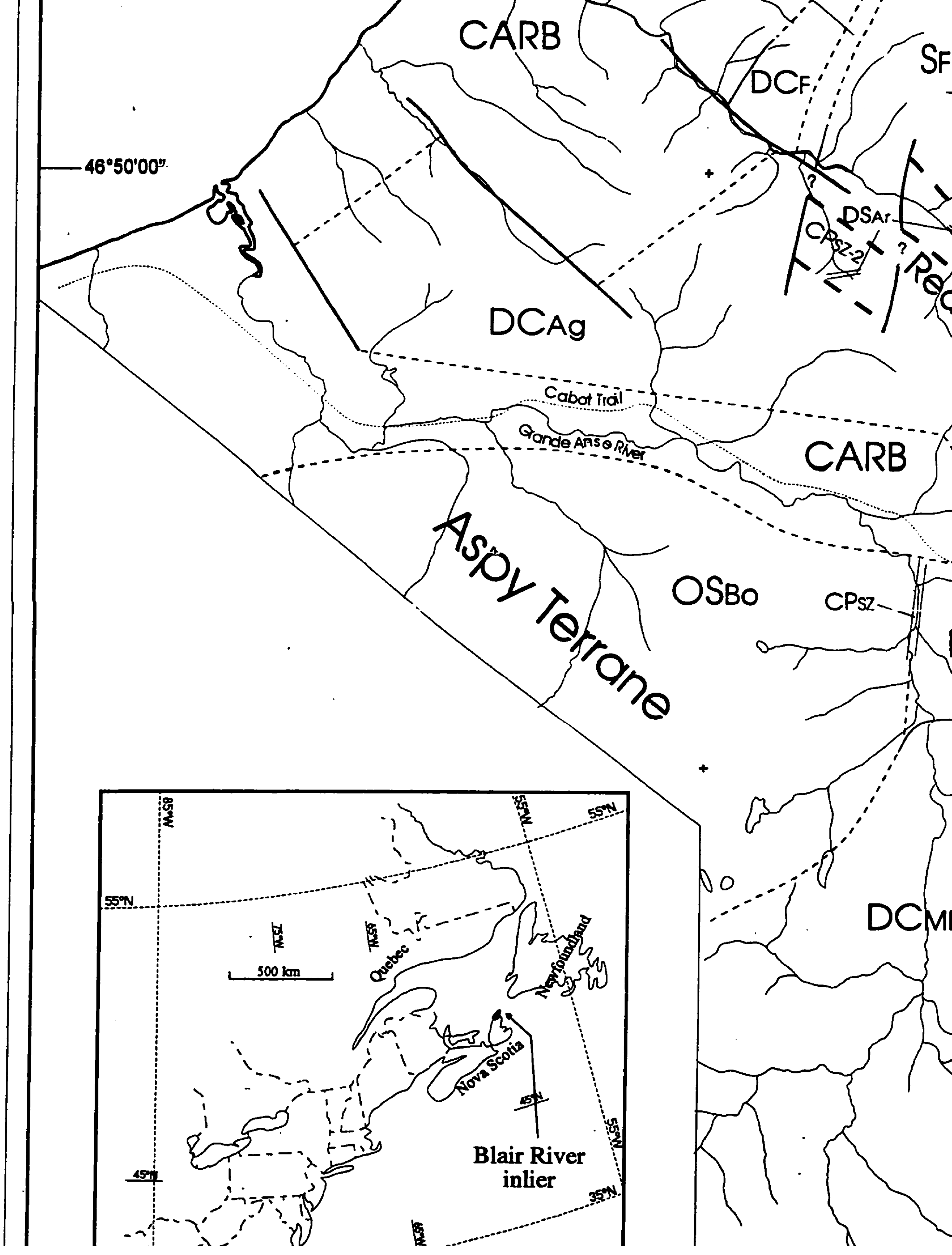
CARB
SF
DCF
46°50'00"
DSAr
CPSZ-2
DCAg
Cabot Trail
Grande Anse River
CARB
Aspy Terrane
OSBo
CPSZ
DCMI
55°N
85°W
55°W
75°W
65°W
500 km
Quebec
Newfoundland
Nova Scotia
45°N
Blair River
inlier
35°N

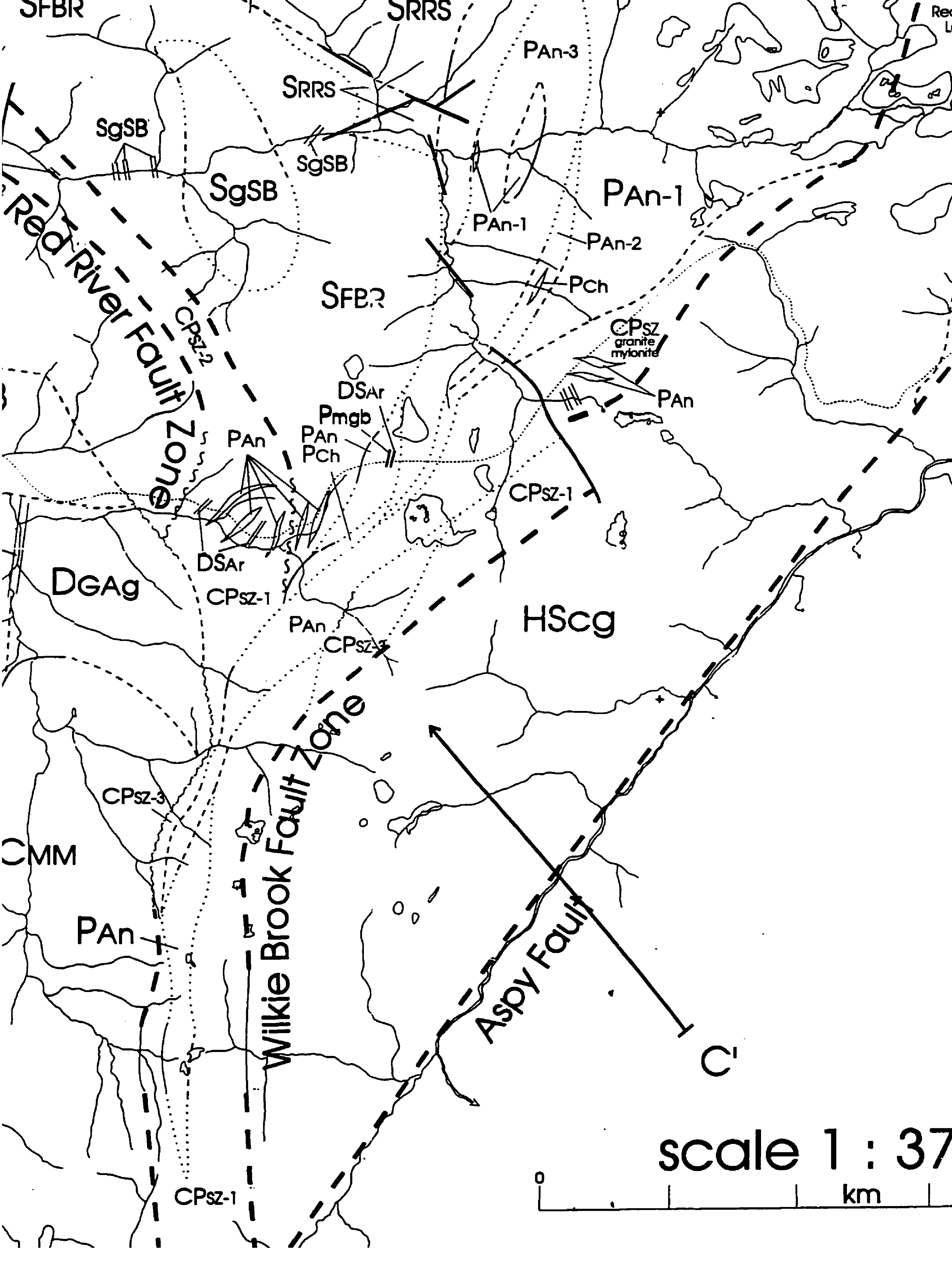
SFBR
SRRS
PAn-3
SRRS
SgSB
SgSB
SgSB
PAn-1
PAn-1
PAn-2
Red River Fault Zone
CPsz-2
SFBR
PCh
CPsz
granite
mylonite
PAn
DSAr
Pmgb
PAn
PCh
PAn
CPsz-1
DSAr
DGAg
CPsz-1
PAn
CPsz-3
HScg
CPsz-3
CMM
PAn
Wilkie Brook Fault Zone
Aspy Fault
C'
CPsz-1
scale 1 : 37
0
km

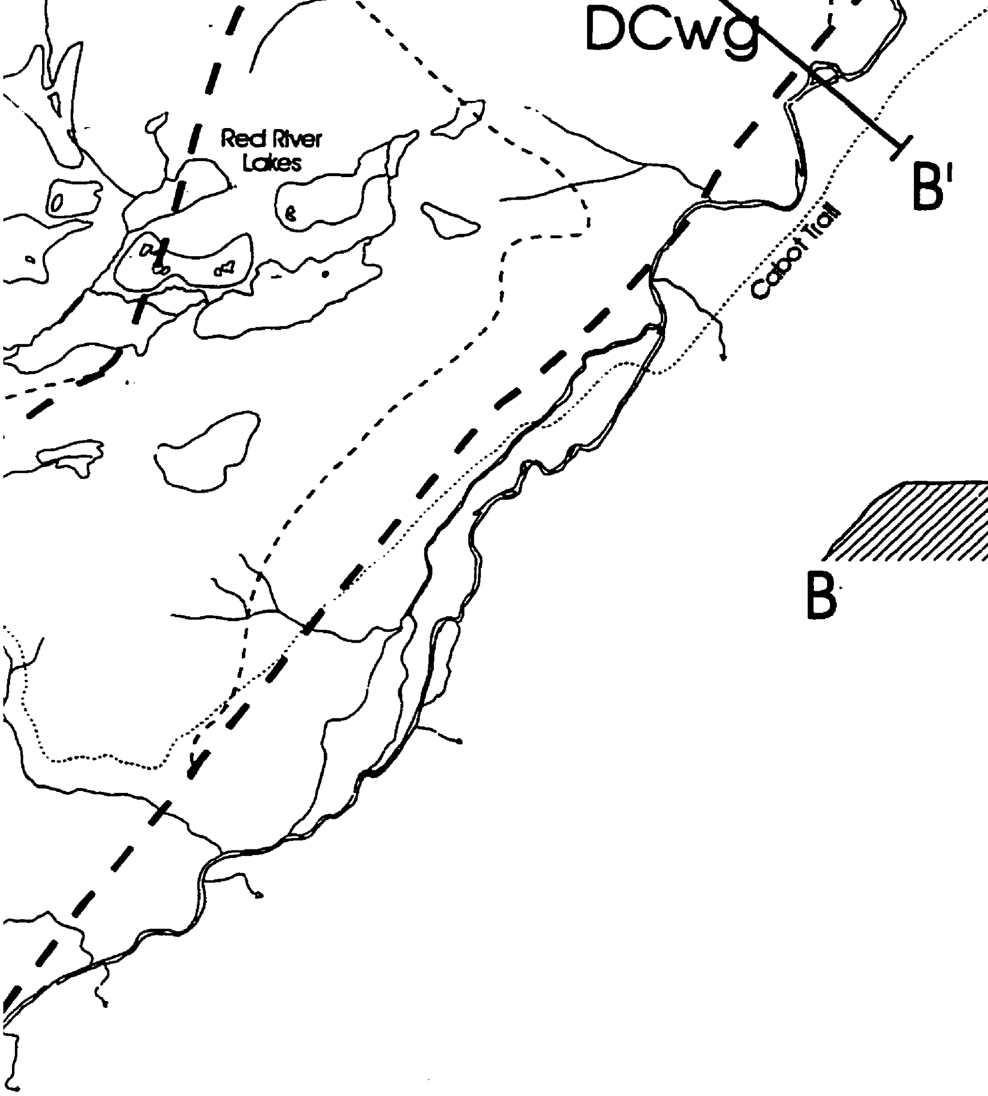

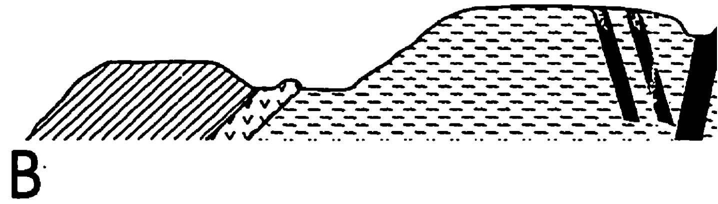

1 : 37,600

REFERENCES:

The units of the Blair River inlier are modified fro

Smith, P.K., and Macdonald, A.S.
1981: The Fisset Brook Formation at Lowland Co
and Energy, Paper 81-1, 18 p.

1983: Geological map of the Red River Anortho

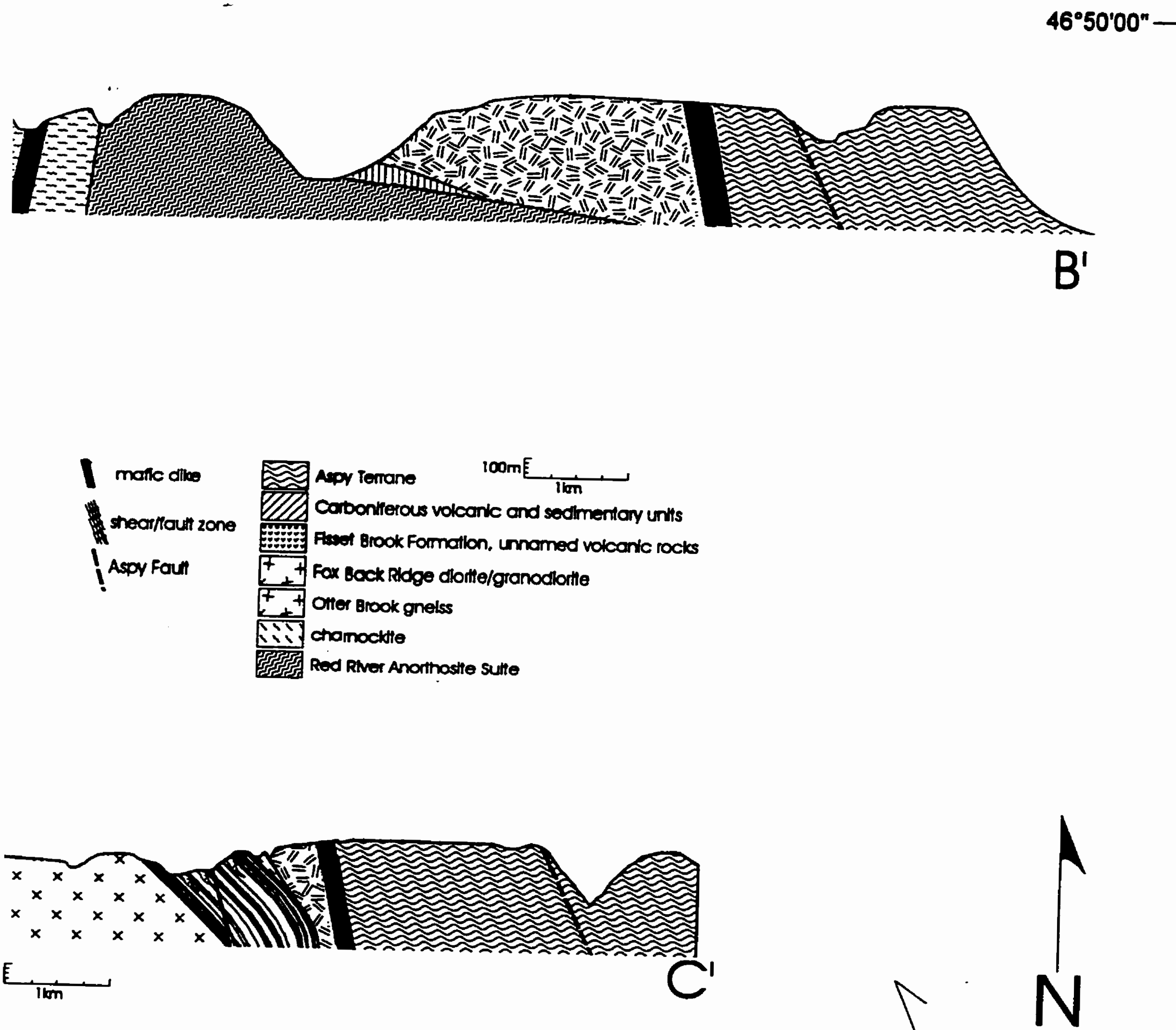

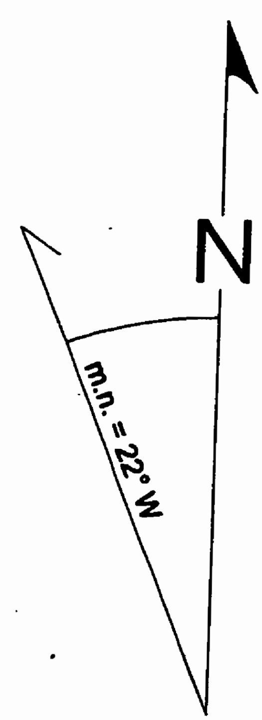

from the previous work of:

Cove, Inverness County, Nova Scotia; Nova Scotia Department of Mines

hosite Complex, Inverness and Victoria counties, Nova Scotia, Nova
D 83-4.

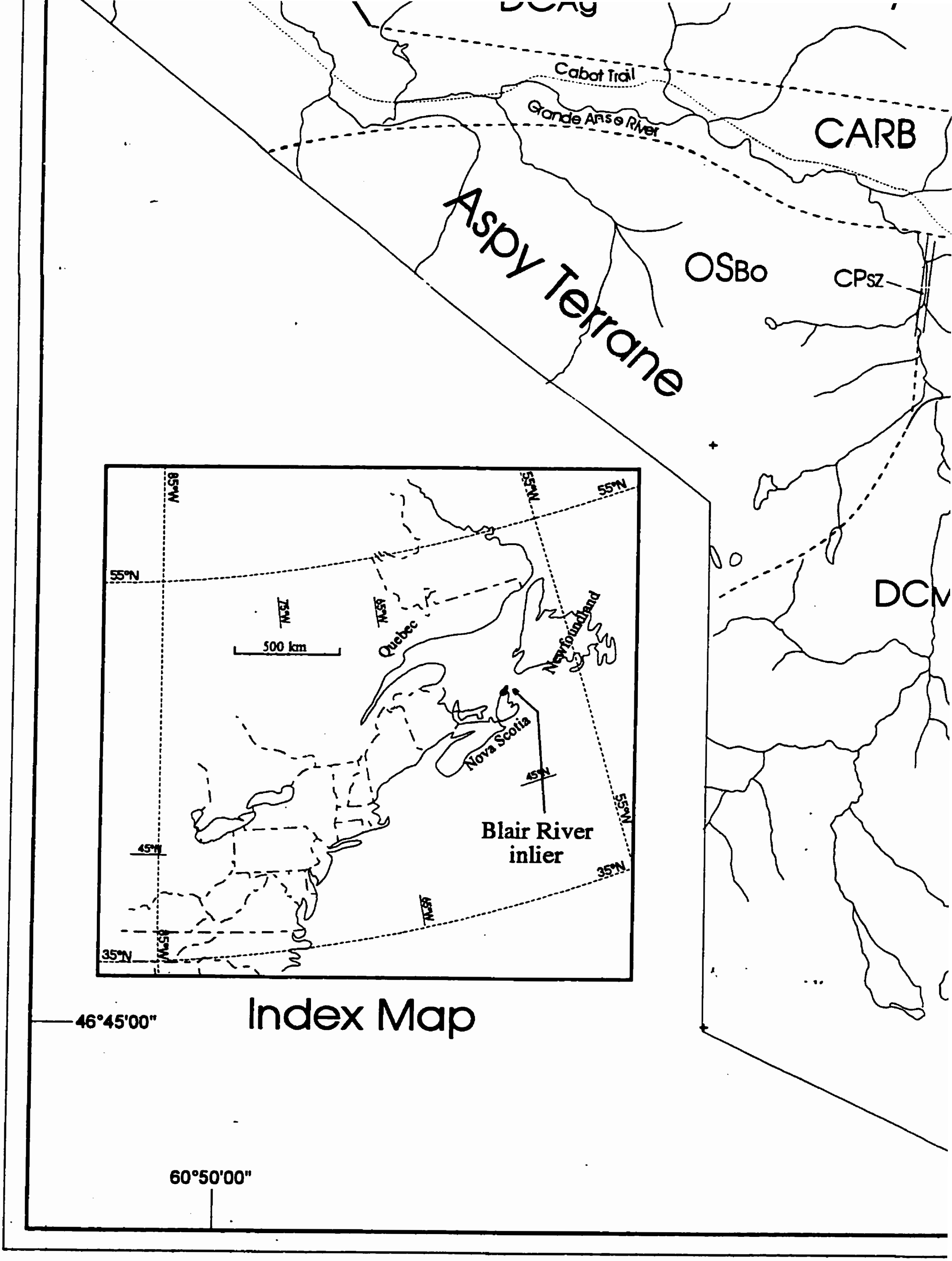
DCAg
Cabot Trail
Grande Anse River
CARB
Aspy Terrane
OSBo
CPsz
DCM
55°N
55°W
65°W
75°W
85°W
45°N
35°N
500 km
Quebec
Newfoundland
Nova Scotia
Blair River
inlier
Index Map
46°45'00"
60°50'00"

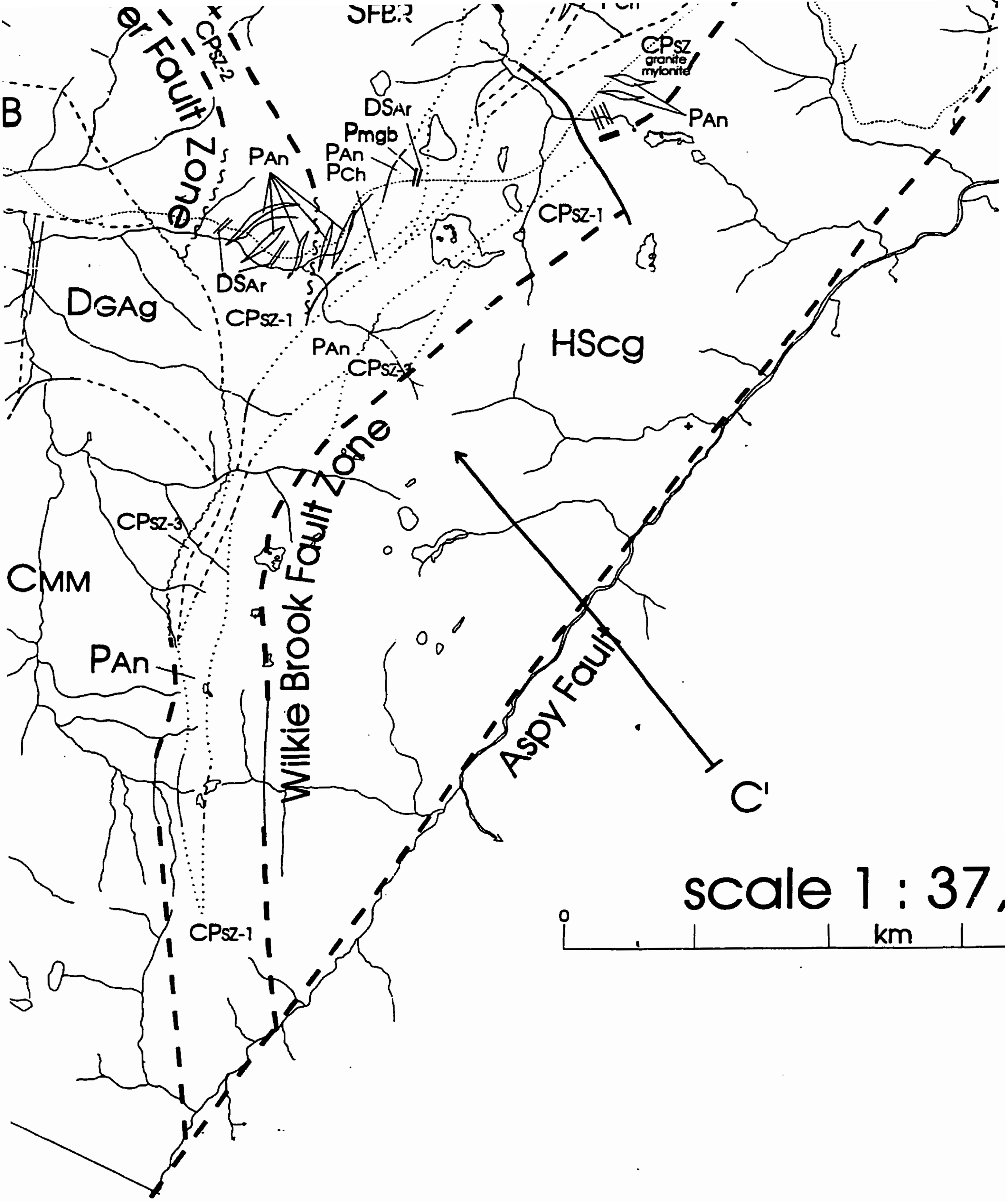
SFBR
B
er Fault Zone
CPsz-2
CPsz
granite
mylonite
DSAr
Pmgb
PAn
PAn
PCh
PAn
CPsz-1
DSAr
DGAg
CPsz-1
PAn
CPsz-3
HScg
Wilkie Brook Fault Zone
CPsz-3
CMM
PAn
Aspy Fault
C'
CPsz-1
scale 1 : 37
0
km

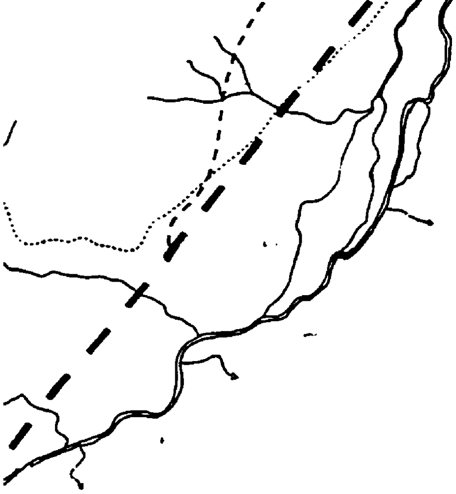

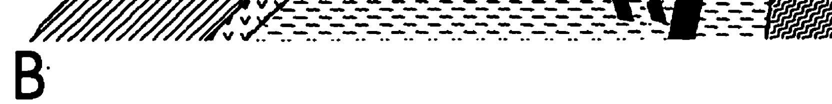

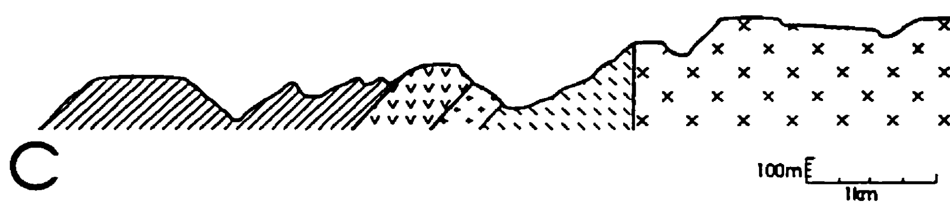

1 : 37,600

km 5

REFERENCES:

The units of the Blair River inlier are modified from the pr

Smith, P.K., and Macdonald, A.S.
1981: The Fisset Brook Formation at Lowland Cove, Inve
and Energy, Paper 81-1, 18 p.

1983: Geological map of the Red River Anorthosite Con
Scotia Department of Mines and Energy, Map 83-4.

Barr, S.M., and Raeside, R.P.
1992: Geology of the northern and eastern Cape Breto
Paper 89-14, 39 p.

Bekkers, R.P.
1993: Petrology and petrogenesis of the anorthosite an
Breton Island, Nova Scotia, (M.Sc. Thesis), Acadia Unive

- mafic dike
- shear/fault zone
- Aspy Fault

- Aspy Terrane
- Carboniferous volcanic and sedimentary units
- Fisset Brook Formation, unnamed volcanic rocks
- Fox Back Ridge diorite/granodiorite
- Otter Brook gneiss
- charnockite
- Red River Anorthosite Suite

100m 1km

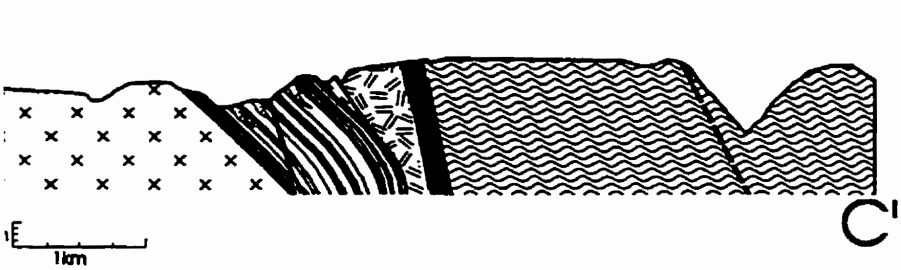

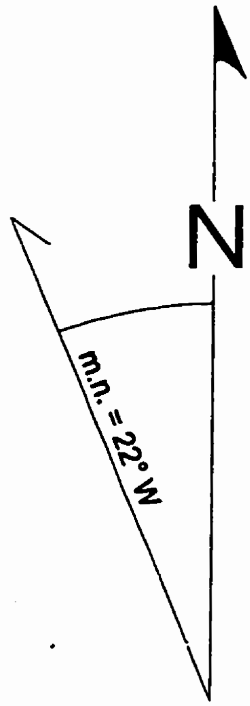

from the previous work of:

Cove, Inverness County, Nova Scotia; Nova Scotia Department of Mines

thosite Complex, Inverness and Victoria counties, Nova Scotia, Nova
ıp 83-4.

Cape Breton Highlands, Nova Scotia, Geological Survey of Canada,

rthosite and associated rocks in the Blair River Complex, Northern Cape
adia University, Wolfville, Nova Scotia, 226 p.

46°45'00"

60°28'30"

NOTE TO USERS

Oversize maps and charts are microfilmed in sections in the following manner:

LEFT TO RIGHT, TOP TO BOTTOM, WITH SMALL OVERLAPS

The following map or chart has been microfilmed in its entirety at the end of this manuscript (not available on microfiche). A xerographic reproduction has been provided for paper copies and is inserted into the inside of the back cover.

Black and white photographic prints (17"x 23") are available for an additional charge.

UMI

Stru
Nort

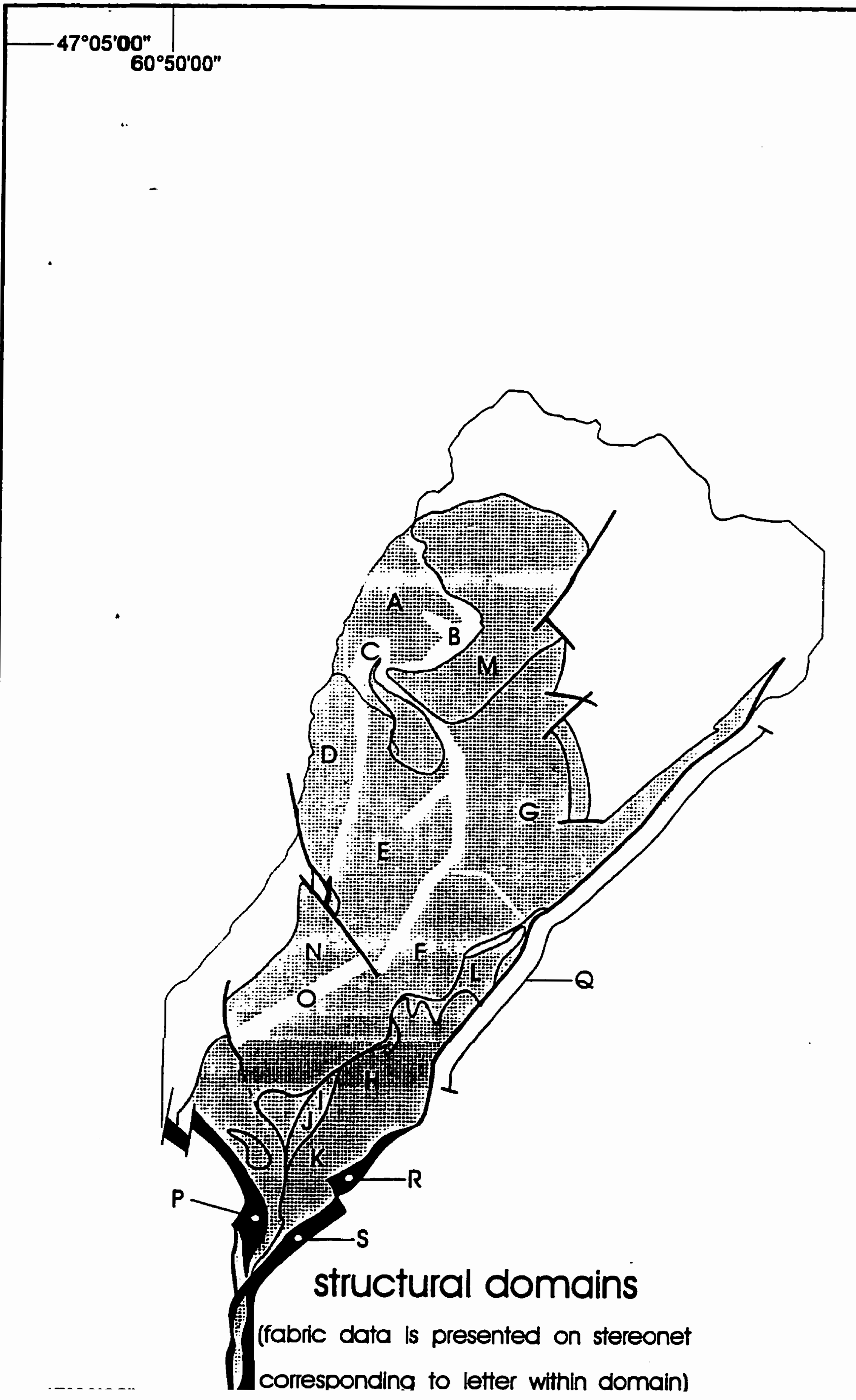

structural domains

(fabric data is presented on stereonet corresponding to letter within domain)

Map B

;cture of the Blair River inlie

ern Cape Breton Island, Nova Scoti

A

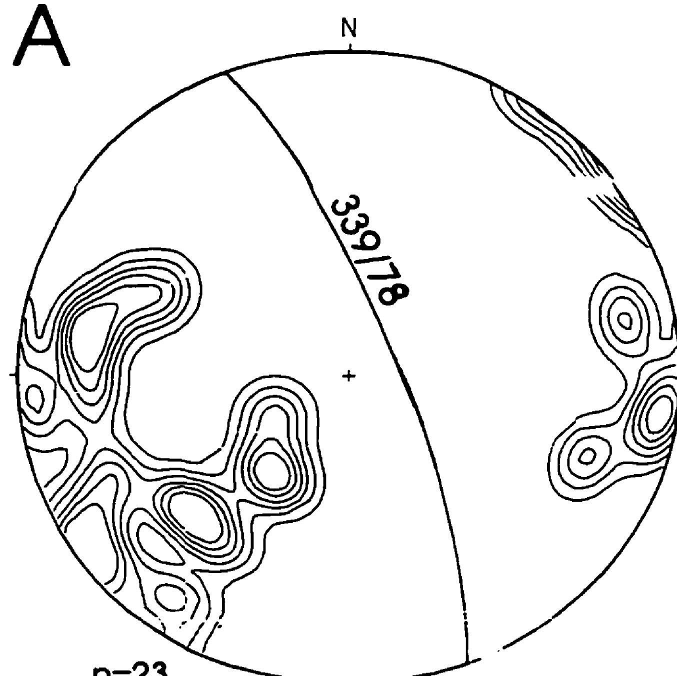

n=23
contours: 1,2,3,4,5,6%
amphibolite facies assemblag
in gneissic foliation in Sailor Bro
gneiss

B

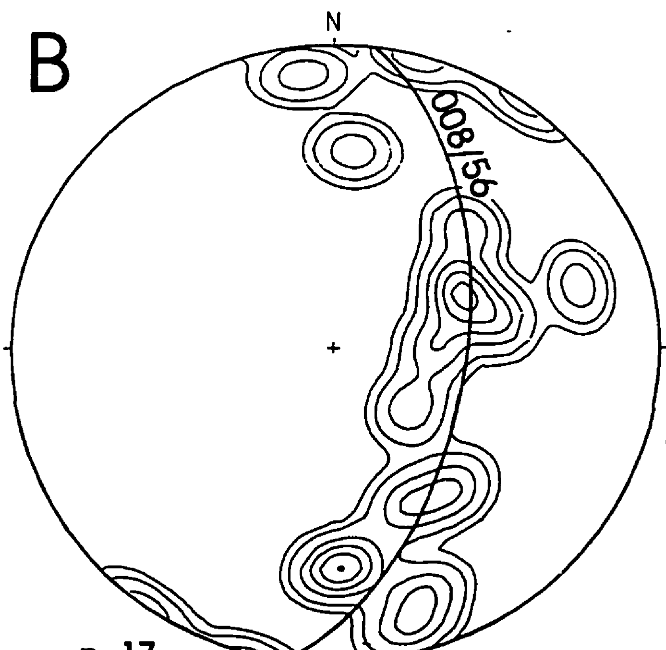

n=17
contours: 1,2,4,5,6,7%
granular compositional
layering in Sailor Brook
gneiss

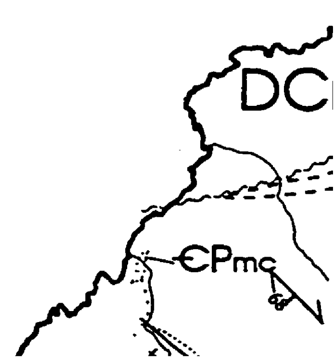

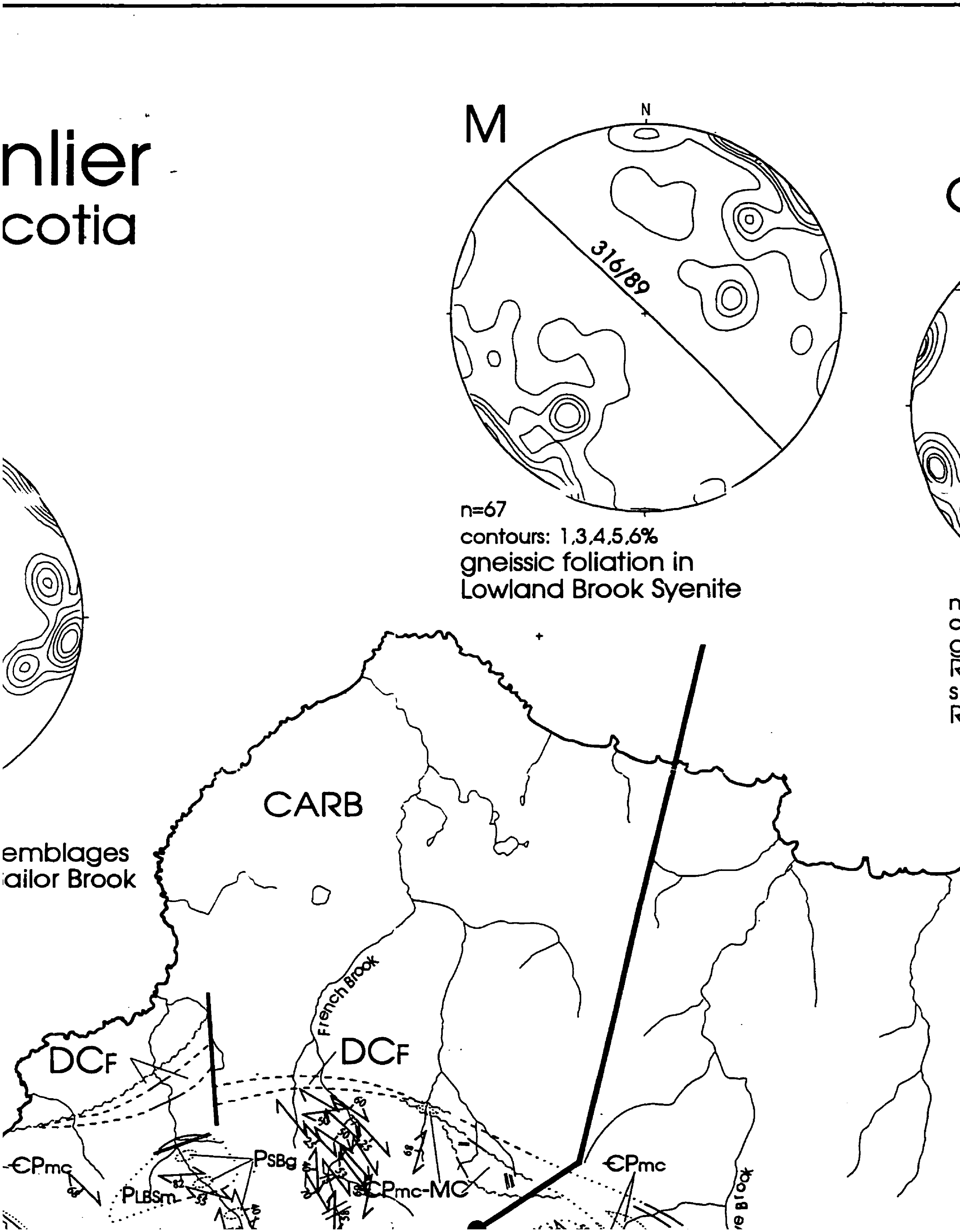

nlier
cotia
M
N
316/89
n=67
contours: 1,3,4,5,6%
gneissic foliation in
Lowland Brook Syenite
emblages
ailor Brook
CARB
French Brook
DCF
DCF
ЄPmc
PSBg
PLBSm
ЄPmc-MC
ЄPmc

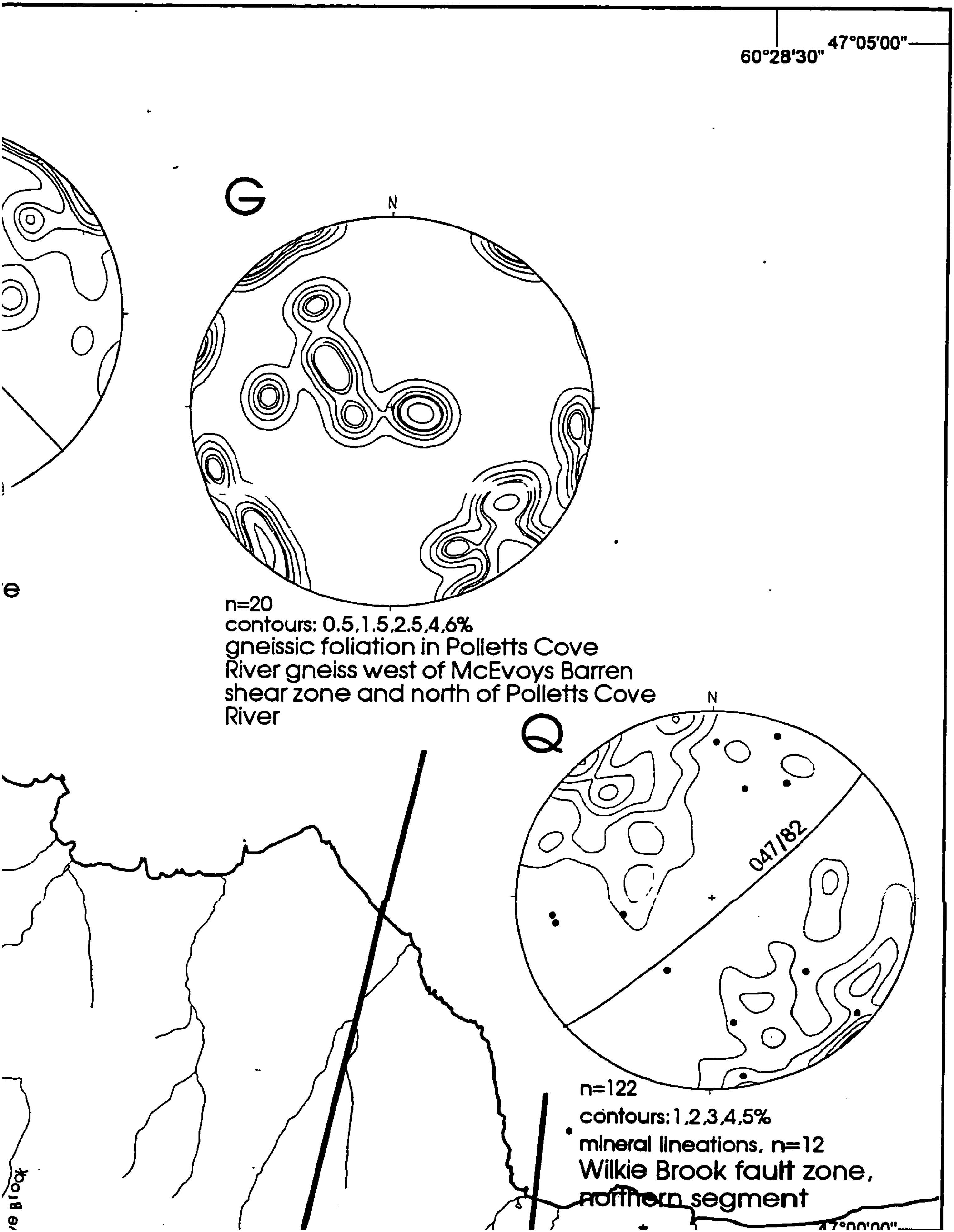
60°28'30"
47°05'00"
G
N
n=20
contours: 0.5,1.5,2.5,4,6%
gneissic foliation in Polletts Cove River gneiss west of McEvoys Barren shear zone and north of Polletts Cove River
Q
N
047/82
n=122
contours: 1,2,3,4,5%
• mineral lineations, n=12
Wilkie Brook fault zone, northern segment

47°00'00"

corresponding to letter within domain)

C

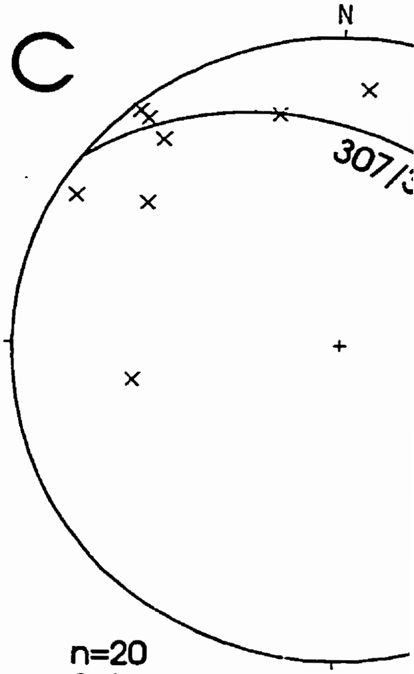

n=20
fabrics around nc
Delaneys Brook A

D

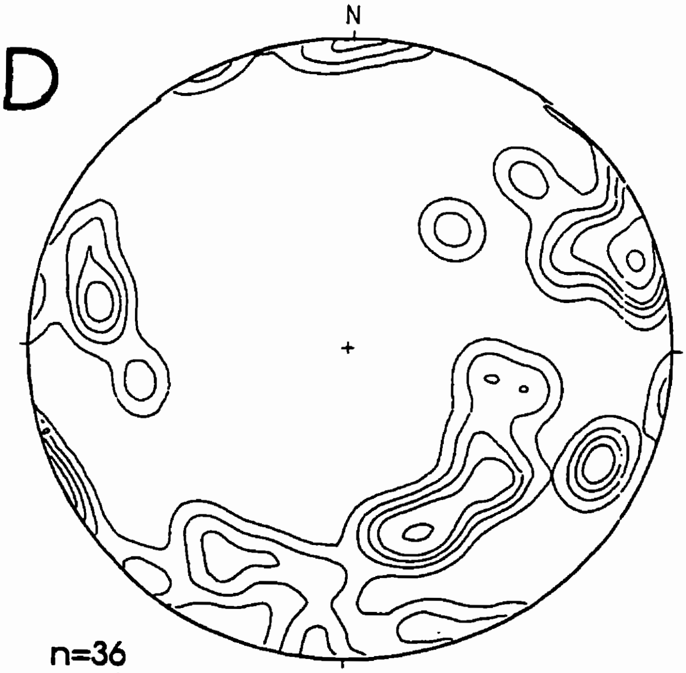

n=36
contours: 1,2,3,4,5%
gneissic foliation in Polletts Cove
River gneiss west of High Capes shec

N

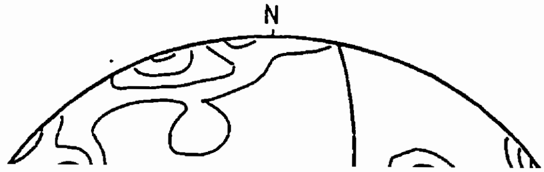

E

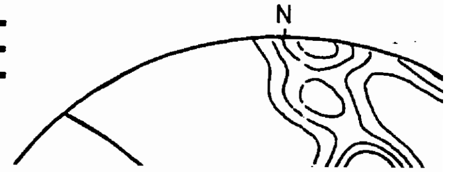

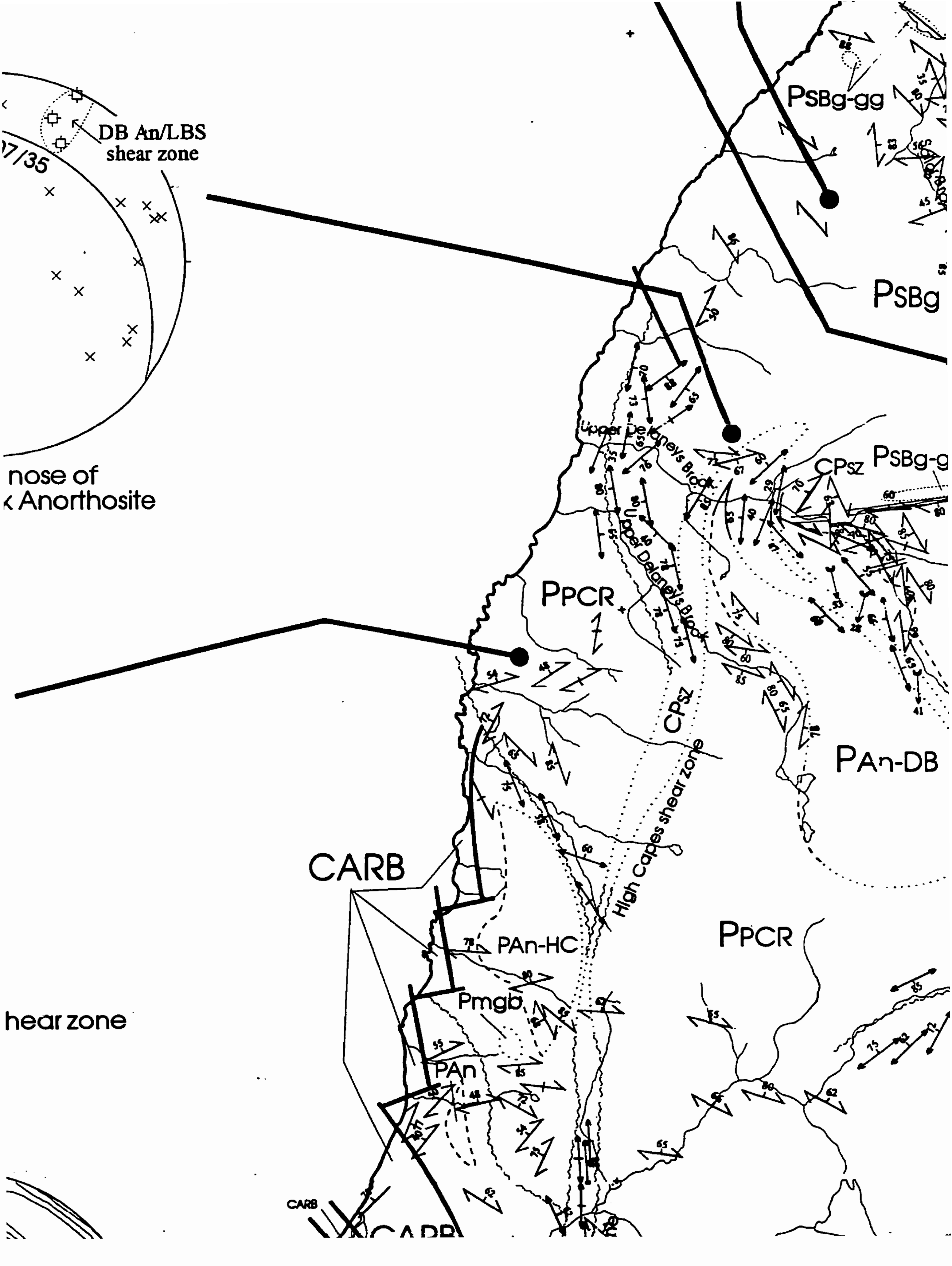

DB An/LBS
shear zone
nose of
Anorthosite
hear zone
PSBg-gg
PSBg
Upper Delaneys Brook
CPsz
PSBg-g
PPCR
Upper Delaneys Brook
CPsz
High Capes shear zone
PAn-DB
CARB
PAn-HC
Pmgb
PAn
PPCR
CARB

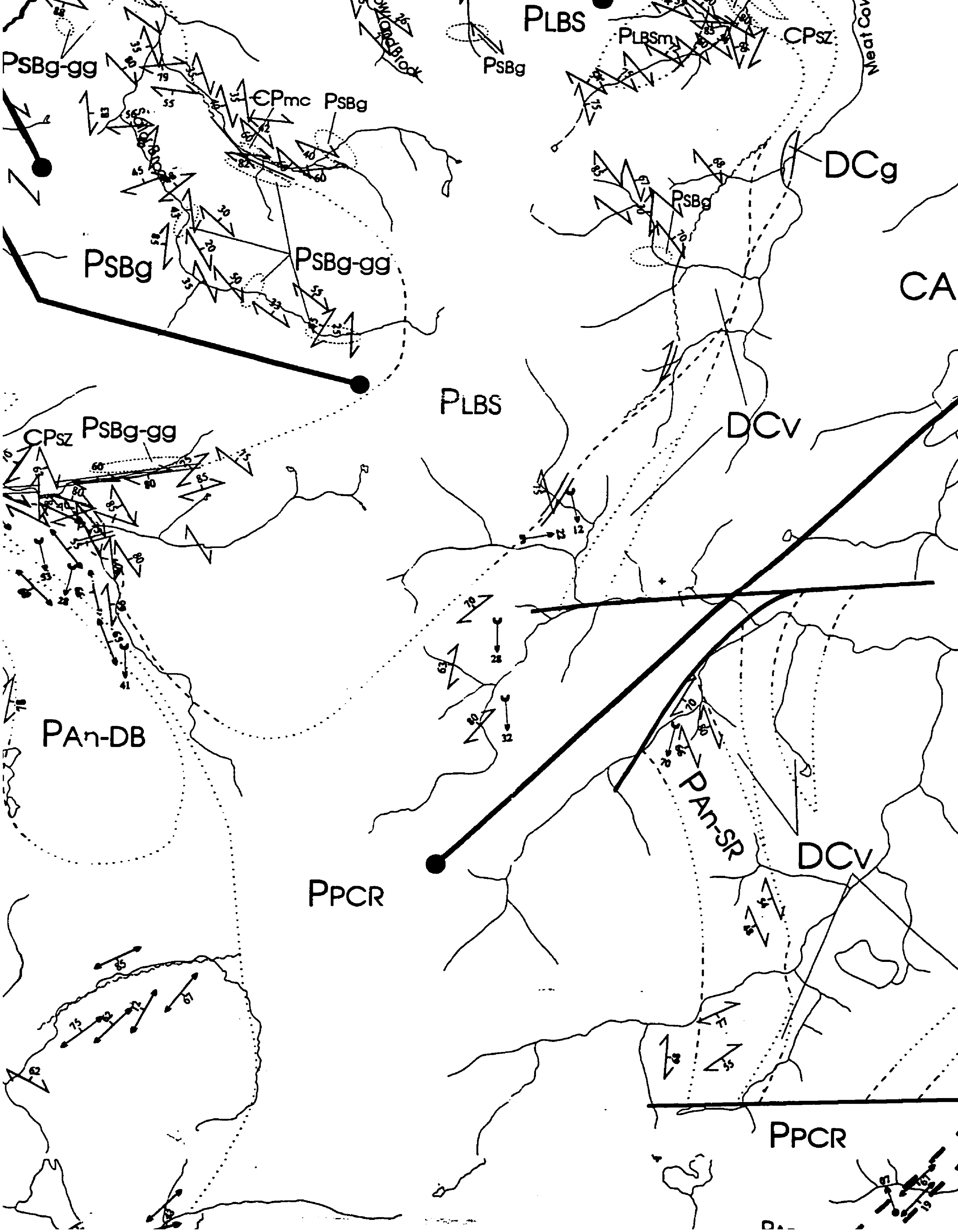

PLBS
PsBg-gg
CPmc
PsBg
PLBSm
CPsz
DCg
PsBg
PsBg-gg
CA
PLBS
DCv
CPsz
PsBg-gg
PAn-DB
PAn-SR
DCv
PPCR
PPCR

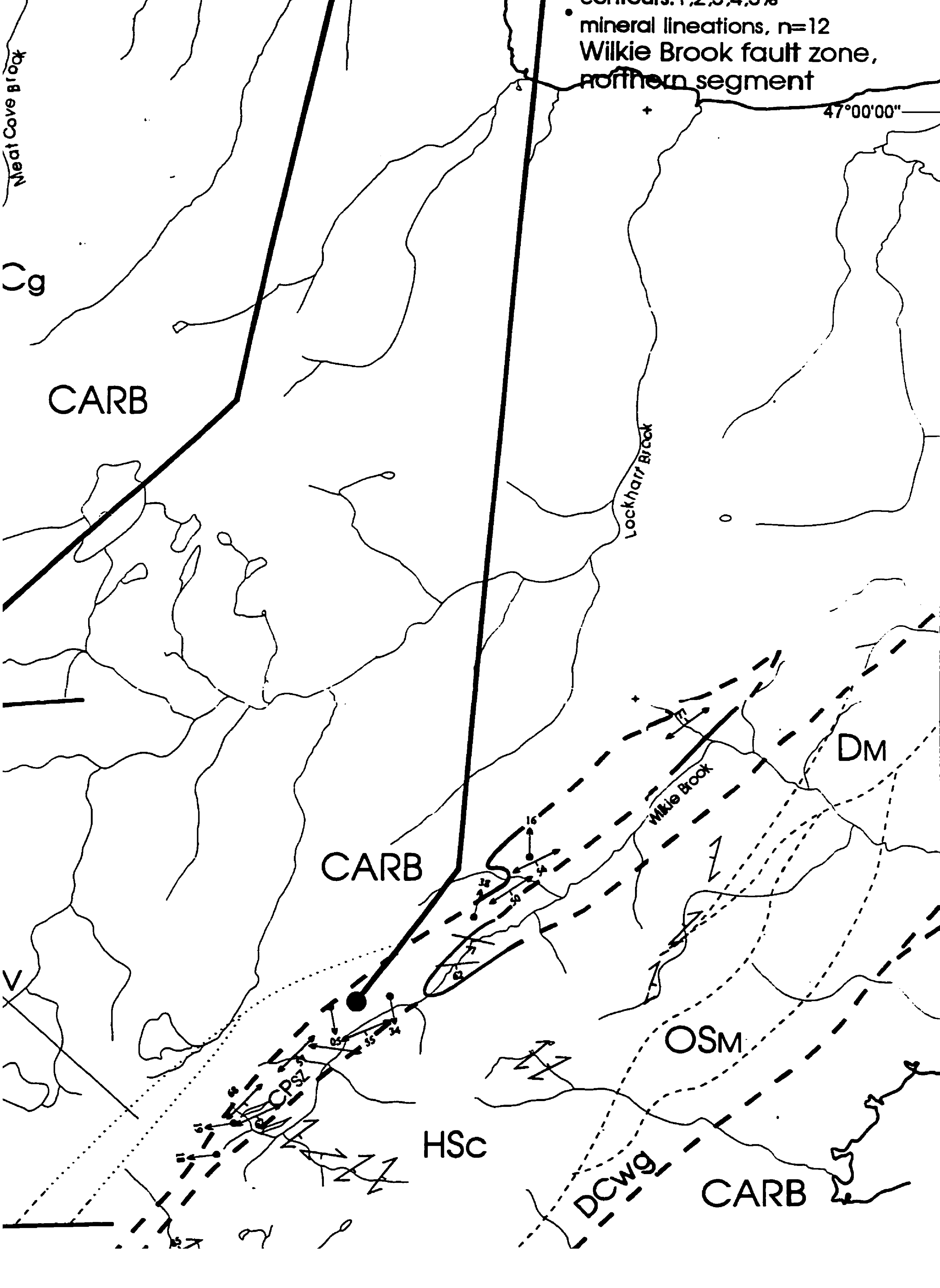

contours: 1,2,3,4,5%
mineral lineations, n=12
Wilkie Brook fault zone, northern segment
47°00'00"
Meat Cove Brook
Cg
CARB
Lockhart Brook
Wilkie Brook
DM
CARB
CPSZ
OSM
HSc
DCwg
CARB

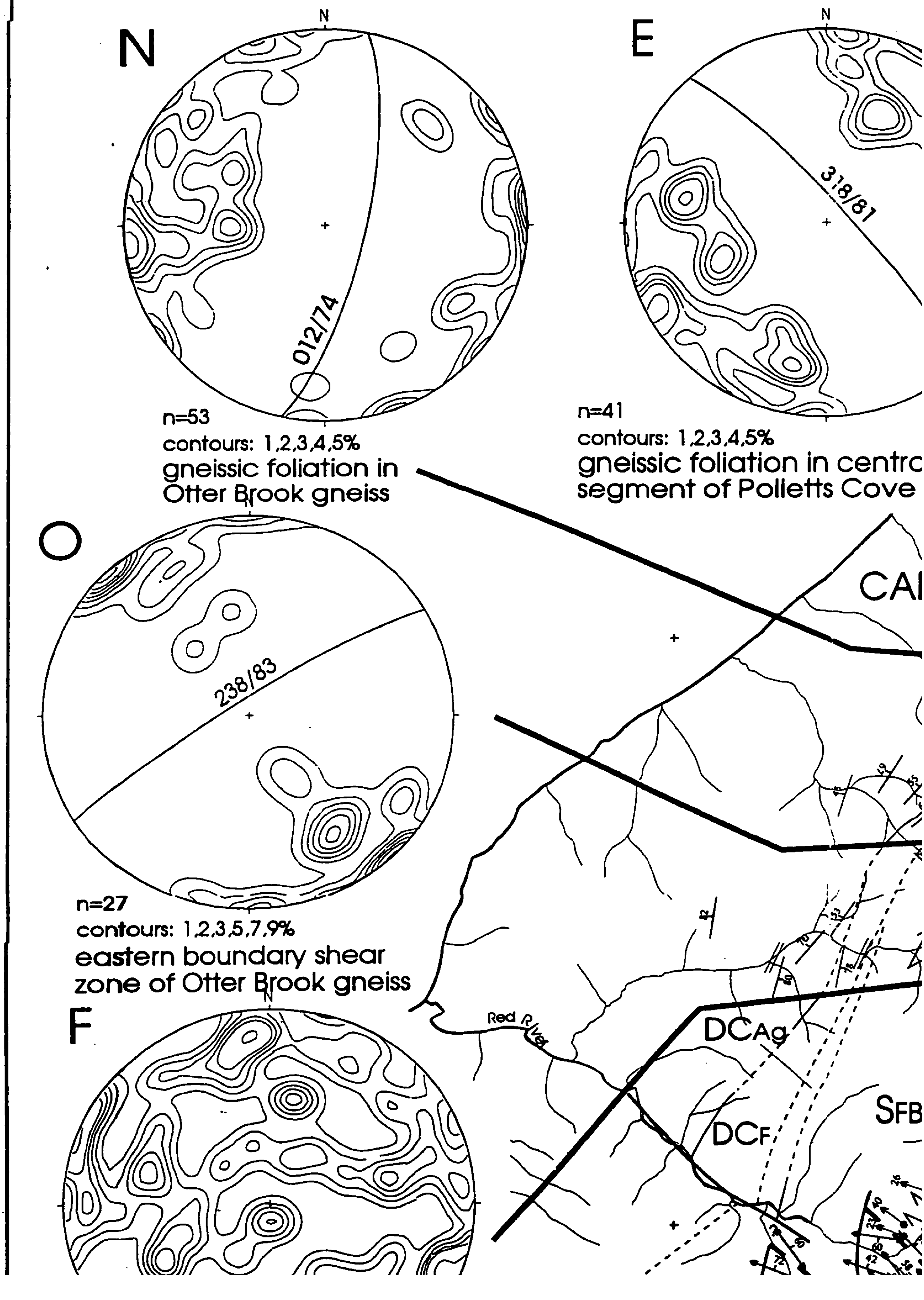
N
N
012/74
n=53
contours: 1,2,3,4,5%
gneissic foliation in
Otter Brook gneiss
E
N
318/81
n=41
contours: 1,2,3,4,5%
gneissic foliation in centra
segment of Polletts Cove
O
N
238/83
n=27
contours: 1,2,3,5,7,9%
eastern boundary shear
zone of Otter Brook gneiss
F
N
CA
Red River
DCAg
DCF
SFB

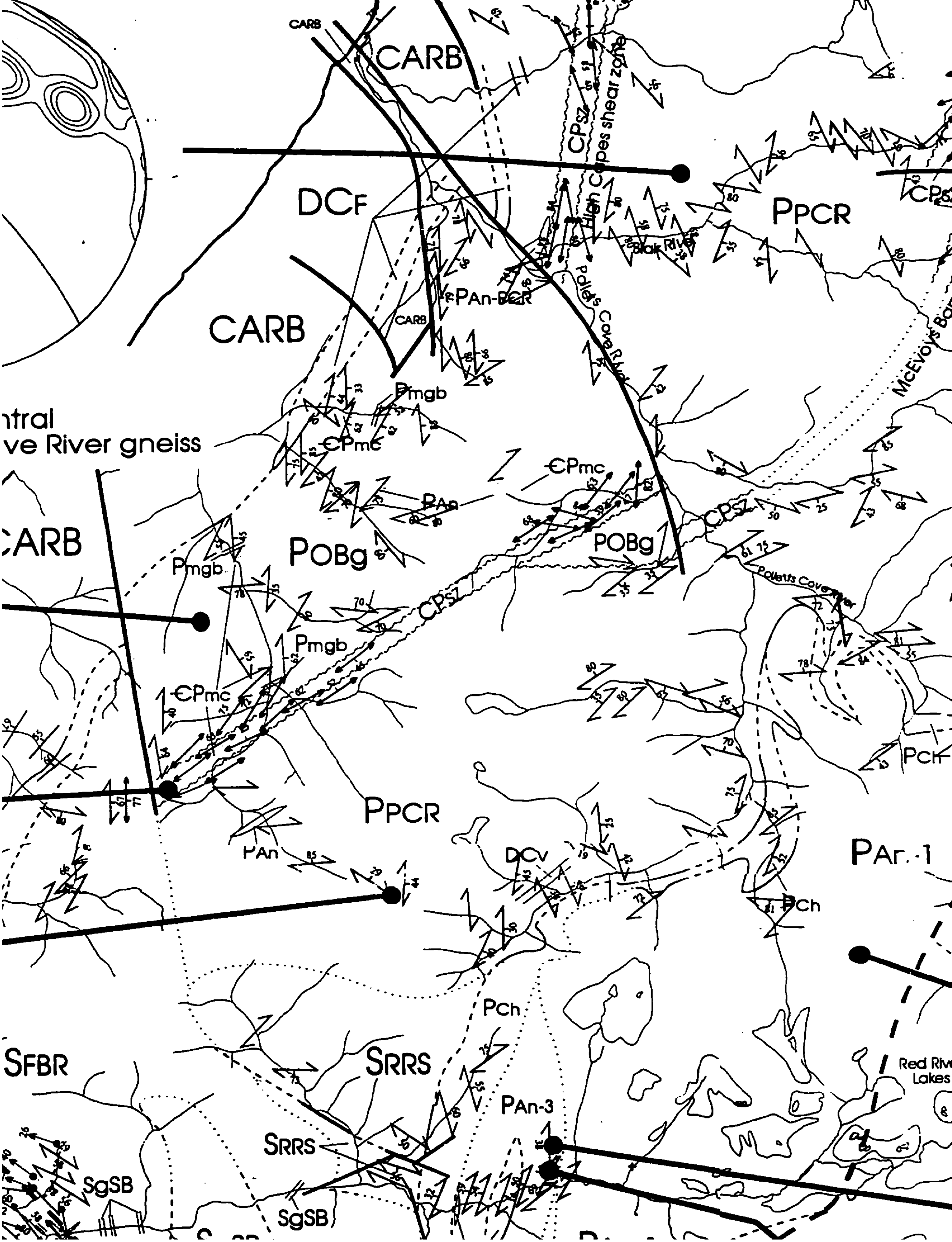
CARB
CARB
CPSZ
High Capes shear zone
DCF
PPCR
Blak River
Polletts Cove River
CARB
PAn-PCR
CARB
Pmgb
ntral
ve River gneiss
€Pmc
PAn
€Pmc
CPSZ
CARB
POBg
POBg
Polletts Cove River
Pmgb
CPSZ
Pmgb
€Pmc
PCh
PPCR
PAn
DCv
PAr. -1
PCh
Pch
SFBR
SRRS
Red River
Lakes
PAn-3
SRRS
SgSB
SgSB

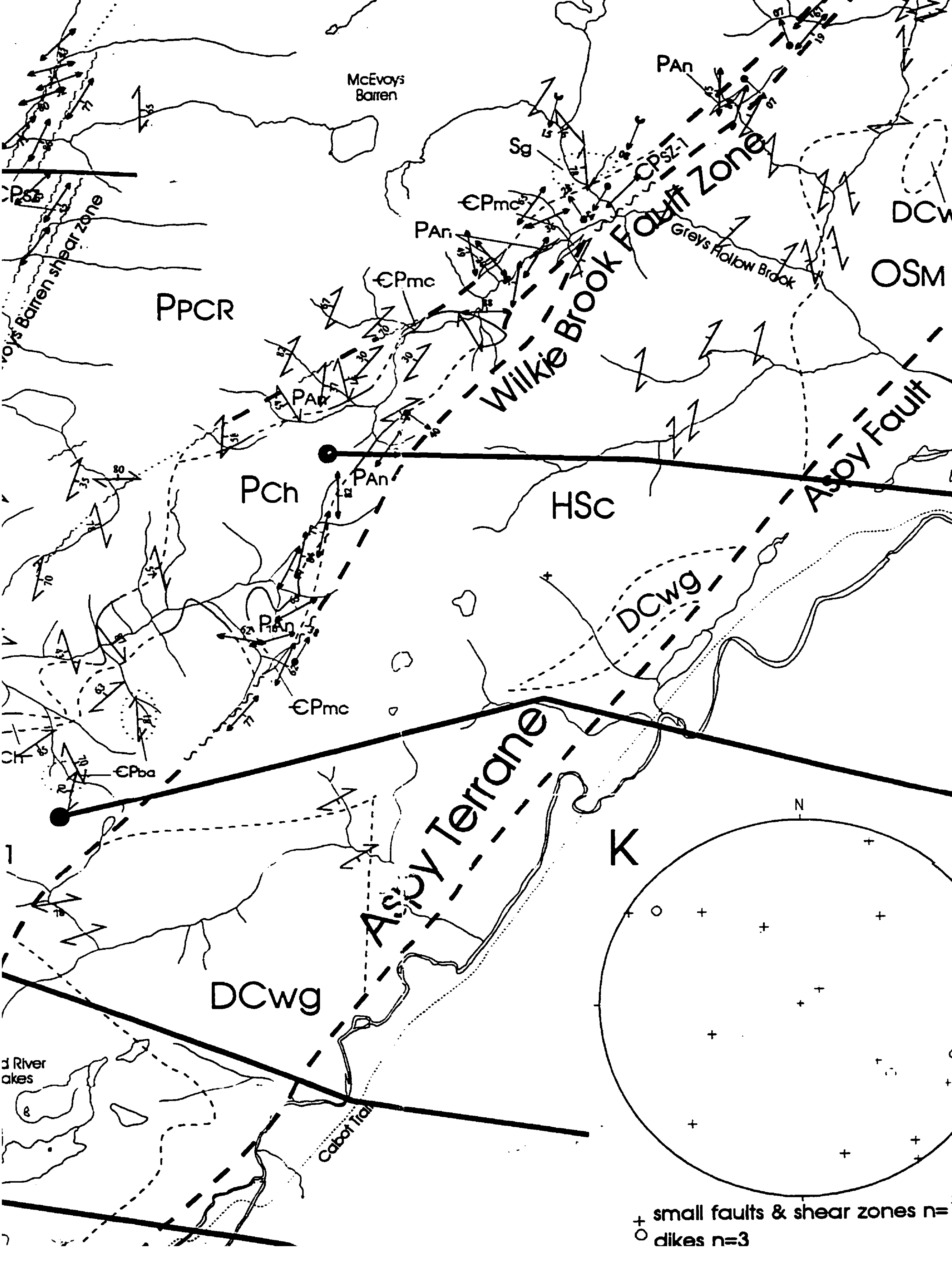

McEvoys Barren
McEvoys Barren shear zone
CPSZ
PPCR
PAn
Sg
CPSZ-1
€Pmc
Wilkie Brook Fault Zone
Greys Hollow Brook
DCw
OSM
Pch
HSc
Aspy Fault
DCwg
€Pba
Aspy Terrane
K
N
DCwg
Cabot Trail
small faults & shear zones n=
dikes n=3

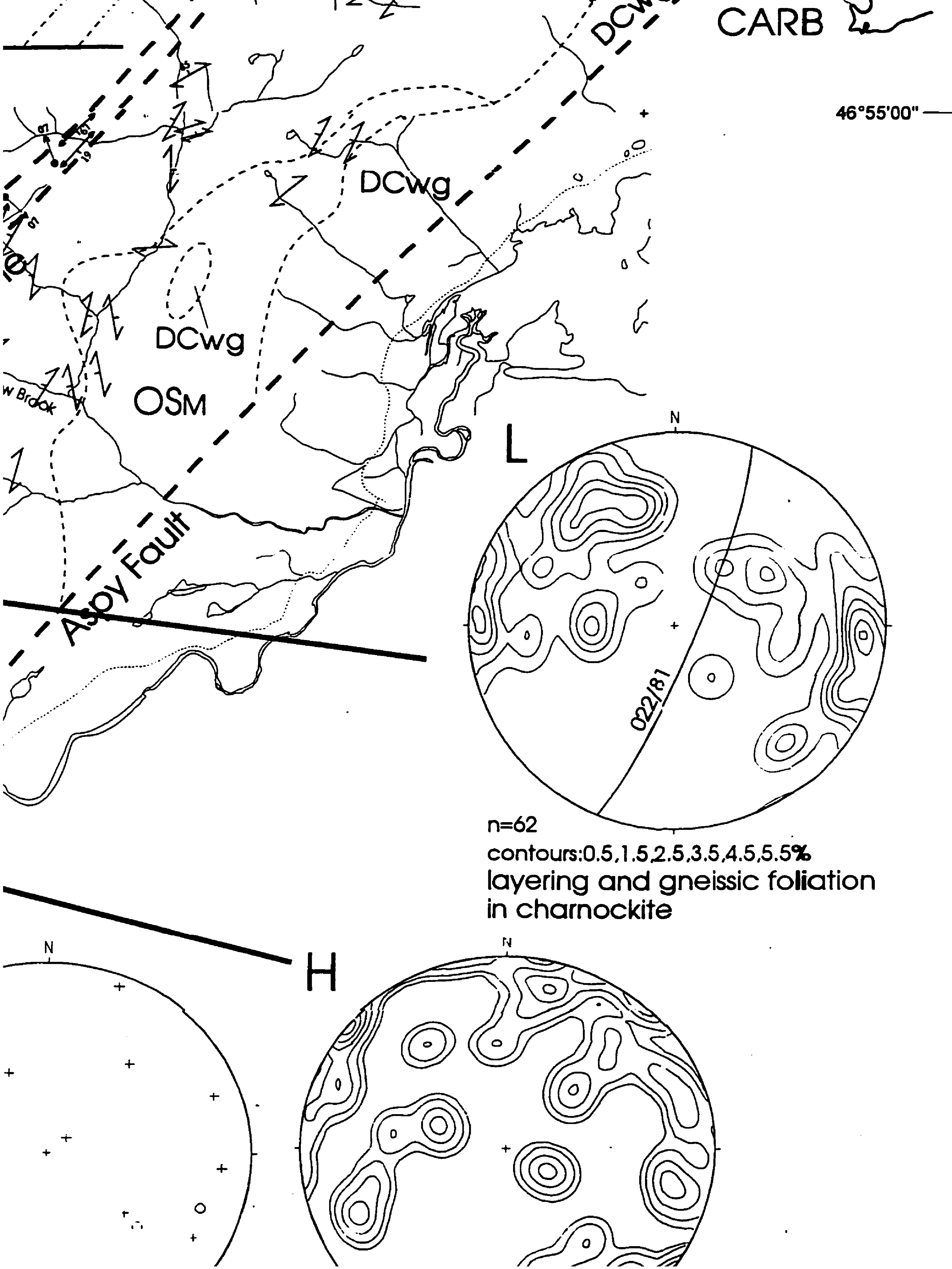
CARB
46°55'00"
DCwg
DCwg
OSM
Aspy Fault
L
N
022/81
n=62
contours:0.5,1.5,2.5,3.5,4.5,5.5%
layering and gneissic foliation
in charnockite
H
N

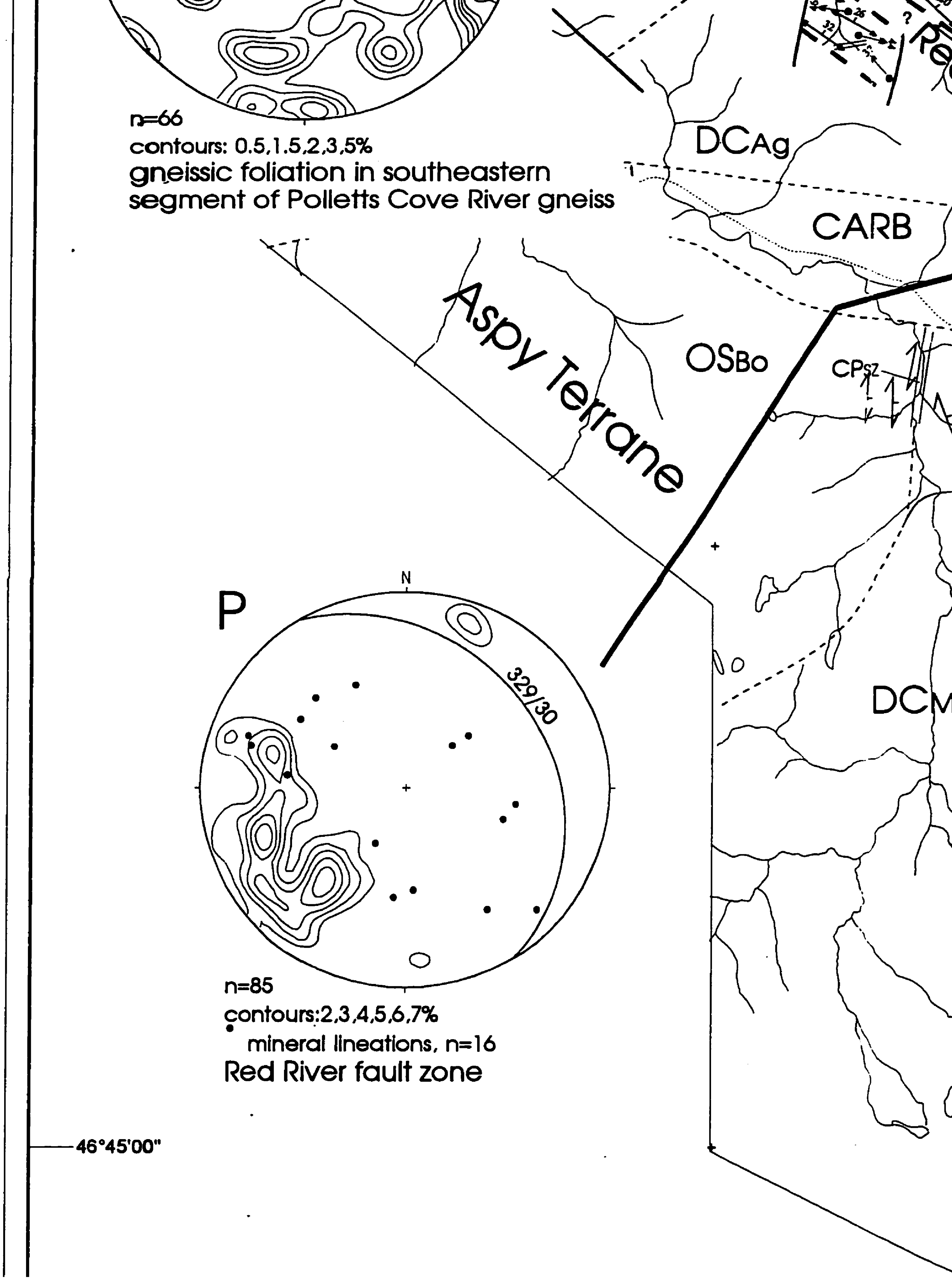
n=66
contours: 0.5,1.5,2,3,5%
gneissic foliation in southeastern segment of Polletts Cove River gneiss
DCAg
CARB
Aspy Terrane
OSBo
CPSZ
P
N
329/30
DCM
n=85
contours:2,3,4,5,6,7%
mineral lineations, n=16
Red River fault zone
46°45'00"

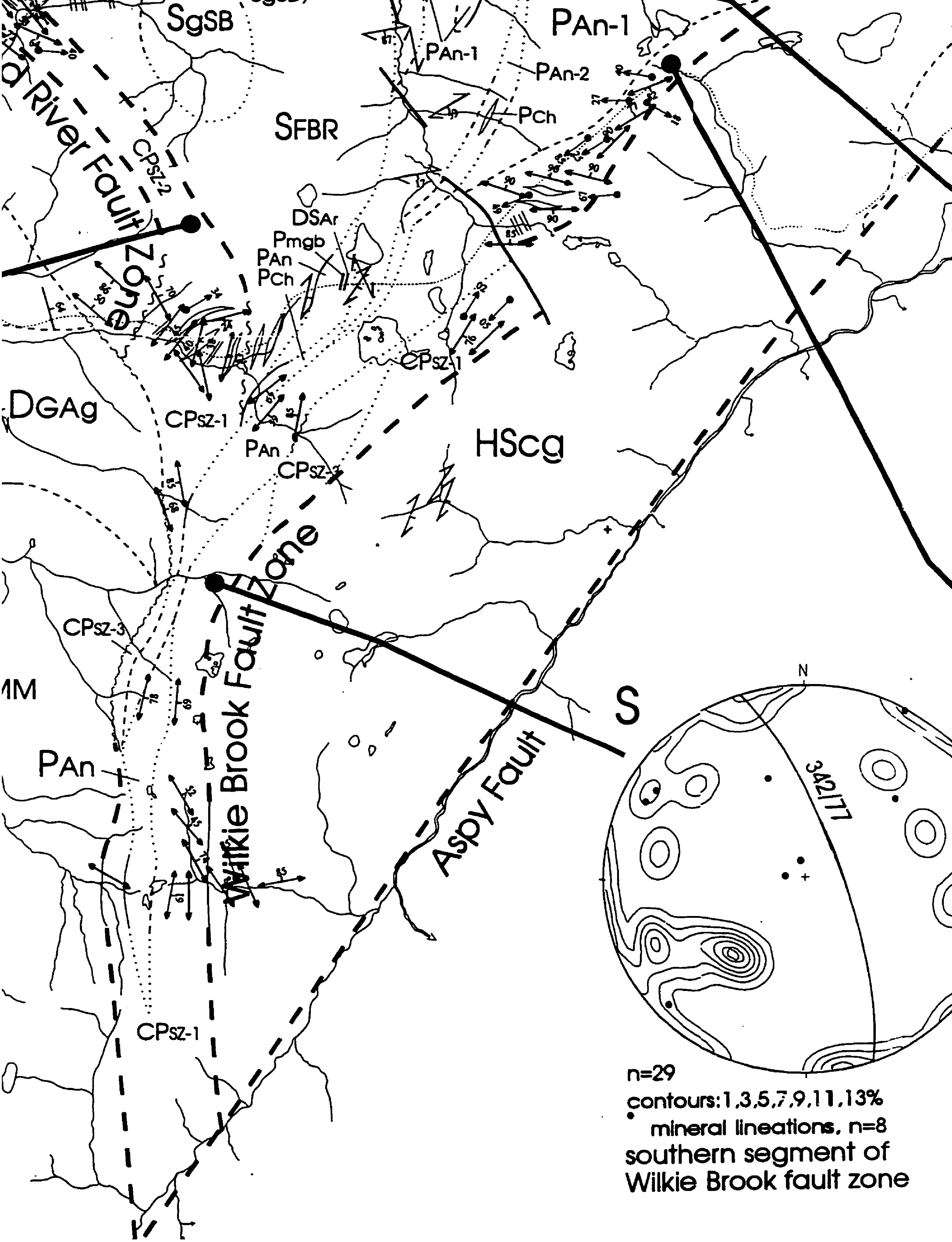

n=29
contours:1,3,5,7,9,11,13%
• mineral lineations, n=8
southern segment of
Wilkie Brook fault zone

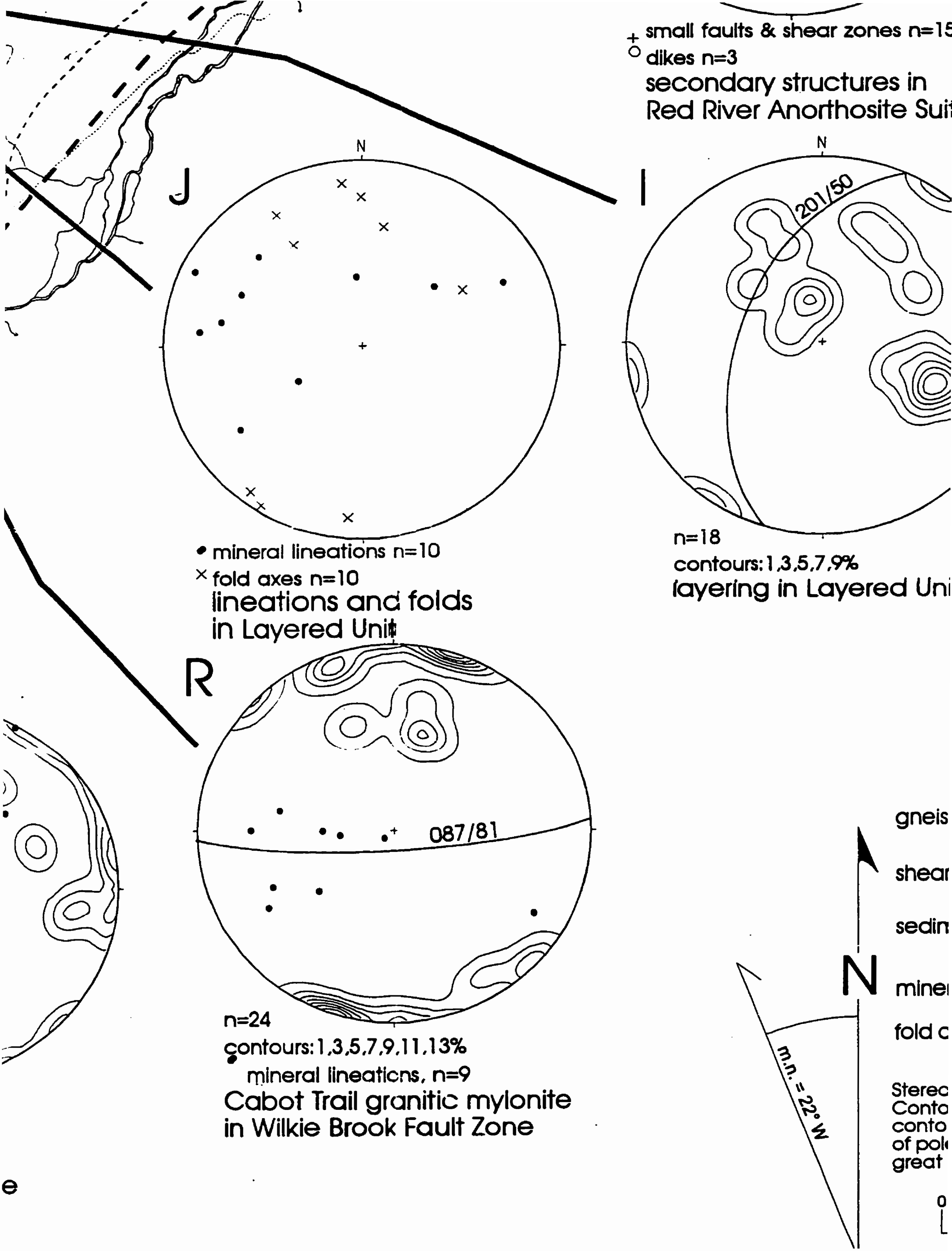
small faults & shear zones n=15
dikes n=3
secondary structures in
Red River Anorthosite Sui
N
J
mineral lineations n=10
fold axes n=10
lineations and folds
in Layered Unit
N
I
201/50
n=18
contours: 1,3,5,7,9%
layering in Layered Uni
R
087/81
n=24
contours: 1,3,5,7,9,11,13%
mineral lineations, n=9
Cabot Trail granitic mylonite
in Wilkie Brook Fault Zone
gneis
shear
sedin
N
mine
fold c
m.n. = 22° W
Stereo
Conto
conto
of pol
great
0
e

ts & shear zones n=15

ary structures in
er Anorthosite Suite

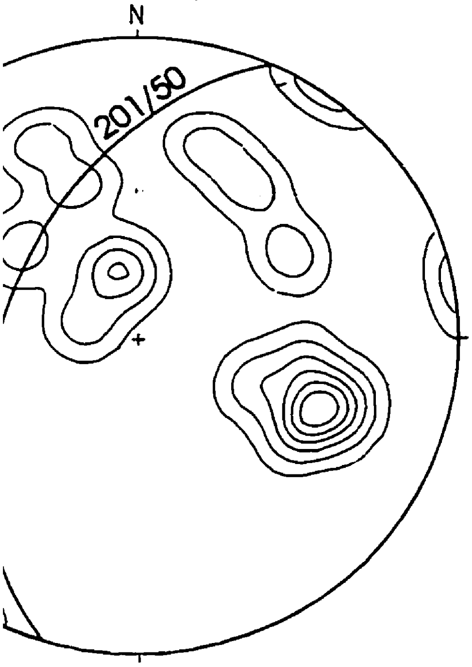

ırs: 1,3,5,7,9%
ng in Layered Unit

n=47
contours: 0.5,1,2,3,4%
deformed mafic clots and wispy
streaks in massive anorthosite

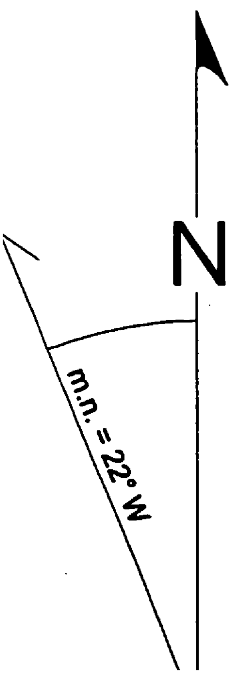

gneissic foliation, schistosity, and banding
(inclined, vertical, horizontal)..........................

shear zone foliation, schistosity, and mylonitic layering
(inclined, vertical, horizontal)..........................

sedimentary bedding and volcanic layering
(inclined, vertical, horizontal)..........................

mineral lineation..

fold axis..

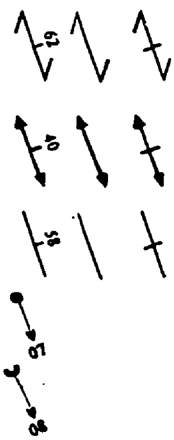

Stereonets are lower-hemispher, equal-area projections. Contoured stereonets are % points (poles) per % area indicated by contour level. Planar data points on uncontoured diagrams are plots of poles. Mean orientation of planar data are indicated by labeled great circles.

46°45'00"

scale 1 : 37,600

0 km 5

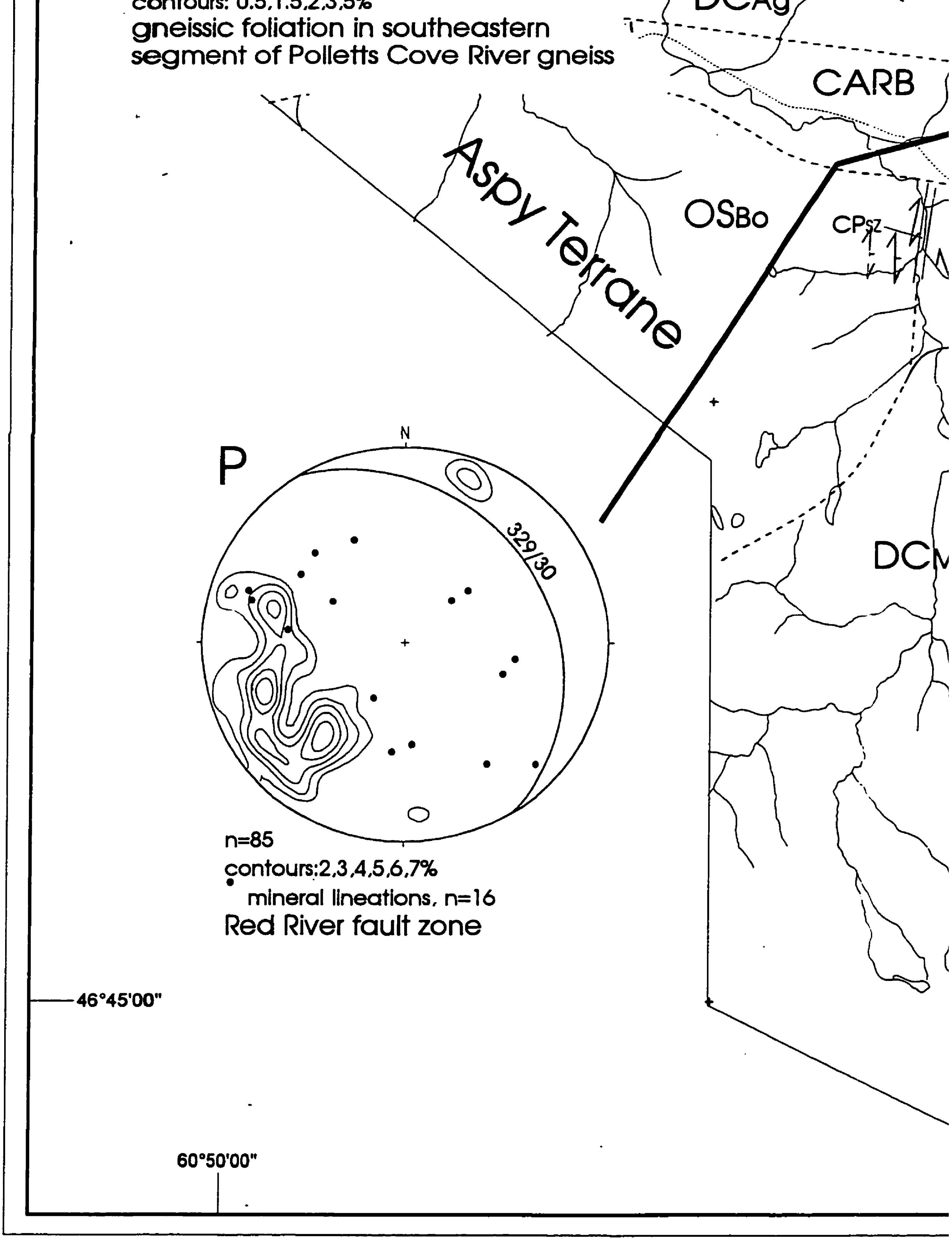

contours: 0.5,1.5,2,3,5%
gneissic foliation in southeastern
segment of Polletts Cove River gneiss
DCAg
CARB
Aspy Terrane
OSBo
CPsz
DCM
P
N
329/30
n=85
contours:2,3,4,5,6,7%
mineral lineations, n=16
Red River fault zone
46°45'00"
60°50'00"

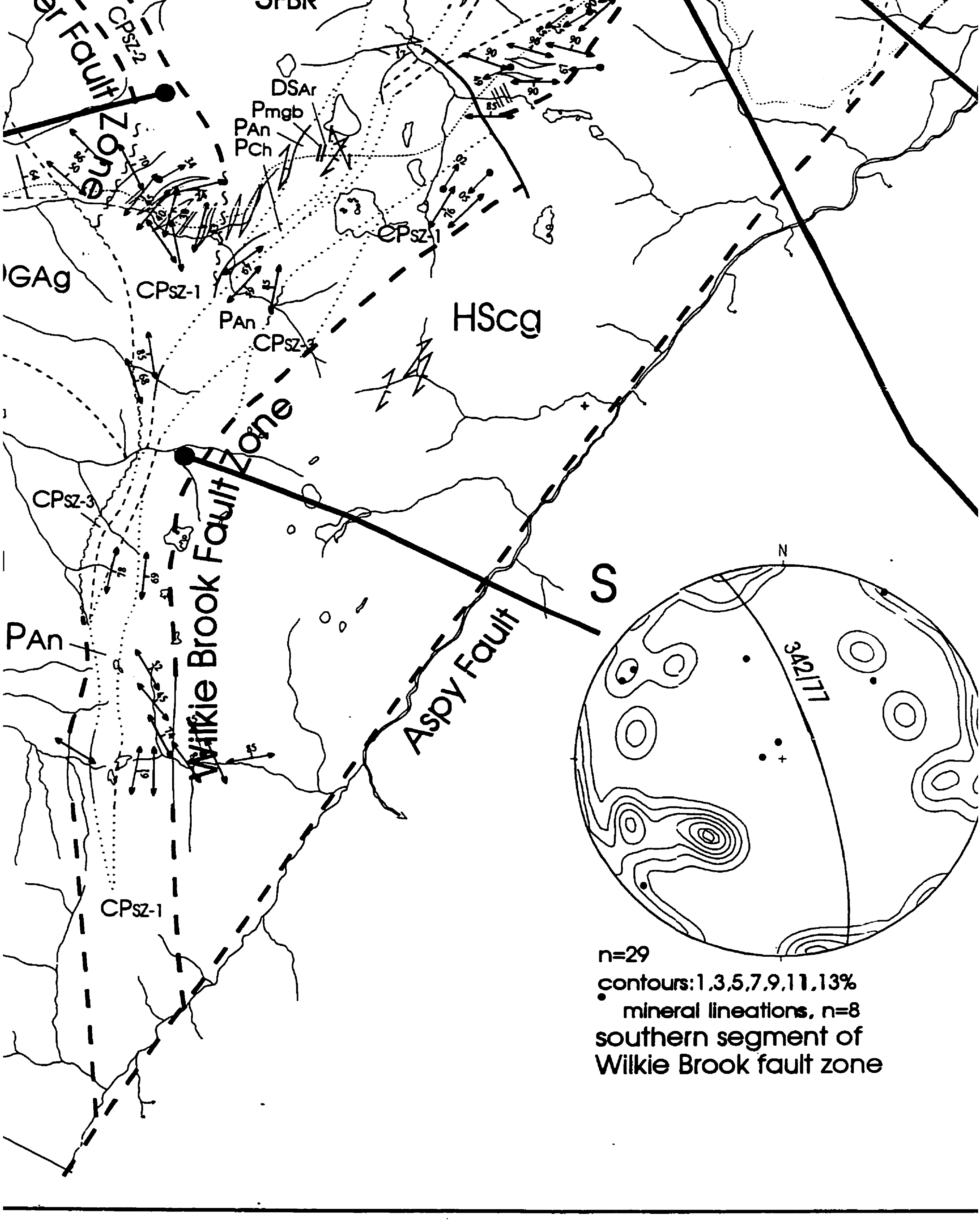

Fault Zone
CPsz-2
DSAr
Pmgb
PAn
PCh
CPsz-1
DGAg
HScg
CPsz-3
Wilkie Brook Fault Zone
Aspy Fault
S
N
342/77
n=29
contours:1,3,5,7,9,11,13%
mineral lineations, n=8
southern segment of
Wilkie Brook fault zone

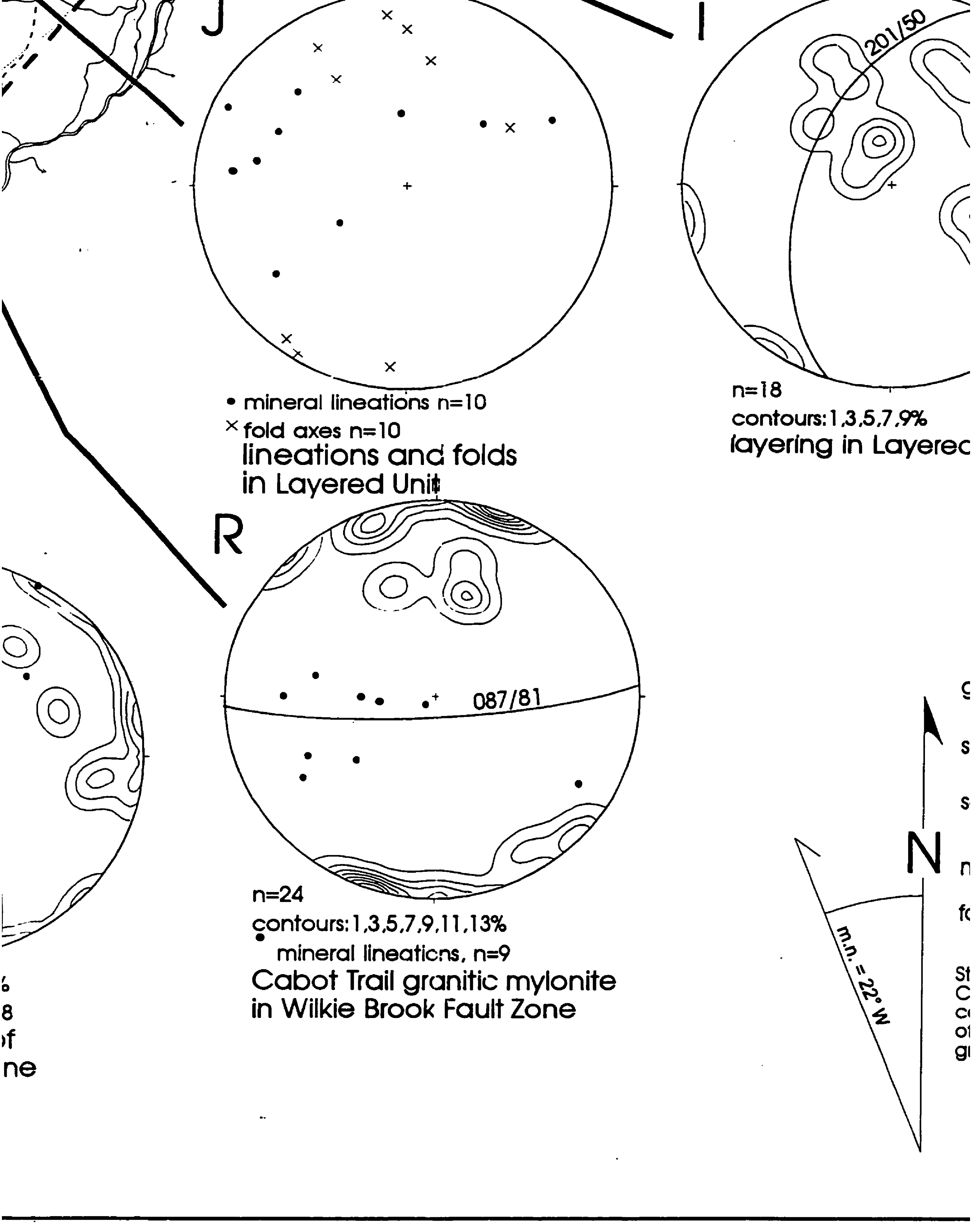
J
I
201/50
mineral lineations n=10
fold axes n=10
lineations and folds
in Layered Unit
n=18
contours:1,3,5,7,9%
layering in Layered
R
087/81
n=24
contours:1,3,5,7,9,11,13%
mineral lineations, n=9
Cabot Trail granitic mylonite
in Wilkie Brook Fault Zone
N
m.n. = 22° W

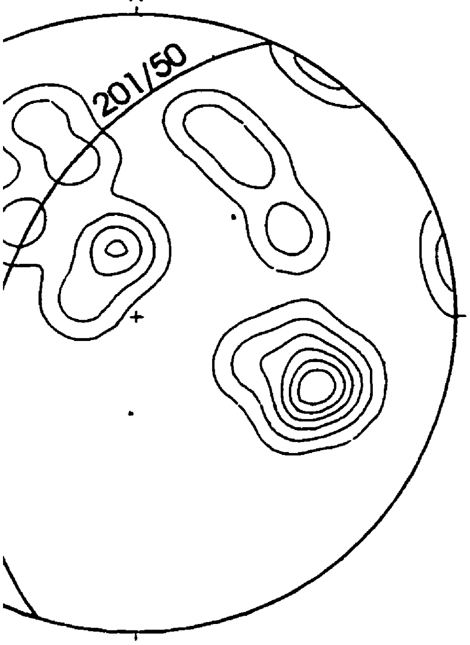

ırs: 1,3,5,7,9%

ng in Layered Unit

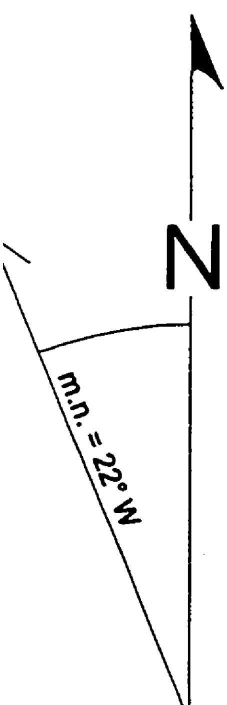

gneissic foliation, schistosity, and banding
(inclined, vertical, horizontal)........................

shear zone foliation, schistosity, and mylonitic layering
(inclined, vertical, horizontal)........................

sedimentary bedding and volcanic layering
(inclined, vertical, horizontal)........................

mineral lineation..

fold axis..

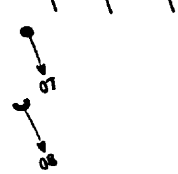

Stereonets are lower-hemispher, equal-area projections. Contoured stereonets are % points (poles) per % area indicated by contour level. Planar data points on uncontoured diagrams are plots of poles. Mean orientation of planar data are indicated by labeled great circles.

46°45'00"

scale 1 : 37,600

60°28'30"

NOTE TO USERS

Oversize maps and charts are microfilmed in sections in the following manner:

LEFT TO RIGHT, TOP TO BOTTOM, WITH SMALL OVERLAPS

The following map or chart has been microfilmed in its entirety at the end of this manuscript (not available on microfiche). A xerographic reproduction has been provided for paper copies and is inserted into the inside of the back cover.

Black and white photographic prints (17"x 23") are available for an additional charge.

UMI

47°05'00"

60°50'00"

Ma

Sample I

(see Map A for u

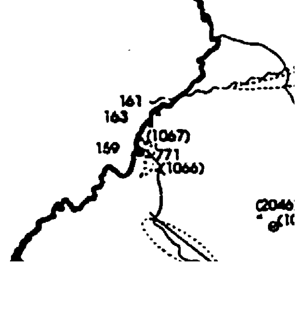

ap C
Locations
units and legend)

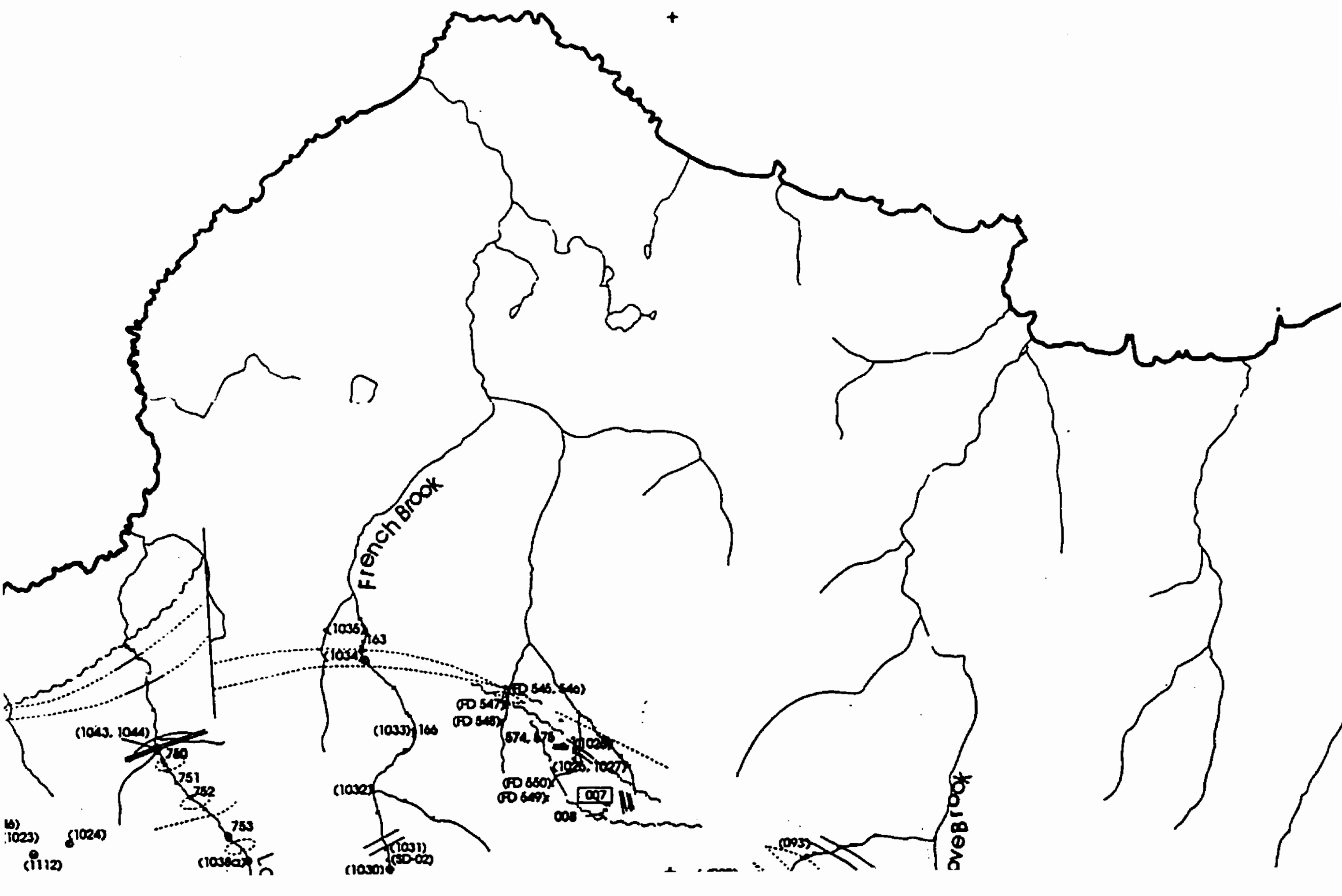

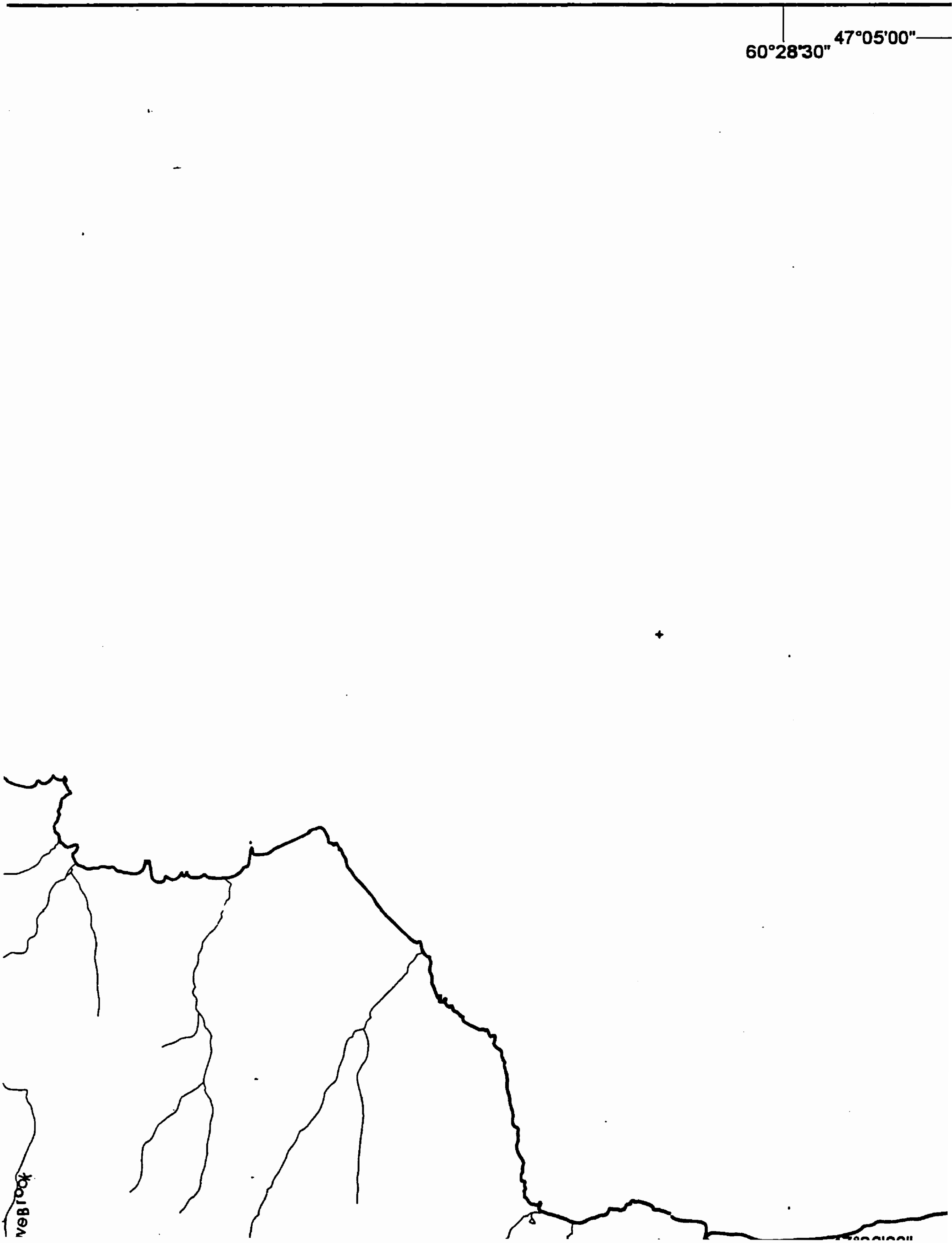
60°28'30"
47°05'00"

47°00'00"

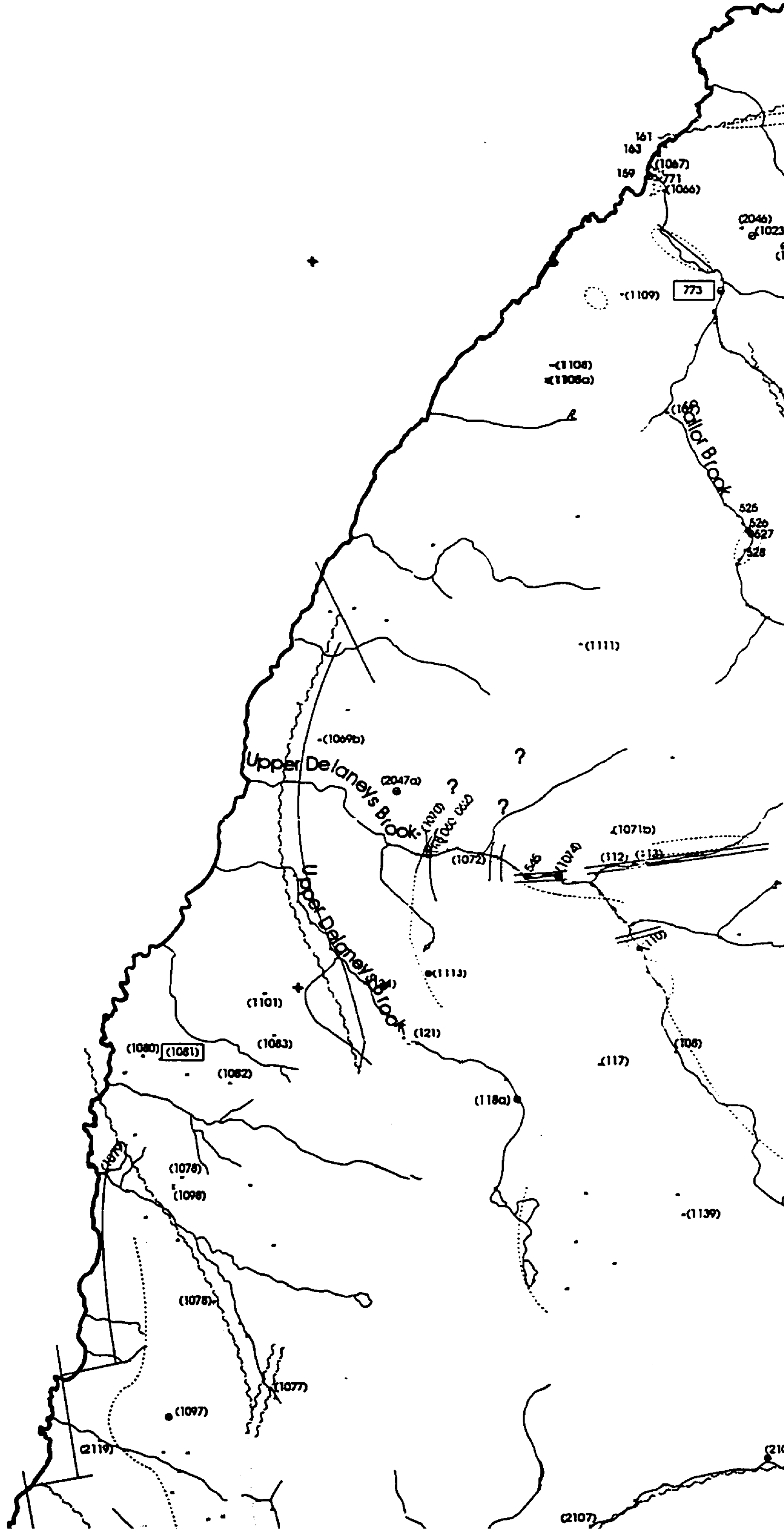

161
163
159
(1067)
771
(1066)
(2046)
(1109)
773
(1108)
(1108a)
525
526
527
528
(1111)
(1069b)
Upper Delaney's Brook
(2047a)
(1071b)
(1072)
(1113)
(1101)
(1083)
(1080)
(1081)
(1082)
(121)
(117)
(108)
(118a)
(1078)
(1098)
(1139)
(1076)
(1077)
(1097)
(2119)
(2107)

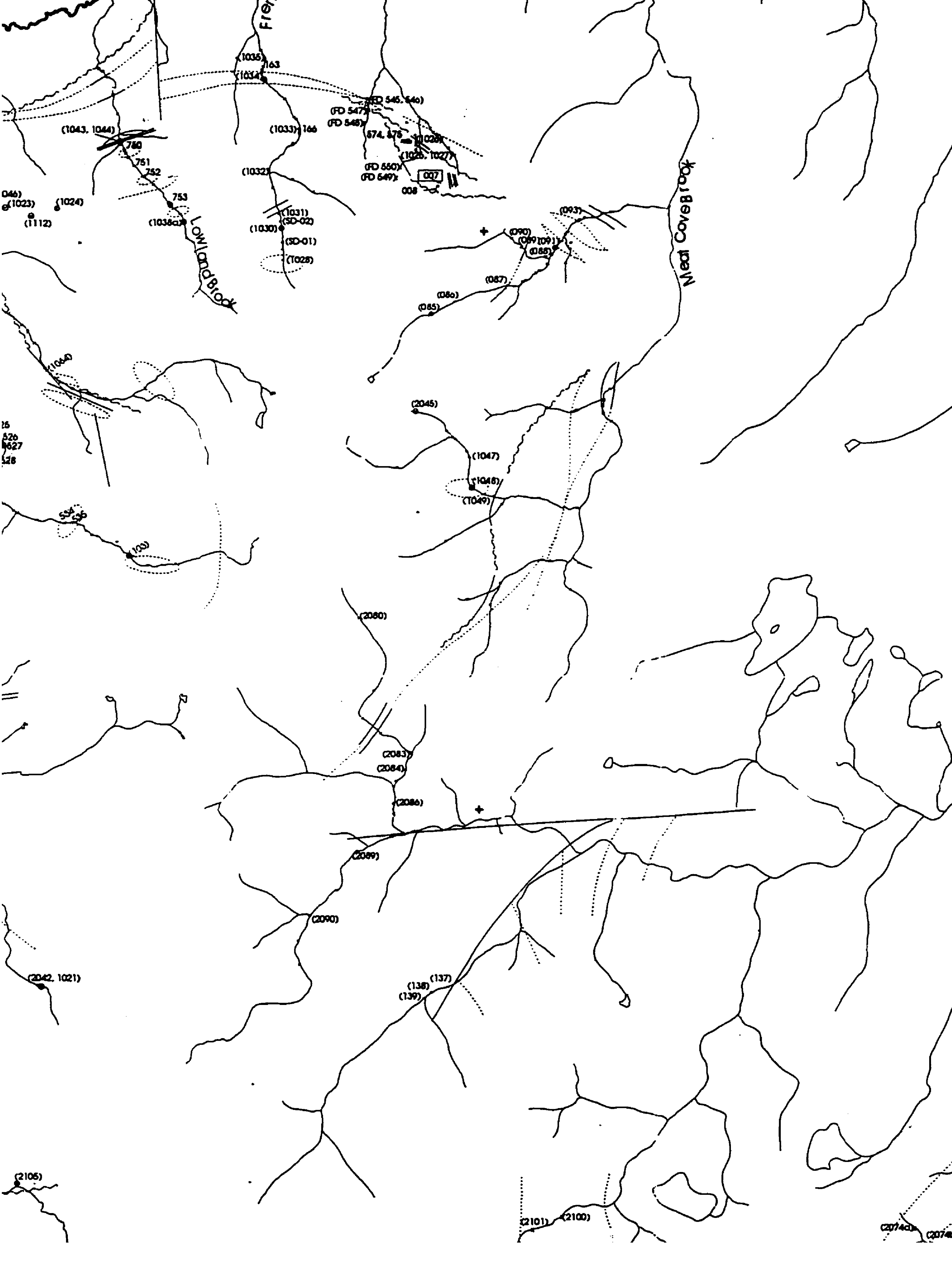

Lowland Brook
Meat Cove Brook
(1035)
163
(1034)
(FD 546, 546)
(FD 547)
(FD 548)
(1043, 1044)
750
751
752
753
(1033)
166
(1032)
574, 575
(1028)
(1026, 1027)
(FD 550)
(FD 549)
007
008
(1023)
(1024)
(1112)
(1038a)
(1031)
(SD-02)
(1030)
(SD-01)
(T028)
(093)
(090)
(089)
(091)
(088)
(087)
(086)
(085)
(1040)
(2045)
(1047)
(1048)
(T049)
(2080)
(2083)
(2084)
(2086)
(2089)
(2090)
(2042, 1021)
(138)
(137)
(139)
(2105)
(2101)
(2100)

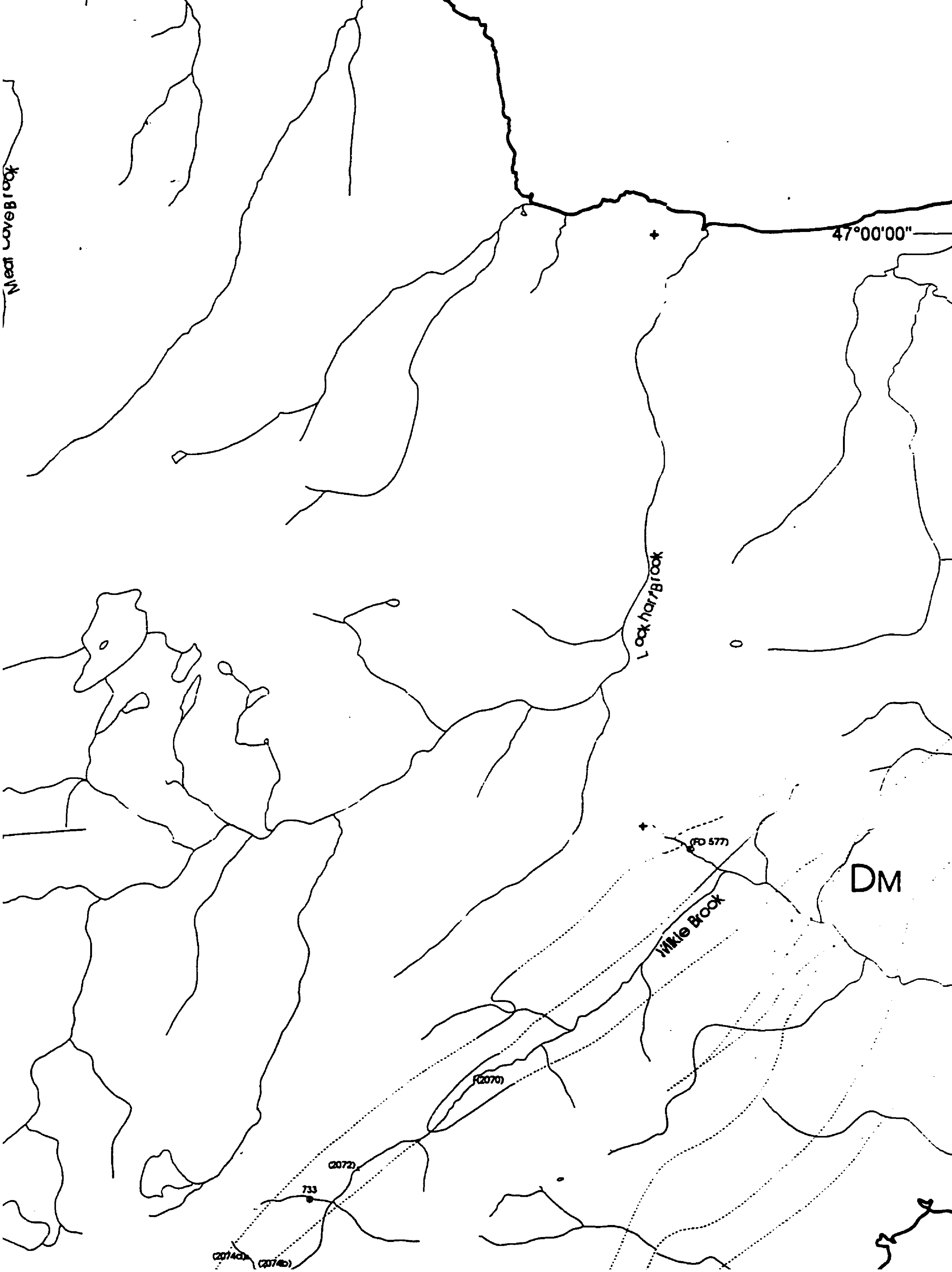

Meat Cove Brook
47°00'00"
Lockhart Brook
(FO 577)
DM
Wilkie Brook
(2070)
(2072)
733
(2074a)
(2074b)

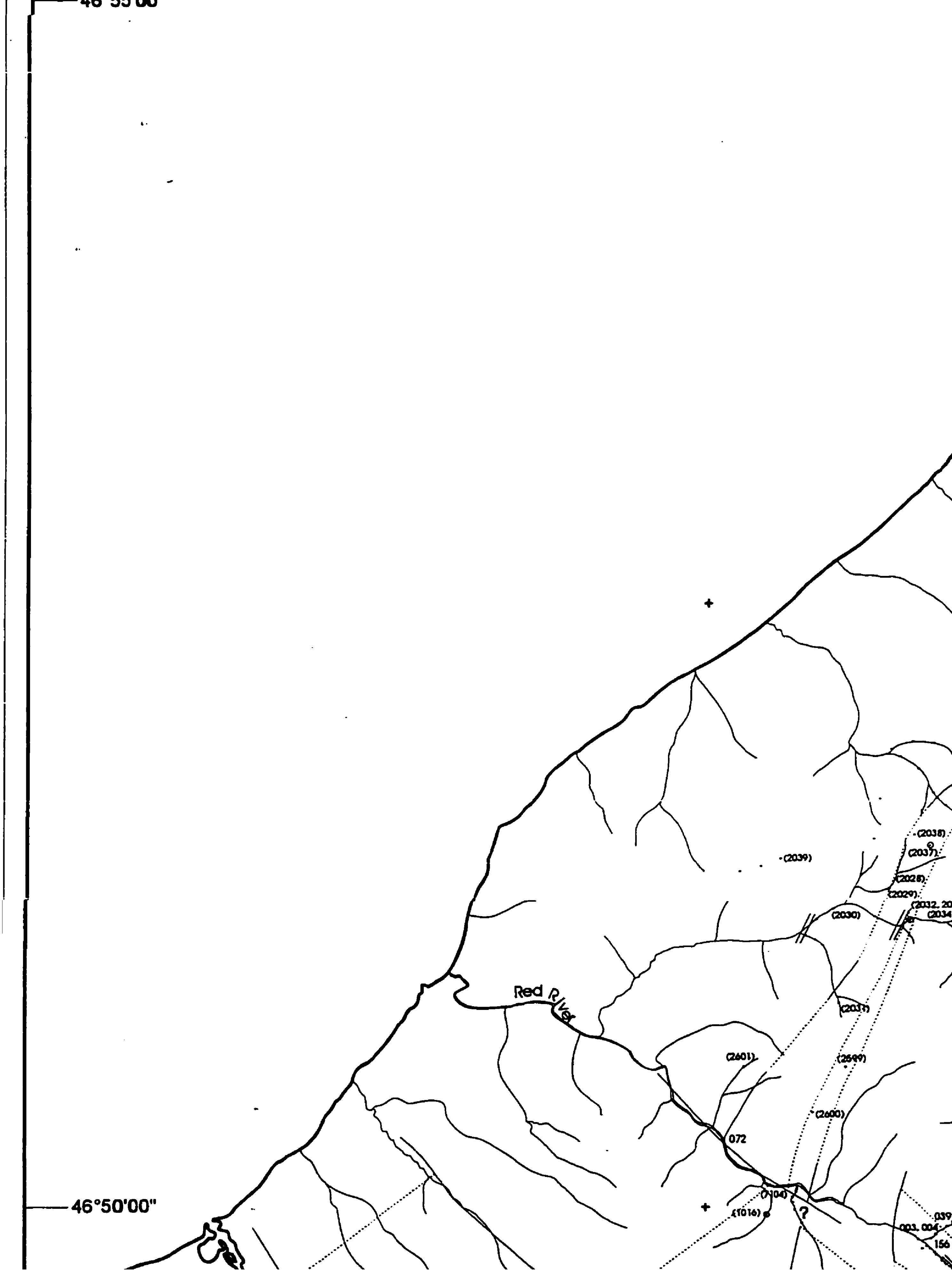
46°50'00"
Red River
(2038)
(2037)
(2039)
(2028)
(2029)
(2030)
(2031)
(2601)
(2599)
(2600)
072
(7104)
(1016)
?
003, 004
156

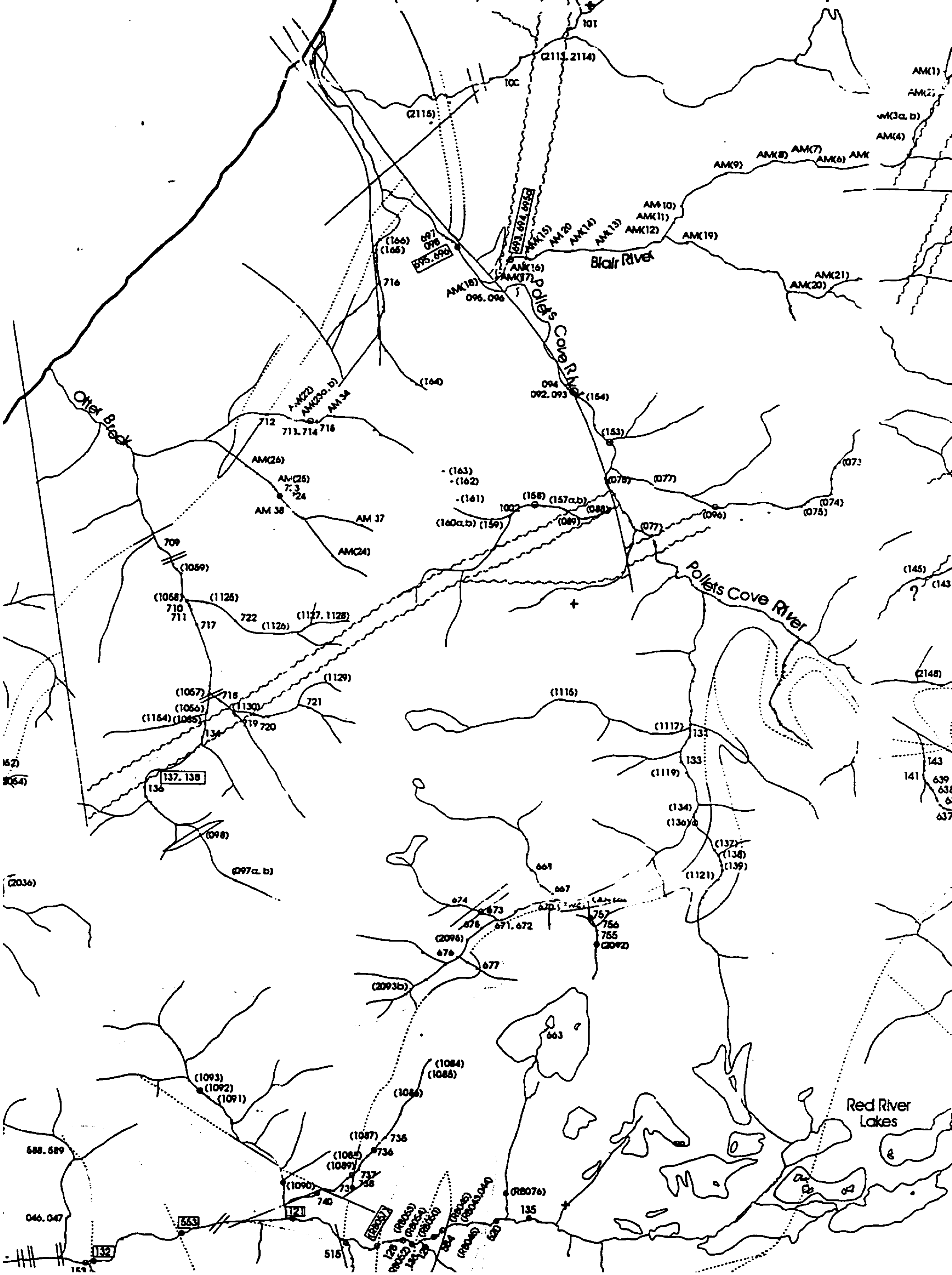

Blair River
Pollets Cove River
Pollets Cove River
Otter Brook
Red River
Lakes
101
(2113, 2114)
(2116)
AM(1)
AM(4)
AM(9)
AM(8)
AM(7)
AM(6)
AM(10)
AM(11)
AM(12)
AM(19)
AM(21)
AM(20)
AM(15)
AM(14)
AM(13)
AM(16)
AM(17)
AM(18)
096, 096
(166)
(165)
697
098
695, 696
693, 694, 695a
716
(164)
094
092, 093
(154)
(153)
AM(22)
AM(23a, b)
AM 34
712
713, 714
715
AM(26)
AM(25)
AM 38
AM 37
AM(24)
(163)
(162)
(161)
(158)
(157a, b)
1002
(160a, b)
(159)
(088)
(089)
(078)
(077)
(077)
(096)
(074)
(075)
709
(1059)
(1058)
710
711
(1125)
717
722
(1126)
(1127, 1128)
(1129)
(1057)
718
(1056)
(1130)
721
(1154)
(1055)
719
720
134
137, 138
136
(098)
(097a, b)
(2036)
(1115)
(1117)
133
(1119)
(134)
(137)
(138)
(139)
(1121)
(145)
(2148)
143
141
639
661
667
674
673
675
671, 672
757
756
755
(2092)
(2095)
676
677
(2093b)
663
(1093)
(1092)
(1091)
(1084)
(1085)
(1086)
(1087)
735
736
(1088)
(1089)
737
738
739
740
(1090)
121
553
588, 589
046, 047
132
515
(RB076)
135

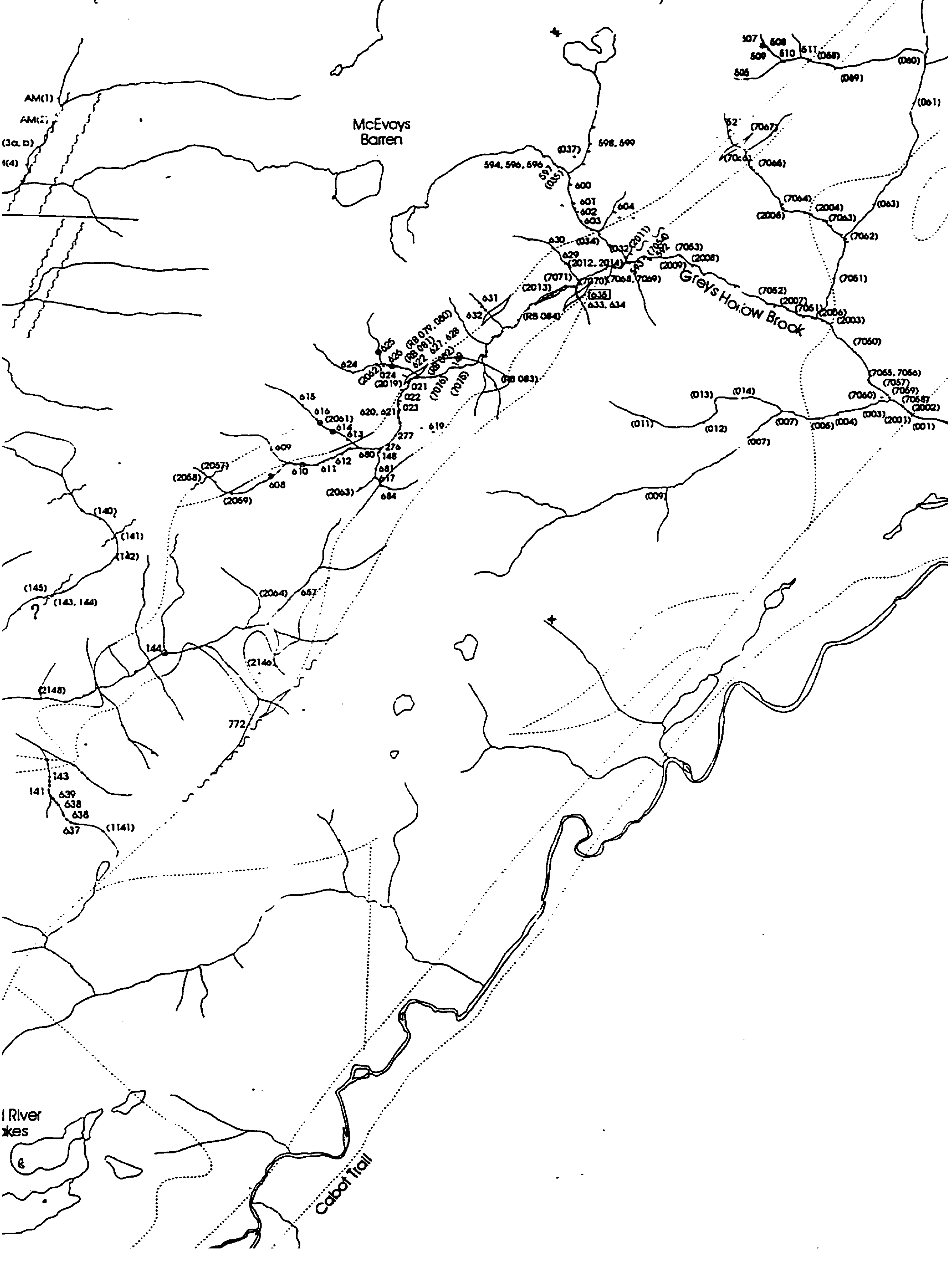
McEvoys
Barren
Greys Hollow Brook
Cabot Trail
River
kes

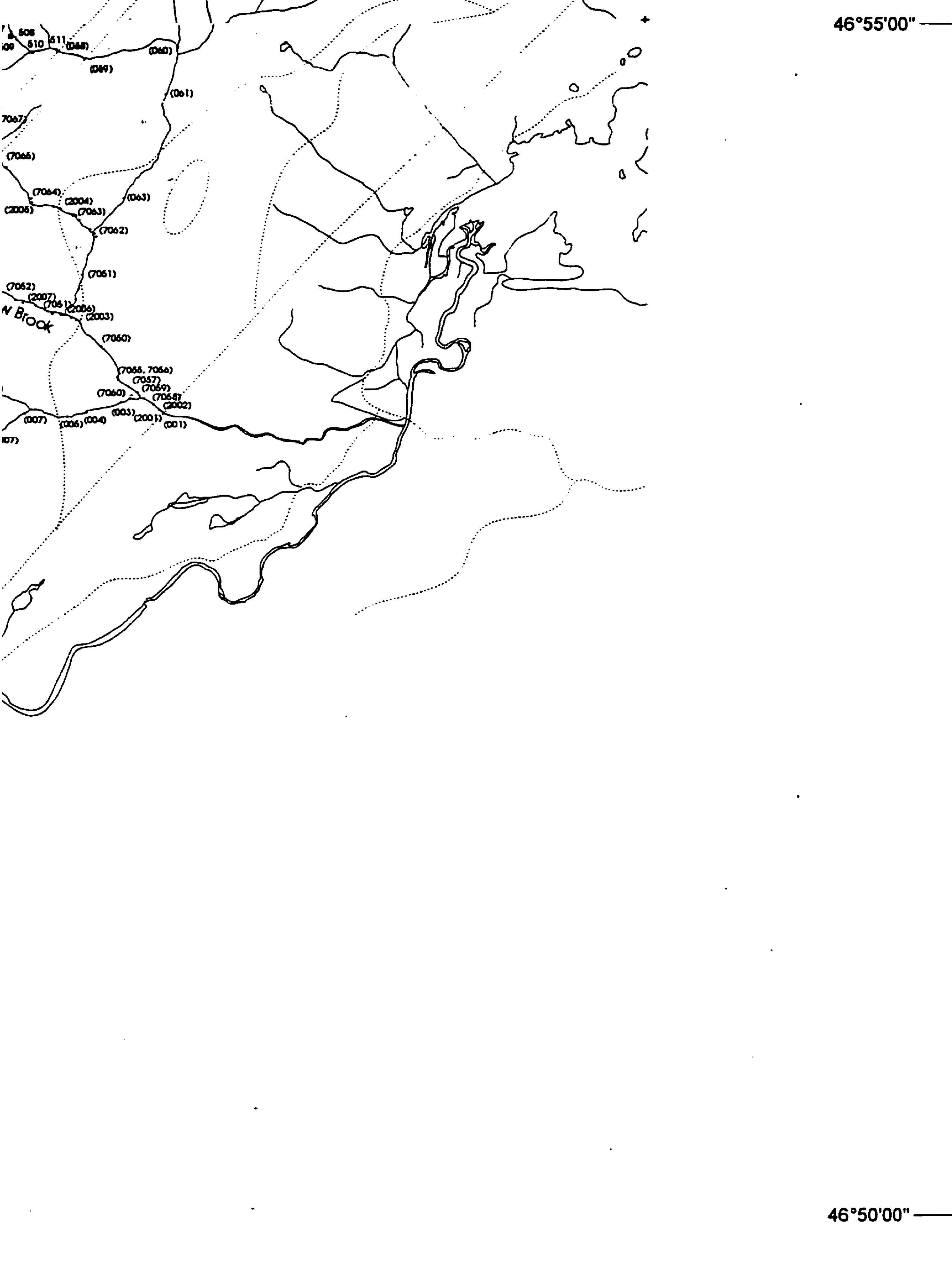
46°55'00"
608
610
611
(060)
(089)
(061)
(7067)
(7066)
(7064)
(2004)
(2005)
(7063)
(063)
(7062)
(7061)
(7052)
(2007)
(7051)
(2006)
(2003)
Brook
(7050)
(7055, 7056)
(7057)
(7059)
(7060)
(7058)
(2002)
(003)
(2001)
(001)
(007)
(006)
(004)
46°50'00"

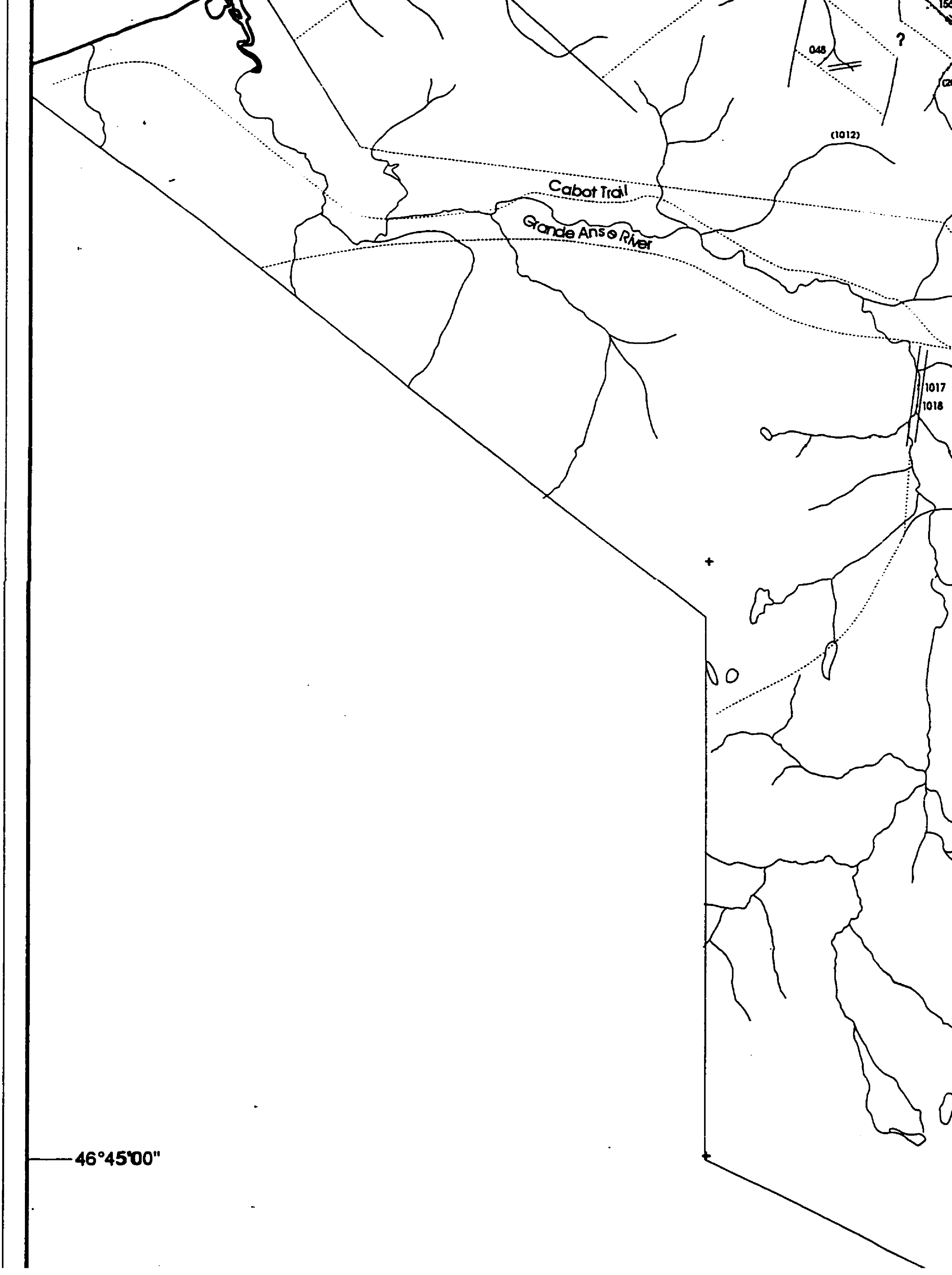
048
?
(1012)
Cabot Trail
Grande Anse River
1017
1018
46°45'00"

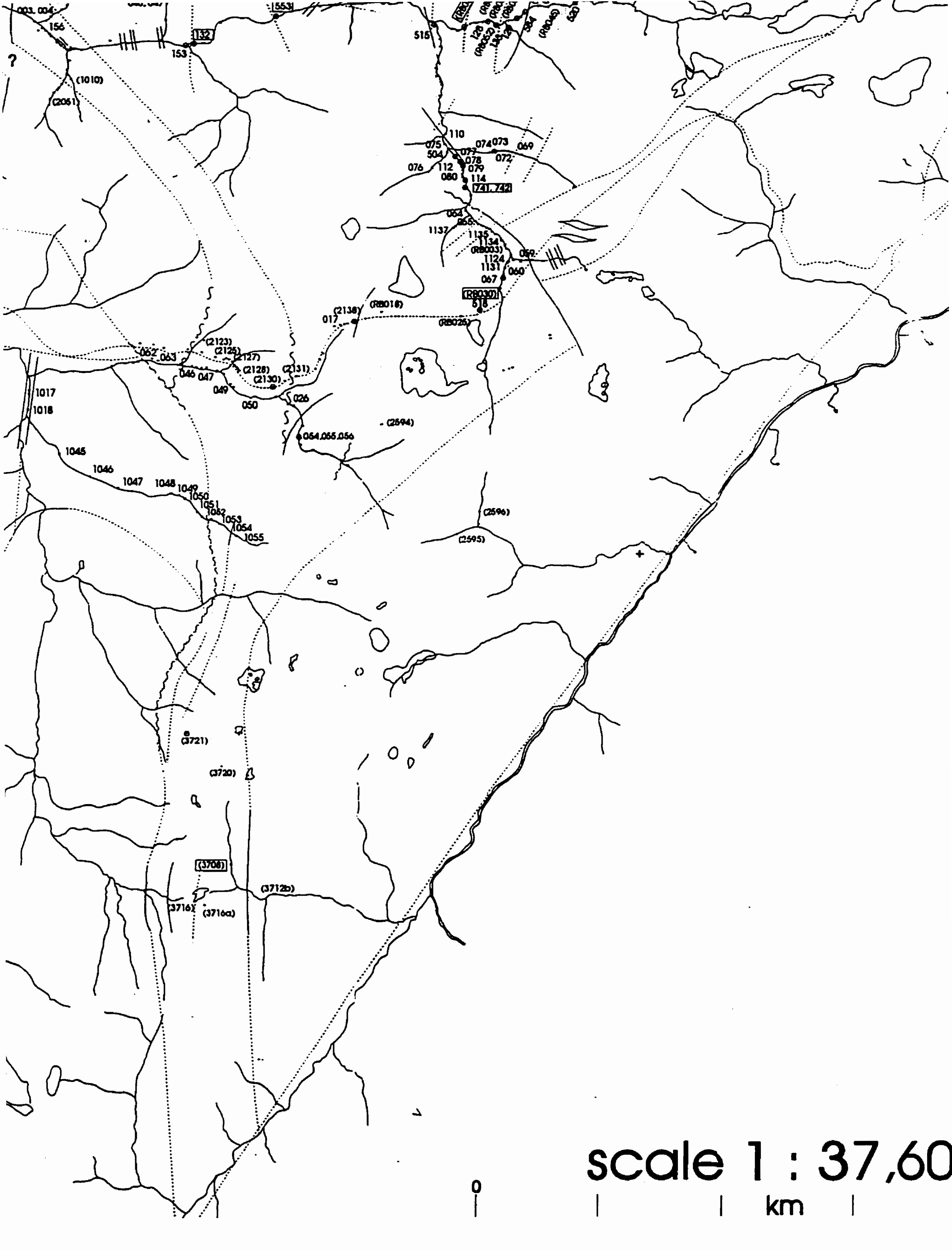
003, 004
156
1553
132
153
?
(1010)
(2061)
515
126
(RB052)
138
584
(RB045)
520
110
075
504
074
073
069
077
078
072
076
112
079
080
114
741, 742
064
065
1137
1135
1134
(RB003)
059
1124
1131
060
067
(RB030)
518
(RB018)
(2138)
017
(RB025)
(2123)
(2125)
062
063
(2127)
(2128)
(2131)
046
047
(2130)
049
050
026
1017
1018
(2594)
054,055,056
1045
1046
1047
1048
1049
1050
1051
1052
1053
1054
1055
(2596)
(2595)
(3721)
(3720)
(3708)
(3712b)
(3716)
(3716a)
scale 1 : 37,60
0
km

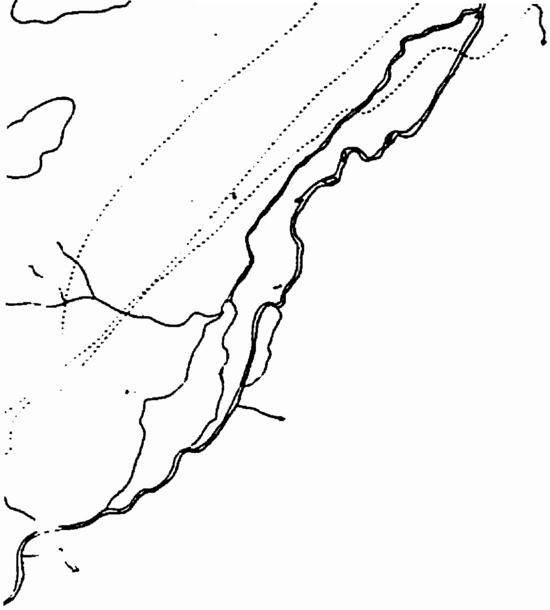

×	examined outcrop location
⊗	geochemistry sample location
$\boxed{065}$	geochronolgy sample location
AM(065)	AM85(001+) samples
(127)	CW85(001+) samples
(514)	FD85(500+) samples
(1082)	SB85(1000+) samples
(2042)	RR85(2000+) samples
065, 553	BVM90(001+). BVM91(500+) samples
(RB, 072)	RB91(001+) samples

,600

5

ɔn
ation
:ation

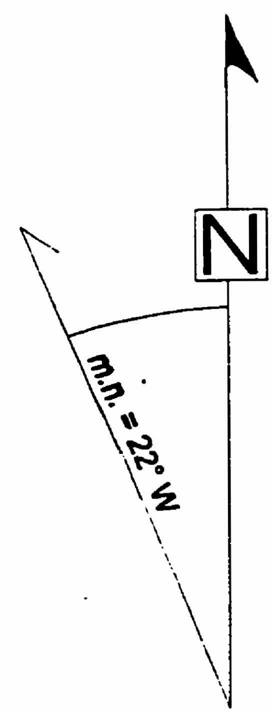

+) samples

46°45'00"

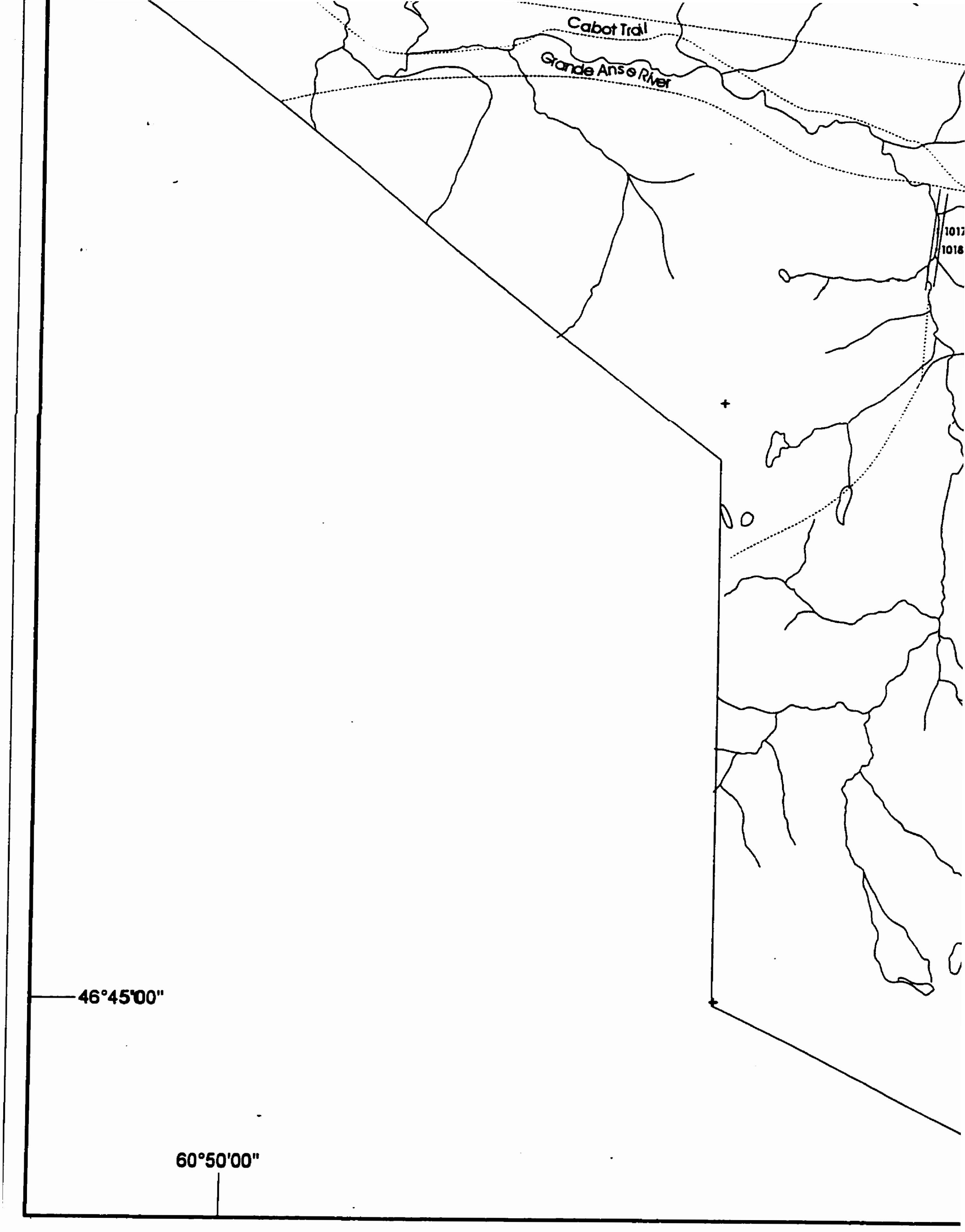

Cabot Trail
Grande Anse River
1017
1018
46°45'00"
60°50'00"

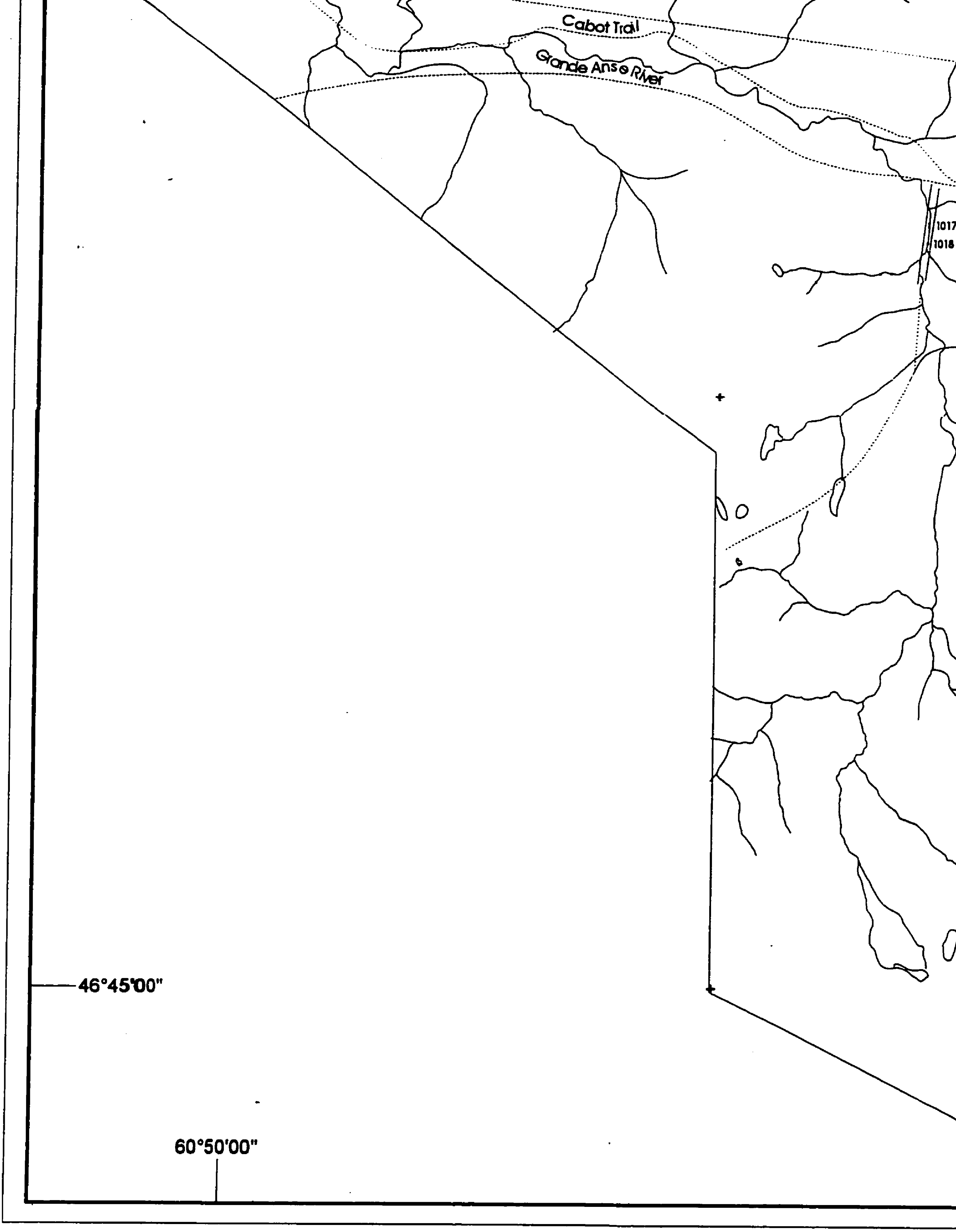

Cabot Trail
Grande Anse River
1017
1018
46°45'00"
60°50'00"

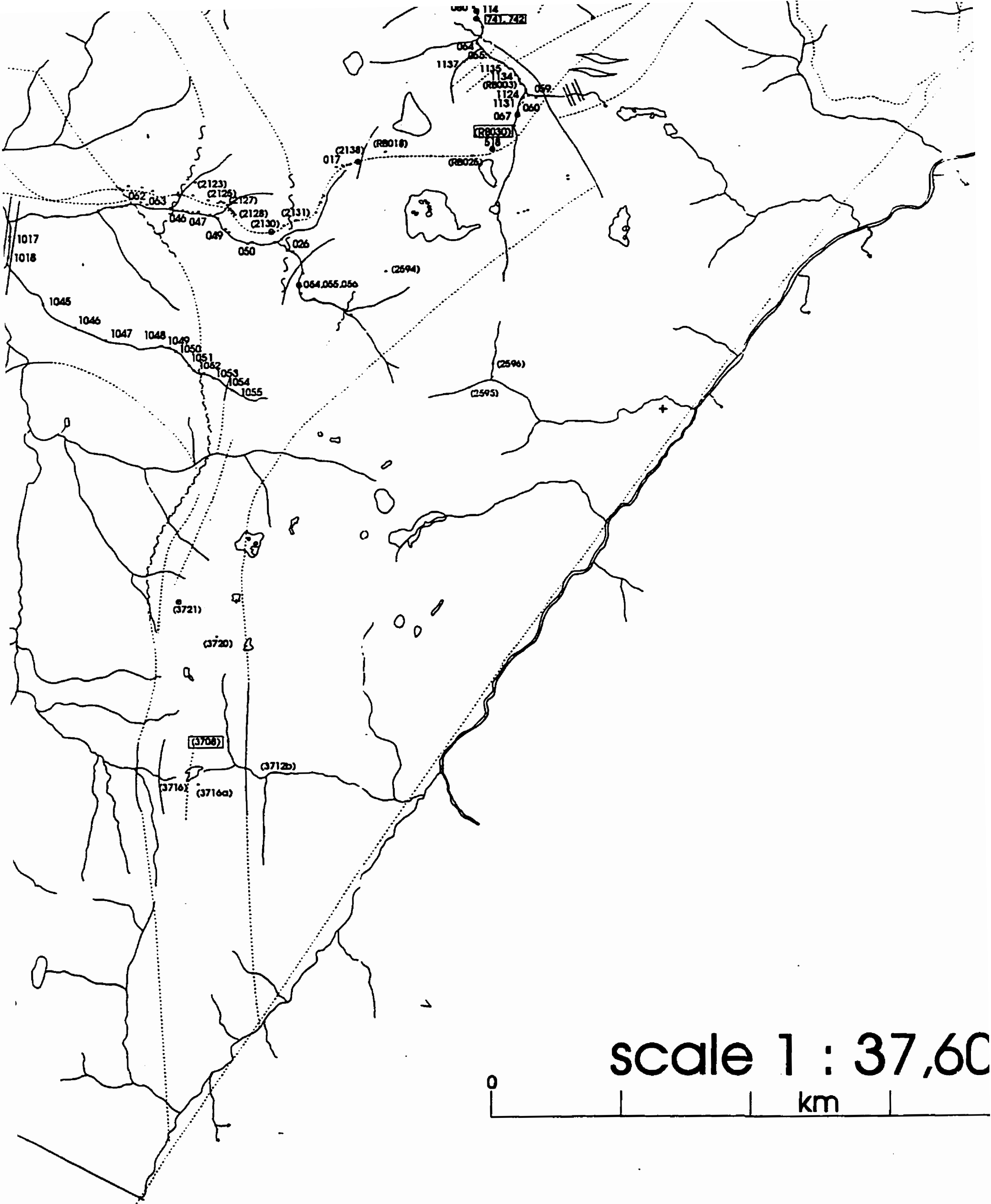

114
741, 742
064
066
1137
1135
1134
(RB003)
1124
1131
059
060
067
(RB030)
518
(RB026)
(RB018)
(2138)
017
(2123)
(2126)
(2127)
(2128)
(2130)
(2131)
062
063
046
047
049
050
026
1017
1018
(2594)
054,055,056
1045
1046
1047
1048
1049
1050
1051
1052
1053
1054
1055
(2596)
(2595)
(3721)
(3720)
(3708)
(3712b)
(3716)
(3716a)
scale 1 : 37,60
0
km

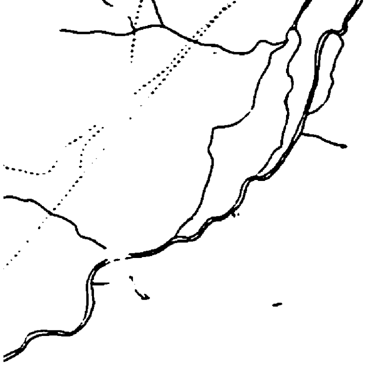

×	examined outcrop location
⊗	geochemistry sample location
$\boxed{065}$	geochronolgy sample location
AM(065)	AM85(001+) samples
(127)	CW85(001+) samples
(514)	FD85(500+) samples
(1082)	SB85(1000+) samples
(2042)	RR85(2000+) samples
065, 553	BVM90(001+). BVM91(500+) samples
(RB, 072)	RB91(001+) samples

7,600

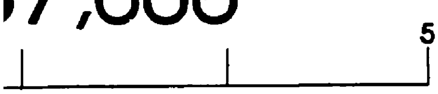

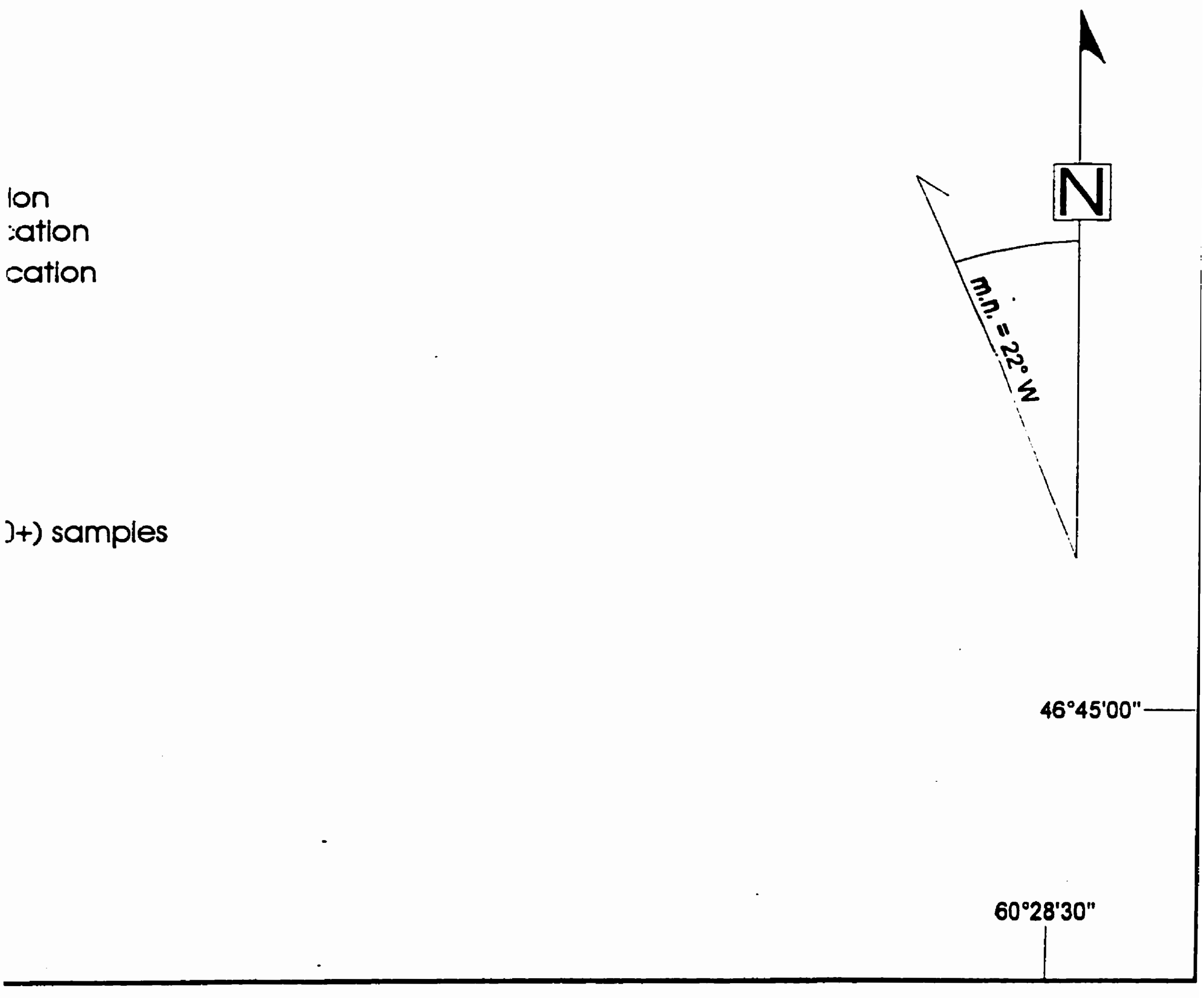
ion
:ation
cation
)+) samples
N
m.n. = 22° W
46°45'00"
60°28'30"

TEST TARGET (QA-3)

150mm

6"

APPLIED IMAGE, Inc

1653 East Main Street
Rochester, NY 14609 USA
Phone: 716/482-0300
Fax: 716/288-5989

© 1993, Applied Image, Inc., All Rights Reserved